frontiers | Research Topics

Emerging technologies and biology for tumor microenvironment and tumor-immune interplay

Edited by
Min Xue, Qihui Shi and Li Cao

Published in
Frontiers in Immunology
Frontiers in Oncology

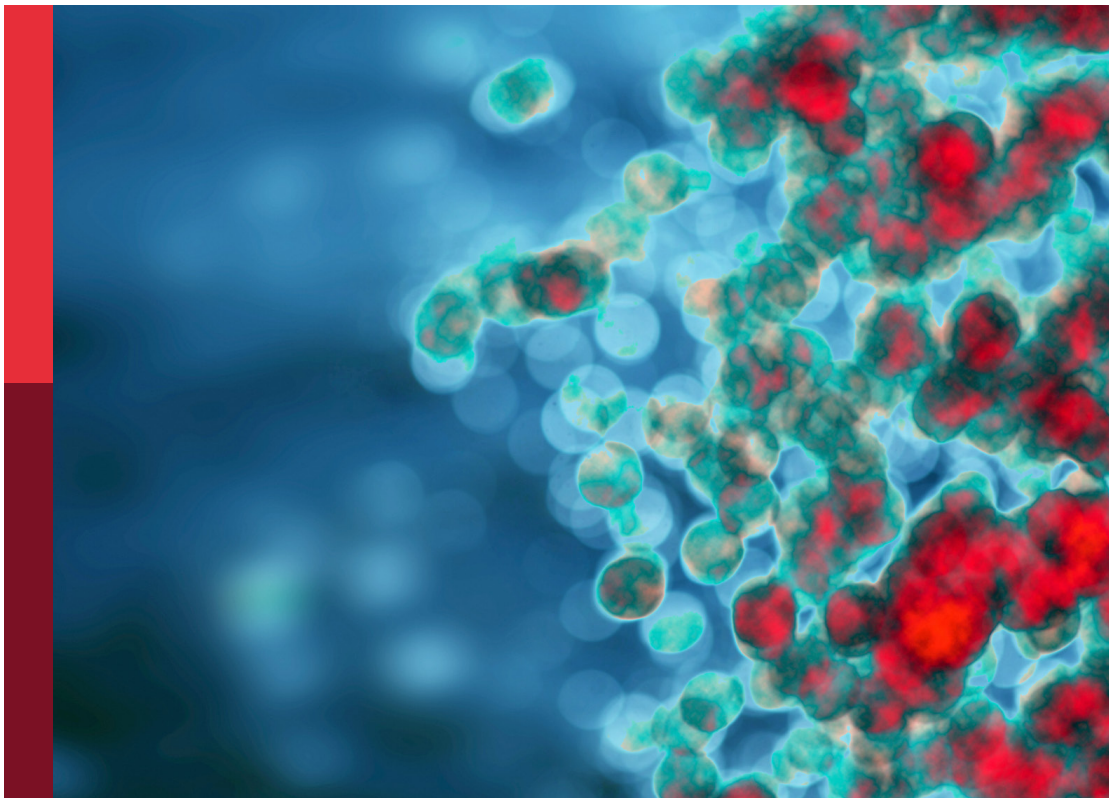

ISSN 1664-8714
ISBN 978-2-83250-904-3
DOI 10.3389/978-2-83250-904-3

About Frontiers

Frontiers is more than just an open access publisher of scholarly articles: it is a pioneering approach to the world of academia, radically improving the way scholarly research is managed. The grand vision of Frontiers is a world where all people have an equal opportunity to seek, share and generate knowledge. Frontiers provides immediate and permanent online open access to all its publications, but this alone is not enough to realize our grand goals.

Frontiers journal series

The Frontiers journal series is a multi-tier and interdisciplinary set of open-access, online journals, promising a paradigm shift from the current review, selection and dissemination processes in academic publishing. All Frontiers journals are driven by researchers for researchers; therefore, they constitute a service to the scholarly community. At the same time, the *Frontiers journal series* operates on a revolutionary invention, the tiered publishing system, initially addressing specific communities of scholars, and gradually climbing up to broader public understanding, thus serving the interests of the lay society, too.

Dedication to quality

Each Frontiers article is a landmark of the highest quality, thanks to genuinely collaborative interactions between authors and review editors, who include some of the world's best academicians. Research must be certified by peers before entering a stream of knowledge that may eventually reach the public - and shape society; therefore, Frontiers only applies the most rigorous and unbiased reviews. Frontiers revolutionizes research publishing by freely delivering the most outstanding research, evaluated with no bias from both the academic and social point of view. By applying the most advanced information technologies, Frontiers is catapulting scholarly publishing into a new generation.

What are Frontiers Research Topics?

Frontiers Research Topics are very popular trademarks of the *Frontiers journals series*: they are collections of at least ten articles, all centered on a particular subject. With their unique mix of varied contributions from Original Research to Review Articles, Frontiers Research Topics unify the most influential researchers, the latest key findings and historical advances in a hot research area.

Find out more on how to host your own Frontiers Research Topic or contribute to one as an author by contacting the Frontiers editorial office: frontiersin.org/about/contact

Emerging technologies and biology for tumor microenvironment and tumor-immune interplay

Topic editors

Min Xue — University of California, Riverside, United States

Qihui Shi — Fudan University, China

Li Cao — Department of Neurology, Shanghai Jiao Tong University Affiliated Sixth People's Hospital, China

Citation

Xue, M., Shi, Q., Cao, L., eds. (2022). *Emerging technologies and biology for tumor microenvironment and tumor-immune interplay*. Lausanne: Frontiers Media SA. doi: 10.3389/978-2-83250-904-3

Table of contents

frontiers | Frontiers in Immunology

ORIGINAL RESEARCH
published: 04 April 2022
doi: 10.3389/fimmu.2022.830158

Analysis of Tumor Glycosylation Characteristics and Implications for Immune Checkpoint Inhibitor's Efficacy for Breast Cancer

Wenchang Lv[1†], Honghao Yu[1†], Mei Han[2], Yufang Tan[1], Min Wu[1], Jun Zhang[3], Yiping Wu[1*] and Qi Zhang[1*]*

[1] Department of Plastic and Cosmetic Surgery, Tongji Hospital, Tongji Medical College, Huazhong University of Science and Technology, Wuhan, China, [2] Department of Anesthesiology, The People's Hospital of China Three Gorges, China Three Gorges University, Yichang, China, [3] Department of Thyroid and Breast Surgery, Shenzhen Qianhai Shekou Free Trade Zone Hospital, Shenzhen, China

OPEN ACCESS

Edited by:
Min Xue,
University of California, Riverside, United States

Reviewed by:
Valeria I. Segatori, National University of Quilmes, Argentina
David Linnaeus Gibbs, Institute for Systems Biology (ISB), United States

***Correspondence:**
Jun Zhang
zhangjunshekou@163.com
Yiping Wu
tongjiplastic@163.com
Qi Zhang
zhangqi06172@163.com

[†]These authors have contributed equally to this work

Specialty section:
This article was submitted to Cancer Immunity and Immunotherapy, a section of the journal Frontiers in Immunology

Received: *06 December 2021*
Accepted: *08 March 2022*
Published: *04 April 2022*

Citation:
Lv W, Yu H, Han M, Tan Y, Wu M, Zhang J, Wu Y and Zhang Q (2022) Analysis of Tumor Glycosylation Characteristics and Implications for Immune Checkpoint Inhibitor's Efficacy for Breast Cancer. Front. Immunol. 13:830158. doi: 10.3389/fimmu.2022.830158

The alterations of glycosylation, which is a common post-translational modification of proteins, have been acknowledged as key events in breast cancer (BC) oncogenesis and progression. The aberrant expression of glycosyltransferases leads to aberrant glycosylation patterns, posing the diagnostic potential in BC outcomes. The present study aims to establish a glycosyltransferase-based signature to predict BC prognosis and response to immune checkpoint inhibitors. We firstly screened 9 glycosyltransferase genes from The Cancer Genome Atlas (TCGA) database and accordingly established a glyco-signature for predicting the prognosis in BC patients. Patients with BC were successfully divided into high-risk and low-risk groups based on the median cutoff point for risk scores in this signature. Next, the combinational analyses of univariate and multivariate Cox regression, Kaplan–Meier, and receiver operating characteristic (ROC) curves were used to prove that this glyco-signature possessed excellent predictive performance for prognosis of BC patients, as the high-risk group possessed worse outcomes, in comparison to the low-risk group. Additionally, the Gene Set Enrichment Analysis (GSEA) and immunologic infiltration analysis were adopted and indicated that there was a more immunosuppressive state in the high-risk group than that in the low-risk group. The clinical sample validation verified that glycosyltransferase genes were differentially expressed in patients in the low- and high-risk groups, while the biomarkers of antitumor M1 macrophages were increased and N-glycosyltransferase STT3A decreased in the low-risk group. The final in vitro assay showed that the silencing of STT3A suppressed the proliferation and migration of BC cells. Collectively, our well-constructed glyco-signature is able to distinguish the high- and low-risk groups and accordingly predict BC prognosis, which will synergistically promote the prognosis evaluation and provide new immunotherapeutic targets for combating BC.

Keywords: breast cancer, prognosis, signature, glycosyltransferase, immune checkpoint

INTRODUCTION

Breast cancer (BC) is the most prevalent malignancy and the primary cause of cancer-related deaths in women worldwide (1). According to the Cancer Statistics 2021, BC accounts for 30% of female cancers, and BC was the major cause of cancer-related mortality among women aged 20 to 59 years (2). Immune checkpoint therapy (ICT) is a promising new treatment, which enhances antitumor immune responses by regulating the activation and effector functions of T lymphocytes (3). Many clinical trials had proved that immune checkpoint inhibitors (ICIs) against programmed cell death protein-1(PD-1)/programmed cell death-ligand 1 (PD-L1) and cytotoxic T lymphocyte-associated protein-4 (CTLA-4) axes can induce durable clinical responses in some BC patients (4). However, a large number of patients derive little or no clinical benefits from some emerging immunotherapeutics, especially in patients with PD-L1-negative, estrogen receptor (ER)-positive BC (5). Therefore, the most urgent thing is to explore novel hallmarks predicting the responsiveness to immunotherapy and to establish reliable prognostic signatures for BC patients, which will allow stratification of patients and precision medicine.

Recently, glycosylation is a typical post-translational modification of proteins, which involves different families of glycan-modifying enzymes, including glycosyltransferases and glycosidases (6). *O*-glycan truncation, sialylation, fucosylation, and *N*-glycan branching are the most common alterations of cancer-related glycosylation, which drive several malignant behaviors of tumors, including tumor cell invasion and dissociation, angiogenesis, metastasis, immune modulation, and cell–matrix interactions (7). For instance, Li et al. suggested that β-1,3-*N*-acetylglucosaminyl transferase (B3GNT3) participated in the PD-1/PD-L1 interaction and B3GNT3-mediated glycosylated PD-L1 suppressed T-cell activity in triple-negative BC (8). ST3GAL1-mediated *O*-linked sialylation of CD55 promoted immune evasion of BC, and ST3GAL1 was overexpressed in high tumor grade (9). Therefore, glycosylation is involved in multiple oncogenesis and progression, as well as immune system modulation in BC.

With the advancements of glycomics, emerging evidence has confirmed that dynamic glycosylation changes are closely associated with tumor progression. It poses that protein glycosylation is a promising biomarker to diagnose and monitor various cancers (10). It is worth noting that low expression of mannosyl(α-1,3-)-glycoprotein β-1,2-*N*-acetylglucosaminyltransferase (MGAT1) was correlated with dedifferentiation of hepatocellular carcinoma, intrahepatic metastasis, and poor prognosis (11). Besides, it has been reported that *N*-acetylgalactosaminyltransferases (GALNT6) increased *O*-glycosylation of α2M to promote the migration and invasion of BC and that the high expression of GALNT6 in BC patients suggested a shorter overall survival (OS) (12). It is meaningful to excavate underlying glycosylation biomarkers and their expression alterations for predicting diagnosis, prognosis, and even therapeutic resistance of cancers.

Therefore, it is intriguing to explore the potential of glycosyltransferases for constructing a prognostic-predicting risk model of BC. In the present study, we firstly screened a profile of 9 differentially expressed glycosyltransferase genes depending on genomic information of 1,089 BC samples and accordingly constructed a prognostic-predicting risk signature. In accordance with the median risk score, the BC cases were successfully classified into low-risk and high-risk groups. These two groups showed distinct differences in OS, gene expression, immune infiltration, ICI response, and chemosensitivity. Meanwhile, clinical sample validation and *in vitro* assay proved that the selected glycosyltransferase genes were associated with the immune state and malignant behaviors of BC. Our results indicated that our model based on glycosyltransferase genes was capable of predicting the prognosis and immune state in BC patients. The detailed flowchart could be seen in **Figure S1**. This study will provide a complimentary screening approach for guiding the prognosis determination and immunotherapy of BC.

MATERIALS AND METHODS

Dataset Source and Preprocessing

Publicly available gene-expression data and related clinical information were obtained from The Cancer Genome Atlas (TCGA) database (https://portal.gdc.cancer.gov/). The detailed clinical information of included BC patients is summarized in **Table S1**. The cases without survival information were excluded from our study. Finally, 1,089 BC cases in TCGA with clinical data were integrated into the analysis. There were 1,089 patients with TCGA data as the training set. Then, half of 1,089 patients were randomly selected as a validation set.

Gene Ontology, Kyoto Encyclopedia of Genes and Genomes, and Gene Set Enrichment Analysis Enrichment Analysis

The Gene Ontology (GO) and Kyoto Encyclopedia of Genes and Genomes (KEGG) pathway analyses are online databases and were used to perform functional enrichment and pathway enrichment regarding the differently expressed glycosyltransferase genes between BC patients and normal samples with the "enrichplot" R package (13). The Gene Set Enrichment Analysis (GSEA) was investigated to explore the enriched pathways in two risk groups using the GSEA software provided by the Broad Institute. False discovery rate (FDR) $q < 0.05$ with $p < 0.05$ after performing 1,000 permutations was determined to be statistically significant.

Construction and Validation of Glyco-Signature

To ascertain prognosis-related glycosyltransferase genes, univariate Cox regression analysis of 169 glycosyltransferase genes was firstly adopted in the training set to select 13 glycosyltransferase genes related to the BC prognosis ($p < 0.05$). The 169 glycosyltransferase genes were extracted from GlycoGene DataBase (GGDB; https://acgg.asia/ggdb2/). The OS of BC patients was considered and calculated for BC prognosis in the Cox regression analysis. In addition, the lasso regression was performed to further compress glycosyltransferase genes. Then,

the glyco-signature for predicting the prognosis of BC patients was established using multivariate Cox regression analyses. The calculation of the risk score was based on the following formula:

$$\text{Risk score} = \sum_{i=1}^{n}(\beta_i * Expi)$$

where n is the number of glycosyltransferase genes, exp indicates the glycosyltransferase gene expression value, and β is the coefficient of multi-Cox regression. Patients were then categorized into the low-risk and high-risk groups depending on the median risk score. The validation set was applied to test the universality of the risk signature. The prognosis difference between the low-risk and high-risk groups was evaluated by the Kaplan–Meier (KM) survival analysis using R language v4.0.2 ($p < 0.05$).

Evaluating Signature Performance and Constructing Nomogram

Independent prognostic analysis and multivariate independent prognostic analysis were conducted because glycemic signatures and other clinical parameters, including age, stage, stages T, N, and M, were covariates. p-Value and hazard ratios (HRs) were displayed in the forest plots. Next, a nomogram was established depending on this glyco-signature and clinical parameters to evaluate the 1-, 3-, and 5-year OS of BC patients using the "rms" R package. Nomogram is a graphical representation of a complex mathematical formula, which could visualize the multivariate Cox regression and predict the OS of BC patients (14). Calibration plots and area under the curve (AUC) were utilized to estimate the predictive accuracy of the nomogram. The principal component analysis (PCA) was employed to cluster the cases in 2D scatterplots.

Mutation and Copy Number Alteration Analysis of Glycosyltransferase Genes

The mutation and copy number alteration (CNA) regarding the 9 glycosyltransferase genes were obtained through segmentation analysis and GISTIC algorithm in the cBioPortal (15). Besides, the 20 genes with the highest mutation frequency in the high-risk and low-risk groups were identified by the waterfall graph.

Immunologic Infiltration Analysis

The fraction scores of 22 immune cell subsets, as well as 29 pivotal pathways in the samples, were calculated using single-sample gene set enrichment analysis (ssGSEA) in the "gsva" R package. ESTIMATE algorithm was then performed to figure out the stromal score and immune score and tumor purity in the BC samples.

Chemosensitivity Analysis

Half of the maximum inhibitory concentration IC50 was applied to evaluate the chemoreceptive difference between the low-risk and high-risk groups. The mRNA profiles and drug sensitivity IC50 values were acquired on the CELLMINER website (https://discover.nci.nih.gov/cellminer/). Wilcoxon's test was conducted to analyze the significance of the difference in IC50 between the two groups.

Quantitative Real-Time PCR

The TRIzol reagent kit (Invitrogen, Carlsbad, CA, USA) was performed to obtain the total RNA of BC tissues. Then, the concentration and purity of total RNA were estimated by using a NanoDrop 2000 spectrophotometer (Thermo Fisher Scientific, Waltham, MA, USA). The RNA was reverse transcribed into complementary DNA (cDNA) using the 1st Strand cDNA Synthesis Kit (Yeasen, Shanghai, China). The qRT-PCR analysis in duplicate samples was carried out with SYBR Green™ Master Mix (Yeasen, China) in a QuantStudio1 PCR (ABI Q1, Foster City, CA, USA). Primer sequences of these 9 glycosyltransferase genes used for RT-qPCR are summarized in **Table S2**.

Histological Evaluation

For immunohistochemistry (IHC), the BC tissue segments were deparaffinized, rehydrated through a graded ethanol series, and retrieved by heating slides at 100°C for 1 h in citrate buffer. The anti-hSTT3A antibodies (all 1:100, ProteinTech, Wuhan China) were applied. Next, the sections were washed in TBST solution and incubated with horseradish peroxidase (HRP)-conjugated secondary antibodies for about 1 h. The antigen–antibody complex was visualized using DAB Peroxidase Substrate Kit (Maxin, Fuzhou, China). The IHC images were obtained under a SOPTOP CX40 microscope (China).

For immunofluorescence (IF), sections were incubated with an anti-hSTT3A antibody (1:100, ProteinTech, China) at 4°C overnight. After being washed 3 times with TBST, the sections were incubated with a cocktail of secondary antibodies (Life Technologies, Carlsbad, CA, USA) for 1 h at room temperature. Nuclear 4,6-diamidino-2-phenylindole (DAPI dye; Vector Laboratories, Burlingame, CA, USA) was utilized for counterstaining the slides. Images were captured using a fluorescence microscope under the corresponding laser wavelength (Olympus, Tokyo, Japan).

In Vitro Verification

The proliferation capabilities of MCF-7 and MDA-MB-231 cells were estimated by using the cell counting kit-8 (CCK-8) assay (Dojindo, Kumamoto, Japan). The cells were inoculated in a 96-well plate (3×10^3/well) with 3 wells for each group. After silencing of STT3A, the CCK-8 assay was performed by adding 10 μl of CCK-8 solution in each well, with subsequent incubation in an incubator for 2 h in a dark environment. Finally, the absorbance was analyzed at a 450-nm wavelength under a microplate reader (BD Biosciences, San Jose, CA, USA).

Transwell migration champers containing 24-well plates (8-μm size; Corning, New York, NY, USA) were used to assess the migration ability. Firstly, a total of 5×10^4 cells/well in the upper cell chamber and 500 μl of DMEM/F12 medium containing 20% fetal bovine serum (FBS) were put in the lower cell chamber as an attractant. At 24 h post-incubation at 37°C, the methanol and 0.1% crystal violet were added to fix and stain the invaded cells in

the lower chambers. Finally, the number of invaded cells was counted by ImageJ software.

Wound healing assay was used to assess the migration of MCF-7 and MDA-MB-231 cells. After the cells confluenced to form a single cell layer, the cell monolayers were lightly scratched with the tip of a 200-μl pipette. Afterward, the cells were incubated in DMEM/F12 medium without FBS at 37°C of 24 h. The horizontal distance of migrated cells from the wound edge was calculated by ImageJ software (NIH, USA).

Lectin blot was applied to assess the expression level of *N*-glycans in BC samples, as well as in MCF-7 and MDA-MB-231 cells. Total proteins were extracted using lysis buffer (Cell Signaling Technology, Danvers, MA, USA), and their concentrations were measured by bicinchoninic acid (BCA) protein assay (Boster, Wuhan, China). The equal content of extracted protein was separated by 12% sodium dodecyl sulfate–polyacrylamide gel electrophoresis (SDS-PAGE) and electrotransferred onto polyvinylidene fluoride (PVDF) membranes (Bio-Rad, Hercules, CA, USA). After being blocked with Carbo-Free Blocking Solution (Vector Laboratories Inc., USA) for 30 min, the membranes were then incubated with biotinylated lectins for 30 min at room temperature, including concanavalin A (ConA), *Phaseolus vulgaris* Leucoagglutinin (PHA-L), and *P. vulgaris* erythroagglutinin (PHA-E) (Vector Laboratories Inc., USA), which were prepared and diluted in PBS at 20 μg/ml concentration. Afterward, the PVDF membranes were incubated with HRP streptavidin (Vector Laboratories Inc., USA) at 1:2,000 dilution for 1 h and detected by using enhanced chemiluminescence (ECL) assay kit (Yeasen, Shanghai, China).

Statistical Analysis

The KM curve was applied to compare the OS among the two risk groups. Univariate and multivariate Cox regression analyses were applied to screen independent prognostic variables. The receiver operating characteristic (ROC) curve was employed to validate the diagnostic value of the signature. Student's t-test was adopted to determine the relationships between the risk score and clinicopathological factors. All statistical analyses were carried out with R language R x64 4.0.5. p-Value <0.05 was regarded as statistically significant.

RESULTS

Consensus Clustering Analysis Deciphered the Potential Cellular Biological Effects of Glycosyltransferase Genes

The GO and KEGG pathway analyses were utilized to reveal the possible cellular biological effects of glycosyltransferase-associated differently expressed genes (DEGs). The top 10 enriched GO terms of biological process (BP), cellular component (CC), and molecular function (MF) for the glycosyltransferase genes are described as a scatter diagram in **Figure 1A**. These enriched GO terms were associated with glycosylation, Golgi stack, and transferring glycosyl group. KEGG analysis also presented that the glycosyltransferase genes were enriched in *O*-glycan, *N*-glycan, and glycosphingolipid biosynthesis as shown in **Figure 1B**.

Development of Glyco-Signature

Through Cox regression analysis, it was found that 13 differently expressed glycosyltransferase genes were associated with BC prognosis ($p < 0.05$) (**Figure 1C**). Lasso regression was applied to further narrow down the number of the genes (**Figure 1D**). Finally, 9 selected glycosyltransferase genes (FUT7, ST3GAL1, ST3GAL3, ST6GALNAC4, B3GNT2, CHPF, POMGNT2, ALG3, and STT3A) were screened out to establish the prognostic risk signature based on the 1,089 cases in TCGA training set (**Figure 1E**). The following formula was used to calculate the risk score for each patient:

$$\begin{aligned}\text{risk score} = {} & \text{ST3GAL1} * 0.0203 - \text{FUT7} * 0.9140 \\ & + \text{ST3GAL3} * 0.1901 + \text{ST6GALNAC4} * 0.0347 \\ & + \text{B3GNT2} * 0.0229 \\ & + \text{CHPF} * 0.0045 - \text{POMGNT2} * 0.0872 \\ & + \text{ALG3} * 0.0180 + \text{STT3A} * 0.0111\end{aligned}$$

Based on the median risk score (0.976), we divided 1,089 BC cases in TCGA training set into the low- and high-risk groups. We confirmed that the high-risk group had a significantly higher percentage of patients with dead status in comparison to the low-risk group. The expression features of the 9 selected glycosyltransferase genes are shown in the heatmap (**Figures 2A, B**). Then, we used the validation set to further validate the universality of the risk signature. With the same risk signature in the training set, the validation set was divided into the low-risk and high-risk groups. The high-risk group also showed a worse prognosis and different gene expression (**Figure 2B**). The KM survival curve showed the low-risk group with markedly longer OS, disease-free survival, and progression-free interval ($p < 0.05$) (**Figures 2C–F**).

Validation of the Glyco-Signature

Based on TCGA datasets, the univariate and multivariate regression analyses revealed that the risk score was correlated with the prognosis ($p < 0.05$) (**Figures 3A, B**), which verified that the glyco-signature was a robust independent prognostic index for BC. To predict survival probability at 1, 3, and 5 years directly and effectively, we then constructed a nomogram including the risk score and the clinicopathological factors (**Figure 3C**). The correction curve was used to correct the accuracy of the 1-, 3-, and 5-year nomogram, which suggested that the nomogram showed high consistency with the actual survival (**Figure 3D**). In addition, we plotted the time-dependent ROC curve to evaluate the risk signature. The AUC values of the 2-, 3-, and 4-year OS probability were 0.702, 0.733, and 0.743, respectively (**Figure 3E**). Besides, the AUC value of risk score was of higher

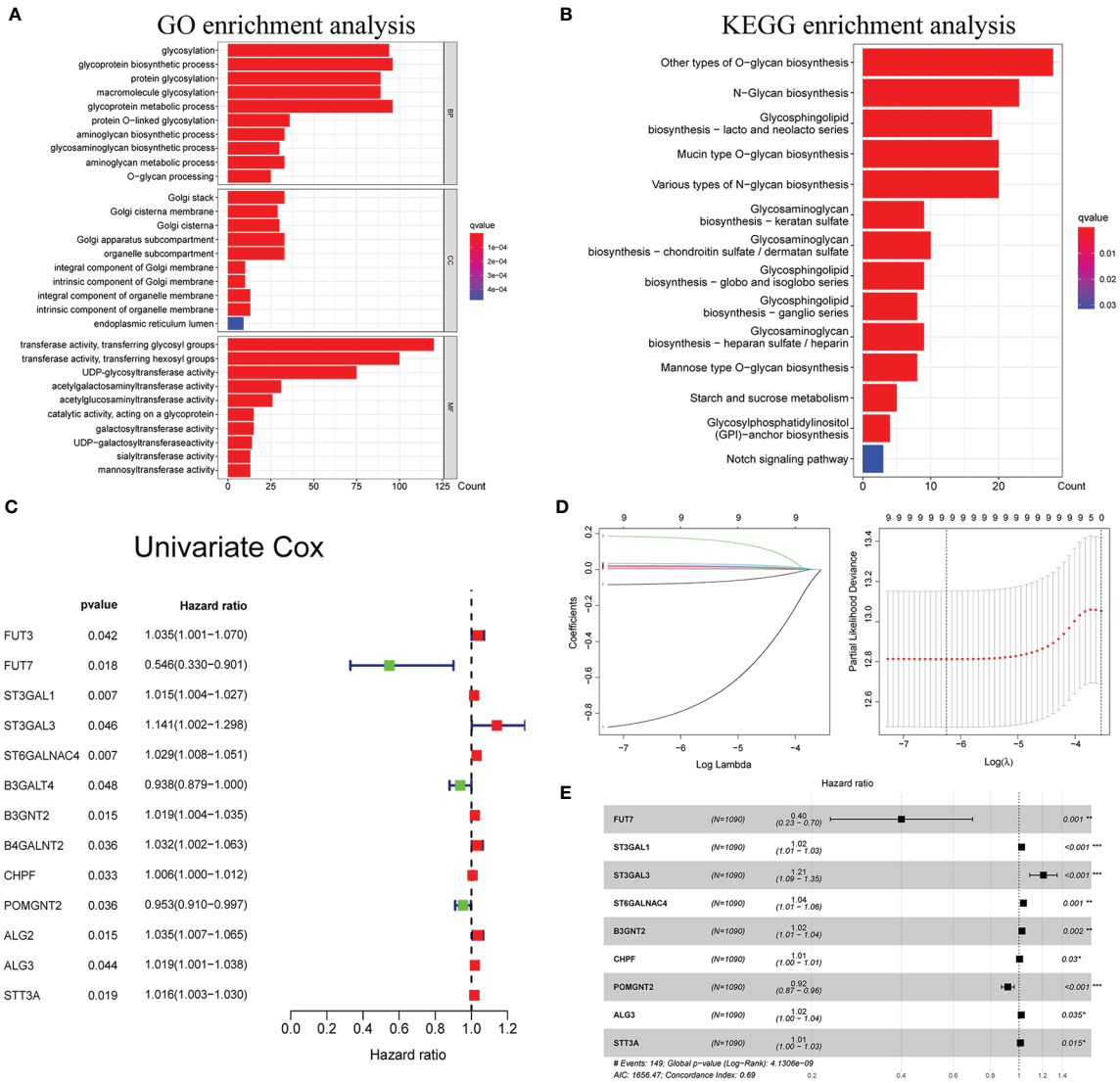

FIGURE 1 | Functional enrichment analysis of glycosyltransferase genes and construction of glyco-signature. Functional annotations of glycosyltransferase-associated DEGs were determined from GO **(A)** and KEGG **(B)** pathway analyses. **(C)** Univariate Cox regression analysis screened 13 glycosyltransferase genes that were related to the BC prognosis ($p < 0.05$). **(D)** Lasso coefficient profiles of the 13 prognosis-associated glycosyltransferase genes with non-zero coefficients validated by the optimal lambda. **(E)** Multivariate Cox regression analysis selected 9 glycosyltransferase genes to construct a risk signature. DEGs, differently expressed genes; GO, Gene Ontology; KEGG, Kyoto Encyclopedia of Genes and Genomes; BC, breast cancer. *$p < 0.05$, **$p < 0.01$, ***$p < 0.001$.

predictive ability than that of age, stage, and stages T, N, and M (**Figure 3F**).

Comparison of Risk Models

Five existing prognostic risk models (16–20) were selected to compare with our glyco-signature, and the ROC and KM curves of the five models were accordingly plotted (**Figures 4A, C**). Then, we calculated the concordance index (C-index) with the "rms" package in R. This result proved that the AUC values at 3 years of this model were higher than those in the five models, and our model had the highest C-index (**Figure 4B**), indicating that our model performed the best among the six prognostic risk models. The HR and p-value of the six models are presented in **Figure 4D**.

Clinical Relevance of Risk Signature

The heatmap was plotted to show the distribution of the clinicopathological factors and the 9 glycosyltransferase genes (**Figure 5A**). The corresponding scatter diagrams further revealed that age (**Figure 5B**), survival status (**Figure 5C**), clinical stage (**Figure 5D**), T stage (**Figure 5E**), and N stage (**Figure 5F**) were related to the risk score, M stage is not significantly related to the risk score (**Figure 5G**), and the result was tested by the Wilcoxon signed-rank test ($p < 0.05$).

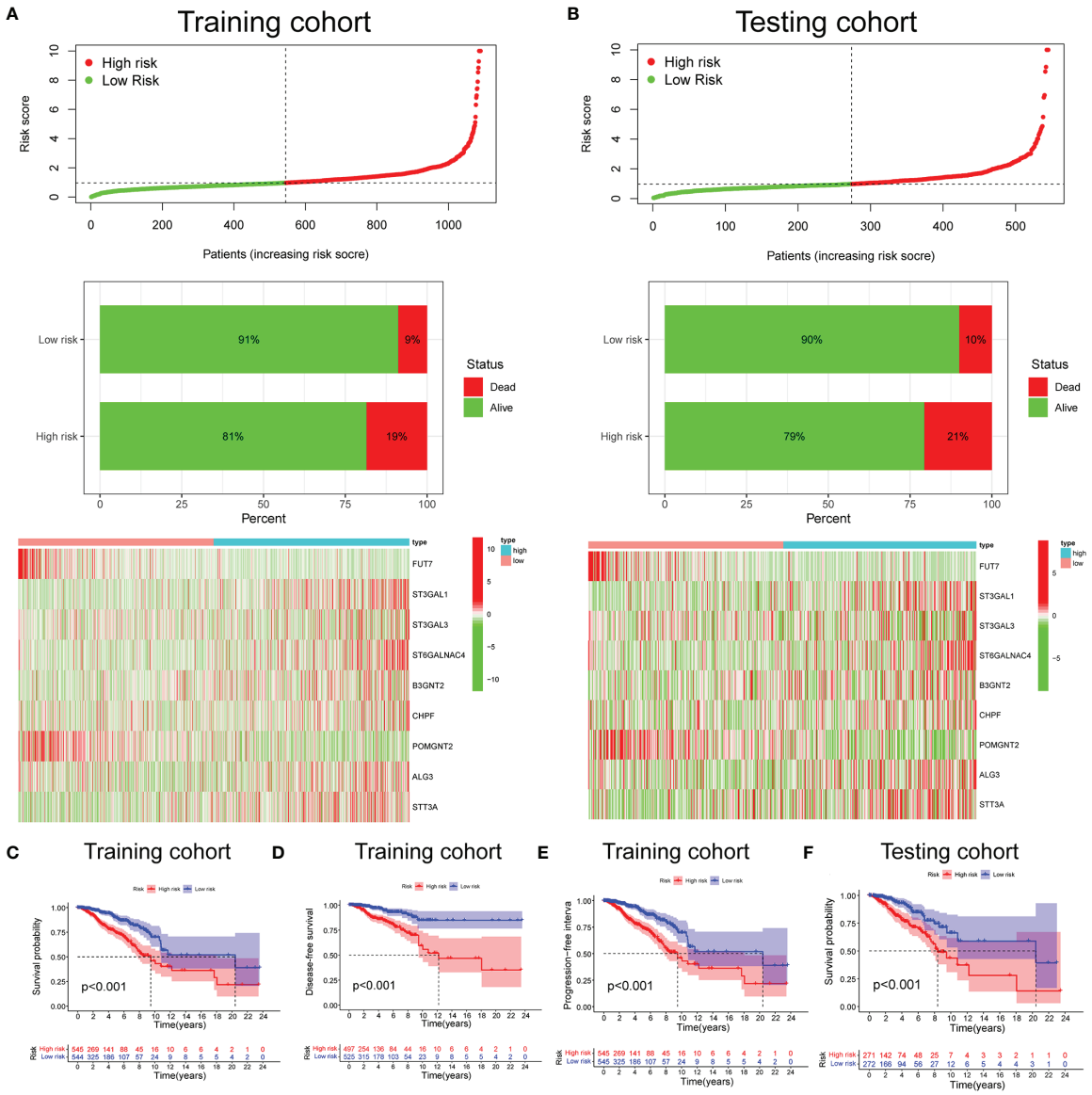

FIGURE 2 | Prognosis and expression of glycosyltransferase genes in the low-risk and high-risk groups of BC patients. Risk plot distribution, survival status, and expression of risk genes of the training set **(A)** and validation set **(B)**. KM survival curve analysis of OS **(C)**, disease-free survival **(D)**, and progression-free interval **(E)** in the training set. **(F)** KM survival curve in the testing set. BC, breast cancer; KM, Kaplan–Meier; OS, overall survival.

In addition, we found that 7 pairs of genes were highly correlated with the risk score in the positive direction and 2 pairs that were negatively correlated (**Figures 5H, I**).

Gene Set Enrichment Analysis of Risk Score-Related Signaling Pathways

To explore the enriched pathways in the 2 groups, we performed GSEA. The result indicated that cajal body, DNA packaging complex, fructose and mannose metabolism, steroid biosynthesis, and tight junction were abundant in the high-risk group and that activation of the immune response, adaptive immune response, B-cell activation, asthma, cytokine–receptor interaction, hematopoietic cell lineage, primary immunodeficiency, and T-cell receptor signaling pathway had a higher enrichment in the low-risk group (**Figures 6A, B**). Many signaling pathways associated with immune response were enriched in the low-risk group, indicating an immunosuppression state in the high-risk group. Then, we performed the PCA based on the total genes (**Figure 6C**), glycosyltransferase genes (**Figure 6D**), and 9 selected glycosyltransferase genes in the signature (**Figure 6E**). The result indicated that expression profiles of the 9 selected glycosyltransferase genes were differentiated well in the low-risk and high-risk groups.

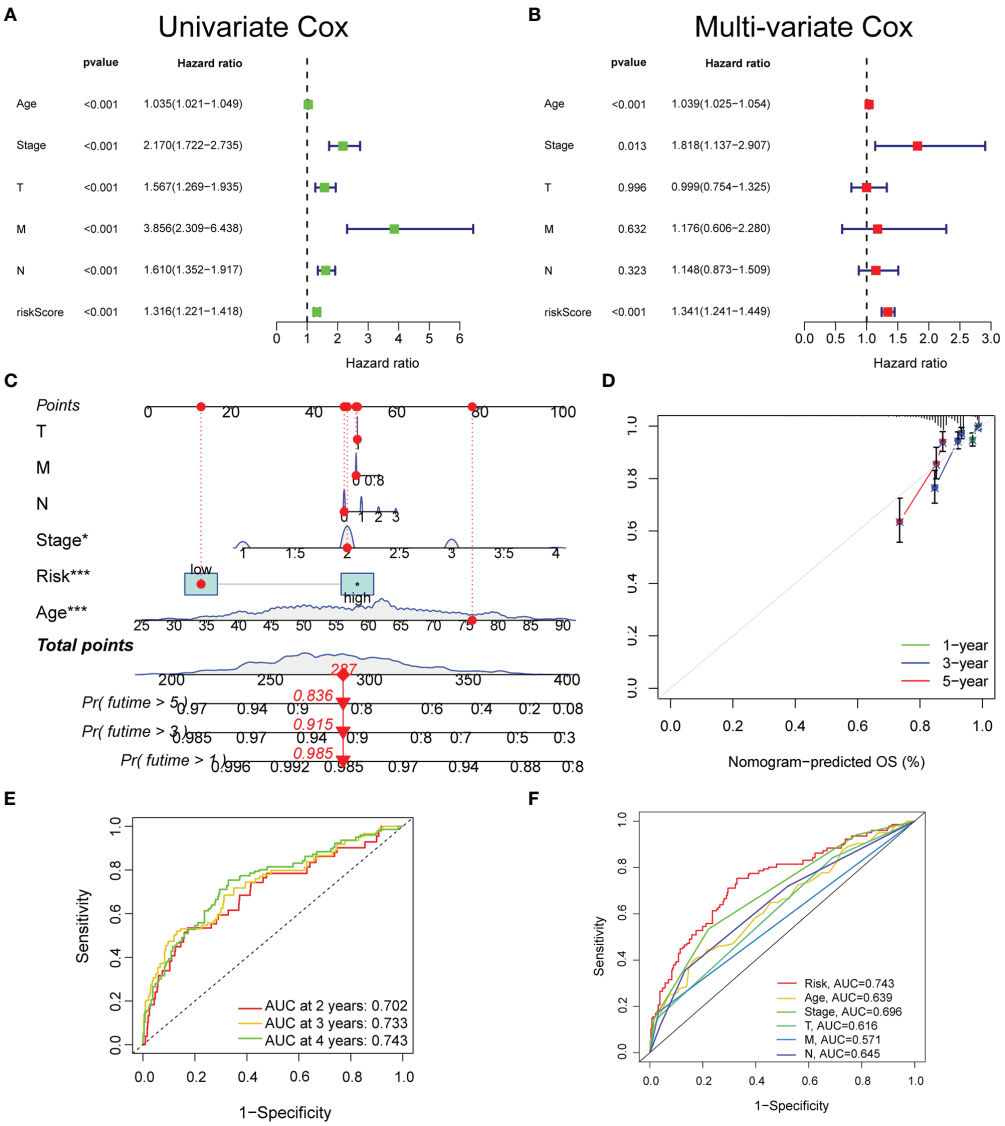

FIGURE 3 | The prognostic value of the glyco-signature. The univariate **(A)** and multivariate **(B)** Cox regression analyses of the prognostic capability of risk score and other clinicopathological features. **(C)** Construction of a nomogram based on the risk score and other clinicopathological factors to predict 1-, 3-, and 5-year OS of BC. **(D)** Calibration curves of the nomograms to validate the consistency between nomogram results and actual 1-, 3-, and 5-year survival outcomes of BC. **(E)** ROC curve analysis and AUC at 2, 3, and 4 years for the risk score. **(F)** ROC curve analysis and AUC at 4 years of the risk score and other clinicopathological factors. OS, overall survival; BC, breast cancer; ROC, receiver operating characteristic; AUC, area under the curve. *p < 0.05, ***p < 0.001.

Mutation and Copy Number Alteration Analysis of 9 Glycosyltransferase Genes

The mutation and CNA analyses of 9 glycosyltransferase genes were performed by us (**Figure 7A**), posing that the frequencies of gene changes, including gene amplification, deep deletions, and missense mutations, ranged from 0.4% to 12%. The amplification of ST3GAL1 was the most frequent CNA among the 9 glycosyltransferase genes. In addition, the frequency of mutation and CNA of 9 glycosyltransferase genes in breast invasive ductal carcinoma, breast invasive mixed mucinous carcinoma, breast invasive carcinoma (NOS), and breast invasive lobular carcinoma is shown in **Figure 7B**, and the breast invasive ductal carcinoma had the highest frequency. The missense mutations and truncating mutation of ST3GAL1 were localized in the glyco_transf_29 area (**Figure 7C**). The waterfall map indicated that the top 20 genes in the two groups had significantly different mutation frequencies (**Figures 7D, E**).

Glyco-Signature Predicts the Immune Cell Infiltration and Responsiveness to Chemotherapy and Target Therapy of Breast Cancer

The ssGSEA was applied to quantify the enriched scores of 22 immune cell subpopulations and 29 related pathways and to

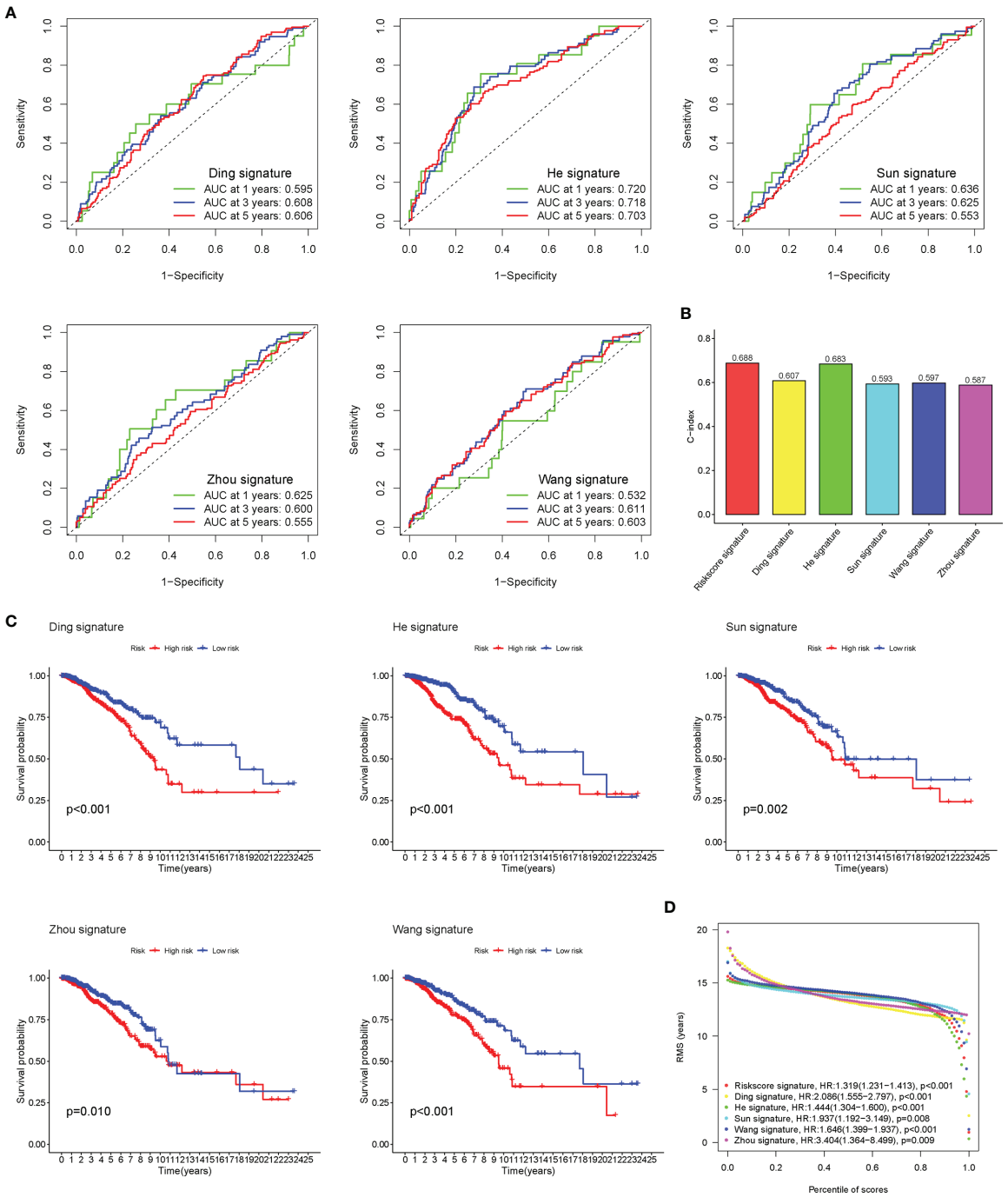

FIGURE 4 | Comparison of risk models. **(A)** The ROC curve of Ding, He, Sun, Wang, and Zhou signatures. **(B)** C-index comparison of six prognostic risk models. **(C)** The KM curve of low-risk and high-risk groups in the signature of Ding, He, Sun, Wang, and Zhou. **(D)** Restricted mean survival (RMS) curves for the six risk models. ROC, receiver operating characteristic; KM, Kaplan–Meier.

compare the fraction of immune cells and the activity of related pathways in the 2 groups (**Figures 8A, B**). The low-risk group possessed a high level of infiltration of immune cells, such as B cells, CD8+ T cells, and plasma cells. Meanwhile, all of the 29 immune-related pathways were of significant enrichment in the low-risk group. Also, CD8 T-cell infiltration was higher in the low-risk group and was positively correlated with the survival rate of BC patient (**Figure S2**). Correlation analysis illustrated that the risk score showed a negative correlation with the fraction of immune cells and a positive relationship with tumor mutation burden (TMB)

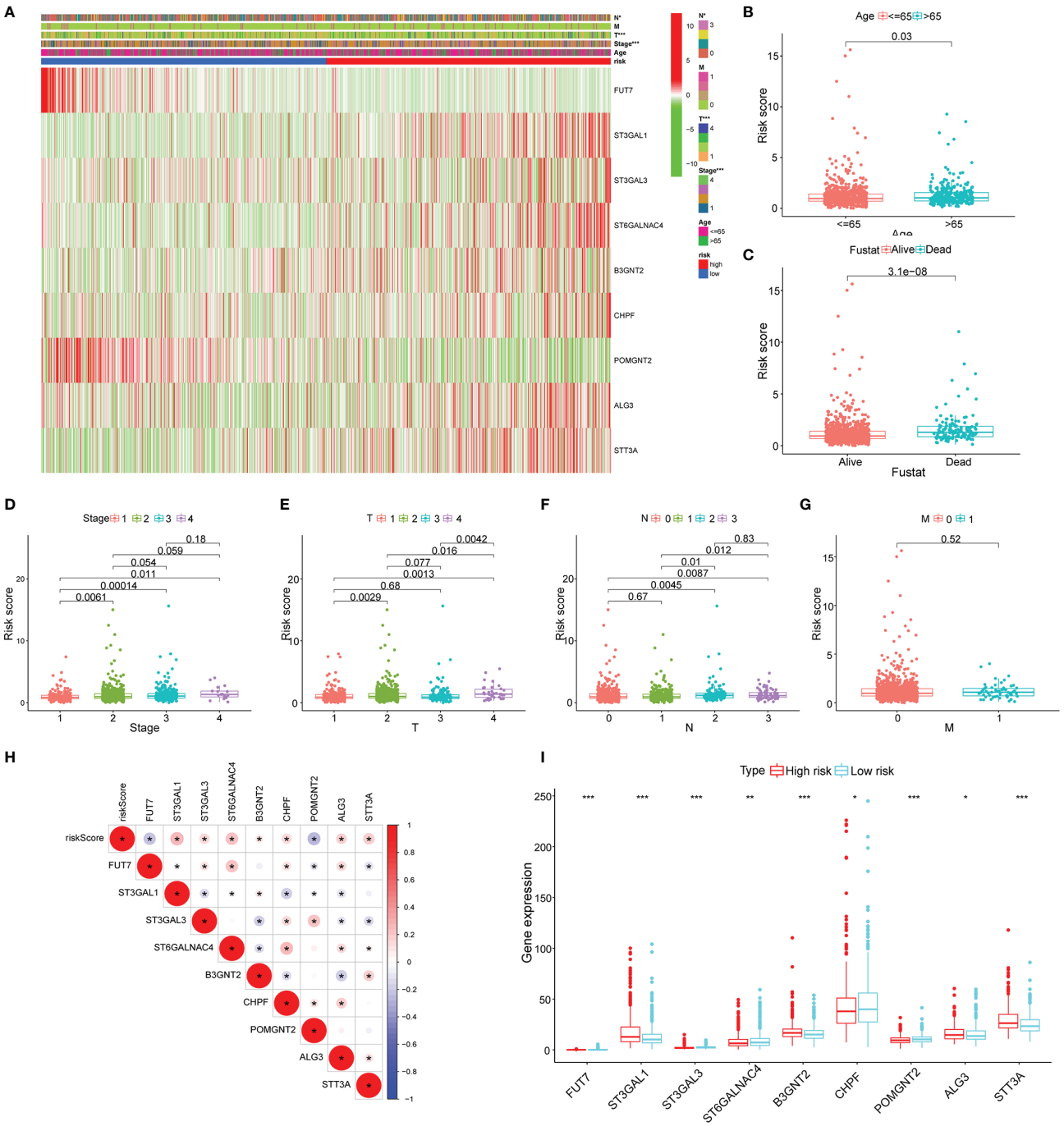

FIGURE 5 | Clinicopathological characteristics evaluation by the glyco-signature. **(A)** A heatmap visualizing the distribution of clinicopathological factors (age, stage, T, N, and M) and expression of 9 glycosyltransferase genes in the low-risk and high-risk groups. The scatter diagram of age **(B)**, survival status **(C)**, stage **(D)**, and stages T **(E)**, N **(F)**, and M **(G)** between groups of high and low risk. **(H)** The correlation of the 9 glycosyltransferase genes with the risk score. **(I)** The expression of 9 glycosyltransferase genes between high- and low-risk groups. *p < 0.05, **p < 0.01, ***p < 0.001.

(**Figures 8C, D**). Also, we analyzed the relevance between the copy number variation (CNV) of 4 glycosyltransferase genes and immune infiltration level in BC, indicating that arm-level deletion CNVs of B3GNT2 and some other CNVs of glycosyltransferase genes were associated with the extent of immune infiltration (**Figure 8E**). The ESTIMATE algorithm confirmed that in the low-risk group, the ESTIMATE score, stromal score, and immune score were dramatically higher and that the tumor purity was lower

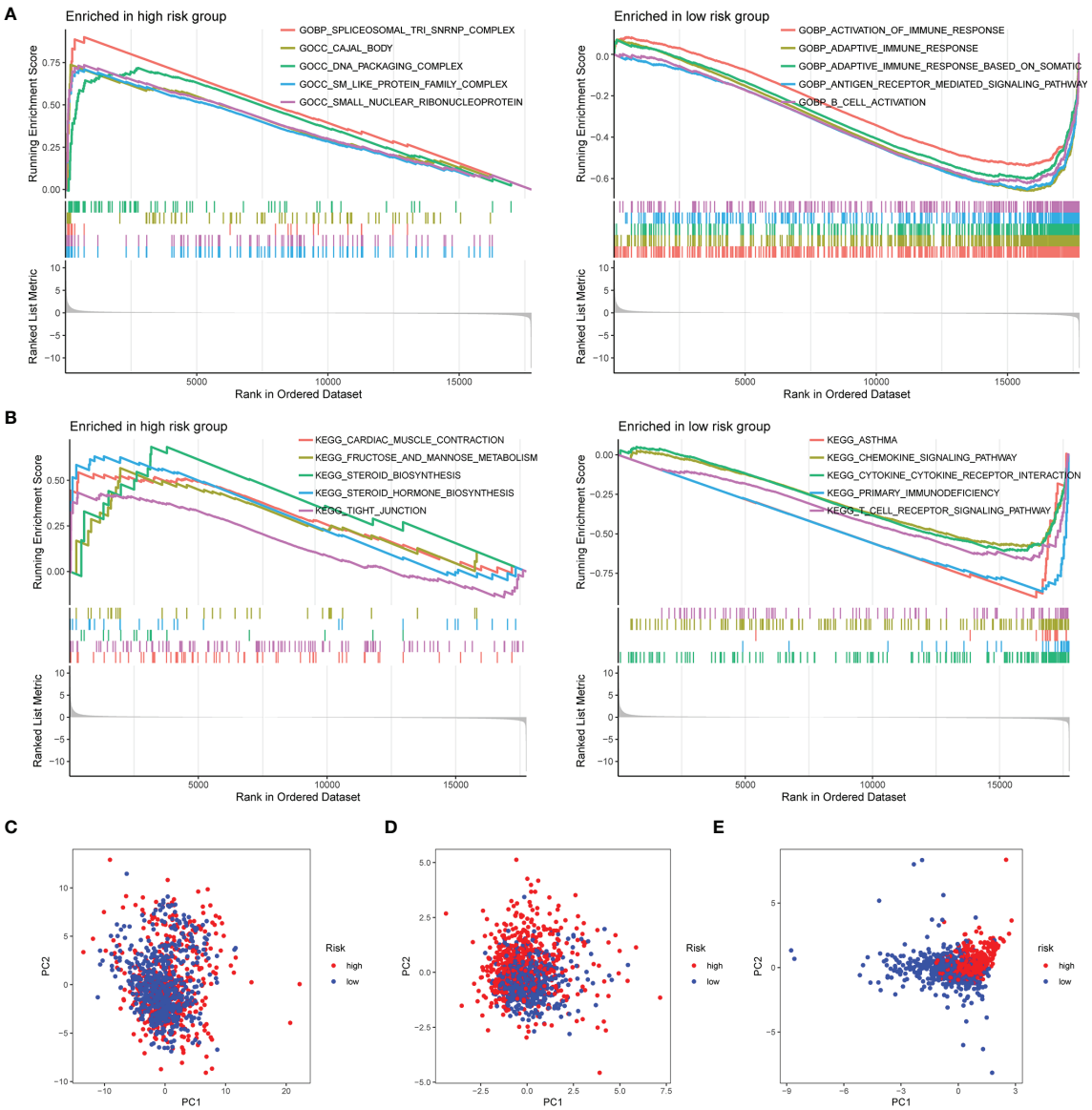

FIGURE 6 | GSEA of risk score-related signaling pathways. Enriched GO terms **(A)** and enriched KEGG pathways **(B)** between high- and low-risk groups. **(C)** PCA for the total mRNA expression profile. **(D)** PCA for glycosyltransferase gene expression profile. **(E)** PCA based on 9 selected glycosyltransferase genes. GSEA, Gene Set Enrichment Analysis; GO, Gene Ontology; KEGG, Kyoto Encyclopedia of Genes and Genomes; PCA, principal component analysis.

($p < 0.05$) (**Figure 9A**). Besides, dysfunction, Tumor Immune Dysfunction and Exclusion (TIDE), and microsatellite instability (MSI), except for exclusion, were distinctly higher in the low-risk group (**Figure 9B**). Also, patients with high TIDE and lower risk scores had the best outcomes (**Figure 9C**). Besides, BC patients in the high-risk group had higher TMB than patients in the low-risk group, supporting that there were more mutant genes in BC patients of the high-risk groups (**Figure 9D**). In addition, the RNA stemness score (RNAss) was correlated with the risk score, as was the DNA stemness score (DNAss) (**Figure 9E**). It indicated that tumors from the high-risk groups had higher tumor stemness. Based on GSE78220, GSE67501, and IMvigor210 cohorts (21), we found that the response of anti-PD-1/PD-L1 therapy was negatively associated with the risk score (**Figure 9F**). The KM curve showed that patients in the IMvigor210 cohort with low-risk scores had a better prognosis for anti-PD-1/PD-L1 and anti-CTLA-4 therapy (**Figure 9G**). Besides, the complete response (CR)/partial response (PR) group had a lower risk score than the stable disease (SD)/progressive disease (PD) group (**Figure 9H**). Also, patients with low levels of immune and tumor cell PD-L1 had higher risk scores, and a high-risk score was strongly correlated with the desert immunophenotype (**Figures 9I–K**). These results suggested that a better prognosis in the low-risk group might result from a promising response to anti-PD-L1 therapy.

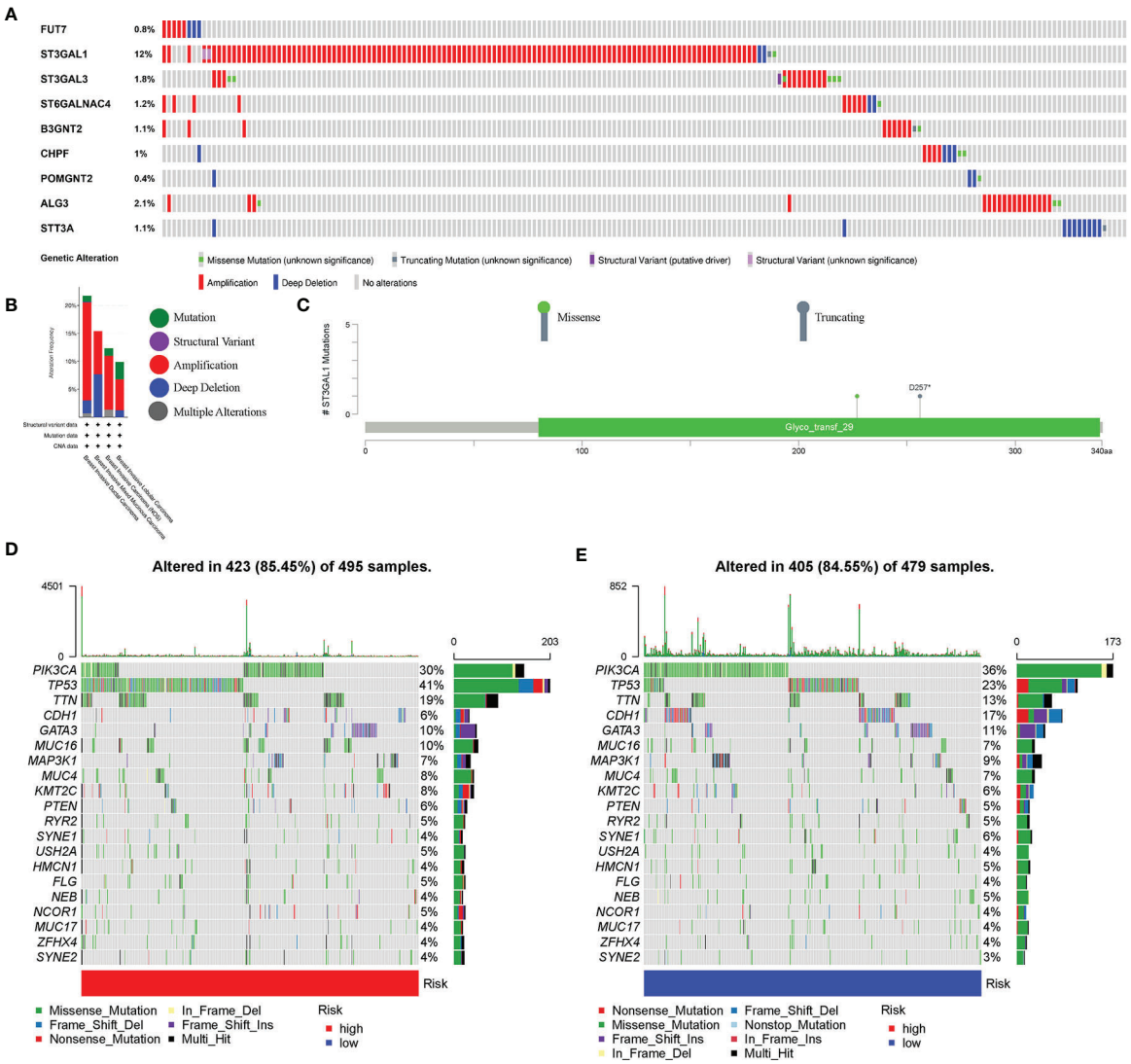

FIGURE 7 | Genetic alterations in BC patients. **(A)** Mutation and copy number alteration (CNA) analysis of 9 selected glycosyltransferase genes. **(B)** Frequency of mutation and CNA in glycosyltransferase genes in 4 types of BC patients. **(C)** Mutation distribution in the functional domains of ST3GAL1. The 20 high-ranking genes with the highest mutation frequency in the high-risk **(D)** and low-risk groups **(E)**. BC, breast cancer.

We used the SubMAP algorithm to speculate the possibility of anti-PD1 and anti-CTLA4 response immunotherapy in the high- and low-risk groups of BC patients. The result demonstrated that the low-risk group might respond better to PD-1 treatment (Bonferroni-corrected $p < 0.01$) (**Figure 10A**). However, there was no significant difference in CTLA4 response immunotherapy between the low- and high-risk groups. The tumor-immune cycle could be divided into 7 steps, including the tumor antigen release, antigen presentation, priming and activation, trafficking of T cells to tumors, infiltration of T cells in tumor entity, T cell-mediated tumor cell recognition, and tumor cell killing (22). The low-risk group possessed higher scores in the seven steps compared with the high-risk group (**Figure 10B**). The expression level of PD1, PDL-1, and CTLA-4 was negatively correlated with the risk score (**Figure 10C**). Also, the relative feasibility to respond to anti-PD-1/PD-L1 and anti-CTLA-4 therapy was higher in the low-risk group (**Figures 10D–G**). To evaluate the efficacy of our signature for chemotherapy response prediction, the estimated IC50 of doxorubicin, rapamycin, etoposide, and epothilone were calculated in each case. It was found that the high-risk group had higher drug sensitivity (**Figure 10H**).

Predictive Ability Validation of the Risk Model in an External Clinical Cohort and *In Vitro* Experiment

To validate the correlation between the expression of glycosyltransferase genes and tumor-infiltrating immune cells

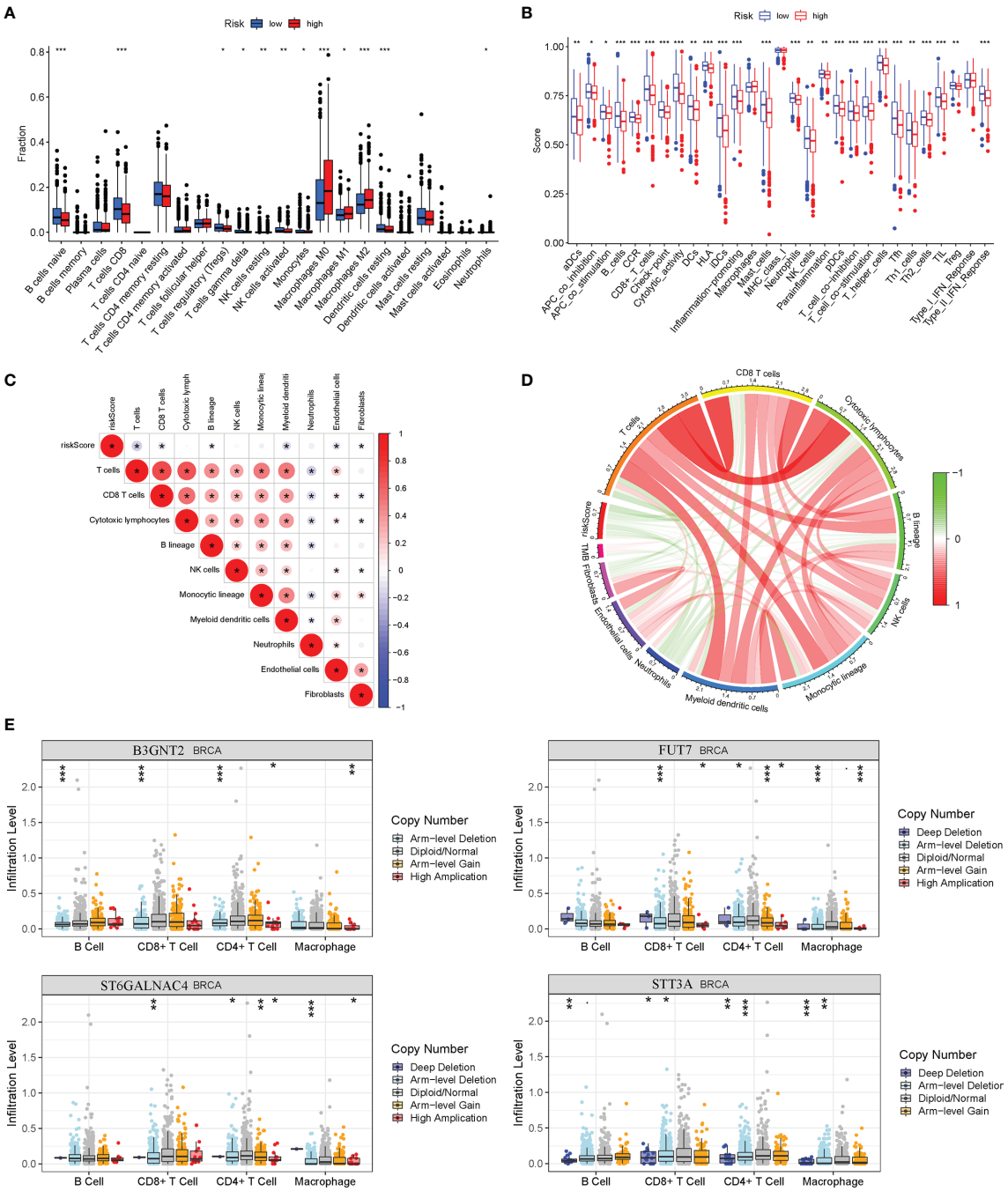

FIGURE 8 | Relationship between risk model and immune status in the high-risk and low-risk groups. **(A)** Differential immune infiltrates of 22 immune cell types. **(B)** Twenty-nine related immune pathways. **(C)** Correlation matrix of the relationship between risk score and differential immune infiltration levels. **(D)** The circular plot of the relationship between the risk score and immune infiltration levels. Green represents the negative association, and red represents the positive association. **(E)** Relationship between copy number variation of 4 glycosyltransferase genes in the signature and immune infiltration level in BC. BC, breast cancer. *p < 0.05, **p < 0.01, ***p < 0.001.

(TIICs), a clinical cohort comprised of 20 BC patients under different clinical stages was involved. The expression level of 9 glycosyltransferase genes detected by qRT-PCR was used to calculate the risk scores of the 20 patients (**Figure 11A**). Afterward, the clinical cohort was divided into the low-risk and high-risk groups. The results are in good agreement with our previous model. The IHC proved that STT3A was overexpressed in high-risk patients (**Figure 11B**). The further

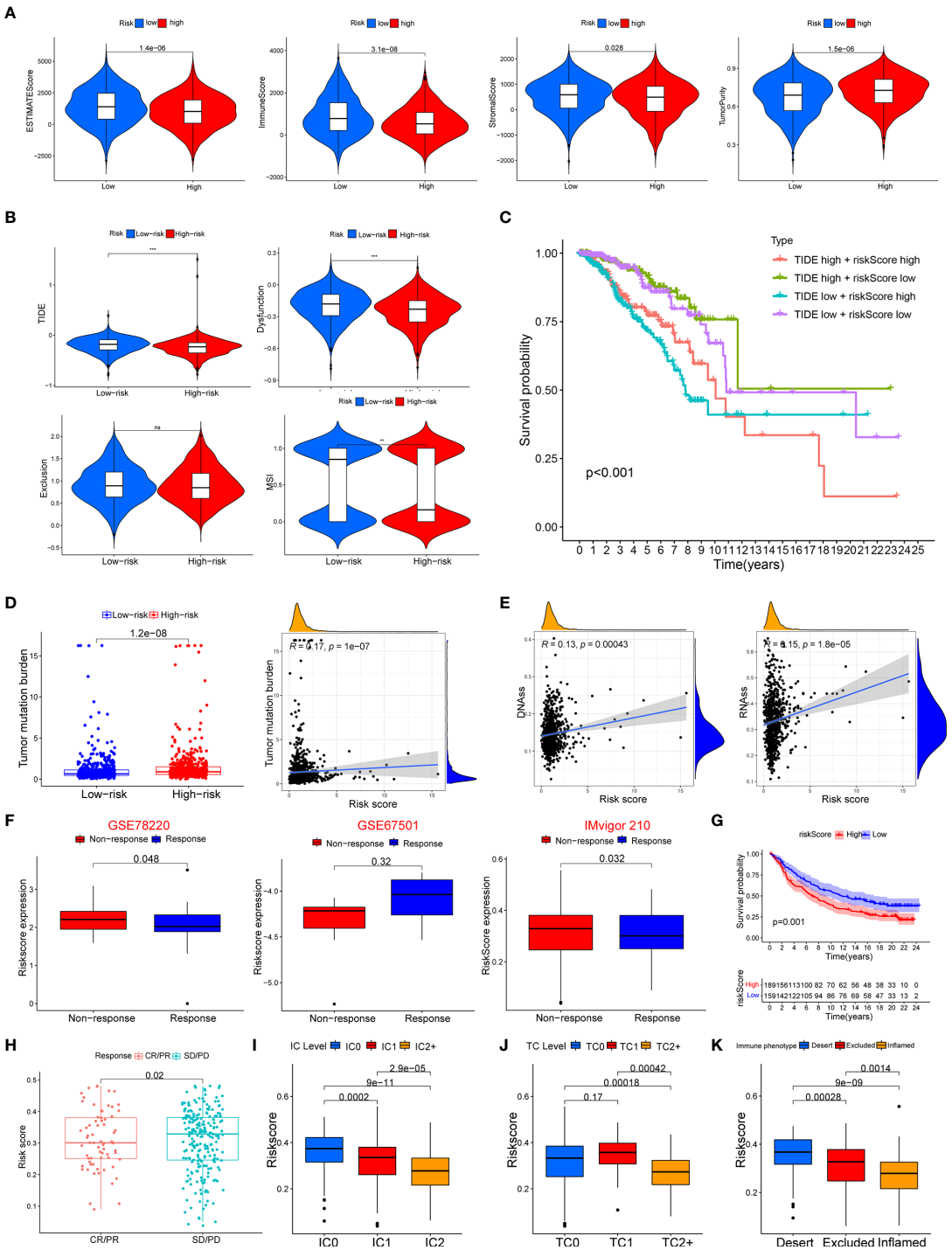

FIGURE 9 | Association between the risk score with tumor microenvironment and response to immune checkpoint inhibitors. **(A)** Association of risk score and tumor microenvironment. **(B)** Relationship of risk score and dysfunction, TIDE, exclusion, and MSI. **(C)** KM survival curve analysis of patients with different combinations of risk scores and TIDE in TCGA cohort. **(D)** Association of the risk score with tumor mutation boundary. **(E)** Relationship of the risk score with RNAss and DNAss. **(F)** The risk score of patients responding or not responding to anti-PD-1/PD-L1 in GSE78220, GSE6750, and IMvigor210 cohorts. **(G)** KM curve in IMvigor210 cohort. **(H)** Association of the risk score with clinical response diagnosis. **(I–K)** Correlation of risk score with immune phenotype and PD-L1 expression on immune cells and tumor cells. TIDE, Tumor Immune Dysfunction and Exclusion; MSI, microsatellite instability; KM, Kaplan–Meier; TCGA, The Cancer Genome Atlas. **p < 0.01, ***p < 0.001. ns, no significance.

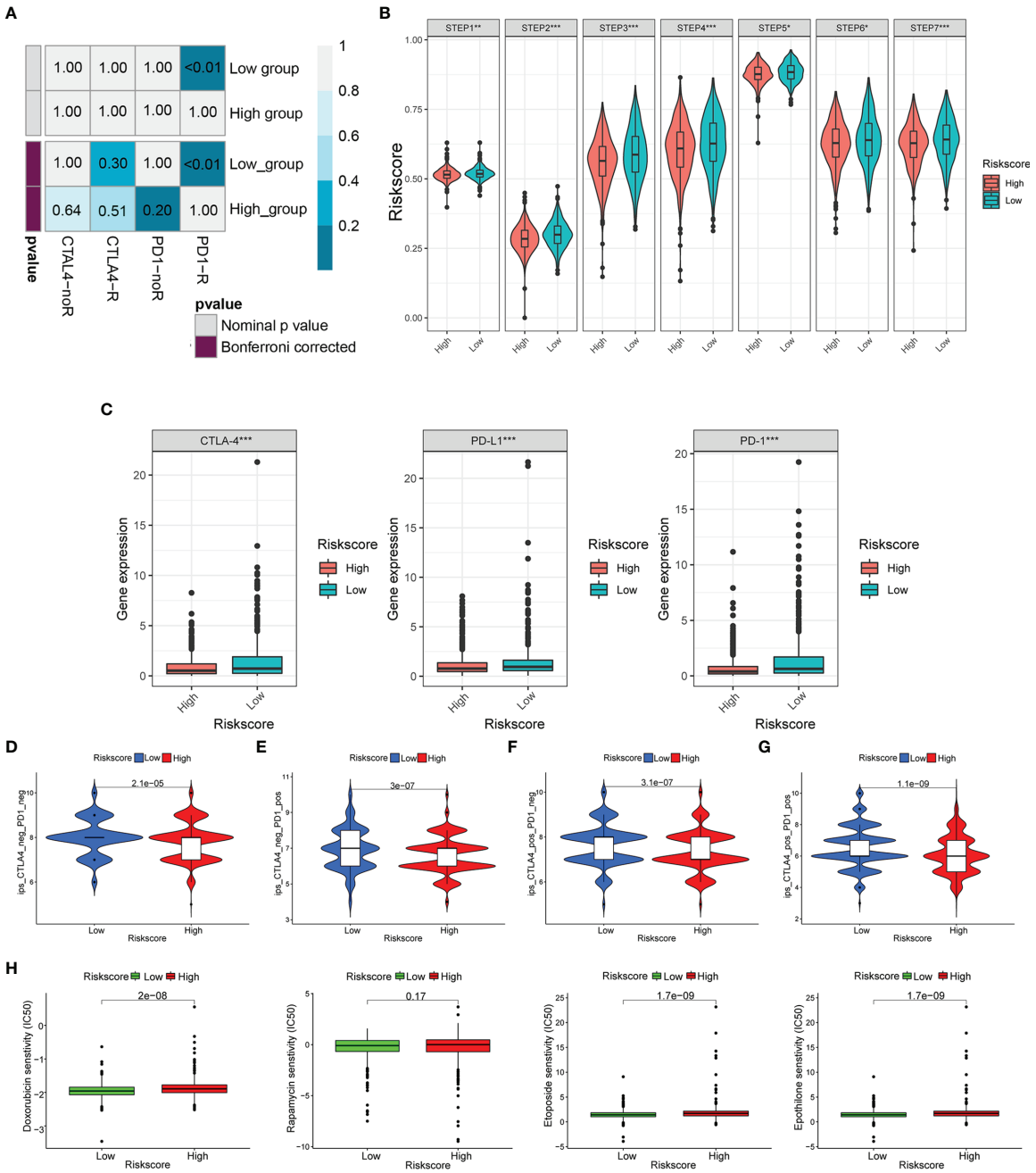

FIGURE 10 | Risk score predicted the responsiveness of BC to chemotherapy and targeted therapy. **(A)** The possibility of anti-PD1 and anti-CTLA4 response immunotherapy in the 2 groups. **(B)** The expression of the seven steps of the tumor-immune cycle. **(C)** The expression of PD1, PD-L1, and CTLA-4. **(D–G)** Four subtypes of IPS values (ips_CTLA-4_pos_PD-1_pos, ips_CTLA-4_neg_PD-1_pos, ips_CTLA-4_pos_PD-1_neg, and ips_CTLA-4_neg_PD-1_neg). **(H)** Drug sensitivity of doxorubicin, rapamycin, etoposide, and epothilone in the high-risk and low-risk groups. BC, breast cancer. *p < 0.05, **p < 0.01, ***p < 0.001.

IF assay indicated that the antitumoral M1 macrophage marker was increased in the low-risk group accompanied by decreased STT3A (**Figure 11C**).

After silencing of STT3A (**Figures 12A, B**), the CCK-8 analysis was performed to explore the role of STT3A in the proliferation of BC cells, which indicated the silence of STT3A suppressed the proliferation of MCF-7 and MDA-MB-231 cells (**Figures 12C, D**). Transwell assay and wound healing deciphered that the silence of STT3A inhibited the migration of MCF-7 and MDA-MB-231 cells (**Figures 12E–H**). In conclusion, the above data proved that STT3A upregulated the proliferation and migration of BC cells. To analyze the

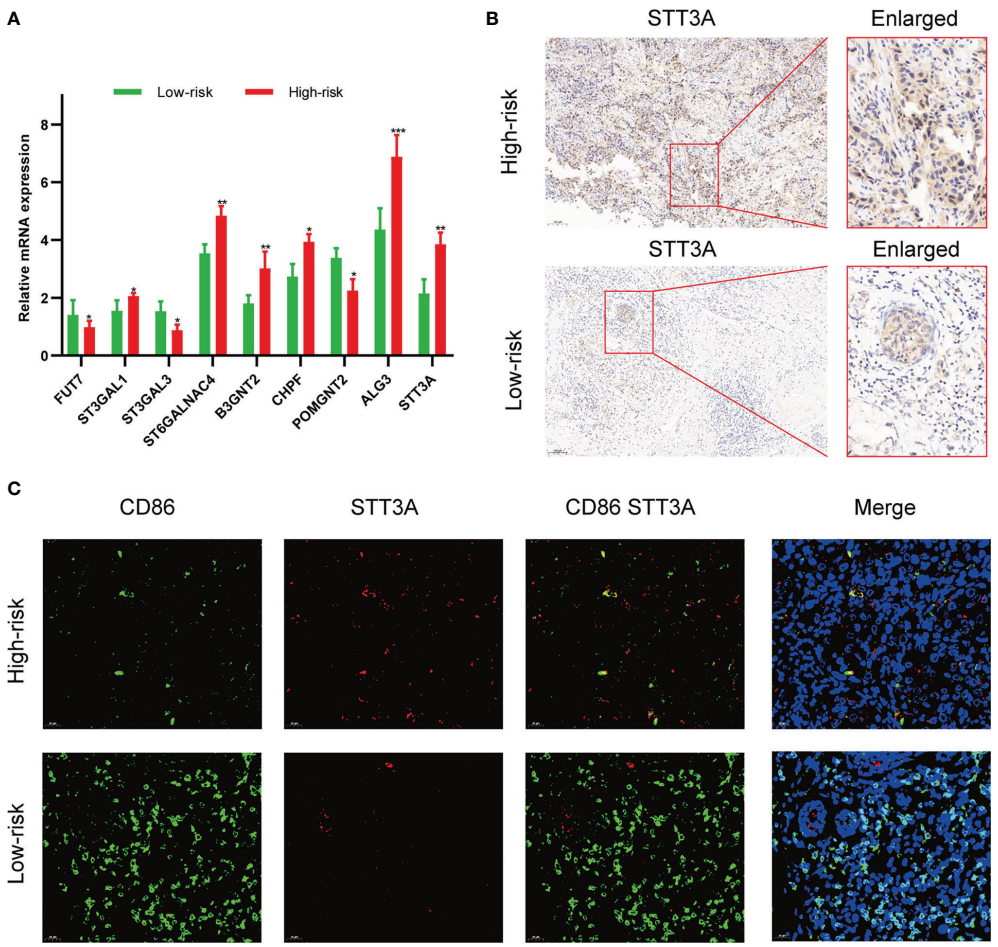

FIGURE 11 | Validation of the association between glycosyltransferase and tumor microenvironment in a clinical cohort. **(A)** Expression of glycosyltransferase genes in the high-risk group and low-risk group. **(B)** STT3A was overexpressed in the high-risk group patient. **(C)** The antitumoral M1 macrophage marker was increased in the low-risk group accompanied by decreased STT3A. *p < 0.05, **p < 0.01, ***p < 0.001.

expression of *N*-glycans in BC samples, we used three lectins (ConA, PHA-L, and PHA-E) to perform lectin blots. ConA binds to α-linked mannose (α-Man). PHA-L could specifically bind β1,6-GlcNAc branched *N*-glycan. PHA-E binds to biantennary galactosylated *N*-glycan with bisecting *N*-acetylglucosamine. Significantly increased intensities of ConA, PHA-L, and PHA-E revealed the higher expression of *N*-glycans in the high-risk group (**Figure 12I**). Also, the silence of STT3A significantly reduced the expression of *N*-glycans in MCF-7 and MDA-MB-231 cells (**Figures 12J, K**).

DISCUSSION

It is well established that BC is a highly heterogeneous tumor phenotype, and its prognosis varied depending on different molecular subtypes. It urgently needs novel and effective strategies to evaluate and improve the BC prognosis. Here, in our study, we have successfully established a risk model based on 9 screened glycosyltransferase genes, including FUT7, ST3GAL1, ST3GAL3, ST6GALNAC4, B3GNT2, CHPF, POMGNT2, ALG3, and STT3A. Moreover, we also confirmed that in comparison to the low-risk group, the high-risk groups depending on these genes are intensively associated with the lower OS, weaker immune effect, higher chemosensitivity, and differential CNV mutation patterns.

Glycosyltransferases belong to a large class of enzymes that influence tumor initiation and metastasis by regulating glycosylation. In this study, the 9 glycosyltransferases involved in our model possess their own different characteristics and functions. FUT7 is a type of α1,3-fucosyltransferase and is necessary for the biosynthesis of functional glycan ligands (23). FUT7 is observed to be abnormally expressed in various cancers and could mediate the malignant behavior change in bladder urothelial carcinoma and follicular thyroid carcinoma (24, 25). ST3GAL1 is an important sialyltransferase that catalyzes α2,3-linked sialic acid to galactose-containing substrates. The overexpression of ST3GAL1 promotes tumorigenesis and is

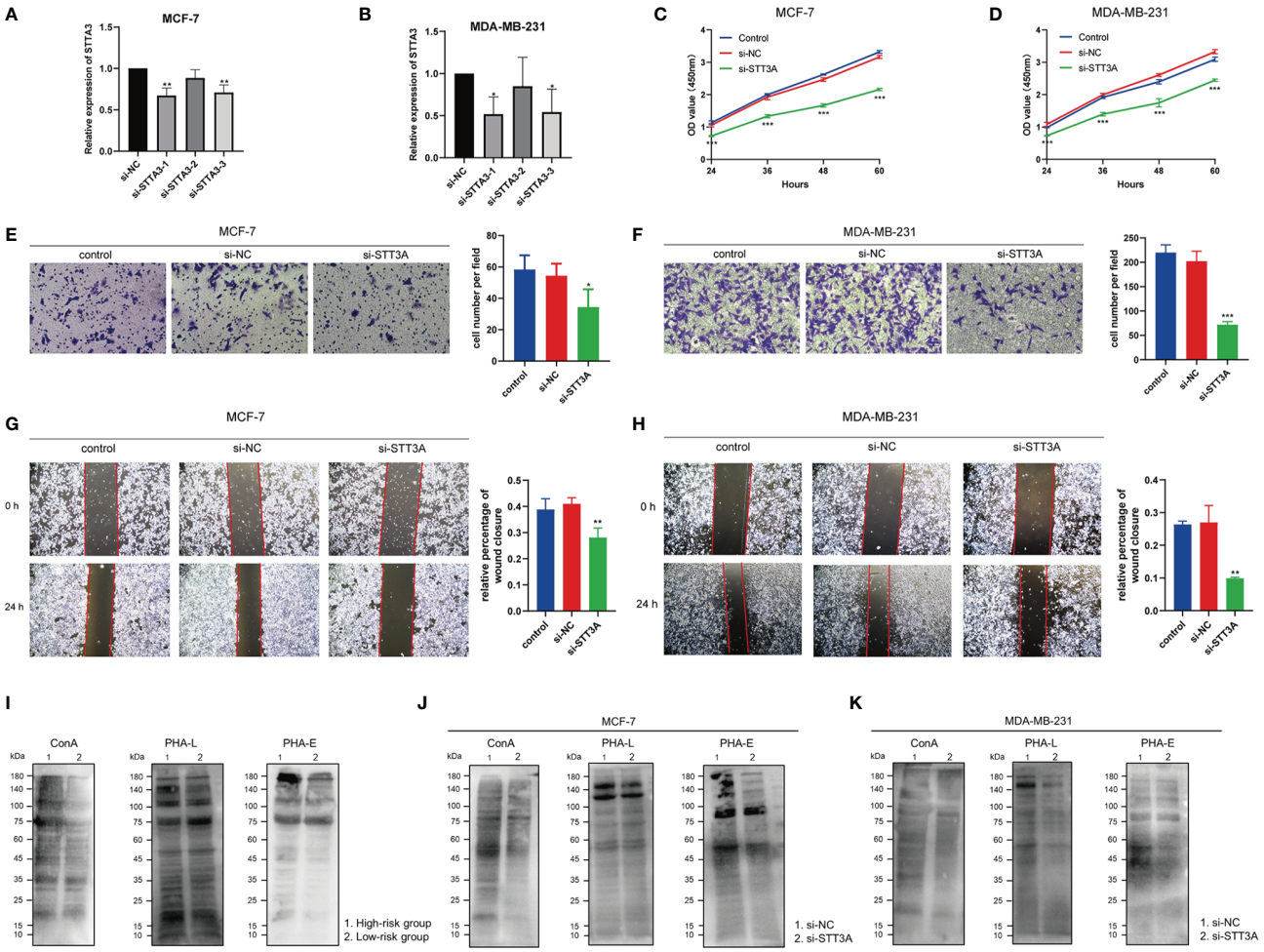

FIGURE 12 | STT3A regulated the proliferation and migration of BC cells. STT3A expression level of MCF-7 **(A)** and MDA-MB-231 **(B)** after silencing. CCK-8 assays were adopted to evaluate the proliferation ability of MCF-7 **(C)** and MDA-MB-231 **(D)** after silencing STT3A. Transwell assay **(E, F)** and wound healing **(H, I)** were performed to evaluate the migration ability of MCF-7 and MDA-MB-231 cells after silencing STT3A. Lectin blots with ConA, PHA-L, and PHA-E were performed in clinical samples in 2 risk groups **(J)** and MCF-7 and MDA-MB-231 cells after silencing STT3A **(K, L)**. BC, breast cancer; CCK-8, cell counting kit-8; ConA, concanavalin A; PHA-L, *Phaseolus vulgaris* leucoagglutinin; PHA-E, *Phaseolus vulgaris* erythroagglutinin.

strongly related to the increased tumor grade in BC (9). That meant that the upregulation of ST3GAL1 is an indicator for predicting a worse prognosis in BC patients. ST3GAL3 is another kind of sialyltransferase that is involved in the biosynthesis of sialyl-Lewis epitopes on the cell surface-expressing glycoproteins (26). ST3GAL3 could serve as a marker gene for circulating tumor cells (CTCs) in patients with BC receiving adjuvant therapy (27). ST6GALNAC4 is also a kind of sialyltransferase that mediates the transfer of sialic acid with an α2,6-linkage to it with terminal GAlNAc residues. ST6GALNAC4 has attracted only a few works and has been reported to promote the invasive properties of human follicular thyroid carcinoma (28). B3GNT2 is mainly involved in the synthesis of a major polylactosamine synthase (29). Some scholars validate that there are enriched mutations in B3GNT2 genes in colon cancer (30). CHPF is an important glycosyltransferase and participates in the biosynthesis of chondroitin sulfate (31). CHPF promotes BC growth, invasion, and metastasis by favoring 6-*O*-sulfated chondroitin sulfate formation in BC cells (32). POMGNT2 is considered an endoplasmic reticulum-resident protein that catalyzes the second step of the *O*-mannosyl glycosylation in the mucin-like domain of α-dystroglycan to generate functional laminin-binding glycans (33). Multiple single-point mutations in POMGNT2 have been detected in patients with the Walker–Warburg syndrome or limb–girdle muscular dystrophy (34). ALG3 has an α1,3-mannosyltransferase activity and is acknowledged as an oncoprotein associated with various malignancies (35). ALG3 promotes cancer cell stemness and decreased radioresistance of BC patients by regulating N-linked glycosylation of TGF-β receptor II (36). Endoplasmic reticulum-associated *N*-glycosyltransferase STT3A catalyzes the glycosylation PD-L1 and sustains the PD-L1 stability (37).

Totally, the role of FUT7, ST3GAL1, ST3GAL3, CHPF, and ALG3 has been partially reported in BC, while that of ST6GALNAC4, B3GNT2, POMGNT2, and STT3A is still not reported in BC yet. Among them, ST3GAL1 is the most reported in various cancer types, including BC. The other not frequently reported 8 glycosyltransferases are also potential targets for BC glycosylation studies in the future.

Nowadays, glycosylation and its dynamic expression changes are diagnostic tools with high efficiency used for early tumor diagnosis, tumor stage determination, and therapeutic strategies. For instance, Abd-El-Halim et al. constructed a glyco-signature based on glycosyltransferase gene expression profiles, which could be utilized for judging the resected and unresectable pancreatic ductal adenocarcinoma (PDAC) (38). Furthermore, the expression of glycosyltransferase genes could contribute to the identification of CTCs in the blood samples of cancer patients using PCR assay (12). It was worth noting that the relative expression of FUT3, GALNT6, and ST3GAL3 was increased in the blood samples of BC (27). This study raised a typical question that although some specific glycosyltransferase genes presented reasonable and satisfying results in the riks model system, there were no significant results that might indicate the presence of blood CTCs. Thus, their clinical application in practice needs further improvement. However, the previously reported studies of prognostic value involved in glycosyltransferase genes were mainly evaluated by a single gene but not by multiple gene-comprising signatures as we did. On the other hand, there have been few studies on the prognosis of BC associated with the glycosyltransferase gene by comprehensive bioinformatics analysis. In the present study, the glycosyltransferase-based signature could reasonably divide the cohort into the high- and low-risk groups. Besides, the low-risk group was markedly related to longer OS, disease-free survival, and progression-free interval as compared with the low-risk group, proposing the feasibility of this model in effectively predicting the outcomes of BC patients.

Next, we also detected the clinicopathological features and prognosis of BC, including the state of infiltration of immune cells, CNVs, and TMB. Glycosylation plays an increasingly pivotal role in regulating immune-related function and antitumor immunity. Xu et al. confirmed that FUT7, IL4I1, and ITGB7 could remodel the glucose metabolism to strengthen the immunotherapy effect (39). The pivotal glycan-binding proteins, including selectins, singles, and galectins, are important orchestrators in regulating the immune response in tumor metastasis (40). In our result, many immune response-related signaling pathways were enriched in the low-risk group, including cytokine–receptor interaction, B-cell activation, and T-cell receptor signaling pathway. Moreover, the immune score and stromal score were both higher in the lower-risk group, whereas the tumor purity was prominently higher in the high-risk group. The BC characterized by hypermutated features is peculiarly prone to benefit from the therapy of PD-1 inhibitors (41). By utilizing the ImmPort database and the univariate Cox analysis, Wang et al. identified the ADRB1 as a prognostic immune gene among mutant genes, and TMB was a key immunotherapy biomarker (42). Moreover, our results revealed that there was a substantial relevance between tumor glycosylation and immune checkpoint expression, especially PD-L1 and PD-1 checkpoints. Existing studies confirmed that patients with high PD-L1 and PD-1 checkpoint expression often exhibited greater sensitivity to immunosuppressive therapy. Here, there was a trend toward increased expression of CTLA-4, PD-L1, and PD-1 in the low-risk group compared to the high-risk group. Meanwhile, we identified that the low-risk score group was more reactive to the response of anti-PD-1/PD-L1 therapy in the GSE78220, GSE6750, and IMvigor210 cohorts. We also found that in BC, the low-risk group might respond better to PD-1 treatment but have no significant difference in CTLA4 response immunotherapy compared with the high-risk group. Moreover, we also found that there are significant differences in chemotherapy response prediction, and the high-risk score group had higher drug sensitivity. Therefore, we speculate that the risk score can better predict the efficiency of anti-PD1/PD-L1 and anti-CTLA4 immunotherapy reactions between the 2 risk groups. The low-risk score group may be more likely to benefit from ICI's efficacy for BC.

ST3Gal1 is an important sialyltransferase that catalyzes α2,3-linked sialic acid to galactose-containing substrates. The ST3GAL1 upregulation is an event that indicates a worse prognosis in patients and is associated with chemoresistance (43). Chong et al. show that the ST3GAL1-related transcriptome programs were indicators for an unfavorable prognosis in glioma patients, accompanied by higher tumor grade higher mesenchymal molecular grading (44). In our study, among the 9 glycosyltransferase genes, ST3GAL1 gene was the most frequent CNA in the BC cohort. It was consistent with our results; Fan et al. demonstrated that in BC, ST3GAL1 and GDNF/GFRA1/RET signaling pathways had positive feedback regulation, and the higher ST3GAL1 expression indicated a poor prognosis in late-stage BC patients (45). These studies together indicate that ST3GAL1 may be a promising target for both diagnosis and treatment strategy development.

The STT3A complex is a key component encoding the catalytic subunit of the oligosaccharide transferase complex to mediate cotranslational glycosylation (46). Notably, several oligosaccharyltransferase (OST) complex, Ribophorin 1 (RPN1), STT3A, and STT3B, were upregulated in BC samples (47). It is worth considering that oncogenic signaling pathways induce glycosylation of coinhibitory molecules to induce immunosuppression. For example, Chan et al. demonstrated that IL-6-activated JAK1 phosphorylates PD-L1, which recruited endoplasmic reticulum-associated *N*-glycosyltransferase STT3A to catalyze glycosylation of PD-L1 and maintain PD-L1 stability in hepatocellular carcinoma (37). Ruan et al. supported that the suppression of the β-catenin/STT3 pathway resulted in reduced PD-L1 stability, thus suppressing immune evasion and promoting apoptosis in colon cancer stem cells (CSCs) (48). Our results verified an upregulated expression pattern of STT3A in BC. We also found the oncogenic function of STT3A that promoted the proliferation and migration behaviors of two BC cell lines. These investigations imply that STT3A might serve as reliable diagnostic and therapeutic targets for BC.

Nevertheless, there are still some concerns needed to be addressed in our study. Firstly, this study is indeed a retrospective study that is mainly constructed by bioinformatics analysis based on TCGA datasets and IMvigor210. There are still some deficiencies lacking clinical prognostic validation of this well-established risk model. Adequate prospective external validations should be performed in the future. Secondly, we only preliminarily conducted the qRT-PCR and IHC assay to validate our bioinformatics results. In the experimental part, we utilized the qRT-PCR and IHC assay of the BC samples to validate the parts of model-related factors. These validated results were not enough to cover all the predicted conclusions. It is still necessary to decipher the multidimensional roles and underlying mechanism of these glycosyltransferase genes in BC oncogenesis, development, and prognosis. Lastly, therefore, the further ongoing prospective studies to evaluate in a large and multicenter cohort can be beneficial to confirm the novelty of the risk score model.

CONCLUSION

To sum up, we successfully constructed a glyco-signature based on 9 glycosyltransferase genes from TCGA database. We confirmed that the high-risk group had a worse prognosis and immunosuppression. Furthermore, this glyco-signature is intensively associated with immune cell infiltration, tumor-immune cycle, responsiveness to ICIs, and chemosensitivity for BC. The comprehensive evaluation of glycosyltransferase levels for BC patients would help us understand immune infiltration and guide more efficacious immunotherapy strategies. The combination of our risk model with the gold standard methods will synergistically promote the prognosis evaluation for combating BC.

DATA AVAILABILITY STATEMENT

The datasets presented in this study can be found in online repositories. The names of the repository/repositories and accession number(s) can be found in the article/**Supplementary Material**.

ETHICS STATEMENT

The studies involving human participants were reviewed and approved by Tongji Hospital affiliated with Tongji Medical College. Written informed consent for participation was not required for this study in accordance with the national legislation and the institutional requirements.

AUTHOR CONTRIBUTIONS

YW, JZ, and QZ conceived the project and supervised all experiments. WL, HY, and YT conducted experiments and analyzed the data. HY and MW wrote and revised the manuscript. MH provided support for experimental techniques. MW edited and revised the manuscript, including figures and tables. All authors have reviewed the manuscript and all approved of the final version.

FUNDING

This work was supported by China Guanghua Science and Technology Foundation (grant number 2019JZXM001) and Wuhan Science and Technology Bureau (grant number 2020020601012241).

SUPPLEMENTARY MATERIAL

The Supplementary Material for this article can be found online at: https://www.frontiersin.org/articles/10.3389/fimmu.2022.830158/full#supplementary-material

Supplementary Figure 1 | The flowchart of this study.

Supplementary Figure 2 | CD8 T cells infiltrating tumors both in the low and high-risk groups. **(A)** The difference of CD8 T cells infiltrating in 2 groups. **(B)** The correlation between CD8 T cells infiltrating and risk score. **(C)** The KM curve analyses of survival rate using the CD8 T cells infiltrating. **(D)** The KM curve analyses of survival rate using the risk score and CD8 T cells infiltrating.

REFERENCES

1. Britt KL, Cuzick J, Phillips KA. Key Steps for Effective Breast Cancer Prevention. *Nat Rev Cancer* (2020) 20(8):417–36. doi: 10.1038/s41568-020-0266-x
2. Siegel RL, Miller KD, Fuchs HE, Jemal A. Cancer Statistics, 2021. *CA Cancer J Clin* (2021) 71(1):7–33. doi: 10.3322/caac.21654
3. Syn NL, Teng MWL, Mok TSK, Soo RA. *De-Novo* and Acquired Resistance to Immune Checkpoint Targeting. *Lancet Oncol* (2017) 18(12):e731–41. doi: 10.1016/S1470-2045(17)30607-1
4. Gaynor N, Crown J, Collins DM. Immune Checkpoint Inhibitors: Key Trials and an Emerging Role in Breast Cancer. *Semin Cancer Biol* (2022) 79:44–57. doi: 10.1016/j.semcancer.2020.06.016
5. Terranova-Barberio M, Pawlowska N, Dhawan M, Moasser M, Chien AJ, Melisko ME, et al. Exhausted T Cell Signature Predicts Immunotherapy Response in ER-Positive Breast Cancer. *Nat Commun* (2020) 11(1):3584. doi: 10.1038/s41467-020-17414-y
6. Munkley J, Elliott DJ. Hallmarks of Glycosylation in Cancer. *Oncotarget* (2016) 7(23):35478–89. doi: 10.18632/oncotarget.8155
7. Pinho SS, Reis CA. Glycosylation in Cancer: Mechanisms and Clinical Implications. *Nat Rev Cancer* (2015) 15(9):540–55. doi: 10.1038/nrc3982
8. Li C-W, Lim S-O, Chung EM, Kim Y-S, Park AH, Yao J, et al. Eradication of Triple-Negative Breast Cancer Cells by Targeting Glycosylated PD-L1. *Cancer Cell* (2018) 33(2):187–201.e10. doi: 10.1016/j.ccell.2018.01.009
9. Lin WD, Fan TC, Hung JT, Yeo HL, Wang SH, Kuo CW, et al. Sialylation of CD55 by ST3GAL1 Facilitates Immune Evasion in Cancer. *Cancer Immunol Res* (2021) 9:113–22. doi: 10.1158/2326-6066.CIR-20-0203
10. Kirwan A, Utratna M, O'Dwyer ME, Joshi L, Kilcoyne M. Glycosylation-Based Serum Biomarkers for Cancer Diagnostics and Prognostics. *BioMed Res Int* (2015) 2015:490531. doi: 10.1155/2015/490531
11. Takayama H, Ohta M, Iwashita Y, Uchida H, Shitomi Y, Yada K, et al. Altered Glycosylation Associated With Dedifferentiation of Hepatocellular Carcinoma: A Lectin Microarray-Based Study. *BMC Cancer* (2020) 20(1):1–8. doi: 10.1186/s12885-020-6699-5
12. Liu C, Li Z, Xu L, Shi Y, Zhang X, Shi S, et al. GALNT6 Promotes Breast Cancer Metastasis by Increasing Mucin-Type O-Glycosylation of α2m. *Aging (Albany NY)* (2020) 12(12):11794–811. doi: 10.18632/aging.103349

13. Yu G, Wang LG, Han Y, He QY. ClusterProfiler: An R Package for Comparing Biological Themes Among Gene Clusters. *Omi A J Integr Biol* (2012) 16 (5):284–7. doi: 10.1089/omi.2011.0118
14. Balachandran VP, Gonen M, Smith JJ, Dematteo P, Sloan M, Cancer K, et al. Nomograms in Oncology. *Lancet Oncol* (2015) 16(4):e173–80. doi: 10.1016/S1470-2045(14)71116-7
15. Gao J, Aksoy BA, Dogrusoz U, Dresdner G, Gross B, Sumer SO, et al. Integrative Analysis of Complex Cancer Genomics and Clinical Profiles Using the cBioPortal. *Sci Signal* (2014) 6(269):1–20. doi: 10.1126/scisignal.2004088
16. Ding S, Sun X, Zhu L, Li Y, Chen W, Shen K. Identification of a Novel Immune-Related Prognostic Signature Associated With Tumor Microenvironment for Breast Cancer. *Int Immunopharmacol* (2021) 100 (March):108122. doi: 10.1016/j.intimp.2021.108122
17. He M, Hu C, Deng J, Ji H, Tian W. Identification of a Novel Glycolysis-Related Signature to Predict the Prognosis of Patients With Breast Cancer. *World J Surg Oncol* (2021) 19(1):1–14. doi: 10.1186/s12957-021-02409-w
18. Sun X, Zhou Z-R, Fang Y, Ding S, Lu S, Wang Z, et al. A Novel Metabolic Gene Signature-Based Nomogram to Predict Overall Survival in Breast Cancer. *Ann Transl Med* (2021) 9(5):367–7. doi: 10.21037/atm-20-4813
19. Zhou D, Wu Y, Jiang K, Xu F, Hong R, Wang S. Identification of a Risk Prediction Model for Clinical Prognosis in HER2 Positive Breast Cancer Patients. *Genomics* (2021) 113(6):4088–97. doi: 10.1016/j.ygeno.2021.10.010.
20. Wang D, Wei G, Ma J, Cheng S, Jia L, Song X, et al. Identification of the Prognostic Value of Ferroptosis-Related Gene Signature in Breast Cancer Patients. *BMC Cancer* (2021) 21(1):1–12. doi: 10.1186/s12885-021-08341-2
21. Mariathasan S, Turley SJ, Nickles D, Castiglioni A, Yuen K, Wang Y, et al. Tgfβ Attenuates Tumour Response to PD-L1 Blockade by Contributing to Exclusion of T Cells. *Nature* (2018) 554(7693):544–8. doi: 10.1038/nature25501
22. Zhang Z, Zeng P, Gao W, Zhou Q, Feng T, Tian X. Circadian Clock: A Regulator of the Immunity in Cancer. *Cell Commun Signal* (2021) 19(1):1–12. doi: 10.1186/s12964-021-00721-2.
23. Ebel ME, Kansas GS. Defining the Functional Boundaries of the Murine α1,3-Fucosyltransferase Fut7 Reveals a Remarkably Compact Locus. *J Biol Chem* (2014) 289(10):6341–9. doi: 10.1074/jbc.M113.511790
24. Liu M, Zheng Q, Chen S, Liu J, Li S. Fut7 Promotes the Epithelial–Mesenchymal Transition and Immune Infiltration in Bladder Urothelial Carcinoma. *J Inflamm Res* (2021) 14:1069–84. doi: 10.2147/JIR.S296597
25. Qin H, Liu J, Yu M, Wang H, Thomas AM, Li S, et al. FUT7 Promotes the Malignant Transformation of Follicular Thyroid Carcinoma Through α1,3-Fucosylation of EGF Receptor. *Exp Cell Res* (2020) 393:112095. doi: 10.1016/j.yexcr.2020.112095.
26. Suzukawa M, Miller M, Rosenthal P, Cho JY, Doherty TA, Varki A, et al. Sialyltransferase ST3Gal-III Regulates Siglec-F Ligand Formation and Eosinophilic Lung Inflammation in Mice. *J Immunol* (2013) 190(12):5939–48. doi: 10.4049/jimmunol.1203455
27. Kölbl AC, Hiller RA, Ilmer M, Liesche F, Heublein S, Schröder L, et al. Glycosyltransferases as Marker Genes for the Quantitative Polymerase Chain Reaction-Based Detection of Circulating Tumour Cells From Blood Samples of Patients With Breast Cancer Undergoing Adjuvant Therapy. *Mol Med Rep* (2015) 12(2):2933–8. doi: 10.3892/mmr.2015.3732
28. Miao X, Jia L, Zhou H, Song X, Zhou M, Xu J, et al. MiR-4299 Mediates the Invasive Properties and Tumorigenicity of Human Follicular Thyroid Carcinoma by Targeting ST6GALNAC4. *IUBMB Life* (2016) 68(2):136–44. doi: 10.1002/iub.1467
29. Togayachi A, Kozono Y, Ishida H, Abe S, Suzuki N, Tsunoda Y, et al. Polylactosamine on Glycoproteins Influences Basal Levels of Lymphocyte and Macrophage Activation. *Proc Natl Acad Sci USA* (2007) 104(40):15829–34. doi: 10.1073/pnas.0707426104
30. Venkitachalam S, Revoredo L, Varadan V, Fecteau RE, Ravi L, Lutterbaugh J, et al. Biochemical and Functional Characterization of Glycosylation-Associated Mutational Landscapes in Colon Cancer. *Sci Rep* (2016) 6:1–11. doi: 10.1038/srep23642
31. Lin X, Han T, Xia Q, Cui J, Zhuo M, Liang Y, et al. CHPF Promotes Gastric Cancer Tumorigenesis Through the Activation of E2F1. *Cell Death Dis* (2021) 12(10):1–11. doi: 10.1038/s41419-021-04148-y
32. Liao W-C, Yen H-R, Chen C-H, Chu Y-H, Song Y-C, Tseng T-J, et al. CHPF Promotes Malignancy of Breast Cancer Cells by Modifying Syndecan-4 and the Tumor Microenvironment. *Am J Cancer Res* (2021) 11(3):812–26.
33. Halmo SM, Singh D, Patel S, Wang S, Edlin M, Boons GJ, et al. Protein O-Linked Mannose β-1,4-N-Acetylglucosaminyltransferase 2 (POMGNT2) Is a Gatekeeper Enzyme for Functional Glycosylation of α-Dystroglycan. *J Biol Chem* (2017) 292(6):2101–9. doi: 10.1074/jbc.M116.764712
34. Yang JY, Halmo SM, Praissman J, Chapla D, Singh D, Wells L, et al. Crystal Structures of β-1,4-N-Acetylglucosaminyltransferase 2: Structural Basis for Inherited Muscular Dystrophies. *Acta Crystallogr Sect D Struct Biol* (2021) 77:486–95. doi: 10.1107/S2059798321001261
35. Ke SB, Qiu H, Chen JM, Shi W, Han C, Gong Y, et al. ALG3 Contributes to the Malignancy of Non-Small Cell Lung Cancer and Is Negatively Regulated by MiR-98-5p. *Pathol Res Pract* (2020) 216(3):152761. doi: 10.1016/j.prp.2019.152761
36. Sun X, He Z, Guo L, Wang C, Lin C, Ye L, et al. ALG3 Contributes to Stemness and Radioresistance Through Regulating Glycosylation of TGF-β Receptor II in Breast Cancer. *J Exp Clin Cancer Res* (2021) 40(1):1–25. doi: 10.1186/s13046-021-01932-8
37. Chan LC, Li CW, Xia W, Hsu JM, Lee HH, Cha JH, et al. IL-6/JAK1 Pathway Drives PD-L1 Y112 Phosphorylation to Promote Cancer Immune Evasion. *J Clin Invest* (2019) 129(8):3324–38. doi: 10.1172/JCI126022
38. Mohamed Abd-El-Halim Y, El Kaoutari A, Silvy F, Rubis M, Bigonnet M, Roques J, et al. A Glycosyltransferase Gene Signature to Detect Pancreatic Ductal Adenocarcinoma Patients With Poor Prognosis. *EBioMedicine* (2021) 71:103541. doi: 10.1016/j.ebiom.2021.103541
39. Xu T, Liu J, Xia Y, Wang Z, Li X, Gao Q. Integrated Analysis Reveals the Participation of IL4I1, ITGB7, and FUT7 in Reshaping the TNBC Immune Microenvironment by Targeting Glycolysis. *Ann Med* (2021) 53(1):916–28. doi: 10.1080/07853890.2021.1937694
40. Rodrigues JG, Balmaña M, Macedo JA, Poças J, Fernandes Â, de-Freitas-Junior JCM, et al. Glycosylation in Cancer: Selected Roles in Tumour Progression, Immune Modulation and Metastasis. *Cell Immunol* (2018) 333:46–57. doi: 10.1016/j.cellimm.2018.03.007
41. Barroso-Sousa R, Jain E, Cohen O, Kim D, Buendia-Buendia J, Winer E, et al. Prevalence and Mutational Determinants of High Tumor Mutation Burden in Breast Cancer. *Ann Oncol* (2020) 31(3):387–94. doi: 10.1016/j.annonc.2019.11.010
42. Wang J, Zhang X, Li J, Ma X, Feng F, Liu L, et al. ADRB1 was Identified as a Potential Biomarker for Breast Cancer by the Co-Analysis of Tumor Mutational Burden and Immune Infiltration. *Aging (Albany NY)* (2020) 13 (1):351–63. doi: 10.18632/aging.104204
43. Yeo HL, Fan TC, Lin RJ, Yu JC, Liao GS, Chen ESW, et al. Sialylation of Vasorin by ST3Gal1 Facilitates TGF-β1-Mediated Tumor Angiogenesis and Progression. *Int J Cancer* (2019) 144(8):1996–2007. doi: 10.1002/ijc.31891
44. Chong YK, Sandanaraj E, Koh LWH, Thangaveloo M, Tan MSY, Koh GRH, et al. ST3GAL1-Associated Transcriptomic Program in Glioblastoma Tumor Growth, Invasion, and Prognosis. *J Natl Cancer Inst* (2016) 108(2):1–12. doi: 10.1093/jnci/djv326
45. Fan TC, Yeo HL, Hsu HM, Yu JC, Ho MY, Lin WD, et al. Reciprocal Feedback Regulation of ST3GAL1 and GFRA1 Signaling in Breast Cancer Cells. *Cancer Lett* (2018) 434:184–95. doi: 10.1016/j.canlet.2018.07.026
46. Lu H, Fermaintt CS, Cherepanova NA, Reid G, Yan N, Lehrman MA. Mammalian STT3A/B Oligosaccharyltransferases Segregate N-Glycosylation at the Translocon From Lipid-Linked Oligosaccharide Hydrolysis. *Proc Natl Acad Sci USA* (2018) 115(38):9557–62. doi: 10.1073/pnas.1806034115
47. Ding J, Xu J, Deng Q, Ma W, Zhang R, He X, et al. Knockdown of Oligosaccharyltransferase Subunit Ribophorin 1 Induces Endoplasmic-Reticulum-Stress-Dependent Cell Apoptosis in Breast Cancer. *Front Oncol* (2021) 11:1–15. doi: 10.3389/fonc.2021.722624
48. Ruan Z, Liang M, Lai M, Shang L, Deng X, Su X. KYA1797K Down-Regulates PD-L1 in Colon Cancer Stem Cells to Block Immune Evasion by Suppressing the β-Catenin/STT3 Signaling Pathway. *Int Immunopharmacol* (2020) 78:106003. doi: 10.1016/j.intimp.2019.106003

Conflict of Interest: The authors declare that the research was conducted in the absence of any commercial or financial relationships that could be construed as a potential conflict of interest.

this article, or claim that may be made by its manufacturer, is not guaranteed or endorsed by the publisher.

GLOSSARY

AUC	area under the curve
BCA	bicinchoninic acid
BP	biological process
BC	breast cancer
CCK-8	cell counting kit-8
CC	cellular component
CTCs	circulating tumor cells
CSCs	colon cancer stem cells
ConA	concanavalin A
cDNA	complementary DNA
CR	complete response
C-index	concordance index
CNV	copy number variation
CTLA-4	cytotoxic T lymphocyte-associated protein-4
DEGs	differently expressed genes
DNAss	DNA stemness score
ECL	enhanced chemiluminescence
FDR	false discovery rate
GEO	Gene Expression Omnibus
GO	Gene Ontology
GSEA	Gene Set Enrichment Analysis
HR	hazard ratio
HRP	horseradish peroxidase
ICIs	immune checkpoint inhibitors
ICT	immune checkpoint therapy
IF	immunofluorescence
IHC	immunohistochemistry
KM	Kaplan–Meier
KEGG	Kyoto Encyclopedia of Genes and Genomes
MGAT1	mannosyl(α-1,3-)-glycoprotein β-1,2-*N*-acetylglucosaminyltransferase
MSI	microsatellite instability
MF	molecular function
GALNT6	*N*-acetylgalactosaminyltransferase 6
OST	oligosaccharyltransferase
OS	overall survival
PDAC	pancreatic ductal adenocarcinoma
PR	partial response
PHA-E	*Phaseolus vulgaris* erythroagglutinin
PHA-L	*Phaseolus vulgaris* leucoagglutinin
PCA	principal component analysis
PVDF	polyvinylidene fluoride
PD-1	programmed cell death protein-1
PD-L1	programmed cell death-ligand 1
PR	progression response
ROC	receiver operating characteristic
RPN1	Ribophorin 1
RNAss	RNA stemness score
ssGSEA	single-sample gene set enrichment analysis
SDS-PAGE	sodium dodecyl sulfate–polyacrylamide gel electrophoresis
SD	stable disease
TCGA	The Cancer Genome Atlas
TIDE	Tumor Immune Dysfunction and Exclusion
TIICs	tumor-infiltrating immune cells
TMB	tumor mutation burden
B3GNT3	β-1,3-*N*-acetylglucosaminyl transferase

frontiers | Frontiers in Immunology

MINI REVIEW
published: 03 May 2022
doi: 10.3389/fimmu.2022.902060

Integration of Tumor Microenvironment in Patient-Derived Organoid Models Help Define Precision Medicine of Renal Cell Carcinoma

Bingran Wang[†], *Yizheng Xue*[†] *and Wei Zhai*[*]

Department of Urology, Renji Hospital, School of Medicine, Shanghai Jiao Tong University, Shanghai, China

Renal cell carcinoma (RCC) is a common urological tumor, with a poor prognosis, as the result of insensitivity to chemotherapy and radiotherapy. About 20%–30% of patients with RCC have metastasis at the first diagnosis, so only systemic treatment is possible. Due to the heterogeneity of renal tumors, responses to drugs differ from person to person. Consequently, patient-derived organoid, highly recapitulating tumor heterogeneity, becomes a promising model for high-throughput *ex vivo* drug screening and thus guides the drug choice of patients with RCC. Systemic treatment of RCC mainly targets the tumor microenvironment, including neovasculature and immune cells. We reviewed several methods with which patient-derived organoid models mimic the heterogeneity of not only tumor epithelium but also the tumor microenvironment. We further discuss some new aspects of the development of patient-derived organoids, preserving *in vivo* conditions in patients with RCC.

Keywords: patient-derived organoids, renal cell carcinoma, tumor microenvironment, precision medicine, immunotherapy

OPEN ACCESS

Edited by:
Qihui Shi,
Fudan University, China

Reviewed by:
Shengzhe Zhang,
University of Texas MD Anderson Cancer Center, United States
Zhuo Wang,
Fudan University, China

***Correspondence:**
Wei Zhai
jacky_zw2002@hotmail.com

[†]*These authors have contributed equally to this work*

Specialty section:
This article was submitted to Cancer Immunity and Immunotherapy, a section of the journal Frontiers in Immunology

Received: *22 March 2022*
Accepted: *04 April 2022*
Published: *03 May 2022*

Citation:
Wang B, Xue Y and Zhai W (2022) Integration of Tumor Microenvironment in Patient-Derived Organoid Models Help Define Precision Medicine of Renal Cell Carcinoma. Front. Immunol. 13:902060. doi: 10.3389/fimmu.2022.902060

INTRODUCTION

In recent years, with the advanced knowledge of tumor biological behaviors, especially in the aspect of tumor heterogeneity, tumor treatment became personalized under the guidance of molecular classification (1–3). To further investigate the mechanisms of oncogenesis, tumor invasion, and metastasis and its translation to novel therapies, *in vitro* models such as cell lines are fundamental. However, a significant gap exists between the modeling system and *in vivo* conditions of patients, resulting in the inaccuracy of the predictive ability of several preclinical models. To shorten the gap, patient-derived models, including patient-derived primary tumor cells (PDTCs), patient-derived organoids (PDOs), and patient-derived xenograft (PDX) have been developed as a preclinical model for nearly all kinds of solid tumors (4).

Renal cell carcinoma (RCC) ranks the 6th most commonly diagnosed cancer in men and 10th in women (5). RCC can be majorly divided into three subtypes, including chromophobe (chRCC), papillary (pRCC), and a most common type clear cell RCC (ccRCC), accounting for 75% of cases of RCC (6). In addition, a large number of patients present with metastatic RCC at the time of the first

diagnosis, which makes radical surgery infeasible (7). Consequently, here we represent the current knowledge of PDO establishment in patients with RCC and its significance in personalized medicine.

EVOLUTION OF PATIENT-DERIVED ORGANOID MODEL IN RENAL CELL CARCINOMA

Organoids are 3D cultured cell models that partially preserve the characteristic architecture of organs, for example, crypt structure in intestinal organoids (8) and tubule structure in kidney organoids (9). PDO models are organoids established from tumor tissues resected from patients, which recapitulate hallmarks of parental tumors both histologically and genetically. Immunohistochemistry, whole-exosome sequencing, and RNA sequencing are routinely used to validate that PDO models are highly consistent with parental tumors and retain inter-tumor heterogeneity (10–12). Moreover, single-cell RNA sequencing (scRNA-seq) technology is expected to provide us with a more comprehensive genetic landscape of PDOs to reveal intra-tumor heterogeneity. Kumar et al. applied scRNA-seq to show the transcriptome profiles of PDO models and validate the preservation of intra-tumor sublineage heterogeneity and transcriptional plasticity of parental gastric cancer tissue (13). In addition, the spatial transcriptome platform has the ability to preserve the spatial architecture of PDOs in the process of scRNA-seq, allowing the investigation of interactions between tumor and microenvironment (14). In the future, more detailed validation of PDO models *via* the latest technologies should be emphasized. As a result, biobanks of PDOs with comprehensive multi-omics information will be established, and researchers will benefit from such a database unprecedentedly.

In comparison to PDX, PDO models take less time to cultivate and have a higher success rate, which is feasible for high-throughput drug screening (15). When compared with PDTC, PDO models show the ability to preserve tumor heterogeneity. Consequently, PDO is a precisely predictive model for drug screening, which mirrors the heterogeneity of drug efficacy. In several cancer types, including lung cancer (16), colorectal cancer (CRC) (17), prostate cancer (12), and glioblastoma (18), PDO models have become a drug screening platform. PDO models also function as valuable models to study tumor evolution. Lee and colleagues have established a PDO bank for bladder cancer and revealed that generally constant truncal mutations with variation in subclonal mutations appear during passaging (19).

In RCC, PDO functions as a model for drug screening and thus guides the selection of effective therapeutic agents. Bolck and colleagues established a biobank of patient-derived 3D ccRCC model, showing a high correspondence to parental tumor and recapitulation of intra- and inter-tumoral heterogeneity, determined by extensive DNA sequencing (20). Furthermore, Fendler et al. characterized and isolated cancer stem cells (CSCs) in ccRCC, which determine the progressiveness of the tumor, and applied CSCs to cultivate ccRCC PDO models. They also validated the significance of the WNT and NOTCH signaling pathways mediating the growth of PDO (21). Na et al. established a concrete protocol of PDO culture directly from surgical resected ccRCC sample. Such PDO preserves the morphology and biomarker expression of parental tumors (22). Grassi et al. also reported an approach to establishing and passaging normal kidney organoids and RCC PDO from surgically resected tissues. They also achieved the transformation between PDO and PDX, which not only guaranteed the long-term establishment of PDO but also paved the way for investigating tumor evolution in RCC (23) (**Table 1**).

TABLE 1 | Published articles on establishment of patient-derived organoids of renal cell carcinoma.

Histological type	Tissue collection	Establishment	Success rate	Maximum passage	Drug screening panel	Reference
ccRCC	Surgical specimen	3D patient-derived cells	26/35 (74%)	N/A	N/A	(20)
ccRCC	Surgical specimen	Cancer stem cells	41/55 (74%)	N/A	N/A	(21)
ccRCC	Surgical specimen	Matrigel submerged tumor cells	N/A	N/A	N/A	(22)
Normal tissue						
ccRCC	Surgical specimen	Matrigel submerged tumor cells	10/15 (67%)	15	Sunitinib	(23)
Normal tissue			13/13 (100%)	15	Temsirolimus	
ccRCC	Surgical specimen	Matrigel submerged tumor cells	15/20 (75%)	15	Sunitinib Axitinib Pazopanib Sorafenib Cabozantinib	(24)
ccRCC	Surgical specimen	Minced tissue in type I collagen matrix ALI system	15/26 (57%)	4	Nivolumab	(25)
pRCC			3/3 (100%)			
chRCC			1/1 (100%)			
Wilms' tumor			1/1 (100%)			
ccRCC	Surgical specimen	Minced tissue in type I collagen matrix ALI system	20/26 (77%)	3	Nivolumab Cabozantinib	(26)
pRCC			4/5 (80%)			
chRCC			0/1 (0%)			
UC			7/8 (88%)			
Oncocytoma			1/3 (33%)			

ccRCC, clear cell renal cell carcinoma; pRCC, papillary renal cell carcinoma; chRCC, chromophobe renal cell carcinoma; UC, urothelial carcinoma; ALI, air–liquid interface. N/A, Not applicable.

TUMOR MICROENVIRONMENT IN RENAL CELL CARCINOMA TREATMENT

In patients with advanced RCC, systemic therapy should be initiated. However, RCC does not show a favorable response to chemotherapies. Recent advances in the molecular mechanism of RCC, especially the inactivation of von Hippel–Lindau (VHL), paved the way for the identification of systemic treatment targeting the tumor microenvironment (TME) (27). Research revealed that the inactivation of VHL contributes to decreased ubiquitin-mediated degradation of a subunit of heterodimeric hypoxia-inducible factor (HIF) transcriptional factor (28). Constitutively accumulated HIF complex enhances the expression of downstream genes, especially vascular endothelial growth factors (VEGF), which leads to the angiogenesis of RCC. Consequently, a specific HIF-2a inhibitor MK-6482 had favorable performance in a recent phase I/II clinical trial (29). Multitargeted, small molecular tyrosine kinase inhibitor (TKI) targeted VEGF, and platelet-derived growth factor (PDGF) such as pazopanib and sunitinib has been proven effective as adjuvant therapy in several clinical trials (30–32). Also, bevacizumab, a monoclonal antibody for VEGF, showed clinical efficacy in metastatic RCC (32). Upon understanding the role of immune escape mechanisms in tumor proliferation and invasion since 2013, several immune checkpoints such as PD-1, PD-L1, and CTLA-4 have emerged as targets to reverse immune exhaustion in TME and counteract negative consequences (34). Such immune checkpoint blockades (ICBs) also benefit patients with advanced RCC. Nivolumab, like a monoclonal antibody for PD-1, has demonstrated a survival benefit in randomized controlled clinical trials (RCTs) (35). Another PD-1 antibody, pembrolizumab, also improves progression-free survival (PFS) of patients with advanced RCC in combination with axitinib compared with sunitinib as a single drug (36).

As illustrated above, unlike a range of solid tumors, systemic therapies of RCC mainly target TME, rather than the malignant epithelium. Consequently, it is necessary to review the mechanisms of TME mediating proliferation and invasion of RCC, which provides precision medicine with targets. Finally, we can work out the importance of integrating TME in PDO as prognostic models and tools for drug screening.

Hypoxia

HIF is composed of one α subunit with three isoforms (HIF-1α, HIF-2α, and HIF-3α) and one β subunit with two isoforms (HIF-1β and HIF-2β). The β subunit of HIF is constitutively expressed, while the α subunit is induced under hypoxia and dimerizes with the β subunit to form a complex, promoting the transcription of target genes (37). However, the isoforms of the α subunit play distinct but also overlapping roles during hypoxia response. HIF-1α preferentially induces apoptotic and glycolytic pathways, while HIF-2α promotes growth, cell proliferation, and angiogenesis. In many types of solid tumors, both HIF-1α and HIF-2α mediate tumorigenesis and are associated with poor prognosis (38). However, in ccRCC, HIF-2α has tumorigenic activity, whereas HIF-1α functions as a tumor suppressor (39). HIF-2α is also proven as a potential therapeutic target for ccRCC (40).

Angiogenesis

VHL gene was originally described as the gene responsible for VHL syndrome, a condition associated with an increased risk of retinal angiomas, hemangioblastomas, and ccRCC (41). Based on advanced knowledge of molecular pathways, genetic alterations in VHL were identified as an essential initiator of the tumorigenesis of ccRCC *via* promoting angiogenesis. Actually, it has been reviewed that up to 90% of sporadic ccRCC have the presence of abnormal VHL function (42). VHL proteins complex with Elongin B, Elongin C, and Cul2, which are components of an E3-ubiquitin ligase complex responsible for the proteasome degradation of two subunits of HIF: HIF-1α and HIF-1β. As the result of insufficient degradation, impaired function of VHL will lead to the accumulation of HIF and upregulated transcription of downstream effector genes, such as VEGF, PDGF, erythropoietin, and transforming growth factor (TGF), which play a crucial role in angiogenesis and tumorigenesis (43).

Immune Cell Infiltration

Historically, the systemic therapy of RCC is initiated by cytokine-based immunotherapy. Interleukin-2 (IL-2) and interferon-α (IFN-α) were considered standard therapy for advanced RCC for a long time (44); even a very small number of patients with advanced RCC have complete responses (CRs) under high-dose IL-2, which is attributed to the mobilization of immune effector cells and the relatively increased number of natural killer cells and CD8+ T cells (45). Among solid tumors, RCC ranks among the highest infiltration of immune cells, with predominantly T cells (50%), followed by tumor-associated macrophages (TAMs, 25%), natural killer (9%), B cells (4%), and other cells (46). However, tumor-infiltrating T cells, different from T cells in normal kidney tissue, are mainly composed of CD8+ T cells with high expression of co-inhibitory receptors such as PD-1 and low levels of proliferation marker Ki-67, which indicate an immune exhaustion state. Moreover, CD8+ T cells in RCC prove to be in a metabolic impaired state with reduced glucose uptake and mitochondrial function, worsening the immune exhaustion state of RCC (47). The immune checkpoint signaling pathway physiologically expressed in normal tissues functions as an inhibitory or stimulatory signaling transducer to protect tissue from autoimmune attack. However, cancer cells evade the immune system and enhance the immune exhaustion state of TME *via* overexpression ligands or receptors of the immune checkpoint. Consequently, ICBs targeting PD-1, PD-L1, and CTLA-4 have shown great effect in reversing immune exhaustion and modulating the metabolism state of immune cells in RCC.

PATIENT-DERIVED ORGANOIDS RECAPITULATE TUMOR MICROENVIRONMENT

RCC is a complex and highly heterogeneous cancer. As a result, treatment responses vary from patient to patient. Nowadays, systemic treatment choices are largely dependent on Memorial Sloan Kettering Cancer Center (MSKCC) scoring (48), suggested

by guidelines while lacking biomarkers or prognostic models to tailor treatment plans to individual patients. However, the advances in PDO during the last two decades shed light on the precision medicine of RCC. PDO as a model preserving majority of the characteristic of patients' tumors is promising in predicting the drug response of individuals. Kazama and colleagues found that RCC PDO models exhibited different responses to TKIs, including sunitinib, pazopanib, cabozantinib, axitinib, and sorafenib. However, responses to PDO require further validation of clinical data (24). A recent prospective clinical study demonstrated the predictive value of PDOs for irinotecan-based chemotherapy in metastatic CRC (49). Wang et al. verified that the drug screening test in PDO models was consistent with clinical efficacy in patients with intrahepatic cholangiocarcinoma (50).

Recent guidelines of RCC stress systemic treatment manipulating TME (51). As illustrated above, multiple targets TKIs inhibit angiogenesis by disturbing the signaling transduction of VEGFR or PDGFR, while ICBs target tumor-infiltrating CD8+ T cells and reverse the immune exhaustion state, both of which modulate TME of RCC instead of tumor epithelium. However, the first-generation PDOs contain exclusively malignant epithelium but impaired TME, thus exhibiting poor performance in predicting clinical outcomes, which hinders the identification of treatment-sensitive patients *via* drug screening based on PDO models and the discovery of predictive biomarkers of drug response (52). Consequently, it is necessary to establish novel PDO models that robustly recapitulate the TME, including immune cell infiltration and interaction with tumor cells, cancer-associated fibroblast (CAF) infiltration, angiogenesis, and extracellular matrix.

Co-Culture

To overcome the lack of immune cell infiltration in first-generation PDOs, thus establishing a drug screening model of ICB and investigating the interactions between immune cells and tumor epithelium, co-culture with immune cells was developed. A few studies have shown promising results. Dijkstra and colleagues obtained tumor-reactive T cells from the co-culture of PDOs from CRC and non-small cell lung cancer (NSCLC) with peripheral blood lymphocytes (PBLs) (53), indicating that the co-culture system can be used to establish individualized PDO models to study immune therapy and interactions between tumor-infiltrating lymphocytes (TILs) and tumor epithelium. In other cancer types, such as melanoma, breast cancer, pancreatic cancer, and lung cancer, PDO co-culture with PBLs or peripheral blood mononuclear cells (PBMCs) has been a feasible platform to study personalized immune therapy responses (54–57). However, the co-culture system has not been widely applied in the establishment of RCC PDOs. Since RCC presents high immune infiltration, and immune therapy is an essential component of systemic treatment of RCC, it is worthwhile to develop a co-culture system in RCC PDO as a model for drug screening or as a model for investigating the interaction between tumor epithelium and infiltrated immune cells. Recently, Rausch et al. developed a 3D spheroid co-culture system of RCC cell lines and immune cells isolated from PBMCs and recapitulated the responses of drug combinations (58). However, the RCC cell lines are homologous, without the representation of inter-tumor heterogeneity. Grassi et al. successfully established PDO in patients with RCC, which preserved the expression of PD-L1 and PD-L2, suggesting a promising application in a co-culture system (23). Consequently, generating PDO models of RCC co-culture with immune cells is substantial and possible in the near future.

Air–Liquid Interface

As illustrated above, RCCs have high immune infiltration and present substantial heterogeneity, which contributes to the difficulty in the prediction of drug responses and creates exigency for establishing PDO models recapitulating the patients' situation as closely as possible for studying personalized medicine. However, co-culture with PBMCs or TILs, albeit preserving immune cells in TME, fails to preserve the diversity of immune cell types in TME, which proves essential in drug responses. Moreover, the physical architecture of TME is also disturbed in the process of co-culture. Consequently, a novel generation of organoids based on the air–liquid interface (ALI), which closely resembles the *in vivo* situation, has been developed and applied as a preclinical tool for the investigation of several diseases (25, 59, 60). ALI-PDO method successfully preserves the complex histological TME architectures *via* mechanically mincing, rather than dissociating tissue with collagenase, which is commonly applied in the first generation. The addition of IL-2 in the medium also plays a central role in preserving the viability of CD3+ TILs (25). The ALI methodology was initially introduced into the culture of murine intestinal organoids to maintain mesenchymal cells and supply paracrine signaling (61–63). Until 2018, Neal and colleagues optimized protocols for establishing the ALI-PDO model in a series of surgically resected tumors, including colon adenocarcinoma, bile duct ampulla adenocarcinoma, lung adenoma, and renal clear cell carcinoma. At the histological level, ALI-PDO accurately presents the heterogeneity and architecture of primary tumor with retention of stromal, CAFs, and diversity of immune cell population. At the gene level, scRNA-seq shows a high concordance in TCR between ALI-PDO and RCC tumors. Moreover, ALI-PDO has been proved to confidently recapitulate the effect of PD-1/PD-L1-dependent immune checkpoint (25). The team of Neal also developed a method for determining the responsiveness of ALI-PDO to immunotherapeutic agents by measuring mRNA or protein markers associated with immune activation, which paved the way for utilizing ALI-PDO as an immunotherapeutic drug screening model (25). Two years later, Esser and colleagues applied the protocols of Neal et al. to cultivate ALI-PDOs from renal tumors and test drug efficacy. ALI-PDOs from RCC showed heterogenic responses to target therapy (TKI) and ICB, which is in line with the clinical situation. By applying this model, researchers also recapitulated that responses of nivolumab are dependent on CD8+ T-cell infiltration, rather

than the expression level of PD-L1 in tissue (26, 64). This study provides the perspective of ALI-PDO in functioning as a preclinical model for tailoring RCC treatment plans. Moreover, Vilgelm and colleagues reported a protocol of PDO cultivation based on fine-needle aspiration (FNA), which is adapted to drug screening. They applied Wnt3A and IL-2-containing medium to effectively preserve the viability of immune cells in RCC PDO (65). Vilgelm et al. demonstrated the ability of predicting clinical outcomes before initiating systemic treatment of RCC patients by cultivating PDOs from diagnostic FNA (65). All of these studies show that ALI-PDO is a promising preclinical model, reliably recapitulating both heterogeneity and architecture of TME, which has the ability to predict responses of first-line treatment of RCC, including TKIs and ICBs, and in turn guide personalized medicine.

Tissue Slice Culture

To retain the heterogeneity and architecture of TME in RCC individualized models, patient-derived tissue slice culture (PDTSC) has been promoted. The first PDTSC for RCC was prompted by Weissinger and colleagues in 2013, functioning as a model to study the oncogenic signaling pathway of RCC (66). Martin and colleagues refined *ex vivo* cultivation procedures of PDTSC for hepatic metastatic CRC (67), which was utilized by Stenzel et al. to examine the effect of nivolumab in RCC by monitoring TILs. Investigators revealed that nivolumab-mediated reduction in PD-1 expression and altered activation status of TILs, especially CD8+ T cells, are indicators for responses to ICBs (68). Roelants et al. also developed a PDTSC model for RCC to evaluate treatment responses (69). Slice culture from RCC showed perfect consistency with parental tumor both histologically and genetically, which had the ability to evaluate the cytotoxic effect of targeted therapies. By applying PDTSC models, CD8+ T cells were predicted as markers indicating immunotherapy responses, which is in line with contemporary research (70).

Here, we concluded the characteristics of PDO models and differences between novel generation PDO models in **Table 2**.

DISCUSSION

PDO is a reliable and economical model for drug screening for various cancer types. The results of drug screening not only indicate clinical treatment choice but also can be used to explore predictive biomarkers of drug responses. In this review, we summarized recent advances in the establishment of PDO models in patients with RCC. Unfortunately, the majority of reported culture methods remain the first generation PDO, which lacks the infiltration of the TME. However, the main targets of systemic treatment in RCC are neo-vasculature and infiltrating immune cells. Consequently, it is urgent to develop PDO models with preserved TME in patients with RCC. In other cancer types, co-culture, ALI, and TSC have been extensively applied to recapitulate the microenvironment. In the future, more effort should be put into the integration of such methods in RCC PDO. Moreover, the peripheral immune system, such as circulating immune cells and peripheral lymph nodes, contributes to the responses of immune therapy (71). Chimeric antigen receptor redirected T (CAR-T) cells also show effects on solid tumors (72). Consequently, in the near future, the interaction between cancer epithelium and peripheral immune system cannot be ignored, especially in RCC, a tumor with highly infiltrated immune cells, which means more holistic models, and integrating systemic conditions in PDO will attract more interest. For example, organ-on-a-chip models highly mimic the physical condition by seeding multiple cell types of the human organ into engineered chambers with perfusion, which provides new perspectives for the investigation of a holistic response to the drug (73). Recently, organ-on-a-chip models are mainly based on microfluidic devices (74). With the development of organoids, "organoids-on-chip" will also appear to recapitulate *in vivo* environment more exactly.

In conclusion, PDO as an essential tool for personalized medicine goes through an evolution during the past few years, with a more accurate recapitulation of *in vivo* conditions. As a result of highly infiltrated immune cells in RCC, progress in mimicking the RCC TME is still needed in the development of PDO.

TABLE 2 | Comparisons between conventional and next-generation patient-derived models of renal cell carcinoma.

		First-generation PDO	PDO plus		
			Co-culture	ALI	TSC
Histological characteristics		Preserved	Preserved	Preserved	Preserved
Genetic alteration		Preserved	Preserved	Preserved	Preserved
Component of TME	ECM	–	–	+	+
	Immune cells	–	+	+	+
	CAFs	–	–	+	+
Architecture of TME		–	–	+	–
Availability of live cell analysis		+	+	+	–
Testable drug classes		TKIs	TKIs; immunotherapy	TKIs; immunotherapy	TKIs; immunotherapy
Reliability as preclinical model		+	++	+++	++

PDO, patient-derived organoid; ALI, air–liquid interface; TSC, tissue slice culture; TME, tumor microenvironment; ECM, extracellular matrix; CAFs, cancer-associated fibroblasts; TKI, tyrosine kinase inhibitors.

#-, does not have or not available; +, perform fine; ++: perform very well; +++: perform excellent.

AUTHOR CONTRIBUTIONS

BW and YX drafted the article, and WZ revised it critically for intellectual content. All authors contributed to the article and approved the submitted version.

FUNDING

This study was supported by the National Natural Science Foundation of China (Nos. 82173214 and 81972369).

REFERENCES

1. Röcken C. Molecular Classification of Gastric Cancer. *Expert Rev Mol Diagn* (2017) 17(3):293–301. doi: 10.1080/14737159.2017.1286985
2. Rodriguez-Canales J, Parra-Cuentas E, Wistuba II. Diagnosis and Molecular Classification of Lung Cancer. *Cancer Treat Res* (2016) 170:25–46. doi: 10.1007/978-3-319-40389-2_2
3. Tsang JYS, Tse GM. Molecular Classification of Breast Cancer. *Adv Anat Pathol* (2020) 27(1):27–35. doi: 10.1097/PAP.0000000000000232
4. Bleijs M, van de Wetering M, Clevers H, Drost J. Xenograft and Organoid Model Systems in Cancer Research. *EMBO J* (2019) 38(15):e101654. doi: 10.15252/embj.2019101654
5. Capitanio U, Bensalah K, Bex A, Boorjian SA, Bray F, Coleman J, et al. Epidemiology of Renal Cell Carcinoma. *Eur Urol* (2019) 75(1):74–84. doi: 10.1016/j.eururo.2018.08.036
6. Kajdasz A, Majer W, Kluzek K, Sobkowiak J, Milecki T, Derebecka N, et al. Identification of RCC Subtype-Specific microRNAs-Meta-Analysis of High-Throughput RCC Tumor microRNA Expression Data. *Cancers (Basel).* (2021) 13(3):548. doi: 10.3390/cancers13030548
7. Wood L. Sunitinib Malate for the Treatment of Renal Cell Carcinoma. *Expert Opin Pharmacother* (2012) 13(9):1323–36. doi: 10.1517/14656566.2012.689130
8. Serra D, Mayr U, Boni A, Lukonin I, Rempfler M, Challet Meylan L, et al. Self-Organization and Symmetry Breaking in Intestinal Organoid Development. *Nature* (2019) 569(7754):66–72. doi: 10.1038/s41586-019-1146-y
9. Yousef Yengej FA, Jansen J, Rookmaaker MB, Verhaar MC, Clevers H. Kidney Organoids and Tubuloids. *Cells* (2020) 9(6):1236. doi: 10.3390/cells9061326
10. Shi R, Radulovich N, Ng C, Liu N, Notsuda H, Cabanero M, et al. Organoid Cultures as Preclinical Models of Non-Small Cell Lung Cancer. *Clin Cancer Res* (2020) 26(5):1162–74. doi: 10.1158/1078-0432.CCR-19-1376
11. Kawasaki K, Toshimitsu K, Matano M, Fujita M, Fujii M, Togasaki K, et al. An Organoid Biobank of Neuroendocrine Neoplasms Enables Genotype-Phenotype Mapping. *Cell* (2020) 183(5):1420–1435.e1421. doi: 10.1016/j.cell.2020.10.023
12. Gao D, Vela I, Sboner A, Iaquinta PJ, Karthaus WR, Gopalan A, et al. Organoid Cultures Derived From Patients With Advanced Prostate Cancer. *Cell* (2014) 159(1):176–87. doi: 10.1016/j.cell.2014.08.016
13. Kumar V, Ramnarayanan K, Sundar R, Padmanabhan N, Srivastava S, Koiwa M, et al. Single-Cell Atlas of Lineage States, Tumor Microenvironment, and Subtype-Specific Expression Programs in Gastric Cancer. *Cancer Discov* (2022) 12(3):670–91. doi: 10.1158/2159-8290.CD-21-0683
14. Bock C, Boutros M, Camp JG, Clarke L, Clevers H, Knoblich JA, et al. The Organoid Cell Atlas. *Nat Biotechnol* (2021) 39(1):13–7. doi: 10.1038/s41587-020-00762-x
15. Yoshida GJ. Applications of Patient-Derived Tumor Xenograft Models and Tumor Organoids. *J Hematol Oncol* (2020) 13(1):4. doi: 10.1186/s13045-019-0829-z
16. Kim M, Mun H, Sung CO, Cho EJ, Jeon HJ, Chun SM, et al. Patient-Derived Lung Cancer Organoids as *In Vitro* Cancer Models for Therapeutic Screening. *Nat Commun* (2019) 10(1):3991. doi: 10.1038/s41467-019-11867-6
17. Pasch CA, Favreau PF, Yueh AE, Babiarz CP, Gillette AA, Sharick JT, et al. Patient-Derived Cancer Organoid Cultures to Predict Sensitivity to Chemotherapy and Radiation. *Clin Cancer Res* (2019) 25(17):5376–87. doi: 10.1158/1078-0432.CCR-18-3590
18. Jacob F, Salinas RD, Zhang DY, Nguyen PTT, Schnoll JG, Wong SZH, et al. A Patient-Derived Glioblastoma Organoid Model and Biobank Recapitulates Inter- and Intra-Tumoral Heterogeneity. *Cell* (2020) 180(1):188–204 e122. doi: 10.1016/j.cell.2019.11.036
19. Lee SH, Hu W, Matulay JT, Silva MV, Owczarek TB, Kim K, et al. Tumor Evolution and Drug Response in Patient-Derived Organoid Models of Bladder Cancer. *Cell* (2018) 173(2):515–528.e517. doi: 10.1016/j.cell.2018.03.017
20. Bolck HA, Corro C, Kahraman A, von Teichman A, Toussaint NC, Kuipers J, et al. Tracing Clonal Dynamics Reveals That Two- and Three-Dimensional Patient-Derived Cell Models Capture Tumor Heterogeneity of Clear Cell Renal Cell Carcinoma. *Eur Urol Focus* (2021) 7(1):152–62. doi: 10.1016/j.euf.2019.06.009
21. Fendler A, Bauer D, Busch J, Jung K, Wulf-Goldenberg A, Kunz S, et al. Inhibiting WNT and NOTCH in Renal Cancer Stem Cells and the Implications for Human Patients. *Nat Commun* (2020) 11(1):929. doi: 10.1038/s41467-020-14700-7
22. Na JC, Kim JH, Kim SY, Gu YR, Jun DY, Lee HH, et al. Establishment of Patient-Derived Three-Dimensional Organoid Culture in Renal Cell Carcinoma. *Investig Clin Urol* (2020) 61(2):216–23. doi: 10.4111/icu.2020.61.2.216
23. Grassi L, Alfonsi R, Francescangeli F, Signore M, De Angelis ML, Addario A, et al. Organoids as a New Model for Improving Regenerative Medicine and Cancer Personalized Therapy in Renal Diseases. *Cell Death Dis* (2019) 10(3):201. doi: 10.1038/s41419-019-1453-0
24. Kazama A, Anraku T, Kuroki H, Shirono Y, Murata M, Bilim V, et al. Development of Patient–Derived Tumor Organoids and a Drug Testing Model for Renal Cell Carcinoma. *Oncol Rep* (2021) 46(4):226. doi: 10.3892/or.2021.8177
25. Neal JT, Li X, Zhu J, Giangarra V, Grzeskowiak CL, Ju J, et al. Organoid Modeling of the Tumor Immune Microenvironment. *Cell* (2018) 175(7):1972–1988.e1916. doi: 10.1016/j.cell.2018.11.021
26. Esser LK, Branchi V, Leonardelli S, Pelusi N, Simon AG, Klumper N, et al. Cultivation of Clear Cell Renal Cell Carcinoma Patient-Derived Organoids in an Air-Liquid Interface System as a Tool for Studying Individualized Therapy. *Front Oncol* (2020) 10:1775. doi: 10.3389/fonc.2020.01775
27. Kim H, Shim BY, Lee SJ, Lee JY, Lee HJ, Kim IH. Loss of Von Hippel-Lindau (VHL) Tumor Suppressor Gene Function: VHL-HIF Pathway and Advances in Treatments for Metastatic Renal Cell Carcinoma (RCC). *Int J Mol Sci* (2021) 22(18):9795. doi: 10.3390/ijms22189795
28. Ivan M, Kondo K, Yang H, Kim W, Valiando J, Ohh M, et al. HIFalpha Targeted for VHL-Mediated Destruction by Proline Hydroxylation: Implications for O2 Sensing. *Science* (2001) 292(5516):464–8. doi: 10.1126/science.1059817
29. Choueiri TK, Bauer TM, Papadopoulos KP, Plimack ER, Merchan JR, McDermott DF, et al. Inhibition of Hypoxia-Inducible Factor-2α in Renal Cell Carcinoma With Belzutifan: A Phase 1 Trial and Biomarker Analysis. *Nat Med* (2021) 27(5):802–5. doi: 10.1038/s41591-021-01324-7
30. Motzer RJ, Haas NB, Donskov F, Gross-Goupil M, Varlamov S, Kopyltsov E, et al. Randomized Phase III Trial of Adjuvant Pazopanib Versus Placebo After Nephrectomy in Patients With Localized or Locally Advanced Renal Cell Carcinoma. *J Clin Oncol* (2017) 35(35):3916–23. doi: 10.1200/JCO.2017.73.5324
31. Motzer RJ, Hutson TE, Tomczak P, Michaelson MD, Bukowski RM, Rixe O, et al. Sunitinib Versus Interferon Alfa in Metastatic Renal-Cell Carcinoma. *N Engl J Med* (2007) 356(2):115–24. doi: 10.1056/NEJMoa065044
32. Sternberg CN, Davis ID, Mardiak J, Szczylik C, Lee E, Wagstaff J, et al. Pazopanib in Locally Advanced or Metastatic Renal Cell Carcinoma: Results of a Randomized Phase III Trial. *J Clin Oncol* (2010) 28(6):1061–8. doi: 10.1200/JCO.2009.23.9764
33. Yang JC, Haworth L, Sherry RM, Hwu P, Schwartzentruber DJ, Topalian SL, et al. A Randomized Trial of Bevacizumab, an Anti-Vascular Endothelial Growth Factor Antibody, for Metastatic Renal Cancer. *N Engl J Med* (2003) 349(5):427–34. doi: 10.1056/NEJMoa021491
34. Tykodi SS. Progress and Potential of Immune Checkpoint Blockade for Treating Advanced Renal Cell Carcinoma. *Immunotherapy* (2013) 5(6):607–19. doi: 10.2217/imt.13.39
35. Motzer RJ, Escudier B, McDermott DF, George S, Hammers HJ, Srinivas S, et al. Nivolumab Versus Everolimus in Advanced Renal-Cell Carcinoma. *N Engl J Med* (2015) 373(19):1803–13. doi: 10.1056/NEJMoa1510665

36. Powles T, Plimack ER, Soulières D, Waddell T, Stus V, Gafanov R, et al. Pembrolizumab Plus Axitinib Versus Sunitinib Monotherapy as First-Line Treatment of Advanced Renal Cell Carcinoma (KEYNOTE-426): Extended Follow-Up From a Randomised, Open-Label, Phase 3 Trial. *Lancet Oncol* (2020) 21(12):1563–73. doi: 10.1016/S1470-2045(20)30436-8
37. Albadari N, Deng S, Li W. The Transcriptional Factors HIF-1 and HIF-2 and Their Novel Inhibitors in Cancer Therapy. *Expert Opin Drug Discov* (2019) 14 (7):667–82. doi: 10.1080/17460441.2019.1613370
38. Martínez-Sáez O, Gajate Borau P, Alonso-Gordoa T, Molina-Cerrillo J, Grande E. Targeting HIF-2 α in Clear Cell Renal Cell Carcinoma: A Promising Therapeutic Strategy. *Crit Rev Oncol Hematol* (2017) 111:117–23. doi: 10.1016/j.critrevonc.2017.01.013
39. Schodel J, Grampp S, Maher ER, Moch H, Ratcliffe PJ, Russo P, et al. Hypoxia, Hypoxia-Inducible Transcription Factors, and Renal Cancer. *Eur Urol* (2016) 69(4):646–57. doi: 10.1016/j.eururo.2015.08.007
40. Isono T, Chano T, Yoshida T, Kageyama S, Kawauchi A, Suzaki M, et al. Hydroxyl-HIF2-Alpha Is Potential Therapeutic Target for Renal Cell Carcinomas. *Am J Cancer Res* (2016) 6(10):2263–76.
41. Chittiboina P, Lonser RR. Von Hippel-Lindau Disease. *Handb Clin Neurol* (2015) 132:139–56. doi: 10.1016/B978-0-444-62702-5.00010-X
42. Pavlovich CP, Schmidt LS. Searching for the Hereditary Causes of Renal-Cell Carcinoma. *Nat Rev Cancer* (2004) 4(5):381–93. doi: 10.1038/nrc1364
43. Pezzuto A, Carico E. Role of HIF-1 in Cancer Progression: Novel Insights. *A Review Curr Mol Med* (2018) 18(6):343–51. doi: 10.2174/1566524018666181109121849
44. Barata PC, Rini BI. Treatment of Renal Cell Carcinoma: Current Status and Future Directions. *CA Cancer J Clin* (2017) 67(6):507–24. doi: 10.3322/caac.21411
45. Janiszewska AD, Poletajew S, Wasiutyński A. Spontaneous Regression of Renal Cell Carcinoma. *Contemp Oncol (Pozn)* (2013) 17(2):123–7. doi: 10.5114/wo.2013.34613
46. Vuong L, Kotecha RR, Voss MH, Hakimi AA. Tumor Microenvironment Dynamics in Clear-Cell Renal Cell Carcinoma. *Cancer Discov* (2019) 9 (10):1349–57. doi: 10.1158/2159-8290.CD-19-0499
47. Siska PJ, Beckermann KE, Mason FM, Andrejeva G, Greenplate AR, Sendor AB, et al. Mitochondrial Dysregulation and Glycolytic Insufficiency Functionally Impair CD8 T Cells Infiltrating Human Renal Cell Carcinoma. *JCI Insight* (2017) 2(12):e93411. doi: 10.1172/jci.insight.93411
48. Motzer RJ, Jonasch E, Boyle S, Carlo MI, Manley B, Agarwal N, et al. NCCN Guidelines Insights: Kidney Cancer, Version 1.2021. *J Natl Compr Canc Netw* (2020) 18(9):1160–70. doi: 10.6004/jnccn.2020.0043
49. Ooft SN, Weeber F, Dijkstra KK, McLean CM, Kaing S, van Werkhoven E, et al. Patient-Derived Organoids can Predict Response to Chemotherapy in Metastatic Colorectal Cancer Patients. *Sci Transl Med* (2019) 11(513): eaay2574. doi: 10.1126/scitranslmed.aay2574
50. Wang Z, Jin Y, Guo Y, Tan Z, Zhang X, Ye D, et al. Conversion Therapy of Intrahepatic Cholangiocarcinoma Is Associated With Improved Prognosis and Verified by a Case of Patient-Derived Organoid. *Cancers (Basel).* (2021) 13(5):1179. doi: 10.3390/cancers13051179
51. Motzer RJ, Jonasch E, Agarwal N, Alva A, Baine M, Beckermann K, et al. Kidney Cancer, Version 3.2022, NCCN Clinical Practice Guidelines in Oncology. *J Natl Compr Canc Netw* (2022) 20(1):71–90. doi: 10.6004/jnccn.2022.0001
52. Liu L, Yu L, Li Z, Li W, Huang W. Patient-Derived Organoid (PDO) Platforms to Facilitate Clinical Decision Making. *J Transl Med* (2021) 19(1):40. doi: 10.1186/s12967-020-02677-2
53. Dijkstra KK, Cattaneo CM, Weeber F, Chalabi M, van de Haar J, Fanchi LF, et al. Generation of Tumor-Reactive T Cells by Co-Culture of Peripheral Blood Lymphocytes and Tumor Organoids. *Cell* (2018) 174(6):1586–1598 e1512. doi: 10.1016/j.cell.2018.07.009
54. Cattaneo CM, Dijkstra KK, Fanchi LF, Kelderman S, Kaing S, van Rooij N, et al. Tumor Organoid-T-Cell Coculture Systems. *Nat Protoc* (2020) 15(1):15–39. doi: 10.1038/s41596-019-0232-9
55. Meng Q, Xie S, Gray GK, Dezfulian MH, Li W, Huang L, et al. Empirical Identification and Validation of Tumor-Targeting T Cell Receptors From Circulation Using Autologous Pancreatic Tumor Organoids. *J Immunother Cancer* (2021) 9(11):e003213. doi: 10.1136/jitc-2021-003213
56. Votanopoulos KI, Forsythe S, Sivakumar H, Mazzocchi A, Aleman J, Miller L, et al. Model of Patient-Specific Immune-Enhanced Organoids for Immunotherapy Screening: Feasibility Study. *Ann Surg Oncol* (2020) 27 (6):1956–67. doi: 10.1245/s10434-019-08143-8
57. Zhou Z, van der Jeught K, Fang Y, Yu T, Li Y, Ao Z, et al. An Organoid-Based Screen for Epigenetic Inhibitors That Stimulate Antigen Presentation and Potentiate T-Cell-Mediated Cytotoxicity. *Nat BioMed Eng* (2021) 5(11):1320–35. doi: 10.1038/s41551-021-00805-x
58. Rausch M, Blanc L, De Souza Silva O, Dormond O, Griffioen AW, Nowak-Sliwinska P. Characterization of Renal Cell Carcinoma Heterotypic 3d Co-Cultures With Immune Cell Subsets. *Cancers (Basel).* (2021) 13(11):2551. doi: 10.3390/cancers13112551
59. Choi KG, Wu BC, Lee AH, Baquir B, Hancock REW. Utilizing Organoid and Air-Liquid Interface Models as a Screening Method in the Development of New Host Defense Peptides. *Front Cell Infect Microbiol* (2020) 10:228. doi: 10.3389/fcimb.2020.00228
60. Gupta AK, Coburn JM, Davis-Knowlton J, Kimmerling E, Kaplan DL, Oxburgh L. Scaffolding Kidney Organoids on Silk. *J Tissue Eng Regener Med* (2019) 13(5):812–22. doi: 10.1002/term.2830
61. Li X, Nadauld L, Ootani A, Corney DC, Pai RK, Gevaert O, et al. Oncogenic Transformation of Diverse Gastrointestinal Tissues in Primary Organoid Culture. *Nat Med* (2014) 20(7):769–77. doi: 10.1038/nm.3585
62. Li X, Ootani A, Kuo C. An Air-Liquid Interface Culture System for 3D Organoid Culture of Diverse Primary Gastrointestinal Tissues. *Methods Mol Biol* (2016) 1422:33–40. doi: 10.1007/978-1-4939-3603-8_4
63. Ootani A, Li X, Sangiorgi E, Ho QT, Ueno H, Toda S, et al. Sustained *In Vitro* Intestinal Epithelial Culture Within a Wnt-Dependent Stem Cell Niche. *Nat Med* (2009) 15(6):701–6. doi: 10.1038/nm.1951
64. Stenzel PJ, Schindeldecker M, Tagscherer KE, Foersch S, Herpel E, Hohenfellner M, et al. Prognostic and Predictive Value of Tumor-Infiltrating Leukocytes and of Immune Checkpoint Molecules PD1 and PDL1 in Clear Cell Renal Cell Carcinoma. *Transl Oncol* (2020) 13(2):336–45. doi: 10.1016/j.tranon.2019.11.002
65. Vilgelm AE, Bergdorf K, Wolf M, Bharti V, Shattuck-Brandt R, Blevins A, et al. Fine-Needle Aspiration-Based Patient-Derived Cancer Organoids. *iScience* (2020) 23(8):101408. doi: 10.1016/j.isci.2020.101408
66. Weissinger D, Tagscherer KE, Macher-Göppinger S, Haferkamp A, Wagener N, Roth W. The Soluble Decoy Receptor 3 is Regulated by a PI3K-Dependent Mechanism and Promotes Migration and Invasion in Renal Cell Carcinoma. *Mol Cancer* (2013) 12(1):120. doi: 10.1186/1476-4598-12-120
67. Martin SZ, Wagner DC, Hörner N, Horst D, Lang H, Tagscherer KE, et al. *Ex Vivo* Tissue Slice Culture System to Measure Drug-Response Rates of Hepatic Metastatic Colorectal Cancer. *BMC Cancer* (2019) 19(1):1030. doi: 10.1186/s12885-019-6270-4
68. Stenzel PJ, Horner N, Foersch S, Wagner DC, Tsaur I, Thomas A, et al. Nivolumab Reduces PD1 Expression and Alters Density and Proliferation of Tumor Infiltrating Immune Cells in a Tissue Slice Culture Model of Renal Cell Carcinoma. *Cancers (Basel).* (2021) 13(18):4511. doi: 10.3390/cancers13184511
69. Roelants C, Pillet C, Franquet Q, Sarrazin C, Peilleron N, Giacosa S, et al. *Ex-Vivo* Treatment of Tumor Tissue Slices as a Predictive Preclinical Method to Evaluate Targeted Therapies for Patients With Renal Carcinoma. *Cancers (Basel).* (2020) 12(1):232. doi: 10.3390/cancers12010232
70. Choueiri TK, Motzer RJ, Rini BI, Haanen J, Campbell MT, Venugopal B, et al. Updated Efficacy Results From the JAVELIN Renal 101 Trial: First-Line Avelumab Plus Axitinib Versus Sunitinib in Patients With Advanced Renal Cell Carcinoma. *Ann Oncol* (2020) 31(8):1030–9. doi: 10.1016/j.annonc.2020.04.010
71. Huang AC, Postow MA, Orlowski RJ, Mick R, Bengsch B, Manne S, et al. T-Cell Invigoration to Tumour Burden Ratio Associated With Anti-PD-1 Response. *Nature* (2017) 545(7652):60–5. doi: 10.1038/nature22079
72. Ma S, Li X, Wang X, Cheng L, Li Z, Zhang C, et al. Current Progress in CAR-T Cell Therapy for Solid Tumors. *Int J Biol Sci* (2019) 15(12):2548–60. doi: 10.7150/ijbs.34213
73. Low LA, Mummery C, Berridge BR, Austin CP, Tagle DA. Organs-On-Chips: Into the Next Decade. *Nat Rev Drug Discov* (2021) 20(5):345–61. doi: 10.1038/s41573-020-0079-3

74. Sontheimer-Phelps A, Hassell BA, Ingber DE. Modelling Cancer in Microfluidic Human Organs-On-Chips. *Nat Rev Cancer* (2019) 19(2):65–81. doi: 10.1038/s41568-018-0104-6

Conflict of Interest: The authors declare that the research was conducted in the absence of any commercial or financial relationships that could be construed as a potential conflict of interest.

Publisher's Note: All claims expressed in this article are solely those of the authors and do not necessarily represent those of their affiliated organizations, or those of the publisher, the editors and the reviewers. Any product that may be evaluated in this article, or claim that may be made by its manufacturer, is not guaranteed or endorsed by the publisher.

frontiers | Frontiers in Immunology

ORIGINAL RESEARCH
published: 04 May 2022
doi: 10.3389/fimmu.2022.895110

Identification of Ferroptosis-Related Prognostic Signature and Subtypes Related to the Immune Microenvironment for Breast Cancer Patients Receiving Neoadjuvant Chemotherapy

Yuhao Xu[1,2†], Yaoqiang Du[3†], Qinghui Zheng[2], Tao Zhou[4], Buyun Ye[1], Yihao Wu[5], Qiuran Xu[6] and Xuli Meng[2*]*

[1] The Second Clinical Medical College, Zhejiang Chinese Medical University, Hangzhou, China, [2] General Surgery, Cancer Center, Department of Breast Surgery, Zhejiang Provincial People's Hospital (Affiliated People's Hospital, Hangzhou Medical College), Hangzhou, China, [3] Laboratory Medicine Center, Department of Transfusion Medicine, Zhejiang Provincial People's Hospital (Affiliated People's Hospital, Hangzhou Medical College), Hangzhou, China, [4] Hangzhou Medical College, Hangzhou, China, [5] College of Pharmacy, Zhejiang University of Technology, Hangzhou, China, [6] Laboratory of Tumor Molecular Diagnosis and Individualized Medicine of Zhejiang Province, Zhejiang Provincial People's Hospital (Affiliated People's Hospital, Hangzhou Medical College), Hangzhou, China

Purpose: To identify molecular clusters associated with ferroptosis and to develop a ferroptosis-related signature for providing novel potential targets for the recurrence-free survival and treatment of breast cancer.

Methods: Ferroptosis-related gene (FRG) signature was constructed by univariate and multivariate Cox regression and least absolute shrinkage and selection operator (LASSO). Receiver operating characteristic curves, Kaplan–Meier survival analysis, principal component analysis, and univariate and multivariate Cox regression analyses in the training and test cohorts were used to evaluate the application of this signature. Quantitative reverse transcriptase–PCR (qRT-PCR) was employed to detect the expression of FRGs in the model. Furthermore, the correlations between the signature and immune microenvironment, somatic mutation, and chemotherapeutic drugs sensitivity were explored.

Results: Internal and external validations affirmed that relapse-free survival differed significantly between the high-risk and low-risk groups. Univariate and multivariate Cox regression analyses indicated that the riskScore was an independent prognostic factor for BRCA. The areas under the curve (AUCs) for predicting 1-, 2-, and 3-year survival in the training and test cohorts were satisfactory. Significant differences were also found in the immune microenvironment and IC50 of chemotherapeutic drugs between different risk groups. Furthermore, we divided patients into three clusters based on 18 FRGs to ameliorate the situation of immunotherapy failure in BRCA.

OPEN ACCESS

Edited by:
Qihui Shi,
Fudan University, China

Reviewed by:
Yu Dong,
Shanghai Jiao Tong University, China
Meiyi Li,
The Chinese University of Hong Kong, China

***Correspondence:**
Xuli Meng
mxlmail@126.com
Qiuran Xu
windway626@sina.com

†These authors have contributed equally to this work

Specialty section:
This article was submitted to Cancer Immunity and Immunotherapy, a section of the journal Frontiers in Immunology

Received: *13 March 2022*
Accepted: *06 April 2022*
Published: *04 May 2022*

Citation:
Xu Y, Du Y, Zheng Q, Zhou T, Ye B, Wu Y, Xu Q and Meng X (2022) Identification of Ferroptosis-Related Prognostic Signature and Subtypes Related to the Immune Microenvironment for Breast Cancer Patients Receiving Neoadjuvant Chemotherapy. Front. Immunol. 13:895110. doi: 10.3389/fimmu.2022.895110

Conclusions: The FRG signature functions as a robust prognostic predictor of the immune microenvironment and therapeutic response, with great potential to guide individualized treatment strategies in the future.

Keywords: breast cancer, ferroptosis, relapse-free survival, neoadjuvant chemotherapy, immune microenvironment

INTRODUCTION

Breast cancer has surpassed lung cancer as being the most commonly diagnosed cancer with approximately 2.3 million new cases in 2020, accounting for 11.7% of all new cancer cases (1). Another scary truth is the drop in average onset age (2). Because breast cancer is a highly heterogeneous systemic disease, advancements in therapy are particularly crucial (3).

Neoadjuvant chemotherapy (NAC) is seen as the standard and first-line treatment for locally advanced breast cancer (4, 5), which not only is beneficial to breast-conserving surgery but also can detect tumor sensitivity to anticancer therapy for locally advanced breast cancer (6), and it could also be employed as a bridge to other therapies (7, 8). Anthracyclines and taxanes serve as the backbone of NAC regimens and are widely used clinically (9).

Ferroptosis is an emerging form of programmed cell death featured by the iron-dependent accumulation of lipid reactive oxygen species (ROS) of metabolic dysfunctions, iron accumulation, and antioxidant vulnerability (10–12). Accumulating evidence showed that the role of ferroptosis in carcinogenesis, progression, and chemoresistance had made progress. Fascin regulates SLC7A11 stability to induce ferroptosis (13). Renovation of SLC7A11 rescues miR-5096-mediated ferroptosis and antitumor effects of breast cancer (14). Ferroptosis-related gene (FRG) GPX4 promotes chemoresistance in nasopharyngeal carcinoma (15). Bufotalin induces ferroptosis by facilitating the ubiquitination and degradation of GPX4 in non-small cell lung cancer cells (16). *Via* ferroptosis, ETS1/miR-23a-3p/ACSL4 axis stimulates sorafenib resistance in HCC (17).

Ferroptosis has the characteristics of inhibiting chemoresistance and enhancing antitumor immunity (18), which may be a potential strategy to overcome the drug resistance mechanism of traditional cancer treatments (12). Previous studies prove the feasibility of ferroptosis-related prognostic markers to predict overall survival and immune characteristics. FRG signatures were constructed to predict overall survival in lung adenocarcinoma (19), colorectal cancer (20), and pancreatic adenocarcinoma (21). However, as far as we are aware, studies focusing on the correlation of ferroptosis with biochemical recurrence and antitumor immunology of BRCA were rather limited. Thus, it is an urgent need to discover a robust biomarker to predict relapse-free survival (RFS) in BRCA.

In this study, we constructed an FRG prognostic signature and identified three ferrClusters in predicting the RFS internally and externally, exploring the status of immune infiltrates and drug sensitivity of BRCA patients receiving NAC for guiding clinical practice. This signature may also serve as a novel and robust prediction tool for evaluating whether BRCA patients can benefit from immunotherapy.

Abbreviations: GEO, Gene Expression Omnibus; TCGA, The Cancer Genome Atlas; NAC, neoadjuvant chemotherapy; CNV, copy number variation; UCSC, University of California, Santa Cruz; ROC, receiver operating characteristic; GDSC, Genomics of Drug Sensitivity in Cancer; IC50, half-maximal inhibitory concentration; AUC, area under the curve; RFS, recurrence-free survival; FRG, ferroptosis-related gene; IS, immune score; SS, stromal score; ES, estimate score; ssGSEA, single-sample gene set enrichment analysis; TIME, tumor immune microenvironment; PCA, principal component analysis; ICI, immune checkpoint inhibitor.

METHODS

Data Acquisition and Processing

Open expression matrix of mRNA (FPKM values) and clinical files of BRCA samples were downloaded from The Cancer Genome Atlas (TCGA) database. Datasets GSE25055 in the Gene Expression Omnibus (GEO) database were used to acquire RNA-sequencing (RNA-Seq) and clinical data of BRCA patients receiving NAC as a training cohort and GSE16446 and GSE25065 as test cohorts. Gene expression file of GSE25055 and GSE25065 was collected using platform GPL96 [HG-U133A] Affymetrix Human Genome U133A Array, and GSE16446 using platform GPL570 [HG-U133_Plus_2] Affymetrix Human Genome U133 Plus 2.0 Array. Batch effects and other unwanted variations in high-throughput experiments were eliminated using the "combat" function in the "sva" package (22) in R 4.1.1. Copy number variation (CNV) data were collected from the University of California, Santa Cruz (UCSC) website.

Construction of the Ferroptosis-Related Signature for Predicting Recurrence-Free Survival

FRGs including 150 drivers, 109 suppressors, and 123 markers were collected from FerrDb (19, 23, 24). A univariate Cox proportional hazards regression analysis was conducted to filtrate prognostic FRGs in the GSE25055 cohort with $p < 0.05$ considered to be statistically significant using the "coxph" function. Subsequently, with the help of the "cv.glmnet" function, the least absolute shrinkage and selection operator (LASSO) was performed for the dimension reduction and K-fold cross-validation, which was multiplied by ten, and the optimal parameter was the λ value that corresponded to the lowest deviation. The optimal penalty parameter was defined as the value within one SD of the minimum cross-validated partial likelihood deviance to obtain the best model. The proteins with non-zero regression coefficients were chosen for subsequent

multivariate Cox regression analyses. The LASSO regression model was as follows:

$$\text{riskScore} = \sum_{N=A,B\ldots n} \text{Coefficient of gene N} \times \text{Expression value of gene N}$$

Validation of the Prognostic Signature

First, in the GSE25055 dataset, the Kaplan–Meier (K-M) survival analysis using the "Surv" function in the "survival" package and univariate and multivariate Cox regression analyses between gene expression and clinical characters using the "coxph" function in the "survival" package were performed to certify that riskScore served as an independent predictor in predicting recurrence-free survival (RFS). Principal component analysis (PCA) using the "prcomp" function was used to visualize sample distribution. Receiver operating characteristic (ROC) using the "timeROC" package was done, and area under the curve (AUC) plots were generated for the 1-year, 2-year, and 3-year survival rates to assess the sensitivity and specificity of the prognostic model. Then, the prognostic signature was validated in the GSE25065 and GSE16446 datasets *via* the above methods.

Cell Culture

Normal breast epithelial cell line MCF-10A and the epithelial BRCA cell lines MCF-7, T47D, MDA-MB-231, MDA-MB-468, and BT-549 were acquired from the American Type and Culture Collection (ATCC; Manassas, VA, USA). MDA-MB-231 and BT-549 cells were cultured in Dulbecco's Modified Eagle's Medium (DMEM) (ATCC; Manassas, VA, USA) supplemented with 10% fetal bovine serum (HyClone, Logan, UT, USA) and 1% antibiotic (100 IU/ml of penicillin and 100 μg/ml of streptomycin; HyClone, Logan, UT, USA). MCF-10A cells were cultured in DMEM/F12 medium supplemented with 20 ng/μl of epidermal growth factor, insulin, hydrocortisone, non-essential amino acid (NEAA), 5% horse serum (HS), and 1% penicillin/streptomycin (P/S) solution (Procell, Wuhan, China). MCF-7 and MDA-MB-468 were cultured in Minimum Essential Medium (MEM) (Gibco BRL, Grand Island, NY, USA) supplemented with 10% fetal bovine serum (HyClone, Logan, UT, USA) and 1% antibiotic (100 IU/ml of penicillin and 100 μg/ml of streptomycin; HyClone, Logan, UT, USA). T-47D cells were cultured in Roswell Park Memorial Institute (RPMI) 1640 (HyClone, Logan, UT, USA) with 10% fetal bovine serum (HyClone, Logan, UT, USA). All the cell lines were incubated at 37°C, with a humidified atmosphere of 5% CO_2.

Quantitative Reverse Transcriptase–PCR

Total RNAs were isolated from cells using the TRIzol reagent (Invitrogen, Carlsbad, CA, USA). PrimeScript™ RT reagent Kit (Takara, Maebashi, Japan) was employed to reverse transcribe into cDNA following the manufacturer's protocol. Then SYBR Green PCRMaster Mix (Applied TaKaRa, Otsu, Japan) was used to conduct Real-time PCR on Applied Biosystems 7500 Fast Real-Time RCR System (Applied Biosystems, Foster City, CA, USA). The primers of FRGs for qRT-PCR utilized in this research were as follows:

Primer name	Primer sequence (5′ to 3′)
SLC7A5-F	GTGGACTTCGGGAACTATCACC
SLC7A5-R	GAACAGGGACCCATTGACGG
ACO1-F	CGCAGCACAAGAACATAGAAGT
ACO1-R	CATTGCAGCAAAGTCAACCAC
ENPP2-F	TCGCTGTGACAACTTGTGTAAG
ENPP2-R	CCAATGCGACTCTCCTTTGC

Drug Sensitive Analysis

With the use of the "pRRophetic" package, the half-maximal inhibitory concentration (IC50) of BRCA patients was calculated on Genomics of Drug Sensitivity in Cancer (GDSC) (25) (https://www.cancerrxgene.org/) based on the given gene expression profiles in these datasets to evaluate the drug sensitivities (26–28).

Immune Infiltration Analyses

The CIBERSORT algorithm was used to explore the proportion of different types of immune cells in BRCA patients using CIBERSORT R script v1.04 (29–31). Based on the expression level of immune cell-related genes, the ESTIMATE algorithm was conducted to calculate the stromal score (SS), estimate score (ES), and immune score (IS) (the SS represents the level of stroma content in a tumor; the IS reflects the infiltration of immune cells in a tumor; the estimated score infers tumor purity) among the high- and low-risk groups using the "estimate" package (32). Single-sample gene set enrichment analysis (ssGSEA) was performed to calculate scores for antitumor immunity and protumor suppression for each sample (33) using "GSEABase" and "GSVA" packages.

Consensus Clustering Analyses for Identifying BRCA Subtypes

Consensus clustering based on Euclidean distance and Ward's linkage was performed for hierarchical clustering to identify different subtypes using the "ConsensusClusterPlus" package and repeated the procedures 1,000 times to guarantee the stability of the classification (34). In consideration of a high consistency of clusters, a low coefficient of variation, and no significant increase in the CDF curve, the optimum cluster number could be determined (35).

Statistical Analysis

Correlation coefficients were calculated by Spearman's and distance correlation analyses. For comparison of more than two groups, the

Kruskal–Wallis and one-way ANOVAs were chosen as non-parametric and parametric methods, while Wilcoxon's t-test was used for two groups. Student's t-test was used to explore the statistical significance of quantitative data. The K-M and log-rank tests were employed to confirm the significance of prognostic differences (22). R 4.1.1 software was the main tool to conduct the statistical analysis. For all statistical results, a p-value of <0.05 was considered to be statistically significant.

RESULTS

Construction of the Ferroptosis-Related Signature Associated With Recurrence-Free Survival

GSE25055 dataset was used as a training cohort; meanwhile, GSE25065 and GSE16446 datasets were used as test cohorts. Batch effects were removed for further study (**Figures 1A, B**). First, we

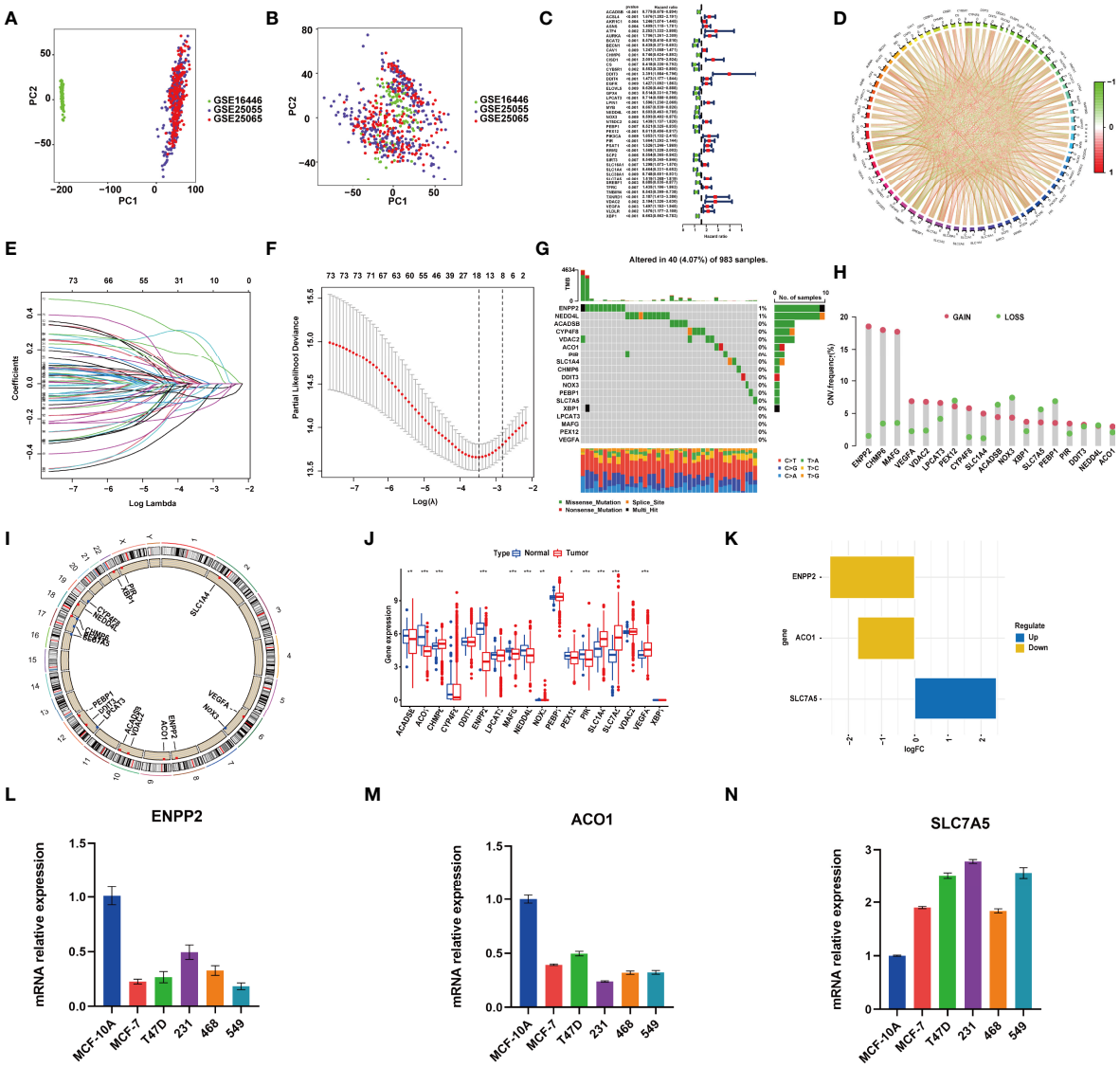

FIGURE 1 | RNA-sequencing (RNA-Seq) data of training and test cohorts before **(A)** and after **(B)** removing batch effects. **(C)** The hazard ratio (HR) and p-value of selected ferroptosis-related genes (FRGs) using the univariable Cox HR regression (criteria: p-value <0.01). **(D)** Expression interaction of the 76 FRGs in BRCA. The lines connecting the FRGs show how they are correlated with each other, with positive associations in red and negative associations in green. **(E)** The least absolute shrinkage and selection operator (LASSO) Cox analysis identified 18 FRGs most related to prognostics. **(F)** The 10-round cross-validation determined the optimal values of the penalty parameter. **(G)** In all, 40 of 983 (4.07%) BRCA patients experienced 18 FRG genetic alterations. **(H)** Copy number variation (CNV) mutation frequency of the 18 FRGs. This column represents the frequency of change. Deletion frequency is represented by green dots, while amplification frequency is represented by pink dots. **(I)** The location of the 18 FRGs in chromosomes. Blue point represents the genes that mainly had CNV deletion; red point represents the genes that mainly had CNV amplification. **(J)** Expression of the 18 FRGs in normal tissues and BRCA tissues. Genes with red color represent the differentially expressed genes. **(K)** The value of logFC of the 18 FRG genes. **(L–N)** qRT-PCR results showed the expression value of the three FRGs in the normal breast and five breast cancer cell lines. *, P < 0.05; **, P < 0.01; ***, P < 0.001.

performed a univariate Cox regression analysis in GSE25055. Among 382 FRGs retrieved from the FerrDB database, 76 FRGs were identified to be associated with RFS, with the standard of $p < 0.01$ (**Figure 1C**). Pearson's correlation analysis revealed a correlation among these genes (**Figure 1D**). Then, LASSO regression analysis was used to establish the FRGs prognostic signature (**Figures 1E, F**):

$$\begin{aligned}\text{riskScore} = {} & \text{ACADSB expression} \times (-0.020510043) \\ & + \text{ACO1 expression} \times (0.007304261) \\ & + \text{CHMP6 expression} \times (-0.086718343) \\ & + \text{CYP4F8 expression} \times (-0.02261864) \\ & + \text{DDIT3 expression} \times (0.289634547) \\ & + \text{ENPP2 expression} \times (0.002930772) \\ & + \text{LPCAT3 expression} \times (-0.054795656) \\ & + \text{MAFG expression} \times (0.015720631) \\ & + \text{NEDD4L expression} \times (-0.154434979) + \text{NOX3} \\ & \times (-0.152413703) + \text{PEBP1} \times (-0.116654913) \\ & + \text{PEX12 expression} \times (0.021389428) + \text{PIR} \\ & \times (0.005001444) + \text{SLC1A4} \times (-0.094069987) \\ & + \text{SLC7A5} \times (0.165365881) + \text{VDAC2} \\ & \times (0.247634891) + \text{VEGFA} \times (0.029115114) \\ & + \text{XBP1} \times (-0.077572219)\end{aligned}$$

Landscape of Gene Mutations and Expression in Ferroptosis-Related Genes in the Model in BRCA

Genomic mutations were common in these genes with 40 (4.07%) of 983 patients having experienced genetic changes, and a mutation frequency of 1% was observed in ENPP2 and NEDD4L (**Figure 1G**). We also found that CNV is prevalent among the 18 FRGs. ENPP2, CHMP6, MAFG, VEGFA, VDAC2, LPCAT3, CYP4F8, SLC1A4, XBP1, PIR, and ACO1 showed copy number amplification, while deletion happened in the other FRGs (**Figure 1H**). The location of the 18 FRGs in human chromosomes could be seen in **Figure 1I**. The result of differential analysis in normal breast tissue and tumor tissue showed that ACO1, CHMP6, ENPP2, MAFG, NEDD4L, PIR, SLC1A4, SLC7A5, and VEGFA had significant differential expression in breast cancer with p-value <0.001; ACADSB and NOX3 with p-value <0.01; and PEX12 with p-value <0.05 (**Figure 1J**). SLC7A5 was seen as a significantly upregulated gene, while ENPP2 and ACO1 were seen as significantly downregulated genes with $|\log FC| > 1$ (**Figure 1K**). The result of RT-PCR provided strong support for our conclusion (**Figures 1L–N**). As described above, FRGs had significant heterogeneity of genetic variation and transcriptomic alteration landscape in BRCA patients, which played an important part in regulating the happening, aggravation, and prognosis of BRCA.

External Validation of the Ferroptosis-Related Gene Model

After the riskScore of each patient based on the risk model was calculated, we divided patients into the high- and low-risk groups with the standard median score in GSE25055 (**Figure 2A**). With the use of the median of GSE25055, patients in GSE25065 (**Figure 2H**) and GSE16446 (**Figures 2H, O**) were separated into the high-risk and low-risk groups in the same manner. The result of PCA showed significant heterogeneity between high-risk and low-risk patients in GSE25055 (**Figures 2B, C**), GSE25065 (**Figures 2I, J**), and GSE16446 (**Figures 2P, Q**), which certified the superior discrimination of the FRG model. For the purpose of exploring whether the signature could represent its prognostic value independently of other clinical factors, we conducted univariate and multivariate Cox regression analyses in the training and test cohorts. In univariate analyses, this risk score was able to independently predict survival outcomes in GEO cohorts (GSE25055, hazard ratio (HR) = 4.690, $p < 0.001$; GSE25065, HR = 6.350, $p < 0.001$; GSE16446, HR = 7.648, $p < 0.001$) (**Figures 2D, K, R**). The same conclusion could be drawn in multivariate analyses (**Figures 2E, L, S**). The results revealed that riskScore and pathologic response served as independent factors affecting receiving NAC BRCA patients' prognosis. The AUCs of the time-dependent ROC curves at 1, 2, and 3 years were 0.818, 0.824, and 0.783 in GSE25055 (**Figure 2F**); 0.812, 0.824, and 0.783 in GSE25065 (**Figure 2M**); and 0.715, 0.725, and 0.723 in GSE16446 (**Figure 2T**). The AUCs in different years and cohorts were relatively high compared with those of other published literature, which suggested high sensitivity and specificity of the signature for predicting RFS. The K-M survival curve showed that patients in the high-risk group had a higher recurrence rate than those in the low-risk group using log-rank tests with $p < 0.001$ (**Figure 2G**), $p < 0.001$(**Figure 2N**), $p = 0.029$ (**Figure 2U**). Ferroptosis is a recently recognized form of regulated cell death that is characterized by lipid peroxidation, which mediates cell death in breast cancer. Among genes in our signature, ferroptosis driver genes such as NOX3 and PEBP1 had negative coefficients, while ferroptosis suppressor genes such as PIR and VDAC2 had positive coefficients. Therefore, high riskScore indicated that ferroptosis was suppressed in breast cancer, which might imply a worse prognosis.

Clinicopathological Parameter Relevance Analysis

We further anatomized the association between riskScore and clinical parameters of BRCA patients. The detailed results depicted that the riskScore had a positive correlation with T stage, N stage, American Joint Committee on Cancer (AJCC) stage, and grade (**Figure 3**). BRCA patients with higher T, N, AJCC stage, and grade, combined with lower age, and negative status of progesterone receptor and estrogen receptor seemed to have higher riskScore, indicating a higher incidence rate of relapse, which was consistent with the conclusions of current accumulated

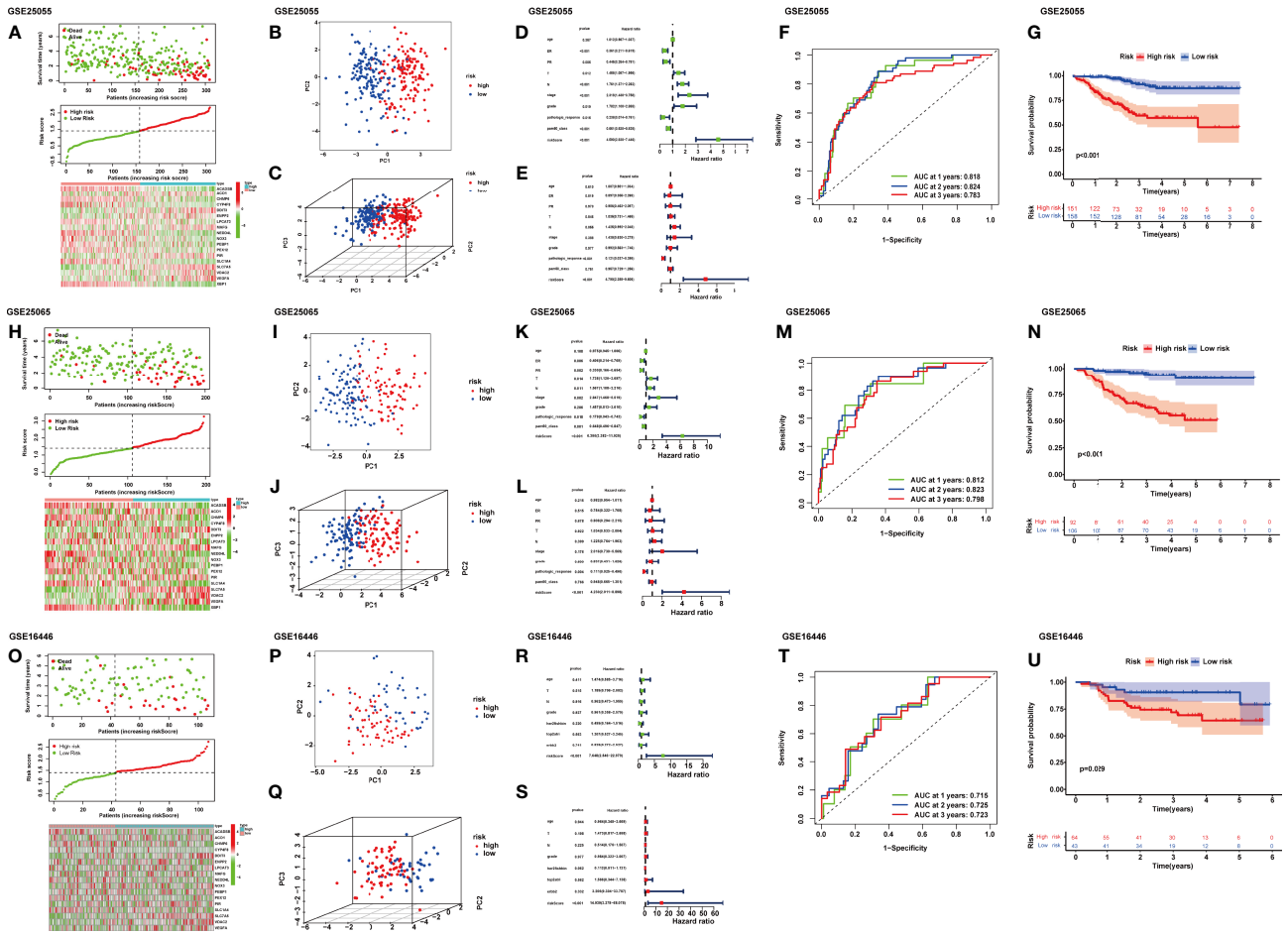

FIGURE 2 | Distribution of riskScore, scatterplot, and heatmap in the high-risk group and the low-risk group in GSE25055 **(A)**, GSE25065 **(H)**, and GSE16446 **(O)**. PCA (principal component analysis) for BRCA based on the riskScore in GSE25055 **(B, C)**, GSE25065 **(I, J)**, and GSE16446 **(P, Q)**. **(D)** Univariate and **(E)** multivariate Cox regression analyses of age, estrogen receptor (ER), progesterone receptor (PR), T, N, stage, grade, pathologic response, pam50 classification, and riskScore in GSE25055. **(K)** Univariate and **(L)** multivariate Cox regression analyses of age, ER, PR, T, N, stage, grade, pathologic response, pam50 classification, and riskScore in GSE25065. **(R)** Univariate and **(S)** multivariate Cox regression analyses of age, T, N, grade, her2-fish, top2atri, erbb2, and riskScore in GSE16446. Time-dependent receiver operating characteristic (ROC) curves for predicting 1-, 2-, and 3-year RFS in GSE25055 **(F)**, GSE25065 **(M)**, and GSE16446 **(T)**. Kaplan–Meier curves of the high- and low-risk subgroup patients in GSE25055 **(G)**, GSE25065 **(N)**, and GSE16446 **(U)**.

literature. In other words, the results implied that the riskScore had a correlation with clinicopathological parameters.

Chemotherapeutic Response Analysis

In order to improve the therapeutic benefit of BRCA patients from neoadjuvant therapy, we further explored whether FRG signature could predict the sensitivity to several chemotherapy drugs widely used in BRCA between two groups. According to the results calculated based on the GDSC database, IC50 values of chemotherapy drugs covering axitinib, bicalutamide, bleomycin, bortezomib, dasatinib, doxorubicin, gefitinib, lapatinib, and paclitaxel were evaluated. Compared with the low-risk group, IC50 values of paclitaxel, gefitinib, doxorubicin, bleomycin, and bortezomib were lower in the high-risk groups, which indicated that high-risk patients were more sensitive to these drugs (**Figures 4A–I**). The above results demonstrated that the riskScore had potential predictive value for chemotherapy and targeted therapy in breast cancer.

Comprehensive Analysis Between Ferroptosis-Related Gene Signature and Immune Microenvironment

We calculated the constitution of tumor-infiltrating immune cells in BRCA through the CIBERSORT algorithm (**Figure 5A**). Compared with the low-risk groups, the proportion of resting mast cells was lower in the high-risk groups (**Figures 5B, C**).

Then, the IS, SS, and ES of patients were evaluated using the ESTIMATE algorithm. Based on the optimum cutoff value of ISs or SSs respectively, BRCA patients were divided into the high and low IS/SS/ES groups. The K-M curves showed that patients with high IS/SS/ES exhibited significantly worse RFS as compared to

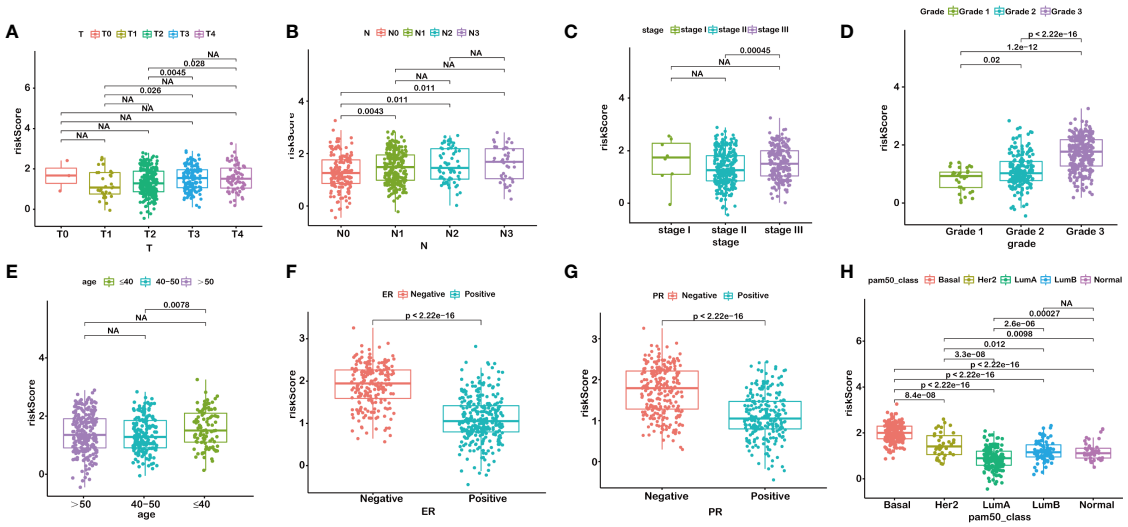

FIGURE 3 | RiskScore is correlated with clinicopathological features of BRCA. T stage **(A)**, N stage **(B)**, AJCC-stage **(C)**, Grade **(D)**, age **(E)**, ER status **(F)**, PR status **(G)**, PAM50 subtypes **(H)**. NA, P>0.05.

the ones with low IS/SS/ES (**Figures 5D–F**). We further explored the relationships between the IS/SS/ES and riskScore. The result of Wilcoxon's rank-sum test displayed that there is no significant difference between the high-risk and low-risk groups in SS (p = 0.53, **Figure 5G**) but significant in IS (p = 5.7e−09, **Figure 5H**) and ES (p = 1.9e−05, **Figure 5I**). Pearson's correlation analysis showed that riskScore was positively associated with IS (R = 0.26, p = 1.6e−10, **Figure 5K**) and ES (R = 0.2, p = 5.1e−07, **Figure 5L**).

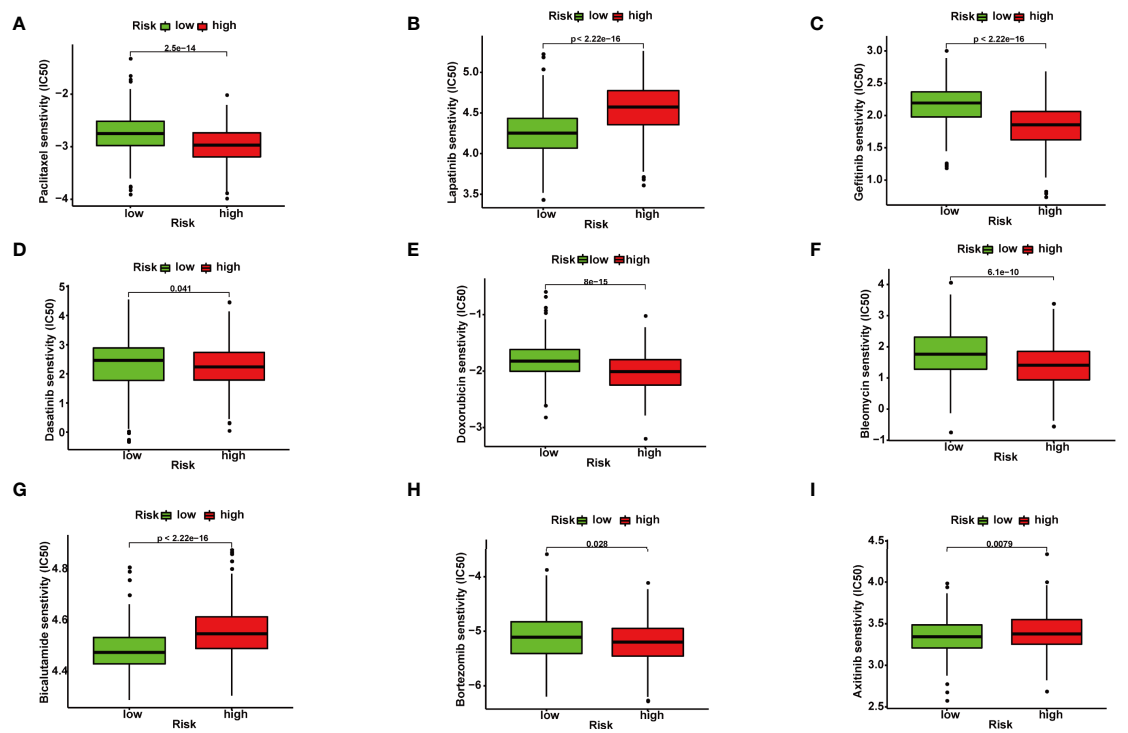

FIGURE 4 | Correlation between ferroptosis-related gene (FRG) signature and drug sensitivity. Box plots for estimated IC50 of drugs between high- and low-risk BRCA patients. Paclitaxel **(A)**, Lapatinib **(B)**, Gefitinib **(C)**, Dasatinib **(D)**, Doxorubicin **(E)**, Bleomycin **(F)**, Bicalutamide **(G)**, Bortezomib **(H)**, Axitinib **(I)**.

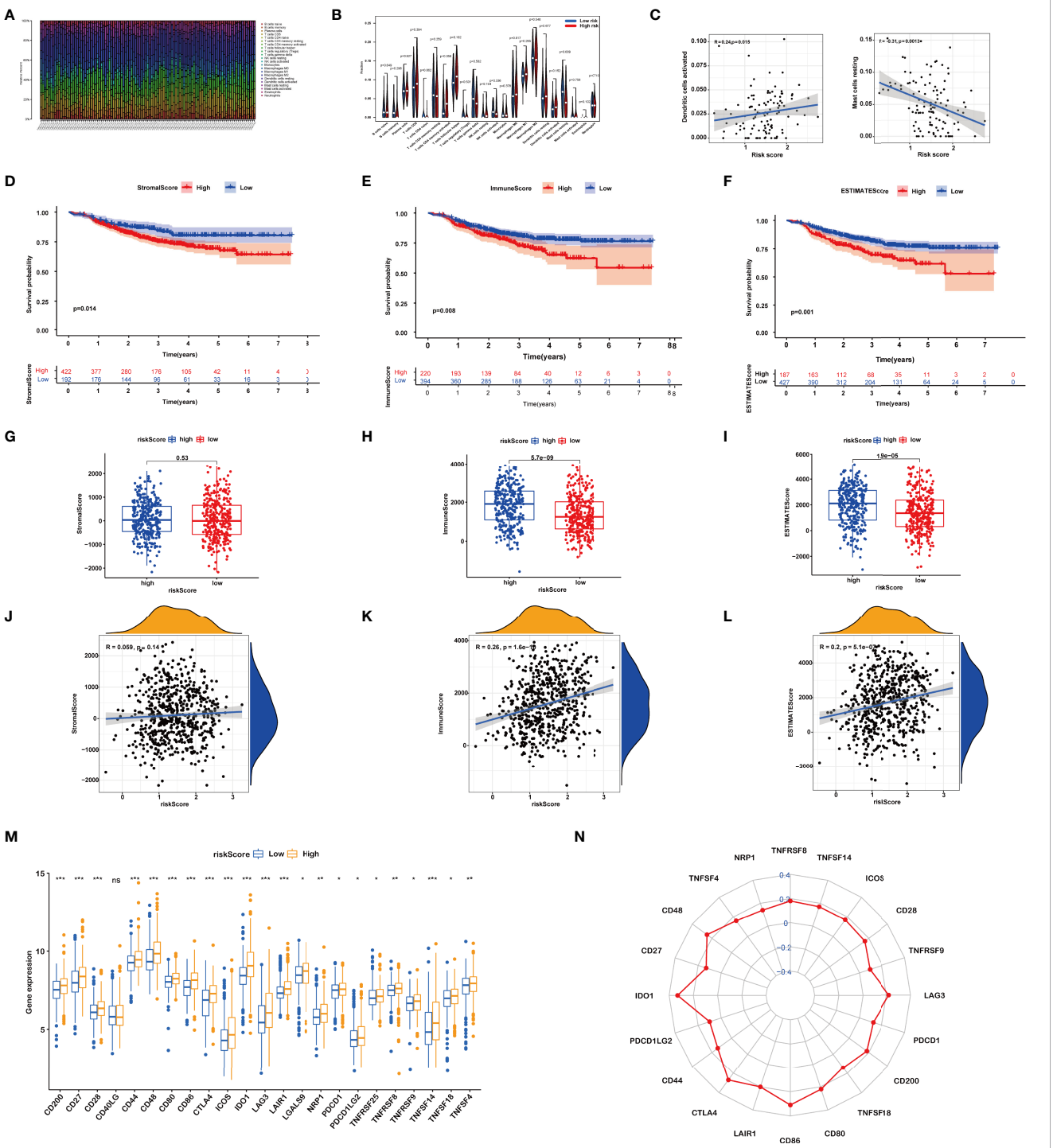

FIGURE 5 | **(A)** Relative percent of different immune cells in each sample. **(B)** Different immune cell contents in low-risk and high-risk patients. **(C)** Correlation between immune cells and riskScore. **(D–F)** Kaplan–Meier curves of the high and low stromal score (SS), immune score (IS), and estimate score (ES) group patients. **(G–L)** Correlation between riskScore and SS, IS, and ES. **(M, N)** Comparisons of the expression levels of immune checkpoints between two groups. ns, P>0.05. *, P < 0.05; **, P < 0.01; ***, P < 0.001.

However, the riskScore was not significantly correlated to the SS (P = 0.14, **Figure 5J**)

Furthermore, we dissected the role of riskScore in immune checkpoint blockade (ICB) treatment. We noticed that the expression levels of all immune checkpoints were significantly higher in the high riskScore group (**Figures 5M, N**). Taken together, the prognostic signature could predict the potential response to immunotherapy in BRCA patients, which provided guidance on whether or what to use for immunotherapy in clinical practice.

Identification of Three Consensus Clustering Subtypes

On the basis of the expression of 18 FRGs in the signature, we employed the "Partition Around Medoids" algorithm, along with Pearson's distance to estimate similarity among patients to identify three clusters. We noticed that K = 3 seemed to be an optimal selection by clustering variable (k) increasing from 2 to 9, in which the intergroup correlations were the lowest and the intragroup correlations were the greatest (**Figure 6B**), indicating the optimal clustering stability of the three molecular phenotypes. The consensus cumulative distribution function (CDF) diagram showed that when k = 3, distribution reached an approximate maximum (**Figure 6C**), implying robust clustering for all samples (**Figure 6A**). The delta area plot depicts the relative change compared to k − 1 showing that the delta area was optimum when k = 3 (**Figure 6D**). Prognostic analysis of the three clusters revealed that patients in ferrCluster A were the least likely to relapse, while in ferrCluster B, they were the most likely to relapse (**Figure 6E**).

We then performed an ssGSEA to quantify the scores of various immune cell subpopulations to further compare the differences in the number of immune cells among the three types of ferrClusters. The results indicated that the contents of monocyte cells were not significantly different. The proportion of immune cells was significantly different among the three clusters. Contents of nearly all types of immune cells in ferrCluster A seemed to be the poorest. The levels of activated CD4+ T cells, CD8+ T cells, dendritic cells, CD56 bright and dim NK cells, γδ-T cells, Tregs, and T helper cells were relatively the highest in ferrCluster B. Hence, we could draw the conclusion that ferrCluster A was a type of immune failure, ferrCluster B was a type of immune-activated characterized by T-cell subset enrichment, and ferrCluster C was a type of immune-activated characterized by B-cell subset enrichment (**Figure 6F**). These results indicated that the FRGs play key roles in immune cell infiltration and characteristic tumor immune microenvironment (TME) formation and affect the prognosis of BRCA patients.

Development of ferrScore to Quantify Individual Ferroptosis Pattern

With a view to the individual heterogeneity and complexity of BRCA patients, we calculated ferrScore to assess the ferroptosis pattern of each patient based on the PCA on the 18 FRGs in the

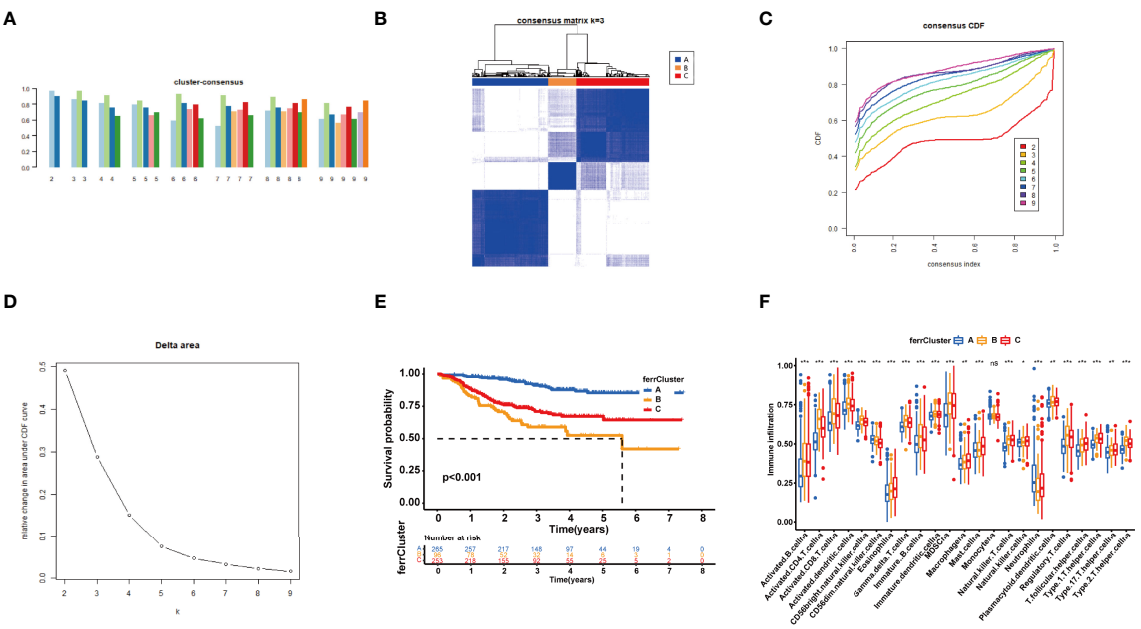

FIGURE 6 | Consensus clustering of 18 ferroptosis-related genes (FRGs) identified three clusters of patients. **(A)** The tracking plot for k = 2 to k = 9. **(B)** The heatmap for K = 3. **(C)** Consensus clustering cumulative distribution function (CDF) with k = 2 to k = 9. **(D)** Relative change in area under CDF curve for k = 2–9. **(E)** Kaplan–Meier (K-M) curve of the survival difference among clusters 1–3. **(F)** Single-sample gene set enrichment analysis of immune status among three ferrClusters. ns, P>0.05. *, P < 0.05; **, P < 0.01; ***, P < 0.001.

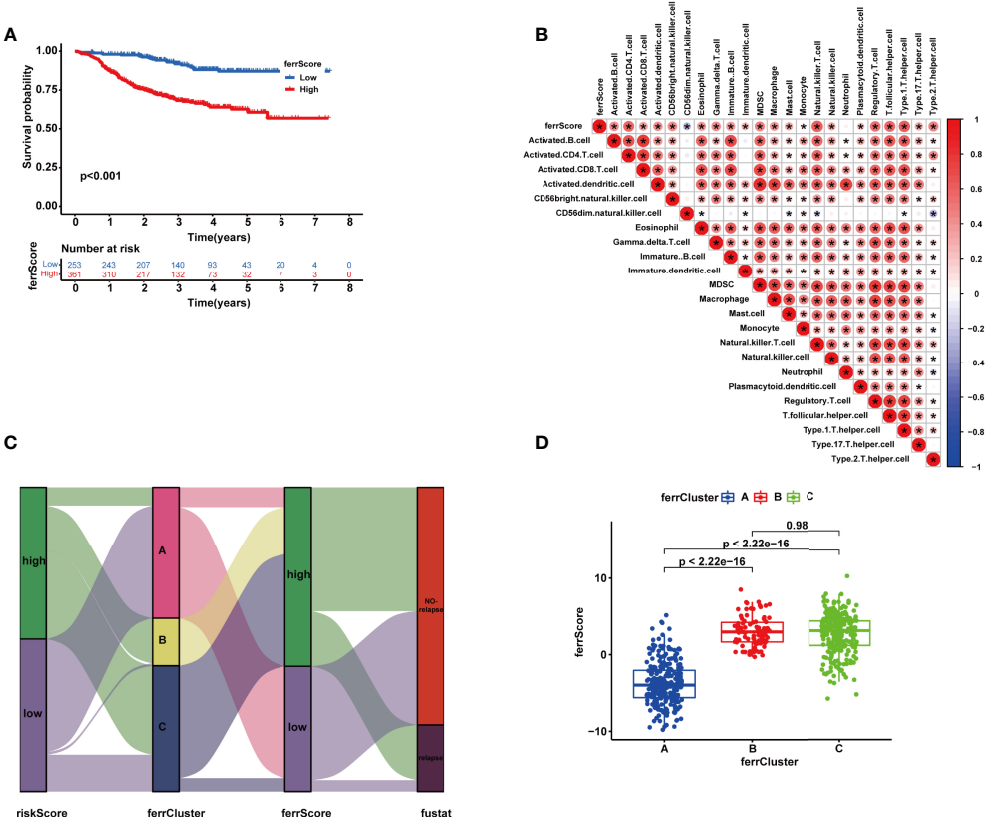

FIGURE 7 | **(A)** Kaplan–Meier (K-M) curve of the survival difference between high and low ferrScore groups. **(B)** Correlation between immune cells and ferrScore. **(C)** Alluvial diagram of riskScore group, ferrCluster group, ferrScore group, and relapse-free status. **(D)** Correlation between ferrCluster and ferrScore *, P < 0.05.

model. The scoring framework was defined as ferrScore = PC1 + PC2 to quantify individual ferroptosis patterns of BRCA patients (36), further facilitating precise treatment. As indicated from the K-M curve, patients with lower ferrScore had a lower probability of relapse (**Figure 7A**). The ferrScore was closely related to immune cells (**Figure 7B**). We also observed that ferrScores of patients in ferrCluster A were significantly lower than those in ferrCluster B and C, while there was no significant difference between ferrClusters B and C (**Figure 7D**). The Sankey diagram shows the attribute changes in riskScore, ferrCluster, ferrScore, and recurrence status, indicating that the higher the riskScore and ferrScore, the higher the risk of relapse after receiving NAC (**Figure 7C**). The above results enriched treatment strategies for BRCA patients not only in targeted therapy and chemotherapy but also in immunotherapy. At last, the expression of CTLA4 was examined to elucidate a potential response to immunotherapy, and the high ferrScore group showed relatively high levels of expression (p = 8.6e−11, **Figure 7B**).

DISCUSSION

Ferroptosis is a newfound programmed cell death pattern distinguished from traditional cell death such as apoptosis, necrosis, and autophagy (37). Accumulating evidence demonstrated that dysregulated expression and genetic variations of FRGs were closely related to cell death, tumor carcinogenesis, and progression (22, 38).

TME is a cradle for tumorigenesis and cancer progression, in which immune infiltrating cells affect therapeutic outcomes (39). The relationships between TME infiltration immune cells and ferroptosis modifications have become a hotspot in the mechanism of tumorigenesis and development (40, 41). MIF secreted by nasopharyngeal carcinoma could suppress ferroptosis of macrophages and then increase the rate of metastasis (42). BEBT-908 induces immunogenic ferroptosis to potentiate cancer immune checkpoint therapy (43). SCD1 and FABP4 could drive ferroptosis, thereby leading to tumor resistance (44). Ferroptotic cells could also release chemotaxis to interact with immune cells, such as CD + T cells, and then modulate the anticancer immunity (45).

High-throughput genomic studies provided cutting-edge sights into the molecular mechanisms and identified new potential targets of breast cancer. Our research developed and verified a stepwise multivariate Cox regression model including 18 FRGs using LASSO and multivariate Cox regression for removing redundant factors to forecast the RFS of individual

patients in GSE25055. The expression of FRGs in the signature was higher in BRCA tissues than in adjacent normal tissues, which was verified in several breast cancer cell lines using real-time PCR. Meanwhile, CNVs and mutation frequencies of FRGs were prevalent. Internal and external validations exhibited an excellent ability to predict the prognosis of BRCA patients. Specifically, a higher riskScore indicated a higher rate of recurrence. Moreover, riskScore was associated closely with clinicopathological features.

With a view to the significance of the immune system in antiviral and antitumor responses, we calculated the proportion of different types of tumor-infiltrating immune cells in BRCA using CIBERSORT and used ESTIMATE to explore IS, SS, and tumor purity. Higher SSs and ISs were observed in high-risk patients, leading to an unfavorable prognosis, which was consistent with a line of evidence from previous research (46, 47).

Extensive interest in cancer immunotherapy is reported according to the clinical importance of CTLA-4 and PD-1/PD-L1 in immune checkpoint therapies (48). The main immune checkpoints for breast cancer include CTLA-4, PD-1/PD-L1, lymphocyte activation gene 3 (LAG-3), T-cell immunoglobulin domain and mucin 3 (TIM-3), and other molecules (49). Clinical trials like SOLTI-1503 PROMETEO TRIAL (50), KEYNOTE-086 (51), NIMBUS (52), KEYNOTE-173 (53), and KEYNOTE-522 (54) showed that immunological checkpoint inhibitors have made significant progress in breast cancer immunotherapy, which is expected to become a new treatment for breast cancer.

Furthermore, for the purpose of exploring the response to chemotherapy sensitivity of patients, we calculated the IC50 value. The sensitivities of chemotherapeutic drugs widely used in BRCA showed a significant difference between the two groups.

In accordance with the expression matrix of the 18 FRGs in the signature, we identified three ferroptosis-related molecular clusters *via* consensus clustering analysis. The rate of relapse was significantly different among the three clusters. ssGSEA identified that the three ferrClusters as three immune types of immune failure, immune-activated characterized by T-cell subset enrichment, and immune-activated characterized by B-cell subset enrichment.

Inevitably, numerous limitations of our study should be included in the consideration. First, although our conclusion came through internal and external validation in TCGA, GSE25055, GSE25065, and GSE16446 cohorts, when it comes to its clinical application, caution is advised. Multicenter large-scale prospective clinical studies were needed rather than only retrospective data from public open databases to verify the signature. Second, the expression matrix of patients in GSE25055 and GSE25065 was extracted *via* platform GPL96 [HG-U133A] Affymetrix Human Genome U133A Array in 2010, which only included 12,549 genes, while GPL570 [HG-U133_Plus_2] Affymetrix Human Genome U133 Plus 2.0 Array for GSE16446 contained 21,655 genes. Due to the relatively small number of detectable genes, bias may be amplified. Finally, detailed molecular mechanisms in the BRCA of the FRGs in the signature had not been fully revealed. Further in-depth studies were required to confirm relationships between FRGs and tumor microenvironment, and between ferroptosis and chemoresistance.

CONCLUSION

In brief, we constructed a novel FRG signature and identified three molecular subtypes for predicting the RFS of BRCA patients, which could predict the immune status of the tumor microenvironment and RFS of patients. It is worth noting that our conclusions provided more clues for the rational choices of chemotherapeutic drugs for patients with BRCA, provided a new immunological perspective and a new basis for immunotherapy of BRCA in the clinic, and had the potential possibility to coach and guide individualized healthcare decisions.

DATA AVAILABILITY STATEMENT

The expression and clinical datasets presented in this study are available in databases of TCGA and Gene Expression Omnibus (GSE25055, GSE25065 and GSE16446), and the copy number variation data are presented in the University of California, Santa Cruz (UCSC) website https://xenabrowser.net/datapages/?dataset=TCGA-BRCA.gistic.tsv&host=https%3A%2F%2Fgdc.xenahubs.net&removeHub=https%3A%2F%2Fxena.treehouse.gi.ucsc.edu%3A443.

AUTHOR CONTRIBUTIONS

XM and QX substantially contributed to the conception of the work. YX, QZ, and TZ contributed to the data collection. YX, YD, and QX wrote the manuscript. QZ and YD helped to perform the enrichment and network analysis. YX, YD, and XM drafted and revised the manuscript. All authors contributed to the article and approved the submitted version.

FUNDING

This research was supported by the Zhejiang Provincial Natural Science Foundation of China (Grant No. LQ21H200007), Zhejiang Provincial Ministry Medical and Health Co-construction Major Project (Grant No. 20214355173), and National Natural Science Foundation of China (Grant No. 81973861).

SUPPLEMENTARY MATERIAL

The Supplementary Material for this article can be found online at: https://www.frontiersin.org/articles/10.3389/fimmu.2022.895110/full#supplementary-material

Supplementary Table 1 | Ferroptosis suppressor, driver and marker genes from FerrDB database.

REFERENCES

1. Sung H, Ferlay J, Siegel RL, Laversanne M, Soerjomataram I, Jemal A, et al. Global Cancer Statistics 2020: GLOBOCAN Estimates of Incidence and Mortality Worldwide for 36 Cancers in 185 Countries. *CA Cancer J Clin* (2021) 71(3):209–49. doi: 10.3322/caac.21660
2. Isik A, Firat D. Bilateral Intra-Areolar Polythelia. *Breast J* (2018) 24(1):89–90. doi: 10.1111/tbj.12838
3. Adams S, Gatti-Mays ME, Kalinsky K, Korde LA, Sharon E, Amiri-Kordestani L, et al. Current Landscape of Immunotherapy in Breast Cancer: A Review. *JAMA Oncol* (2019) 5(8):1205–14. doi: 10.1001/jamaoncol.2018.7147
4. Early Breast Cancer Trialists' Collaborative G. Long-Term Outcomes for Neoadjuvant Versus Adjuvant Chemotherapy in Early Breast Cancer: Meta-Analysis of Individual Patient Data From Ten Randomised Trials. *Lancet Oncol* (2018) 19(1):27–39. doi: 10.1016/S1470-2045(17)30777-5
5. Cortazar P, Zhang L, Untch M, Mehta K, Costantino JP, Wolmark N, et al. Pathological Complete Response and Long-Term Clinical Benefit in Breast Cancer: The CTNeoBC Pooled Analysis. *Lancet* (2014) 384(9938):164–72. doi: 10.1016/S0140-6736(13)62422-8
6. Hamy AS, Pierga JY, Sabaila A, Laas E, Bonsang-Kitzis H, Laurent C, et al. Stromal Lymphocyte Infiltration After Neoadjuvant Chemotherapy Is Associated With Aggressive Residual Disease and Lower Disease-Free Survival in HER2-Positive Breast Cancer. *Ann Oncol* (2017) 28(9):2233–40. doi: 10.1093/annonc/mdx309
7. Kuijer A, Straver M, den Dekker B, van Bommel ACM, Elias SG, Smorenburg CH, et al. Impact of 70-Gene Signature Use on Adjuvant Chemotherapy Decisions in Patients With Estrogen Receptor-Positive Early Breast Cancer: Results of a Prospective Cohort Study. *J Clin Oncol* (2017) 35(24):2814–9. doi: 10.1200/JCO.2016.70.3959
8. Harbeck N, Gnant M. Breast Cancer. *Lancet* (2017) 389(10074):1134–50. doi: 10.1016/S0140-6736(16)31891-8
9. Chaudhary LN. Early Stage Triple Negative Breast Cancer: Management and Future Directions. *Semin Oncol* (2020) 47(4):201–8. doi: 10.1053/j.seminoncol.2020.05.006
10. Xie Y, Hou W, Song X, Yu Y, Huang J, Sun X, et al. Ferroptosis: Process and Function. *Cell Death Differ* (2016) 23(3):369–79. doi: 10.1038/cdd.2015.158
11. Stockwell BR, Friedmann Angeli JP, Bayir H, Bush AI, Conrad M, Dixon SJ, et al. Ferroptosis: A Regulated Cell Death Nexus Linking Metabolism, Redox Biology, and Disease. *Cell* (2017) 171(2):273–85. doi: 10.1016/j.cell.2017.09.021
12. Sun LL, Linghu DL, Hung MC. Ferroptosis: A Promising Target for Cancer Immunotherapy. *Am J Cancer Res* (2021) 11(12):5856–63.
13. Chen C, Xie B, Li Z, Chen L, Chen Y, Zhou J, et al. Fascin Enhances the Vulnerability of Breast Cancer to Erastin-Induced Ferroptosis. *Cell Death Dis* (2022) 13(2):150. doi: 10.1038/s41419-022-04579-1
14. Yadav P, Sharma P, Sundaram S, Venkatraman G, Bera AK, Karunagaran D. SLC7A11/ xCT is a Target of miR-5096 and its Restoration Partially Rescues miR-5096-Mediated Ferroptosis and Anti-Tumor Effects in Human Breast Cancer Cells. *Cancer Lett* (2021) 522:211–24. doi: 10.1016/j.canlet.2021.09.033
15. Yuan L, Li S, Chen Q, Xia T, Luo D, Li L, et al. EBV Infection-Induced GPX4 Promotes Chemoresistance and Tumor Progression in Nasopharyngeal Carcinoma. *Cell Death Differ* (2022). doi: 10.1038/s41418-022-00939-8
16. Zhang W, Jiang B, Liu Y, Xu L, Wan M. Bufotalin Induces Ferroptosis in non-Small Cell Lung Cancer Cells by Facilitating the Ubiquitination and Degradation of GPX4. *Free Radic Biol Med* (2022) 180:75–84. doi: 10.1016/j.freeradbiomed.2022.01.009
17. Lu Y, Chan YT, Tan HY, Zhang C, Guo W, Xu Y, et al. Epigenetic Regulation of Ferroptosis *via* ETS1/miR-23a-3p/ACSL4 Axis Mediates Sorafenib Resistance in Human Hepatocellular Carcinoma. *J Exp Clin Cancer Res* (2022) 41(1):3. doi: 10.1186/s13046-021-02208-x
18. Lin HY, Ho HW, Chang YH, Wei CJ, Chu PY. The Evolving Role of Ferroptosis in Breast Cancer: Translational Implications Present and Future. *Cancers (Basel)* (2021) 13(18):4576. doi: 10.3390/cancers13184576
19. Wang S, Xie Z, Wu Z. Establishment and Validation of a Ferroptosis-Related Gene Signature to Predict Overall Survival in Lung Adenocarcinoma. *Front Genet* (2021) 12:793636:793636. doi: 10.3389/fgene.2021.793636
20. Du S, Zeng F, Sun H, Liu Y, Han P, Zhang B, et al. Prognostic and Therapeutic Significance of a Novel Ferroptosis Related Signature in Colorectal Cancer Patients. *Bioengineered* (2022) 13(2):2498–512. doi: 10.1080/21655979.2021.2017627
21. Yang J, Wei X, Hu F, Dong W, Sun L. Development and Validation of a Novel 3-Gene Prognostic Model for Pancreatic Adenocarcinoma Based on Ferroptosis-Related Genes. *Cancer Cell Int* (2022) 22(1):21. doi: 10.1186/s12935-021-02431-8
22. Liu DL, Wu MY, Zhang TN, Wang CG. Ferroptosis Regulator Modification Patterns and Tumor Microenvironment Immune Infiltration Characterization in Hepatocellular Carcinoma. *Front Mol Biosci* (2022) 9:807502:807502. doi: 10.3389/fmolb.2022.807502
23. Ke ZB, You Q, Sun JB, Zhu JM, Li XD, Chen DN, et al. A Novel Ferroptosis-Based Molecular Signature Associated With Biochemical Recurrence-Free Survival and Tumor Immune Microenvironment of Prostate Cancer. *Front Cell Dev Biol* (2021) 9:774625:774625. doi: 10.3389/fcell.2021.774625
24. Li X, Huang J, Chen J, Zhan Y, Zhang R, Lu E, et al. A Novel Prognostic Signature Based on Ferroptosis-Related Genes Predicts the Prognosis of Patients With Advanced Bladder Urothelial Carcinoma. *Front Oncol* (2021) 11:726486:726486. doi: 10.3389/fonc.2021.726486
25. Chen Z, Zou Y, Zhang Y, Chen Z, Wu F, Jin H, et al. A Pyroptosis-Based Prognostic Model for Immune Microenvironment Estimation of Hepatocellular Carcinoma. *Dis Markers* (2022) 2022:8109771. doi: 10.1155/2022/8109771
26. Qin M, Ma Y, Wang Z, Fang D, Wei J. Using Immune-Related lncRNAs to Construct Novel Biomarkers and Investigate the Immune Landscape of Breast Cancer. *Transl Cancer Res* (2021) 10(6):2991–3003. doi: 10.21037/tcr-21-783
27. Zhao Z, Liu H, Zhou X, Fang D, Ou X, Ye J, et al. Necroptosis-Related lncRNAs: Predicting Prognosis and the Distinction Between the Cold and Hot Tumors in Gastric Cancer. *J Oncol* (2021) 2021:6718443. doi: 10.1155/2021/6718443
28. Jia X, Chen B, Li Z, Huang S, Chen S, Zhou R, et al. Identification of a Four-Gene-Based SERM Signature for Prognostic and Drug Sensitivity Prediction in Gastric Cancer. *Front Oncol* (2021) 11:799223:799223. doi: 10.3389/fonc.2021.799223
29. Zhang S, Zhang W, Zhang J. Comprehensive Analysis of Immune Cell Infiltration and Significant Genes in Head and Neck Squamous Cell Carcinoma. *Oral Oncol* (2022) 126:105755. doi: 10.1016/j.oraloncology.2022.105755
30. Zhang H, Wang X, Hou C, Yang Z. Identification of Driver Genes and Interaction Networks Related to Brain Metastasis in Breast Cancer Patients. *Dis Markers* (2022) 2022:7631456. doi: 10.1155/2022/7631456
31. Chen B, Khodadoust MS, Liu CL, Newman AM, Alizadeh AA. Profiling Tumor Infiltrating Immune Cells With CIBERSORT. *Methods Mol Biol* (2018) 1711:243–59. doi: 10.1007/978-1-4939-7493-1_12
32. Yoshihara K, Shahmoradgoli M, Martinez E, Vegesna R, Kim H, Torres-Garcia W, et al. Inferring Tumour Purity and Stromal and Immune Cell Admixture From Expression Data. *Nat Commun* (2013) 4:2612. doi: 10.1038/ncomms3612
33. Kong G, Wang Y, Huang Y, Shi Z. Identification and Verification of Tumor Immune Microenvironment-Related Prognostic Genes in Kidney Renal Clear Cell Carcinoma. *BioMed Res Int* (2022) 2022:5563668. doi: 10.1155/2022/5563668
34. Wilkerson MD, Hayes DN. ConsensusClusterPlus: A Class Discovery Tool With Confidence Assessments and Item Tracking. *Bioinformatics* (2010) 26 (12):1572–3. doi: 10.1093/bioinformatics/btq170
35. Quan Y, Zhang X, Ping H. Construction of a Risk Prediction Model Using M6a RNA Methylation Regulators in Prostate Cancer: Comprehensive Bioinformatic Analysis and Histological Validation. *Cancer Cell Int* (2022) 22(1):33. doi: 10.1186/s12935-021-02438-1
36. Zhang X, Wei X, Wang Y, Wang S, Ji C, Yao L, et al. Pyroptosis Regulators and Tumor Microenvironment Infiltration Characterization in Clear Cell Renal Cell Carcinoma. *Front Oncol* (2021) 11:774279:774279. doi: 10.3389/fonc.2021.774279
37. Dixon SJ, Lemberg KM, Lamprecht MR, Skouta R, Zaitsev EM, Gleason CE, et al. Ferroptosis: An Iron-Dependent Form of Nonapoptotic Cell Death. *Cell* (2012) 149(5):1060–72. doi: 10.1016/j.cell.2012.03.042
38. Sun X, Ou Z, Chen R, Niu X, Chen D, Kang R, et al. Activation of the P62-Keap1-NRF2 Pathway Protects Against Ferroptosis in Hepatocellular Carcinoma Cells. *Hepatology* (2016) 63(1):173–84. doi: 10.1002/hep.28251

39. Hassannia B, Vandenabeele P, Vanden Berghe T. Targeting Ferroptosis to Iron Out Cancer. *Cancer Cell* (2019) 35(6):830–49. doi: 10.1016/j.ccell.2019.04.002
40. Xu H, Ye D, Ren M, Zhang H, Bi F. Ferroptosis in the Tumor Microenvironment: Perspectives for Immunotherapy. *Trends Mol Med* (2021) 27(9):856–67. doi: 10.1016/j.molmed.2021.06.014
41. Shi ZZ, Fan ZW, Chen YX, Xie XF, Jiang W, Wang WJ, et al. Ferroptosis in Carcinoma: Regulatory Mechanisms and New Method for Cancer Therapy. *Onco Targets Ther* (2019) 12:11291–304. doi: 10.2147/OTT.S232852
42. Chen W, Zuo F, Zhang K, Xia T, Lei W, Zhang Z, et al. Exosomal MIF Derived From Nasopharyngeal Carcinoma Promotes Metastasis by Repressing Ferroptosis of Macrophages. *Front Cell Dev Biol* (2021) 9:791187:791187. doi: 10.3389/fcell.2021.791187
43. Fan F, Liu P, Bao R, Chen J, Zhou M, Mo Z, et al. A Dual PI3K/HDAC Inhibitor Induces Immunogenic Ferroptosis to Potentiate Cancer Immune Checkpoint Therapy. *Cancer Res* (2021) 81(24):6233–45. doi: 10.1158/0008-5472.CAN-21-1547
44. Luis G, Godfroid A, Nishiumi S, Cimino J, Blacher S, Maquoi E, et al. Tumor Resistance to Ferroptosis Driven by Stearoyl-CoA Desaturase-1 (SCD1) in Cancer Cells and Fatty Acid Biding Protein-4 (FABP4) in Tumor Microenvironment Promote Tumor Recurrence. *Redox Biol* (2021) 43:102006. doi: 10.1016/j.redox.2021.102006
45. Wang W, Green M, Choi JE, Gijon M, Kennedy PD, Johnson JK, et al. CD8(+) T Cells Regulate Tumour Ferroptosis During Cancer Immunotherapy. *Nature* (2019) 569(7755):270–4. doi: 10.1038/s41586-019-1170-y
46. Turley SJ, Cremasco V, Astarita JL. Immunological Hallmarks of Stromal Cells in the Tumour Microenvironment. *Nat Rev Immunol* (2015) 15 (11):669–82. doi: 10.1038/nri3902
47. Huang Y, Chen S, Xiao L, Qin W, Li L, Wang Y, et al. A Novel Prognostic Signature for Survival Prediction and Immune Implication Based on SARS-CoV-2-Related Genes in Kidney Renal Clear Cell Carcinoma. *Front Bioeng Biotechnol* (2021) 9:744659:744659. doi: 10.3389/fbioe.2021.744659
48. Son HY, Jeong HK. Immune Evasion Mechanism and AXL. *Front Oncol* (2021) 11:756225:756225. doi: 10.3389/fonc.2021.756225
49. Zhang W, Kong X, Ai B, Wang Z, Wang X, Wang N, et al. Research Progresses in Immunological Checkpoint Inhibitors for Breast Cancer Immunotherapy. *Front Oncol* (2021) 11:582664:582664. doi: 10.3389/fonc.2021.582664
50. Pascual T, Cejalvo JM, Oliveira M, Vidal M, Vega E, Ganau S, et al. SOLTI-1503 PROMETEO TRIAL: Combination of Talimogene Laherparepvec With Atezolizumab in Early Breast Cancer. *Future Oncol* (2020) 16(24):1801–13. doi: 10.2217/fon-2020-0246
51. Adams S, Loi S, Toppmeyer D, Cescon DW, De Laurentiis M, Nanda R, et al. Pembrolizumab Monotherapy for Previously Untreated, PD-L1-Positive, Metastatic Triple-Negative Breast Cancer: Cohort B of the Phase II KEYNOTE-086 Study. *Ann Oncol* (2019) 30(3):405–11. doi: 10.1093/annonc/mdy518
52. Harris KM, Smilek DE, Byron M, Lim N, Barry WT, McNamara J, et al. Effect of Costimulatory Blockade With Abatacept After Ustekinumab Withdrawal in Patients With Moderate to Severe Plaque Psoriasis: The PAUSE Randomized Clinical Trial. *JAMA Dermatol* (2021) 157(11):1306–15. doi: 10.1001/jamadermatol.2021.3492
53. Schmid P, Salgado R, Park YH, Munoz-Couselo E, Kim SB, Sohn J, et al. Pembrolizumab Plus Chemotherapy as Neoadjuvant Treatment of High-Risk, Early-Stage Triple-Negative Breast Cancer: Results From the Phase 1b Open-Label, Multicohort KEYNOTE-173 Study. *Ann Oncol* (2020) 31(5):569–81. doi: 10.1016/j.annonc.2020.01.072
54. Cetin B, Gumusay O. Pembrolizumab for Early Triple-Negative Breast Cancer. *N Engl J Med* (2020) 382(26):e108. doi: 10.1056/NEJMc2006684

Conflict of Interest: The authors declare that the research was conducted in the absence of any commercial or financial relationships that could be construed as a potential conflict of interest.

Publisher's Note: All claims expressed in this article are solely those of the authors and do not necessarily represent those of their affiliated organizations, or those of the publisher, the editors and the reviewers. Any product that may be evaluated in this article, or claim that may be made by its manufacturer, is not guaranteed or endorsed by the publisher.

frontiers | Frontiers in Immunology

ORIGINAL RESEARCH
published: 16 May 2022
doi: 10.3389/fimmu.2022.895513

Dissecting Tissue Compartment-Specific Protein Signatures in Primary and Metastatic Oropharyngeal Squamous Cell Carcinomas

Habib Sadeghirad[1†], *James Monkman*[1†], *Ahmed M. Mehdi*[1,2], *Rahul Ladwa*[3,4], *Ken O'Byrne*[3], *Brett G. M. Hughes*[4,5] *and Arutha Kulasinghe*[1,4*]

[1] The University of Queensland Diamantina Institute, The University of Queensland, Woolloongabba, QLD, Australia, [2] Queensland Cyber Infrastructure Foundation Ltd., QCIF Facility for Advanced Bioinformatics, Brisbane, QLD, Australia, [3] Princess Alexandra Hospital, Woolloongabba, QLD, Australia, [4] Faculty of Medicine, University of Queensland, Herston, QLD, Australia, [5] Cancer Care Services, Royal Brisbane and Women's Hospital, Herston, QLD, Australia

OPEN ACCESS

Edited by:
Qihui Shi,
Fudan University, China

Reviewed by:
Liu Yang,
Shanghai General Hospital, China
Chunying Wang,
Fudan University, China

***Correspondence:**
Arutha Kulasinghe
Arutha.kulasinghe@uq.edu.au

[†]*These authors share first authorship*

Specialty section:
This article was submitted to Cancer Immunity and Immunotherapy, a section of the journal Frontiers in Immunology

Received: *13 March 2022*
Accepted: *08 April 2022*
Published: *16 May 2022*

Citation:
Sadeghirad H, Monkman J, Mehdi AM, Ladwa R, O'Byrne K, Hughes BGM and Kulasinghe A (2022) Dissecting Tissue Compartment-Specific Protein Signatures in Primary and Metastatic Oropharyngeal Squamous Cell Carcinomas. Front. Immunol. 13:895513. doi: 10.3389/fimmu.2022.895513

Head and neck squamous cell carcinoma (HNSCC) often presents with locoregional or distant disease, despite multimodal therapeutic approaches, which include surgical resection, chemoradiotherapy, and more recently, immunotherapy for metastatic or recurrent HNSCC. Therapies often target the primary and nodal regional HNSCC sites, and their efficacy at controlling occult distant sites remains poor. While our understanding of the tumor microenvironment conducive to effective therapies is increasing, the biology underpinning locoregional sites remains unclear. Here, we applied targeted spatial proteomic approaches to primary and lymph node metastasis from an oropharyngeal SCC (OPSCC) cohort to understand the expression of proteins within tumors, and stromal compartments of the respective sites in samples of both matched and unmatched patients. In unmatched analyses of n = 43 primary and 11 nodal metastases, our data indicated that tumor cells in nodal metastases had higher levels of Ki-67, PARP, BAD, and cleaved caspase 9, suggesting a role for increased proliferation, DNA repair, and apoptosis within these metastatic cells. Conversely, in matched analyses (n = 7), pro-apoptotic markers BIM and BAD were enriched in the stroma of primary tumors. Univariate, overall survival (OS) analysis indicated CD25 in tumor regions of primary tumors to be associated with reduced survival (HR = 3.3, p = 0.003), while progesterone receptor (PR) was associated with an improved OS (HR = 0.33, p = 0.015). This study highlights the utility of spatial proteomics for delineating the tumor and stromal compartment composition, and utility toward understanding these properties in locoregional metastasis. These findings indicate unique biological properties of lymph node metastases that may elucidate further understanding of distant metastatic in OPSCC.

Keywords: oropharangeal cancer, spatial proteomics, head and neck cancer, metastasis, lymph node metastasis, digital spatial profiling

INTRODUCTION

Head and neck squamous cell carcinoma (HNSCC) is the 7th leading cause of cancer worldwide, with approximately 890,000 new cases and 450,000 deaths (1). HNSCC is considered a heterogeneous malignancy arising from the upper aerodigestive tract, particularly from the squamous mucosal line. The lip, oral and nasal cavity, paranasal sinuses, larynx, nasopharynx, oropharynx, and hypopharynx are the areas involved in HNSCC (1). Several risk factors contribute to the development of HNSCC, including both tobacco and alcohol consumption. Viral-driven HNSCC is also found, with Epstein–Barr Virus (EBV) and human papillomavirus (HPV) responsible for the nasopharynx and oropharynx malignancies, respectively (1).

Oropharyngeal SCC (OPSCC) is responsible for a quarter of HNSCC (2), with a tendency to occur more commonly in non-smokers and frequent nodal involvement. Treatment of OPSCC is aimed at curing and organ preservation using a multimodality approach. In locoregional disease, patients are often treated with chemoradiation. Most notably, HPV-induced OPSCC has a better prognosis compared to HPV-negative OPSCC, namely, better radiation sensitivity and overall survival. The 5-year survival rate for patients with HPV-negative and HPV-positive OPSCC is 46 and 57.4%, respectively (3).

In approximately two-thirds of OPSCC patients, locoregional metastasis has been reported. Advanced nodal status, especially extranodal extension, is a poor prognostic predictor, and defining the molecular phenotypes of these multiple sites is important to understand not only the primary tumor, but also the influence of lymph node metastasis to develop effective therapies (4). To gain a deeper understanding of the primary and metastatic tissues, studies of the tumor microenvironment (TME) are needed, ideally by comparing primary and lymph node metastasis, and where possible, where these are from matched patients. The identification and characterization of potential TME biomarkers could have significant predictive and prognostic value in the treatment selection for OPSCC patients (5). However, this can be challenging due to inter- or intra-tumoral heterogeneity (6). The cellular composition and molecular interactions between the TME and the host immune cells could play a role in disease progression and treatment resistance. It is thought that locoregional metastasis are immune-cold and therefore treatment-resistant to any immuno-modulatory treatment strategies (1, 7).

To delineate primary and nodal disease in OPSCC, we applied digital spatial profiling (DSP) of the TME using targeted-panel multiplex immunohistochemistry of tumor- and stromal-compartments. Our study found in unmatched analyses that the tumor compartments of the primary were enriched for ARG1, PD-L1, and nodal metastases were enriched for Ki-67, PARP, BAD, and cleaved caspase 9. Stromal compartments of the primary were enriched for VISTA and IDO1. In matched analyses, BIM and BAD were enriched in the stroma of primary tumors. Furthermore, protein signatures were identified to discriminate matched primary/nodal tissues, and survival associations were investigated compartmentally by tumor sample site.

MATERIAL AND METHODS

This study has the approval of the Queensland University of Technology Human Research Ethics Committee (UHREC #2000000494) and University of Queensland ratification. A tissue microarray (TMA) of OPSCC specimens was sourced from the Tristar Technologies Group (USA) and contained forty-three primary tumors, eleven nodal metastases, and seven matched pairs of primary tumor/nodal metastases with concordant clinicopathological annotations.

Nanostring GeoMx Digital Spatial Profiling (DSP)

The TMA slides from OPSCC samples were obtained and analyzed using the Nanostring GeoMX Digital Spatial Profiling (DSP) technology by the Systems Biology and Data Science Group at Griffith University (Gold Coast, Australia). Pan-cytokeratin and CD45 were the visualization markers used by the instrument to stain the tumor and lymphocytes, respectively. A protein panel of 68 antibodies was used, namely, immune activation, pan-tumor, immuno-oncology (IO) drug target, cell death, immune cell typing, human immune cell core panel, and PI3K/AKT panels. The slides were prepared according to the instructions of the manufacturer, and the tumor/stroma distinction was achieved by masking on $PanCK^+$ or $PanCK^-$ regions, respectively. Using the Nanostring nCounter® platform, antibody barcodes were counted in accordance with the instructions of the manufacturer. In DSP analysis, external RNA Controls Consortium (ERCC) QC was employed to prepare the data for further bioinformatic analysis.

Bioinformatic Analysis

Data analysis was conducted in collaboration with the Queensland Cyber Infrastructure Foundation (QCIF, QLD, Australia). The quality of data was investigated using principal component analysis, and the suitability of the RUV-III normalization method was determined using coefficients of variation (8, 9). Differential analysis was carried out using Limma packages (10). Sparse partial least squares-discriminant analysis (sPLS-DA) within the mixOmics package was used to identify multivariate minimal protein signatures (11). The Kaplan–Meier survival analysis and Cox proportional hazards models were constructed within R studio (12) using Survival package (13) and plots generated by ggplot2 (14). Data shown are not adjusted for multiple testing. The false discovery rate (FDR) adjusted results were not significant within this cohort.

RESULTS

OPSCC Patient Cohort

To investigate protein expression in primary tumors and nodal metastases, we evaluated tissue from a tissue microarray (TMA). The TMA included unmatched specimens from forty-three primary tumors and eleven nodal metastases, and seven matched primary and nodal metastases. All primary tumors were resected from oropharyngeal regions and had squamous

cell carcinoma histology (**Table 1**). The TNM staging (8th edition) ranged from T2-4, N0-2, and M0 (**Table 1**). Only one patient within the cohort was HPV-16 positive.

Identification of Differentially Expressed Proteins by the Nanostring GeoMX DSP Assay

Nanostring Digital Spatial Profiler (DSP) was applied to investigate the protein expression of 68 TMA cores. By masking on $PanCK^+/PanCK^-$ regions, we compartmentalized protein expression within the tumor and stromal compartments (**Figures 1A–D**). Differential expression (DE) was performed on normalized protein counts to identify compartmental enrichment of proteins in unmatched primary tumors compared to nodal metastases and between patient-matched primary tumors and nodal metastases. We discovered significant differences in key deregulated proteins between the two comparison groups. Additionally, DE within the stroma between unmatched primary tumors and nodal metastasis revealed that V-domain IG suppressor of T cell activation (VISTA) and Indoleamine 2,3-dioxygenase 1 (IDO1) exhibited higher expression in primary tumors (**Figures 2A, B**). Parallel analysis of tumor compartments uncovered DE proteins. Programmed death-ligand 1 (PD-L1), Fibroblast activation protein-alpha (FAP-a), Poly (ADP-ribrose) polymerase (PARP), Ki-67, Progesterone receptor (PR), Arginase 1 (ARG1), CD56, BCL2-antagonist of cell death (BAD), and Cleaved Caspase 9. Accordingly, PD-L1, FAP-a, PR, and ARG1 had higher expression in primary tumors, while PARP, Ki-67, CD56, BAD, and Cleaved Caspase 9 were enriched in nodal metastases (**Figures 2C, D**). Furthermore, analysis of stromal compartments across matched primary and nodal metastasis specimens unveiled seven significant differentially expressed proteins, namely, smooth muscle actin (SMA), phosphatase and tensin homolog deleted on chromosome 10 (PTEN), CD163, Bcl-2-like protein 11 (BIM), BAD, PD-L1, and CD25. BIM, BAD, and CD25 were enriched in matched primary tumors, while SMA, PTEN, CD163, and PD-L1 were higher in matched nodal metastases (**Figures 3A, B**). Analysis of tumor compartments between matched primary and nodal metastasis specimens indicated no significant DE proteins.

Survival Associations of OPSCC Primary Tumor and Nodal Metastases

To assess the association between our protein expression and overall survival (OS), we performed a Cox proportional hazards model on all proteins. Analysis of the stromal compartment in primary tumor specimens revealed that the expression of NF1 (HR = 0.748, p = 0.025), CD27 (HR = 0.279, p = 0.035), and CD80 (HR = 0.703, p = 0.02) was associated with a better OS (**Figure 4A**). Moreover, tumoral compartment analysis across primary tumor samples indicated that PR (HR = 0.332, p = 0.015) was associated with better OS, while CD25 (HR = 3.311, p = 0.003) was associated with worse OS (**Figure 4B**). Survival analysis within the stromal compartment from nodal metastasis specimens showed that NY.ESO.1 (HR = 0.309, p = 0.016), and B7.H3 (HR = 0.249, p = 0.026) were associated with better OS (**Figure 4C**). Evaluation of tumoral compartment of nodal metastasis samples found several proteins associated with better OS, namely, SMA (HR = 0.685, p = 0.034), CD45 (HR = 0.463, p = 0.045), CD8 (HR = 0.251, p = 0.028), Fibronectin (HR = 0.472, p = 0.035), and STING (HR = 0.239, p = 0.024), however, BIM (HR = 1.979, p = 0.048), GZMA (HR = 4.332, p = 0.036), FOXP3 (HR = 3.258, p = 0.011), and PR (HR = 9.34, p = 0.017) were associated with worse OS (**Figure 4D**).

Multivariate Discrimination of OPSCC Primary Tumors From Nodal Metastases

Multivariate analysis by sparse partial least-squares discriminant analysis (sPLSDA) was employed to identify minimal protein signatures that collectively distinguish primary tumors from nodal metastases. Signatures within the stroma of matched primary vs nodal metastases stratified samples effectively (**Figure 5A**). The first signature (**Figure 5B**) included levels of SMA, PTEN, cleaved caspase 9, and CD25 (AUC = 0.979)

TABLE 1 | OPSCC cohort characteristics.

	Nodal Metastasis, n = 11	Primary, n = 43	Matched Nodal Met/Primary, n = 7
Gender			
Female	0 (0%)	7 (16%)	1 (14%)
Male	11 (100%)	36 (84%)	6 (86%)
Age			
25–50	5 (45%)	5 (12%)	3 (42%)
50–95	6 (55%)	38 (88%)	4 (58%)
Status			
Alive	9 (82%)	28 (65%)	2 (29%)
Deceased	2 (18%)	15 (35%)	5 (71%)
Radiation			
Yes	3 (27%)	21 (49%)	1 (14%)
No	0	22 (51%)	6 (86%)
N/A	8 (73%)	N/A	N/A
Adjuvant chemotherapy			
Yes	1 (9.1%)	8 (19%)	3 (43%)
No	2 (18%)	35 (81%)	4 (57%)
N/A	8 (73%)	N/A	N/A

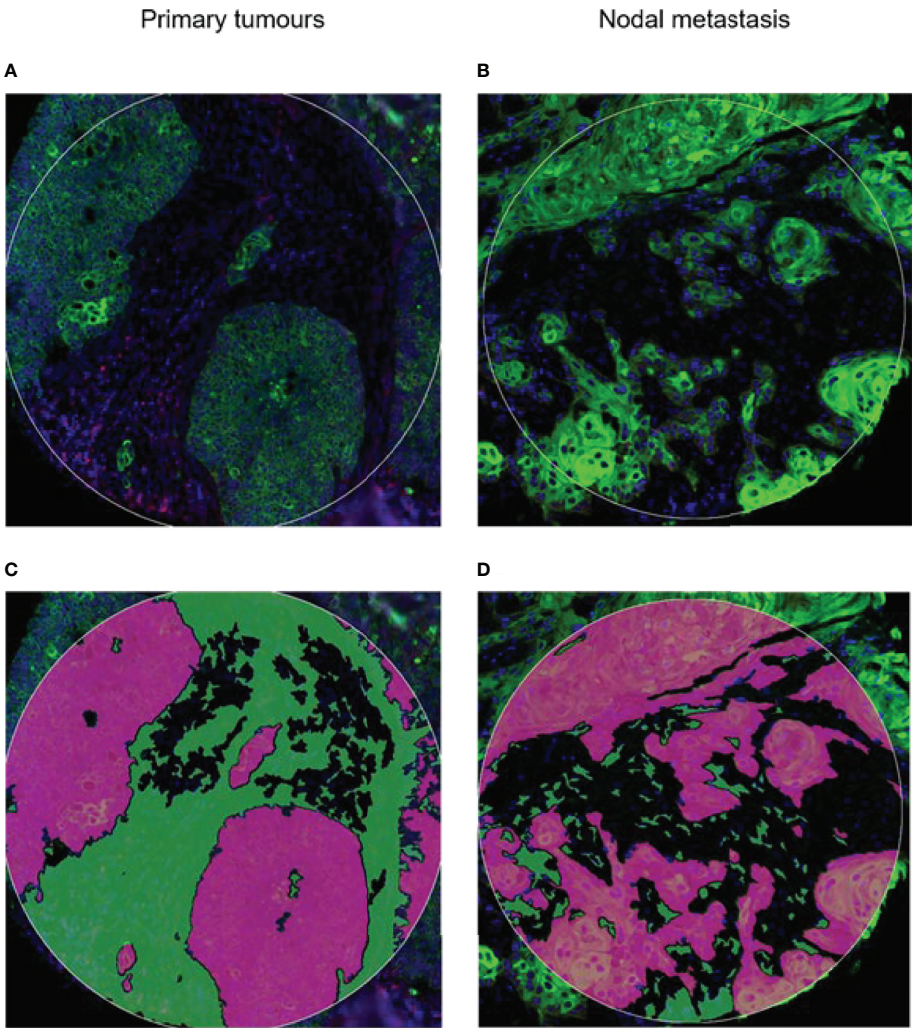

FIGURE 1 | Spatial profiling was performed on tumor microarray cores from **(A)** primary and **(B)** nodal metastasis. Tissues were stained for PanCK^{+} (Tumor) and PanCK^{-} (Stroma) areas. Green, PanCK; Red, CD45. Tissue segmentation strategy to capture **(C)** Tumor mask in purple and **(D)** stromal regions in green. Masks were generated per PanCK$^{+/-}$ feature to liberate barcodes for digital counting by nCounter.

(**Figure 5C**). A second signature comprised of CD95, CD80, and CD27 distinguished matched sample types as well (AUC = 0.918) (**Figure 5D**).

DISCUSSION

HNSCC has a high risk of locoregional nodal metastasis, which affects patient prognosis and treatment outcomes (15). Patients with nodal metastasis are considered to have locoregionally advanced disease with a lower chance of remission (16). Currently, the predictors of nodal metastasis include tumor thickness and size, which have been shown to be unreliable predictors (17). It has been difficult to manage clinically negative neck nodes (N0) due to a lack of reliable predictors of occult metastasis (16, 18). In a study conducted by Shah et al., the authors found that there was a 40% chance of nodal metastasis in clinically node-negative neck dissections (19). For the purpose of distinguishing patients with a high risk of nodal metastasis, various pathological and clinical factors, namely, lymphovascular invasion, tumor differentiation, depth of invasion (DOI), and pattern of invasion (POI), have been reported (20, 21). Moreover, modern imaging modalities such as MRI, CT imaging, and PET/CT scanning, have been used to aid in the detection of locoregional nodal metastases. However, some radiographic features, namely, "subclinical", or "microscopic", or "occult" disease, remain difficult to diagnose using any of these approaches (22, 23). Therefore, companion diagnostics tools are needed to improve the prediction of the likelihood of the development of locoregional metastasis. Ideally, this would be possible by interrogating the primary tissue to determine its aggressiveness and propensity for metastasis.

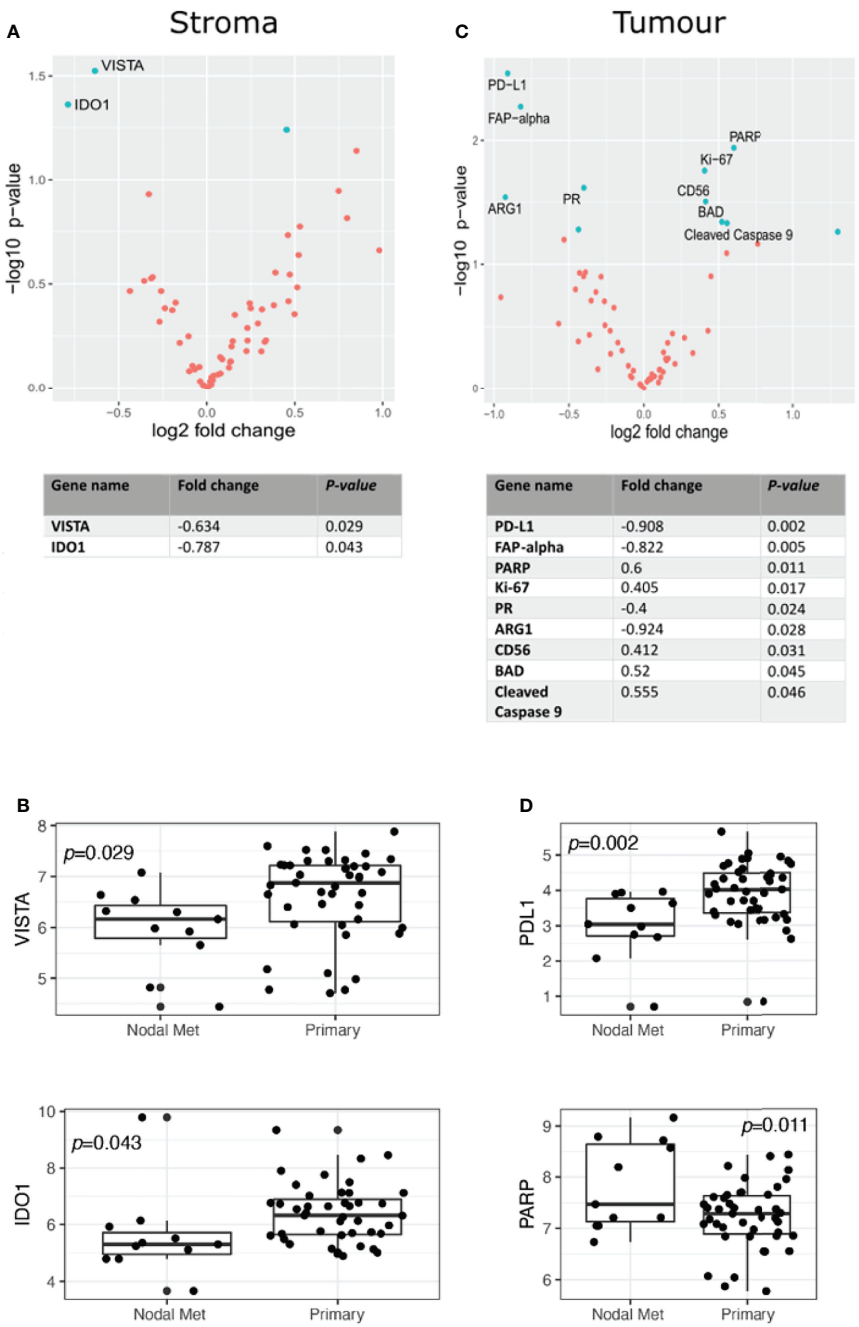

Gene name	Fold change	*P-value*
VISTA	-0.634	0.029
IDO1	-0.787	0.043

Gene name	Fold change	*P-value*
PD-L1	-0.908	0.002
FAP-alpha	-0.822	0.005
PARP	0.6	0.011
Ki-67	0.405	0.017
PR	-0.4	0.024
ARG1	-0.924	0.028
CD56	0.412	0.031
BAD	0.52	0.045
Cleaved Caspase 9	0.555	0.046

FIGURE 2 | Differential protein expression compared to specimens from unmatched OPSCC primary (n = 43) and nodal metastasis (n = 11). **(A)** Upper panel. Volcano scatter plot showing stromal enrichment of proteins in primary (left) vs nodal metastases (right) ranked by significance (–log10 *P*-value). Lower panel. List of top two significant deregulated proteins ranked by *P*-value. **(B)** Boxplots indicating VISTA and IDO1 enrichment in primary tumors. **(C)** Upper panel. Volcano scatter plot showing tumor region enrichment of proteins from primary (left) vs nodal metastases (right) ranked by significance (–log10 *P*-value). Lower panel. List of top nine significant deregulated proteins ranked by *P*-value. **(D)** Boxplots indicating enrichment of PD-L1 and PARP in primary tumors and nodal metastases, respectively.

Tumor tissue analysis by bulk expression or single cell RNA sequencing offers an overview of the molecular features of HNSCC tumors and their TME. These methods are incapable of revealing the spatial cellular properties required for the anti-tumor immune responses (24). Spatial proteomic approaches can provide compartment-specific tumor information to aid in delineating tumor composition. To garner insight into these properties that distinguish primary OPSCC tumors from their metastatic nodal counterparts, we have employed Digital Spatial Profiling to address a targeted profile of proteins and present this

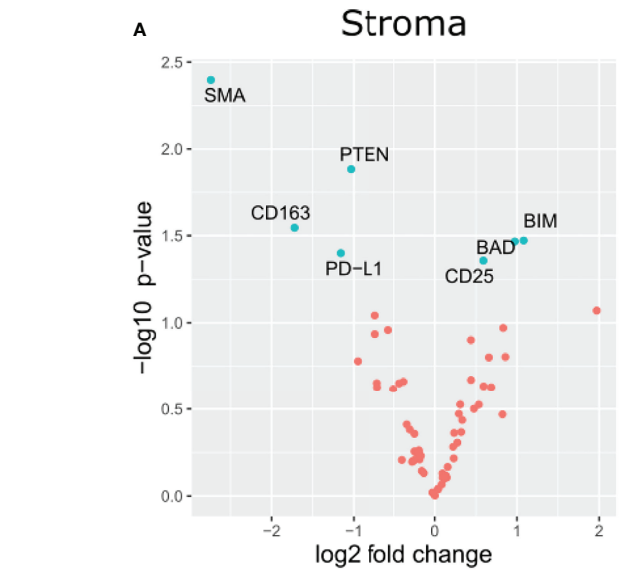

Gene name	Fold change	*P-value*
SMA	-2.739	0.004
PTEN	-1.032	0.013
CD163	-1.721	0.028
BIM	1.082	0.033
BAD	0.974	0.034
PD-L1	-1.158	0.039
CD25	0.592	0.043

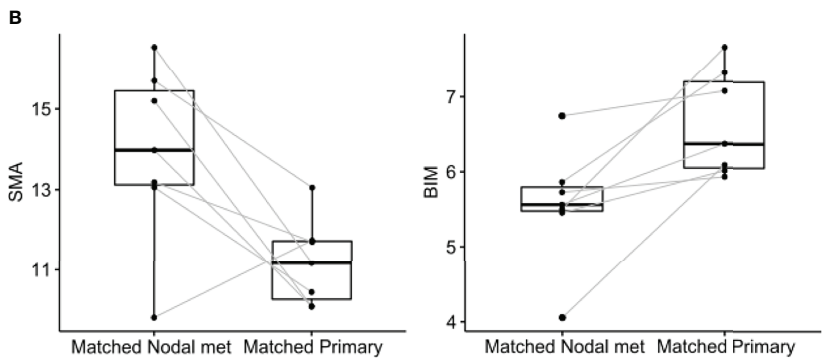

FIGURE 3 | Differential protein expression comparing specimens from matched OPSCC primary tumors and nodal metastasis (n = 7). **(A)** Upper panel. Volcano scatter plot showing stromal enrichment of proteins from nodal metastases (left) vs primary tumors (right) ranked by significance (–log10 *P*-value). Lower panel. List of top seven significant deregulated proteins ranked by *P*-value. **(B)** Representative boxplots indicating SMA and BIM enrichment in matched nodal metastasis and matched primary specimens, respectively.

data as a first step in profiling HNSCC nodal involvement in an OPSCC cohort.

Unmatched analyses between primary tumors (n = 43) and nodal metastases (n = 11) provided insight into the potential dysregulation of several proteins, despite the inherent limitations associated with such a sampling strategy. VISTA, IDO1, and PD-L1 are key immune checkpoints, with VISTA and IDO1 appearing more abundant in the stromal compartment of primary tumors, whereas PD-L1 indicated higher expression in their respective tumor compartments. The V-domain Ig suppressor of T cell activation (VISTA) is an inhibitory immune checkpoint protein that is typically expressed on naïve $CD4^+$ and $Foxp3^+$ Tregs and functions by inhibiting T-cell proliferation and promoting naive to Treg conversion (25). VISTA was associated with several immune cell regions in the stroma but not in HNSCC tumors (26). Blockade of VISTA was found to boost anti-tumor immunity in

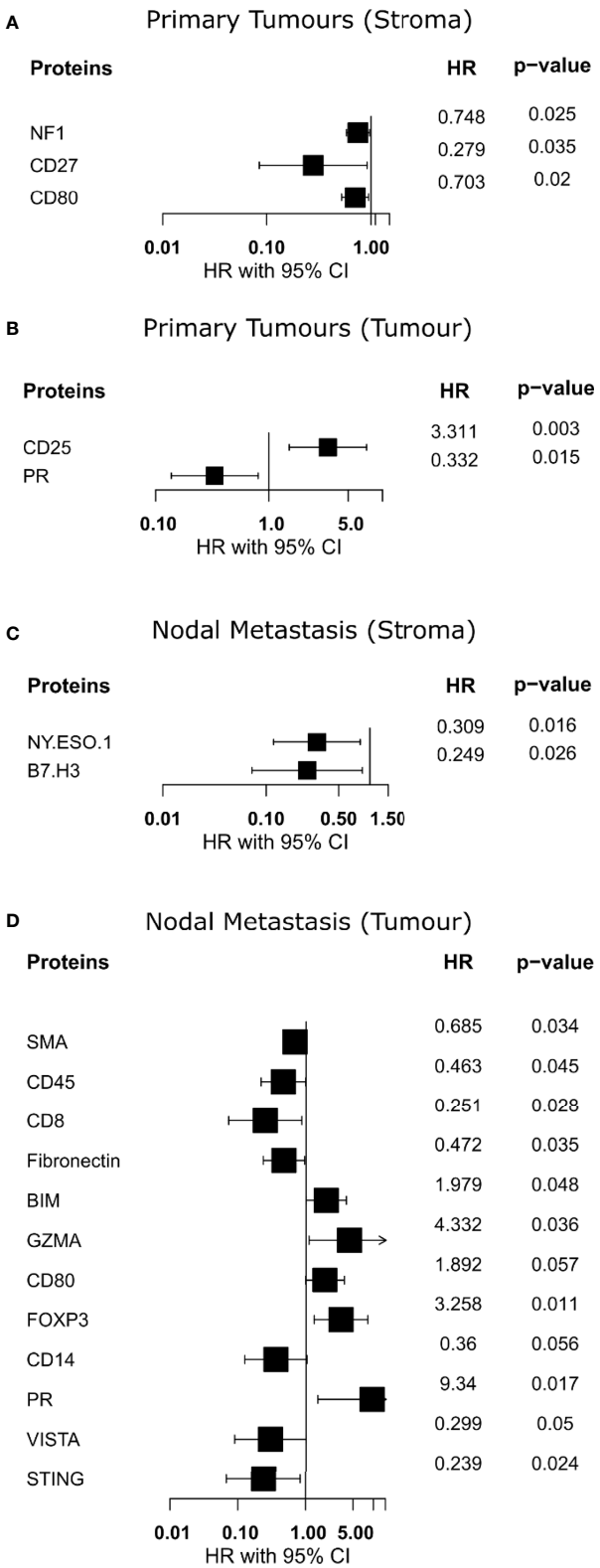

FIGURE 4 | Identification of proteins with overall survival associations. **(A, B)** Forest plot indicating hazard ratio with 95% confidence interval for proteins from primary specimens. **(C, D)** Forest plot indicating hazard ratio with 95% confidence interval for proteins from nodal metastases. HR >1 demonstrates association with poorer outcome.

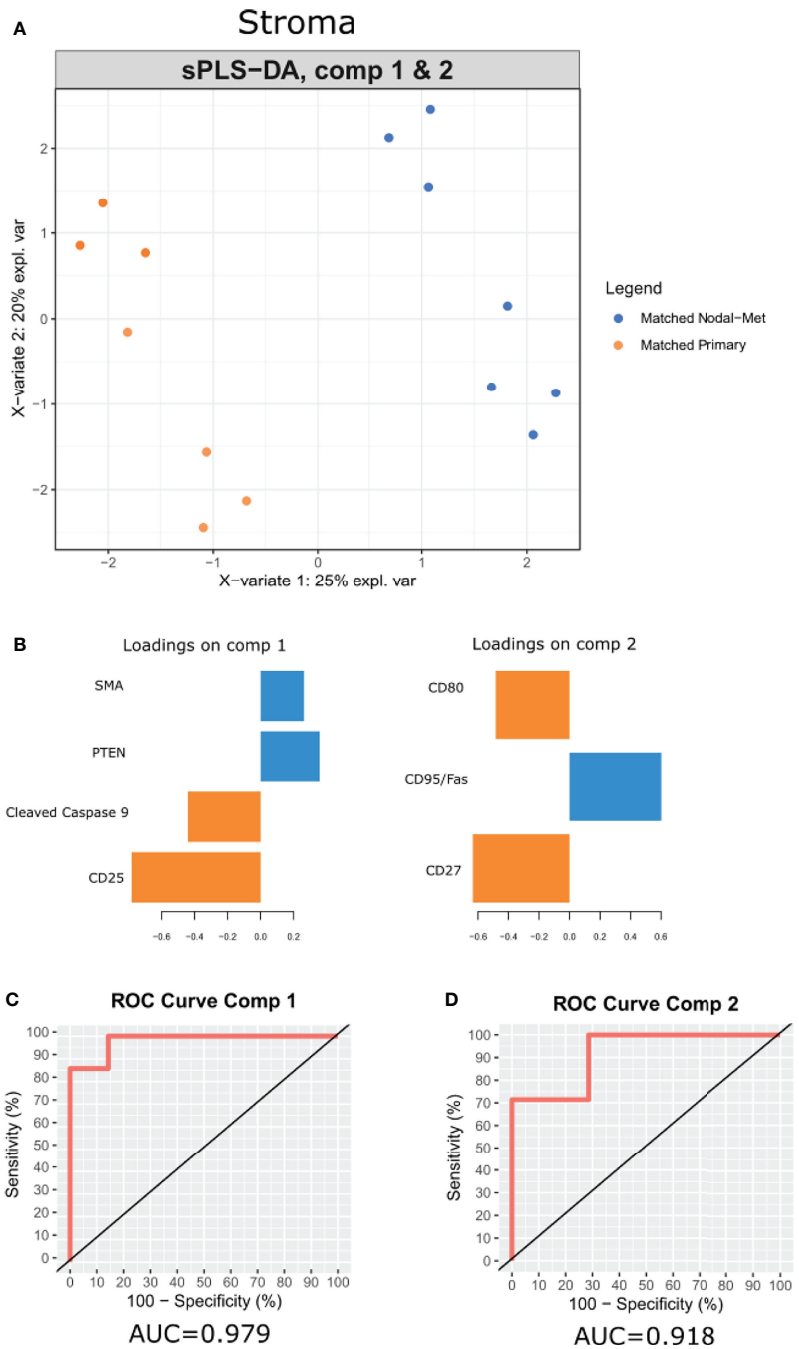

FIGURE 5 | A multi-protein signature differentiates OPSCC tumor progression. **(A)** sPLSDA distinguishes the groups (Matched Primary vs Matched Nodal Mets) by protein signatures in stroma. **(B)** Features of discriminating proteins per component in stroma. **(C, D)** ROC curve of each signature was used to differentiate the groups (Matched Primary vs Matched Nodal Mets). Color of component loadings indicates patient group in which feature was maximally expressed. Positive or negative values in bar chart indicate positive or negative loading to the discriminant signature.

the tumor microenvironment by increasing the number of activated dendritic cells (DCs) and decreasing the number of myeloid-derived suppressor cells (MDSCs). IDO1 induces T-cell apoptosis through activation of caspase 8 and releases mitochondrial cytochrome C, functioning in an immunosuppressive capacity (27). Programmed death-ligand 1 (PD-L1) is a canonical inhibitory immune checkpoint that binds PD-1 on the surface of tumors and immune cells (28). PD-L1 expression on the surface of HNSCC tumor cells is associated with a more robust anti-tumor immune response (29, 30).

Apoptotic pathways play an important role in tumorigenesis, and our results indicate that pro-apoptotic BAD and cleaved caspase 9 were enriched in tumor cells of unmatched nodal metastases. Conversely, in the matched analysis, BIM and BAD were enriched in the stroma of primary tumors. Under various physiological and patho-physiological conditions, Bcl-2 interacting mediator of cell death (BIM) promotes the intrinsic apoptotic pathway (31). Bcl2-associated agonist of cell death (BAD) is a member of the BCL2 family of proteins that act as pro-apoptotic regulators (32). The expression of BAD has been linked to chemoresistance in cancer patients (33, 34). Caspase 9 functions as a pro-apoptotic regulator, allowing the activation of effector caspases 3 and 7 (35). Caspase 9-induced apoptosis has been linked to chemotherapy response. Studies have shown that HNSCC tumors may be resistant to cisplatin if they have a reduced expression of caspase 9 (36).

It is interesting to note that despite an imbalance in samples in the unmatched analysis, several proteins appear enriched within nodal metastases relative to primary tumors. In addition to the pro-apoptotic markers above, Ki-67 and PARP appear enriched in nodal tumor cells. Ki-67 is an established proliferation marker (37), while PARP responds to DNA damage by recruiting effector proteins to repair single-strand breaks (38, 39). PARP inhibitors have been studied as a promising drug to overcome the limitations of conventional therapies that cause DNA damage, such as chemotherapy or radiotherapy (40). This pro-apoptotic, proliferative, and DNA damage phenotype of unmatched nodal metastatic cells is a novel finding in our data that requires further validation, perhaps indicating tumor evolution or response to changes in the cellular ecosystem of the lymph node.

Several other notable features of our data include increased expression of CD25 in the stroma of matched primary tumors. CD25, also known as the IL-2 receptor alpha, is a protein found on activated T cells, specifically Tregs (41). Interestingly, we found that it was CD25 expression within primary tumor regions, not stroma, that was associated with poorer OS. Additionally, PR expression appeared associated with better survival within primary tumors and was also enriched within their tumor regions relative to nodal metastases.

In addition to the differential expression of each individual protein, we applied a multivariate statistical model (sPLSDA) to further discern features that collectively discriminated between our matched patient samples. Of note, this model only performed effectively in stratifying these sample types by their stroma. Expression of CD25 and cleaved caspase 9 in the primary samples and PTEN and SMA in nodal samples could discern samples. Similarly, levels of CD80 and CD27 within primary samples and CD95 in nodal samples could separate these samples. This method offers an alternative to traditional differential expression that may provide insight into contributing differences in observed phenotypes using a multivariate approach.

A protein association with overall survival (OS) was investigated using the Univariate Cox proportional hazards model. Stromal expression of CD27 in primary tumor specimens, and NY-ESO.1 and B7-H3 expression in the nodal metastasis samples, was associated with improved OS. In nodal metastases tumor regions, CD8 and STING were associated with improved OS; however, GZMA was associated with poorer OS. Interestingly, the expression of PR in the tumoral compartment of primary and nodal metastasis tumors demonstrated a different survival pattern. Although the PR expression was associated with improved OS in primary tumors, it was associated with worse OS in nodal metastasis specimens. Immune response protein markers, CD27, and NY.ESO.1 within the stromal compartment of primary and nodal metastasis specimens, were associated with improved OS in our study. Cluster of differentiation 27 (CD27) belongs to the tumor necrosis factor (TNF) receptor superfamily and is involved in T and B cell co-stimulation (42). New York esophageal squamous cell carcinoma 1 (NY.ESO.1) is a member of the cancer testis antigen (CTA) family, which regulates both humoral and cellular immune responses. NY-ESO.1 expression has been linked to higher tumor differentiation grade and stage, and lymph node metastasis (43). In our study, we found that B7.H3 and STING protein expression, NF-κB pathway markers, were linked to improved OS. B7.H3, also known as CD276, promotes anti-tumor immune response by activating T and NK cells (44). STING, on the other hand, contributes to the immune response to tumor cells through the upregulation of interferon gamma 1 (IFN1) (45). Progesterone receptor (PR) is a type of androgen receptor and a member of the nuclear receptor family of transcription factors that regulates target gene expression networks in response to its ligand progesterone (46).

Our study has identified tumor and stromal compartment-specific proteins and signatures that may have predictive and prognostic implications for HNSCC and the development of nodal metastasis. Nevertheless, the study is impacted by the number of samples for each cohort, in particular the matched group. We propose further investigation to profile primary, locoregional, and distant metastasis from matched patient samples to understand the molecular features driving the development of metastasis in OPSCC.

DATA AVAILABILITY STATEMENT

The data presented in the study are deposited in the Geo repository, under accession number GEO Submission GSE200601.

ETHICS STATEMENT

This study has the approval from the Queensland University of Technology Human Research Ethics Committee (UHREC #2000000494). The patients/participants provided their written informed consent to participate in this study.

AUTHOR CONTRIBUTIONS

Experimental design: HR, BH, and AK. Methodology: HR, JM, AM, BH, and AK. Data analysis and reporting: HR, JM, AM, KO, BGMH,

and AK. Manuscript preparation and critical review: all authors. All authors listed have made a substantial, direct, and intellectual contribution to the work and approved it for publication.

FUNDING

This project is funded by the Garnett Passe and Rodney Williams Memorial Foundation (GPRWMF) conjoint grant for AK and BH. AK is supported by a fellowship from the NHMRC (1157741). KO'B and AK are supported by the PA Research Foundation.

ACKNOWLEDGMENTS

The authors acknowledge the researchers in the Systems Biology and Data Science Research Facility (Griffith University) and QCIF Bioinformatics.

REFERENCES

1. Johnson DE, Burtness B, Leemans CR, Lui VWY, Bauman JE, Grandis JR. Head and Neck Squamous Cell Carcinoma. *Nat Rev Dis Primers* (2020) 6 (1):92. doi: 10.1038/s41572-020-00224-3
2. Sabatini ME, Chiocca S. Human Papillomavirus as a Driver of Head and Neck Cancers. *Br J Cancer* (2020) 122(3):306–14. doi: 10.1038/s41416-019-0602-7
3. Chen T-C, Wu C-T, Ko J-Y, Yang T-L, Lou P-J, Wang C-P, et al. Clinical Characteristics and Treatment Outcome of Oropharyngeal Squamous Cell Carcinoma in an Endemic Betel Quid Region. *Sci Rep* (2020) 10(1):526. doi: 10.1038/s41598-019-57177-1
4. Argiris A, Karamouzis MV, Raben D, Ferris RL. Head and Neck Cancer. *Lancet* (2008) 371(9625):1695–709. doi: 10.1016/S0140-6736(08)60728-X
5. Sadeghi Rad H, Monkman J, Warkiani ME, Ladwa R, O'Byrne K, Rezaei N, et al. Understanding the Tumor Microenvironment for Effective Immunotherapy. *Medicinal Res Rev* (2021) 41(3):1474–98. doi: 10.1002/med.21765
6. Stern PL, Dalianis T. Oropharyngeal Squamous Cell Carcinoma Treatment in the Era of Immune Checkpoint Inhibitors. *Viruses* (2021) 13(7):1234. doi: 10.3390/v13071234
7. Kulasinghe A, Taheri T, O'Byrne K, Hughes BGM, Kenny L, Punyadeera C. Highly Multiplexed Digital Spatial Profiling of the Tumor Microenvironment of Head and Neck Squamous Cell Carcinoma Patients. *Front Oncol* (2021) 10. doi: 10.3389/fonc.2020.607349
8. Risso D, Ngai J, Speed TP, Dudoit S. Normalization of RNA-Seq Data Using Factor Analysis of Control Genes or Samples. *Nat Biotechnol* (2014) 32 (9):896–902. doi: 10.1038/nbt.2931
9. Molania R, Gagnon-Bartsch JA, Dobrovic A, Speed TP. A New Normalization for Nanostring Ncounter Gene Expression Data. *Nucleic Acids Res* (2019) 47 (12):6073–83. doi: 10.1093/nar/gkz433
10. Ritchie ME, Phipson B, Wu D, Hu Y, Law CW, Shi W, et al. Limma Powers Differential Expression Analyses for RNA-Sequencing and Microarray Studies. *Nucleic Acids Res* (2015) 43(7):e47. doi: 10.1093/nar/gkv007
11. Rohart F, Gautier B, Singh A, KA LC. Mixomics: An R Package for 'Omics Feature Selection and Multiple Data Integration. *PloS Comput Biol* (2017) 13 (11):e1005752. doi: 10.1371/journal.pcbi.1005752
12. Team R. *RStudio: Integrated Development for R*. Boston, MA: RStudio (2020). Available at: http://www.rstudio.com/.
13. Therneau TM. *A Package for Survival Analysis in R* (2021). Available at: https://CRAN.R-project.org/package=survival.
14. Hadley W. *Ggplot2: Elegrant Graphics for Data Analysis*. Springer (2016).
15. Chow LQM. Head and Neck Cancer. *N Engl J Med* (2020) 382(1):60–72. doi: 10.1056/NEJMra1715715
16. Ampil FL, Nathan CA, Sangster G, Caldito G. Head and Neck Cancer With Lower Neck Nodal Metastases: Management of 23 Cases and Review of the Literature. *Oral Oncol* (2012) 48(4):325–8. doi: 10.1016/j.oraloncology.2011.11.016
17. Puram SV, Tirosh I, Parikh AS, Patel AP, Yizhak K, Gillespie S, et al. Single-Cell Transcriptomic Analysis of Primary and Metastatic Tumor Ecosystems in Head and Neck Cancer. *Cell* (2017) 171(7):1611–24.e24. doi: 10.1016/j.cell.2017.10.044
18. De Silva RK, Siriwardena B, Samaranayaka A, Abeyasinghe W. Tilakaratne WM. A Model to Predict Nodal Metastasis in Patients With Oral Squamous Cell Carcinoma. *PloS One* (2018) 13(8):e0201755. doi: 10.1371/journal.pone.0201755
19. Shah JP. Patterns of Cervical Lymph Node Metastasis From Squamous Carcinomas of the Upper Aerodigestive Tract. *Am J Surg* (1990) 160 (4):405–9. doi: 10.1016/S0002-9610(05)80554-9
20. Tai SK, Li WY, Yang MH, Chu PY, Wang YF. Perineural Invasion in T1 Oral Squamous Cell Carcinoma Indicates the Need for Aggressive Elective Neck Dissection. *Am J Surg Pathol* (2013) 37(8):1164–72. doi: 10.1097/PAS.0b013e318285f684
21. Rajapakshe RM, Pallegama RW, Jayasooriya PR, Siriwardena BS, Attygalla AM, Hewapathirana S, et al. A Retrospective Analysis to Determine Factors Contributing to the Survival of Patients With Oral Squamous Cell Carcinoma. *Cancer Epidemiol* (2015) 39(3):360–6. doi: 10.1016/j.canep.2015.02.011
22. Sohn B, Koh YW, Kang WJ, Lee JH, Shin NY, Kim J. Is There an Additive Value of 18 F-FDG PET-CT to CT/MRI for Detecting Nodal Metastasis in Oropharyngeal Squamous Cell Carcinoma Patients With Palpably Negative Neck? *Acta Radiol* (2016) 57(11):1352–9. doi: 10.1177/0284185115587544
23. Kann BH, Aneja S, Loganadane GV, Kelly JR, Smith SM, Decker RH, et al. Pretreatment Identification of Head and Neck Cancer Nodal Metastasis and Extranodal Extension Using Deep Learning Neural Networks. *Sci Rep* (2018) 8 (1):14036. doi: 10.1038/s41598-018-32441-y
24. Sadeghi Rad H, Bazaz SR, Monkman J, Ebrahimi Warkiani M, Rezaei N, O'Byrne K, et al. The Evolving Landscape of Predictive Biomarkers in Immuno-Oncology With a Focus on Spatial Technologies. *Clin Trans Immunol* (2020) 9(11):e1215. doi: 10.1002/cti2.1215
25. ElTanbouly MA, Croteau W, Noelle RJ, Lines JL. VISTA: A Novel Immunotherapy Target for Normalizing Innate and Adaptive Immunity. *Semin Immunol* (2019) 42:101308. doi: 10.1016/j.smim.2019.101308
26. Lines JL, Pantazi E, Mak J, Sempere LF, Wang L, O'Connell S, et al. VISTA is an Immune Checkpoint Molecule for Human T Cells. *Cancer Res* (2014) 74 (7):1924–32. doi: 10.1158/0008-5472.CAN-13-1504
27. Fallarino F, Grohmann U, Vacca C, Bianchi R, Orabona C, Spreca A, et al. T Cell Apoptosis by Tryptophan Catabolism. *Cell Death Differ* (2002) 9 (10):1069–77. doi: 10.1038/sj.cdd.4401073
28. Liebl MC, Hofmann TG. Identification of Responders to Immune Checkpoint Therapy: Which Biomarkers Have the Highest Value? *J Eur Acad Dermatol Venereol* (2019) 33:52–6. doi: 10.1111/jdv.15992
29. Cohen EE, Soulières D, Le Tourneau C, Dinis J, Licitra L, Ahn M-J, et al. Pembrolizumab Versus Methotrexate, Docetaxel, or Cetuximab for Recurrent or Metastatic Head-and-Neck Squamous Cell Carcinoma (KEYNOTE-040): A Randomised, Open-Label, Phase 3 Study. *Lancet* (2019) 393(10167):156–67. doi: 10.1016/S0140-6736(18)31999-8
30. Brahmer JR, Tykodi SS, Chow LQ, Hwu W-J, Topalian SL, Hwu P, et al. Safety and Activity of Anti–PD-L1 Antibody in Patients With Advanced Cancer. *N Engl J Med* (2012) 366(26):2455–65. doi: 10.1056/NEJMoa1200694
31. Shukla S, Saxena S, Singh BK, Kakkar P. BH3-Only Protein BIM: An Emerging Target in Chemotherapy. *Eur J Cell Biol* (2017) 96(8):728–38. doi: 10.1016/j.ejcb.2017.09.002
32. Boac BM, Abbasi F, Ismail-Khan R, Xiong Y, Siddique A, Park H, et al. Expression of the BAD Pathway is a Marker of Triple-Negative Status and Poor Outcome. *Sci Rep* (2019) 9(1):1–14. doi: 10.1038/s41598-019-53695-0
33. Bansal N, Marchion DC, Bicaku E, Xiong Y, Chen N, Stickles XB, et al. BCL2 Antagonist of Cell Death Kinases, Phosphatases, and Ovarian Cancer Sensitivity to Cisplatin. *J Gynecol Oncol* (2012) 23(1):35–42. doi: 10.3802/jgo.2012.23.1.35

34. Marchion DC, Cottrill HM, Xiong Y, Chen N, Bicaku E, Fulp WJ, et al. BAD Phosphorylation Determines Ovarian Cancer Chemosensitivity and Patient Survival. *Clin Cancer Res* (2011) 17(19):6356–66. doi: 10.1158/1078-0432.CCR-11-0735
35. Thornberry NA, Lazebnik Y. Caspases: Enemies Within. *Science* (1998) 281 (5381):1312–6. doi: 10.1126/science.281.5381.1312
36. Kuwahara D, Tsutsumi K, Oyake D, Ohta T, Nishikawa H, Koizuka I. Inhibition of Caspase-9 Activity and Apaf-1 Expression in Cisplatin-Resistant Head and Neck Squamous Cell Carcinoma Cells. *Auris Nasus Larynx* (2003) 30:85–8. doi: 10.1016/S0385-8146(02)00129-3
37. Sun X, Kaufman PD. Ki-67: More Than a Proliferation Marker. *Chromosoma* (2018) 127(2):175–86. doi: 10.1007/s00412-018-0659-8
38. Langelier M-F, Riccio AA, Pascal JM. PARP-2 and PARP-3 are Selectively Activated by 5′ Phosphorylated DNA Breaks Through an Allosteric Regulatory Mechanism Shared With PARP-1. *Nucleic Acids Res* (2014) 42 (12):7762–75. doi: 10.1093/nar/gku474
39. Eustermann S, Wu W-F, Langelier M-F, Yang J-C, Easton LE, Riccio AA, et al. Structural Basis of Detection and Signaling of DNA Single-Strand Breaks by Human PARP-1. *Mol Cell* (2015) 60(5):742–54. doi: 10.1016/j.molcel.2015.10.032
40. Lord CJ, Ashworth A. PARP Inhibitors: Synthetic Lethality in the Clinic. *Science* (2017) 355(6330):1152–8. doi: 10.1126/science.aam7344
41. Flynn MJ, Hartley JA. The Emerging Role of Anti-CD 25 Directed Therapies as Both Immune Modulators and Targeted Agents in Cancer. *Br J Haematol* (2017) 179(1):20–35. doi: 10.1111/bjh.14770
42. Starzer AM, Berghoff AS. New Emerging Targets in Cancer Immunotherapy: CD27 (Tnfrsf7). *ESMO Open* (2019) 4:e000629. doi: 10.1136/esmoopen-2019-000629
43. Thomas R, Al-Khadairi G, Roelands J, Hendrickx W, Dermime S, Bedognetti D, et al. NY-ESO-1 Based Immunotherapy of Cancer: Current Perspectives. *Front Immunol* (2018) 9:947. doi: 10.3389/fimmu.2018.00947
44. Luo L, Chapoval AI, Flies DB, Zhu G, Hirano F, Wang S, et al. B7-H3 Enhances Tumor Immunity *In Vivo* by Costimulating Rapid Clonal Expansion of Antigen-Specific CD8+ Cytolytic T Cells. *J Immunol* (2004) 173(9):5445–50. doi: 10.4049/jimmunol.173.9.5445
45. Ishikawa H, Barber GN. STING Is an Endoplasmic Reticulum Adaptor That Facilitates Innate Immune Signalling. *Nature* (2008) 455(7213):674–8. doi: 10.1038/nature07317
46. Grimm SL, Hartig SM, Edwards DP. Progesterone Receptor Signaling Mechanisms. *J Mol Biol* (2016) 428(19):3831–49. doi: 10.1016/j.jmb.2016.06.020

Conflict of Interest: AM is employed by QCIF Bioinformatics.

The remaining authors declare that the research was conducted in the absence of any commercial or financial relationships that could be construed as a potential conflict of interest.

Publisher's Note: All claims expressed in this article are solely those of the authors and do not necessarily represent those of their affiliated organizations, or those of the publisher, the editors and the reviewers. Any product that may be evaluated in this article, or claim that may be made by its manufacturer, is not guaranteed or endorsed by the publisher.

frontiers | Frontiers in Immunology

ORIGINAL RESEARCH
published: 20 May 2022
doi: 10.3389/fimmu.2022.914236

Single-Cell Transcriptomics Revealed Subtype-Specific Tumor Immune Microenvironments in Human Glioblastomas

Yong Xiao[1,2,3†], Zhen Wang[2,3†], Mengjie Zhao[3†], Yanxiang Deng[1], Mingyu Yang[1], Graham Su[1], Kun Yang[2], Chunfa Qian[2], Xinhua Hu[2], Yong Liu[2], Liangyuan Geng[2], Yang Xiao[1], Yuanjie Zou[2], Xianglong Tang[3], Hongyi Liu[2], Hong Xiao[3*] and Rong Fan[1,4,5*]*

[1] Department of Biomedical Engineering, Yale University, New Haven, CT, United States, [2] Department of Neurosurgery, Nanjing Brain Hospital Affiliated to Nanjing Medical University, Nanjing, China, [3] Department of Neuro-Psychiatric Institute, Nanjing Brain Hospital Affiliated to Nanjing Medical University, Nanjing, China, [4] Yale Stem Cell Center and Yale Cancer Center, Yale School of Medicine, New Haven, CT, United States, [5] Human and Translational Immunology Program, Yale School of Medicine, New Haven, CT, United States

Human glioblastoma (GBM), the most aggressive brain tumor, comprises six major subtypes of malignant cells, giving rise to both inter-patient and intra-tumor heterogeneity. The interaction between different tumor subtypes and non-malignant cells to collectively shape a tumor microenvironment has not been systematically characterized. Herein, we sampled the cellular milieu of surgically resected primary tumors from 7 GBM patients using single-cell transcriptome sequencing. A lineage relationship analysis revealed that a neural-progenitor-2-like (NPC2-like) state with high metabolic activity was associated with the tumor cells of origin. Mesenchymal-1-like (MES1-like) and mesenchymal-2-like (MES2-like) tumor cells correlated strongly with immune infiltration and chronic hypoxia niche responses. We identified four subsets of tumor-associated macrophages/microglia (TAMs), among which TAM-1 co-opted both acute and chronic hypoxia-response signatures, implicated in tumor angiogenesis, invasion, and poor prognosis. MES-like GBM cells expressed the highest number of M2-promoting ligands compared to other cellular states while all six states were associated with TAM M2-type polarization and immunosuppression *via* a set of 10 ligand–receptor signaling pathways. Our results provide new insights into the differential roles of GBM cell subtypes in the tumor immune microenvironment that may be deployed for patient stratification and personalized treatment.

Keywords: single-cell RNA sequencing, glioblastoma, cellular state, tumor-associated macrophage, hypoxia, M2-type polarization, cell-to-cell interaction

OPEN ACCESS

Edited by:
Qihui Shi,
Fudan University, China

Reviewed by:
Yin Tang,
Institute for Systems Biology (ISB), United States
Zhuo Wang,
Fudan University, China

***Correspondence:**
Hongyi Liu
njnkyylhy@163.com
Hong Xiao
xiaohong63xx@163.com
Rong Fan
rong.fan@yale.edu

†These authors have contributed equally to this work

Specialty section:
This article was submitted to Cancer Immunity and Immunotherapy, a section of the journal Frontiers in Immunology

Received: *06 April 2022*
Accepted: *20 April 2022*
Published: *20 May 2022*

Citation:
Xiao Y, Wang Z, Zhao M, Deng Y, Yang M, Su G, Yang K, Qian C, Hu X, Liu Y, Geng L, Xiao Y, Zou Y, Tang X, Liu H, Xiao H and Fan R (2022) Single-Cell Transcriptomics Revealed Subtype-Specific Tumor Immune Microenvironments in Human Glioblastomas. Front. Immunol. 13:914236. doi: 10.3389/fimmu.2022.914236

INTRODUCTION

Isocitrate dehydrogenase (IDH)-wild-type glioblastoma (GBM) is an incurable brain tumor, and the main underlying challenge to treatment is heterogeneity (1). At least three determinants drive GBM heterogeneity: (i) genetic alterations reshape cellular transformation, which induces tumorigenesis; (ii) cellular lineages and the epigenetic programs contribute to key phenotype; and (iii) the tumor microenvironment (TME) (2). Although GBM differs in individuals, investigations have attempted to uncover the common ground shared among most patients, in hopes of providing new insights into treatment. In the bulk sequencing era, The Cancer Genome Atlas (TCGA) Research Network generated a blueprint of GBM genomic subtypes, namely, classical, mesenchymal, neural, and proneural subtypes each having a unique signature (3). However, multiple TCGA subtypes can co-exist in the same tumor of the same patient either in different regions or even in close proximity, and these subtypes can change over time and evolve through treatment as seen by longitudinal genomic analysis (4). The advent of single-cell RNA sequencing (scRNA-seq) provides an opportunity to dissect the lineage identity and heterogeneity of cancers with unprecedented resolution. Neftel et al. used scRNA-seq to examine GBM tumor cells and found that the malignant cells share a limited set of cellular states, namely, astrocyte-like (AC-like), mesenchymal-1-like (MES1-like), mesenchymal-2-like (MES2-like), oligodendrocyte-progenitor-like (OPC-like), neural-progenitor-1-like (NPC1-like), and neural-progenitor-2-like (NPC2-like) states (5). Moreover, these cellular states are partially enriched for select genetic events: amplifications of *EGFR*, *PDGFRA*, and *CDK4* are more common in AC-like, OPC-like, and NPC-like states, respectively, whereas mutations of *NF1* are more common in MES-like states. These works provide a basis for studying the heterogeneity of GBM malignant cells, but the specific characteristics of different cellular states and their roles in shaping the tumor immune microenvironment and subsequently patient outcomes need to be systematically studied. The interactions between different tumor cellular states and non-malignant cells (e.g., vascular and immune cells) are yet to be elucidated in order to gain a holistic view of the TME in GBM patients.

TME is composed of malignant tumor cells together with surrounding non-malignant stromal cells including vascular and immune cells as well as non-cellular components such as the extracellular matrix. These cell types communicate with each other *via* ligand–receptor interactions, which play crucial roles in inflammation, immune infiltration, tumorigenesis, and therapeutic resistance (6). Although scRNA-seq has emerged as a powerful method to dissect cellular states within tumors and to study the cross-talk between cells (7), in the field of human GBM research, scRNA-seq studies were mostly concentrated on quantitating the heterogeneity of malignant tumor cells or tumor stem/progenitor cells (5, 8, 9). In glioma, stromal cells comprise normal astrocytes, oligodendrocytes, immune cells, and endothelial cells (5, 10). Lines of evidence from experimental and clinical studies have shown that tumor-associated macrophages/microglia (TAMs) make up most of the immune cells in GBM (>95%) (11–13), but we have a limited understanding of the heterogeneity of GBM TAMs and the subtypes of TAMs contributing to GBM patient bleak prognosis (14, 15). TAMs have been functionally divided into M1 and M2 polarized cells, and the latter is associated with tumor cell invasion, angiogenesis, and suppressive antitumor immunity, resulting in poor prognosis (16–18). Yuan et al. and Zhang et al. used the same published dataset to examine the interactions between glioma tumor cells and TAMs (19, 20), but have yet to investigate the differential roles of the GBM subtypes and these interactions in TAM M2-type polarization. Although some studies indicate that glioma cells may recruit TAMs through the generation of soluble factors, such as *CSF*, *MCP*, *CX3CL1*, *CCL2*, and *EGF* (21), the contributions of major regulatory pathways and their modulators or targets involved in TAM polarization are inadequately studied. Thus, researchers have yet to systematically examine the role of six GBM cellular states in cell–cell communication and TAM polarization in order to elucidate the mechanisms underlying TAM polarization to discover new strategies for treating glioma by intervening cell–cell interactions.

Here, we report on the scRNA-seq of primary IDH-wild-type tumors surgically resected from 7 GBM patients and obtained 28,279 single-cell transcriptomes. We dissociated the tumor specimens immediately after procurement at the operating room to prepare samples for scRNA-seq without cell sorting with *CD45* antibody conducted in previous studies (5, 22) and therefore all major cell types in the GBM samples including tumor cells and stromal cells were retained and analyzed in our data, which enabled us to explore important questions such as which tumor cellular states could be associated with GBM progenitor cells, which cell types were poor-prognosis indicators, how GBM tumor cells reprogram TAMs into an immunosuppressive phenotype, and how they communicate with other stromal cells to shape the subtype-specific TME. We found that NPC2-like tumor cells functioned as tumor cells of origin, and that hypoxia-response MES-like tumor cells and hypoxia-response TAMs were involved in angiogenesis and the invasion niche development. Additionally, our work provided the first systematic study of the landscape of cell–cell interaction and gene regulation network in shaping the GBM microenvironments including promoting TAM M2-type polarization, endothelial angiogenesis, and their relationship with different GBM cellular states, which may shed new light to the development of therapeutic approaches by targeting TME components.

METHODS

Tumor Tissue Acquisition and Processing

Fresh tumor samples were acquired when patients underwent surgical resection of primary GBM. Sample use was approved by the Institutional Review Board at the Nanjing Brain Hospital Affiliated to Nanjing Medical University. The experiments performed here conform to the principles set out in the WMA Declaration of Helsinki and the Department of Health and

Human Services Belmont report. All patients signed informed consent. Their pathological results were confirmed as IDH-wild-type GBM according to the WHO 2016 Classification. Fresh tumor samples were immediately stored in the GEXSCOPE Tissue Preservation Solution (Singleron Biotechnologies) at 2–8°C after resection. Prior to tissue dissociation, the specimens were washed three times with Hanks' Balanced Salt Solution (HBSS) and minced into 1- to 2-mm pieces. Subsequently, these pieces were digested in 2 ml of GEXSCOPE Tissue Dissociation Solution (Singleron Biotechnologies) at 37°C for 15 min in a 15-ml centrifuge tube with continuous agitation. Following digestion, a 40-micron sterile strainer (Corning) was used to separate cells from cell debris and other impurities. Then, cells were centrifuged at 1,000 rpm, 4°C, for 5 min and cell pellets were resuspended into 1 ml of PBS (HyClone). To remove red blood cells, 2 ml of GEXSCOPE Red Blood Cell Lysis Buffer (Singleron Biotechnologies) was added to the cell suspension and incubated at 25°C for 10 min. The mixture was then centrifuged at 1,000 rpm for 5 min and the cell pellets were resuspended in PBS. Cells were counted with a TC20 automated cell counter (Bio-Rad) and the concentration was adjusted to 1×10^5 cells/ml in PBS.

Single-Cell RNA Sequencing

A single-cell state suspension was obtained by pipetting up and down using a glass pipette. Single-cell suspension was then loaded onto a microfluidic chip and scRNA-seq libraries were constructed according to the manufacturer's instructions (Singleron GEXSCOPE Single Cell RNAseq Library Kit, Singleron Biotechnologies). Sequencing was performed on an Illumina HiSeq X10 instrument with 150-bp paired-end reads.

Single-Cell RNA Sequencing Alignment and Expression Quantitation

Raw reads were processed to generate gene expression matrices by scopetools (https://anaconda.org/singleronbio/scopetools). Briefly, read 1 contained the cell and molecular barcodes, while all genomic information was contained in read 2. Reads without poly T tails at the intended positions were filtered out, and then for each read, cell barcode and unique molecular identifier (UMI) were extracted. Adapters and poly A tails were trimmed before aligning read 2 to GRCh38 with ensemble version 92 gene annotation. Reads with the same cell barcode, UMI, and gene were grouped together to generate the number of UMIs per gene per cell. Cell number was then determined based on the inflection point of the number of UMI versus sorted cell barcode curve. Finally, the digital gene expression matrix was generated based on the remaining barcode–UMI–gene triplets. In total, we sequenced 28,279 single cells of 7 primary GBM samples.

Data Filtering, Unsupervised Clustering, Cell-Type Annotation, and Function Analysis

The Seurat package (v.3.2.3) and the DoubletFinder package (v. 2.0.3) in R (v.3.6.3) were applied to filter cells and genes among 28,279 cells. Cells were kept in further data analysis only if they met the following quality control criteria: (i) the number of detected genes was less than twice and more than half the mean number of expression genes across cells coming from the same sample; (ii) expression of mitochondrial genes was less than 20% of total counts in one cell; and (iii) passing the standard workflow of the DoubletFinder package to remove the doublets. Seven samples were merged into one object and clustered without supervision using the harmony package (v.1.0) after filters of cells, and then genes were kept only when they were expressed in at least 10 cells. Uniform Manifold Approximation and Projection (UMAP) was applied to project single cells onto a two-dimensional map to discover heterogeneity among cells. Differentially expressed genes (DEGs) in each cluster were identified by the Seurat function FindMarkers, which can return the gene names, average log fold change, and adjusted *p*-value of genes enriched in every cluster. The package clusterProfiler (3.14.3) was used to accomplish the GO analysis of DEGs, and significant biological processes were picked out by setting "pvalueCutoff=0.05" and "qvalueCutoff=0.05". Enrichment analysis of specific gene sets was done by the package GSVA (v.1.34.0) by setting "method=ssgsea".

Malignant tumor cells were distinguished from non-tumor cells by copy number variations (CNVs) as Yuan et al. reported (10). Raw count matrix should first be transformed into log2 (counts per thousand molecules +1), and genes that were expressed in less than 100 cells were discarded; subsequently, the average of log2(counts per thousand molecules +1) was computed across the genes on each chromosome; finally, the resulting average of each cell were z-scored and the principal components (PCs) of the resulting z-matrix were calculated. Here, HLA genes on chromosome 6 were also excluded because they could manifest as CNVs in immune cells. For all cells, the first PC yielded the malignant score that can differentiate tumor cells from non-tumor cells. Furthermore, the CNV subclones in different patients were confirmed by the infercnv package (v.1.2.1). Non-tumor cells were annotated to the specific cell types according to the expression of cell marker genes.

Identification of Tumor Cell Cellular States and Stem-Like Cells

Single-sample gene set enrichment analysis (ssGSEA) (4) was done with the gene signatures for the GBM tumor cell six cellular states (5) and GBM stem-like tumor cell (23) as previously reported compared to a permutated data set (permutation = 1000). The cutoff used here was p-value < 0.05. Firstly, tumor cells were annotated as stem-like cell if the p-value of stem-like gene set was less than 0.05 and the matching enrichment score was more than 0. Among the remaining un-annotated tumor cells, cancer cells were annotated to the specific cellular state according to the lowest p-value when p-value was less than 0.05 and related enrichment score was more than 0. If the enrichment score was less than 0, this tumor cell would be marked as un-annotated tumor cells.

Developmental Linage of Six Cellular States

The velocyto python package was applied to recount the spliced reads and unspliced reads based on previously aligned bam files, then the velocyto.R package (v.0.6) was used to calculate RNA velocity values for each gene from each cell and embed RNA velocity vector to the 2-D diffusion map space.

Construction of Regulon Network

Simultaneous gene regulatory networks of the six tumor cell cellular states and non-tumor cells were constructed by the SCENIC package (v.1.1.1.10 and v.1.2.2). The databases used were "hg19-500bp-upstream-7species.mc9nr.feather" and "hg19-tss-centered-10kb-7species.mc9nr.feather". Genes were included in analysis only if they were expressed in at least 10 cells and were contained in the former two databases. The regulon specificity score was calculated by the function calcRSS.

Analysis of Public GBM Datasets

The mRNA expression data and metadata containing survival information for TCGA and Chinese Glioma Genome Atlas (CGGA) GBM patients were downloaded from http://www.cbioportal.org/ and http://www.cgga.org.cn/, respectively. We ranked the GBM patients from high to low according to their enrichment scores of specific cell-type marker signatures, then labeled the upper 50% of the patients as the higher group and the lower 50% of the patients as the lower group. Survival curves were performed by Kaplan–Meier analysis in the package survival (3.2-7) between the higher and the lower group, and were tested for significance using the Mantel-Cox log-rank test. A value of $p < 0.05$ was considered statistically significant.

Cell-to-Cell Interactions

Cross-talks between the GBM tumor cell six cellular states and other microenvironmental cells were done using the CellChat package (v.0.5.5), and CellChatDB.huma was used as the ligand–receptor interaction reference database. The function computeCommun ProbPathway inferred the cell–cell communication at a signaling pathway level, and then we explored how signaling pathways coordinate together among multiple cell types by using the function identifyCommunicationPatterns.

Investigating the Role of Six Cellular States in TAM M2-Type Polarization

We did NicheNet (v.1.0.0) analysis to link ligands secreted by the six tumor cell cellular states to TAM M2-type marker genes (**Supplementary Figure 8C**). The ligand–target prior model, database for ligand–receptor network, and weighted integrated network were provided by NicheNet. If the gene was detected in at least 10% of cells among the same cellular state or TAMs, it was considered as expressed gene and was used in this part analysis. We computed the ligand activity compared to the background set of genes and ranked ligands based on the presence of their target genes in the M2-type marker gene sets. In the ligand–receptor network analysis, only bona fide ligand–receptor interactions documented in literature and publicly available databases were remained.

Immunofluorescence

Formalin-fixed paraffin-embedded sections of primary GBM were collected from the same 7 patients whose samples underwent scRNA-seq in this study. The protein expression levels of the marker genes were detected by immunofluorescence for human primary GBM specimens with antibodies shown in **Supplementary Table 7**. The samples were incubated with the first primary antibody against *CD14* (1:200 for IF, Servicebio) overnight at 4°C and then with the first corresponding secondary antibody at room temperature for 50 min under dark conditions. Later, the sample slides were incubated with the second antibody *ERO1A* (1:200 for IF, DF12984) overnight at 4°C and then with the second corresponding secondary antibody at room temperature for 50 min under dark conditions. Slides were counterstained with DAPI for nuclei visualization. Finally, the slides were imaged using Imaging System from Nikon. We used CaseViewer software (3DHISTECH) to unmix and remove autofluorescence and to analyze the multispectral images.

RESULTS

Dissecting GBM Cellular States and Correlation With TCGA Subtypes

We conducted single-cell 3' mRNA sequencing of 7 GBM patient samples and obtained 28,279 single-cell transcriptomes at a depth of 100,000 mean reads per cell (**Figure 1A** and **Supplementary Tables 1**, **2**). The median number of genes detected per sample ranged from 1,053 to 2,098. In total, 25,467 genes in 20,289 cells passed the quality control filtering (see the *Methods* section) and were used in further downstream data analysis. The whole transcriptome of all single cells after batch effect correction was used to perform unsupervised clustering analysis and the results were visualized using the UMAP for dimension reduction (**Figure 1B**). The distribution of single cells from different patients was also shown (**Figure 1C**).

Firstly, we dissected the GBM cell composition. Large CNVs and aneuploidies are readily detected by scRNA-seq and can be applied to distinguish malignantly transformed tumor cells from non-malignant cells (22). We adopted a computational pipeline reported previously (10) to calculate the malignancy score based on CNVs, which was subsequently used to identify GBM tumor cells. When compared to normal oligodendrocytes, malignant cells had higher malignancy scores (**Figure 1D**) with distinct CNVs (**Figure 1E**). Furthermore, non-tumor cells were annotated to specific cell types by marker genes (**Figures 1F, G**) (5, 24). Notably, *SOX2* was pervasively expressed in tumor cells (**Figure 1F** and **Supplementary Figure 1B**), which is consistent with the previous study (10). Compared to non-malignant oligodendrocytes, tumor cells usually exhibited a loss of chromosome 10 (**Figure 1E**), which is the earliest and one of the most common genetic alterations in adult GBMs (25). All GBM patients had their own main unique CNV subclones, indicating the existence of genetically heterogeneous malignant

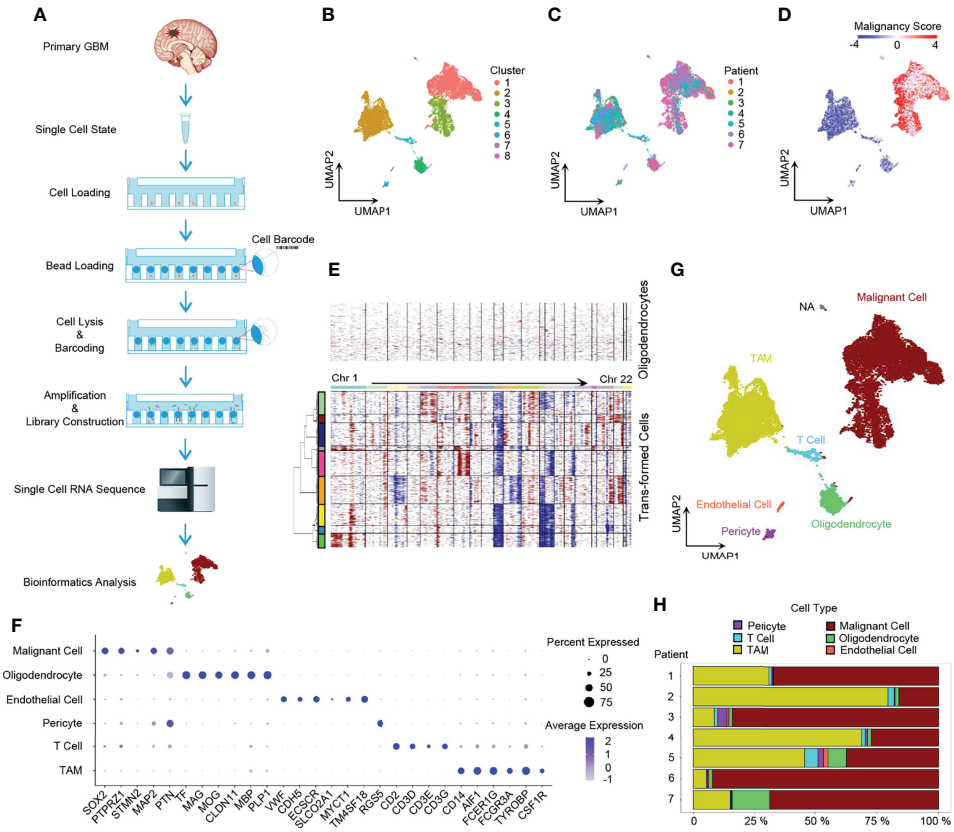

FIGURE 1 | Dissection of primary GBM by scRNA-seq. **(A)** Scheme of the workflow in our study. **(B)** UMAP projection of all 20,289 GBM cells including tumor cells and stromal cells. Eight clusters were found when index Resolution in Seurat FindClusters was set as 0.05. **(C)** UMAP visualization showing cells of individuals. **(D)** UMAP of malignancy scores. Transformed cells had higher malignancy scores and were colored with red, while non-tumor cells had lower malignancy scores and were in blue. **(E)** Evaluation of copy number variations (CNVs). Compared to oligodendrocytes, malignant cells presented with obvious CNVs. Red, amplification; blue, deletion. **(F)** Dot plot of cell marker gene expression level. **(G)** Annotation of cell types in GBM. The majority of GBM cells were malignant cells and TAMs, and GBM still had a small number of normal oligodendrocytes, endothelial cells, pericytes, and T cells. **(H)** Composition ratio of cell types in individual GBM. See also **Supplementary Figure 1**.

cells (**Supplementary Figure 1A**). The majority of cells were malignant tumor cells and TAMs (**Figure 1H**).

Next, we performed ssGSEA with the gene meta-modules (5) and identified the six cellular states, namely, AC-like, MES1-like, MES2-like, OPC-like, NPC1-like, and NPC2-like states. We found that nearly 72% of malignant cells can be successfully annotated to one of the six specific cellular states with p-value < 0.05 (**Figure 2A** and **Supplementary Figure 2B**; **Supplementary Table 3**), whereas 28% of cells had gene signatures associated with multiple cellular states, suggesting the existence of a developmental lineage continuum within the tumor cell compartment. To correlate the transcriptional cellular states to TCGA GBM subtypes defined by genomic alterations, we also performed the ssGSEA analysis with the gene signatures of the TCGA GBM genomic subtype. Our results revealed that AC-like cells were correlated to TCGA-classical subtype (**Figure 2B**) with higher expression of *EGFR* (**Figure 2C**). MES-like cells were enriched for the TCGA-mesenchymal subtype (**Figure 2B**). We observed that the tumors in patients 1, 2, and 4 with a higher percentage of MES-like cells also contained a higher proportion of TAMs (**Figures 2D, E**). Thus, as shown in the TCGA-mesenchymal subtype data, MES-like cells were correlated with infiltrating TAMs (**Figure 2F**). However, no significant difference was observed between OPC-like and NPC-like states in the enrichment score between the TCGA-neural subtype and TCGA-proneural subtype (**Figure 2B**), indicating an overlap of TCGA-proneural and TCGA-neural subtypes at the transcriptional level.

Developmental Trajectory, Lineage Analysis, and Cells of GBM Origin

In order to explore the developmental lineages of the six cellular states of GBM tumor cells, we used RNA Velocity to construct the trajectory (26). All tumor cells from 7 patients were integrated together to construct the developmental trajectory because not all patients contained all the six cellular states (**Figure 2D**). Apart from the six cellular states, GBM stem cells were annotated individually (**Figure 2A**), which can also help us to confirm the root cell of origin. In the RNA Velocity lineages, we found that NPC2-like cells and GBM stem-like cells were at

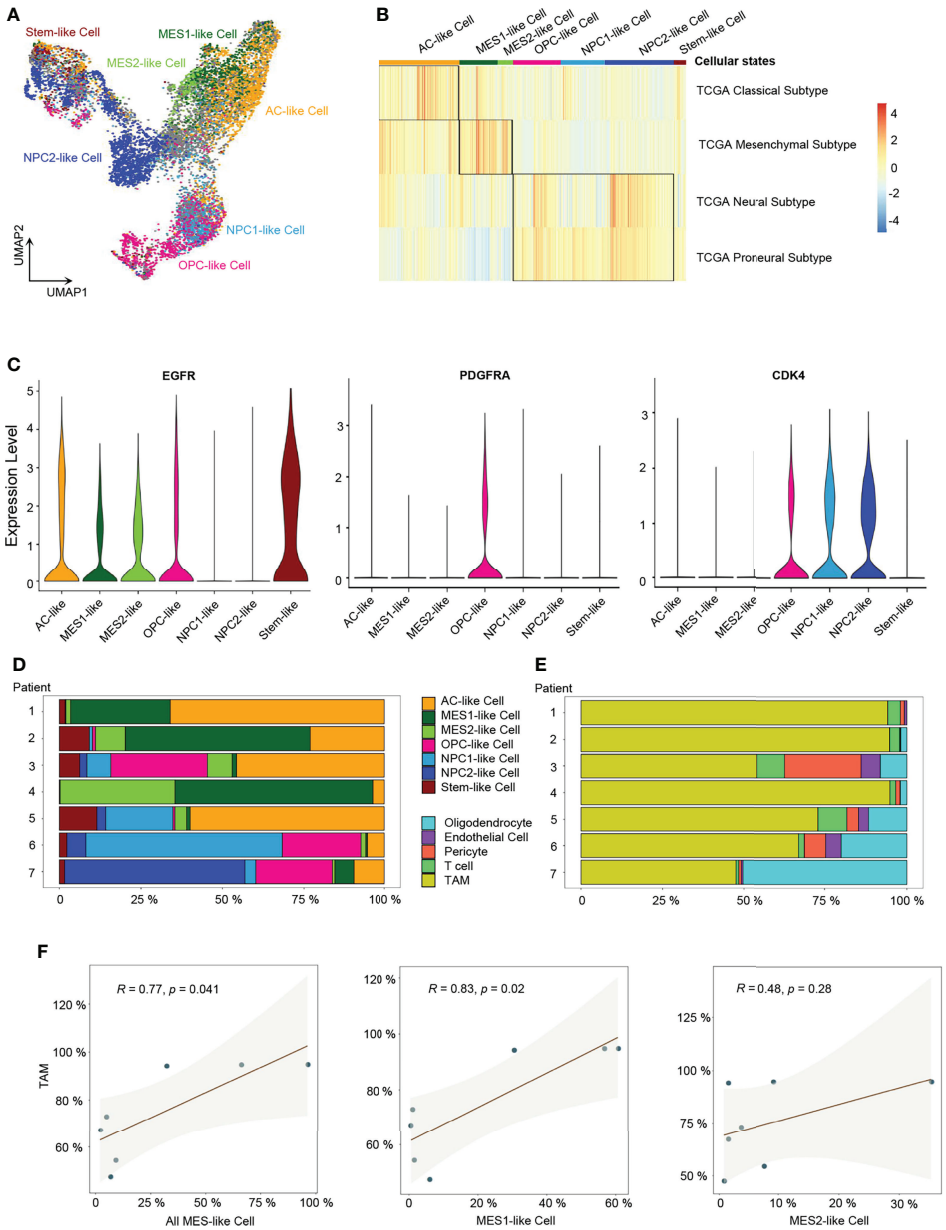

FIGURE 2 | Identification of six GBM tumor cell cellular states. **(A)** UMAP projection of the six GBM tumor cell cellular states and stem-like cells. **(B)** Heatmap of the four GBM TCGA transcription subtype scores. **(C)** Violin plot of *EGFR*, *PDGFRA*, and *CDK4* expression level in different cellular states. **(D)** Composition ratio of the six cellular states in tumor cells. **(E)** Composition ratio of stromal cells in non-tumor cells. **(F)** Correlation between the number of MES-like cells and TAMs. See also **Supplementary Figure 2** and **Supplementary Table 3**.

the root of the developmental tree, which implied that NPC2-like tumor cells could be the cells of origin among all six cellular states in GBM (**Figure 3A** and **Supplementary Figure 3**). Next, we analyzed the transcription factor (TF)-mediated gene regulatory networks using regulon, a gene set that is regulated as a unit, in the NPC2-like cells (**Figure 3B**). Some of these top activated TFs were related to cell cycle (e.g., *E2F1*, *E2F2*, *MYBL2*, and *YBX1*) (27); cell fate determination, proliferation, and differentiation (e.g., *BHLHE22*, *HDAC2*, *NEUROD1*, and *NPDC1*) (28); nervous system development (*POU3F3*); and proneural-stem marker (*EZH2*) (29). This implied that NPC2-like tumor cells were in the proliferative state and could be the cells of origin in the tumor cell lineages. Then, we further conducted enrichment analysis of cancer-related gene sets, and these results were consistent with the former finding that NPC2-like GBM cells were in cell cycle (**Figures 3C, D**). Every cellular activity requires energy, and if one cell is in proliferation and cell cycle, it needs more energy than the quiescent cell. Thus, we

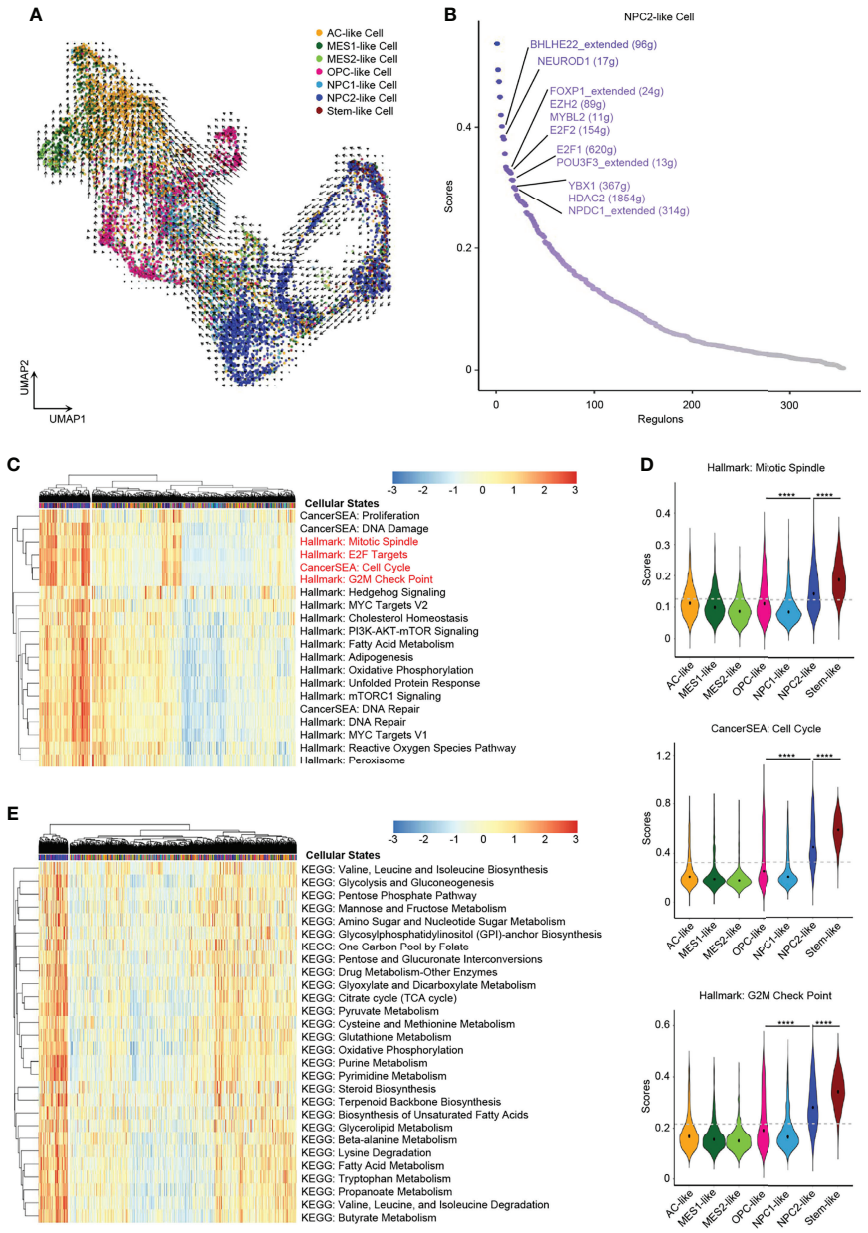

FIGURE 3 | NPC2-like cells, the original root cell of GBM. **(A)** Inferred developmental trajectory of the six GBM tumor cell cellular states by RNA velocity, which implied that the NPC2-like cells, like stem-like cells, were the root cell of the developmental trajectory. **(B)** The activated regulons ranked by regulon specificity score from high to low in the NPC2-like cells. **(C)** Heatmap of cancer-specific gene sets in the six cellular states and stem-like cells. **(D)** Violin plot of the Mitotic Spindle, Cell Cycle, and G2M Check Point gene set scores in the six cellular states and stem-like cells. NPC2-like cells, like stem-like cells, were in the cell cycle. **(E)** Heatmap of metabolism gene sets in the six cellular states and stem-like cells. NPC2-like cells had a higher metabolism level than other cellular states. Gray dash line, average score; ****$p < 0.0001$. See also **Supplementary Figure 3** and **Supplementary Table 4**.

compared the metabolic level among the six cellular states and found that the NPC2-like cells had higher metabolic activities as compared to other tumor cell states, for example, with elevated citrate cycle (TCA cycle), oxidative phosphorylation, and fatty acid metabolism (**Figure 3E**). Thus, the NPC2-like cells in proliferative state with high metabolic activity could be the cells of origin in the developmental trajectory of human GBM.

Subtype-Specific Immune Mediators and Hypoxia-Response Tumor Cells

Although recent single-cell studies determined that GBMs consist of diverse cellular states, we still do not know how different tumor cellular states differentially affect the TME and the potential impact on the prognosis of GBM patients. Herein, we conducted a cancer subtype-specific gene set enrichment

analysis and found that MES1-like and MES2-like tumor cells were associated with the hypoxia niche (**Figures 4A, D**). Another characteristic of MES-like cells was the induction of immune mediators, including activation of *IL2/STAT5* Signaling, *TNFA* Signaling *via NFKB*, *IL6/JAK/STAT3* Signaling, Interferon-α Response, and Interferon-β Response. Furthermore, MES1-like and MES2-like tumor cells had high expression levels of immune factors (**Figure 4B**) (e.g., *CSF1*, *CCL2*, *CXCL2*, *CXCL3*, *CXCL8*, *CXCL14*, *IFITM3*, *IFI6*, *IFI27*, *IL1B*, *IL1RAP*, *IL6ST*, *IL13RA2*, and *IL32*), which play important roles in the formation of an immunosuppressive TME (21). This was consistent with the former result that the MES-like cells were correlated with infiltrating TAMs, which can promote the immunosuppressive environment and tumor progression. Although the MES-like cells were in quiescence state, non-cycling, they were associated with an invasion-promoting microenvironment with elevated *TGF-β* signaling activation and epithelial–mesenchymal transition (EMT) (**Figures 4A, C, E**). These results suggested that MES1-like and MES2-like cellular state cells were the GBM tumor cells that produce soluble mediators to modulate the TME and potentially lead to poor prognosis.

Then, we constructed the regulon networks in MES1-like and MES2-like state cells. Although both *HIF1A* and *EPAS1* genes were upregulated in MES1-like and MES2-like tumor cells (**Figure 4C**), only *EPAS1* regulon (not *HIF1A* regulon) was activated in both MES1-like and MES2-like cells among the top activated regulons (**Figures 4F, G**). While cells respond to chronic hypoxia *via* the *EPAS1* pathway, the *HIF1A* pathway is activated when an acute decrease of oxygen level (30). These results suggested that MES-like tumor cells were in a chronic hypoxia environment. *STAT3* is one of the major mediators of tumor-induced immunosuppression and was activated in MES-like state tumor cells, and *NFKB1*, an inflammatory regulon, was also upregulated in MES-like cells. Therefore, these cells were likely related to an immunosuppressive microenvironment. Other top activated regulons, such as *RELB* and *RUNX1*, are oncogenic drivers of mesenchymal GBM subtype and contributed to EMT *via* the *TGF-β* pathway (31, 32). Results of enrichment analysis and regulon networks coincided in MES1-like and MES2-like cells, suggesting that it was MES-like cellular state tumor cells that gave rise to the TME known to be associated with poor clinical outcomes. This was confirmed by using public GBM datasets, TCGA and the CGGA (**Figures 4H, I**). GBM patients with a lower MES-like signature score had longer survival time than those with a higher score.

Heterogeneity of TAMs in GBM

While infiltrating macrophages and activated microglia are the primary immune cells that reside in and around the glioma TME, there is no clear distinction between them and it is still difficult to distinguish these two cell types due to their common myeloid lineage origin (10, 33). We noticed that TAMs expressed not only macrophage genes, but also microglia markers, and TAMs distributed together in the principal component analysis (PCA) reduction analysis based on the macrophage and microglia markers (**Supplementary Figures 5A–C**). Additionally, a significant correlation in the enrichment scores between macrophage and microglia marker genes in TAMs was uncovered (**Supplementary Figure 5D**). Therefore, we used TAMs, namely, tumor-associated macrophage/microglia, in our study, as these two immune cells are difficult to distinguish and are functionally similar in GBM. TAMs made up the majority of GBM stromal cells. We discovered an inconsistent expression pattern in malignant cells as well as TAMs from the heatmap of top DEGs (**Supplementary Figure 1B**), indicating that TAMs were also heterogeneous in nature and depended on GBM subtypes. Herein, we identified 4 TAM clusters with different expression patterns using clustering and reduction (**Figure 5A**) and TAMs were also shown from different individuals (**Figure 5B**). These TAM clusters had distinct transcriptional profiles and associated functions. TAM-0 cluster was related to cytokine production and lipoprotein metabolism with high expression levels of chemokines (e.g., *CCL3*, *CCL4*, *CCL3L1*, and *CCL4L2*) and lipoprotein receptors (e.g., *APOE*, *APOC1*, and *OLR1*) (**Supplementary Figures 5E, F**). *MKI67*+ TAMs, namely, the TAM-2 cluster, were in cell cycle, and overexpressed other cell cycle-related genes, such as *TOP2A*, *CENPF*, and *NUSAP1* (**Supplementary Figures 5E, F**). TAM-3 cluster had high expression levels of *RSAD2*, *IFIT1*, *IFIT2*, *IFIT3*, and *ISG15*, and could respond to interferon in GBM (**Supplementary Figures 5E, F**). The TAM-1 cluster, which responded to decreased oxygen levels in GBM, was also identified (**Figures 5C, H, I**), which is of particular interest. After revealing the heterogeneity in TAMs, we set out to investigate which types of these TAMs could affect the TME and potentially the survival of patients.

Hypoxia Niches and TAM-1 Signature in Prognosis

Firstly, we confirmed the existence of the TAM-1 cluster by scRNA-seq in mRNA level and using immunohistochemistry to verify the protein marker expression (*CD14+ERO1A+*) (**Figures 5D, E** and **Supplementary Figures 6**). We further compared the relationship between MES-like cellular state and different TAM clusters, because the quantity of MES-like tumor cells and all TAMs were positively correlated (**Figure 2F**). In particular, there was a significant association between MES-like cells and the TAM-1 cluster (**Figures 5F, G** and **Supplementary Figure 5G**), and they were both related to the GBM hypoxia niche. Thus, we speculated that the hypoxia-response TAMs, namely, the TAM-1 cluster, could associate with poor prognosis. By constructing the regulon networks in TAMs, we found that hypoxia-related regulons, *EPAS1* and *HIF1A*, were both activated in the TAM-1 cluster (**Figure 5J** and **Supplementary Table 5**), which differs from the hypoxia response in MES1-like and MES2-like tumor cells. This suggested that the GBM hypoxia niche could be divided into two conditions, namely, acute and chronic hypoxia microenvironments: MES-like tumor cells were only in the chronic hypoxia niche, while TAM-1 distributed in both hypoxia niches. However, the TAM-1 cluster signature was also enriched in the process of invasion and extracellular matrix organization (**Figure 5H** and **Supplementary Figure 5H**). Thus, TAM-1 was involved in the hypoxia and progressively invasive niche as well. Ultimately, we checked the differential survival

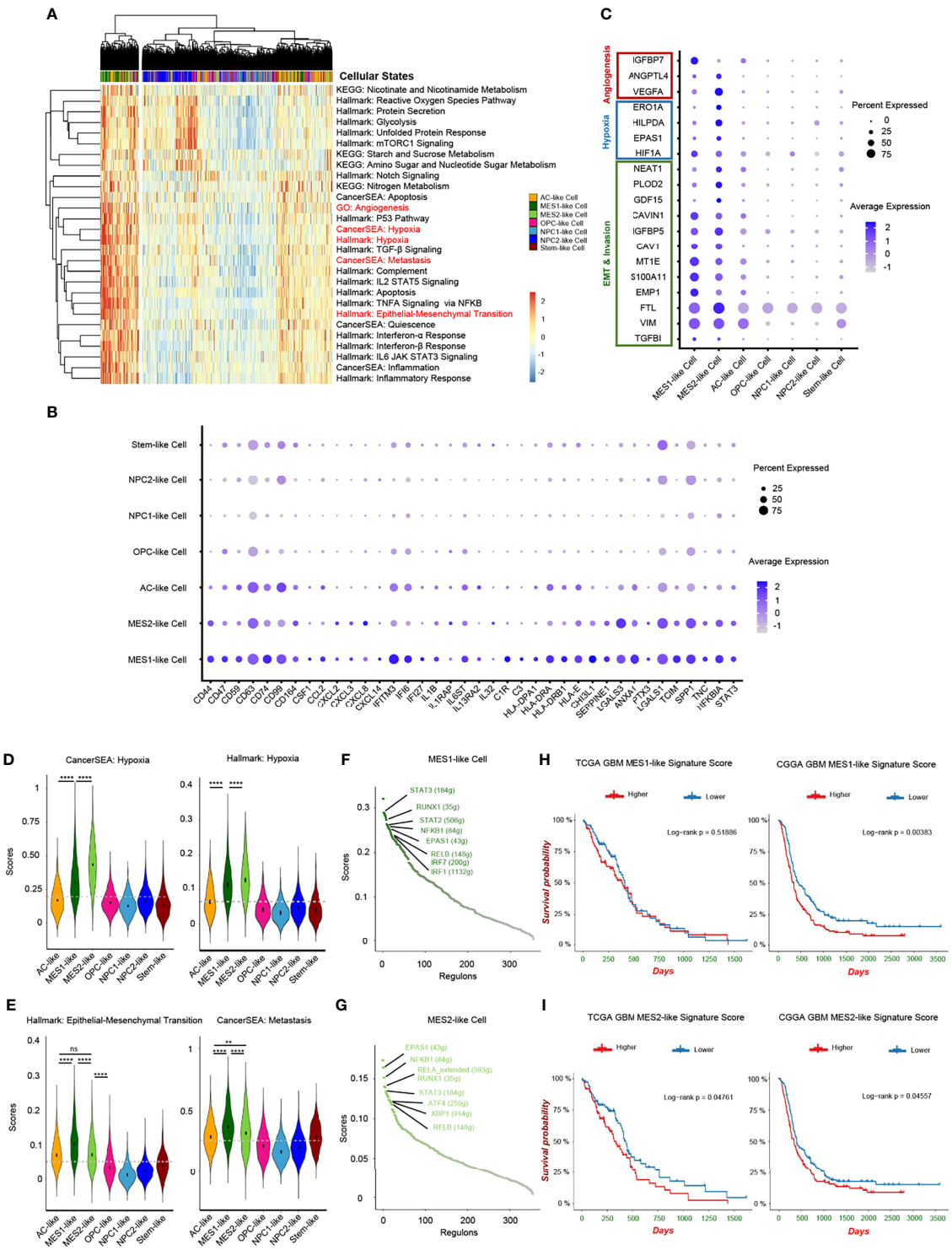

FIGURE 4 | Hypoxia-response tumor cells in GBM. **(A)** Heatmap of cancer-specific gene sets in the six cellular states and stem-like cells. **(B)** Upregulated immune gene pattern in MES1-like and MES2-like cells. **(C)** High expressed genes related to angiogenesis, hypoxia, and invasion in MES1-like and MES2-like cells. Violin plot of the hypoxia **(D)**, and epithelial–mesenchymal transition and metastasis **(E)** gene set scores in the six cellular states and stem-like cells. MES1-like and MES2-like cells were the hypoxia-response tumor cells in GBM. The activated regulons in the MES1-like **(F)** and MES2-like **(G)** cells ranked by regulon specificity score from high to low. Survival analysis of the MES1-like **(H)** and MES2-like **(I)** cell signatures in TCGA and CGGA GBM databases, respectively. Gray dash line, average score; ns, no significance; $^{**}p < 0.01$; $^{****}p < 0.0001$. See also **Supplementary Figure 4** and **Supplementary Table 4**.

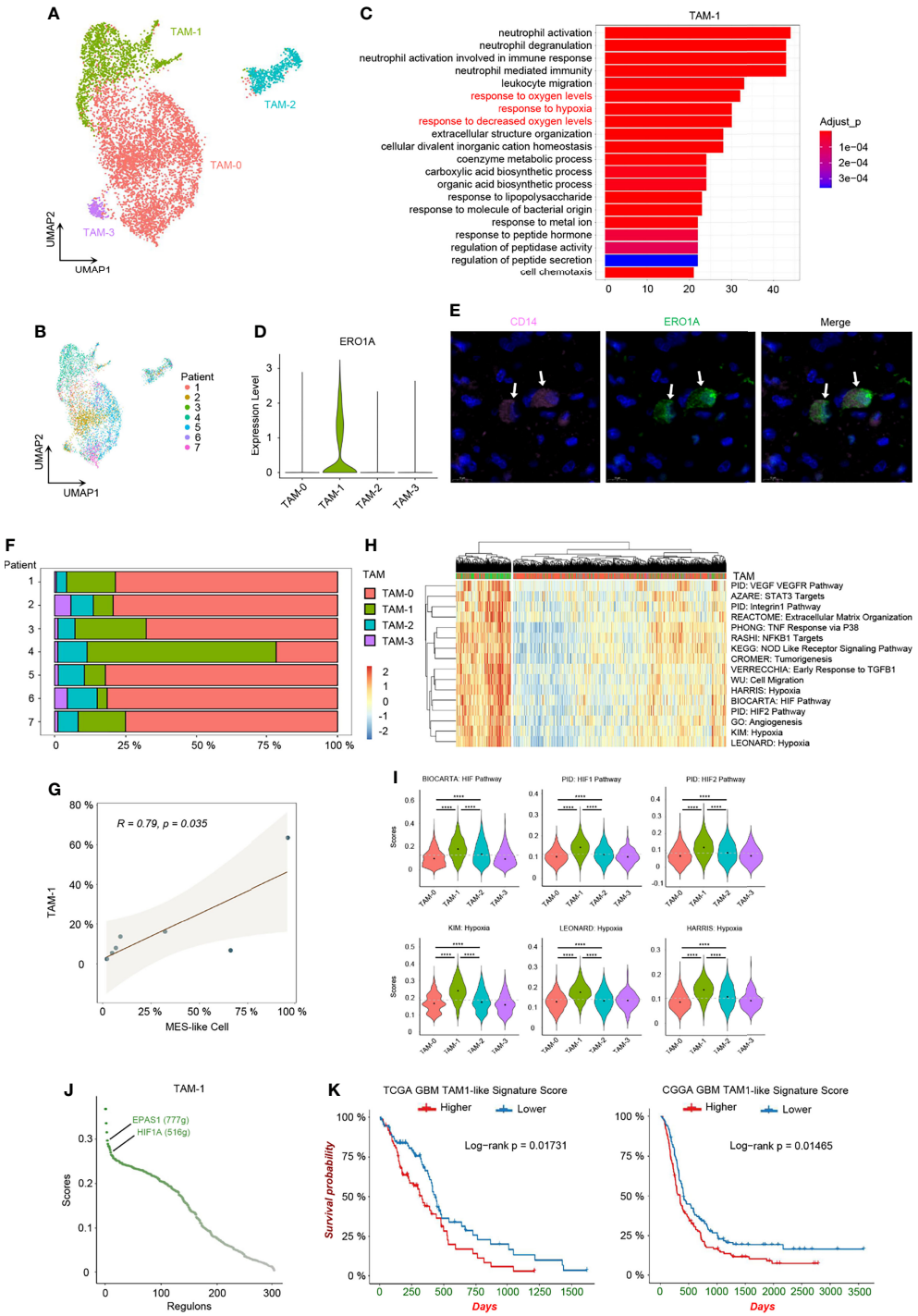

FIGURE 5 | Hypoxia-response TAMs in GBM. **(A)** UMAP visualization of TAMs. **(B)** UMAP visualization showing TAMs of individuals. **(C)** Top 20 function analysis results of TAM-1 cluster. Hypoxia-related biological processes were colored in red. **(D)** Violin plot of *ERO1A* expression level in different TAM clusters. **(E)** Immunofluorescence staining for TAM-1 cluster (*CD14+ERO1A+*) in patient tumor sample. The staining was performed for seven patients, one section each, and a representative image from patient 6 with TAM-1 pointed out by white arrows was shown; scale, 10 μm. The other images are shown in Supplementary **Supplementary Figure 6**. **(F)** Composition ratio of the TAM clusters in individual GBM. **(G)** Correlation between the number of MES-like and TAM-1 cells. **(H)** Heatmap of specific gene sets in TAMs. **(I)** Violin plot of the hypoxia gene set scores in TAMs. TAM-1 was the hypoxia-response cluster in TAMs. **(J)** The activated regulons in the TAM-1 cluster ranked by the regulon specificity score from high to low. **(K)** Survival analysis of the TAM-1 cluster signatures in TCGA and CGGA GBM databases, respectively. Gray dash line, average score; ****$p < 0.0001$. See also **Supplementary Figures 5** and **6**, and **Supplementary Tables 3** and **6**.

curves of patients in relation to different TAM clusters in the TCGA and CGGA GBM database (**Figure 5K** and **Supplementary Figures 5I–K**). We observed that it was the TAM-1 cluster that is mostly significantly associated with poor prognosis. Patients with a lower TAM-1 signature score had a longer survival time than those with a higher score.

Hypoxia-Specific Inter-Cellular Communication and Angiogenesis

We identified a hypoxia-specific intercellular communication network and the potential impact on promoting angiogenesis. Firstly, we identified significant ligand–receptor interactions between different cell types using CellChat (34). Then, we inferred cell–cell communication at a signaling pathway level from ligand–receptor pairs (**Supplementary Figures 7A, B**). Finally, these cell–cell communication signaling pathways were clustered to generate the cell–cell specific communication pattern (**Figure 6A** and **Supplementary Figure 7C**).

Pattern 5 was revealed to be specific to these GBM hypoxia-response cells, namely, MES1-like tumor cells, MES2-like tumor cells, and TAM-1; the remaining immune cells were grouped in pattern 1, and the remaining tumor cellular states were clustered together in pattern 2 (**Figure 6A**). As the communication pattern from endothelial cells to other cell types was similar to pericytes, they were in the same group, pattern 3 (**Figure 6A**). Oligodendrocyte was the only normal glial-lineage cell type; thus, it was different from other GBM cell types in cellular communication pattern (**Figure 6A**). Because TAM-1 and MES-like cells were clustered in the same pattern, we further checked the purity of TAM-1 to rule out the possibility that TAM-1 was formed as doublets of tumor cells and TAMs even though the standard pipeline of DoubletFinder was taken into the data filtering process (35). Apart from the malignancy score (**Figure 1D**), we also constructed the CNVs in TAM-1 compared to oligodendrocytes without filtration of HLA genes. TAM-1 cells had amplification in chromosome 6, which reflected the TAMs with high expression of HLA genes, but no CNVs in chromosome 7 and 10 which was different from tumor cells (**Figures 1E**, **6B**). From these results, we confirmed the purity of the TAM-1 cluster. Next, we wanted to clarify the former finding from the cellular interaction perspective that GBM hypoxia-response cells contributed to the TME associated with poor survival of GBM patients. Pattern 5 included *CALCR*, *ANGPTL*, *GDF*, and *VEGF* pathways (**Figure 6C**). We further deciphered the significant ligand–receptor pairs in pattern 5, and the majority of these interactions were from source cells targeting endothelial cells (**Figure 6D**). In addition, we found that these ligands secreted by hypoxia-related GBM cell types, namely, MES1-like tumor cells, MES2-like tumor cells, and TAM-1, may stimulate angiogenesis *via*, for example, *ADM*, *ANGPTL4*, *GDF15*, and *VEGFA* (36–38). Then, we also explored the expression of *VEGF* pathway-related ligands, because *VEGFA* is the principal agonist during the formation of vasculature. We discovered that only MES1-like tumor cells, MES2-like tumor cells, and TAM-1 expressed the *VEGFA* in GBM (**Figure 6E**). These results indicated that hypoxia-dependent GBM cell types promoted angiogenesis (**Figures 4A**, **5H**, **6F**), because solid tumors are unable to grow beyond a couple of millimeters without neo-vascularization providing oxygen and nutrients to tumor cells. Extensive tumor angiogenesis and endothelial proliferation is a hallmark of GBM, and tumor vascularity is significantly correlated with poor survival (39). In short, hypoxia-specific cellular communication attributed in part to these hypoxia-response GBM cell types could induce poor outcomes in GBM patients.

Role of GBM Tumor Cells in TAM M2-Type Polarization

We found it hard to divide TAMs into the M1 or M2 phenotype. While TAMs had relatively higher enrichment score of M2-type TAM marker genes than M1-type TAM marker genes (**Figures 7A–D**), GBM TAMs still over-expressed some markers of M1-type TAMs, such as *TSPO*, *CD86*, and *IL1B* (**Supplementary Figure 8A**), which was consistent with literature (17). Considering that TAMs had mixed M1/M2 phenotypes, we took a method that predicts the ligand–target links from GBM tumor cells to TAMs based on scRNA-seq data (40). The expression of each TAM M2-type marker gene used in the analysis is listed in **Figure 7D** and **Supplementary Figure 8B**. We discovered that tumor cells from all six GBM cellular states secreted ligands, which may target TAM M2-type marker genes to induce activation (**Supplementary Figure 8C**). Thus, these TAMs would gradually shift to an M2-like phenotype and then may promote GBM progression. It was found that MES-like tumor cells had a higher number of promoting ligands than other cellular states (**Supplementary Figure 8C**), which also explained in part why MES-like tumor cells correlate with poor prognosis (**Figures 4H, I**). To clarify the cross-talk between different cellular states and TAMs, we linked the ligands secreted by the six cellular states of GBM and receptors of TAMs (**Figure 7E**). Because many ligand–receptor (L–R) pairs were speculated, we only chose the L–R networks that have been reported in literature and publicly available databases. We observed that ten L–R pairs may take part in the M2-type polarization of TAMs (**Figure 7F**).

One of these L–R pairs has been confirmed experimentally in human glioma. *CSF1* was reported for recruitment and polarization of TAMs in several cancers, and receptor inhibition of *CSF1* in GBM could block TAMs from M2-type polarization and inhibit tumor progression (12, 41). We found that only MES1-like tumor cells secreted *CSF1* that interacted with *CSF1R* on TAMs.

Some of the L–R axes have also been reported in other cancers. *ANXA1* is an immune-modulating protein that plays a central role in the anti-inflammatory and neuroprotection in brain (42). The *ANXA1–FPR2* axis between tumor cells and TAMs may enhance cancer cell growth and migration by promoting M2-type polarization of TAMs, and furthermore, the *ANXA1*-deficient breast cancer mouse model showed enhanced survival due to increased M1 TAMs within the tumor environment (43). However, *ANXA1–FPR1* and *ANXA1–FPR3* pairs (not *ANXA1–FPR2* pairs) were found to be involved in the polarization process in our results. AC-like and MES-like tumor cells expressed ligand

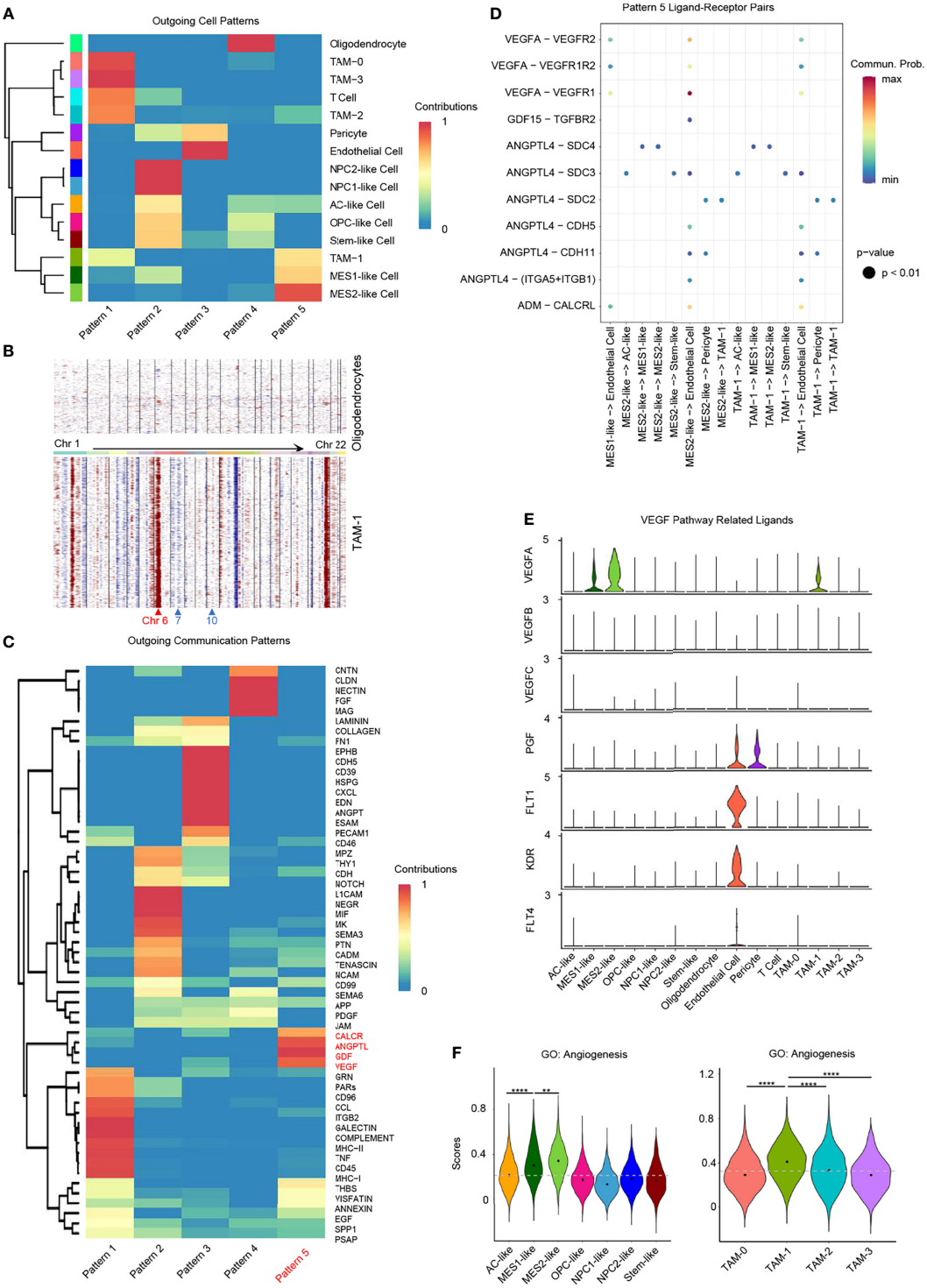

FIGURE 6 | Role of hypoxia-response cells in angiogenesis. **(A)** Cluster of GBM cell types according to the source cell functions in cell–cell communication. Hypoxia-response cell types, namely, MES1-like, MES2-like, and TAM-1 cells, were in the same pattern 5. **(B)** Compared to oligodendrocytes, TAM-1 cells presented with obvious CNVs in chromosome 6, but no CNVs in chromosomes 7 and 10. Red, amplification; blue, deletion. **(C)** Cell–cell communication-related pathways in different outgoing cell patterns. **(D)** Dot plot of outgoing cell pattern 5-related ligand–receptor pairs. **(E)** Violin plot of *VEGF* pathway-related ligand expression levels. **(F)** Violin plot of the angiogenesis gene set scores in GBM tumor cells and TAMs, respectively. Hypoxia-response cells, namely, MES1-like, MES2-like, and TAM-1 cells, had the highest score. Commun., communication; Prob., probability; gray dash line, average score; $^{**}p < 0.01$; $^{****}p < 0.0001$. See also **Supplementary Figure 7**.

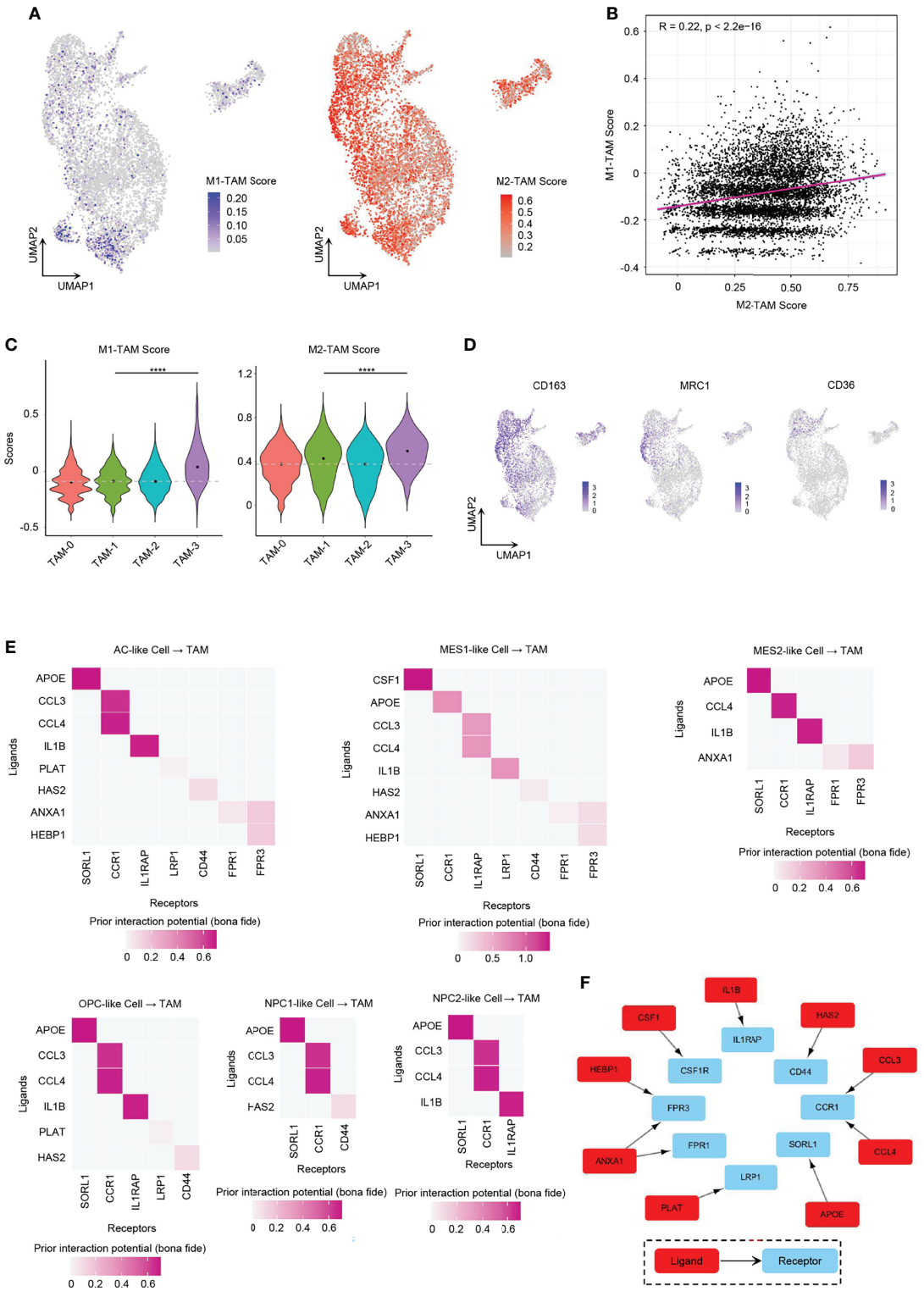

FIGURE 7 | Role of GBM tumor cells in promoting TAM M2-type polarization. **(A)** UMAP projection showed the M1-TAM score and M2-TAM score in TAMs. **(B)** Correlation between M1-TAM score and M2-TAM score in TAMs. **(C)** Violin plot of the M1-TAM score and M2-TAM score in different TAM clusters. **(D)** Expression levels of M2-TAM marker genes, namely, *CD163*, *MRC1*, and *CD36*, in TAMs. **(E)** Ligand–receptor pairs from different GBM tumor cellular state cells to TAMs took part in TAM M2-type polarization. **(F)** Ten L–R pairs, in total, could promote TAM M2-type polarization. Gray dash line, average score; ****$p < 0.0001$. See also **Supplementary Figure 8**.

ANXA1. Tumor cell-derived *IL1B* cross-talks with *IL1RAP* in TAMs could establish an immunosuppressive environment by activating M2 TAMs in pancreatic cancer, which required *NF-κB* activation (16). All tumor cells except NPC1-like cells expressed the ligand *IL1B*. Various tumor cell types produce *CCL4* that has been shown to promote colon cancer progression through inducing M2 TAM infiltration together with other chemokines such as *CCL3* (44). As *CCR1* exhibits nearly 100-fold lower affinity for *CCL4* than for *CCL3*, *CCR5* is the specific receptor for *CCL4* (45). However, in our analysis, it showed that both *CCL3* and *CLL4* interacted with *CCR1* (not *CCR5*) in human GBM. All six GBM cellular states expressed *CCL3* and *CCL4*. Tumor cell-associated hyaluronan (HA) and the associated extracellular matrix trigger TAM M2-like polarization *via* CD44 in breast cancer (46).

The remaining L–R signal pathways are documented in other diseases or have not been reported in M2 polarization. *APOE* can downregulate M1 phenotype macrophage markers and upregulate markers of anti-inflammatory M2 macrophages *via* surface *APOE* receptors in the development of atherosclerosis (47). Further experimental works still need to be done to confirm the role of *PLAT* and *HEBP1* in TAM polarization.

DISCUSSION

Genetic, epigenetic, and microenvironmental cues drive GBM heterogeneity, which remains one of the greatest barriers for therapy. Previous work uncovered that GBM tumor cells could be mapped to six dominant cellular states (AC-like, MES1-like, MES2-like, OPC-like, NPC1-like, and NPC2-like) with specific gene expression signatures (5). Our work further explored the correlation of six transcriptional cellular states to GBM TCGA subtypes, developmental lineages, regulon networks, and cell–cell communication with stromal cells, which can link single-cell transcriptional states to GBM genotypes, improving our understanding of intratumor heterogeneity and the differential roles of tumor subtypes in shaping TME. Although previous studies have focused on malignant cells in GBM (8, 9), it is believed that stromal cells including immune and vascular cells also play essential roles in tumor development and progression. All these cell types were included in our study, allowing us to explore cell-to-cell communications between GBM tumor cells and stromal cells in a subtype-specific manner. Our results provided the first systematic portrait at the single-cell level of the differential roles of six GBM cellular states, dissected the heterogeneity of TAM, and revealed the unique mechanisms in driving M2-type polarization of TAMs.

In 2010, TCGA classified GBM into four genotypes based on genetic alterations, but the transcriptomic profiles from each subtype were also obtained by bulk RNA sequencing (3). Xiao assigned human GBM scRNA-seq data to four TCGA GBM subtypes, but only 33% of tumor cells were annotated (48). In our study, we were able to identify 72% of GBM tumor cells that could be successfully annotated to unique GBM cellular states. The improvement of subtype-specific annotation may be affected by technical issues such as high dropout rates in scRNA-seq as well as the intrinsic heterogeneity within the continuum of tumor cell lineage differentiation trajectories. As reported, functional gene set enrichment analysis of MES-like cells is related to VERHAAK_GLIOBLASTOMA_MESENCHYMAL; enrichment analysis of OPC-like cells and NPC-like cells is related to VERHAAK_GLIOBLASTOMA_PRONEURAL (5). Our results also confirmed that MES1-like and MES2-like cells correlated with the TCGA-mesenchymal subtype, and OPC-like, NPC1-like, and NPC2-like cells were related to TCGA-proneural subtypes. Furthermore, we found that AC-like tumor cells were similar to the TCGA-classical subtype and expressed high levels of *EGFR*. Recently, researchers suggested the removal of the TCGA-neural subtype due to its overlap with the TCGA-proneural subtype (4, 23), and this overlap was also reflected in the overlapping relationship with OPC-like, NPC1-like, and NPC2-like cells in our study. We observed that individual GBM samples contained at least three cellular states and their own unique CNV subclone groups, suggesting a high degree of intratumor and inter-tumor heterogeneity of GBM.

Previous studies on the origin of glioma cells indicated that neural progenitor cells, oligodendrocyte progenitor cells, and astrocytes, upon pathological insult, all have the ability to induce tumorigenesis (49); Neftel and colleagues demonstrated GBM cellular transition by comparing the cellular composition of the GBM mouse PDX model (5). Through developmental trajectory analysis using RNA velocity in our study, NPC2-like state cells developed into other tumor cellular states. Many upregulated regulons in NPC2-like cells are correlated with cell cycle and proliferation (e.g., *E2F1*, *E2F2*, *MYBL2*, *YBX1*, *BHLHE22*, *HDAC2*, *NEUROD1*, *NPDC1*, and *POU3F3*). Because tumor cell proliferation and invasion are stochastically mutually exclusive events—actively proliferating cells tend to be stationary, while rapidly migrating tumor cells divide more slowly, namely, the "Go-or-Grow" hypothesis (50), we also discovered activated regulons suppressing glioma cell invasion and migration (e.g., *FOXP1*) (**Figure 3B**). Furthermore, the NPC2-like tumor cells had higher metabolic activities than other tumor cellular states. Therefore, NPC2-like state cells were in the proliferating state and functioned as GBM progenitor cells, which could be a potential therapeutic target.

GBM is the most aggressive malignant brain tumor with bleak prognosis, and it contains numerous cell types. However, we still know little about which cell type may cause the poor clinical outcome of GBM patients. The gene signature of blood-derived TAMs, but not microglial TAMs, correlates with significantly inferior survival in low-grade glioma (17). Our work was the first to reveal the hypoxia-response TAMs and tumor cells in GBM strongly associated with poor prognosis. We further uncovered the chronic and acute GBM hypoxia niches that were not only related to EMT and invasion microenvironment but also involved in promoting angiogenesis. This may be one of the reasons for driving GBM progression.

TAMs are the major players in TME and are broadly divided into two phenotypes: classical M1 type involved in inflammatory response and antitumor immunity, and alternatively activated

M2 type, which elicits an anti-inflammatory response and pro-tumorigenic properties (18). TAMs can shift to M2 phenotypes in response to various microenvironmental signals secreted by malignant tumor cells and stromal cells, which results in progression of tumors and poor prognosis of patients. Our work portrayed the landscape of potential ligand–receptor cross-talk pathways between GBM tumor cells and TAMs. Although MES-like tumor cells had the most ligands in promoting TAM M2 polarization and NPC-like malignant cells expressed the least relevant ligands, all GBM cellular states could participate in TAM M2-type polarization. The majority of all ten L–R pairs we identified were consistent with that reported previously in glioma and other cancers, and the remaining ones need further experimental verification. However, these findings provided new strategies to target tumor-induced M2 polarization for potential therapy.

In summary, our results revealed that NPC2-like tumor cells were in a proliferative and high energy-consumption state and could be the origin of cells in human GBM. We identified the hypoxia-response GBM cell subset, consisting of MES1-like and MES2-like tumor cells, and hypoxia-response TAMs, which were associated with worse prognosis in GBM patients through promoting invasion and angiogenesis. This study delineated the landscape of potential ligand–receptor pathways in TAM M2-like polarization, which may lead to the proposal of new strategies for the treatment of GBM.

DATA AVAILABILITY STATEMENT

The datasets presented in this study can be found in online repositories. The names of the repository/repositories and accession number(s) can be found at: https://www.ncbi.nlm.nih.gov/geo/, GSE135045.

ETHICS STATEMENT

The studies involving human participants were reviewed and approved by the Institutional Review Board at the Nanjing Brain Hospital Affiliated to Nanjing Medical University. The patients/participants provided their written informed consent to participate in this study.

AUTHOR CONTRIBUTIONS

YoX, HL, HX, and RF designed the project. KY, CQ, XH, YL, LG, and YZ prepared the tumor tissue for scRNA-seq. YoX, ZW, MZ, and XT conducted the scRNA-seq experiments. YoX analyzed the data. YoX, YD, MY, GS, and YaX wrote the original draft. RF reviewed and edited the manuscript. HL provided the research funding. All authors contributed to the article and approved the submitted version.

FUNDING

The research work was supported by grants from the National Natural Science Foundation of China (81972350 and 81902535), the Jiangsu Science and Education Strengthening Engineering Innovation Team Project (CXTDA2017050), the Medical Research Foundation of Jiangsu Health Commission (H2019059), and the Medical Science and Technology Development Foundation of Nanjing (ZDX16011). YoX as a visiting student researcher who received tuition support for a year from Prof. Fan's unrestricted faculty support funds (RF).

ACKNOWLEDGMENTS

We thank Prof. Peter A. Sims for help in data analysis of distinguishing malignant cells from non-tumor cells based on copy number variations.

SUPPLEMENTARY MATERIAL

The Supplementary Material for this article can be found online at: https://www.frontiersin.org/articles/10.3389/fimmu.2022.914236/full#supplementary-material

Supplementary Figure 1 | Cell type Annotation.

Supplementary Figure 2 | Correlations between GBM Cellular States and TCGA Subtypes.

Supplementary Figure 3 | Developmental Trajectory of GBM Tumor Cells.

Supplementary Figure 4 | Survival Analysis of GBM Cellular State Signatures.

Supplementary Figure 5 | Heterogeneity of TAMs.

Supplementary Figure 6 | Immunofluorescence staining for TAM-1 cluster (*CD14+ERO1A+*) in GBM.

Supplementary Figure 7 | Cell-cell Communications in GBM.

Supplementary Figure 8 | TAMs M2-type Polarization.

Supplementary Table 1 | Patient Information.

Supplementary Table 2 | Evaluation of scRNA-seq Data Quality.

Supplementary Table 3 | GBM Cellular States and Cell Type Constitutions.

Supplementary Table 4 | Top20 Regulons in Cellular States.

Supplementary Table 5 | Top20 Regulons in TAMs.

Supplementary Table 6 | DEG signatures of TAMs.

Supplementary Table 7 | Antibodies used in this study.

REFERENCES

1. Dagogo-Jack I, Shaw AT. Tumour Heterogeneity and Resistance to Cancer Therapies. *Nat Rev Clin Oncol* (2018) 15(2):81–94. doi: 10.1038/nrclinonc.2017.166
2. Tirosh I, Suva ML. Dissecting Human Gliomas by Single-Cell Rna Sequencing. *Neuro Oncol* (2018) 20(1):37–43. doi: 10.1093/neuonc/nox126
3. Verhaak RG, Hoadley KA, Purdom E, Wang V, Qi Y, Wilkerson MD, et al. Integrated Genomic Analysis Identifies Clinically Relevant Subtypes of Glioblastoma Characterized by Abnormalities in Pdgfra, Idh1, Egfr, and Nf1. *Cancer Cell* (2010) 17(1):98–110. doi: 10.1016/j.ccr.2009.12.020
4. Wang Q, Hu B, Hu X, Kim H, Squatrito M, Scarpace L, et al. Tumor Evolution of Glioma-Intrinsic Gene Expression Subtypes Associates With Immunological Changes in the Microenvironment. *Cancer Cell* (2018) 33 (1):152. doi: 10.1016/j.ccell.2017.12.012
5. Neftel C, Laffy J, Filbin MG, Hara T, Shore ME, Rahme GJ, et al. An Integrative Model of Cellular States, Plasticity, and Genetics for Glioblastoma. *Cell* (2019) 178(4):835–49.e21. doi: 10.1016/j.cell.2019.06.024
6. Choi H, Sheng J, Gao D, Li F, Durrans A, Ryu S, et al. Transcriptome Analysis of Individual Stromal Cell Populations Identifies Stroma-Tumor Crosstalk in Mouse Lung Cancer Model. *Cell Rep* (2015) 10(7):1187–201. doi: 10.1016/j.celrep.2015.01.040
7. Kumar MP, Du J, Lagoudas G, Jiao Y, Sawyer A, Drummond DC, et al. Analysis of Single-Cell Rna-Seq Identifies Cell-Cell Communication Associated With Tumor Characteristics. *Cell Rep* (2018) 25(6):1458–68.e4. doi: 10.1016/j.celrep.2018.10.047
8. Richards LM, Whitley OKN, MacLeod G, Cavalli FMG, Coutinho FJ, Jaramillo JE, et al. Gradient of Developmental and Injury Response Transcriptional States Defines Functional Vulnerabilities Underpinning Glioblastoma Heterogeneity. *Nat Cancer* (2021) 2(2):157–73. doi: 10.1038/s43018-020-00154-9
9. Couturier CP, Ayyadhury S, Le PU, Nadaf J, Monlong J, Riva G, et al. Single-Cell Rna-Seq Reveals That Glioblastoma Recapitulates a Normal Neurodevelopmental Hierarchy. *Nat Commun* (2020) 11(1):3406. doi: 10.1038/s41467-020-17186-5
10. Yuan J, Levitin HM, Frattini V, Bush EC, Boyett DM, Samanamud J, et al. Single-Cell Transcriptome Analysis of Lineage Diversity in High-Grade Glioma. *Genome Med* (2018) 10(1):57. doi: 10.1186/s13073-018-0567-9
11. Ellert-Miklaszewska A, Wisniewski P, Kijewska M, Gajdanowicz P, Pszczolkowska D, Przanowski P, et al. Tumour-Processed Osteopontin and Lactadherin Drive the Protumorigenic Reprogramming of Microglia and Glioma Progression. *Oncogene* (2016) 35(50):6366–77. doi: 10.1038/onc.2016.55
12. Stafford JH, Hirai T, Deng L, Chernikova SB, Urata K, West BL, et al. Colony Stimulating Factor 1 Receptor Inhibition Delays Recurrence of Glioblastoma After Radiation by Altering Myeloid Cell Recruitment and Polarization. *Neuro Oncol* (2016) 18(6):797–806. doi: 10.1093/neuonc/nov272
13. Ochocka N, Segit P, Walentynowicz KA, Wojnicki K, Cyranowski S, Swatler J, et al. Single-Cell Rna Sequencing Reveals Functional Heterogeneity of Glioma-Associated Brain Macrophages. *Nat Commun* (2021) 12(1):1151. doi: 10.1038/s41467-021-21407-w
14. Friebel E, Kapolou K, Unger S, Nunez NG, Utz S, Rushing EJ, et al. Single-Cell Mapping of Human Brain Cancer Reveals Tumor-Specific Instruction of Tissue-Invading Leukocytes. *Cell* (2020) 181(7):1626–42.e20. doi: 10.1016/j.cell.2020.04.055
15. Klemm F, Maas RR, Bowman RL, Kornete M, Soukup K, Nassiri S, et al. Interrogation of the Microenvironmental Landscape in Brain Tumors Reveals Disease-Specific Alterations of Immune Cells. *Cell* (2020) 181(7):1643–60.e17. doi: 10.1016/j.cell.2020.05.007
16. Das S, Shapiro B, Vucic EA, Vogt S, Bar-Sagi D. Tumor Cell-Derived Il1beta Promotes Desmoplasia and Immune Suppression in Pancreatic Cancer. *Cancer Res* (2020) 80(5):1088–101. doi: 10.1158/0008-5472.CAN-19-2080
17. Muller S, Kohanbash G, Liu SJ, Alvarado B, Carrera D, Bhaduri A, et al. Single-Cell Profiling of Human Gliomas Reveals Macrophage Ontogeny as a Basis for Regional Differences in Macrophage Activation in the Tumor Microenvironment. *Genome Biol* (2017) 18(1):234. doi: 10.1186/s13059-017-1362-4
18. Roesch S, Rapp C, Dettling S, Herold-Mende C. When Immune Cells Turn Bad-Tumor-Associated Microglia/Macrophages in Glioma. *Int J Mol Sci* (2018) 19(2):1–20. doi: 10.3390/ijms19020436
19. Zhang J, Guan M, Wang Q, Zhang J, Zhou T, Sun X. Single-Cell Transcriptome-Based Multilayer Network Biomarker for Predicting Prognosis and Therapeutic Response of Gliomas. *Brief Bioinform* (2019) 21:1–18. doi: 10.1093/bib/bbz040
20. Yuan D, Tao Y, Chen G, Shi T. Systematic Expression Analysis of Ligand-Receptor Pairs Reveals Important Cell-To-Cell Interactions Inside Glioma. *Cell Commun Signal* (2019) 17(1):48. doi: 10.1186/s12964-019-0363-1
21. Hambardzumyan D, Gutmann DH, Kettenmann H. The Role of Microglia and Macrophages in Glioma Maintenance and Progression. *Nat Neurosci* (2016) 19(1):20–7. doi: 10.1038/nn.4185
22. Filbin MG, Tirosh I, Hovestadt V, Shaw ML, Escalante LE, Mathewson ND, et al. Developmental and Oncogenic Programs in H3k27m Gliomas Dissected by Single-Cell Rna-Seq. *Science* (2018) 360(6386):331–5. doi: 10.1126/science.aao4750
23. Patel AP, Tirosh I, Trombetta JJ, Shalek AK, Gillespie SM, Wakimoto H, et al. Single-Cell Rna-Seq Highlights Intratumoral Heterogeneity in Primary Glioblastoma. *Science* (2014) 344(6190):1396–401. doi: 10.1126/science.1254257
24. Darmanis S, Sloan SA, Croote D, Mignardi M, Chernikova S, Samghababi P, et al. Single-Cell Rna-Seq Analysis of Infiltrating Neoplastic Cells at the Migrating Front of Human Glioblastoma. *Cell Rep* (2017) 21(5):1399–410. doi: 10.1016/j.celrep.2017.10.030
25. Cheng YK, Beroukhim R, Levine RL, Mellinghoff IK, Holland EC, Michor F. A Mathematical Methodology for Determining the Temporal Order of Pathway Alterations Arising During Gliomagenesis. *PloS Comput Biol* (2012) 8(1): e1002337. doi: 10.1371/journal.pcbi.1002337
26. La Manno G, Soldatov R, Zeisel A, Braun E, Hochgerner H, Petukhov V, et al. Rna Velocity of Single Cells. *Nature* (2018) 560(7719):494–8. doi: 10.1038/s41586-018-0414-6
27. Zhang X, Lv QL, Huang YT, Zhang LH, Zhou HH. Akt/Foxm1 Signaling Pathway-Mediated Upregulation of Mybl2 Promotes Progression of Human Glioma. *J Exp Clin Cancer Res* (2017) 36(1):105. doi: 10.1186/s13046-017-0573-6
28. Dennis DJ, Han S, Schuurmans C. Bhlh Transcription Factors in Neural Development, Disease, and Reprogramming. *Brain Res* (2019) 1705:48–65. doi: 10.1016/j.brainres.2018.03.013
29. Jin X, Kim LJY, Wu Q, Wallace LC, Prager BC, Sanvoranart T, et al. Targeting Glioma Stem Cells Through Combined Bmi1 and Ezh2 Inhibition. *Nat Med* (2017) 23(11):1352–61. doi: 10.1038/nm.4415
30. Bronisz A, Salinska E, Chiocca EA, Godlewski J. Hypoxic Roadmap of Glioblastoma-Learning About Directions and Distances in the Brain Tumor Environment. *Cancers (Basel)* (2020) 12(5):1–12. doi: 10.3390/cancers12051213
31. Zhao K, Cui X, Wang Q, Fang C, Tan Y, Wang Y, et al. Runx1 Contributes to the Mesenchymal Subtype of Glioblastoma in a Tgfbeta Pathway-Dependent Manner. *Cell Death Dis* (2019) 10(12):877. doi: 10.1038/s41419-019-2108-x
32. Lee DW, Ramakrishnan D, Valenta J, Parney IF, Bayless KJ, Sitcheran R. The Nf-Kappab Relb Protein Is an Oncogenic Driver of Mesenchymal Glioma. *PloS One* (2013) 8(2):e57489. doi: 10.1371/journal.pone.0057489
33. Prionisti I, Buhler LH, Walker PR, Jolivet RB. Harnessing Microglia and Macrophages for the Treatment of Glioblastoma. *Front Pharmacol* (2019) 10:506. doi: 10.3389/fphar.2019.00506
34. Jin S, Guerrero-Juarez CF, Zhang L, Chang I, Ramos R, Kuan CH, et al. Inference and Analysis of Cell-Cell Communication Using Cellchat. *Nat Commun* (2021) 12(1):1088. doi: 10.1038/s41467-021-21246-9
35. McGinnis CS, Murrow LM, Gartner ZJ. Doubletfinder: Doublet Detection in Single-Cell Rna Sequencing Data Using Artificial Nearest Neighbors. *Cell Syst* (2019) 8(4):329–37.e4. doi: 10.1016/j.cels.2019.03.003
36. Chen L, Qiu JH, Zhang LL, Luo XD. Adrenomedullin Promotes Human Endothelial Cell Proliferation. *Via Hif-1alpha. Mol Cell Biochem* (2012) 365 (1-2):263–73. doi: 10.1007/s11010-012-1267-1
37. Fernandez-Hernando C, Suarez Y. Angptl4: A Multifunctional Protein Involved in Metabolism and Vascular Homeostasis. *Curr Opin Hematol* (2020) 27(3):206–13. doi: 10.1097/MOH.0000000000000580

38. Rochette L, Meloux A, Zeller M, Cottin Y, Vergely C. Functional Roles of Gdf15 in Modulating Microenvironment to Promote Carcinogenesis. *Biochim Biophys Acta Mol Basis Dis* (2020) 1866(8):165798. doi: 10.1016/j.bbadis.2020.165798
39. D'Alessio A, Proietti G, Sica G, Scicchitano BM. Pathological and Molecular Features of Glioblastoma and Its Peritumoral Tissue. *Cancers (Basel)* (2019) 11(4):1–39. doi: 10.3390/cancers11040469
40. Browaeys R, Saelens W, Saeys Y. Nichenet: Modeling Intercellular Communication by Linking Ligands to Target Genes. *Nat Methods* (2019) 17:1–11. doi: 10.1038/s41592-019-0667-5
41. Pyonteck SM, Akkari L, Schuhmacher AJ, Bowman RL, Sevenich L, Quail DF, et al. Csf-1r Inhibition Alters Macrophage Polarization and Blocks Glioma Progression. *Nat Med* (2013) 19(10):1264–72. doi: 10.1038/nm.3337
42. Gimenes AD, Andrade BFD, Pinotti JVP, Oliani SM, Galvis-Alonso OY, Gil CD. Annexin A1-Derived Peptide Ac2-26 in a Pilocarpine-Induced Status Epilepticus Model: Anti-Inflammatory and Neuroprotective Effects. *J Neuroinflamm* (2019) 16(1):32. doi: 10.1186/s12974-019-1414-7
43. Moraes LA, Kar S, Foo SL, Gu T, Toh YQ, Ampomah PB, et al. Annexin-A1 Enhances Breast Cancer Growth and Migration by Promoting Alternative Macrophage Polarization in the Tumour Microenvironment. *Sci Rep* (2017) 7(1):17925. doi: 10.1038/s41598-017-17622-5
44. De la Fuente Lopez M, Landskron G, Parada D, Dubois-Camacho K, Simian D, Martinez M, et al. The Relationship Between Chemokines Ccl2, Ccl3, and Ccl4 With the Tumor Microenvironment and Tumor-Associated Macrophage Markers in Colorectal Cancer. *Tumour Biol* (2018) 40(11):1010428318810059. doi: 10.1177/1010428318810059
45. Neote K, DiGregorio D, Mak JY, Horuk R, Schall TJ. Molecular Cloning, Functional Expression, and Signaling Characteristics of a C-C Chemokine Receptor. *Cell* (1993) 72(3):415–25. doi: 10.1016/0092-8674(93)90118-a
46. Witschen PM, Chaffee TS, Brady NJ, Huggins DN, Knutson TP, LaRue RS, et al. Tumor Cell Associated Hyaluronan-Cd44 Signaling Promotes Pro-Tumor Inflammation in Breast Cancer. *Cancers (Basel)* (2020) 12(5):1–23. doi: 10.3390/cancers12051325
47. Baitsch D, Bock HH, Engel T, Telgmann R, Muller-Tidow C, Varga G, et al. Apolipoprotein E Induces Antiinflammatory Phenotype in Macrophages. *Arterioscler Thromb Vasc Biol* (2011) 31(5):1160–8. doi: 10.1161/ATVBAHA.111.222745
48. Xiao Y, Kim D, Dura B, Zhang K, Yan R, Li H, et al. Ex Vivo Dynamics of Human Glioblastoma Cells in a Microvasculature-On-a-Chip System Correlates With Tumor Heterogeneity and Subtypes. *Adv Sci (Weinh)* (2019) 6(8):1801531. doi: 10.1002/advs.201801531
49. Lu QR, Qian L, Zhou X. Developmental Origins and Oncogenic Pathways in Malignant Brain Tumors. *Wiley Interdiscip Rev Dev Biol* (2019) 8:e342. doi: 10.1002/wdev.342
50. Mehta S, Lo Cascio C. Developmentally Regulated Signaling Pathways in Glioma Invasion. *Cell Mol Life Sci* (2018) 75(3):385–402. doi: 10.1007/s00018-017-2608-8

Conflict of Interest: RF is co-founder of IsoPlexis and Singleron Biotechnologies with financial interest.

The remaining authors declare that the research was conducted in the absence of any commercial or financial relationships that could be construed as a potential conflict of interest.

frontiers | Frontiers in Immunology

ORIGINAL RESEARCH
published: 23 May 2022
doi: 10.3389/fimmu.2022.903297

Identification of New Prognostic Markers and Therapeutic Targets for Non-Muscle Invasive Bladder Cancer: HER2 as a Potential Target Antigen

Han Kyu Chae[1], Wook Nam[1], Han Gwun Kim[1], Sharon Lim[2], Byeong-Joo Noh[2], So Won Kim[3], Gil Hyun Kang[2], Jong Yeon Park[1], Dae-Woon Eom[2] and Sung Jin Kim[1]**

[1] Department of Urology, Gangneung Asan Hospital, University of Ulsan College of Medicine, Gangneung, South Korea, [2] Department of Pathology, Gangneung Asan Hospital, University of Ulsan College of Medicine, Gangneung, South Korea, [3] Department of Parmacology, Asan Medical Center, University of Ulsan College of Medicine, Seoul, South Korea

OPEN ACCESS

Edited by:
Qihui Shi,
Fudan University, China

Reviewed by:
Jie Chen,
Shanghai Jiao Tong University, China
Yin Tang,
Institute for Systems Biology (ISB), United States

***Correspondence:**
Sung Jin Kim
bop1004@gmail.com
Dae-Woon Eom
edwjyh@gnah.co.kr

Specialty section:
This article was submitted to Cancer Immunity and Immunotherapy, a section of the journal Frontiers in Immunology

Received: 24 March 2022
Accepted: 25 April 2022
Published: 23 May 2022

Citation:
Chae HK, Nam W, Kim HG, Lim S, Noh B-J, Kim SW, Kang GH, Park JY, Eom D-W and Kim SJ (2022) Identification of New Prognostic Markers and Therapeutic Targets for Non-Muscle Invasive Bladder Cancer: HER2 as a Potential Target Antigen. Front. Immunol. 13:903297. doi: 10.3389/fimmu.2022.903297

Bacillus Calmette–Guérin (BCG) is the gold standard adjuvant treatment for non-muscle-invasive bladder cancer (NMIBC). However, given the current global shortage of BCG, new treatments are needed. We evaluated tumor microenvironment markers as potential BCG alternatives for NMIBC treatment. Programmed death-ligand 1, human epidermal growth factor receptor-2 (HER2), programmed cell death-1 (PD1), CD8, and Ki67 levels were measured in treatment-naïve NMIBC and MIBC patients (pTa, pT1, and pT2 stages). Univariate and multivariate Cox proportional hazard models were used to determine the impact of these markers and other clinicopathological factors on survival, recurrence, and progression. EP263, IM142, PD1, and Ki67 levels were the highest in the T2 stage, followed by the T1 and Ta stages. HER2 and IM263 expressions were higher in the T1 and T2 stages than in the Ta stage. In NMIBC, the significant prognostic factors for recurrence-free survival were adjuvant therapy, tumor grade, and HER2 positivity, whereas those for progression-free survival included age, T-stage, and IM263. Age, T-stage, EP263, PD1, CD8, and Ki67 levels were significant factors associated with overall survival. IM263 and HER2 are potential biomarkers for progression and recurrence, respectively. Therefore, we propose HER2 as a potential target antigen for intravesical therapeutics as a BCG alternative.

Keywords: HER2 (human epidermal growth factor receptor-2), PD-L1, PD1, CD8, ki67, ADC (antibody-drug conjugate), BCG (Bacillus Calmette–Guérin)

INTRODUCTION

Urothelial carcinoma (UC) is the ninth most common cancer with the thirteenth highest mortality rate among cancers worldwide (1). Of all diagnosed bladder cancers, approximately 75% are non-muscle-invasive bladder cancer (NMIBC), and the remaining are muscle-invasive bladder cancer (MIBC) (2). High-risk NMIBC patients require adjuvant intravesical therapy due to the risk of recurrence and progression to MIBC.

Intravesical Bacillus Calmette–Guérin (BCG) for UC, the first immunotherapeutic anti-cancer agent approved by the US Food and Drug Administration (FDA) (3), still remains the gold standard for adjuvant treatment of high-risk NMIBC patients. BCG therapy is challenging in terms of its ineffectiveness and adverse effects. Even among patients who respond well to initial BCG treatment, 10-20% of patients relapse and eventually progress to MIBC (4, 5). Since no other effective treatments are available, additional use of BCG is recommended in such cases based on each patient's situation, despite insufficient evidence of its effectiveness (6). Radical cystectomy is the only option for patients who fail to achieve remission after initial BCG therapy, which has high morbidity (2). Of the 15% of patients who discontinue treatment after first course of BCG treatment, 35% of them are known to have difficulty in continuing treatment due to side effects of bacterial or chemical cystitis, hematuria, and systemic febrile events (7). Globally, BCG shortage exists because the BCG strain (Connaught, Tice) is lacking (6). Research on reduction in dose and frequency of BCG treatment was also conducted; however, recurrence-related prognosis was reported to be inferior (8).Thus, developing an alternative therapy to BCG is necessary.

Recently, there have been several advancements in UC treatment, including immune checkpoint blockers (ICBs) (9, 10). Several clinical studies have evaluated the therapeutic efficacy of ICBs for high-risk NMIBC patients who have failed to respond to BCG therapy (11, 12). Enfortumab vedotin (EV), a novel antibody-drug conjugate (ADC) targeting nectin-4, was approved by the FDA as a therapeutic agent for metastatic UC (mUC) (13). Before the development of ADCs, human epidermal growth factor receptor-2 (HER2) received attention as a therapeutic target but was shown to be ineffective (14). Following the approval of monomethyl auristatin E (MMAE) as a cytotoxic agent in EV, RC48 has been used to develop a HER2-targeting ADC for the treatment of mUC (15). ADC's novel mechanism is the direct injection of cytotoxic drugs into cancer cells. After identifying a target antigen, there is an opportunity to develop an intravesical therapeutic agent for this identified target antigen by mediating ADCs (16).

At a time when new trends are emerging in the field of anticancer drugs, we are interested in studying the underestimated potential of known biomarkers. Therefore, this study aimed to evaluate changes in the expression of tumor microenvironment markers, such as programmed death-ligand 1 (PD-L1), HER2, programmed death-1 (PD1), CD8, and Ki67, in NMIBC patients during the initial course of the disease and compare them with the expressions in MIBC patients to study the effects of tumor microenvironment and clinicopathological factors on recurrence, progression, and overall prognosis in NMIBC.

MATERIALS AND METHODS

This retrospective study was approved by the Institutional Review Board of Gangneung Asan Hospital, Gangneung, Republic of Korea (approval number: 2018-05-017) according to the principles of the Declaration of Helsinki. The requirement for informed consent was waived due to the retrospective nature of the study.

Patients

Patients who had undergone transurethral resection of bladder tumor (TURB) between 2000 and 2013 (n=322, pTa: 131, pT1: 102, and pT2: 89) were screened for eligibility. We excluded 55 patients from 233 screened NMIBC patients (**Figure 1**). Exclusion criteria and the matched number of patients were as follows: 1) previous bladder cancer diagnosis (n=11); 2) incomplete medical history for initial bladder cancer (n=11); 3) inadequate follow-up for recurrence or progression (n=9); 4) clinically advanced bladder cancer that required invasive procedures (radical cystectomy, radiation therapy, and chemotherapy) (n=9); 5) pathological slides in which interpreting more than two microenvironmental markers after staining was difficult (n=15). Furthermore, we excluded 19 patients from 89 screened MIBC patients (**Figure 1**). Exclusion criteria and the matched number of patients were as follows: 1) pathologically, the bladder cancer was not a urothelial carcinoma (n=3); 2) renal pelvis urothelial carcinoma (n=1); 3) previous radiotherapy or chemotherapy (n=4); 5) pathological slides in which interpreting more than two microenvironmental markers after staining was difficult (n=11). We enrolled 248 patients with NMIBC (n=178, pTa: 99, pT1:79) and MIBC (n=70, pT2:70). All included NMIBC patients were diagnosed with bladder cancer for the first time at our hospital and had well-preserved specimens for analysis. The MIBC patients also had well-preserved pT2 specimens for analysis and clear medical records regardless of bladder cancer recurrence or adjuvant intravesical therapy. All patients were treatment-naïve and had no history of chemotherapy or radiotherapy. The expression levels of tumor microenvironment markers—EP263, EP142, IM263, IM142, HER2, PD1, CD8, and Ki67—were determined in all 248 patients. To evaluate prognosis related to survival, recurrence, and progression, we included clinicopathological factors (tumor number, tumor size, prior recurrence rate, T-stage, tumor grade, and association of carcinoma in situ) based on the European Organization for Research and Treatment of Cancer (EORTC) guidelines (17) in the analysis. Other patient information regarding sex, age, tumor characteristics, and history of adjuvant therapy were also collected.

Follow-Up and Endpoint

The routine follow-up included cystoscopy performed every 3 months and upper tract imaging (computed tomography and

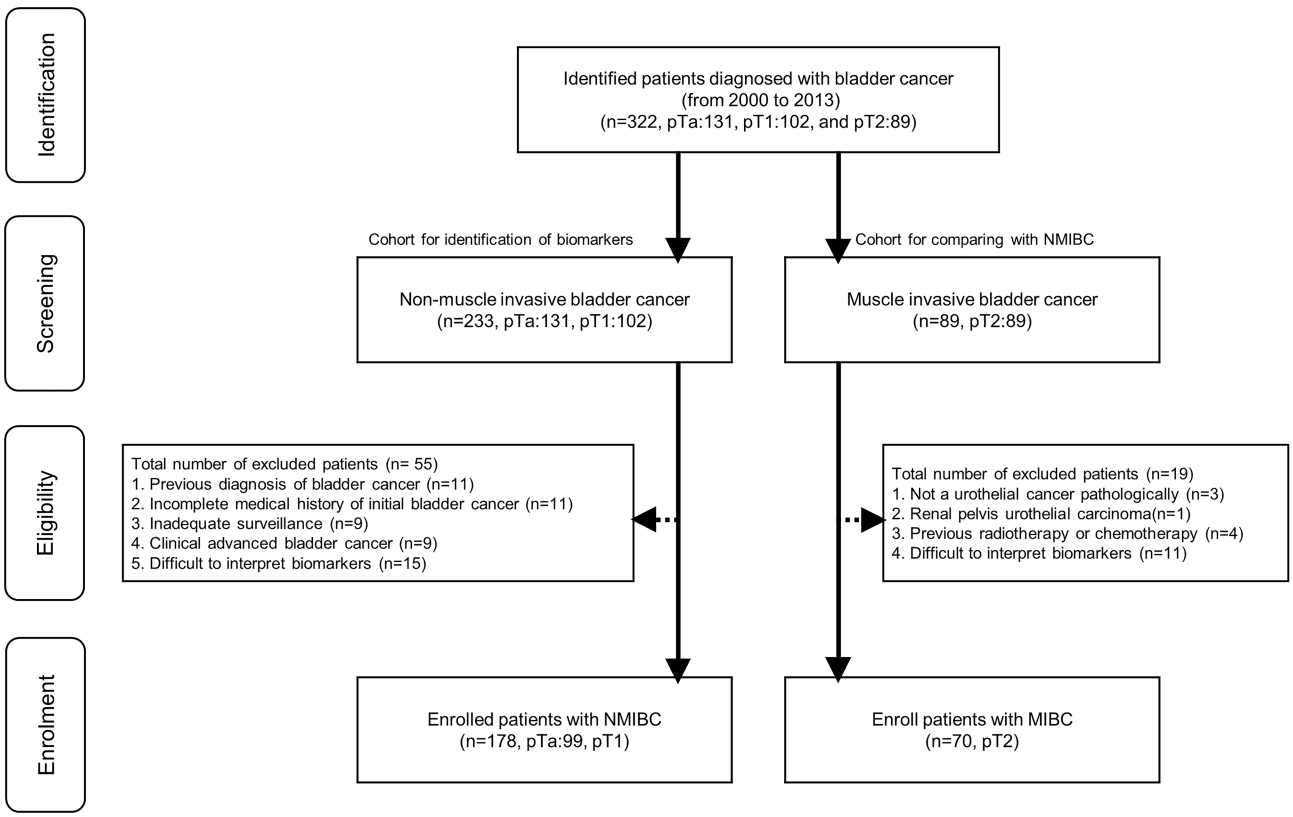

FIGURE 1 | Flowchart for enrolled patients. NMIBC, non-muscle invasive bladder cancer; MIBC, muscle invasive bladder cancer.

ultrasonography) performed every year. Urine cytology was performed during cystoscopy. Lesions suspected of recurrence were biopsied during cystoscopy or elective surgery. Suspected lesions that were pathologically confirmed as UC were defined as recurrence, and the recurrence time was defined as the time when the suspected lesion was identified. Progression was defined as recurrent UC that was confirmed to be at a pathologically higher stage than the pT2 stage. Clinically definite progression was determined if the recurrent lesions required more invasive procedures (radical cystectomy, radiation therapy, and chemotherapy), and progression was also defined even if pT2 was not confirmed pathologically.

Tissue Microarray

Formalin-fixed, paraffin-embedded tumor samples from specimens of 178 TURB diagnosed as UC were collected and arrayed using a tissue microarrayer (Quick-Ray®, Unitma Co., Ltd., Seoul, Republic of Korea). Briefly, representative areas from each tumor sample were selected and marked on hematoxylin and eosin-stained slides, and the corresponding tissue blocks were collected. Matching areas in each tumor block were punched with two tissue cylinders (2 mm diameter), and each core was transferred to its recipient microarray block. Sections (4 μm thick) were cut from the tissue microarray (TMA) paraffin blocks for immunohistochemical (IHC) staining.

Immunohistochemistry

IHC staining of PD-L1 was performed using two different anti-PDL1 antibody clones (Ventana SP142 and SP263, Ventana Medical Systems, Tucson, USA) and the Benchmark automated staining system (Ventana) for the FDA-approved SP263 and SP142 assay kits, according to the package inserts. Rabbit monoclonal negative control immunoglobulin (Ventana) was used as a negative control. IHC staining of CD8 (SP16; Thermo Fisher Scientific, Runcorn, UK; 1:100) and PD1 (EPR4877; Abcam, Cambridge, UK; 1:100) was performed on TMA blocks using a Bond-Max automatic immunostaining device (Leica Biosystems, Newcastle, UK). IHC staining of HER2 (4B5; Roche Diagnostics, Tucson, USA; pre-dilution) and Ki67 (SP6; Cell Marque, California, USA; 1:300) was performed on TMA blocks using the Benchmark automated staining system (Ventana). As positive controls, we used placental tissue sections for PD-L1 and tonsil tissue sections for PD1, CD8, and Ki67. Negative controls were performed by omitting the primary antibody.

Immunohistochemical Analyses

PD-L1 immunoreactivity was evaluated semi-quantitatively by a pathologist (DW EOM) blinded to the clinicopathological data. Membrane-based immunostaining of PD-L1 (SP263 and SP142) was interpreted based on the proportion of more than

unequivocal positivity (any intensity) in both epithelial tumor cells and infiltrating immune cells. The proportion of positively stained epithelial tumor cells was graded as 0 (<1%), 1 (≥1% to <5%), 2 (≥5% to <50%), or 3 (≥50%). The proportion of positively stained tumor immune cells was graded as 0 (<1%), 1 (≥1% to <5%), 2 (≥5% to <10%), or 3 (≥10%). Based on the guideline's interpretation, a positive 1%-cutoff value score was used (18).

Sections immunostained for PD1 and CD8 were assessed for tumor-infiltrating lymphocytes (TILs) in the tumor bed area. Immune cells were evaluated in each section by microscopic examination (400; BX51; Olympus, Tokyo, Japan). Five noncontiguous microscopic areas with TILs were randomly selected in each sample to corroborate representativeness and homogeneity. The mean number of immune cells in these five fields was calculated based on a 200× microscopic field (0.1590 mm^2/field). The number of nuclear Ki67 positive cells (per 1,000 cells) was counted visually in the hotspots at high magnification, and the Ki67 value was scored by the labeling index (19). HER2 expression levels were examined according to breast cancer guidelines (20) as follows: HER2 0: no staining (**Figure 2A**, IHC score 0); HER2 1^+: faint or partial membrane staining in ≤10% of tumor cells (**Figure 2B**, IHC score 1); HER2 2^+: weak or moderate complete membrane staining in >10% of tumor cells (**Figure 2C**, IHC score 2); and HER2 3^+: strong complete membrane staining in >10% of tumor cells (**Figure 2D**, IHC score 3). HER2+ (HER2 positive) staining was defined as expression levels of "HER2 1^+ or HER2 2^+ or HER2 3^+" (**Figures 2B–D**).

Statistical Analyses

We analyzed the relationship between bladder cancer-related outcomes and the variables previously mentioned using Pearson's χ^2 test or Fisher's exact test. Continuous variables were analyzed using an independent t-test. The relationship between survival and clinicopathological factors was estimated using Kaplan–Meier models and analyzed using the log-rank test.

We also evaluated the impact of clinicopathological factors and microenvironmental markers on the overall survival (OS) in

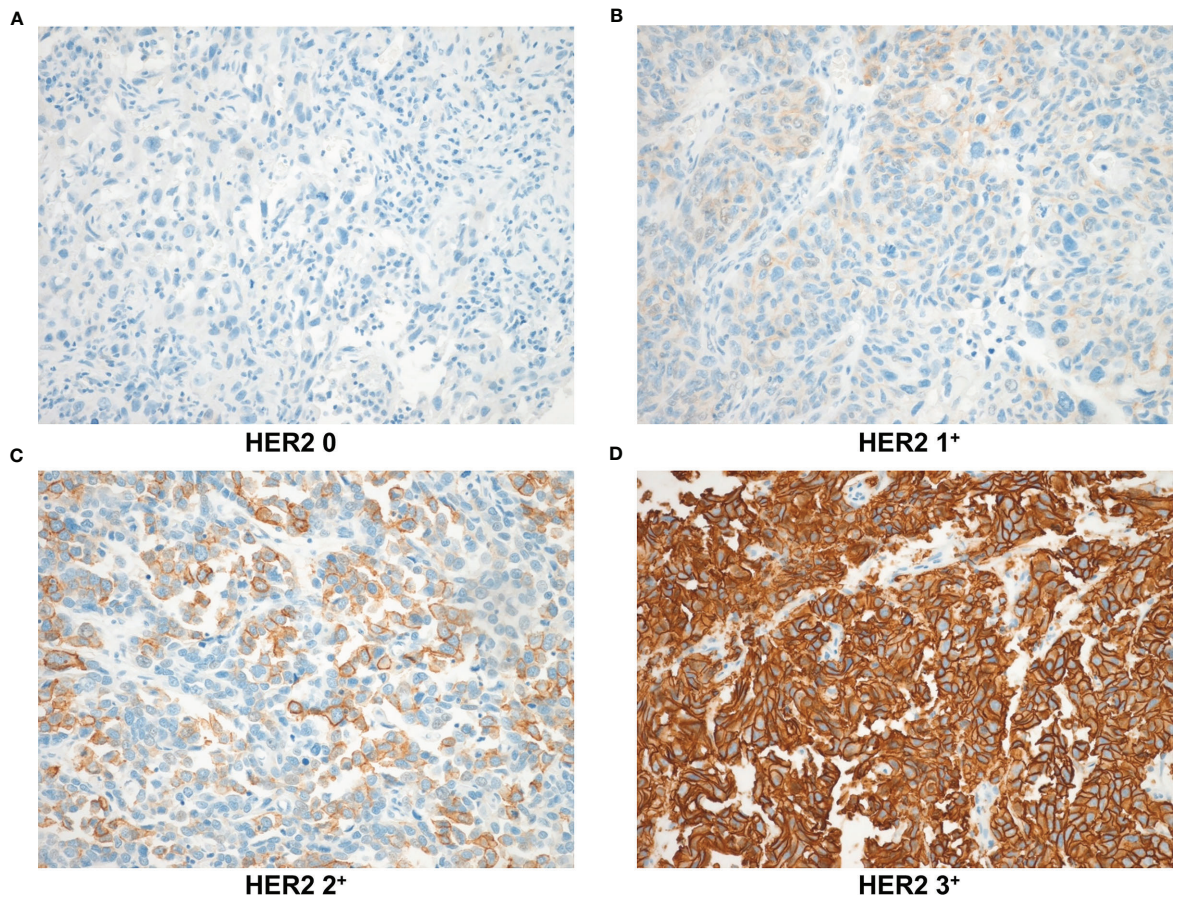

FIGURE 2 | HER2 expression levels based on immunohistochemical staining were observed at 200× magnification. **(A)** HER2 0: no staining **(B)** HER2 1^+: faint or partial membrane staining in ≤10% of tumor cells **(C)** HER2 2^+: weak or moderate complete membrane staining in >10% of tumor cells **(D)** HER2 3^+: strong complete membrane staining in >10% of tumor cells. HER2, human epidermal growth factor receptor-2.

all stage (pTa-T2) patients using univariate and multivariate Cox proportional hazard models. To analyze recurrence-free survival (RFS) and progression-free survival (PFS) in NMIBC patients, variables were selected using the stepwise backward elimination method. All variables with p<0.2 in the univariate analysis were included in the multivariate analysis. Each multivariate model was built using PDL-1-related factors, including EP263, IM263, EP142, and IM142 along with the other variables, to prevent overlapping inclusion of factors. The multivariate model of NMIBC included factors that were found to be significant in the univariate analysis. Statistical significance was set at p<0.05. Statistical analyses were performed using the SPSS software (IBM Corp. Released 2011, version 20.0. Armonk, NY: IBM Corp.).

RESULTS

Patient Clinicopathological Characteristics

Table 1 summarizes the characteristics and clinical features of the patients according to disease stage (pTa, pT1, and pT2). We included 178 NMIBC patients in the analysis, 99 of which were diagnosed with pTa (39.9%), and 79 of which were diagnosed with pT1 (31.8%). To compare the tumor microenvironment between NMIBC and MIBC patients, we included 70 (28.2%) patients diagnosed with pT2 tumors (by TURB). Of the 248 patients, 201 (81.0%) were male. Patients in the pTa group tended to be younger than those in the pT1 or pT2 groups. Sex, diabetes, and hypertension were comparable among the three groups. Gross tumor appearance was evaluated; compared with pTa tumors, pT1 and pT2 tumors tended have a solid appearance more frequently (p<0.01). The proportion of patients with tumors >3 cm in size was higher in the pT1 group than in the pTa group and higher in the pT2 group than in the pT1 group (both p<0.01). The three groups showed no significant difference in tumor number. Pathological results were evaluated; regarding tumor grade, patients with pTa tumors had a lower incidence of high-grade disease at 40/93 (43.0%), whereas this incidence was 70/75 (93.3%) and 64/64 (100%) in patients with pT1 and pT2 tumors, respectively (p<0.01). The three groups showed no significant difference in the incidence of carcinoma in situ. Adjuvant therapy was administered to 40/99 (40.4%) patients in the pTa group and 44/79 (55.7%) in the pT1 group. Among the pTa patients, 27 (27.3%) received intravesical BCG, while 13 (13.1%) received intravesical mitomycin. Among the

TABLE 1 | Patient characteristics.

	Total	pTa	pT1	pT2	p-value
Number of patients, n (%)	248 (100)	99 (39.9)	79 (31.9)	70 (28.2)	
Age, years (mean ± SD)	69.3 ± 10.9	66.5 ± 11.0	71.3 ± 10.4	70.9 ± 10.7	<0.01*
Sex, n (%), Male	201 (81.0)	81 (81.8)	64 (81.0)	56 (80.0)	0.95***
BMI (kg/m^2)	24.0 ± 2.8	24.8 ± 2.9	23.5 ± 2.6	23.2 ± 2.6	<0.01**
DM, n (%)	30 (12.1)	13 (13.1)	10 (12.7)	7 (10.0)	0.94***
HTN, n (%)	70 (28.2)	34 (34.3)	24 (30.4)	12 (17.1)	0.09***
Tumor description, n (%)	247 (100)	99 (100)	79 (100)	69 (100)	<0.01***
Papillary	191 (77.3)	96 (97.0)	64 (81.0)	31 (44.9)	
Solid	11 (4.5)	0 (0.0)	6 (7.6)	5 (7.2)	
Mixed	45 (18.2)	3 (3.0)	9 (11.4)	33 (47.8)	
Not reported	1	0	0	1	
Tumor grade, n (%)	229 (100)	93 (100)	75 (100)	64 (100)	<0.01***
Low	58 (25.3)	53 (57.0)	5 (6.7)	0 (0)	
High	171 (74.7)	40 (43.0)	70 (93.3)	64 (100)	
Not reported	19	6	4	6	
Tumor number, n (%)	219 (100)	88 (100)	68 (100)	63 (100)	0.09***
1	151 (68.9)	56 (63.6)	43 (63.2)	52 (82.5)	
2–4	57 (26.0)	27 (30.7)	20 (29.4)	10 (15.9)	
>4	11 (5.0)	5 (5.7)	5 (7.4)	1 (1.6)	
Not reported	29	11	11	7	
Tumor size (cm), n (%)	225 (100)	88 (100)	72 (100)	65 (100)	<0.01***
1	30 (13.3)	17 (19.3)	9 (12.5)	4 (6.2)	
1–3	86 (38.2)	48 (54.5)	26 (36.1)	12 (18.5)	
>3	109 (48.5)	23 (26.1)	37 (51.4)	49 (75.4)	
Not reported	23	11	7	5	
Concurrent CIS, n (%)	14 (5.6)	6 (6.1)	6 (7.6)	2 (2.9)	0.45***
Adjuvant therapy, n (%)	178 (100)	99 (100)	79 (100)	-	
BCG	69 (38.8)	27 (27.3)	42 (53.2)	-	
Mitomycin	15 (8.4)	13 (13.1)	2 (2.5)	-	
None	94 (52.8)	59 (59.6)	35 (44.3)	-	
Recurrence, n (%)		58 (58.6)	56 (70.9)	–	0.12***
Progression, n (%)		2 (2.0)	16 (20.3)	–	<0.01***
Expire, n (%)	132 (53.2)	28 (28.3)	42 (53.2)	62 (88.6)	<0.01***

*Analysis of variance; **Kruskal–Wallis; ***Pearson's χ-2 test or Fisher's exact test.

SD, standard deviation; BMI, body mass index; DM, diabetes mellitus; HTN, hypertension; CIS, carcinoma in situ; BCG, Bacillus Calmette–Guérin.

pT1 patients, 42 (53.2%) received intravesical BCG, and 2 (2.5%) received intravesical mitomycin. The median (interquartile range [IQR]) follow-up period in the pTa, pT1, and pT2 groups was 91.0 (69.5–122), 73.0 (38–123), and 16.0 (5–46.5) months, respectively. During the follow-up period, 58 (58.6%) pTa and 56 (70.9%) pT1 patients reported recurrence. The disease progressed to the pT2 stage in 2 (2.0%) pTa and 16 (20.3%) pT1 patients. During the follow-up period, 28 (28.3%), 42 (53.2%), and 62 (88.6%) patients expired in the pTa, pT1, and pT2 groups, respectively.

Expression of Tumor Microenvironment Markers

Figure 3 and **Supplementary Table 1** show the expression of different markers of the tumor microenvironment at each stage of the disease. EP263 and IM142 positivity rates were significantly higher in the pT2 group than in the pTa and pT1 groups (**Figures 3A, D** and **Supplementary Table 1**). EP142 expression was significantly higher in pT2 patients than in pTa patients (**Figure 3B** and **Supplementary Table 1**). However, EP142 expression in pT1 patients was comparable to that in pTa and pT2 patients. The IM263 and HER2 positivity rates were higher in pT1 patients than in pTa patients, while no significant difference was noted between the pT1 and pT2 patients (**Figures 3C, E** and **Supplementary Table 1**). PD1 and Ki67 expression were highest in pT2 patients, followed by pT1 and pTa patients (**Figures 3F, H** and **Supplementary Table 1**). CD8 expression was highest in pT2 patients, and was comparable in pTa and pT1 patients (**Figure 3G** and **Supplementary Table 1**).

Correlation Between Tumor Microenvironment Markers and Survival in UC

Table 2 shows the results of the univariate and multivariate analyses of OS, including the clinicopathological factors and tumor microenvironment markers in all patients (pTa, pT1, and pT2 stages). Based on the univariate analysis, age ($p<0.01$), T-stage ($p<0.01$), tumor grade ($p<0.01$), EP263 ($p<0.01$), HER2 ($p<0.01$), PD1 ($p<0.01$), CD8 ($p<0.05$), and Ki67 ($p<0.01$) were significant prognostic factors. Through the multivariate analysis, we found that age ($p<0.01$), T-stage ($p<0.01$), EP263 ($p<0.05$), PD1 ($p<0.01$), CD8 ($p<0.05$), and Ki67 ($p<0.05$) were significant prognostic factors. **Figure 4** was generated using the Kaplan–Meier survival curves based on significant factors derived from the univariate and

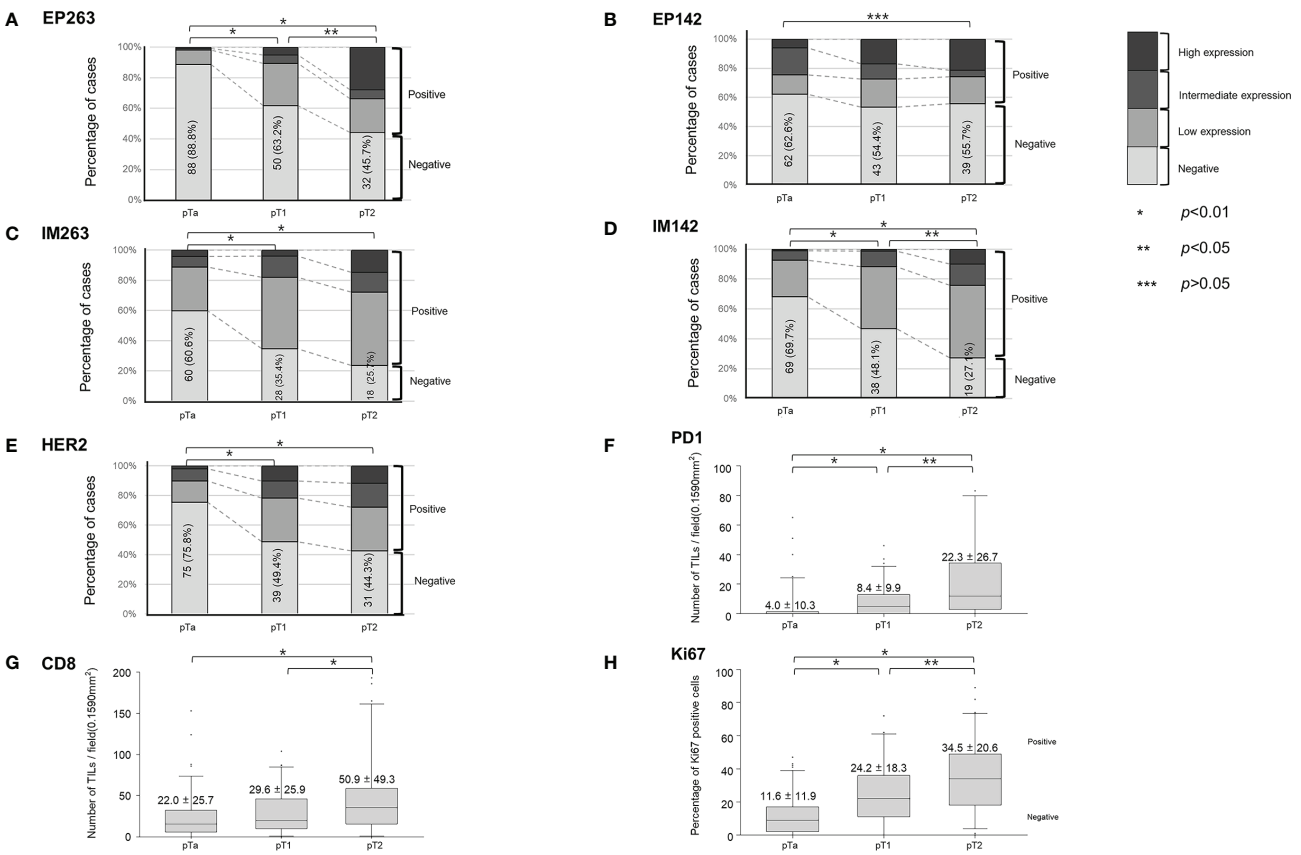

FIGURE 3 | Baseline expression of tumor microenvironment markers according to T-stage. The percent of positive cases are shown for **(A)** EP263, **(B)** EP142, **(C)** IM263, **(D)** IM142, and **(E)** HER2 according to T-stage. The expression levels of **(F)** PD1, **(G)** CD8, and **(H)** Ki67 according to T-stage are also shown. TILs, tumor-infiltrating lymphocytes; HER2, human epidermal growth factor receptor-2; PD1, programmed cell death protein 1.

TABLE 2 | Univariate and multivariate analyses of OS in all patients.

	Univariate (OS)		Multivariate (OS)	
	HR (95% CI)	**p-value**	**HR (95% CI)**	**p-value**
Age (continuous)	1.070 (1.050–1.090)	<0.01	1.064 (1.043–1.084)	<0.01
Sex	0.950 (0.600–1.490)	0.82		
Bladder tumor				
- T-stage				
Ta	Reference		3.270 (2.360–4.531)	<0.01
T1	2.168 (1.333–3.526)	<0.01		
T2	8.190 (5.159–13.001)	<0.01		
- Grade (High vs. Low)	3.120 (1.820–5.370)	<0.01		
- Concurrent CIS	1.150 (0.560–2.350)	0.71		
Microenvironment markers				
- EP263 (positive vs. negative)	1.970 (1.380–2.800)	<0.01	1.568 (1.025–2.398)	<0.05
- IM263 (positive vs. negative)	1.390 (0.970–1.990)	0.07		
- EP142 (positive vs. negative)	0.940 (0.660–1.330)	0.71		
- IM142 (positive vs. negative)	1.350 (0.950–1.910)	0.09		
- HER2 (positive vs. negative)	1.690 (1.200–2.400)	<0.01		
- PD1 (continuous)	1.020 (1.010–1.030)	<0.01	1.023 (1.007–1.040)	<0.01
- CD8 (continuous)	1.010 (1.000–1.010)	<0.05	0.989 (0.981–0.997)	<0.05
- Ki67 (continuous)	1.010 (1.010–1.020)	<0.01	0.985 (0.974–0.997)	<0.05

OS, overall survival; NMIBC, non-muscle-invasive bladder cancer; HR, hazard ratio; CI, confidence interval; CIS, carcinoma in situ; HER2, human epidermal growth factor receptor-2; PD1, programmed cell death protein 1.

multivariate analysis, including age (p<0.01, **Figure 4A**), T-stage (p<0.01, **Figure 4B**), grade (p<0.01, **Figure 4C**), EP263 (p<0.01, **Figure 4D**), PD1 (p<0.01, **Figure 4E**), and Ki67 (p<0.01, **Figure 4F**).

Correlation of Tumor Microenvironment Markers With RFS and PFS in NMIBC

Table 3 summarizes the results of the univariate and multivariate analyses for RFS and PFS, including the clinicopathologic factors and tumor microenvironment markers in NMIBC patients. In the univariate analysis, adjuvant therapy (p=0.05), tumor grade (p<0.05), and HER2+ (p<0.05) were evaluated as significant biomarkers for RFS. In multivariate analyses, we found that RFS had a significant correlation with two Cox proportional hazard models: model[a] and model[b]. Model[a] was built using adjuvant therapy (p<0.01) and tumor grade (p<0.01), and model[b] was built using adjuvant therapy (p<0.05) and HER2+ (p<0.05). Using a Kaplan–Meier model, **Figure 5** was generated from significant factors of adjuvant therapy (p<0.05, **Figure 5A**), tumor grade (p<0.05, **Figure 5B**), and HER2+ (p<0.05, **Figure 5C**).

In the univariate analysis of PFS, age (p<0.05), T-stage (p<0.01), tumor grade (p<0.05), and IM263 (p<0.05) were significant prognostic factors. In the multivariate analysis, we found that PFS was significantly correlated with two Cox proportional hazard models: model[c] and model[d]. Model[c] was built using age (p=0.05) and T-stage (p<0.01), and model[d] was built using age (p<0.01) and IM263 (p<0.05). **Figure 6** was generated based on significant factors from the log-rank test of the Kaplan–Meier model that were screened for factors in the univariate analysis, including age (p<0.01, **Figure 6A**), T-stage (p<0.01, **Figure 6B**), tumor grade (p<0.05, **Figure 6C**), IM263 (p<0.05, **Figure 6D**), and HER2+ (p<0.05, **Figure 6E**).

Statistical analyses were performed between HER2 positive and HER2 negative patient groups in the gray area of **Supplementary Figure 1**, based on the tendency of the recurrence-free survival curve appearing to have narrowing trends. Baseline patient characteristics of the HER2 positive group without relapse by 72 months are shown in **Supplementary Table 2**; characteristics of biomarker expression in this subgroup are shown in **Supplementary Table 3**. The proportion of HER2 2^+ or HER2 3^+ was significantly higher in patients with relapse or censor before 72 months (p<0.05, **Supplementary Table 3**).

DISCUSSION

In this study, an increase in bladder cancer stage (Ta–T2) correlated with increased Ki67, PD1, EP263, and IM142 expression levels. The T1 and T2 stages had higher expression levels of HER2 and IM263 than the Ta stage, and there was no significant difference between the expression levels in the T1 and T2 stages. CD8 levels in the Ta and T1 stages were comparable but were lower than those in the T2 stage. No significant differences were noted in the EP142 levels across the three stages. Based on a multivariate analysis model including adjuvant therapy and tumor grade in NMIBC, RFS was associated with HER2+, while OS was associated with age, T-stage, EP263, PD1, CD8, and Ki67 levels.

In NMIBC patients, a higher disease stage correlated with a higher expression of PD1 and EP263. EP263 was found to be a predictive factor for progression. On the contrary, cytotoxic lymphocyte infiltration assessed by CD8 levels did not vary significantly in the different stages of NMIBC; therefore, it does not appear to be a prognostic factor. For over 40 years, adjuvant intravesical BCG has been the gold standard treatment for UC,

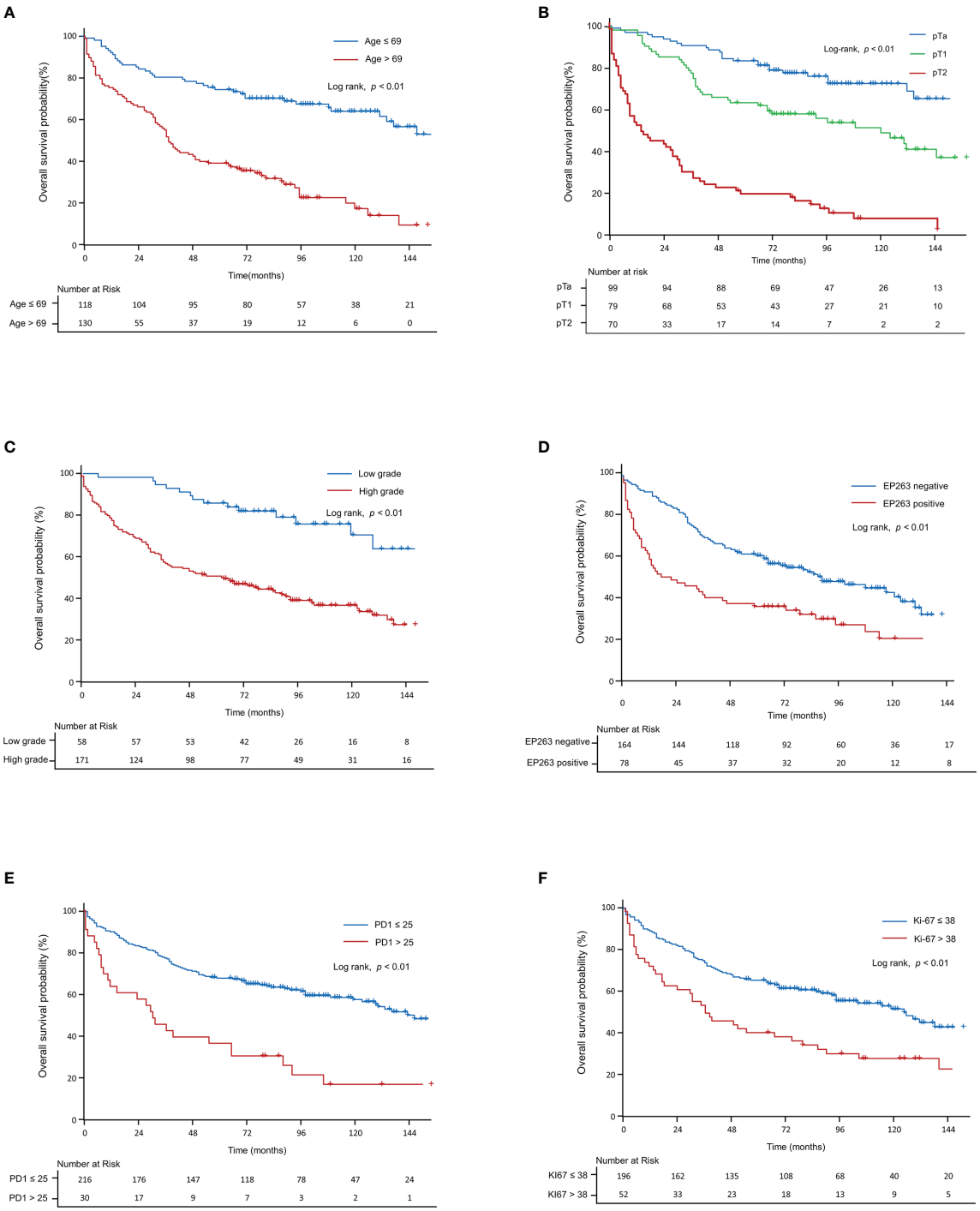

FIGURE 4 | Kaplan–Meier curve for overall survival in all patients. The Kaplan–Meier curves show overall survival according to **(A)** age, **(B)** T-stage, **(C)** grade, **(D)** EP263, **(E)** PD1, and **(F)** Ki67. PD1, programmed cell death protein 1.

although its mechanism of action, including the target antigen, remains unclear. However, with the development of PD-L1 therapeutics, there has been an increased interest in this mechanism, and strategies targeting PD-L1 have been approved by the FDA for advanced UC patients (9, 10, 21). In a study on NMIBC, patients with advanced disease showed higher levels of PD-L1 in BCG granulomas. Although there is no conclusive evidence that T-cell-related immunity is related to

TABLE 3 | Univariate and multivariate analyses of RFS and PFS in NMIBC patients.

	Univariate (RFS)		Multivariate (RFS)		Univariate (PFS)		Multivariate (PFS)	
	HR (95% CI)	p-value	HR (95% CI)	p-value	HR (95% CI)	p-value	HR (95% CI)	p-value
Age (continuous)	1.020 (1.000–1.030)	0.07			1.071 (1.023-1.121)	<0.05	1.051 (0.999–1.106) 1.076 (1.024–1.131)	0.05[c] <0.01[d]
Sex	0.720 (0.420–1.220)	0.22			0.950 (0.280–3.300)	0.94		
Adjuvant therapy	1.454 (0.997–2.120)	0.05	0.582 (0.390–0.870) 1.510 (1.033–2.207)	<0.01[a] <0.05[b]	0.660 (0.260–1.700)	0.39		
Bladder tumor								
- T-stage	1.300 (0.900–1.880)	0.16			27.73 (3.671–209.4)	<0.01	11.70 (2.660–51.45)	<0.01[c]
- Grade (High vs. Low)	1.605 (1.048–2.458)	<0.05	1.890 (1.215–2.940)	<0.01[a]	10.09 (1.337–76.09)	<0.05		
- Concurrent CIS	1.070 (0.520–2.200)	0.85			1.170 (0.160–8.870)	0.88		
- Tumor size	1.080 (0.730–1.620)	0.69			1.030 (0.380–2.790)	0.95		
- Multiple tumor	1.310 (0.820–2.080)	0.26			0.480 (0.110–2.120)	0.34		
- Solid or Mixed	0.880 (0.470–1.630)	0.68			1.140 (0.260–4.980)	0.86		
Microenvironment markers								
- EP263 (positive vs. negative)	1.300 (0.850–2.000)	0.23			1.360 (0.440–4.170)	0.59		
- IM263 (positive vs. negative)	1.080 (0.740–1.570)	0.70			3.831 (1.244–11.780)	<0.05	3.659 (1.183–11.32)	<0.05[d]
- EP142 (positive vs. negative)	0.790 (0.540–1.160)	0.23			0.890 (0.340–2.290)	0.80		
- IM142 (positive vs. negative)	1.070 (0.730–1.570)	0.73			1.320 (0.520–3.370)	0.56		
- HER2 (positive vs. negative)	1.480 (1.010–2.160)	<0.05	1.532 (1.048–2.238)	<0.05[b]	2.552 (1.006–6.473)	<0.05		
- PD1 (continuous)	1.000 (0.980–1.020)	0.75			0.980 (0.920–1.040)	0.55		
- CD8 (continuous)	1.000 (0.990–1.010)	0.59			1.000 (0.980–1.020)	0.99		
- Ki67 (continuous)	1.083 (0.744–1.576)	0.68			1.002 (0.973–1.032)	0.87		

In the multivariate analysis for RFS, Cox proportional hazard model[a] included adjuvant therapy and grade, while model[b] included adjuvant therapy and HER2+.
In the multivariate analysis for PFS, Cox proportional hazard model[c] included age and grade, while model[d] included age and IM263.
RFS, recurrence-free survival; PFS, progression-free survival; NMIBC, non-muscle-invasive bladder cancer; HR, hazard ratio; CI, confidence interval; CIS, carcinoma in situ; HER2, human epidermal growth factor receptor-2; PD1, programmed cell death protein 1.

BCG treatment, this may hint at a link between BCG failure and T-cell depletion (22). Therefore, the systemic immune-related adverse effects of ICBs should be considered when treating BCG-resistant UC. An evaluation of the levels of tumor microenvironment markers at baseline can help predict the outcome of ICB treatment in NMIBC patients. While the relationship between PD1 and CD8 has been widely reported for MIBC (23, 24), only a few reports describe their association in NMIBC (25, 26). Therefore, while EP263 has the potential to be a prognostic marker for progression, CD8 appears to have a limited role in these patients.

The reason for conflicting results with respect to measurement results of the TME in bladder cancer was that, due to molecular heterogeneity, different TMEs were reported to coexist, even in the case of bladder cancer extracted from a single mass (27). Furthermore, due to co-localization of PD-L1, PD-1, and CD8+ cell characteristics, other reasons may include the presence of parts rich or low in PD-L1, depending on the part measured by the TME environment (28, 29). In addition to these tumor-related biases that were partly extracted, problems due to test methods and scoring were present; however, there is no standardization of tests for PD-L1 IHC expression, and there were several analyses utilizing different clones and scoring algorithms (30). Currently, four commercially available antibodies are SP142 (Ventana), SP256 (Ventana), 22C3 (Dako), and 29-8 (Dako). In this study, we used a Ventana analysis system of PD-L1 antibodies (SP142, SP256) system. SP142 antibody is the most widely used method of PD-L1 because the immune cell (IC) count score measured from SP142 is indicates use of atezolizumab (Tecentriq®) in muscle invasive bladder cancer; furthermore, since SP142 is specifically designed to stain IC, it is advantageous in being more sensitive and allowing for a clearer view of immune infiltrates (31). In a previous study using the above four antibodies in muscle invasive specimens, a concordance rate of 80-90% was reported; however, some specimens that used IM142 antibody reported inconsistency in the staining pattern that varied from other specimens (32). and Some reports criticized SP142 for poor reproducibility compared to other PD-L1 antibodies (33) The authors designed the study to use multiple antibodies from the same tumor rather than relying on a single slide to reduce bias in the testing methods for these antibodies. In NMIBC particularly, each marker was analyzed for each prognosis competitively because there was no report on concordance or prognostic significance according to use of each antibody in NMIBC.

We evaluated the role of high HER2 expression in the recurrence of superficial UC. HER2, a mediator of tumor cell growth through the regulation of a tyrosine kinase, is amplified in UC, as shown by genome sequencing (34) and immunohistochemistry (35). HER2 overexpression is a biomarker that correlates with poor prognosis and represents a potential target marker for anti-HER2 therapy based on experience with breast cancer or gastric cancer (36, 37). In order for HER2-related therapeutics to be effective in bladder cancer, investigation of HER2 expression is needed because HER2 expression is directly related to the treatment mechanism. The relationship between HER2 expression and bladder cancer that is known to date has been reported at the level that correlated with advanced bladder cancer. It was reported that HER2 overexpression was already observed in a

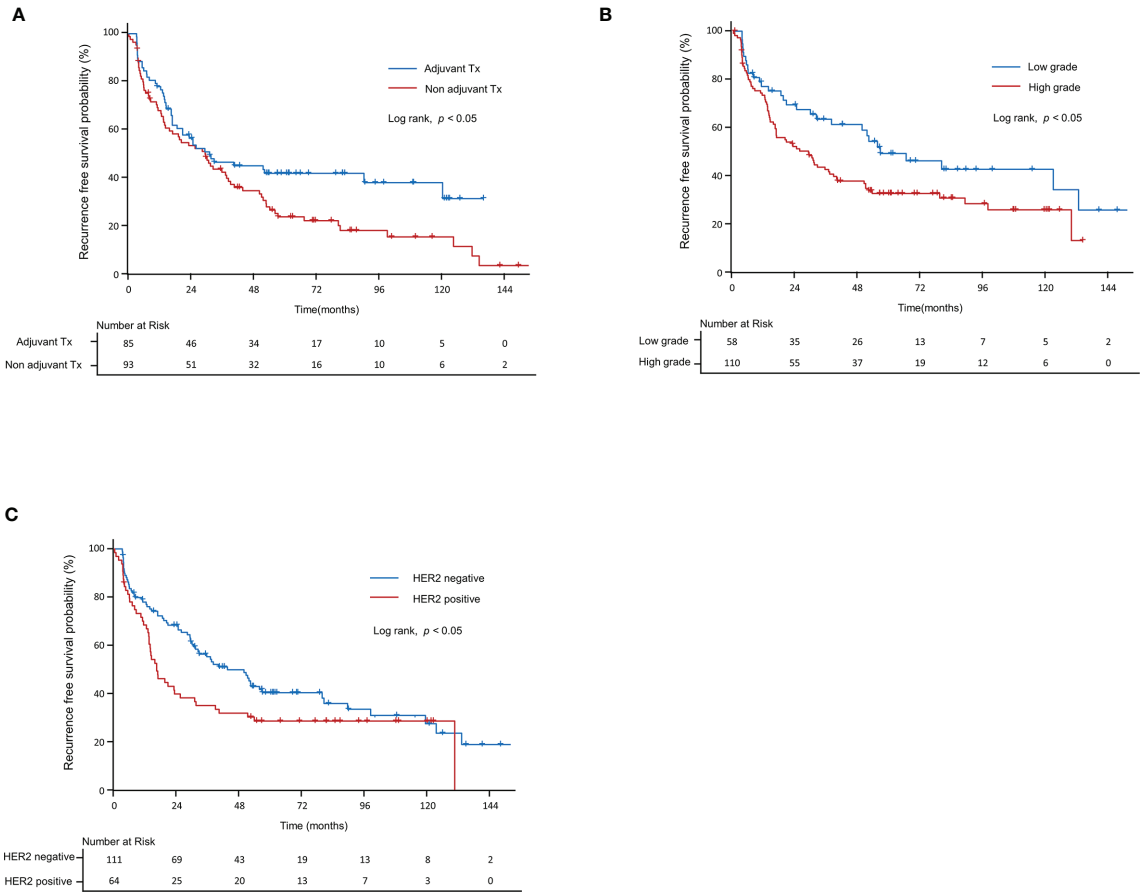

FIGURE 5 | Kaplan–Meier curve for recurrence-free survival in non-muscle-invasive bladder cancer patients. Recurrence-free survival according to **(A)** grade, **(B)** adjuvant therapy, and **(C)** HER2+. HER2, human epidermal growth factor receptor-2.

specimen before progression, and was consequently observed after progression (38, 39); genetic changes also showed similar patterns to these reports (40). Therefore, the known onset point of HER2 expression was at the level of previous advanced bladder cancer lesions. This study revealed HER2 overexpression is also observed at a level of early diagnosis of NMIBC and correlates with bladder cancer recurrence and progression. The recent emergence of novel ADCs has renewed the interest in HER2-targeted therapies for UC. Since ADCs deliver high concentrations of a cytotoxic agent to tumor cells with specific target antigens, they effectively kill tumor cells with minimal systemic side effects. Most agents targeting HER2 require genome amplification of HER2 for effective treatment (34). However, studies on RC48-ADC in IHC 2^+ or IHC 3^+ UC patients suggest that only a moderate level of protein expression is sufficient to induce a response (15). In line with these findings, this study provides information on HER2 expression as a prognostic biomarker in NMIBC, thus identifying high-risk patients with this biomarker and providing a potential patient group that may be targeted for anti-Her2 therapies. In particular, among HER2 2^+ or HER2 3^+ characteristics; only two patients without recurrence or a 72-month censor were followed-up. Hence, we recommend intensive surveillance for patients with initially expressed HER2 2^+ or HER2 3^+. Further research is needed to confirm these results and to explore whether HER2 is an effective target antigen of this treatment.

Oportuzumab monatox (OM), an ADC that uses Pseudomonas exotoxin A (ETA 252-608) as a cytotoxic agent and targets EpCAM expressing tumor cells, has shown potential as an intravesical therapeutic agent (16). Phase II trials of OM for BCG-refractory NMIBC have demonstrated its potential as a method of intravesical therapy (16). Unlike mUC and MIBC, NMIBC has a relatively good prognosis, with a few exceptions (2). Studies on the natural course of NMIBC patients have evaluated various clinicopathological factors that can predict recurrence and progression. Although a guideline has been developed for appropriate adjuvant therapy (2), many NMIBC patients are at risk of repeated relapses and progression (4, 5). Furthermore, due to the current chronic shortage of BCG, urology oncologists often have to treat patients not based on these guidelines (2) but on the amounts of BCG available at their

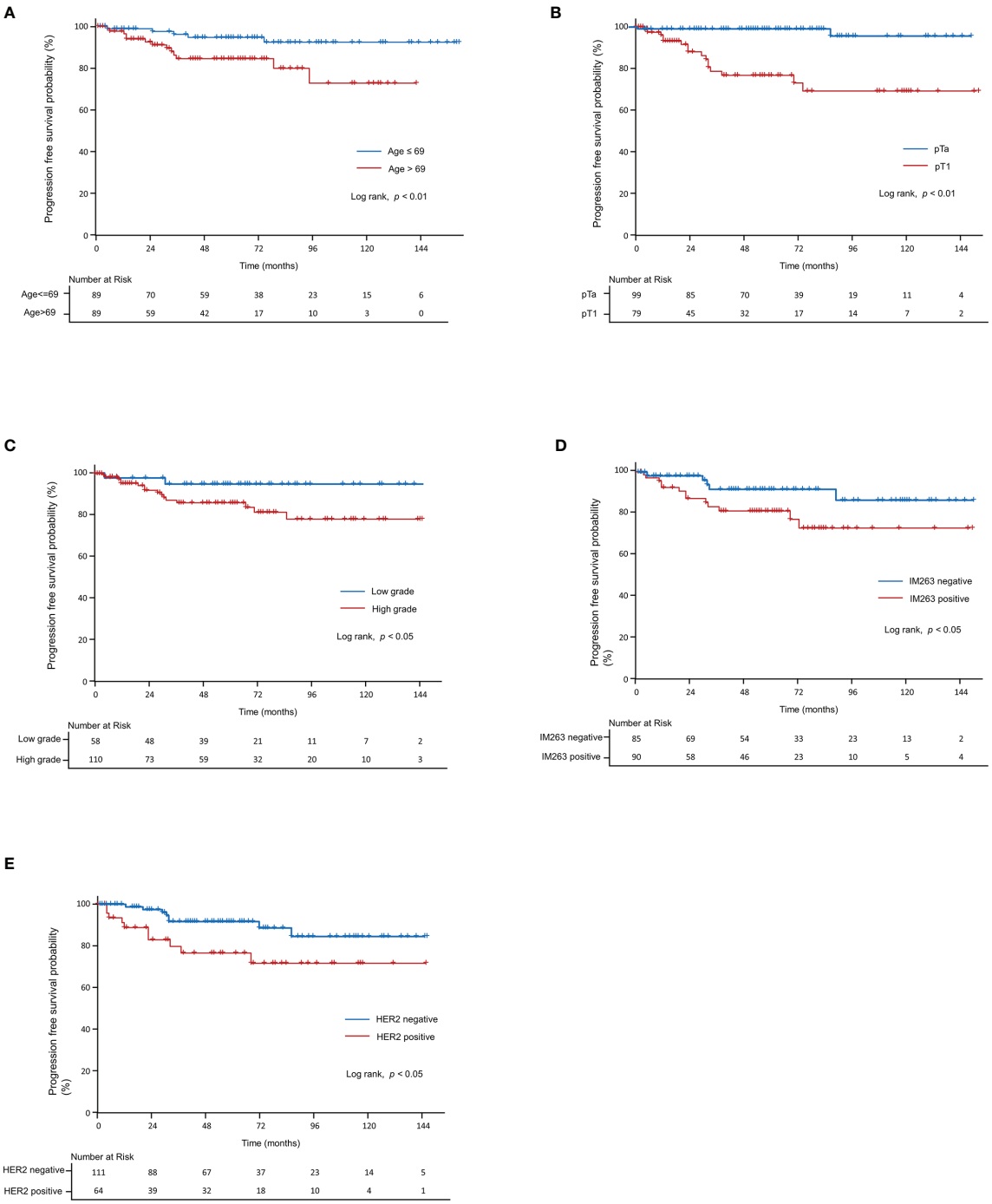

FIGURE 6 | Kaplan–Meier curve for progression-free survival in non-muscle-invasive bladder cancer patients. Progression-free survival according to **(A)** age, **(B)** T-stage, **(C)** grade, **(D)** IM263, and **(E)** HER2+. HER2, human epidermal growth factor receptor-2.

hospitals (41). Under these circumstances, ADCs are promising intravesical drugs that directly exert cytotoxic effects on tumor cells by targeting specific tumor antigens, with reduced systemic adverse effects (16). ADCs are particularly beneficial for patients whose cancer risk is not high enough to tolerate the systemic side effects or those who developed side effects when treated with BCG. In this study, HER2+ expression showed a significant association with RFS and is therefore a potential target antigen for the development of ADC-mediated intravesical therapeutic agents and an alternative adjuvant therapy to BCG.

Ki67 is a DNA-bound protein activated only during the proliferation phase and is not detected during cell cycle quiescence. Studies on Ki67 in UC have reported it as a prognostic factor for recurrence and progression in upper tract UC (19, 42) NMIBC after TURB (43, 44). In the present study, we found a correlation between higher stages of UC and increased Ki67 expression levels. Ki67 was analyzed as a significant prognostic factor in a survival model including patients with all stages of UC but was not a prognostic factor for recurrence or progression in NMIBC patients. Patients who undergo radical surgery, such as the upper ureter tract UC, can be classified into risk groups based on the pathology of the full ureter's layers, which is a better indicator of the depth of tumor invasion than the TURB specimen. In this patient group, most cases of recurrence occur in the form of local recurrence, and since most cases of local recurrence are explained by pathological results of surgically removed ureter cancer, the pathologic results have a close relationship with patient prognosis (19, 42). However, in NMIBC patients, many recurrences are not related to primary UC that was surgically removed, such as by incomplete TURB. For the reasons mentioned here, unlike previous studies reporting that Ki67 is related to prognosis under certain conditions, in NMIBC (43, 44), we found no significant relationship between Ki67 expression levels and recurrence/progression.

A limitation of this study is that the number of patients included was relatively small; therefore, it will be necessary to assess whether the results can be replicated in a large-scale study. In addition, since this was a retrospective study, the stored samples had been stained and previously handled. All formalin-fixed and paraffin-embedded specimens were archived in closed wooden boxes, protected from light, in a dry dedicated deposit at constant room temperature between 18-25° C. In our study, as at 2020, for immunostaining, there were two specimens stored for 20 years. Including the two cases, 32 cases in total had been archived for more than 15 years. We performed immunostaining for Vimentin, which is known to efficiently reflect preserved immunoreactivity of the old paraffin block specimen for all the cases included in the study, and confirm whether mesenchymal cells and endothelial cells were well stained. Moreover, in order to obtain good immunostaining properties, at least 500 micrometers were cut out during the TMA block manufacturing process and immunostaining was performed on the deep portion of the tissue. Two Vimentin-stained specimens were stored for 20 years (**Supplementary Figure 2**). Therefore, although only the results from well-preserved samples were included in the study, errors caused by the use of old samples could not be avoided. There are also limitations in the analysis due to the assumption of a causal relationship between expression level and prognosis. However, although performed on a small-scale, this was a well-designed study in the field of therapeutic agent development, which has received increasing interest in recent years. Several studies have reported that PD-L1 or HER2 expression varies depending on the patient's status, such as additional treatment for tumors and site of lesion collection (primary or metastatic) (45–47). The diagnostic criteria for "high PD-L1 expression" depends on the staining method, antibodies used, and infiltrating cells (tumor or immune cells) (48). PD-L1 expression has been shown to increase after chemotherapy in patients with mUC (46). A study on patients with recurrent NMIBC reported increased HER2 expression when cancer relapsed after adjuvant intravesical therapy (45). Moreover, since metastatic lesions have higher HER2 expression than primary lesions (47), results might vary depending on adjuvant therapy or status of recurrence. In this study, we included only patients diagnosed with UC for the first time with no history of UC-related diagnosis or therapy. Therefore, our results are significant because they reveal the initial changes in the tumor microenvironment at different stages of the disease. We also evaluated the prognostic role of these tumor microenvironment markers by comparing them with other clinicopathological factors to identify their potential as therapeutic agents. Given the shortage of BCG, we believe our findings will help identify a target antigen for developing therapies alternative to BCG for the treatment of NMIBC.

CONCLUSIONS

In NMIBC patients, the expression of IM263, an immune cell marker, and HER2 increased as the disease stage increased. IM263 and HER2 levels were significant predictors of PFS and RFS, respectively, suggesting their potential as biomarkers for progression and recurrence. Additionally, HER2 is a promising target antigen for use in an ADC for adjuvant intravesical therapeutics as an alternative to BCG.

DATA AVAILABILITY STATEMENT

The original contributions presented in the study are included in the article/**Supplementary Material**. Further inquiries can be directed to the corresponding authors.

ETHICS STATEMENT

The studies involving human participants were reviewed and approved by Institutional Review Board of Gangneung Asan Hospital. The ethics committee waived the requirement of written informed consent for participation.

AUTHOR CONTRIBUTIONS

SJK and D-WE were responsible for conceptualization and design. Acquisition of data was conducted by SL, B-JN, and GK. HC, SJK, and D-WE analyzed and interpreted the data. HC and SJK drafted the manuscript. WN, HK, SWK, JP, SJK, and D-WE were responsible for critical revision of the manuscript. SJK and D-WE supervised the project. All authors contributed to the to the article and approved the submitted version.

FUNDING

This work was supported by the Gangneung Asan Hospital Medical Institute and the Asan Foundation under Grant number 2020–IB008.

SUPPLEMENTARY MATERIAL

The Supplementary Material for this article can be found online at: https://www.frontiersin.org/articles/10.3389/fimmu.2022.903297/full#supplementary-material

REFERENCES

1. Antoni S, Ferlay J, Soerjomataram I, Znaor A, Jemal A, Bray F. Bladder Cancer Incidence and Mortality: A Global Overview and Recent Trends. *Eur Urol* (2017) 71:96–108. doi: 10.1016/j.eururo.2016.06.010
2. Babjuk M, Burger M, Compérat EM, Gontero P, Mostafid AH, Palou J, et al. European Association of Urology Guidelines on non-Muscle-Invasive Bladder Cancer (TaT1 and Carcinoma in Situ) –2019 Update. *Eur Urol* (2019) 76:639–57. doi: 10.1016/j.eururo.2019.08.016
3. Morales A, Eidinger D, Bruce AW. Intracavitary Bacillus Calmette-Guerin in the Treatment of Superficial Bladder Tumors. *J Urol* (1976) 116:180–3. doi: 10.1016/S0022-5347(17)58737-6
4. Solsona E, Iborra I, Dumont R, Rubio-Briones J, Casanova J, Almenar S. The 3-Month Clinical Response to Intravesical Therapy as a Predictive Factor for Progression in Patients With High Risk Superficial Bladder Cancer. *J Urol* (2000) 164:685–9. doi: 10.1016/S0022-5347(05)67281-3
5. Herr HW, Dalbagni G. Defining Bacillus Calmette-Guerin Refractory Superficial Bladder Tumors. *J Urol* (2003) 169:1706–8. doi: 10.1097/01.ju.0000062605.92268.c6
6. Nadler RB, Catalona WJ, Hudson MA, Ratliff TL. Durability of the Tumor-Free Response for Intravesical Bacillus Calmette-Guerin Therapy. *J Urol* (1994) 152:367–73. doi: 10.1016/S0022-5347(17)32741-6
7. Witjes JA, Palou J, Soloway M, Lamm D, Kamat AM, Brausi M, et al. Current Clinical Practice Gaps in the Treatment of Intermediate- and High-Risk non-Muscle-Invasive Bladder Cancer (NMIBC) With Emphasis on the Use of Bacillus Calmette–Guérin (BCG): Results of an International Individual Patient Data Survey (IPDS). *BJU Int* (2013) 112:742–50. doi: 10.1111/bju.12012
8. Grimm MO, van der Heijden AG, Colombel M, Muilwijk T, Martínez-Piñeiro L, Babjuk MM, et al. Treatment of High-Grade non-Muscle-Invasive Bladder Carcinoma by Standard Number and Dose of BCG Instillations Versus Reduced Number and Standard Dose of BCG Instillations: Results of the European Association of Urology Research Foundation Randomised Phase III Clinical Trial "Nimbus". *Eur Urol* (2020) 78:690–8. doi: 10.1016/j.eururo.2020.04.066
9. Balar AV, Castellano D, O'Donnell PH, Grivas P, Vuky J, Powles T, et al. First-Line Pembrolizumab in Cisplatin-Ineligible Patients With Locally Advanced and Unresectable or Metastatic Urothelial Cancer (KEYNOTE-052): A Multicentre, Single-Arm, Phase 2 Study. *Lancet Oncol* (2017) 18:1483–92. doi: 10.1016/S1470-2045(17)30616-2
10. Balar AV, Galsky MD, Rosenberg JE, Powles T, Petrylak DP, Bellmunt J, et al. Atezolizumab as First-Line Treatment in Cisplatin-Ineligible Patients With Locally Advanced and Metastatic Urothelial Carcinoma: A Single-Arm, Multicentre, Phase 2 Trial. *Lancet* (2017) 389:67–76. doi: 10.1016/S0140-6736(16)32455-2
11. Balar AV, Kamat AM, Kulkarni GS, Uchio EM, Boormans JL, Roumiguié M, et al. Pembrolizumab Monotherapy for the Treatment of High-Risk non-Muscle-Invasive Bladder Cancer Unresponsive to BCG (KEYNOTE-057): An Open-Label, Single-Arm, Multicentre, Phase 2 Study. *Lancet Oncol* (2021) 22:919–30. doi: 10.1016/S1470-2045(21)00147-9
12. Soria F, Giordano A, Shariat SF, Gontero P. Bladder Sparing Landscape for Bacillus Calmette–Guérin Unresponsive Bladder Cancer. *Curr Opin Urol* (2020) 30:542–6. doi: 10.1097/MOU.0000000000000789
13. Rosenberg J, Sridhar SS, Zhang J, Smith D, Ruether D, Flaig TW, et al. EV-101: A Phase I Study of Single-Agent Enfortumab Vedotin in Patients With Nectin-4-Positive Solid Tumors, Including Metastatic Urothelial Carcinoma. *J Clin Oncol* (2020) 38:1041–9. doi: 10.1200/JCO.19.02044
14. Hussain MH, MacVicar GR, Petrylak DP, Dunn RL, Vaishampayan U, Lara PNJr., et al. Trastuzumab, Paclitaxel, Carboplatin, and Gemcitabine in Advanced Human Epidermal Growth Factor Receptor-2/Neu-Positive Urothelial Carcinoma: Results of a Multicenter Phase II National Cancer Institute Trial. *J Clin Oncol* (2007) 25:2218–24. doi: 10.1200/JCO.2006.08.0994
15. Sheng X, Yan X, Wang L, Shi Y, Yao X, Luo H, et al. Open-Label, Multicenter, Phase II Study of RC48-ADC, a HER2-Targeting Antibody-Drug Conjugate, in Patients With Locally Advanced or Metastatic Urothelial Carcinoma. *Clin Cancer Res* (2021) 27:43–51. doi: 10.1158/1078-0432.CCR-20-2488
16. Kowalski M, Guindon J, Brazas L, Moore C, Entwistle J, Cizeau J, et al. A Phase II Study of Oportuzumab Monatox: An Immunotoxin Therapy for Patients With Noninvasive Urothelial Carcinoma *in Situ* Previously Treated With Bacillus Calmette–Guérin. *J Urol* (2012) 188:1712–8. doi: 10.1016/j.juro.2012.07.020
17. Sylvester RJ, van der Meijden AP, Oosterlinck W, Witjes JA, Bouffioux C, Denis L, et al. Predicting Recurrence and Progression in Individual Patients With Stage Ta T1 Bladder Cancer Using EORTC Risk Tables: A Combined Analysis of 2596 Patients From Seven EORTC Trials. *Eur Urol* (2006) 49:466–5. doi: 10.1016/j.eururo.2005.12.031
18. Schildhaus HU. Predictive Value of PD-L1 Diagnostics. *Pathologe* (2018) 39:498–519. doi: 10.1007/s00292-018-0507-x
19. Krabbe LM, Bagrodia A, Haddad AQ, Kapur P, Khalil D, Hynan LS, et al. Multi-Institutional Validation of the Predictive Value of Ki-67 in Patients With High Grade Urothelial Carcinoma of the Upper Urinary Tract. *J Urol* (2015) 193:1486–93. doi: 10.1016/j.juro.2014.11.007
20. Wolff AC, Hammond MEH, Allison KH, Harvey BE, Mangu PB, Bartlett JMS, et al. Human Epidermal Growth Factor Receptor 2 Testing in Breast Cancer: American Society of Clinical Oncology/College of American Pathologists Clinical Practice Guideline Focused Update. *Arch Pathol Lab Med* (2018) 142:1364–82. doi: 10.5858/arpa.2018-0902-SA
21. Topalian SL, Taube JM, Anders RA, Pardoll DM. Mechanism-Driven Biomarkers to Guide Immune Checkpoint Blockade in Cancer Therapy. *Nat Rev Cancer* (2016) 16:275–87. doi: 10.1038/nrc.2016.36
22. Inman BA, Sebo TJ, Frigola X, Dong H, Bergstralh EJ, Frank I, et al. PD-L1 (B7-H1) Expression by Urothelial Carcinoma of the Bladder and BCG-Induced Granulomata: Associations With Localized Stage Progression. *Cancer* (2007) 109:1499–505. doi: 10.1002/cncr.22588
23. Baras AS, Drake C, Liu JJ, Gandhi N, Kates M, Hoque MO, et al. The Ratio of CD8 to Treg Tumor-Infiltrating Lymphocytes is Associated With Response to Cisplatin-Based Neoadjuvant Chemotherapy in Patients With Muscle Invasive Urothelial Carcinoma of the Bladder. *Oncoimmunology* (2016) 5:e1134412. doi: 10.1080/2162402X.2015.1134412
24. Jiang LR, Zhang N, Chen ST, He J, Liu YH, Han YQ, et al. PD-1-Positive Tumor-Associated Macrophages Define Poor Clinical Outcomes in Patients With Muscle Invasive Bladder Cancer Through Potential CD68/PD-1 Complex Interactions. *Front Oncol* (2021) 11:679928. doi: 10.3389/fonc.2021.679928
25. Kubon J, Sikic D, Eckstein M, Weyerer V, Stöhr R, Neumann A, et al. Analysis of CXCL9, PD1 and PD-L1 mRNA in Stage T1 non-Muscle Invasive Bladder Cancer and Their Association With Prognosis. *Cancers (Basel)* (2020) 12(10):2794. doi: 10.3390/cancers12102794
26. Lim CJ, Nguyen PHD, Wasser M, Kumar P, Lee YH, Nasir NJM, et al. Immunological Hallmarks for Clinical Response to BCG in Bladder Cancer. *Front Immunol* (2020) 11:615091. doi: 10.3389/fimmu.2020.615091
27. Thomsen MBH, Nordentoft I, Lamy P, Vang S, Reinert L, Mapendano CK, et al. Comprehensive Multiregional Analysis of Molecular Heterogeneity in Bladder Cancer. *Sci Rep* (2017) 7:11702. doi: 10.1038/s41598-017-11291-0
28. Eich ML, Chaux A, Guner G, Taheri D, Mendoza Rodriguez MA, Rodriguez Peña MDC, et al. Tumor Immune Microenvironment in non-Muscle-Invasive Urothelial Carcinoma of the Bladder. *Hum Pathol* (2019) 89:24–32. doi: 10.1016/j.humpath.2019.04.003
29. Kates M, Matoso A, Choi W, Baras AS, Daniels MJ, Lombardo K, et al. Adaptive Immune Resistance to Intravesical BCG in non-Muscle Invasive

Bladder Cancer: Implications for Prospective BCG-Unresponsive Trials. *Clin Cancer Res* (2020) 26:882–91. doi: 10.1158/1078-0432.CCR-19-1920
30. Eckstein M, Erben P, Kriegmair MC, Worst TS, Weiß CA, Wirtz RM, et al. Performance of the Food and Drug Administration/EMA-Approved Programmed Cell Death Ligand-1 Assays in Urothelial Carcinoma With Emphasis on Therapy Stratification for First-Line Use of Atezolizumab and Pembrolizumab. *Eur J Cancer* (2019) 106:234–43. doi: 10.1016/j.ejca.2018.11.007
31. Schwamborn K, Ammann JU, Knüchel R, Hartmann A, Baretton G, Lasitschka F, et al. Multicentric Analytical Comparability Study of Programmed Death-Ligand 1 Expression on Tumor-Infiltrating Immune Cells and Tumor Cells in Urothelial Bladder Cancer Using Four Clinically Developed Immunohistochemistry Assays. *Virchows Arch* (2019) 475:599–608. doi: 10.1007/s00428-019-02610-z
32. Rijnders M, van der Veldt AAM, Zuiverloon TCM, Grünberg K, Thunnissen E, de Wit R, et al. PD-L1 Antibody Comparison in Urothelial Carcinoma. *Eur Urol* (2019) 75:538–40. doi: 10.1016/j.eururo.2018.11.002
33. Aggen DH, Drake CG. Biomarkers for Immunotherapy in Bladder Cancer: A Moving Target. *J Immunother Cancer* (2017) 5:94. doi: 10.1186/s40425-017-0299-1
34. Zehir A, Benayed R, Shah RH, Syed A, Middha S, Kim HR, et al. Mutational Landscape of Metastatic Cancer Revealed From Prospective Clinical Sequencing of 10,000 Patients. *Nat Med* (2017) 23:703–13. doi: 10.1038/nm.4333
35. Yan M, Schwaederle M, Arguello D, Millis SZ, Gatalica Z, Kurzrock R. HER2 Expression Status in Diverse Cancers: Review of Results From 37,992 Patients. *Cancer Metastasis Rev* (2015) 34:157–64. doi: 10.1007/s10555-015-9552-6
36. Piccart-Gebhart MJ, Procter M, Leyland-Jones B, Goldhirsch A, Untch M, Smith I, et al. Trastuzumab After Adjuvant Chemotherapy in HER2-Positive Breast Cancer. *N Engl J Med* (2005) 353:1659–72. doi: 10.1056/NEJMoa052306
37. Bang YJ, Van Cutsem E, Feyereislova A, Chung HC, Shen L, Sawaki A, et al. Trastuzumab in Combination With Chemotherapy Versus Chemotherapy Alone for Treatment of HER2-Positive Advanced Gastric or Gastro-Oesophageal Junction Cancer (ToGA): A Phase 3, Open-Label, Randomised Controlled Trial. *Lancet* (2010) 376:687–97. doi: 10.1016/S0140-6736(10)61121-X
38. Chen PC, Yu HJ, Chang YH, Pan CC. Her2 Amplification Distinguishes a Subset of non-Muscle-Invasive Bladder Cancers With a High Risk of Progression. *J Clin Pathol* (2013) 66:113–9. doi: 10.1136/jclinpath-2012-200944
39. Latif Z, Watters AD, Dunn I, Grigor KM, Underwood MA, Bartlett JM. HER2/neu Overexpression in the Development of Muscle-Invasive Transitional Cell Carcinoma of the Bladder. *Br J Cancer* (2003) 89:1305–9. doi: 10.1038/sj.bjc.6601245
40. Simon R, Atefy R, Wagner U, Forster T, Fijan A, Bruderer J, et al. HER-2 and TOP2A Coamplification in Urinary Bladder Cancer. *Int J Cancer* (2003) 107:764–72. doi: 10.1002/ijc.11477
41. Nikas CV, Smith AB. Goldilocks and the BCG: Bacillus Calmette–Guérin Dose Reduction in the Age of Shortage. *Eur Urol* (2020) 78:699–700. doi: 10.1016/j.eururo.2020.05.021
42. Yang CH, Weng WC, Ou YC, Lin YS, Huang LH, Lu CH, et al. Diffusive Ki67 and Vimentin are Associated With Worse Recurrence-Free Survival of Upper Tract Urothelial Carcinoma: A Retrospective Cohort Study From Bench to Bedside. *Urol Oncol* (2022) 40:109.e21–30. doi: 10.1016/j.urolonc.2021.09.018
43. Semeniuk-Wojtaś A, Lubas A, Cierniak S, Brzóskowska U, Syryło T, Zieliński H, et al. Selected Protein Expression in a New Prognostic Model for Patients With non-Muscle-Invasive Bladder Cancer. *J Cancer Res Clin Oncol* (2020) 146:2099–108. doi: 10.1007/s00432-020-03202-0
44. Stec R, Cierniak S, Lubas A, Brzóskowska U, Syryło T, Zieliński H, et al. Intensity of Nuclear Staining for Ki-67, P53 and Survivin as a New Prognostic Factor in non-Muscle Invasive Bladder Cancer. *Pathol Oncol Res* (2020) 26:1211–9. doi: 10.1007/s12253-019-00678-1
45. Moustakas G, Kampantais S, Nikolaidou A, Vakalopoulos I, Tzioufa V, Dimitriadis G. HER-2 Overexpression is a Negative Predictive Factor for Recurrence in Patients With non-Muscle-Invasive Bladder Cancer on Intravesical Therapy. *J Int Med Res* (2020) 48:300060519895847. doi: 10.1177/0300060519895847
46. McDaniel AS, Alva A, Zhan T, Xiao H, Cao X, Gursky A, et al. Expression of PDL1 (B7-H1) Before and After Neoadjuvant Chemotherapy in Urothelial Carcinoma. *Eur Urol Focus* (2016) 1:265–8. doi: 10.1016/j.euf.2015.03.004
47. Jimenez RE, Hussain M, Bianco FJJr., Vaishampayan U, Tabazcka P, Sakr WA, et al. Her-2/Neu Overexpression in Muscle-Invasive Urothelial Carcinoma of the Bladder: Prognostic Significance and Comparative Analysis in Primary and Metastatic Tumors. *Clin Cancer Res* (2001) 7:2440–7.
48. Davick JJ, Frierson HF, Smolkin M, Gru AA. PD-L1 Expression in Tumor Cells and the Immunologic Milieu of Bladder Carcinomas: A Pathologic Review of 165 Cases. *Hum Pathol* (2018) 81:184–91. doi: 10.1016/j.humpath.2018.06.028

Conflict of Interest: The authors declare that the research was conducted in the absence of any commercial or financial relationships that could be construed as a potential conflict of interest.

Publisher's Note: All claims expressed in this article are solely those of the authors and do not necessarily represent those of their affiliated organizations, or those of the publisher, the editors and the reviewers. Any product that may be evaluated in this article, or claim that may be made by its manufacturer, is not guaranteed or endorsed by the publisher.

frontiers | Frontiers in Immunology

ORIGINAL RESEARCH
published: 30 May 2022
doi: 10.3389/fimmu.2022.903882

Tumor-Derived Exosomes Regulate Apoptosis of CD45$^+$EpCAM$^+$ Cells in Lung Cancer

Shixiang Lu[1†], Zhen Sun[2†], Lili Liu[3†], Peng Li[4], Bin Li[2], Wenjing Li[2], Zhaojun Wu[2], Mingming Zhao[2], Wenna Liu[2], Yongjie Wang[4] and Bin Wang[1*]*

[1] Department of Special Medicine, School of Basic Medicine, Qingdao University, Qingdao, China, [2] Department of Research and Development, Sino-Cell Biomed Co., Ltd., Qingdao, China, [3] School of Basic Medicine, Qingdao University, Qingdao, China, [4] Department of Thoracic Surgery, The Affiliated Hospital of Qingdao University, Qingdao, China

OPEN ACCESS

Edited by:
Min Xue,
University of California, Riverside, United States

Reviewed by:
Zhili Guo,
Quantum-Si, Inc., United States
Siwen Wang,
Ligand Pharmaceuticals, United States

***Correspondence:**
Yongjie Wang
wangyongjie@qduhospital.cn
Bin Wang
wangbin532@126.com

[†]These authors have contributed equally to this work

Specialty section:
This article was submitted to Cancer Immunity and Immunotherapy, a section of the journal Frontiers in Immunology

Received: *24 March 2022*
Accepted: *27 April 2022*
Published: *30 May 2022*

Citation:
Lu S, Sun Z, Liu L, Li P, Li B, Li W, Wu Z, Zhao M, Liu W, Wang Y and Wang B (2022) Tumor-Derived Exosomes Regulate Apoptosis of CD45$^+$EpCAM$^+$ Cells in Lung Cancer. Front. Immunol. 13:903882. doi: 10.3389/fimmu.2022.903882

Lung cancer has the highest mortality rate among human cancers, and the majority of deaths result from metastatic spread. The tumor microenvironment plays an important role in suppressing the immune surveillance and elimination of tumor cells. A few studies have reported the presence of CD45$^+$EpCAM$^+$ double-positive cells in cancer, but the underlying mechanism remains unclear with respect to how these cells originate and their function in cancer biology. In this study, we analyzed 25 lung tumor samples. We confirmed the presence of CD45$^+$EpCAM$^+$ cells in lung cancer, and these cells exhibited higher apoptosis than CD45$^+$EpCAM$^-$ cells. Using co-culture of lung cancer cell-derived exosomes with healthy donor peripheral blood mononuclear cells, we recapitulated CD45$^+$EpCAM$^+$ cell formation and increased apoptosis that occurs in patients with primary lung cancer. Further analysis suggested that microRNAs in lung cancer cell-derived exosomes may alter the gene expression profile of CD45$^+$EpCAM$^+$ cells, resulting in elevated *TP53* expression and increased apoptosis. To our knowledge, this is the first report of cancer cell-derived exosomes that can inhibit the immune system by promoting immune cell apoptosis.

Keywords: CD45$^+$EpCAM$^+$ cells, HCC827 cells, tumor-derived exosomes, PBMC, apoptosis

INTRODUCTION

Lung cancer is one of the leading causes of cancer-related deaths in both men and women (1) and remains the most commonly diagnosed cancer in the world (2). It is divided into two histological subtypes: non-small cell lung cancer (NSCLC), which accounts for 85% of the cases, and small cell lung cancer, which accounts for the remaining 15% (3). Surgical treatment, chemotherapy, radiotherapy, and targeted therapy are currently the most effective modalities for treating lung cancer. Unfortunately, the outcome for lung cancer patients remains unsatisfactory. Many studies have indicated that the chemical resistance and highly metastatic nature of epithelial tumors are associated with epithelial-mesenchymal transformation (EMT) (4, 5). Ishizawa et al. demonstrated that CD45$^+$EpCAM$^+$ cells exist in both solid cancer tissues and malignant pleural effusions in patients with NSCLC (6). The CD45$^+$EpCAM$^+$ cell population was found in three patients with EGFR mutation, and this cell population was highly suspected of exhibiting the EMT phenotype (6).

Moreover, $CD45^+EpCAM^+$ cells are not only less sensitive to standard drug regimens but also more invasive and equipped to avoid natural killer (NK) cell-mediated immune surveillance in human epithelial ovarian carcinoma (EOC) (7). However, there are few studies regarding the manner in which $CD45^+EpCAM^+$ cells are formed.

Exosomes are secreted by almost all types of cancer cells; these are extracellular vesicles, 30–150 nm in diameter (8). Nucleic acids (9), proteins (10), and lipids (11) are delivered to neighboring or remote cells and modulate recipient cells by cancer-derived exosomes. Recently, high levels of microRNAs (miRNAs) have been identified in cancer-derived exosomes, which provide an advantageous microenvironment for promoting tumorigenesis (12), tumor metastasis (9, 10), angiogenesis (13), chemoresistance (14), and immune escape (15). For example, lung cancer cell-derived exosomes that upregulate miR-28-5p, were shown to facilitate mesenchymal stem cell function in phosgene-induced acute lung injury (16).

An increasingly number of exosomes are identified as a mode of long-distance intercellular communication from sites in tissues to the circulation (17, 18). When released into the extracellular milieu, exosomes communicate *via* signals by intercellular shuttling that transports macromolecules, to promote tumor growth and immunological tolerance, locally and systemically (19–21). Acting as cellular substitutions, exosomes are important contributors to the damnification of the immune system (22). Although the role of exosomes in attenuating immunoreaction is not well known, recent research indicates that immune cells can be guided toward a tumor-promoting phenotype by cancer-derived exosomes and facilitate tumorigenesis, intrusion of the peripheral tissues, angiogenesis, formation of pre-metastatic niches, and metastatic dissemination (23). Several investigations indicate that exosomes from tumor cells possess dissimilar immunosuppressive effects, including the inhibition of effector T cell activity (24), differentiation of fibroblasts to a myofibroblastic phenotype (25), and the functional enhancement of regulatory T cells.

In this study, we report the presence of $CD45^+EpCAM^+$ cells in NSCLC tumor tissue, and these cells are prone to undergoing apoptosis. Co-culture of exosomes derived from HCC827 human lung cancer cells with PBMCs resulted in the formation of $CD45^+EpCAM^+$ cells. Further studies showed that miRNA from exosomes may play a role in changing the gene expression profiles of $CD45^+EpCAM^+$ cells to impair their antitumor activity. The p53 pathway may be one of the targets of the miRNA in exosomes, which renders these cells susceptible to apoptosis. Our data reveal a new potential mechanism of how tumor cells inhibit the immune system by producing exosomes that deliver molecules to alter immune cell function.

MATERIALS AND METHODS

Human Lung Cancer Cells

Twenty-five patients with lung cancer were recruited from a local hospital in Qingdao, China, between 2021 and 2022. This research was approved by the Ethics Committee of the Medical College of Qingdao University, under the accession number QDU-HEC-2022157. The patients were histopathologically diagnosed by at least two pathologists, according to the World Health Organization classification. No history of cancer and any antitumor therapy occurred prior to the primary diagnosis. Fresh tumor specimens were acquired using minimally invasive surgery followed by single-cell preparation as described further. Fresh lung tumor specimens were cut into small pieces of about 1–3 mm, followed by the addition of an appropriate amount of RPMI-1640 medium (CM31800; G-Clone) containing 10% FBS (SV30087.02; HyClone) on a 40-mm cell strainer (352340; FALCON) and gentle trituration with a 20-ml syringe plunger until homogeneous cell suspensions were acquired. Subsequently, the suspended cells were filtered with cell strainers followed by centrifugation at 400*g* for 10 min. Finally, the cell pellets were resuspended in RPMI-1640 medium with 10% FBS after washing twice using 1× PBS.

PBMCs Extraction and Culture

PBMCs were isolated from healthy donors using Density Reagent (DAKEWE). After density gradient centrifugation for 30 min at 700*g*, the PBMCs that settled at the interphase were carefully collected and washed twice with 1× PBS. PBMCs were cultivated in RPMI-1640 medium replenished with 10% human AB serum (Gemcell), 1% penicillin and 1% streptomycin (Gibco), CD3 (50 ng/ml; Beijing T&L Biotechnology), and Interleukin-2 (300 U/ml; Kingsley). PBMCs were conventionally sustained in a humidified incubator at 37°C with 5% CO_2, and the culture medium was substituted every other day.

Cell Culture of HCC827 Cells

The HCC827 human lung cancer cell line was acquired from the American Type Culture Collection and cultivated in RPMI-1640 medium supplemented with 10% exosome-free fetal bovine serum (C3801-0100; VivaCell), 1% penicillin and 1% streptomycin. HCC827 cells were conventionally sustained in a humidified incubator at 37°C with 5% CO_2, and the culture medium was substituted every second day. HCC827 cells were secondary cultured until they reached 80%–90% confluence.

Flow Cytometry and Cell Sorting

Cells for surface staining were obtained from the tumors or peripheral blood. The following fluorochrome-conjugated antibodies were utilized: anti-human CD19 (4G7), anti-human CD4 (OKT4), anti-human CD8 (SK1), anti-human CD3 (OKT3), anti-human EpCAM (9C4), anti-human CD45 (2D1), anti-human PD-1 (A17188B), and anti-human CD69 (FN50) (all from BioLegend). Flow cytometry data was acquired from a CytoFLEX (Beckman-Coulter, Fullerton, CA, USA) and analyzed by FlowJo software (TreeStar). The surface-stained cells were sorted using a FACSAria II (BD Biosciences) to reach more than 90% purity.

Analysis of Apoptosis

After cell surface staining, apoptosis assays were performed by staining cells with Annexin V detection kit (559763;

BD Pharmingen). Flow cytometry data was collected from a CytoFLEX and analyzed by FlowJo software.

Immunofluorescent Histochemical Staining

Tumor samples from patients with lung cancer were frozen with OCT (Sakura Finetek) in liquid nitrogen. Cryostat Microtome System was used for cutting tissues into 8-μm thick sections. The tissue sections were fixed in 4% paraformaldehyde (P0099; Beyotime) for 30 min and permeabilized by incubating in PBST (0.2% Triton X-100 in PBS) (T8787; Sigma-Aldrich) at 25°C for 20 min. The samples were blocked for 1 h at room temperature in PBS with 5% bovine serum albumin (A8010; Solarbio), and 0.05% Tween 20 (P9416; Sigma-Aldrich). The sections were then incubated with anti-EpCAM antibody (ab71916; Abcam; 1:100). Subsequently, Cy3-conjugated goat anti-rabbit IgG (GB21303; Servicebio; 1:300) and FITC conjugated CD45 antibodies (ab197730; Abcam; 1:100) were used for incubating the sections. The PBS was used to wash slides at least thrice after each procedure. The sections were immobilized and mounted with an antifade kit including DAPI (P0131; Beyotime Biotechnology) and subsequently inspected with a confocal fluorescence microscope.

Exosome Isolation, Characterization, and Treatment

As described, exosomes were obtained from cell culture supernatants by differential centrifugation (26). HCC827 cells were cultured in RPMI-1640 medium using exosome-free serum. After the supernatant was collected, centrifugation at 300g for 10 min at 4°C was used for the removal of non-adherent cells. The second centrifugation at 2,000g for 10 min at 4°C was followed by a third one at 10,000g for 30 min at 4°C, with the supernatant being transferred to a clean tube during each round. Finally, the exosomes were pelleted *via* ultracentrifugation at 120,000g for 70 min at 4°C. Subsequently, the exosome pellet was washed with 1× PBS and centrifuged at 120,000g for another 70 min, followed by resuspension in 1× PBS. The BCA protein assay kit (PC0020; Solarbio) was used to measure the exosome concentration. The exosome characterization was ascertained by HT7700 (Hitachi, Japan) TEM and exosome size by N30E Nanoparticle Tracking analysis (NanoFCM, China). $CD63^+$ human exosomes were analyzed from a pre-enriched exosome solution prepared using ultracentrifugation for flow cytometry analysis using the Human CD63 Isolation/Detection kit (10606D; Invitrogen). Purified HCC827 cell-derived exosomes were used for experimental procedures. For *in vitro* experiments, PBMCs from healthy donors were incubated with exosomes for 24 h (10, 50, and 100 μg/ml).

RNA Isolation, Reverse Transcription, and Quantitative RT-PCR

Total RNA was extracted using the RNAfast200 kit (Fastagen, China). RNA was reverse-transcribed using the HiScript® III RT SuperMix (Vazyme, China). Relative gene expression levels were analyzed by quantitative RT-PCR (qRT-PCR) with the ChamQ Universal SYBR qPCR Master Mix (Vazyme, China) on a Roche Light Cycler 480 System (Roche, Basel, Switzerland). The primer sequences were: *PTPRC*: 5′-ATA CTG GCC GTC AAT GGA AGA-3′ and 5′-CAG TTT GAG GAG CAA GTG AGG A-3′, *VIM*: 5′-CAT GAC CTC TAC GAG GAG GAG ATG C-3′ and 5′-TGT CTG AAA GAT TGC AGG GTG T-3′, *ZEB1*: 5′-AGG TGT AAG CGC AGA AAG CAG-3′ and 5′-CCT CCC AGC AGT TCT TAG CAT T-3′, *EPCAM*: 5′-ATG ATC CTG ACT GCG ATG AGA G-3′ and 5′-TGA TAA CGC GTT GTG ATC TCC T-3′, *CDH1*: 5′-CCA CCA AAG TCA CGC TGA ATA C-3′ and 5′-CTG ATG GGA GGA ATA ACC CAG T-3′, *TP53*: 5′-AGC ATC TTA TCC GAG TGG AAG G-3′ and 5′-CAG TGT GAT GAT GGT GAG GAT G-3′, and *IFNG*: 5′-TCG GTA ACT GAC TTG AAT GTC CA-3′ and 5′-TCG CTT CCC TGT TTT AGC TG C-3′, and *GAPDH*: 5′-CAT GTT CGT CAT GGG TGT GAA-3′ and 5′-CAT GGA CTG TGG TCA TGA GTC CT-3′.

siRNA Transfection

siRNA duplexes, both siRNA-control (sc-37007) and siRNA-p53 (sc-29435), as well as siRNA transfection reagent (sc-29528) were purchased from Santa Cruz Biotech. The procedure was performed according to the manufacturer's instructions. Briefly, 2×10^6 PBMCs were plated into each well and transfected with 20 nM siRNA in a six well plates. After 6 hours, 1 ml of HCC827 culture supernatant containing 20% exosome-free fetal bovine serum, 2% penicillin and 2% streptomycin were added into each well without removing the transfection mixture followed by incubating for an additional 18-24 hours. Afterwards, PBMCs were harvested and replaced with HCC827 culture supernatant containing 10% exosome-free fetal bovine serum, 1% penicillin and 1% streptomycin. 24 hours later, apoptosis assays and RT-PCR were performed.

Small RNA Sequencing and Data Analysis

Total RNA from HCC827 cell-derived exosomes was isolated with the exoRNeasy Maxi Kit (Qiagen). Next, the sequencing library was established using the high-quality RNA; 3 μg total RNA was used as raw material for the small RNA library. The NEBNext Multiplex Small RNA Library Prep Set for Illumina (NEB, USA) was used for establishing small RNA libraries. An Illumina platform from Novogene Corporation (Beijing, China) was used to sequence the libraries. For miRNA-seq data analysis, the raw data quality was evaluated with FastQC. Clean data was aligned to the latest miRBase20.0 database, and the remaining readings were aligned with the latest human genome.

Statistical Analysis

Using GraphPad Prism software (version 8.0), the statistical significance of the differences between the groups was confirmed by a two-tailed, unpaired Student's *t*-test with 95% confidence interval. Differences with $P \geq 0.05$ were considered insignificant (NS). *P* values <0.05 were considered statistically significant ($^*P < 0.05$; $^{**}P < 0.01$; $^{***}P < 0.001$).

RESULTS

$CD45^+EpCAM^+$ Cells Are Detected in Early Stages of Lung Cancer

CD45 is a marker for leukocytes, and EpCAM is a marker for epithelial cells. In 25 tumor tissues from patients with early lung

cancer, we confirmed the existence of $CD45^+EpCAM^+$ cells by FACS and immunofluorescent histochemical staining (**Figures 1A, B**). The expression levels of CD45 and EpCAM were markedly higher in $CD45^+EpCAM^+$ cells than in $CD45^+EpCAM^-$ cells (**Figures 1C, D**). Next, we examined the percentage of different immune cell subsets in the $CD45^+EpCAM^+$ population. Flow cytometry revealed a significantly higher percent of $CD3^+$ T cells in the $CD45^+EpCAM^+$ subsets than of $CD45^+EpCAM^-$ cells (**Figures 1E, F**). In contrast, significantly fewer $CD19^+$ and $CD16^+$ cells in the $EpCAM^+CD45^+$ subsets were present than $CD45^+EpCAM^-$ cells (**Figures 1E, F**).

Majority of $EpCAM^+CD45^+$ Cells Expressing PD-1 and CD69

The programmed death 1 receptor (PD-1), known as an immunoinhibitory receptor, is expressed by chronically stimulated CD8 T cells (27–29). These $PD\text{-}1^+$ CD8 T cells demonstrate a reduced proliferation capacity and express effector cytokines. CD69 is known as an activation marker and is expressed on infiltrated leukocytes at inflammatory sites under various chronic human inflammatory diseases, such as rheumatoid arthritis (30), systemic sclerosis (31), allergic asthma (32), and atopic dermatitis (33). Therefore, we first analyzed the proportion of $CD8^+$ and $CD4^+$ T cells associated

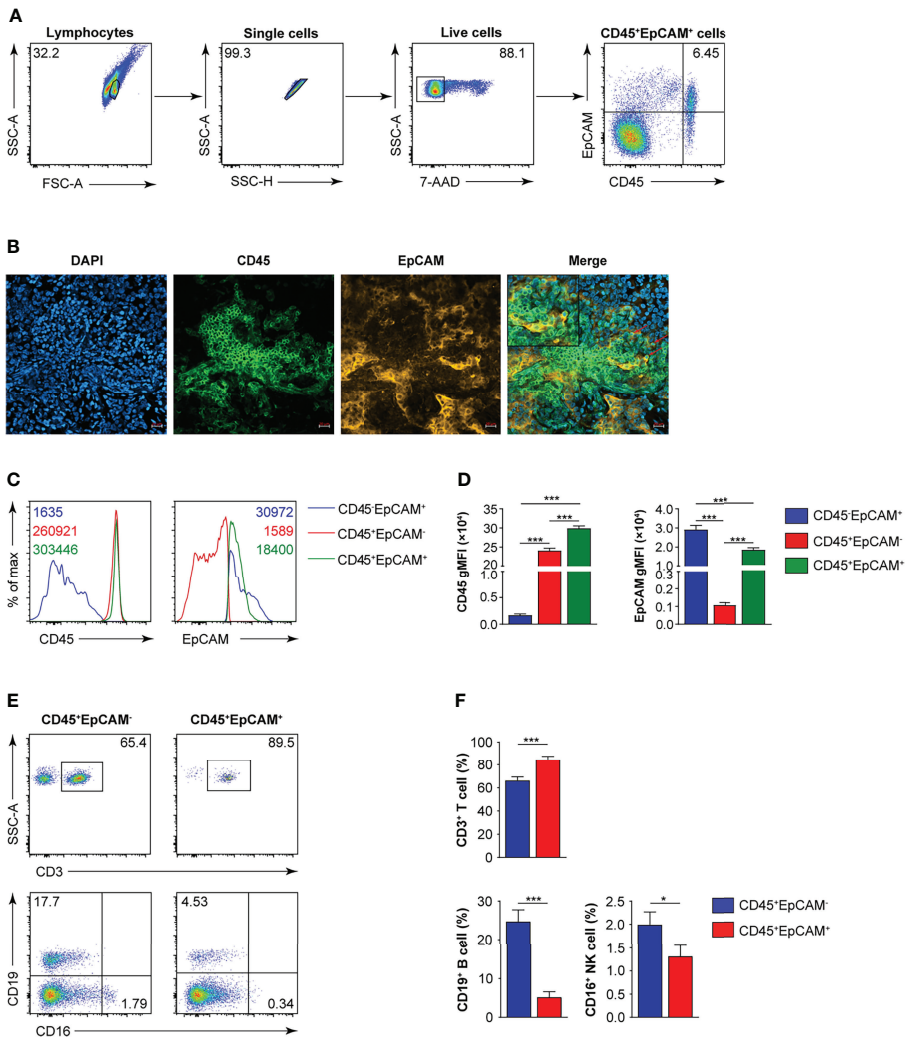

FIGURE 1 | $CD45^+EpCAM^+$ cells are detected in lung cancer tissue by FACS and immune-fluorescence microscopy. **(A)** Flow cytometry analysis of $CD45^+EpCAM^+$ cells gated on live cells from solid tumors of patients with lung cancer with representative pseudocolor plot, respectively (average of $CD45^+EpCAM^+$ in lung cancer is 6.25%, $n = 25$). **(B)** Confocal microscopy analysis of $CD45^+EpCAM^+$ cells in solid tumors from patients with lung cancer. Green: CD45, red: EpCAM. Scale bar: 20 μm. Representative figures are presented from two independent experiments. **(C, D)** Expression of CD45 and EpCAM on $CD45^+EpCAM^+$ cells was analyzed using flow cytometry with typical histograms and quantification data in **(C, D)**, respectively ($n = 25$). **(E, F)** Flow cytometry analysis of $CD3^+$ T, $CD19^+$ B, and $CD16^+$ cells gated on $CD45^+EpCAM^+$ cells or $CD45^+EpCAM^-$ cells from tumors of patients with lung cancer with typical pseudocolor plots and cumulative data in **(E, F)**, respectively ($n = 25$). Data are representative of 25 separate experiments. Error bars represent SEM. $^*P < 0.05$, and $^{***}P < 0.001$ (Student's *t*-test).

with CD45$^+$EpCAM$^+$ cells. The results indicated that there was no difference in the ratio of CD4$^+$ T to CD8$^+$ T cells in CD45$^+$EpCAM$^+$ cells compared with CD45$^+$EpCAM$^-$ cells (**Figures 2A, B**). Moreover, there was no difference in PD-1 and CD69 expression in CD8$^+$ T and CD4$^+$ T cells between CD45$^+$EpCAM$^+$ and CD45$^+$EpCAM$^-$ cells (**Figures 2C, D**). There was also no considerable difference in IFNγ production between CD45$^+$EpCAM$^+$ and CD45$^+$EpCAM$^-$ cells (**Figure 2E**). These results indicated that CD45$^+$EpCAM$^+$ T cells display an effective antitumor immune response.

CD45$^+$EpCAM$^+$ Cells Display Elevated Apoptosis

To determine whether CD45$^+$EpCAM$^+$ cells are different from CD45$^+$EpCAM$^-$ cell with respect to viability, we used Annexin V staining to quantitate apoptosis levels. We found a significantly higher rate of apoptotic cells in the CD45$^+$EpCAM$^+$ versus CD45$^+$EpCAM$^-$ cell population (**Figures 3A, B**). These data suggest that increased apoptosis of CD45$^+$EpCAM$^+$ cells may contribute to immune suppression in lung cancer.

HCC827 Lung Cancer Cell-Derived Exosomes Fuse With Healthy Donor PBMCs to Form CD45$^+$EpCAM$^+$ Cells

There are several potential mechanisms of CD45$^+$EpCAM$^+$ cell formation in cancer tissue. One possibility is the direct contact of cancer cells (expressing EpCAM) with CD45$^+$ blood cells, which may result in fusion to form CD45$^+$EpCAM$^+$ cells. The second possibility is that exosomes derived from cancer cells (or blood cells) fuse with blood (or cancer) cells. The majority of the CD45$^+$EpCAM$^+$ cells from the FACS analysis are in a single-cell gate, which suggests that the cells are unlikely to result from cell–cell fusion. Thus, we focused on the second possibility, which is to determine whether exosomes derived from cancer cells (or blood cells) induce CD45$^+$EpCAM$^+$ cell formation. We first added conditioned media from human lung cancer cell line HCC827 to peripheral blood mononuclear cells (PBMCs) and did the same vice versa. We observed a significant level of CD45$^+$EpCAM$^+$ cell formation when conditional media from HCC827 was added to the PBMCs culture system. In contrast, there were few CD45$^+$EpCAM$^+$ cells present when PBMCs conditional media was added to HCC827 cells (data not shown). The cell growth rate was not affected in either experiment indicating that conditioned media did not affect cell growth.

To identify the components in the conditioned media of the HCC827 human lung cancer cell line that mediated this phenotypic switch of CD45$^+$ immune cells, we determined whether the exosomes were a significant contributor. Exosomes were isolated from the culture supernatants of HCC827 cells through multiple rounds of centrifugation. Using transmission electron microscopy (TEM), the HCC827-derived exosomes were perceived to be circular vesicles (**Figure 4A**), and exosome sizes in the range of 30–150 nm were detected by nanoparticle tracking analysis (**Figure 4B**). Flow cytometry revealed that CD63 and EpCAM were co-expressed in the isolated exosomes (**Figure 4C**). We isolated PBMCs from healthy donors and cocultured them under various conditions (**Figure 4D**). We observed CD45$^+$EpCAM$^+$ cells when PBMCs were cocultured with HCC827, with HCC827 conditioned media, and with different amounts of purified exosomes (**Figures 4D, E**). The formation of CD45$^+$EpCAM$^+$ cells in PBMCs/exosome co-culture occurred in an exosome

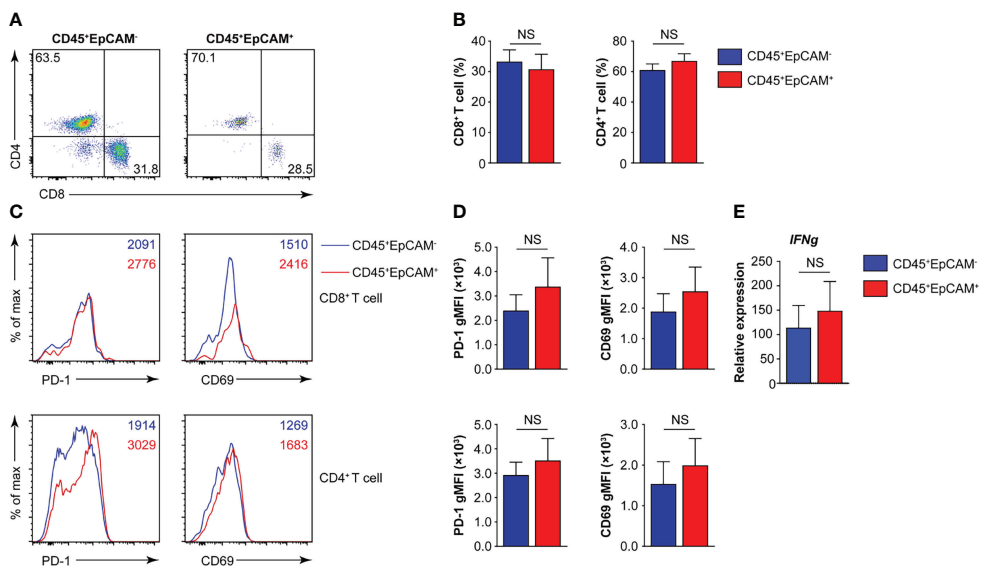

FIGURE 2 | CD45$^+$EpCAM$^+$CD8$^+$ T cells in lung cancer express PD-1 and CD69. **(A, B)** Flow cytometry analysis of CD8$^+$ T and CD4$^+$ T cells gated on CD45$^+$EpCAM$^+$CD3$^+$ and CD45$^+$EpCAM$^-$CD3$^+$ cells from tumors of patients with lung cancer with representative pseudocolor plot and cumulative data in **(A)** and **(B)**, respectively ($n = 8$). **(C, D)** Expression of PD-1 and CD69 on CD8$^+$ T and CD4$^+$ T cells was analyzed using flow cytometry with typical histograms and quantification data in **(C)** and **(D)**, respectively ($n \geq 8$). **(E)** Quantitative RT-PCR analysis of *IFNg* from sorted CD45$^+$EpCAM$^+$ and CD45$^+$EpCAM$^-$ cells after PBMCs cultured with HCC827 cell conditioned media ($n \geq 4$) NS, no significance.

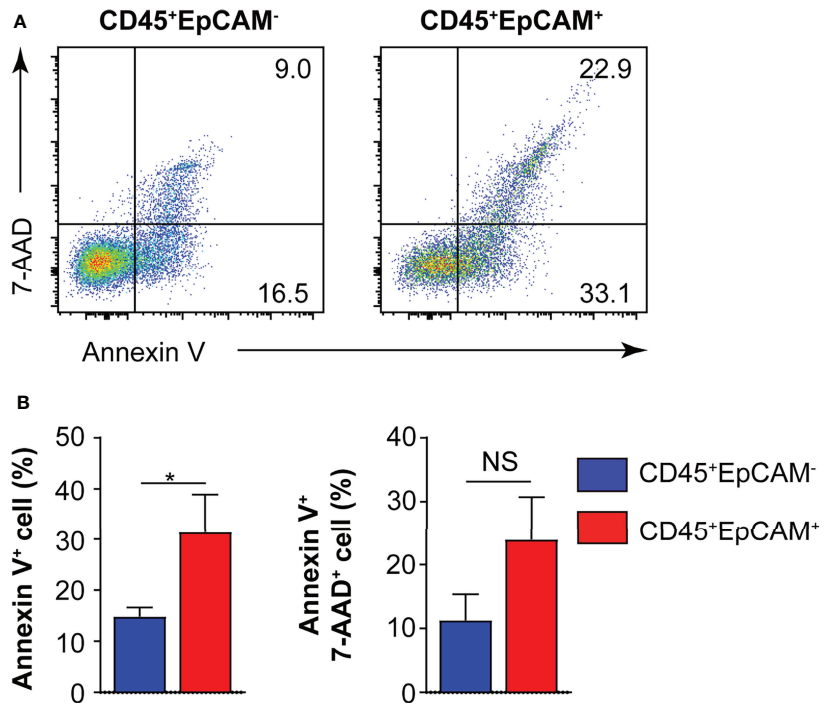

FIGURE 3 | $CD45^+EpCAM^+$ cells undergo apoptosis in the tumor microenvironment. **(A)** $CD45^+EpCAM^+$ and $CD45^+EpCAM^-$ cells from tumors of patients with lung cancer were stained with Annexin V/7-AAD kit to assess viability by flow cytometry. **(B)** The ratio of apoptosis in $CD45^+EpCAM^+$ and $CD45^+EpCAM^-$ cells is shown in **(B)**, respectively ($n = 6$). Data are representative of six separate experiments. Error bars represent SEM. $^*P < 0.05$ (Student's *t*-test). NS, no significance.

dose-dependent manner. Next, we sorted $CD45^+EpCAM^+$ and $CD45^+EpCAM^-$ cells to examine gene expression. We found that the expression of the epithelial cell-related genes, *EPCAM* and *CDH1*, was markedly increased in $CD45^+EpCAM^+$ cells by quantitative RT-PCR analysis (**Figure 4F**). In contrast, the expression of mesenchymal cell-relevant genes *PTPRC*, *VIM*, and *ZEB1* did not show significant differences in $CD45^+EpCAM^+$ cells compared with $CD45^+EpCAM^-$ cells (**Figure 4F**).

$CD45^+EpCAM^+$ Cells From PBMCs and Exosome Co-Culture Show Increased Apoptosis

We measured the apoptosis rate of $CD45^+EpCAM^+$ and $CD45^+EpCAM^-$ cells in PBMCs after HCC827 cell-derived exosome treatment. We found that the apoptosis ratio was increased in $CD45^+EpCAM^+$ cells compared with $CD45^+EpCAM^-$ cells from PBMCs co-cultured with HCC827 cells, HCC827 media, and different amounts of exosomes (**Figures 5A, B**). Moreover, apoptosis was increased in $CD45^+EpCAM^+$ cells when PBMCs were co-cultured with higher amounts of HCC827-derived exosomes.

HCC827 Cell-Derived Exosomes Promote $CD45^+EpCAM^+$ Cell Apoptosis *via* the p53 Pathway

To identify the mechanisms of HCC827 cell-derived exosomes in regulating $CD45^+EpCAM^+$ cell apoptosis, we analyzed the miRNA profiles of the exosomes. The miRNA data analysis revealed that numerous miRNAs were encapsulated within the exosomes (**Table S1**). GO and KEGG pathway enrichment analyses were performed for miRNA-targeted genes in HCC827 cell-derived exosomes, and the results are presented in **Figures 6A, B**. Based on the results, miRNA target genes were enriched in multiple GO categories including cellular process, metabolic process, cell organelle, and so on (**Figure 6A**). Simultaneously, miRNA-targeted genes were enriched in several signaling pathways, including pathways in cancer, PI3K-Akt signaling, JAK-STAT signaling, apoptosis, NSCLC, and particularly the p53 signaling pathway (**Figure 6B**). The miRNAs targeting genes of the p53 signaling pathway were detected in HCC827 cell-derived exosomes (**Figure 6C**). Using quantitative RT-PCR, we confirmed the *TP53* gene alterations. We found increased expression of the apoptotic-related gene, *TP53*, in $CD45^+EpCAM^+$ cells compared with $CD45^+EpCAM^-$ cells (**Figure 6D**). To further confirm the regulatory role of p53 signaling pathway in $CD45^+EpCAM^+$ cell apoptosis, we used siRNA-p53 to knock down *TP53* gene in the PBMCs-exosome co-culture system (**Figure 6E**). In $CD45^+EpCAM^+$ cell population, we found significantly decreased apoptosis in siRNA-p53 treated group compared with siRNA-control treated group (**Figures 6F, G**). Overall, these results suggest that HCC827 cell-derived exosomal miRNAs induce $CD45^+EpCAM^+$ cell apoptosis *via* the p53 pathway. However, since miRNAs can regulate multiple apoptosis-related signaling

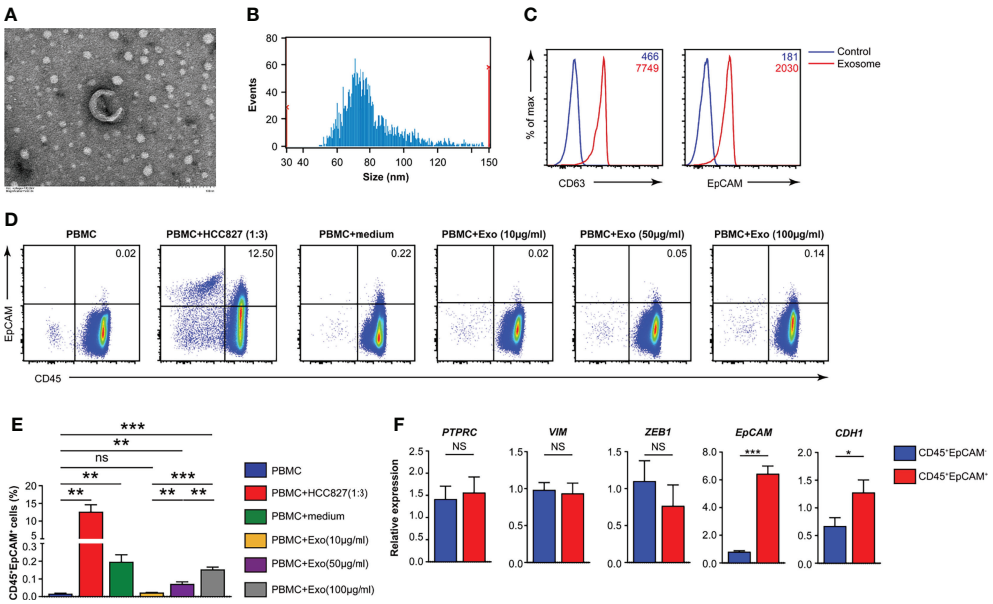

FIGURE 4 | HCC827 cell-derived exosomes play a critical role in CD45$^+$EpCAM$^+$ cell formation. **(A)** Representative TEM pictures of HCC827 cell-derived exosomes. Scale bar: 100 nm. **(B)** Nanoparticle tracking the size distribution of HCC827 cell-derived exosomes. **(C)** Detection of protein levels of CD63 and EpCAM in HCC827 cell-derived exosomes by flow cytometry (representative of 3 independent experiments). **(D, E)** Flow cytometry analysis of CD45$^+$EpCAM$^+$ cells from PBMCs cocultured with HCC827 cells, cultured with HCC827 cell media, or with HCC827 cell-derived exosomes (10, 50, and 100 μg/ml) for 24 h. Analysis of CD45$^+$EpCAM$^+$ and CD45$^+$EpCAM$^-$ cells was from the same sample, and 5 × 10^5 live cells were analyzed for each sample. Representative pseudocolor plot and cumulative data are demonstrated in **(D, E)**, respectively (n = 3). **(F)** Quantitative RT-PCR analysis of epithelial and mesenchymal marker genes described as above in CD45$^+$EpCAM$^+$ and CD45$^+$EpCAM$^-$ cells from PBMCs cultured with HCC827 cell conditioned media ($n \geq 4$). Data are representative of at the latest three separate experiments. Error bars delegate SEM. *P < 0.05, **P < 0.01, and ***P < 0.001 (Student's t-test). NS, no significance.

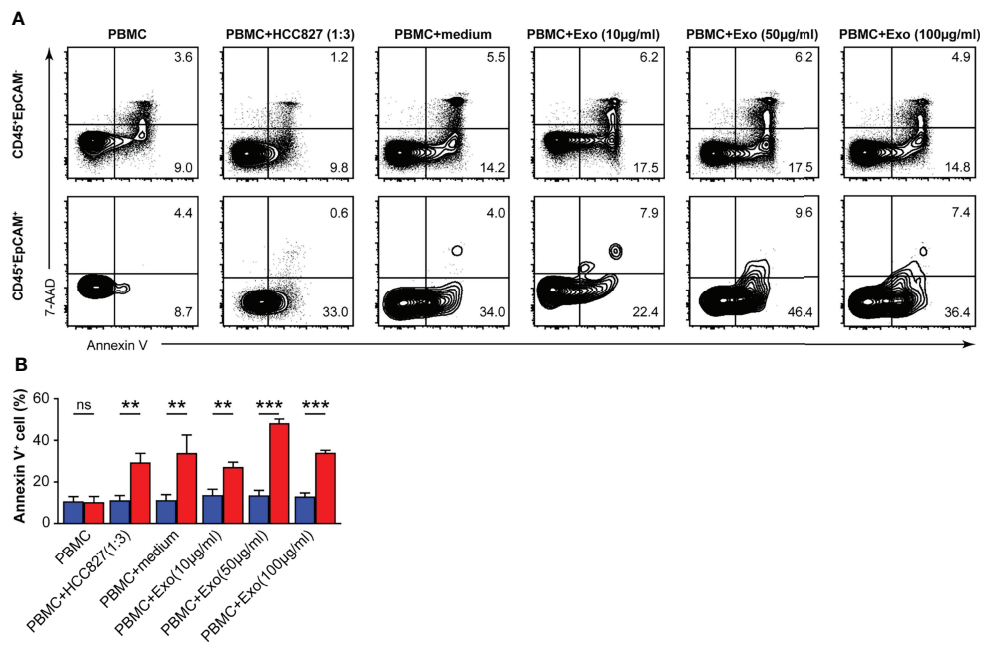

FIGURE 5 | HCC827 cell-derived exosomes induce CD45$^+$EpCAM$^+$ cells from PBMCs that are prone to apoptosis. **(A)** Contour plots represent Annexin V$^+$ cells gated on CD45$^+$EpCAM$^-$ (top panel) and CD45$^+$EpCAM$^+$ cells (bottom panel) from PBMCs, cocultured with HCC827 cells, or with HCC827 cell media, or with different amounts of HCC827 cell-derived exosomes (10, 50, and 100 μg/ml) for 24 h. Data are representative of three separate experiments. **(B)** Quantification data on the ratio of Annexin V$^+$ cells are demonstrated (n = 3). Error bars represent SEM. **P < 0.01, and ***P < 0.001 (Student's t-test). NS, no significance.

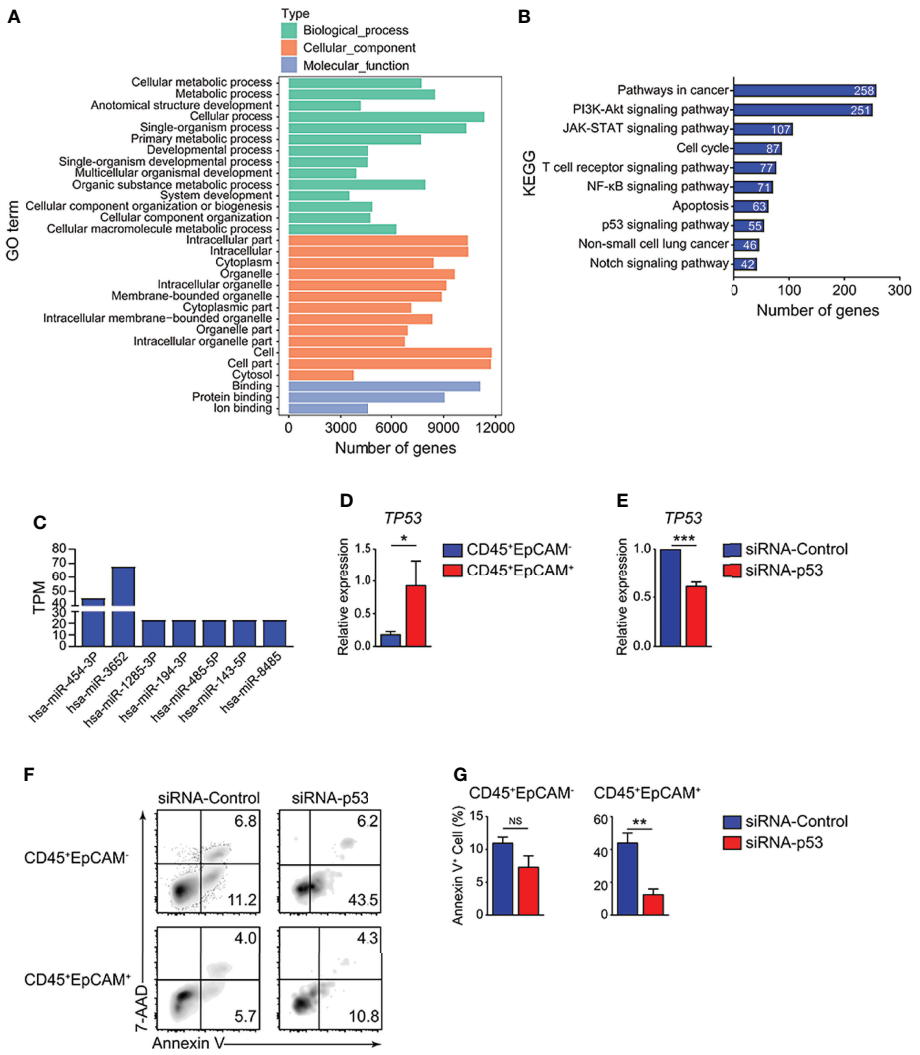

FIGURE 6 | HCC827 cell-derived exosomes promote CD45$^+$EpCAM$^+$ cell apoptosis *via* the p53 pathway. **(A)** GO function analysis for miRNA-targeted genes in HCC827 cell-derived exosomes. **(B)** KEGG pathway analysis of miRNA-targeted genes in HCC827 cell-derived exosomes. **(C)** Expression of miRNAs targeting gene *TP53* in HCC827 cell-derived exosomes. **(D)** Quantitative RT-PCR analysis of the cell apoptosis-related gene, *TP53*, in CD45$^+$EpCAM$^+$ and CD45$^+$EpCAM$^-$ cells from PBMCs cultured with HCC827 cell conditioned media ($n \geq 4$). **(E)** Quantitative RT-PCR analysis of *TP53* in siRNA-control group and siRNA-p53 group from PBMCs cultured with HCC827 cell conditioned media ($n = 3$). **(F, G)** Flow cytometry analysis of Annexin V$^+$ cells gated on CD45$^+$EpCAM$^-$ (top panel) and CD45$^+$EpCAM$^+$ cells (bottom panel) from PBMCs cultured with HCC827 cell conditioned media, treated with siRNA-control or siRNA-p53 treatment respectively. Data are presented by typical density plots and quantification data shown in **(F, G)**, ($n = 3$). Data are representative of at any rate two separate experiments. Error bars delegate SEM. $^*P < 0.05$, and $^{**}P < 0.01$, and $^{***}P < 0.001$ (Student's *t*-test). NS, no significance.

pathways, there may be other regulatory mechanisms that require further investigation.

DISCUSSION

Previous studies showed that CD45$^+$EpCAM$^+$ cells are associated with the EMT. CD45$^+$EpCAM$^+$ cells display the main tumor burden and more drug-resistance than EpCAM$^+$ tumor cells in patients with NSCLC and EOC (6, 7). In this study, we showed that varying percentages of CD45$^+$EpCAM$^+$ cells exist in all of the 25 patient lung tumor tissues examined (**Figure 1**). The majority CD45$^+$EpCAM$^+$ cells are activated CD3$^+$ T cells expressing both PD-1 and CD69 (**Figure 2**). Interestingly, our data have shown that CD45$^+$EpCAM$^+$ cells display elevated levels of apoptosis (**Figure 3**). This data suggest it may be another mechanism by which tumor cells suppress immune cell activity.

Latest research demonstrates that the exosome-mediated cellular material exchange between cells is a significant method of intercellular communication (34–36). Tumor-derived exosomes regulate intercellular communication and signaling pathways that influence cancer progression by transferring

nucleic acids and proteins between varieties of cell genres. The latest evidence indicates that tumor-derived exosomes can also regulate immunoreaction (37). For instance, tumor-derived exosomes can be efficiently taken up by dendritic cells (DCs), and the antigen is processed and cross-presented to tumor-specific CTLs (38, 39). Du et al. revealed that LLC-derived exosomes are taken up by immune cells in the lung (40). In the present study, $CD45^+EpCAM^+$ cells were observed when PBMCs were co-cultured with HCC827, HCC827 conditioned media, and different amounts of purified exosomes. Moreover, the formation of $CD45^+EpCAM^+$ cells under PBMCs/exosome co-culture conditions occurs in an exosome dose-dependent manner (**Figures 4D, E**). We also observed $CD45^+EpCAM^+$ cell formation when the media after ultracentrifugation were used for PBMCs co-culture, although at less level compared with the purified exosomes (data not show) or media before ultracentrifugation. This suggests that ultracentrifugation did not recover all the exosomes in HCC827 conditioned media. Other components in HCC827 conditioned media may also exist and play roles to enhance the $CD45^+EpCAM^+$ cell formation to assist exosome or independently. In tumor environment, cellular mechanisms may also be involved in $CD45^+EpCAM^+$ cell formation such as recently reported " trogocytosis" when immune cells steal tumor cell membranes carrying surface protein (41). The expression of the epithelial cell-related genes, *EPCAM* and *CDH1*, was markedly increased in $CD45^+EpCAM^+$ cells as determined by quantitative RT-PCR analysis (**Figure 4F**). These results indicate that tumor cells may influence the gene expression of immune cells through exosomes.

An increasing number of evidence demonstrates that exosomes contribute to tumor progression by transmitting immunosuppressive molecules (42). Exosomal miRNAs are vital carriers that can affect the function of immune cells containing DCs and T cells in cancer (43). Lung tumor cell-derived exosomes can transfer miR-21/29a to activate TLR7 and TLR8 in immune cells, which were promoted to tumor development and metastasis (44). In addition, the study demonstrated that tumor cell-derived exosomes can deliver miR-214 to CD4 T cells in human cancers, which ultimately reduced phosphatase and tensin homolog production and accelerated Treg cell expansion and tumor growth (45). In our study, we found a significantly higher rate of apoptotic cells in $CD45^+EpCAM^+$ versus $CD45^+EpCAM^-$ cells from solid tumors of patients with lung cancer (**Figure 3**). We recapitulated these results by co-culturing PBMCs with HCC827 cell-derived exosomes. $CD45^+EpCAM^+$ cells formed from co-culture of PBMCs with HCC827 cell derived exosomes showed increased apoptosis (**Figure 5**).

In the current research, miRNA sequencing analysis was used to confirm the functional miRNAs encapsulated in tumor derived exosomes that contribute to elevated $CD45^+EpCAM^+$ cell apoptosis. The miRNA-targeted genes were enriched in apoptotic-related signaling pathways by KEGG pathway analysis. All types of responses containing cell cycle arrest and apoptosis were generated by activated p53 (46, 47). The miRNA sequencing results indicate that the miRNAs targeting genes of the p53 signaling pathway were detected in HCC827 cell-derived exosomes, including miR454-3P, miR3652, miR1285-3P, miR194-3P, miR485-3P, miR143-3P, and miR8485 (**Figure 6C**). We confirmed that the expression of the apoptosis-related gene, *TP53*, markedly increased in $CD45^+EpCAM^+$ cells, by quantitative RT-PCR analysis (**Figure 6D**).

In summary, we demonstrated that $CD45^+EpCAM^+$ cell formation and increased apoptosis occur in patients with primary lung cancer and from PBMCs treated with HCC827 cell-derived exosomes. Further analysis suggests that miRNAs from lung cancer cell-derived exosomes may alter the gene expression profiles of $CD45^+EpCAM^+$ cells, resulting in elevated *TP53* expression and increased apoptosis. As far as we know, this research is the first to report that cancer cell-derived exosomes can inhibit the immune system by promoting immune cell apoptosis. Overall, this work disclosed a novel mechanism that is capable of inducing immune inhibition in the tumor microenvironment.

DATA AVAILABILITY STATEMENT

The datasets presented in this study can be found in online repositories. The names of the repository/repositories and accession number(s) can be found below: https://www.ncbi.nlm.nih.gov/geo/, GSE197975.

ETHICS STATEMENT

The studies involving human participants were reviewed and approved by Approval document of Ethics Committee Medical College of Qingdao University. The patients/participants provided their written informed consent to participate in this study.

AUTHOR CONTRIBUTIONS

SL and ZS performed and analyzed all experiments and were involved in drafting the manuscript. LL contributed to data analysis. PL provided tumors from patients with lung cancer. ZW analyzed the miRNA-seq data. BL, WJL, MZ, and WNL assisted with the total experiments. YW and BW supervised the project and designed the experiments. All authors have read and endorsed the ultimate manuscript.

FUNDING

This work was supported in part by grants from the Wu Jieping Medical Foundation to YW (320.6750.2021-01-4) and the Project for "Clinical Medicine + X" supported by the Affiliated Hospital of Qingdao University to YW (QYFY-X2021032/3731).

SUPPLEMENTARY MATERIAL

The Supplementary Material for this article can be found online at: https://www.frontiersin.org/articles/10.3389/fimmu.2022.903882/full#supplementary-material

REFERENCES

1. Siegel RL, Miller KD, Jemal A. Cancer Statistics, 2017. *CA Cancer J Clin* (2017) 67(1):7–30. doi: 10.3322/caac.21387
2. Fan H, Shao ZY, Xiao YY, Xie ZH, Chen W, Xie H, et al. Incidence and Survival of Non-Small Cell Lung Cancer in Shanghai: A Population-Based Cohort Study. *BMJ Open* (2015) 5(12):e009419. doi: 10.1136/bmjopen-2015-009419
3. Oser MG, Niederst MJ, Sequist LV, Engelman JA. Transformation From Non-Small-Cell Lung Cancer to Small-Cell Lung Cancer: Molecular Drivers and Cells of Origin. *Lancet Oncol* (2015) 16(4):e165–72. doi: 10.1016/S1470-2045(14)71180-5
4. Wang Z, Li Y, Kong D, Banerjee S, Ahmad A, Azmi AS, et al. Acquisition of Epithelial-Mesenchymal Transition Phenotype of Gemcitabine-Resistant Pancreatic Cancer Cells Is Linked With Activation of the Notch Signaling Pathway. *Cancer Res* (2009) 69(6):2400–7. doi: 10.1158/0008-5472.CAN-08-4312
5. Ahmed N, Abubaker K, Findlay J, Quinn M. Epithelial Mesenchymal Transition and Cancer Stem Cell-Like Phenotypes Facilitate Chemoresistance in Recurrent Ovarian Cancer. *Curr Cancer Drug Targets* (2010) 10(3):268–78. doi: 10.2174/156800910791190175
6. Ishizawa K, Yamanaka M, Saiki Y, Miyauchi E, Fukushige S, Akaishi T, et al. CD45(+)CD326(+) Cells Are Predictive of Poor Prognosis in Non-Small Cell Lung Cancer Patients. *Clin Cancer Res* (2019) 25(22):6756–63. doi: 10.1158/1078-0432.CCR-19-0545
7. Akhter MZ, Sharawat SK, Kumar V, Kochat V, Equbal Z, Ramakrishnan M, et al. Aggressive Serous Epithelial Ovarian Cancer is Potentially Propagated by EpCAM(+)CD45(+) Phenotype. *Oncogene* (2018) 37(16):2089–103. doi: 10.1038/s41388-017-0106-y
8. Ruivo CF, Adem B, Silva M, Melo SA. The Biology of Cancer Exosomes: Insights and New Perspectives. *Cancer Res* (2017) 77(23):6480–8. doi: 10.1158/0008-5472.CAN-17-0994
9. Fang T, Lv H, Lv G, Li T, Wang C, Han Q, et al. Tumor-Derived Exosomal miR-1247-3p Induces Cancer-Associated Fibroblast Activation to Foster Lung Metastasis of Liver Cancer. *Nat Commun* (2018) 9(1):191. doi: 10.1038/s41467-017-02583-0
10. Zhang H, Deng T, Liu R, Bai M, Zhou L, Wang X, et al. Exosome-Delivered EGFR Regulates Liver Microenvironment to Promote Gastric Cancer Liver Metastasis. *Nat Commun* (2017) 8:15016. doi: 10.1038/ncomms15016
11. Skotland T, Sandvig K, Llorente A. Lipids in Exosomes: Current Knowledge and the Way Forward. *Prog Lipid Res* (2017) 66:30–41. doi: 10.1016/j.plipres.2017.03.001
12. Melo SA, Sugimoto H, O'Connell JT, Kato N, Villanueva A, Vidal A, et al. Cancer Exosomes Perform Cell-Independent microRNA Biogenesis and Promote Tumorigenesis. *Cancer Cell* (2014) 26(5):707–21. doi: 10.1016/j.ccell.2014.09.005
13. Zeng Z, Li Y, Pan Y, Lan X, Song F, Sun J, et al. Cancer-Derived Exosomal miR-25-3p Promotes Pre-Metastatic Niche Formation by Inducing Vascular Permeability and Angiogenesis. *Nat Commun* (2018) 9(1):5395. doi: 10.1038/s41467-018-07810-w
14. Deng Z, Rong Y, Teng Y, Zhuang X, Samykutty A, Mu J, et al. Exosomes miR-126a Released From MDSC Induced by DOX Treatment Promotes Lung Metastasis. *Oncogene* (2017) 36(5):639–51. doi: 10.1038/onc.2016.229
15. Song Y, Dou H, Li X, Zhao X, Li Y, Liu D, et al. Exosomal miR-146a Contributes to the Enhanced Therapeutic Efficacy of Interleukin-1beta-Primed Mesenchymal Stem Cells Against Sepsis. *Stem Cells* (2017) 35(5):1208–21. doi: 10.1002/stem.2564
16. Shao Y, Zhou F, He D, Zhang L, Shen J. Overexpression of CXCR7 Promotes Mesenchymal Stem Cells to Repair Phosgene-Induced Acute Lung Injury in Rats. *BioMed Pharmacother* (2019) 109:1233–9. doi: 10.1016/j.biopha.2018.10.108
17. Thery C, Zitvogel L, Amigorena S. Exosomes: Composition, Biogenesis and Function. *Nat Rev Immunol* (2002) 2(8):569–79. doi: 10.1038/nri855
18. Raposo G, Stoorvogel W. Extracellular Vesicles: Exosomes, Microvesicles, and Friends. *J Cell Biol* (2013) 200(4):373–83. doi: 10.1083/jcb.201211138
19. Zomer A, Vendrig T, Hopmans ES, van Eijndhoven M, Middeldorp JM, Pegtel DM. Exosomes: Fit to Deliver Small RNA. *Commun Integr Biol* (2010) 3(5):447–50. doi: 10.4161/cib.3.5.12339
20. Valadi H, Ekstrom K, Bossios A, Sjostrand M, Lee JJ, Lotvall JO. Exosome-Mediated Transfer of mRNAs and microRNAs Is a Novel Mechanism of Genetic Exchange Between Cells. *Nat Cell Biol* (2007) 9(6):654–9. doi: 10.1038/ncb1596
21. Thery C, Ostrowski M, Segura E. Membrane Vesicles as Conveyors of Immune Responses. *Nat Rev Immunol* (2009) 9(8):581–93. doi: 10.1038/nri2567
22. Ricklefs FL, Alayo Q, Krenzlin H, Mahmoud AB, Speranza MC, Nakashima H, et al. Immune Evasion Mediated by PD-L1 on Glioblastoma-Derived Extracellular Vesicles. *Sci Adv* (2018) 4(3):eaar2766. doi: 10.1126/sciadv.aar2766
23. Sceneay J, Smyth MJ, Moller A. The Pre-Metastatic Niche: Finding Common Ground. *Cancer Metastasis Rev* (2013) 32(3-4):449–64. doi: 10.1007/s10555-013-9420-1
24. Clayton A, Al-Taei S, Webber J, Mason MD, Tabi Z. Cancer Exosomes Express CD39 and CD73, Which Suppress T Cells Through Adenosine Production. *J Immunol* (2011) 187(2):676–83. doi: 10.4049/jimmunol.1003884
25. Webber J, Steadman R, Mason MD, Tabi Z, Clayton A. Cancer Exosomes Trigger Fibroblast to Myofibroblast Differentiation. *Cancer Res* (2010) 70(23):9621–30. doi: 10.1158/0008-5472.CAN-10-1722
26. Plebanek MP, Angeloni NL, Vinokour E, Li J, Henkin A, Martinez-Marin D, et al. Pre-Metastatic Cancer Exosomes Induce Immune Surveillance by Patrolling Monocytes at the Metastatic Niche. *Nat Commun* (2017) 8(1):1319. doi: 10.1038/s41467-017-01433-3
27. Chen L. Co-Inhibitory Molecules of the B7-CD28 Family in the Control of T-Cell Immunity. *Nat Rev Immunol* (2004) 4(5):336–47. doi: 10.1038/nri1349
28. Greenwald RJ, Freeman GJ, Sharpe AH. The B7 Family Revisited. *Annu Rev Immunol* (2005) 23:515–48. doi: 10.1146/annurev.immunol.23.021704.115611
29. Sharpe AH, Wherry EJ, Ahmed R, Freeman GJ. The Function of Programmed Cell Death 1 and its Ligands in Regulating Autoimmunity and Infection. *Nat Immunol* (2007) 8(3):239–45. doi: 10.1038/ni1443
30. Afeltra A, Galeazzi M, Ferri GM, Amoroso A, De Pita O, Porzio F, et al. Expression of CD69 Antigen on Synovial Fluid T Cells in Patients With Rheumatoid Arthritis and Other Chronic Synovitis. *Ann Rheum Dis* (1993) 52(6):457–60. doi: 10.1136/ard.52.6.457
31. Radstake TR, van Bon L, Broen J, Hussiani A, Hesselstrand R, Wuttge DM, et al. The Pronounced Th17 Profile in Systemic Sclerosis (SSc) Together With Intracellular Expression of TGFbeta and IFNgamma Distinguishes SSc Phenotypes. *PloS One* (2009) 4(6):e5903. doi: 10.1371/journal.pone.0005903
32. Julius P, Luttmann W, Knoechel B, Kroegel C, Matthys H, Virchow JC Jr. CD69 Surface Expression on Human Lung Eosinophils After Segmental Allergen Provocation. *Eur Respir J* (1999) 13(6):1253–9. doi: 10.1183/09031936.99.13612609
33. Toma T, Mizuno K, Okamoto H, Kanegane C, Ohta K, Ikawa Y, et al. Expansion of Activated Eosinophils in Infants With Severe Atopic Dermatitis. *Pediatr Int* (2005) 47(1):32–8. doi: 10.1111/j.1442-200x.2004.02004.x
34. Wang P, Wang H, Huang Q, Peng C, Yao L, Chen H, et al. Exosomes From M1-Polarized Macrophages Enhance Paclitaxel Antitumor Activity by Activating Macrophages-Mediated Inflammation. *Theranostics* (2019) 9(6):1714–27. doi: 10.7150/thno.30716
35. Wang QL, Zhuang X, Sriwastva MK, Mu J, Teng Y, Deng Z, et al. Blood Exosomes Regulate the Tissue Distribution of Grapefruit-Derived Nanovector *via* CD36 and IGFR1 Pathways. *Theranostics* (2018) 8(18):4912–24. doi: 10.7150/thno.27608
36. Liu Y, Bai L, Guo K, Jia Y, Zhang K, Liu Q, et al. Focused Ultrasound-Augmented Targeting Delivery of Nanosonosensitizers From Homogenous Exosomes for Enhanced Sonodynamic Cancer Therapy. *Theranostics* (2019) 9(18):5261–81. doi: 10.7150/thno.33183
37. Robbins PD, Morelli AE. Regulation of Immune Responses by Extracellular Vesicles. *Nat Rev Immunol* (2014) 14(3):195–208. doi: 10.1038/nri3622
38. Wolfers J, Lozier A, Raposo G, Regnault A, Thery C, Masurier C, et al. Tumor-Derived Exosomes are a Source of Shared Tumor Rejection Antigens for CTL Cross-Priming. *Nat Med* (2001) 7(3):297–303. doi: 10.1038/85438
39. Andre F, Schartz NE, Movassagh M, Flament C, Pautier P, Morice P, et al. Malignant Effusions and Immunogenic Tumour-Derived Exosomes. *Lancet* (2002) 360(9329):295–305. doi: 10.1016/S0140-6736(02)09552-1
40. Du C, Duan X, Yao X, Wan J, Cheng Y, Wang Y, et al. Tumour-Derived Exosomal miR-3473b Promotes Lung Tumour Cell Intrapulmonary Colonization by Activating the Nuclear factor-kappaB of Local Fibroblasts. *J Cell Mol Med* (2020) 24(14):7802–13. doi: 10.1111/jcmm.15411

41. Hasim MS, Marotel M, Hodgins JJ, Vulpis E, Makinson OJ, Asif S, et al. When Killers Become Thieves: Trogocytosed PD-1 Inhibits NK Cells in Cancer. *Sci Adv* (2022) 8(15):eabj3286. doi: 10.1126/sciadv.abj3286
42. Greening DW, Gopal SK, Xu R, Simpson RJ, Chen W. Exosomes and Their Roles in Immune Regulation and Cancer. *Semin Cell Dev Biol* (2015) 40:72–81. doi: 10.1016/j.semcdb.2015.02.009
43. Sun Z, Shi K, Yang S, Liu J, Zhou Q, Wang G, et al. Effect of Exosomal miRNA on Cancer Biology and Clinical Applications. *Mol Cancer* (2018) 17(1):147. doi: 10.1186/s12943-018-0897-7
44. Fabbri M, Paone A, Calore F, Galli R, Gaudio E, Santhanam R, et al. MicroRNAs Bind to Toll-Like Receptors to Induce Prometastatic Inflammatory Response. *Proc Natl Acad Sci USA* (2012) 109(31):E2110–6. doi: 10.1073/pnas.1209414109
45. Yin Y, Cai X, Chen X, Liang H, Zhang Y, Li J, et al. Tumor-Secreted miR-214 Induces Regulatory T Cells: A Major Link Between Immune Evasion and Tumor Growth. *Cell Res* (2014) 24(10):1164–80. doi: 10.1038/cr.2014.121
46. Vousden KH, Lu X. Live or Let Die: The Cell's Response to P53. *Nat Rev Cancer* (2002) 2(8):594–604. doi: 10.1038/nrc864
47. Vogelstein B, Lane D, Levine AJ. Surfing the P53 Network. *Nature* (2000) 408 (6810):307–10. doi: 10.1038/35042675

Conflict of Interest: ZS, BL, WJL, ZW, MZ, and WNL are employed by Sino-Cell Biomed Co., Ltd. BW is a consultant for Sino-Cell Biomed Co., Ltd.

The remaining authors declare that the research was conducted in the absence of any commercial or financial relationships that could be construed as a potential conflict of interest.

frontiers | Frontiers in Immunology

REVIEW
published: 01 June 2022
doi: 10.3389/fimmu.2022.907550

Immune Microenvironment in Osteosarcoma: Components, Therapeutic Strategies and Clinical Applications

Tianyi Zhu[†], *Jing Han*[†], *Liu Yang*, *Zhengdong Cai*, *Wei Sun*[*], *Yingqi Hua*[*] *and Jing Xu*[*]

Department of Orthopedics, Shanghai General Hospital, Shanghai Jiao Tong University School of Medicine, Shanghai Bone Tumor Institution, Shanghai, China

OPEN ACCESS

Edited by:
Qihui Shi,
Fudan University, China

Reviewed by:
Zhuo Cheng,
Eastern Hepatobiliary Surgery Hospital, China
Qihui Liu,
Jilin University, China

***Correspondence:**
Jing Xu
jingxu6000@163.com
Yingqi Hua
yhua@shsmu.edu.cn
Wei Sun
vivsun@163.com

[†]*These authors have contributed equally to this work and share first authorship*

Specialty section:
This article was submitted to Cancer Immunity and Immunotherapy, a section of the journal Frontiers in Immunology

Received: *29 March 2022*
Accepted: *26 April 2022*
Published: *01 June 2022*

Citation:
Zhu T, Han J, Yang L, Cai Z, Sun W, Hua Y and Xu J (2022) Immune Microenvironment in Osteosarcoma: Components, Therapeutic Strategies and Clinical Applications. Front. Immunol. 13:907550. doi: 10.3389/fimmu.2022.907550

Osteosarcoma is a primary malignant tumor that tends to threaten children and adolescents, and the 5-year event-free survival rate has not improved significantly in the past three decades, bringing grief and economic burden to patients and society. To date, the genetic background and oncogenesis mechanisms of osteosarcoma remain unclear, impeding further research. The tumor immune microenvironment has become a recent research hot spot, providing novel but valuable insight into tumor heterogeneity and multifaceted mechanisms of tumor progression and metastasis. However, the immune microenvironment in osteosarcoma has been vigorously discussed, and the landscape of immune and non-immune component infiltration has been intensively investigated. Here, we summarize the current knowledge of the classification, features, and functions of the main infiltrating cells, complement system, and exosomes in the osteosarcoma immune microenvironment. In each section, we also highlight the complex crosstalk network among them and the corresponding potential therapeutic strategies and clinical applications to deepen our understanding of osteosarcoma and provide a reference for imminent effective therapies with reduced adverse effects.

Keywords: osteosarcoma, immune microenvironment, therapeutic strategies, clinical applications, immune cells, non-immune cells, complement, exosomes

Abbreviations: ABC, ATP-binding cassette transporter; CAR-NK, chimeric antigen receptor-NK cells; CAR-T cells, chimeric antigen receptor T cells; CSC, cancer stem cell; CTCs, circulating tumor cells; CTLs, cytotoxic T lymphocytes; DCs, dendritic cells; EVs, extracellular vesicles; G-MDSCs, granulocytic MDSCs; IFN-γ, interferon-gamma; Ig, immunoglobulin; IL, interleukin; MCs, mast cells; MDSCs, myeloid-derived suppressor cells; M-MDSCs, monocytic MDSCs; MSCs, mesenchymal stem cells; NK cells, natural killer cells; NKG2D, natural killer group 2 member D; PD-1, programmed cell death protein-1; PMN-MDSCs, polymorphonuclear MDSCs; STAT, signal transducer and activator of transcription; TAMs, tumor-associated macrophages; TANs, tumor-associated neutrophils; TGF-β, transforming growth factor-β; Th, helper T cells; TIM-3, T cell immunoglobulin and mucin domain-containing protein-3; Tregs, regulatory T cells.

1 INTRODUCTION

Osteosarcoma is a rare primary cancer, characterized by the production of an abnormal and immature osteoid matrix (1). Despite its rarity in the whole spectrum of diseases, with an annual incidence rate of 4.7 per million, osteosarcoma ranks first among malignant bone tumors in young people (0–19 years) and has complex heterogeneity (2). In certain circumstances, osteosarcoma is associated with or secondary to other diseases, such as Paget's disease, retinoblastoma, Li–Fraumeni syndrome, Rothmund–Thomson syndrome, and Bloom syndrome, which may be rooted in genetic risks, adding to the complexity of the condition (3, 4). The primary clinical manifestations of osteosarcoma are bone pain, swelling, and functional impairment. As the onset is usually insidious, it may not be taken seriously in the early stages. Another terrible situation is misdiagnosis as osteomyelitis, benign tumors, or metastatic bone tumors, which consequently leads to improper treatment (5). Osteosarcoma treatment is based on its classification and staging. A combination of surgery and chemotherapy is the first choice of treatment for high-grade osteosarcoma. Chemotherapy is considered to be applied preoperatively or postoperatively, according to specific conditions. For low-grade osteosarcoma, surgery alone is no worse than surgery plus chemotherapy (6). Surgery is also the preferred option for resectable metastases and pathological fractures (5, 7). The MAP regimen, comprising doxorubicin, cisplatin, and high-dose methotrexate, is the cornerstone of chemotherapy. It is worth noting that the impact of methotrexate on older adult patients is unpredictable and lacks positive evidence. Therefore, replacing methotrexate with ifosfamide is recommended for patients over 40 years of age. Second-line chemotherapy includes ifosfamide, cyclophosphamide, etoposide, carboplatin, gemcitabine, docetaxel, sorafenib, regorafenib, and samarium (8–15). Muramyl tripeptide is an innate immunomodulatory drug that has already been approved in Europe for the treatment of patients under the age of 30 years with resected osteosarcoma (16). Despite such exploration, the 5-year event-free survival rate of 70% for patients with osteosarcoma has not improved significantly over the last three decades, which indicates that existing regimens remain insufficient and limited. There is great variation among different individuals in response to the same regimen of therapeutic management. Therefore, there is still a long way to go for osteosarcoma treatment research.

Currently, the focus on tumors has expanded from the tumor cell itself to the tumor environment, in which tumor cells are promoted to uncontrollably proliferate, migrate, and resist apoptosis and drugs. An increasing number of studies have shown that changes in the tumor microenvironment are important (17). The immune microenvironment is a novel perspective to view and interpret, and its overall feature is immune suppression to help tumor cells escape immune surveillance. Components of the immune microenvironment of osteosarcoma are mainly divided into two categories: cellular and acellular substances. The former includes immunocytes, such as tumor-associated macrophages (TAMs), tumor-associated neutrophils (TANs), myeloid-derived suppressor cells (MDSCs), mast cells (MCs), T cells, B cells, natural killer cells (NK cells), and dendritic cells (DCs). Non-immune cells, including mesenchymal stem cells (MSCs) and circulating tumor cells (CTCs), can actively interact with the immune system and promote the formation of inhibitory immune networks (18). The complement system and exosomes with special immune effects are also hot spots in the field of microenvironment research.

Surgery and stereotactic radiotherapy can largely remove localized tumors at early stages. However, both approaches are limited by space and cannot eradicate all osteosarcoma cells in the body, especially metastatic and circulating osteosarcoma cells, which may lead to relapse and progression (19, 20). Studies have shown that tumor cells may be in constant confrontation with the immune system, and the balance can be disrupted at a certain time point. Once tumors are generated, they are difficult to completely remove. Immunity is promising for eliminating tumor cells from the body at the cellular level (21). Drugs that target the immune microenvironment are gradually stepping onto the stage with great application potential.

Few reviews have focused on the panorama of the immune microenvironment in osteosarcoma specially. Instead of rigidly borrowing conclusions from other studies on the immune microenvironment in other solid tumors, this review systematically summarizes the main components in the immune microenvironment of osteosarcoma and their functional characteristics, as is shown in **Figure 1**. In each column, we also list relevant therapeutic strategies and clinical applications in progress. The ultimate aim is to provide more information and insight into the understanding and treatment of osteosarcoma.

2 CELLS

2.1 Myeloid Cells

2.1.1 Tumor-Associated Macrophages

TAMs are the most abundant tumor cells in the immune microenvironment of osteosarcoma and account for approximately 50% of the total tumor volume (22). TAMs play important roles in matrix remodeling, inflammation, vascularization, immune defense, and regulation. There are two TAM phenotypes: M1 which is classically activated and M2 which is alternatively activated. Generally, the M1 phenotype participates in inflammation with a reversed impact on metastasis, whereas the M2 phenotype is involved in wound healing and immune regulation with an accelerative impact on metastasis (23). The exact mechanisms of the complex impact include gene alteration, Notch pathway abnormality, macrophage polarization, and helper T cells (Th) 1/Th2 cytokine disturbance (24–26). Therefore, as the understanding of TAMs has deepened, researchers have attempted to inhibit M2 polarization in various ways to prevent tumor progression.

Therapeutic Strategies

All-trans retinoic acid prevents the migration of osteosarcoma cells both *in vitro* and *in vivo* by inhibiting interleukin (IL) 13- or IL14-induced M2 polarization (23). Another study indicated that

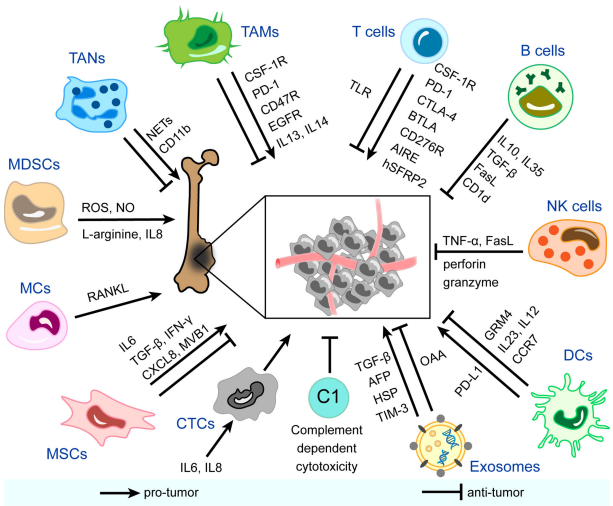

FIGURE 1 | Immune and non-immune components in the immune microenvironment of osteosarcoma and mechanisms of their pro-tumor/anti-tumor effects. CSF-1R, colony-stimulating factor 1 receptor; PD-1, programmed cell death protein-1; EGFR, epidermal growth factor receptor; IL, interleukin; NETs, neutrophil extracellular traps; ROS, reactive oxygen species; NO, nitric oxide; RANKL, receptor activator NF-κB ligand; TGF-β, transforming growth factor-beta; IFN-γ, interferon-gamma; CXCL8, C-X-C motif chemokine ligand 8; AFP, α-fetoprotein; HSP, heat shock protein; TIM-3, T cell immunoglobulin and mucin domain-containing protein-3; OAA, osteosarcoma-associated antigens; PD-L1, programmed cell death protein ligand-1; GRM4, glutamate metabotropic receptor 4; CCR7, chemokine receptor 7; TNF-α, tumor necrosis factor-alpha; CTLA-4, cytotoxic T-lymphocyte-associated protein-4; BTLA, B And T-lymphocyte attenuator; AIRE, autoimmune regulator expression; hSFRP2, humanized secreted frizzled-related protein 2; TLR, toll-like receptor; TAMs, tumor-associated macrophages; TANs, tumor-associated neutrophils; MDSCs, myeloid-derived suppressor cells; MCs, mast cells; MSCs, mesenchymal stem cells; CTCs, circulating tumor cells; C, complement; DCs, dendritic cells; NK cells, natural killer cells.

all-trans retinoic acid could decrease cancer stem cell (CSC) properties strengthened by the M2 phenotype, increasing the number of $CD117^{+}Stro\text{-}1^{+}$ cells and the overexpression of CD133, CXCR4, Nanog, and Oct4 (27). Therefore, all-trans retinoic acid is expected to be added to the existing standard regimens. Paradoxically, studies have suggested that the M2 phenotype might be anti-tumor and anti-metastatic in osteosarcoma (24, 28). Classifying TAMs into M1 and M2 subgroups to analyze their influence on osteosarcoma pathogenesis, metastasis, and drug resistance may be crude and one-sided. Researchers are also attempting other approaches targeting TAMs to treat osteosarcoma. In human osteosarcoma implantation mice, scientists utilized a specific macrophage-eliminating liposome to ablate TAMs, which led to decreased tumor growth. Moreover, when epidermal growth factor receptor was silenced by short hairpin RNA in implanted osteosarcoma cells, tumor growth stimulated by recruited and polarized macrophages was suppressed (29). TAM-specific surface molecules are ideal targets for drug development. CD47R and programmed cell death protein-1 (PD-1) are two popular surface molecules that can be used to generate immune checkpoint inhibitors. Mifamotide and camrelizumab are being tested for their pharmacological effects on blood and lymphatic vessel formation, immunosuppression, and drug resistance (22). Pexidartinib (PLX3397), an inhibitor of colony-stimulating factor 1 receptor, has the potential to reprogram TAMs and activate T cells infiltration in osteosarcoma, resulting in decreased tumor growth and lung metastasis (30). In summary, TAMs are potential target candidates for new therapies.

2.1.2 Tumor-Associated Neutrophils

Most research on neutrophils in patients with osteosarcoma focuses on the neutrophil-lymphocyte ratio or circulating neutrophils. Increased pre-treatment or preoperative neutrophil-lymphocyte ratio might be correlated with poor outcomes, which means that neutrophil-lymphocyte ratio can be investigated as a prognostic biomarker (31–35). However, there has been insufficient research on neutrophil infiltration in osteosarcoma microenvironment. Neutrophils in the tumor immune environment, known as TANs, exhibit phenotypic heterogeneity and functional versatility (36). In osteosarcoma, research on TANs is still in its early stages. The lifespan of TANs may be longer than that of circulating neutrophils under stimulation by pro-inflammatory factors such as interferon-gamma (IFN-γ) (37, 38). Neutrophil extracellular traps are web-like chromatin structures formed by granule proteins and chromatin secreted by neutrophils. Unlike traditional phagocytosis and killing factor secretion, neutrophil extracellular traps can promote metastasis *via* the DNA receptor coiled-coil domain containing protein 25 (39). Leshner et al. (40) also found that peptidylarginine deiminase 4, which is vital for extensive chromatin decondensation to form neutrophil extracellular traps, is overexpressed in osteosarcoma. Similar to the M1 and M2 subtypes of TAMs, Fridlender et al. (41) reported that TANs could also be polarized to the anti-tumor N1 phenotype and pro-tumor N2 phenotype.

Yang et al. (42) found that the number of neutrophils in non-metastatic tissues (detected by the neutrophil-specific marker CD11b) was higher than that in metastatic tissues. The infiltrated neutrophils exerted anti-tumor effects by coordinating the recruitment of immune cells, but also mediating antibody–dependent cellular cytotoxicity. In addition, neutrophil infiltration has been suggested to correlate with hypoxia-associated genes. Emerging evidence indicates that the hypoxic microenvironment plays a pivotal role in tumor progression, and a retrospective study assessed the validation of hypoxia-associated risk score as a prognostic factor of metastasis. The results of this study indicated that TANs were downregulated in the high hypoxia-risk group. The authors concluded that hypoxia might downregulate anti-tumor immune cells, which contribute to immune escape and metastasis (43). Unfortunately, both studies mentioned above did not take functional differences between subtypes into consideration, but merely counted the total number of TANs. This may be because of the difficulty in identifying the ideal markers. More detailed research is needed to uncover the complex role of TANs in the immune microenvironment of osteosarcoma. Development of therapeutic strategies associated with TANs in osteosarcoma is still ongoing and require creative ideas based on basic scientific research.

2.1.3 Myeloid-Derived Suppressor Cells

MDSCs are a population of heterogeneous immunosuppressive immature myeloid cells that can differentiate into TAMs, TANs, and tumor-associated DCs. MDSCs not only interact with immune substances but also closely interact with osteoclasts, osteoblasts, chondrocytes, and other stromal cells in the bone and joint microenvironment to promote the pathogenesis and metastasis of osteosarcoma. MDSCs are classified as granulocytic MDSCs/polymorphonuclear MDSCs (G-MDSCs/PMN-MDSCs) and monocytic MDSCs (M-MDSCs). Recent studies have identified early bone marrow mesenchymal stem cells (e-MDSCs) that act as precursors of both PMN-MDSCs and M-MDSCs (44).

Among all immune cells, MDSCs interact with T cells most closely, which exerts the effect of inhibiting proliferation of T cells, reducing T cell-mediated immune responses and promoting T cell apoptosis by consuming L-arginine and producing reactive oxygen species in the microenvironment. Different MDSC subpopulations undergo different pathways to inhibit T cell function. PMN-MDSCs produce reactive oxygen species mainly by activating signal transducer and activator of transcription (STAT) 3 and upregulating nicotinamide adenine dinucleotide phosphate oxidase, whereas M-MDSCs produce nitric oxide mainly by activating STAT1 and upregulating inducible nitric oxide synthase to inhibit the effect of T cells. MDSCs suppress not only acquired anti-tumor immunity but also innate anti-tumor immunity. In addition to T cells, MDSCs inhibit the function of NK cells and DCs (45–47). Interestingly, stimulated by the hypoxic microenvironment, MDSCs express high levels of vascular endothelial growth factor, vascular endothelial growth factor analog Bv8, basic fibroblast growth factor, and matrix metalloprotease 9 to facilitate angiogenesis and the formation of a pre-metastatic niche, which has a strong relationship with osteosarcoma metastasis (48).

Therapeutic Strategies and Clinical Applications

Because MDSCs extensively infiltrate osteosarcoma lesions and inhibit anti-tumor immunity, researchers have been inspired to develop related therapies. The process of obliterating osteosarcoma cells with some existing drugs involves modulation of MDSCs immune responses. Studies have shown that current neoadjuvant chemotherapeutic drugs (doxorubicin, cisplatin, ifosfamide) could reduce the number of MDSCs in osteosarcoma patients, boost local immune states, and increase immune sensitivity (49). All-trans retinoic acid has been found to affect not only TAMs but also MDSCs by reducing the number of M-MDSCs and the potency of PMN-MDSCs (50, 51). Metformin has been shown to modulate the metabolism of MDSCs to play an anti-tumor role in osteosarcoma by downregulating oxidative phosphorylation and upregulating glycolysis, which is also related to the enhancement of T cell immunity (52). MDSCs can also be targets of the drugs themselves. Tumor cell surface vimentin-targeted interleukin 12 alters the immune profile (IFN-$\gamma^{Hi}CD8^{Hi}FOXP3^{Low}CD33^{Low}$) in mice transplanted with osteosarcoma and lowers the number of MDSCs, thereby controlling tumor recurrence and metastasis (53). Because infiltrating MDSCs in the osteosarcoma microenvironment express the chemokine receptor CXCR4, Jiang et al. (54) designed an antagonist of CXCR4, AMD3100, and tested its synergistic effect in combination with an anti-PD-1 antibody in an osteosarcoma murine model. In addition, Shi et al. (55) combined a functional inhibitor of PMN-MDSCs *via* selectively suppressing PI3Kδ/γ, (S)-(–)-N-[2-(3-Hydroxy-1H-indol-3-yl)-methyl]-acetamide (SNA), with an anti-PD-1 antibody to treat mice bearing osteosarcoma, and they validated that tumor growth was restrained and survival time was prolonged. Other studies have attempted to inhibit osteosarcoma progression by preventing the migration of MDSCs to the tumor microenvironment. Guan et al. (56) found that in an osteosarcoma murine model, anti-IL18 therapy significantly reduced the abnormal upregulation of MDSCs in peripheral blood, thus effectively curbing chemotaxis and infiltration, and finally inhibiting tumor progression. In addition to serving as a drug target, the number of MDSCs in the peripheral blood or tumor microenvironment of osteosarcoma is also a promising candidate as a prognostic biomarker (57). However, owing to the lack of highly specific markers for MDSCs, MDSCs-related therapy of osteosarcoma has not been sufficiently safe, and further research on its identification markers is needed. The mechanisms of accumulation, migration, and interaction with other immune and non-immune cells of MDSCs are also a mystery and require more effort.

2.1.4 Mast Cells

MCs rank among the top five infiltrating cells in osteosarcoma and can be classified into resting MCs and activated MCs. The level of activated MCs in the osteosarcoma microenvironment is significantly higher than that in the normal set (58–60). The infiltration of MCs ($CD117^+$ and $tryptase^+$) was lower in the center of the tumor mass and more distributed at the normal-tumor interface where osteolysis occurs. The special distribution

of MCs may be related to their function. Heymann et al. (61) found that under the influence of osteosarcoma cells, MCs could maintain viability and activity and produce receptor activator NF-κB ligand, a key molecular triad controlling bone remodeling. The dissolution and reconstruction of bone can help immunosuppressive cells further infiltrate the tumor microenvironment and shield the immune escape of tumor cells. Therefore, Inagaki et al. (62) proposed that MCs could function as biomarkers for osteolysis.

Clinical Applications

The most popular application of MCs in osteosarcoma is as a prognostic marker. MCs have been found to have the potential to predict metastasis and survival. Fan et al. (63) reported that the abundance of activated MCs in osteosarcoma microenvironment is associated with negative outcomes, which might indicate the prognosis of patients. Wei et al. (64) detected a correlation between immune-related genes and long noncoding RNAs to compare the different landscapes of immune-related long noncoding RNA pairs in localized and metastatic osteosarcoma. A significant difference in immune infiltration was observed between localized and metastatic osteosarcoma, and the high abundance of activated MCs indicated unsatisfactory outcomes. Le et al. (58) found that the proportion of MCs in patients who died was higher than that in living patients, implying a negative association between MCs and prognosis. In general, because of the unclear role of MCs in the immune microenvironment, related therapies are just beginning and urgently require further development.

2.1.5 Dendritic Cells

DCs are derived from the bone marrow and can be divided into three major subgroups: plasmacytoid DC, myeloid/conventional DC1, and myeloid/conventional DC2. DCs act as a bridge between innate and adaptive immunity and are the most important antigen-presenting cells (65). Inflammatory infiltration varies markedly among different types of sarcomas, and DCs do not differ. There are more infiltrating cells represented by (DC-SIGN/CD11c$^+$) DCs, CD14$^+$/CD68$^+$ TAMs, and CD3$^+$ T cells in conventional high-grade osteosarcoma, undifferentiated pleomorphic sarcoma, and giant cell tumor of the bone than in Ewing's sarcoma, chordoma, and chondrosarcoma (62). Another study found that the quantity of resting DCs was significantly higher in tissues with high immune scores in contrast to the low immune score group, and the degree of DC activation was positively correlated with outcomes (60). Furthermore, the infiltration of DCs into osteosarcoma tissues was found to be related to autophagy. Zhang et al. (66) tested the correlation between immune cell infiltration and 13 autophagy-related long noncoding RNAs, one of which was named RUSC1-AS1 and was negatively associated with the proportion of infiltrating immature DCs, macrophages, and mast cells. The study also illustrated that the level of plasmacytoid DCs was higher in the osteosarcoma microenvironment of the high-risk group than in the low-risk group, whereas the levels of total DCs and immature DCs were lower and associated with poor prognosis. However, the subgroup and quantity of DCs in the tumor microenvironment of the same patient are not static but dynamic in the trend of first increasing and then decreasing in quantity. DCs can trigger further immune responses by detecting tumor antigens and presenting them to helper and cytotoxic T cells, during which time they transform from immature DCs to mature DCs. Therefore, in the early stages, DCs proliferate actively and mature to activate helper and cytotoxic T cells. As the tumor grows, osteosarcoma cells develop variants resistant to DCs and phagocytes, leading to less stimulation of DC activation and eventual immune escape (67).

DCs are known to drive the pathogenesis of osteosarcoma through oncogenes and the tumor suppressor glutamate metabotropic receptor 4. Glutamate metabotropic receptor 4$^{-/-}$ DCs secrete more IL23 and IL12 than wild-type DCs, leading to rapid tumor growth and accelerated progression in mouse models. DCs cultivated with osteosarcoma cells express increased IL23 and decreased IL12, and the higher ratio of IL23/IL12 can be reduced by augmented glutamate metabotropic receptor 4 signaling. Agonists of glutamate metabotropic receptor 4 or an antibody against IL23 may be promising treatment candidates (68, 69). DCs may also be associated with metastasis in patients with advanced osteosarcoma. A study on the single-cell RNA landscape revealed that CCR7 participates in the deformation, chemotaxis, migration, and survival of DCs, which are crucial to tumor metastasis. The study also demonstrated that compared with primary and recurrent lesions, the proportion of CD1c$^+$ DCs is large in lung metastatic lesions (70). Although several lines of evidence have drawn a beneficial portrait of DCs in osteosarcoma, some studies have reported contradictory results. Koirala et al. (71) examined the role of PD-L1 and explored its prognostic value. They concluded that PD-L1 is significantly associated with DCs, T cells, and NK cells. Furthermore, DCs (28.3% vs. 83.9%, P=0.001) and TAMs (45.5% vs. 84.4%, P=0.032) were significantly associated with worse 5-year event-free survival. Another study investigating the immune classification in osteosarcoma also showed a negative association between DCs and prognosis. Their analysis suggested that the number of DCs in live patients was less than that in dead patients, in contrast to NK cells and CD8$^+$ T cells (58).

Therapeutic Strategies

Scientific research has shed light on the therapeutic potential of DCs, and scientists have achieved some inspiring success. Some agents or partial components of the agents enhance the impact of DCs. For example, capsaicin was reported to enhance the phagocytosis of osteosarcoma cells (MG-63) by DCs *in vitro* (72). The most popular treatment approach for DCs is vaccination. Several vaccines have shown encouraging efficacy, such as the CD1c$^+$ DC vaccine and vaccination with polyinosinic:polycytidylic acid (poly I:C) activated and tumor antigen-loaded CD103$^+$ myeloid/conventional DC1s (70, 73). In addition to vaccines, liposomal-muramyl tripeptide phosphatidylethanolamine has a good chance of extending overall survival and survival without metastasis by charging DCs or producing T cells, not only when used alone but also in combination with other approaches (74). Scientists have already investigated the effect of DCs to explore the possibility of their application in combination with anti-

transforming growth factor-β (TGF-β) antibodies, agonist anti-glucocorticoid-induced tumor necrosis factor receptor antibodies, and doxorubicin (60, 67, 75). For example, Kawano et al. (76) combined DCs and anti-TGF-β antibodies to treat osteosarcoma and detected enhanced systematic immune responses *in vivo*. Existing attempts to utilize DCs to maximize tumor killing by virtue of upregulating the immunocompetence of lymphocytes. Nevertheless, the studies mentioned above also focused on the pro-tumor activity of DCs, which is a vital risk when using DC-associated therapy. Making full use of the advantages and avoiding the disadvantages with further precision therapy is the key to DCs application in the future.

2.2 Lymphoid Cells

2.2.1 T Cells

T cells are thymus-derived lymphocytes that mature and reside in thymus-dependent areas of peripheral immune organs. T cells play a vital role in both cellular and humoral immunities. The classification of T cells according to different criteria is very complex. In the activation stage, T cells can be divided into naive, effector, and memory T cells. According to the T cell receptor characteristics, including distribution and major histocompatibility complex restriction, T cells can be divided into αβT and γδT. On the principle of function, T cells can be divided into Th, including Th1, Th2, Th9, Th17, Th22, and follicular helper T cells, cytotoxic T lymphocytes (CTLs), and regulatory T cells (Tregs), including natural Tregs, inducible Tregs, and other Tregs.

T cell infiltration plays a critical role in osteosarcoma anti-tumor immunity, and its classification is highly heterogeneous. In osteosarcoma, tumor-infiltrating lymphocytes are mainly distributed in the region expressing human leukocyte antigen Class I, whereas $CD4^+$ and $CD8^+$ T cells are mainly clustered at the interface between pulmonary metastases and normal tissues (57). The number of T cells in metastatic lesions is significantly higher than that in primary and recurrent lesions *in situ* (77). In metastatic lesions, checkpoint and immunoregulatory molecules were calculated to be higher than those in primary lesions, including PD-1, lymphocyte activation gene-3, T cell immunoglobulin and mucin domain-containing protein-3 (TIM-3), indoleamine 2,3-dioxygenase 1, and IFN-γ (57). Han et al. (78) analyzed the biopsy tissue and peripheral blood of 16 patients with primary osteosarcoma and concluded that there were more $TIM\text{-}3^+PD\text{-}1^-$ T and $TIM\text{-}3^+PD\text{-}1^+$ T cells in biopsy tissue than in peripheral blood, suggesting that the immune microenvironment in tumor lesions was inhibitory. They also reported that immune cells could interact with each other to form a vicious cycle, in which the immune activity of T cells could be inhibited by pro-tumor macrophages, and depletion of $CD163^+$ macrophages could increase T cell growth and pro-inflammatory factor production *in vitro*. Another interesting case report from Japanese Hiroshima University was the case of extraosseous osteosarcoma with partial spontaneous regression and $CD8^+$T cells, T cell-restricted intracellular antigen-1^+ T cells, and granzyme B^+ T cells in the tumor mass (79). These studies suggest that sophisticated T cell infiltration occurs in osteosarcoma in terms of regions, subtypes, and molecules.

Therapeutic Strategies and Clinical Applications

Given that T cells play a significant role in the immune microenvironment of osteosarcoma, T cell-related applications show vigorous vitality, the mechanisms of which can mainly be divided into the following aspects: 1) T cell infiltration profile used as an auxiliary indicator of diagnosis, such as disease staging, patient clustering, prediction of metastasis, drug resistance, and survival outcomes; 2) immunotherapies targeting T cell-related immune responses, including strengthening the function of effector T cells and weakening the inhibitory effect of Tregs; 3) adoptive T cell therapy, including CTL, γδT, and gene-engineered tumor-specific T cells; and 4) non-immunotherapies involving T cell-related pathways. All four aspects are discussed in order below, which is illustrated in **Figure 2**.

First, T cells are potential prognostic predictors and assistant indicators for clinical diagnosis. Weak immunosuppressive signals and strong T-cell immune responses have been found to be significantly associated with improved outcomes in osteosarcoma patients (57). The number of activated $CD8^+$ T cells in tumor lesions of osteosarcoma patients has been found to be higher in men than in women (80). A study claimed that $CD8^+$ T cells might be associated with a good prognosis, whereas γδT cells have a poor prognosis (58). Autoimmune regulator expression is an indispensable transcription factor for T cells, resulting in peripheral immune tolerance, which develops and obtains central tolerance in the thymus. Matsuda et al. (81) analyzed 43 biopsy samples of conventional osteosarcoma and found that autoimmune regulator expression was expressed in 58.1% of the samples and was related to increased Tregs ($FOXP3^+$), lung metastasis, and reduced overall survival. The results suggest that autoimmune regulator expression might be an ideal prognostic indicator and a satisfying target for drug design. Based on the above studies, it is not difficult to conclude that if the infiltration of T cells in the surgically removed tumor biopsy can be carefully analyzed, it may provide guidance for the next step of treatment and predict the prognosis.

Second, T cell and T cell-induced immune responses are common targets in immunotherapies. Toll-like receptor is a key molecule involved in innate immunity, and acts as a bridge between nonspecific and specific immunity. Yahiro et al. (82) found that activation of the Toll-like receptor 4 signaling pathway could further stimulate $CD8^+$ T cells in murine models, thereby inhibiting osteosarcoma progression. Fujiwara et al. (30) reported that the colony-stimulating factor 1 receptor inhibitor PLX3397 could consume TAMs and Tregs ($FOXP3^+$) and enhance $CD8^+$ T cell infiltration in primary and metastatic lesions. This phenomenon has been observed both *in vitro* and *in vivo*. *In vitro*, PLX3397 inhibited colony-stimulating factor-1 or tumor-conditioned media stimulation of pERK1/2 and reduced the pro-tumor M2 polarization of TAMs. In an osteosarcoma orthotopic xenograft model, systemic administration of PLX3397 significantly inhibited primary tumor growth and lung metastasis, contributing to improved metastasis-free survival. Currently, popular immune checkpoint inhibitors are being explored in the field of osteosarcoma treatment. Yoshida et al.

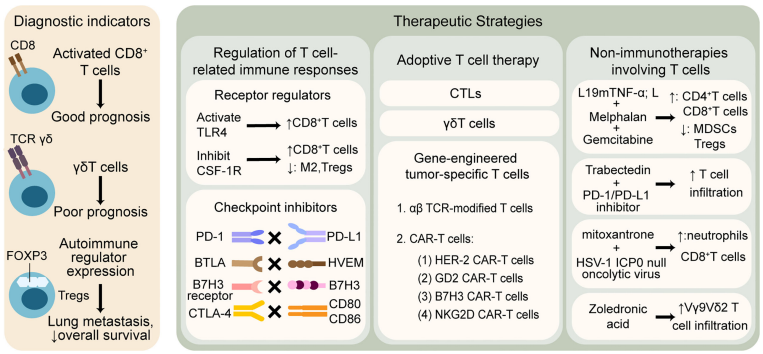

FIGURE 2 | T cell-related therapeutic strategies and clinical applications in osteosarcoma. T cells are widely explored to predict outcomes and promote anti-tumor treatment. The left column shows that T cell infiltration profile may be associated with different prognosis. The right column illustrates that therapies involving T cells are mainly divided into three categories: 1) regulation of T cell-related immune responses by modulating receptors and blocking checkpoints, 2) adoptive T cell therapy based on CTLs, γδT cells and gene-engineered tumor-specific T cells, 3) non-immunotherapies containing T cell-related mechanisms. TLR, toll-like receptor; CSF-1R, colony-stimulating factor 1 receptor; M2, tumor associated macrophages M2 phenotype; PD-1, programmed cell death protein-1; PD-L1, programmed cell death protein ligand-1; BTLA, B And T-lymphocyte attenuator; HVEM, herpesvirus entry mediator; CTLA-4, cytotoxic T-lymphocyte-associated protein-4; CTLs, cytotoxic T lymphocytes; TCR, T cell receptor; CAR-T cells, chimeric antigen receptor T cells; HER-2, human epidermal growth factor receptor-2; GD2, disialoganglioside; NKG2D, natural killer group 2 member D; TNF-α, tumor necrosis factor-alpha; MDSCs, myeloid-derived suppressor cells; HSV, herpes simplex virus.

(83) validated that anti-PD-1 antibody (4H2) could decrease Treg infiltration in subcutaneously implanted models of murine osteosarcoma cell line LM8, and finally, tumor volume decreased in size and overall survival was prolonged. Cascio et al. (84) reported that PD-1/PD-L1 was not the only immune checkpoint axis in human osteosarcoma lesions; herpesvirus entry mediator (HVEM/CD270) and indeterminate receptor to B7H3/CD276 were also expressed. The expression of these three immune checkpoints was significantly higher in metastatic lesions than in the primary lesions. The levels of the three ligands were positively correlated with each other and with peritumoral T-cell infiltration. Therefore, owing to low intratumor effector T cell infiltration in osteosarcoma, combined therapies of immune checkpoint inhibitors may be used to magnify immune infiltration, improve the immune microenvironment, and finally repress tumors in the future. Some researchers have combined immune checkpoint inhibitors with other therapies to further optimize osteosarcoma treatment. He et al. (85) observed that PD-1/PD-L1 therapy combined with L-arginine improved the therapeutic effect in immunocompetent BALB/c mouse models. L-arginine significantly increased the infiltration of $CD8^+$ T cells, splenic $CD8^+$ T cells, serum IFN-γ, and anti-α-PD-L1 antibody to prevent the exhaustion of $CD8^+$ T cells and promote the expression of IFN-γ, granzyme B, and perforin. The combination of L-arginine and PD-1/PD-L1 immunotherapy significantly increased overall survival in mice; therefore, the addition of L-arginine may be a future direction. Takahashi et al. (86) found that a combination of dual checkpoint blockade therapy (anti-PD-L1 and anti-cytotoxic T-lymphocyte-associated protein-4) and X-ray irradiation could control primary osteosarcoma and diminish metastasis *in vivo*, which was associated with increased recruitment of $CD8^+$ T cells and decreased infiltration of Tregs. Immune checkpoint inhibitors have not been shown to be significantly effective in all the studies. Nasarre et al. (87) investigated the role of a monoclonal antibody targeting humanized secreted frizzled-related protein 2, a protein that promotes angiogenesis and metastasis, in metastatic osteosarcoma resistance to PD-1/PD-L1 inhibitors, and its impact on T cells. They found that humanized secreted frizzled-related protein 2 monoclonal antibody inhibited T cell proliferation and osteosarcoma metastasis by lowering the expression of NFATc3, CD38, and PD-1.

Third, adoptive T-cell therapy is popular and is flourishing in osteosarcoma. Adoptive T cell transfer is one of the current research hotspots, which involves the introduction of specific T cells amplified *in vitro* into patients to supplement and enhance T cell-related immunity. Common applicable T cells include CTL, γδT, and gene-engineered tumor-specific T cells (88). In particular, gene engineering is moving to the center stage of osteosarcoma. Osteosarcoma-associated antigens are numerous and complicated, mainly represented by activated leukocyte cell adhesion molecules (CD166), B7H3, and epidermal growth factor receptor. T cells can be loaded with specific osteosarcoma-associated antigens by gene engineering, among which αβT cell receptor-modified T cells, chimeric antigen receptor T cells (CAR-T cells), especially HER-2 CAR-T cells, disialoganglioside GD2 CAR-T cells, and B7H3 CAR-T cells have been discussed the most (89). CAR-T cell therapy has progressed to the third generation with preliminary advances in hematologic tumors and neuroblastoma, but is still in the exploratory stage in osteosarcoma (90). Fernandez et al. (91) verified the safety and effectiveness of installing natural killer group 2 member D (NKG2D) CARs containing 4-1BB and CD3z signaling domains in $CD45RA^-$ T cells through lentiviral transduction *in vivo* and *in vitro*. They found that the anti-tumor activity of NKG2D-CAR memory T cells was enhanced by

strengthening the interactions between NKG2D ligands and receptors in osteosarcoma. However, it is not enough to increase the adaptation of effector T cells to osteosarcoma; it is also crucial to facilitate their proliferation, prolong their lifespan, enhance their resistance to the inhibitory immune microenvironment, and promote their susceptibility to tumor cells. Gene-engineered T cells can be used in treatment in the future, with more precise targets, flexible controllability, and richer functions.

Fourth, many non-immunotherapies are relevant to the regulation of immune microenvironmental pathways. Mortara et al. (92) found a significant increase in $CD4^+$ and $CD8^+$ T cells and a decrease in MDSCs and Tregs in the microenvironment of osteosarcoma syngeneic mouse tumor models, which responded well to the combination of targeting angiogenesis L19 tumor necrosis factor alpha (L19mTNF-α; L), melphalan, and gemcitabine. Atti et al. (93) showed increased T cell infiltration in the microenvironment of an osteosarcoma murine model treated with the alkylating agent trabectedin. However, $CD8^+$ T cells were exhausted in no time, which may be due to the high expression of PD-1. Therefore, the team suggested the addition of PD-1/PD-L1 blockers to compensate for this failure to achieve better anti-tumor effects. Belisario et al. (94) found that the ratio of ATP-binding cassette transporter (ABC)-A1, an activator of anti-tumor Vγ9Vδ2 T cells, to ABC-B1, an inducer of chemotherapy resistance, could indicate chemo-immune resistance. In addition, zoledronic acid increased the sensitivity of drug-resistant osteosarcoma cells by enhancing intratumor apoptosis and the ratio of ABC-A1 to ABC-B1 and Vγ9Vδ2 T-cell infiltration. Workenhe et al. (95) reported that the combination of HSV-1 ICP0 null oncolytic virus KM100 and mitoxantrone, an immunogenic cell death-inducing chemotherapeutic drug, could significantly increase the survival benefit by increasing the infiltration of $CD8^+$ T cells and neutrophils in the osteosarcoma microenvironment of BALB/c mice bearing HER-2/neu TUBO-derived tumors. The oncolytic HSV-1 did not reverse tumor immune tolerance *in vitro*, indicating that the two drugs might share some overlap in pharmacological mechanisms to achieve the effect that one plus one was greater than two.

Furthermore, some T cell-associated therapies have not yet achieved initial success, but they can inspire researchers. The addition of immunomodulatory cytokines such as IL2, IL15, and liposomal-muramyl tripeptide phosphatidylethanolamine might induce T cell proliferation and differentiation to improve the survival outcomes of osteosarcoma patients, but the evidence is insufficient. Studies on specific monoclonal antibodies and bispecific antibodies targeting osteosarcoma cells are also ongoing, but there is abundant evidence. Anti-tumor vaccines are thought to be able to clear small residual lesions in the body by inducing active or passive specific immunity, and several clinical trials of sarcoma are underway (**Table 1**), which is expected in the field of osteosarcoma (90). In summary, the function of T cells in the immune microenvironment of osteosarcoma and their interactions with other components have not been fully recognized, and relevant therapies remain in the preliminary stage of exploration. Further research is required to expand this field and inspire applications.

2.2.2 B Cells and Antibodies

B cells are derived from lymphoid stem cells in the bone marrow and reside in the lymphoid follicles of the peripheral lymphoid organs when they mature. B cells are not only the protagonists of humoral immunity by producing antibodies but are also a type of antigen-presenting cells involved in immunoregulation. According to the activation stage, B cells can be divided into three categories: initial B cells, memory B cells, and effector B cells/plasma cells, among which the latter is the main source of antibodies. Regulatory B cells are a type of B cells with immunosuppressive effects. Regulatory B cells inhibit $CD4^+$ T cells, CTLs, macrophages, and DCs by secreting inhibitory cytokines such as IL10, TGF-β, IL35, and expressing membrane surface regulatory molecules such as FasL and CD1d, and promote the transformation of T cells into Tregs, thus weakening anti-tumor immune responses (96). Although humoral immunity is not the predominant mechanism of the anti-tumor immune responses, it plays an indispensable role. Overall, B cells and humoral immunity are receiving increasing attention in anti-tumor immunity, and breakthroughs are expected in this area.

Therapeutic Strategies and Clinical Applications

The infiltration of B cells in osteosarcoma is complex, with differences in cell subtypes and patient sex. Yang et al. (80) obtained data on osteosarcoma cases from The Cancer Genome Atlas and performed a comprehensive assessment of the infiltration of immune cells. They found more memory B cells and activated B cells in osteosarcoma lesions in men than in women. Li et al. (97) analyzed the immune cells in the microenvironment of osteosarcoma, Ewing's sarcoma, multiple myeloma, and cancer bone metastases and found that osteosarcoma patients with high infiltration of B cells had a better prognosis and activated B cells were positively correlated with survival.

Therefore, infiltration of effector B cells may be a good prognostic indicator. Research on B cells in osteosarcoma is still very limited, and new therapies based on B cells lack satisfactory results.

Antibodies produced by B cells and plasma cells proliferate and differentiate from memory B cells and mainly exist in serum, tissue fluids, secretory fluids, and on the surface of certain cells.

Antibodies regulate tumor growth and metastasis through antibody-dependent cell-mediated cytotoxicity, modulatory effects, activation of complement, closure of tumor cell receptors, and alteration of tumor cell adhesion. Contrary to common sense, some antibodies can bind to antigens on the surface of tumor cells and block killing (98–100). Immunoglobulins are globulins with antibody activity or similar chemical structure domain antibodies that are mainly distributed in the serum or on B-cell membranes. Studies on antibodies and immunoglobulins in osteosarcoma are relatively few and need to be further investigated. IgE has been found to be associated with osteosarcoma development. Zhang et al. (101) conducted bioinformatic analysis on 19 osteosarcoma cases and

TABLE 1 | Clinical trials of anti-tumor vaccines in sarcoma.

NCT number	Phases	Diseases	Vaccines
NCT00923351	I, II	Ewing's sarcoma, undifferentiated/embryonal sarcoma, desmoplastic small round cell tumor, synovial cell sarcoma, rhabdomyosarcoma	Tumor purged/CD25 depleted lymphocytes with tumor lysate/KLH pulsed dendritic cell vaccine
NCT00405327	II	Sarcoma, neuroblastoma, Wilm's tumor	Tumor lysate-pulsed dendritic cell vaccine
NCT00001566	II	Ewing's sarcoma, rhabdomyosarcoma	Autologous dendritic cell vaccine
NCT01141491	II	Sarcoma	Trivalent ganglioside vaccine
NCT01241162	I	Ewing's sarcoma, osteogenic sarcoma, rhabdomyo sarcoma, synovial sarcoma, neuroblastoma	Autologous dendritic cell vaccine
NCT00069940	I	Sarcoma, central nervous system tumors, gastrointestinal stromal tumor	Telomerase 540-548 peptide vaccine
NCT00003023	I	Sarcoma, neuroblastoma	BCG vaccine, monoclonal antibody A1G4 anti-idiotype vaccine
NCT00199849	I	Sarcoma, prostate cancer, bladder cancer, non-small cell lung cancer, esophageal cancer	NY-ESO-1 plasmid DNA cancer vaccine

six normal samples obtained from the Gene Expression Omnibus database and compared the differentially expressed genes, differentially methylated regions, copy number, and functional enrichment of the two groups. The results showed that hypermethylation in the fragment crystallizable region of immunoglobulin (Ig) E, high-affinity I, receptor for γ polypeptide was significantly associated with osteosarcoma development. IgE elevation is often seen in allergic diseases; therefore, the specific role of IgE epigenetic alterations in osteosarcoma immunity needs to be further explored.

Therapeutic Strategies and Clinical Applications

Immunoglobulins, their receptors, and their transporters can be used as predictors and diagnostic factors. Wang et al. (102) found that positive expression of polymeric immunoglobulin receptor, the transporter of dimeric IgA, and pentameric IgM, was significantly associated with poor prognosis in patients with osteosarcoma, indicating that polymeric immunoglobulin receptor might be a good prognostic biomarker. Guerra et al. (103) analyzed biochemical and immunological parameters in the saliva of healthy children and children with cancer before and after antineoplastic treatment, including osteosarcoma. The total concentration of IgA in the saliva of children with cancer was significantly lower than that in healthy children, independent of antineoplastic treatment. This noninvasive test provides a new clue for the diagnosis and treatment of childhood cancer. In addition, antibodies specific for osteosarcoma-associated antigens are the mainstay of humoral immunity and the raw material for the design of anti-tumor drugs. Receptor tyrosine kinase-like orphan receptor 2 has been found to be a highly expressed osteosarcoma-associated antigen, and its antibodies are potential drugs. Hellmann et al. (104) fabricated a clinically used monoclonal antibody with high affinity to receptor tyrosine kinase-like orphan receptor 2 using human Ig transgenic animals, providing a new idea for osteosarcoma immunotherapy. Autoantibodies can also be used for etiological studies. Mazzoni et al. (105) discovered that IgG reacting with Simian virus 40 mimotopes was significantly higher in the sera of osteosarcoma patients than in those of breast cancer patients, undifferentiated nasopharyngeal carcinoma patients, and healthy people, demonstrating an association between Simian virus 40 and osteosarcoma pathogenesis. The Ig superfamily may conceal the secrets to osteosarcoma progression and metastasis. Leukocyte-associated immunoglobulin-like receptor-1 is a collagen receptor of the Ig superfamily, and the related pathways in lymphocytes and monocytes have received increasing attention. Leukocyte-associated immunoglobulin-like receptor-1 overexpression decreased Glut1 and epithelial-mesenchymal transition-related molecules, thereby inhibiting osteosarcoma cell metabolism and metastasis and providing a new target for slowing osteosarcoma progression (106). Although studies on antibodies and immunoglobulins in osteosarcoma are scarce, they may exert considerable influence on the diagnosis, treatment, and scientific research of osteosarcoma in the future.

2.2.3 Natural Killer Cells

NK cells are a class of innate lymphoid cells that express the intracellular transcription factors E4BP4$^+$ and CD3$^-$CD19$^-$ CD56$^+$CD16$^+$ on their surface. NK cells are widely distributed in the blood, peripheral lymphoid tissues, liver, and spleen. NK cells have been found to not only kill tumor cells directly but also control tumor progression and metastasis. NK cells express a

variety of cytokine receptors related to chemotaxis and activation and can be recruited to the tumor microenvironment to kill tumor cells by releasing perforin, granzyme, and tumor necrosis factor-α and expressing FasL (107). The PD-1/PD-L1 axis can regulate the anti-tumor effects of NK cells. Zhang et al. (108) found that blocking the PD-1/PD-L1 axis with a PD-L1 antibody, which inhibited NK cell toxicity by secreting granzyme B, could enhance the killing effect of NK cells on human osteosarcoma cells. Yang et al. (80) conducted a comprehensive analysis of immune infiltration in the osteosarcoma microenvironment and concluded that male patients had more NK cells than did female patients. Lazarova et al. (109) discovered that NK cells were suppressed, but TGF-β expression increased in the osteosarcoma microenvironment. The mechanisms explained were that TGF-β could promote angiogenesis, bone remodeling, and cell migration by inhibiting the expression of activation receptor NKG2D and reducing the release of killing perforin of NK cells. To overcome these negative effects and induce resistance of NK cells to TGF-β, Kisseberth et al. (110) continuously exposed NK cells to low-dose TGF-β and IL2 *in vitro*, thereby alleviating the degree of immunosuppression in the canine osteosarcoma microenvironment, which might be applied to the treatment of human NK cells in the future.

Therapeutic Strategies

For cancer cells evading adaptive immune surveillance by antigen shedding, lowering major histocompatibility complex-I, and inhibiting T cells, NK cells alone or in combination show great application prospects. Attempts have been focused in three directions: adoptive NK cells, cytokine-based targeting therapies that enhance the immune activity of NK cells, and chimeric antigen receptor-NK cells (CAR-NK). Adoptive NK cells have achieved initial success in the treatment of osteosarcoma. The basic principle is to compensate for the hypothetically existing immune deficiency and reactivate the suppressed NK anti-tumor immunity. NK cells used for treatment can be obtained from sources such as autologous or alien peripheral blood, umbilical cord blood, hematopoietic progenitors, and pluripotent stem cells. The advantage is that it is safe, and there is no graft vs. host disease, such as CAR-T cells and immune checkpoint inhibitors (111). Mismatched allogeneic donors may have a greater anti-tumor effect than matched or autologous NK cells in osteosarcoma (112). Chu et al. (113) combined N-803 (IL15 super agonist) and dinutuximab (monoclonal antibody targeting disialoganglioside GD2) to treat *ex vivo* expanded peripheral blood NK cells. They found that the toxicity of expanded peripheral blood NK cells was enhanced, and this effect was verified *in vivo*, with significantly longer survival in osteosarcoma mice. In addition, Buddingh et al. (114) found that utilizing IL15 to treat allogeneic and autologous NK cells could restore the sensitivity of chemotherapy-resistant osteosarcoma through DNAX accessory molecule-1 and NKG2D pathways. These two studies emphasized the application value of IL15, an NK cell-activating agent, in osteosarcoma. CAR-NK is a novel and promising therapy for loading NK cells with specific antibodies, which has been observed to have therapeutic effects in Ewing's sarcoma and B-cell leukemia (115). However, there is still a lack of research on CAR-NK cells in osteosarcoma. Research on NK cell biology, checkpoint inhibition, CAR technology, and the expansion of autologous and allogeneic NK cells is of great value and urgently needed.

2.3 Non-Immune Cells

2.3.1 Mesenchymal Stem Cells

CSCs are competitive clones that drive tumorigenesis. CSCs are considered the key reason for the huge heterogeneity of osteosarcoma and cause recurrence, metastasis, and drug resistance (116). Xu et al. (117) divided osteosarcoma patients into two clusters based on osteosarcoma tumor stem cell-related genes. Cluster 1 had a higher immune infiltration score and a better prognosis than Cluster 2. The Cluster 1 immune microenvironment is characterized by fewer follicular helper T cells, M0 macrophages, and more $CD8^+$ T cells. These results suggest that CSCs are potentially associated with the immune microenvironment landscape in osteosarcoma, which means that different CSCs may develop different immune infiltrates and have different prognoses. There is a lot of research indicating that osteosarcoma originates from MSCs. MSCs are adult multipotent stem cells distributed in various tissues of the body, especially in the bone, adipose tissue, and dental pulp.

MSCs play an important role in osteosarcoma tumorigenesis by regulating immune responses and by inducing cell fusion and differentiation (118). A study on osteosarcoma histogenesis suggested that naive MSCs and tumor-derived MSCs may exert different effects on osteosarcoma development. Naive MSCs were found to have both anti-tumor and pro-tumor effects. Tumor-derived MSCs have been shown to promote tumor cell proliferation, increase CSCs proportion, facilitate epithelial-mesenchymal transition, and exhibit strong immunosuppressive activity (119). There are two non-immune mechanisms by which MSCs promote osteosarcoma cell proliferation and metastasis: first, the interaction between osteosarcoma cells and MSCs involving IL8 and aquaporin 1; second, abnormal gene expression, such as *Rb*, *C-MYC*, *TP53*, *K-Ras*, and *IHH* promote the transformation of MSCs into osteosarcoma cells (120–125). MSCs have also been found to transform into cancer-associated fibroblasts when exposed to osteosarcoma cells, which could significantly accelerate the proliferation, migration, and invasion of osteosarcoma cells. This process involves monocyte chemotactic protein 1, growth-related oncogene-alpha, TGF-β, and intercellular adhesion molecule 1. Cancer-associated fibroblasts can also secrete extracellular matrix responsible for intercellular communication, cell adhesion, and proliferation to shield malignant phenotypes and enrich tumor heterogeneity. Moreover, the effects of MSCs and osteosarcoma cells were similar. Under MSC stimulation, osteosarcoma cells can induce endothelial cell migration and invasion and promote angiogenesis (126–129). When it comes to immunity, MSCs could secrete anti-inflammatory substances and inhibit pro-inflammatory substances to help osteosarcoma cells escape immune surveillance, mediated by autocrine or paracrine extracellular vesicles (EVs), particularly exosomes (130). Lagerweij et al. (131) found that MSCs inhibit T cell proliferation and immune responses by secreting EVs containing miRNAs/RNA and proteins. Zhang et al. (132) reported that MSC-EV-associated TGF-β and

IFN-γ can promote the transformation of mononuclear cells into Tregs. In addition to influencing T cell-associated immune responses, MSCs have been found to inhibit the immune effects of B cells. Khare et al. (133) found that MSC-EVs increased the levels of C-X-C motif chemokine ligand 8 and MVB1 RNA, which could reduce IgM in B cells. MSCs can also promote the M2 polarization of TAMs by secreting IL6 (134). Some cytokines, such as IL10, hepatocyte growth factor, leukemia inhibitory factor, C-C motif chemokine ligand 2, vascular endothelial growth factor-C, and C-C motif chemokine ligand 20 (135) are also very important in the increased migration of MSC-EVs to the tumor microenvironment and inflammation inhibition.

Therapeutic Strategies

The application of MSCs has focused on two aspects: 1) regulation of the signaling pathways and secretion behavior of MSCs and 2) delivery of drugs by MSCs. For example, Alvaro et al. (136) loaded MSCs with an oncolytic virus and granulocyte-colony stimulating factor to increase immune infiltration and alleviate tumor growth. However, it should be noted that the pharmacokinetic characteristics of MSCs vectors require extensive studies to ensure both efficacy and safety (118). However, a few studies have shown that MSCs can effectively inhibit osteosarcoma recurrence, proliferation, and metastasis. Aanstoos et al. (137) injected MSCs directly into the tumor mass of osteosarcoma mice and found that tumor expansion and local recurrence were controlled. In contrast, the intravenous administration of MSCs to osteosarcoma mice promoted lung metastasis. The researchers attributed the anti-tumor activity to the promotion of apoptosis, restraint of angiogenesis, and regulation of immune responses. The reason for this contradiction may lie in an unclear understanding of the different sources and functional characteristics of MSCs in the academic community. In the field of osteosarcoma, attempts to target pro-tumor MSCs subtypes or amplify anti-tumor MSCs subtypes are still in the exploration stage, and research on the development of MSC-associated exosomes or other EVs is still insufficient. It is hoped that a breakthrough will be realized in the near future.

2.3.2 Circulating Tumor Cells

Osteosarcoma cells exist not only in the tumor mass, but also in circulation, and are called CTCs. CTCs can escape local treatment, such as surgical resection and radiotherapy and survive in small quantities under systemic treatment, which results in the metastasis and recurrence of osteosarcoma. Several studies have shown that CTCs play a specific role in the immune microenvironment of osteosarcoma. Zhang et al. (138) found that the inhibition of IL6 could suppress osteosarcoma cell proliferation and reduced CTCs. The phenomenon observed in *in vitro* experiments was that recommendation human interleukin 6 activated Janus-activated kinase/signal transducers and activators of transcription 3 and mitogen-activated protein kinase/extracellular signal regulated kinase1/2 pathways. Both pathways promote osteosarcoma cell proliferation, but only the former promotes cell migration. This effect was also confirmed in a nude mouse model of human osteosarcoma. Given that activated Janus-activated kinase/signal transducers and activators of transcription 3 can enhance immunosuppression, it is not difficult to speculate that CTCs are related to the formation of an immunosuppressive microenvironment in osteosarcoma.

In addition to IL6, IL8 has also been found to be a positive factor in the promotion of osteosarcoma progression by CTCs. The main biological activity of IL8 is to attract and activate neutrophils, eosinophils, basophils, and lymphocytes. Liu et al. (139) successfully isolated and cultivated self-seeded CTCs and discovered that IL8 could promote tumor growth and lung metastasis *in vitro* and *in vivo*. Therefore, inhibiting IL8 might exert a therapeutic effect, and a combination with activators or inhibitors of other cytokines would be encouraged. Although the mechanisms of the interaction between CTCs and tumor immunity are not clear, CTCs are potential predictive markers and drug targets. Elimination of CTCs is expected to be a symbol of a more thorough efficacy of anti-tumor therapies.

3 COMPLEMENT SYSTEM

The complement system is a protein reaction system consisting of more than 30 components with precise regulation and is widely present in the serum, tissue fluid, and cell membrane surface. In addition to innate immunity to pathogens, the complement system participates in the immune regulation of inflammation and tumors. The majority of current studies suggest that complement system activation has anti-tumor effects by killing tumor cells through complement-dependent cytotoxicity, whereas other studies suggest that complement system activation has pro-tumor potential in a special immune microenvironment.

Clinical Applications

Chen et al. (140) found that the expression level of C1q (C1qA, C1qB, and C1qC) was positively correlated with the survival time of patients with osteosarcoma and negatively correlated with the percentage of surgical pathological necrosis, indicating that C1q is likely to be a positive prognostic factor. Gene set enrichment analysis showed that immune-related genes were significantly enriched in the group with high C1q expression, indicating that high expression of C1q implies strong immune function and better prognosis. CiberSort proportional analysis showed that the expression level of C1q was positively correlated with M1 and M2 macrophages and $CD8^+$ T cells, which added to the specific mechanisms by which C1q interacts with various cells in the immune microenvironment. Similarly, another study published in 2021 suggested that C1q could predict osteosarcoma metastasis and prognosis. Huang et al. (141) found that C1qA, C1qB, and C1qC levels were positively correlated with the number of follicular helper T cells, $CD8^+$ T cells, and memory B cells. Moreover, the expression of these three key genes was significantly lower in metastatic osteosarcoma cell lines than in non-metastatic osteosarcoma cell lines. This finding also indicates that C1q is a positive

prognostic factor. However, Jeon et al. (142) found that after the addition of normal human serum, human bone osteosarcoma epithelial cells (U2-OS) activated the alternative pathway of the complement system, resulting in the generation of more vascular endothelial growth factor-A and fibroblast growth factor 1 and promotion of angiogenesis in models *in vitro*, regulated by the phospho-ERK signaling pathway. Moreover, the expression of negative complement regulatory proteins, such as CD46, CD55, and CD59 and endogenously expressed properdin or C3, was reduced in normal human serum-treated U2-OS cells. Despite the above research, the entire landscape of the complement system and its role in the immune microenvironment of osteosarcoma are still unknown, which may be an interesting direction for future research.

4 EXOSOMES

EVs are lipid-coated vesicles secreted by cells into the extracellular space, containing nucleic acids (DNA, RNA, and microRNAs), proteins, lipids (eicosanes, fatty acids, and cholesterol), and intact organelles. In osteosarcoma, exosomes are representative special heterogeneous vesicles with a diameter of 30–150 nm produced by direct outward budding of the cell membrane (143). Exosomes play an important role in the proliferation, metastasis, and drug resistance of osteosarcoma. Many reviews have elaborated on these mechanisms, and this review attempts to summarize the role and application of exosomes related to immunity.

Immune effects of exosomes have been observed in other tumors also. For example, in mesothelioma, TGF-β1 in exosomes significantly downregulates NKG2D on the surface of $CD8^+$ T cells and NK cells, inhibits lymphocyte activation, and further impedes tumor cell recognition (144). Exosomes containing TGF-β1 in mesothelioma have also been found to inhibit IL2-mediated lymphocyte proliferation more strongly than does soluble TGF-β1, thereby increasing immune escape (145). In breast cancer, TGF-β in exosomes induces monocyte differentiation and accumulation of immature MDSCs (146). Exosomes produced by osteosarcoma cells have been reported to have a bidirectional effect on tumors; however, there are only a few studies on their immune effects. Exosomes have tumor-associated antigens on their surfaces, which can interact with antigen-presenting cells and induce tumor-specific toxic T-cell immune responses (75). Similar to exosomes secreted by osteoblasts, exosomes secreted by osteosarcoma cells also have immunosuppressive effects, even at a much higher degree. Exosomes containing TGF-β, α-fetoprotein, and heat shock proteins slow T cell proliferation, prevent effector T cells from working, promote a regulatory ($FOXP3^+$) $CD4^+$ phenotype, and lower the expression of the activation marker CD25 on $CD8^+$ cells (147). Exosomes secreted by metastasized osteosarcoma cells have been found to induce M2 polarization *via* TGF-β2, thus promoting further invasion and metastasis (148). Exosomes can also disrupt the activity of NK cells and DCs *via* TIM-3 (149, 150).

Therapeutic Strategies and Clinical Applications

The application of exosomes mainly includes two aspects: 1) exosomes as diagnostic and prognostic indicators, and 2) exosomes as drug carriers because of their good biocompatibility and low immunogenicity. Wang et al. (151) reported that the serum levels of exosomal PD-L1 and N-cadherin in patients with osteosarcoma could accurately predict metastasis. Shimbo et al. (152) encapsulated artificial synthetic therapeutic miRNA-143 in exosomes and released them into the osteosarcoma microenvironment, and found that the therapy significantly reduced osteosarcoma cell migration. Although exosomes are expected to be potential drug delivery vectors in cancer, packaging drugs and modifying exosomes creatively to obtain more controlled and stable release and fewer adverse effects is one of the directions for future research. **Table 2** lists clinical trials on exosomes in other malignant tumors, indicating that exosomes may also be versatile in osteosarcoma research.

5 CONCLUSIONS, LIMITATIONS, AND PERSPECTIVES

Osteosarcoma is a primary malignant bone tumor that mainly occurs in children, adolescents, and the elderly, with a poor prognosis. The immune microenvironment of osteosarcoma is a complex system with high heterogeneity, which is closely related to the escape of tumor cells from immune surveillance, uncontrolled proliferation, and metastasis. Amplifying the effect of anti-tumor immunity and inhibiting pro-tumor immunity may be a promising approach to eliminate microscopic tumor lesions and CTCs. This review systematically summarizes the roles of cellular and non-cellular components in the immune microenvironment of osteosarcoma and the progress in related therapeutic strategies and clinical applications over the last 10 years, especially in the last 5 years, providing a reference for future research, diagnosis, and treatment of osteosarcoma.

However, the research above is far from sufficient for the following reasons. 1) First, the tumor immune microenvironment is variable, as reflected by variations in disease type and subtype, disease course, and individual. The current understanding of the roles of components of the immune microenvironment of osteosarcoma is still at the stage of borrowing analogous findings from other solid tumor types, which may be vague and one-sided. 2) Second, most studies remain in the preclinical stage, and evidence of translational medicine is insufficient. 3) Finally, the immune system influences the entire body, and immune-related therapies should be both safe and effective. If not employed properly, they can lead to new and serious diseases; therefore, adverse effects should be considered seriously.

Based on this, some future directions are proposed: 1) Diagnosis: Explore the multi-factor predictive model, diagnosis model, and grading scores of osteosarcoma that contain immune

TABLE 2 | Clinical trials on exosomes in other malignant tumors.

NCT number	Diseases	Exosomes	Functions
NCT02702856	Prostate cancer	Urinary exosome gene signature	Diagnosis
NCT03830619	Lung cancer	Serum exosomal long noncoding RNAs	Diagnosis
NCT03032913	Pancreatic ductal adenocarcinoma	CTCs and onco-exosomes	Diagnosis
NCT04720599	Urologic cancer	ExoDx Prostate Intelliscore	Diagnosis
NCT02662621	Malignant solid tumors	HSP70-exosomes in the blood and urine	Diagnosis
NCT03911999	Prostate cancer	Urinary exosomal microRNA	Prediction
NCT03031418	Prostate cancer	ExoDx Prostate Intelliscore	Prediction
NCT03895216	Bone metastases	Deregulated miRNAs in the circulating exosomes	Prediction
NCT02862470	Thyroid cancer	Urinary exosomes	Prediction
NCT01159288	Non-small cell lung cancer	Vaccination with tumor antigen-loaded dendritic cell-derived exosomes	Treatment

components to promote precision treatment. 2) Treatment: Develop new approaches that are more effective than existing treatment schemes under the premise of safety, try to combine immunotherapy with other therapies, and pursue cheaper and faster manufacturing. 3) Research: Find more ideal identification markers of immune cells and non-immune cells, determine interactions among immune microenvironment components, find more ideal therapeutic targets, and combine multidisciplinary knowledge and multi-technical assistance for research.

AUTHOR CONTRIBUTIONS

TZ and JH contributed to conception, designed of the outline, and wrote the manuscript. LY and ZC helped to search for and systematically sort out the literature and material. LY, WS, YH, and JX polished up the writing. WS, YH, and JX conducted oversight and took leadership responsibility for the whole research planning and execution. All authors contributed to manuscript revision, read, and approved the submitted version.

FUNDING

This work was supported by National Natural Science Foundation of China (grant number 81872177; 81972517) and Shanghai Rising-Star Program (grant number 20QA1408000).

ACKNOWLEDGMENTS

We would like to express sincere gratitude to our colleagues in Shanghai Bone Tumor Institution for their kind support and technical help, including Tao Zhang, Yinghua Gao, Zhuoying Wang, Xinglong Ma, Yafei Jiang, Mengkai Yang, Xinmeng Jin, Ke Zeng, Haoran Mu, Linghang Xue and Huanliang Meng.

REFERENCES

1. Durfee, RA, Mohammed, M, and Luu, HH. Review of Osteosarcoma and Current Management. *Rheumatol Ther* (2016) 3(2):221–43. doi: 10.1007/s40744-016-0046-y
2. Ottaviani, G, and Jaffe, N. The Epidemiology of Osteosarcoma. *Cancer Treat Res* (2009) 152:3–13. doi: 10.1007/978-1-4419-0284-9_1
3. Appelman-Dijkstra, NM, and Papapoulos, SE. Paget's Disease of Bone. *Best Pract Res Clin Endocrinol Metab* (2018) 32(5):657–68. doi: 10.1016/j.beem.2018.05.005
4. Hameed, M, and Mandelker, D. Tumor Syndromes Predisposing to Osteosarcoma. *Adv Anat Pathol* (2018) 25(4):217–22. doi: 10.1097/PAP.0000000000000190
5. Casali, PG, Bielack, S, Abecassis, N, Aro, HT, Bauer, S, Biagini, R, et al. Bone Sarcomas: ESMO-PaedCan-EURACAN Clinical Practice Guidelines for Diagnosis, Treatment and Follow-Up. *Ann Oncol* (2018) 29(Suppl 4):iv79–95. doi: 10.1093/annonc/mdy096
6. Harrison, DJ, Geller, DS, Gill, JD, Lewis, VO, and Gorlick, R. Current and Future Therapeutic Approaches for Osteosarcoma. *Expert Rev Anticancer Ther* (2018) 18(1):39–50. doi: 10.1080/14737140.2018.1413939
7. Grimer, RJ. Surgical Options for Children With Osteosarcoma. *Lancet Oncol* (2005) 6(2):85–92. doi: 10.1016/S1470-2045(05)01734-1
8. Ferrari, S, Ruggieri, P, Cefalo, G, Tamburini, A, Capanna, R, Fagioli, F, et al. Neoadjuvant Chemotherapy With Methotrexate, Cisplatin, and Doxorubicin With or Without Ifosfamide in Nonmetastatic Osteosarcoma of the Extremity: An Italian Sarcoma Group Trial ISG/OS-1. *J Clin Oncol* (2012) 30(17):2112–8. doi: 10.1200/JCO.2011.38.4420
9. Le Deley, MC, Paulussen, M, Lewis, I, Brennan, B, Ranft, A, Whelan, J, et al. Cyclophosphamide Compared With Ifosfamide in Consolidation Treatment of Standard-Risk Ewing Sarcoma: Results of the Randomized Noninferiority Euro-EWING99-R1 Trial. *J Clin Oncol* (2014) 32(23):2440–8. doi: 10.1200/JCO.2013.54.4833
10. Goorin, AM, Harris, MB, Bernstein, M, Ferguson, W, Devidas, M, Siegal, GP, et al. Phase II/III Trial of Etoposide and High-Dose Ifosfamide in Newly Diagnosed Metastatic Osteosarcoma: A Pediatric Oncology Group Trial. *J Clin Oncol* (2002) 20(2):426–33. doi: 10.1200/JCO.2002.20.2.426
11. Meyer, WH, Pratt, CB, Poquette, CA, Rao, BN, Parham, DM, Marina, NM, et al. Carboplatin/ifosfamide Window Therapy for Osteosarcoma: Results of the St Jude Children's Research Hospital OS-91 Trial. *J Clin Oncol* (2001) 19(1):171–82. doi: 10.1200/JCO.2001.19.1.171
12. Palmerini, E, Jones, RL, Marchesi, E, Paioli, A, Cesari, M, Longhi, A, et al. Gemcitabine and Docetaxel in Relapsed and Unresectable High-Grade Osteosarcoma and Spindle Cell Sarcoma of Bone. *BMC Cancer* (2016) 16:280. doi: 10.1186/s12885-016-2312-3
13. Grignani, G, Palmerini, E, Ferraresi, V, D'Ambrosio, L, Bertulli, R, Asaftei, SD, et al. Sorafenib and Everolimus for Patients With Unresectable High-Grade Osteosarcoma Progressing After Standard Treatment: A non-Randomised Phase 2 Clinical Trial. *Lancet Oncol* (2015) 16(1):98–107. doi: 10.1016/S1470-2045(14)71136-2

14. Duffaud, F, Mir, O, Boudou-Rouquette, P, Piperno-Neumann, S, Penel, N, Bompas, E, et al. Efficacy and Safety of Regorafenib in Adult Patients With Metastatic Osteosarcoma: A non-Comparative, Randomised, Double-Blind, Placebo-Controlled, Phase 2 Study. *Lancet Oncol* (2019) 20(1):120–33. doi: 10.1016/S1470-2045(18)30742-3
15. Anderson, PM, Wiseman, GA, Dispenzieri, A, Arndt, CA, Hartmann, LC, Smithson, WA, et al. High-Dose Samarium-153 Ethylene Diamine Tetramethylene Phosphonate: Low Toxicity of Skeletal Irradiation in Patients With Osteosarcoma and Bone Metastases. *J Clin Oncol* (2002) 20 (1):189–96. doi: 10.1200/JCO.2002.20.1.189
16. Meyers, PA, Schwartz, CL, Krailo, MD, Healey, JH, Bernstein, ML, Betcher, D, et al. Osteosarcoma: The Addition of Muramyl Tripeptide to Chemotherapy Improves Overall Survival–A Report From the Children's Oncology Group. *J Clin Oncol* (2008) 26(4):633–8. doi: 10.1200/JCO.2008.14.0095
17. Corre, I, Verrecchia, F, Crenn, V, Redini, F, and Trichet, V. The Osteosarcoma Microenvironment: A Complex But Targetable Ecosystem. *Cells* (2020) 9(4):976. doi: 10.3390/cells9040976
18. Zheng, Y, Wang, G, Chen, R, Hua, Y, and Cai, Z. Mesenchymal Stem Cells in the Osteosarcoma Microenvironment: Their Biological Properties, Influence on Tumor Growth, and Therapeutic Implications. *Stem Cell Res Ther* (2018) 9(1):22. doi: 10.1186/s13287-018-0780-x
19. Koebel, CM, Vermi, W, Swann, JB, Zerafa, N, Rodig, SJ, Old, LJ, et al. Adaptive Immunity Maintains Occult Cancer in an Equilibrium State. *Nature* (2007) 450(7171):903–7. doi: 10.1038/nature06309
20. Balakrishnan, A, George, IA, and Kumar, P. Circulating Tumor Cells as an Emerging Tool in Cancer Therapy. *Front Biosci (Landmark Ed)* (2020) 25:606–31. doi: 10.2741/4824
21. Locy, H, de Mey, S, de Mey, W, De Ridder, M, Thielemans, K, and Maenhout, SK. Immunomodulation of the Tumor Microenvironment: Turn Foe Into Friend. *Front Immunol* (2018) 9:2909. doi: 10.3389/fimmu.2018.02909
22. Huang, Q, Liang, X, Ren, T, Huang, Y, Zhang, H, Yu, Y, et al. The Role of Tumor-Associated Macrophages in Osteosarcoma Progression - Therapeutic Implications. *Cell Oncol (Dordr)* (2021) 44(3):525–39. doi: 10.1007/s13402-021-00598-w
23. Zhou, Q, Xian, M, Xiang, S, Xiang, D, Shao, X, Wang, J, et al. All-Trans Retinoic Acid Prevents Osteosarcoma Metastasis by Inhibiting M2 Polarization of Tumor-Associated Macrophages. *Cancer Immunol Res* (2017) 5(7):547–59. doi: 10.1158/2326-6066.CIR-16-0259
24. Buddingh, EP, Kuijjer, ML, Duim, RA, Bürger, H, Agelopoulos, K, Myklebost, O, et al. Tumor-Infiltrating Macrophages are Associated With Metastasis Suppression in High-Grade Osteosarcoma: A Rationale for Treatment With Macrophage Activating Agents. *Clin Cancer Res* (2011) 17(8):2110–9. doi: 10.1158/1078-0432.CCR-10-2047
25. Ren, S, Zhang, X, Hu, Y, Wu, J, Ju, Y, Sun, X, et al. Blocking the Notch Signal Transduction Pathway Promotes Tumor Growth in Osteosarcoma by Affecting Polarization of TAM to M2 Phenotype. *Ann Transl Med* (2020) 8(17):1057. doi: 10.21037/atm-20-3881
26. Dumars, C, Ngyuen, JM, Gaultier, A, Lanel, R, Corradini, N, Gouin, F, et al. Dysregulation of Macrophage Polarization Is Associated With the Metastatic Process in Osteosarcoma. *Oncotarget* (2016) 7(48):78343–54. doi: 10.18632/oncotarget.13055
27. Shao, XJ, Xiang, SF, Chen, YQ, Zhang, N, Cao, J, Zhu, H, et al. Inhibition of M2-Like Macrophages by All-Trans Retinoic Acid Prevents Cancer Initiation and Stemness in Osteosarcoma Cells. *Acta Pharmacol Sin* (2019) 40(10):1343–50. doi: 10.1038/s41401-019-0262-4
28. Punzo, F, Bellini, G, Tortora, C, Pinto, DD, Argenziano, M, Pota, E, et al. Mifamurtide and TAM-Like Macrophages: Effect on Proliferation, Migration and Differentiation of Osteosarcoma Cells. *Oncotarget* (2020) 11(7):687–98. doi: 10.18632/oncotarget.27479
29. Xiao, Q, Zhang, X, Wu, Y, and Yang, Y. Inhibition of Macrophage Polarization Prohibits Growth of Human Osteosarcoma. *Tumour Biol* (2014) 35(8):7611–6. doi: 10.1007/s13277-014-2005-y
30. Fujiwara, T, Yakoub, MA, Chandler, A, Christ, AB, Yang, G, Ouerfelli, O, et al. CSF1/CSF1R Signaling Inhibitor Pexidartinib (PLX3397) Reprograms Tumor-Associated Macrophages and Stimulates T-Cell Infiltration in the Sarcoma Microenvironment. *Mol Cancer Ther* (2021) 20(8):1388–99. doi: 10.1158/1535-7163.MCT-20-0591
31. Yang, S, Wu, C, Wang, L, Shan, D, and Chen, B. Pretreatment Inflammatory Indexes as Prognostic Predictors for Survival in Osteosarcoma Patients. *Int J Clin Exp Pathol* (2020) 13(3):515–243. doi: 10.1038/s41598-018-21093-7
32. Liu, B, Huang, Y, Sun, Y, Zhang, J, Yao, Y, Shen, Z, et al. Prognostic Value of Inflammation-Based Scores in Patients With Osteosarcoma. *Sci Rep* (2016) 6:39862. doi: 10.1038/srep39862
33. Xia, WK, Liu, ZL, Shen, D, Lin, QF, Su, J, and Mao, WD. Prognostic Performance of Pre-Treatment NLR and PLR in Patients Suffering From Osteosarcoma. *World J Surg Oncol* (2016) 14:127. doi: 10.1186/s12957-016-0889-2
34. Vasquez, L, León, E, Beltran, B, Maza, I, Oscanoa, M, and Geronimo, J. Pretreatment Neutrophil-To-Lymphocyte Ratio and Lymphocyte Recovery: Independent Prognostic Factors for Survival in Pediatric Sarcomas. *J Pediatr Hematol Oncol* (2017) 39(7):538–46. doi: 10.1097/MPH.0000000000000911
35. Yapar, A, Tokgöz, MA, Yapar, D, Atalay, İB, Ulucaköy, C, and Güngör, B. Diagnostic and Prognostic Role of Neutrophil/Lymphocyte Ratio, Platelet/Lymphocyte Ratio, and Lymphocyte/Monocyte Ratio in Patients With Osteosarcoma. *Jt Dis Relat Surg* (2021) 32(2):489–96. doi: 10.52312/jdrs.2021.79775
36. Wu, L, Saxena, S, Awaji, M, and Singh, RK. Tumor-Associated Neutrophils in Cancer: Going Pro. *Cancers (Basel)* (2019) 11(4):564. doi: 10.3390/cancers11040564
37. Pillay, J, den Braber, I, Vrisekoop, N, Kwast, LM, de Boer, RJ, Borghans, JA, et al. *In Vivo* Labeling With 2H2O Reveals a Human Neutrophil Lifespan of 5.4 Days. *Blood* (2010) 116(4):625–7. doi: 10.1182/blood-2010-01-259028
38. Akgul, C, Moulding, DA, and Edwards, SW. Molecular Control of Neutrophil Apoptosis. *FEBS Lett* (2001) 487(3):318–22. doi: 10.1016/S0014-5793(00)02324-3
39. Papayannopoulos, V. Neutrophil Extracellular Traps in Immunity and Disease. *Nat Rev Immunol* (2018) 18(2):134–47. doi: 10.1038/nri.2017.105
40. Leshner, M, Wang, S, Lewis, C, Zheng, H, Chen, XA, Santy, L, et al. PAD4 Mediated Histone Hypercitrullination Induces Heterochromatin Decondensation and Chromatin Unfolding to Form Neutrophil Extracellular Trap-Like Structures. *Front Immunol* (2012) 3:307. doi: 10.3389/fimmu.2012.00307
41. Fridlender, ZG, Sun, J, Kim, S, Kapoor, V, Cheng, G, Ling, L, et al. Polarization of Tumor-Associated Neutrophil Phenotype by TGF-Beta: "N1" Versus "N2" TAN. *Cancer Cell* (2009) 16(3):183–94. doi: 10.1016/j.ccr.2009.06.017
42. Yang, B, Su, Z, Chen, G, Zeng, Z, Tan, J, Wu, G, et al. Identification of Prognostic Biomarkers Associated With Metastasis and Immune Infiltration in Osteosarcoma. *Oncol Lett* (2021) 21(3):180. doi: 10.3892/ol.2021.12441
43. Fu, Y, Bao, Q, Liu, Z, He, G, Wen, J, Liu, Q, et al. Development and Validation of a Hypoxia-Associated Prognostic Signature Related to Osteosarcoma Metastasis and Immune Infiltration. *Front Cell Dev Biol* (2021) 9:633607. doi: 10.3389/fcell.2021.633607
44. Ling, Z, Yang, C, Tan, J, Dou, C, and Chen, Y. Beyond Immunosuppressive Effects: Dual Roles of Myeloid-Derived Suppressor Cells in Bone-Related Diseases. *Cell Mol Life Sci* (2021) 78(23):7161–83. doi: 10.1007/s00018-021-03966-9
45. Rodríguez, PC, and Ochoa, AC. Arginine Regulation by Myeloid Derived Suppressor Cells and Tolerance in Cancer: Mechanisms and Therapeutic Perspectives. *Immunol Rev* (2008) 222:180–91. doi: 10.1111/j.1600-065X.2008.00608.x
46. Yang, Y, Li, C, Liu, T, Dai, X, and Bazhin, AV. Myeloid-Derived Suppressor Cells in Tumors: From Mechanisms to Antigen Specificity and Microenvironmental Regulation. *Front Immunol* (2020) 11:1371. doi: 10.3389/fimmu.2020.01371
47. Gabrilovich, DI. Myeloid-Derived Suppressor Cells. *Cancer Immunol Res* (2017) 5(1):3–8. doi: 10.1158/2326-6066.CIR-16-0297
48. Marvel, D, and Gabrilovich, DI. Myeloid-Derived Suppressor Cells in the Tumor Microenvironment: Expect the Unexpected. *J Clin Invest* (2015) 125 (9):3356–64. doi: 10.1172/JCI80005
49. Deng, C, Xu, Y, Fu, J, Zhu, X, Chen, H, Xu, H, et al. Reprograming the Tumor Immunologic Microenvironment Using Neoadjuvant Chemotherapy in Osteosarcoma. *Cancer Sci* (2020) 111(6):1899–909. doi: 10.1111/cas.14398

50. Bauer, R, Udonta, F, Wroblewski, M, Ben-Batalla, I, Santos, IM, Taverna, F, et al. Blockade of Myeloid-Derived Suppressor Cell Expansion With All-Trans Retinoic Acid Increases the Efficacy of Antiangiogenic Therapy. *Cancer Res* (2018) 78(12):3220–32. doi: 10.1158/0008-5472.CAN-17-3415
51. Long, AH, Highfill, SL, Cui, Y, Smith, JP, Walker, AJ, Ramakrishna, S, et al. Reduction of MDSCs With All-Trans Retinoic Acid Improves CAR Therapy Efficacy for Sarcomas. *Cancer Immunol Res* (2016) 4(10):869–80. doi: 10.1158/2326-6066.CIR-15-0230
52. Uehara, T, Eikawa, S, Nishida, M, Kunisada, Y, Yoshida, A, Fujiwara, T, et al. Metformin Induces CD11b+-Cell-Mediated Growth Inhibition of an Osteosarcoma: Implications for Metabolic Reprogramming of Myeloid Cells and Anti-Tumor Effects. *Int Immunol* (2019) 31(4):187–98. doi: 10.1093/intimm/dxy079
53. Zhao, Q, Hu, J, Mitra, A, Cutrera, J, Zhang, W, Zhang, Z, et al. Tumor-Targeted IL-12 Combined With Tumor Resection Yields a Survival-Favorable Immune Profile. *J Immunother Cancer* (2019) 7(1):154. doi: 10.1186/s40425-019-0631-z
54. Jiang, K, Li, J, Zhang, J, Wang, L, Zhang, Q, Ge, J, et al. SDF-1/CXCR4 Axis Facilitates Myeloid-Derived Suppressor Cells Accumulation in Osteosarcoma Microenvironment and Blunts the Response to Anti-PD-1 Therapy. *Int Immunopharmacol* (2019) 75:105818. doi: 10.1016/j.intimp.2019.105818
55. Shi, X, Li, X, Wang, H, Yu, Z, Zhu, Y, and Gao, Y. Specific Inhibition of PI3Kδ/γ Enhances the Efficacy of Anti-PD1 Against Osteosarcoma Cancer. *J Bone Oncol* (2019) 16:100206. doi: 10.1016/j.jbo.2018.11.001
56. Guan, Y, Zhang, R, Peng, Z, Dong, D, Wei, G, and Wang, Y. Inhibition of IL-18-Mediated Myeloid Derived Suppressor Cell Accumulation Enhances Anti-PD1 Efficacy Against Osteosarcoma Cancer. *J Bone Oncol* (2017) 9:59–64. doi: 10.1016/j.jbo.2017.10.002
57. Ligon, JA, Choi, W, Cojocaru, G, Fu, W, Hsiue, EH, Oke, TF, et al. Pathways of Immune Exclusion in Metastatic Osteosarcoma are Associated With Inferior Patient Outcomes. *J Immunother Cancer* (2021) 9(5):e001772. doi: 10.1136/jitc-2020-001772
58. Le, T, Su, S, and Shahriyari, L. Immune Classification of Osteosarcoma. *Math Biosci Eng* (2021) 18(2):1879–97. doi: 10.3934/mbe.2021098
59. Cao, H, Quan, S, Zhang, L, Chen, Y, and Jiao, G. BMPR2 Expression Level is Correlated With Low Immune Infiltration and Predicts Metastasis and Poor Survival in Osteosarcoma. *Oncol Lett* (2021) 21(5):391. doi: 10.3892/ol.2021.12652
60. Zhang, C, Zheng, JH, Lin, ZH, Lv, HY, Ye, ZM, Chen, YP, et al. Profiles of Immune Cell Infiltration and Immune-Related Genes in the Tumor Microenvironment of Osteosarcoma. *Aging (Albany NY)* (2020) 12 (4):3486–501. doi: 10.18632/aging.102824
61. Heymann, MF, Lézot, F, and Heymann, D. The Contribution of Immune Infiltrates and the Local Microenvironment in the Pathogenesis of Osteosarcoma. *Cell Immunol* (2019) 343:103711. doi: 10.1016/j.cellimm.2017.10.011
62. Inagaki, Y, Hookway, E, Williams, KA, Hassan, AB, Oppermann, U, Tanaka, Y, et al. Dendritic and Mast Cell Involvement in the Inflammatory Response to Primary Malignant Bone Tumours. *Clin Sarcoma Res* (2016) 6:13. doi: 10.1186/s13569-016-0053-3
63. Fan, L, Ru, J, Liu, T, and Ma, C. Identification of a Novel Prognostic Gene Signature From the Immune Cell Infiltration Landscape of Osteosarcoma. *Front Cell Dev Biol* (2021) 9:718624. doi: 10.3389/fcell.2021.718624
64. Wei, J, Fang, DL, Huang, CK, Hua, SL, and Lu, XS. Screening a Novel Signature and Predicting the Immune Landscape of Metastatic Osteosarcoma in Children *via* Immune-Related lncRNAs. *Transl Pediatr* (2021) 10(7):1851–66. doi: 10.21037/tp-21-226
65. Collin, M, and Bigley, V. Human Dendritic Cell Subsets: An Update. *Immunology* (2018) 154(1):3–20. doi: 10.1111/imm.12888
66. Zhang, GZ, Wu, ZL, Li, CY, Ren, EH, Yuan, WH, Deng, YJ, et al. Development of a Machine Learning-Based Autophagy-Related lncRNA Signature to Improve Prognosis Prediction in Osteosarcoma Patients. *Front Mol Biosci* (2021) 8:615084. doi: 10.3389/fmolb.2021.615084
67. Le, T, Su, S, Kirshtein, A, and Shahriyari, L. Data-Driven Mathematical Model of Osteosarcoma. *Cancers (Basel)* (2021) 13(10):2367. doi: 10.3390/cancers13102367
68. Kansara, M, Thomson, K, Pang, P, Dutour, A, Mirabello, L, Acher, F, et al. Infiltrating Myeloid Cells Drive Osteosarcoma Progression *via* GRM4 Regulation of IL23. *Cancer Discov* (2019) 9(11):1511–9. doi: 10.1158/2159-8290.CD-19-0154
69. Jones, KB. Dendritic Cells Drive Osteosarcomagenesis Through Newly Identified Oncogene and Tumor Suppressor. *Cancer Discov* (2019) 9 (11):1484–6. doi: 10.1158/2159-8290.CD-19-0994
70. Zhou, Y, Yang, D, Yang, Q, Lv, X, Huang, W, Zhou, Z, et al. Single-Cell RNA Landscape of Intratumoral Heterogeneity and Immunosuppressive Microenvironment in Advanced Osteosarcoma. *Nat Commun* (2020) 11 (1):6322. doi: 10.1038/s41467-020-20059-6
71. Koirala, P, Roth, ME, Gill, J, Piperdi, S, Chinai, JM, Geller, DS, et al. Immune Infiltration and PD-L1 Expression in the Tumor Microenvironment are Prognostic in Osteosarcoma. *Sci Rep* (2016) 6:30093. doi: 10.1038/srep30093
72. Jin, T, Wu, H, Wang, Y, and Peng, H. Capsaicin Induces Immunogenic Cell Death in Human Osteosarcoma Cells. *Exp Ther Med* (2016) 12(2):765–70. doi: 10.3892/etm.2016.3368
73. Zhou, Y, Slone, N, Chrisikos, TT, Kyrysyuk, O, Babcock, RL, Medik, YB, et al. Vaccine Efficacy Against Primary and Metastatic Cancer With *In Vitro*-Generated CD103(+) Conventional Dendritic Cells. *J Immunother Cancer* (2020) 8(1):e000474. doi: 10.1136/jitc-2019-000474
74. Mori, K, Rédini, F, Gouin, F, Cherrier, B, and Heymann, D. Osteosarcoma: Current Status of Immunotherapy and Future Trends (Review). *Oncol Rep* (2006) 15(3):693–700. doi: 10.3892/or.15.3.693
75. Pu, F, Chen, F, Zhang, Z, Liu, J, and Shao, Z. Information Transfer and Biological Significance of Neoplastic Exosomes in the Tumor Microenvironment of Osteosarcoma. *Onco Targets Ther* (2020) 13:8931–40. doi: 10.2147/OTT.S266835
76. Kawano, M, Itonaga, I, Iwasaki, T, Tsuchiya, H, and Tsumura, H. Anti-TGF-β Antibody Combined With Dendritic Cells Produce Antitumor Effects in Osteosarcoma. *Clin Orthop Relat Res* (2012) 470(8):2288–94. doi: 10.1007/s11999-012-2299-2
77. Sundara, YT, Kostine, M, Cleven, AH, Bovée, JV, Schilham, MW, and Cleton-Jansen, AM. Increased PD-L1 and T-Cell Infiltration in the Presence of HLA Class I Expression in Metastatic High-Grade Osteosarcoma: A Rationale for T-Cell-Based Immunotherapy. *Cancer Immunol Immunother* (2017) 66(1):119–28. doi: 10.1007/s00262-016-1925-3
78. Han, Q, Shi, H, and Liu, F. CD163(+) M2-Type Tumor-Associated Macrophage Support the Suppression of Tumor-Infiltrating T Cells in Osteosarcoma. *Int Immunopharmacol* (2016) 34:101–6. doi: 10.1016/j.intimp.2016.01.023
79. Matsuo, T, Shimose, S, Kubo, T, Mikami, Y, Arihiro, K, Yasunaga, Y, et al. Extraskeletal Osteosarcoma With Partial Spontaneous Regression. *Anticancer Res* (2009) 29(12):5197–201.
80. Yang, H, Zhao, L, Zhang, Y, and Li, FF. A Comprehensive Analysis of Immune Infiltration in the Tumor Microenvironment of Osteosarcoma. *Cancer Med* (2021) 10(16):5696–711. doi: 10.1002/cam4.4117
81. Matsuda, K, Miyoshi, H, Moritsubo, M, Hiraoka, K, Hamada, T, Shiba, N, et al. Clinicopathological and Immunohistochemical Analysis of Autoimmune Regulator Expression in Patients With Osteosarcoma. *Clin Exp Metastasis* (2018) 35(7):641–8. doi: 10.1007/s10585-018-9928-4
82. Yahiro, K, Matsumoto, Y, Yamada, H, Endo, M, Setsu, N, Fujiwara, T, et al. Activation of TLR4 Signaling Inhibits Progression of Osteosarcoma by Stimulating CD8-Positive Cytotoxic Lymphocytes. *Cancer Immunol Immunother* (2020) 69(5):745–58. doi: 10.1007/s00262-020-02508-9
83. Yoshida, K, Okamoto, M, Sasaki, J, Kuroda, C, Ishida, H, Ueda, K, et al. Anti-PD-1 Antibody Decreases Tumour-Infiltrating Regulatory T Cells. *BMC Cancer* (2020) 20(1):25. doi: 10.1186/s12885-019-6499-y
84. Cascio, MJ, Whitley, EM, Sahay, B, Cortes-Hinojosa, G, Chang, LJ, Cowart, J, et al. Canine Osteosarcoma Checkpoint Expression Correlates With Metastasis and T-Cell Infiltrate. *Vet Immunol Immunopathol* (2021) 232:110169. doi: 10.1016/j.vetimm.2020.110169
85. He, X, Lin, H, Yuan, L, and Li, B. Combination Therapy With L-Arginine and α-PD-L1 Antibody Boosts Immune Response Against Osteosarcoma in Immunocompetent Mice. *Cancer Biol Ther* (2017) 18(2):94–100. doi: 10.1080/15384047.2016.1276136
86. Takahashi, Y, Yasui, T, Tamari, K, Minami, K, Otani, K, Isohashi, F, et al. Radiation Enhanced the Local and Distant Anti-Tumor Efficacy in Dual

Immune Checkpoint Blockade Therapy in Osteosarcoma. *PloS One* (2017) 12(12):e0189697. doi: 10.1371/journal.pone.0189697
87. Nasarre, P, Garcia, DI, Siegel, JB, Bonilla, IV, Mukherjee, R, Hilliard, E, et al. Overcoming PD-1 Inhibitor Resistance With a Monoclonal Antibody to Secreted Frizzled-Related Protein 2 in Metastatic Osteosarcoma. *Cancers (Basel)* (2021) 13(11):2696. doi: 10.3390/cancers13112696
88. Wang, Z, Li, B, Ren, Y, and Ye, Z. T-Cell-Based Immunotherapy for Osteosarcoma: Challenges and Opportunities. *Front Immunol* (2016) 7:353. doi: 10.3389/fimmu.2016.00353
89. DeRenzo, C, and Gottschalk, S. Genetically Modified T-Cell Therapy for Osteosarcoma: Into the Roaring 2020s. *Adv Exp Med Biol* (2020) 1257:109–31. doi: 10.1007/978-3-030-43032-0_10
90. Roberts, SS, Chou, AJ, and Cheung, NK. Immunotherapy of Childhood Sarcomas. *Front Oncol* (2015) 5:181. doi: 10.3389/fonc.2015.00181
91. Fernández, L, Metais, JY, Escudero, A, Vela, M, Valentín, J, Vallcorba, I, et al. Memory T Cells Expressing an NKG2D-CAR Efficiently Target Osteosarcoma Cells. *Clin Cancer Res* (2017) 23(19):5824–35. doi: 10.1158/1078-0432.CCR-17-0075
92. Mortara, L, Orecchia, P, Castellani, P, Borsi, L, Carnemolla, B, and Balza, E. Schedule-Dependent Therapeutic Efficacy of L19mTNF-α and Melphalan Combined With Gemcitabine. *Cancer Med* (2013) 2(4):478–87. doi: 10.1002/cam4.89
93. Ratti, C, Botti, L, Cancila, V, Galvan, S, Torselli, I, Garofalo, C, et al. Trabectedin Overrides Osteosarcoma Differentiative Block and Reprograms the Tumor Immune Environment Enabling Effective Combination With Immune Checkpoint Inhibitors. *Clin Cancer Res* (2017) 23(17):5149–61. doi: 10.1158/1078-0432.CCR-16-3186
94. Belisario, DC, Akman, M, Godel, M, Campani, V, Patrizio, MP, Scotti, L, et al. ABCA1/ABCB1 Ratio Determines Chemo- and Immune-Sensitivity in Human Osteosarcoma. *Cells* (2020) 9(3):647. doi: 10.3390/cells9030647
95. Workenhe, ST, Pol, JG, Lichty, BD, Cummings, DT, and Mossman, KL. Combining Oncolytic HSV-1 With Immunogenic Cell Death-Inducing Drug Mitoxantrone Breaks Cancer Immune Tolerance and Improves Therapeutic Efficacy. *Cancer Immunol Res* (2013) 1(5):309–19. doi: 10.1158/2326-6066.CIR-13-0059-T
96. Sarvaria, A, Madrigal, JA, and Saudemont, A. B Cell Regulation in Cancer and Anti-Tumor Immunity. *Cell Mol Immunol* (2017) 14(8):662–74. doi: 10.1038/cmi.2017.35
97. Li, GQ, Wang, YK, Zhou, H, Jin, LG, Wang, CY, Albahde, M, et al. Application of Immune Infiltration Signature and Machine Learning Model in the Differential Diagnosis and Prognosis of Bone-Related Malignancies. *Front Cell Dev Biol* (2021) 9:630355. doi: 10.3389/fcell.2021.630355
98. Murphy, MA, O'Leary, JJ, and Cahill, DJ. Assessment of the Humoral Immune Response to Cancer. *J Proteom* (2012) 75(15):4573–9. doi: 10.1016/j.jprot.2012.01.021
99. Kinker, GS, Vitiello, GAF, Ferreira, WAS, Chaves, AS, Cordeiro de Lima, VC, and Medina, TDS. B Cell Orchestration of Anti-Tumor Immune Responses: A Matter of Cell Localization and Communication. *Front Cell Dev Biol* (2021) 9:678127. doi: 10.3389/fcell.2021.678127
100. Janiszewska, M, Primi, MC, and Izard, T. Cell Adhesion in Cancer: Beyond the Migration of Single Cells. *J Biol Chem* (2020) 295(8):2495–505. doi: 10.1074/jbc.REV119.007759
101. Zhang, K, Gao, J, and Ni, Y. Screening of Candidate Key Genes Associated With Human Osteosarcoma Using Bioinformatics Analysis. *Oncol Lett* (2017) 14(3):2887–93. doi: 10.3892/ol.2017.6519
102. Wang, X, Du, J, Gu, P, Jin, R, and Lin, X. Polymeric Immunoglobulin Receptor Expression is Correlated With Poor Prognosis in Patients With Osteosarcoma. *Mol Med Rep* (2014) 9(6):2105–10. doi: 10.3892/mmr.2014.2110
103. Guerra, RN, Oliveira-Junior, JJ, Mouchrek-Filho, JC, Liberio, SA, Lima, MV, Paim, DB, et al. Salivary Evaluation of Pediatric Patients With Cancer, Before and After Antineoplasic Treatment. *J Oral Pathol Med* (2012) 41(7):527–32. doi: 10.1111/j.1600-0714.2012.01165.x
104. Hellmann, I, Waldmeier, L, Bannwarth-Escher, MC, Maslova, K, Wolter, FI, Grawunder, U, et al. Novel Antibody Drug Conjugates Targeting Tumor-Associated Receptor Tyrosine Kinase ROR2 by Functional Screening of Fully Human Antibody Libraries Using Transpo-mAb Display on Progenitor B Cells. *Front Immunol* (2018) 9:2490. doi: 10.3389/fimmu.2018.02490
105. Mazzoni, E, Benassi, MS, Corallini, A, Barbanti-Brodano, G, Taronna, A, Picci, P, et al. Significant Association Between Human Osteosarcoma and Simian Virus 40. *Cancer* (2015) 121(5):708–15. doi: 10.1002/cncr.29137
106. Zhang, J, Zhang, Y, Cheng, S, Mu, Y, Liu, Y, Yi, X, et al. LAIR-1 Overexpression Inhibits Epithelial-Mesenchymal Transition in Osteosarcoma *via* GLUT1-Related Energy Metabolism. *World J Surg Oncol* (2020) 18(1):136. doi: 10.1186/s12957-020-01896-7
107. Prager, I, and Watzl, C. Mechanisms of Natural Killer Cell-Mediated Cellular Cytotoxicity. *J Leukoc Biol* (2019) 105(6):1319–29. doi: 10.1002/JLB.MR0718-269R
108. Zhang, ML, Chen, L, Li, YJ, and Kong, DL. PD–L1/PD–1 Axis Serves an Important Role in Natural Killer Cell–Induced Cytotoxicity in Osteosarcoma. *Oncol Rep* (2019) 42(5):2049–56. doi: 10.3892/or.2019.7299
109. Lazarova, M, and Steinle, A. Impairment of NKG2D-Mediated Tumor Immunity by TGF-β. *Front Immunol* (2019) 10:2689. doi: 10.3389/fimmu.2019.02689
110. Kisseberth, WC, and Lee, DA. Adoptive Natural Killer Cell Immunotherapy for Canine Osteosarcoma. *Front Vet Sci* (2021) 8:672361. doi: 10.3389/fvets.2021.672361
111. Choucair, K, Duff, JR, Cassidy, CS, Albrethsen, MT, Kelso, JD, Lenhard, A, et al. Natural Killer Cells: A Review of Biology, Therapeutic Potential and Challenges in Treatment of Solid Tumors. *Future Oncol* (2019) 15(26):3053–69. doi: 10.2217/fon-2019-0116
112. Delgado, D, Webster, DE, DeSantes, KB, Durkin, ET, and Shaaban, AF. KIR Receptor-Ligand Incompatibility Predicts Killing of Osteosarcoma Cell Lines by Allogeneic NK Cells. *Pediatr Blood Cancer* (2010) 55(7):1300–5. doi: 10.1002/pbc.22665
113. Chu, Y, Nayyar, G, Jiang, S, Rosenblum, JM, Soon-Shiong, P, Safrit, JT, et al. Combinatorial Immunotherapy of N-803 (IL-15 Superagonist) and Dinutuximab With Ex Vivo Expanded Natural Killer Cells Significantly Enhances In Vitro Cytotoxicity Against GD2(+) Pediatric Solid Tumors and *In Vivo* Survival of Xenografted Immunodeficient NSG Mice. *J Immunother Cancer* (2021) 9(7):e002267. doi: 10.1136/jitc-2020-002267
114. Buddingh, EP, Schilham, MW, Ruslan, SE, Berghuis, D, Szuhai, K, Suurmond, J, et al. Chemotherapy-Resistant Osteosarcoma is Highly Susceptible to IL-15-Activated Allogeneic and Autologous NK Cells. *Cancer Immunol Immunother* (2011) 60(4):575–86. doi: 10.1007/s00262-010-0965-3
115. Kailayangiri, S, Altvater, B, Spurny, C, Jamitzky, S, Schelhaas, S, Jacobs, AH, et al. Targeting Ewing Sarcoma With Activated and GD2-Specific Chimeric Antigen Receptor-Engineered Human NK Cells Induces Upregulation of Immune-Inhibitory HLA-G. *Oncoimmunology* (2017) 6(1):e1250050. doi: 10.1080/2162402X.2016.1250050
116. Schiavone, K, Garnier, D, Heymann, MF, and Heymann, D. The Heterogeneity of Osteosarcoma: The Role Played by Cancer Stem Cells. *Adv Exp Med Biol* (2019) 1139:187–200. doi: 10.1007/978-3-030-14366-4_11
117. Xu, A, Qian, C, Lin, J, Yu, W, Jin, J, Liu, B, et al. Cell Differentiation Trajectory-Associated Molecular Classification of Osteosarcoma. *Genes (Basel)* (2021) 12(11):1685. doi: 10.3390/genes12111685
118. Chang, X, Ma, Z, Zhu, G, Lu, Y, and Yang, J. New Perspective Into Mesenchymal Stem Cells: Molecular Mechanisms Regulating Osteosarcoma. *J Bone Oncol* (2021) 29:100372. doi: 10.1016/j.jbo.2021.100372
119. Sun, Z, Wang, S, and Zhao, RC. The Roles of Mesenchymal Stem Cells in Tumor Inflammatory Microenvironment. *J Hematol Oncol* (2014) 7:14. doi: 10.1186/1756-8722-7-14
120. Kawano, M, Tanaka, K, Itonaga, I, Iwasaki, T, and Tsumura, H. Interaction Between Human Osteosarcoma and Mesenchymal Stem Cells *via* an Interleukin-8 Signaling Loop in the Tumor Microenvironment. *Cell Commun Signal* (2018) 16(1):13. doi: 10.1186/s12964-018-0225-2
121. Du, L, Han, XG, Tu, B, Wang, MQ, Qiao, H, Zhang, SH, et al. CXCR1/Akt Signaling Activation Induced by Mesenchymal Stem Cell-Derived IL-8 Promotes Osteosarcoma Cell Anoikis Resistance and Pulmonary Metastasis. *Cell Death Dis* (2018) 9(7):714. doi: 10.1038/s41419-018-0745-0
122. Pelagalli, A, Nardelli, A, Fontanella, R, and Zannetti, A. Inhibition of AQP1 Hampers Osteosarcoma and Hepatocellular Carcinoma Progression Mediated by Bone Marrow-Derived Mesenchymal Stem Cells. *Int J Mol Sci* (2016) 17(7):1102. doi: 10.3390/ijms17071102
123. Wang, JY, Wu, PK, Chen, PC, Lee, CW, Chen, WM, and Hung, SC. Generation of Osteosarcomas From a Combination of Rb Silencing and C-

Myc Overexpression in Human Mesenchymal Stem Cells. *Stem Cells Transl Med* (2017) 6(2):512–26. doi: 10.5966/sctm.2015-0226
124. Saalfrank, A, Janssen, KP, Ravon, M, Flisikowski, K, Eser, S, Steiger, K, et al. A Porcine Model of Osteosarcoma. *Oncogenesis* (2016) 5(3):e210. doi: 10.1038/oncsis.2016.19
125. Deng, Q, Li, P, Che, M, Liu, J, Biswas, S, Ma, G, et al. Activation of Hedgehog Signaling in Mesenchymal Stem Cells Induces Cartilage and Bone Tumor Formation *via* Wnt/β-Catenin. *Elife* (2019) 8:e50208. doi: 10.7554/eLife.50208
126. Baglio, SR, Lagerweij, T, Pérez-Lanzón, M, Ho, XD, Léveillé, N, Melo, SA, et al. Blocking Tumor-Educated MSC Paracrine Activity Halts Osteosarcoma Progression. *Clin Cancer Res* (2017) 23(14):3721–33. doi: 10.1158/1078-0432.CCR-16-2726
127. Lin, L, Huang, K, Guo, W, Zhou, C, Wang, G, and Zhao, Q. Conditioned Medium of the Osteosarcoma Cell Line U2OS Induces hBMSCs to Exhibit Characteristics of Carcinoma-Associated Fibroblasts *via* Activation of IL-6/STAT3 Signalling. *J Biochem* (2020) 168(3):265–71. doi: 10.1093/jb/mvaa044
128. Pietrovito, L, Leo, A, Gori, V, Lulli, M, Parri, M, Becherucci, V, et al. Bone Marrow-Derived Mesenchymal Stem Cells Promote Invasiveness and Transendothelial Migration of Osteosarcoma Cells *via* a Mesenchymal to Amoeboid Transition. *Mol Oncol* (2018) 12(5):659–76. doi: 10.1002/1878-0261.12189
129. Mannerström, B, Kornilov, R, Abu-Shahba, AG, Chowdhury, IM, Sinha, S, Seppänen-Kaijansinkko, R, et al. Epigenetic Alterations in Mesenchymal Stem Cells by Osteosarcoma-Derived Extracellular Vesicles. *Epigenetics* (2019) 14(4):352–64. doi: 10.1080/15592294.2019.1585177
130. Chang, AI, Schwertschkow, AH, Nolta, JA, and Wu, J. Involvement of Mesenchymal Stem Cells in Cancer Progression and Metastases. *Curr Cancer Drug Targets* (2015) 15(2):88–98. doi: 10.2174/1568009615666150126154151
131. Lagerweij, T, Pérez-Lanzón, M, and Baglio, SR. A Preclinical Mouse Model of Osteosarcoma to Define the Extracellular Vesicle-Mediated Communication Between Tumor and Mesenchymal Stem Cells. *J Vis Exp* (2018) 135:56932. doi: 10.3791/56932
132. Zhang, Q, Fu, L, Liang, Y, Guo, Z, Wang, L, Ma, C, et al. Exosomes Originating From MSCs Stimulated With TGF-β and IFN-γ Promote Treg Differentiation. *J Cell Physiol* (2018) 233(9):6832–40. doi: 10.1002/jcp.26436
133. Khare, D, Or, R, Resnick, I, Barkatz, C, Almogi-Hazan, O, and Avni, B. Mesenchymal Stromal Cell-Derived Exosomes Affect mRNA Expression and Function of B-Lymphocytes. *Front Immunol* (2018) 9:3053. doi: 10.3389/fimmu.2018.03053
134. Jia, XH, Feng, GW, Wang, ZL, Du, Y, Shen, C, Hui, H, et al. Activation of Mesenchymal Stem Cells by Macrophages Promotes Tumor Progression Through Immune Suppressive Effects. *Oncotarget* (2016) 7(15):20934–44. doi: 10.18632/oncotarget.8064
135. Mardpour, S, Hamidieh, AA, Taleahmad, S, Sharifzad, F, Taghikhani, A, and Baharvand, H. Interaction Between Mesenchymal Stromal Cell-Derived Extracellular Vesicles and Immune Cells by Distinct Protein Content. *J Cell Physiol* (2019) 234(6):8249–58. doi: 10.1002/jcp.27669
136. Morales-Molina, A, Gambera, S, Leo, A, and García-Castro, J. Combination Immunotherapy Using G-CSF and Oncolytic Virotherapy Reduces Tumor Growth in Osteosarcoma. *J Immunother Cancer* (2021) 9(3):e001703. doi: 10.1136/jitc-2020-001703
137. Aanstoos, ME, Regan, DP, Rose, RJ, Chubb, LS, and Ehrhart, NP. Do Mesenchymal Stromal Cells Influence Microscopic Residual or Metastatic Osteosarcoma in a Murine Model? *Clin Orthop Relat Res* (2016) 474(3):707–15. doi: 10.1007/s11999-015-4362-2
138. Zhang, Y, Ma, Q, Liu, T, Guan, G, Zhang, K, Chen, J, et al. Interleukin-6 Suppression Reduces Tumour Self-Seeding by Circulating Tumour Cells in a Human Osteosarcoma Nude Mouse Model. *Oncotarget* (2016) 7(1):446–58. doi: 10.18632/oncotarget.6371
139. Liu, T, Ma, Q, Zhang, Y, Wang, X, Xu, K, Yan, K, et al. Self-Seeding Circulating Tumor Cells Promote the Proliferation and Metastasis of Human Osteosarcoma by Upregulating Interleukin-8. *Cell Death Dis* (2019) 10(8):575. doi: 10.1038/s41419-019-1795-7
140. Chen, LH, Liu, JF, Lu, Y, He, XY, Zhang, C, and Zhou, HH. Complement C1q (C1qA, C1qB, and C1qC) May Be a Potential Prognostic Factor and an Index of Tumor Microenvironment Remodeling in Osteosarcoma. *Front Oncol* (2021) 11:642144. doi: 10.3389/fonc.2021.642144
141. Huang, H, Tan, M, Zheng, L, Yan, G, Li, K, Lu, D, et al. Prognostic Implications of the Complement Protein C1Q and Its Correlation With Immune Infiltrates in Osteosarcoma. *Onco Targets Ther* (2021) 14:1737–51. doi: 10.2147/OTT.S295063
142. Jeon, H, Han, SR, Lee, S, Park, SJ, Kim, JH, Yoo, SM, et al. Activation of the Complement System in an Osteosarcoma Cell Line Promotes Angiogenesis Through Enhanced Production of Growth Factors. *Sci Rep* (2018) 8(1):5415. doi: 10.1038/s41598-018-23851-z
143. De Martino, V, Rossi, M, Battafarano, G, Pepe, J, Minisola, S, and Del Fattore, A. Extracellular Vesicles in Osteosarcoma: Antagonists or Therapeutic Agents? *Int J Mol Sci* (2021) 22(22):12586. doi: 10.3390/ijms222212586
144. Clayton, A, Mitchell, JP, Court, J, Linnane, S, Mason, MD, and Tabi, Z. Human Tumor-Derived Exosomes Down-Modulate NKG2D Expression. *J Immunol* (2008) 180(11):7249–58. doi: 10.4049/jimmunol.180.11.7249
145. Clayton, A, Mitchell, JP, Court, J, Mason, MD, and Tabi, Z. Human Tumor-Derived Exosomes Selectively Impair Lymphocyte Responses to Interleukin-2. *Cancer Res* (2007) 67(15):7458–66. doi: 10.1158/0008-5472.CAN-06-3456
146. Xiang, X, Poliakov, A, Liu, C, Liu, Y, Deng, ZB, Wang, J, et al. Induction of Myeloid-Derived Suppressor Cells by Tumor Exosomes. *Int J Cancer* (2009) 124(11):2621–33. doi: 10.1002/ijc.24249
147. Troyer, RM, Ruby, CE, Goodall, CP, Yang, L, Maier, CS, Albarqi, HA, et al. Exosomes From Osteosarcoma and Normal Osteoblast Differ in Proteomic Cargo and Immunomodulatory Effects on T Cells. *Exp Cell Res* (2017) 358(2):369–76. doi: 10.1016/j.yexcr.2017.07.011
148. Wolf-Dennen, K, Gordon, N, and Kleinerman, ES. Exosomal Communication by Metastatic Osteosarcoma Cells Modulates Alveolar Macrophages to an M2 Tumor-Promoting Phenotype and Inhibits Tumoricidal Functions. *Oncoimmunology* (2020) 9(1):1747677. doi: 10.1080/2162402X.2020.1747677
149. Cheng, Z, Wang, L, Wu, C, Huang, L, Ruan, Y, and Xue, W. Tumor-Derived Exosomes Induced M2 Macrophage Polarization and Promoted the Metastasis of Osteosarcoma Cells Through Tim-3. *Arch Med Res* (2021) 52(2):200–10. doi: 10.1016/j.arcmed.2020.10.018
150. Wolf, Y, Anderson, AC, and Kuchroo, VK. TIM3 Comes of Age as an Inhibitory Receptor. *Nat Rev Immunol* (2020) 20(3):173–85. doi: 10.1038/s41577-019-0224-6
151. Wang, J, Zhang, H, Sun, X, Wang, X, Ren, T, Huang, Y, et al. Exosomal PD-L1 and N-Cadherin Predict Pulmonary Metastasis Progression for Osteosarcoma Patients. *J Nanobiotechnol* (2020) 18(1):151. doi: 10.1186/s12951-020-00710-6
152. Shimbo, K, Miyaki, S, Ishitobi, H, Kato, Y, Kubo, T, Shimose, S, et al. Exosome-Formed Synthetic microRNA-143 is Transferred to Osteosarcoma Cells and Inhibits Their Migration. *Biochem Biophys Res Commun* (2014) 445(2):381–7. doi: 10.1016/j.bbrc.2014.02.007

Conflict of Interest: The authors declare that the research was conducted in the absence of any commercial or financial relationships that could be construed as a potential conflict of interest.

The handling editor declared a past co-authorship with the authors LY and YH.

Publisher's Note: All claims expressed in this article are solely those of the authors and do not necessarily represent those of their affiliated organizations, or those of the publisher, the editors and the reviewers. Any product that may be evaluated in this article, or claim that may be made by its manufacturer, is not guaranteed or endorsed by the publisher.

frontiers | Frontiers in Immunology

REVIEW
published: 15 July 2022
doi: 10.3389/fimmu.2022.958360

Liquid Biopsy in Pre-Metastatic Niche: From Molecular Mechanism to Clinical Application

Zaoqu Liu[1,2,3†], Ying Kong[1†], Qin Dang[4†], Siyuan Weng[1], Youyang Zheng[5], Yuqing Ren[6], Jinxiang Lv[1], Na Li[1], Yilin Han[1] and Xinwei Han[1,2,3]*

[1] Department of Interventional Radiology, The First Affiliated Hospital of Zhengzhou University, Zhengzhou, China, [2] Interventional Institute of Zhengzhou University, Zhengzhou, China, [3] Interventional Treatment and Clinical Research Center of Henan Province, Zhengzhou, China, [4] Department of Colorectal Surgery, The First Affiliated Hospital of Zhengzhou University, Zhengzhou, China, [5] Department of Cardiology, The First Affiliated Hospital of Zhengzhou University, Zhengzhou, China, [6] Department of Respiratory and Critical Care Medicine, The First Affiliated Hospital of Zhengzhou University, Zhengzhou, China

OPEN ACCESS

Edited by:
Min Xue,
University of California, Riverside, United States

Reviewed by:
Jindong Xie,
Sun Yat-sen University Cancer Center (SYSUCC), China
Zheyu Kong,
Peking University People's Hospital, China

***Correspondence:**
Xinwei Han
fcchanxw@zzu.edu.cn

[†]These authors have contributed equally to this work and share the first authorship

Specialty section:
This article was submitted to Cancer Immunity and Immunotherapy, a section of the journal Frontiers in Immunology

Received: 31 May 2022
Accepted: 22 June 2022
Published: 15 July 2022

Citation:
Liu Z, Kong Y, Dang Q, Weng S, Zheng Y, Ren Y, Lv J, Li N, Han Y and Han X (2022) Liquid Biopsy in Pre-Metastatic Niche: From Molecular Mechanism to Clinical Application. Front. Immunol. 13:958360. doi: 10.3389/fimmu.2022.958360

Metastatic dissemination represents a hallmark of cancer that is responsible for the high mortality rate. Recently, emerging evidence demonstrates a time-series event—pre-metastatic niche (PMN) has a profound impact on cancer metastasis. Exosomes, cell-free DNA (cfDNA), circulating tumor cells (CTC), and tumor microenvironment components, as critical components in PMN establishment, could be monitored by liquid biopsy. Intensive studies based on the molecular profile of liquid biopsy have made it a viable alternative to tissue biopsy. Meanwhile, the complex molecular mechanism and intercellular interaction are great challenges for applying liquid biopsy in clinical practice. This article reviews the cellular and molecular components involved in the establishment of the PMN and the promotion of metastasis, as well as the mechanisms of their interactions. Better knowledge of the characteristics of the PMN may facilitate the application of liquid biopsy for clinical diagnosis, prognosis, and treatment.

Keywords: pre-metastatic niche, liquid biopsy, tumor microenvironment, molecular mechanism, clinical application

INTRODUCTION

Distant metastasis was the terminal stage of tumor progression and the crucial cause of tumor death (1, 2). The immaturity of early diagnostic techniques and drug resistance indirectly promoted distant metastasis, leading to a high mortality rate of cancer (3, 4). Cancer progression is a dynamic process. Metastasis is an organ-selective and multi-stepping complex process that requires in-depth

Abbreviations: BMDCs, bone marrow-derived cells; CAFs, carcinoma-associated fibroblasts; CCRS, CRC related survival; CEA, carcinoembryonic antigen; CECs, circulating endothelial cells; cfDNA, circulating cell-free DNA; CRC, colorectal cancer; CSF, cerebrospinal fluid; CTCs, circulating tumor cells; ctDNA, circulating tumor DNA; CTECs, circulating tumor-derived endothelial cells; EGF, epidermal growth factor; EMT, epithelial–mesenchymal transformation; EVs, extracellular vesicles; EVPs, extracellular vesicles and particles; LECs, lymphatic endothelial cells; LN, lymph node; MDSCs, myeloid-derived suppressor cells; MIF, migration inhibitory factor; MMP, matrix metalloproteinases; MRD, minimal residual disease; MSCs, mesenchymal stem cells; NSCLC, non-small cell lung cancer; PDACs, pancreatic ductal adenocarcinomas; PMNs, pre-metastatic niches; PSA, prostate-specific antigen; PSO, particle-swarm optimization; RFS, recurrence-free survival; TAM, tumor-associated macrophages; TDEs, tumor-derived exosomes; TDSFs, tumor-derived soluble factors; EPs, tumor-educated blood platelets; TF, transcription factor.

study, in order to find a better approach to diagnosis and treatment (5). The early perspective was that tumor cells migrated out of the primary site into the lymphatics or the bloodstream, survived in the circulation, and extravasated into the tissue, eventually forming metastasis (6). However, this theory was not enough to guide tumor-specific diagnosis and treatment. Stephen et al. first proposed the concept of "seed and soil" theory, which emphasized the importance of the microenvironment and revealed the organotropism of metastasis. The secondary site has established an abnormal, tumor growth-favoring microenvironment before tumor cells arrive (7). These predetermined soil microenvironments were termed "pre-metastatic niches", which actively attracted the colonization of tumor cells (8). With the characteristics of inflammation, immunosuppression, angiogenesis/vascular permeability, reprogramming, organotropism, and lymphangiogenesis, the indispensable role of the PMN in metastasis has attracted increasing attention in recent years (9–13) (**Figure 1**).

Nowadays, tissue biopsy, as the gold standard of cancer identification, remains the first-line clinical mean (14). However, conventional tissue biopsies are invasive and sometimes only small samples can be obtained (15), making it impossible to characterize tumor heterogeneity or dynamically monitor tumor progression (16, 17). Moreover, it is restricted by tissue excision site, adverse accuracy and sensitivity, and high procedural expenses (18–20). Therefore, a novel diagnostic method has emerged—liquid biopsy. It is a neoteric skill to

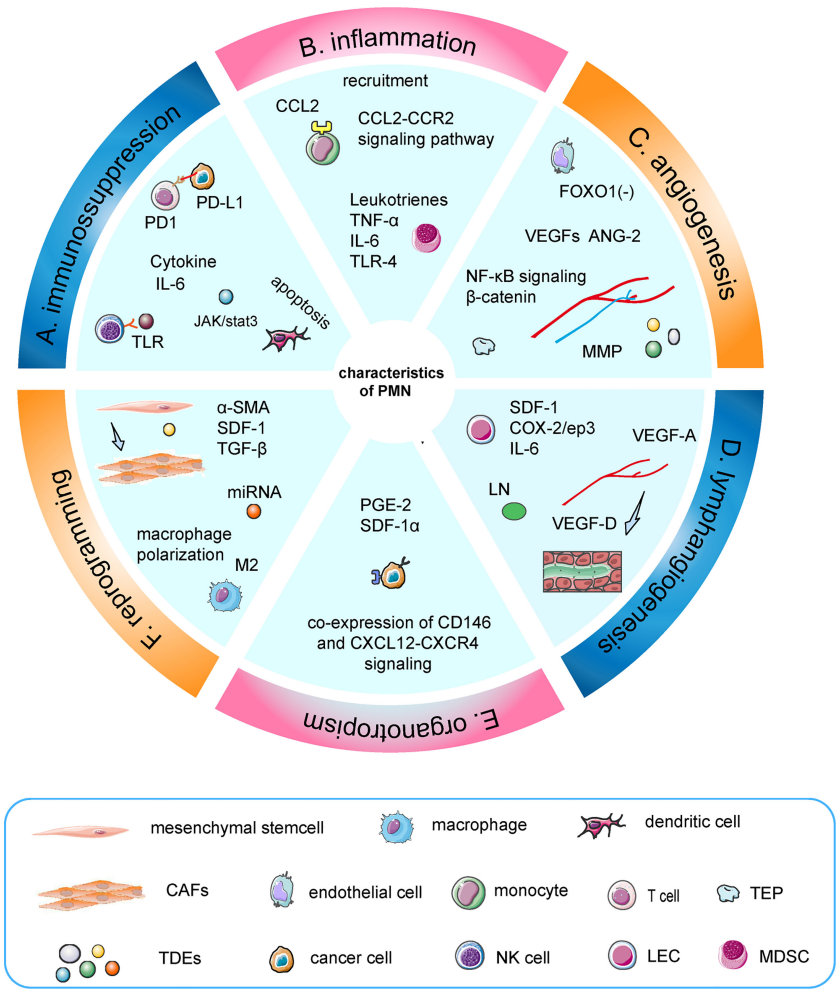

FIGURE 1 | Characteristics of the PMN. **(A)** TDEs induced apoptosis of dendritic cells, increased secretion of IL-6, and inhibited the function of T cells and NK cells. **(B)** TNF-α induced S100A8-SAA3-TLR4 signaling and maintained an inflammatory state, which was mediated by MDSC. Similarly, IL-6, leukotrienes, and CCL2–CCR2 signaling pathways were involved. **(C)** Upregulation of angiopoietin-2 and VEGFs could regulate the angiogenic switch, in which TEPs and MMPs had a synergistic effect. Moreover, miR-135b promotes angiogenesis by inhibiting FOXO1 expression in endothelial cells. **(D)** VEGF-A and VEGF-D are crucial factors in the induction of premetastatic lymphangiogenesis. Furthermore, dendritic cells induce a PMN during LN metastasis through COX-2/ep3-dependent induction of SDF-1. **(E)** Tumor cells interacted with resident mesenchymal stem cells/pericytes around the surrounding blood vessels to achieve organotropism through co-expressed CD146 and Sdf-1/CXCL12-CXCR4 signaling. **(F)** Exosomes induced the transformation of mesenchymal stem cells into CAFs and macrophage M2-like polarization.

identify tumor markers among the accessible samples, such as cfDNA or RNA, circulating tumor DNA (ctDNA), CTCs, exosomes, circulating tumor-derived endothelial cells (CTECs), tumor-educated blood platelets (TEPs), and protein molecules (21–25). Biomarkers for liquid biopsies can be derived from cerebrospinal fluid (CSF), saliva, blood, ascites, urine, stool, and pleural fluid (26–28). Better than tissue biopsy, liquid biopsy is non-invasive, easier to repeat, and could better overcome tumor heterogeneity due to the wide range of samples (16, 29). In accord with the patient's will not only from the macro perspective but also from the micro mechanism analysis, the progress of gene detection technology supports the development of the clinical application. Whole-exome sequencing or whole-genome sequencing data analysis explores the changes of genes and tumor burden in the course of patients (30), carries out comprehensive dynamic monitoring at the molecular level in a non-invasive manner, predicts tumor progression, and provides support for the formulation of subsequent precise treatment programs (31). Fortunately, cellular and molecular components such as exosomes, CTCs, and TEPs, which promote the formation of the PMN, are also widely present in plasma, urine, ascites, and other body fluids, making the application of liquid biopsy feasible (32, 33).

In this review, we focus on the critical molecular and cellular components that could be used in liquid biopsy at various stages of tumor metastasis niche formation and explain their clinical applications in prediction, prognosis, and treatment.

THE EVOLUTION OF PMN AND THE PROCESS OF PROMOTING METASTASIS

PMNs evolve in phased, sequential, and distinct ways, with each stage contributing to the metastasis process in its way (8, 9). Complex molecular and cellular changes have taken place in PMN to support the growth of metastatic tumors in the future (34, 35). Some molecules or cells could serve as markers of liquid biopsy. To simplify the complex development of time series events and more clearly explain the mechanism of liquid biopsy, the formation and metastasis promotion process of PMN can be divided into the following four temporal phases in sequence (9) (**Figure 2**).

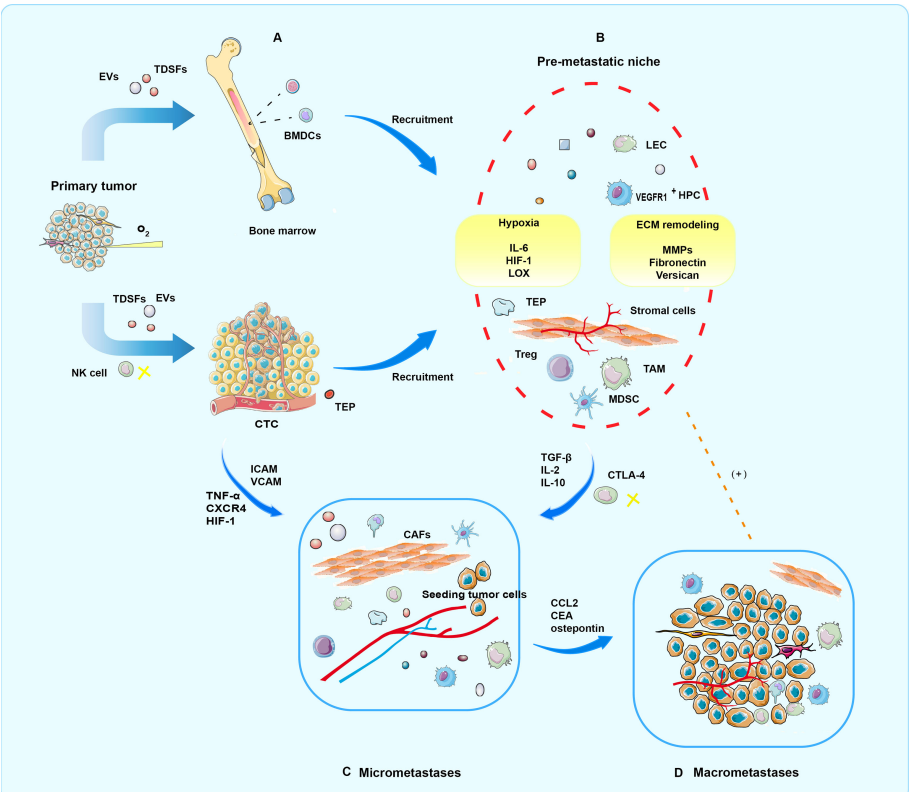

FIGURE 2 | Four periods of PMN formation. **(A)** In the priming phase, produced by primary tumor cells, TDSFs, EVs, and other molecular components trigger an immature PMN formation in the secondary organ site or the same organ outside the primary tumor. **(B)** In the licensing phase, BMDC, regulatory, and suppressive immune cells involved in ECM remodeling are mobilized and recruited into the secondary sites. Finally, a mature PMN prepared well for potential seeding and colonization of CTCs. In addition, hypoxia is a critical condition for progress. **(C)** In the initiation phase, partial CTCs arrive and survive at the fertile PMN, where tumor cell seeding, colonization, and outgrowth occur, eventually resulting in micrometastases. **(D)** In the progression phase, PMNs attract more tumor cells to colonize. Moreover, mutual promotion of tumor cells and PMN is locked in a vicious circle, which culminates in macrometastases.

Priming

During the priming period, when the primary tumor proliferates uncontrollably, hypoxia and inflammation are produced, which induces the secretion of extracellular vesicles (EVs), tumor-derived soluble factors (TDSFs), and other molecular components (36). Exosomes secreted by cancer cells under hypoxic conditions may remodel distant PMN. Exosomes were isolated from human prostate cancer cells under normoxic and hypoxic conditions, and their effects on key biomarkers associated with PMN in nude mice were observed. It was found that the exosomes produced under hypoxic conditions increased the levels of matrix metalloproteinases (MMP) and extracellular matrix proteins (fibronectin and collagen) as well as enhanced the number of CD11b+ cells at selective PMN sites (37). In addition, abnormal glycolysis and high lactate production may reduce tissue pH, which has been verified in the tumor mouse model. The average pH of the tumor stroma was prominently lower than the surrounding tissue.

Moreover, acidifying the tumor microenvironment is not conducive to roving immune cells, establishing an anergic state in human tumor-specific CD8+ T lymphocytes, and facilitating immune escape (38, 39). Acidic conditions also alter key phenotypes of malignancies and determine the type and quantity of exosomes released from tumor cells. Likewise, in prostate cancer, the microenvironment acidity exerts selective pressure to induce an upregulation of nanovesicle production, expressing both the exosome biomarker CD81 and prostate-specific antigen (PSA). The ratio of PSA-expressing exosomes in the plasma of cancer patients is significantly higher compared to benign prostatic hyperplasia and healthy individuals (40). Therefore, as a tool for early diagnosis and screening, PSA cancer exosomes are considered novel and non-invasive.

Pervasively, TDSFs would serve as tumor precursors for organ-specific preparation of PMNs prior to CTC colonization. TDSFs, mainly including cytokines, chemokines, and growth factors, can contribute to the recruitment and activation of inflammatory cells (41). Many types of cancer are characterized by aberrant IL-6/JAK/STAT3 activation, which strongly inhibits the antitumor immune response (42). Besides IL-6, TNF-α and TGF-β also affect the myeloid-derived suppressor cell (MDSC) recruitment in the premetastatic lung, which is modulated by the generation of inflammatory chemoattractants S100A9 and S100A8 (43). In breast cancer, with CCR2 (the chemokine receptor for CCL2) expressed, inflammatory monocytes are more promising to accumulate in the pulmonary metastases than in primary tumors. Metastatic seeding is also suppressed by inhibition of the CCL2–CCR2 pathway and exhaustion of tumor-derived CCL2. All these suggest that a CCL2 overexpression improves macrophage infiltration and worsens the prognosis of human breast cancer (44). Moreover, CXCR2-positive MDSCs are attracted to metastatic sites by CXCL1 derived from tumor-associated macrophages (TAM) due to the stimulation of VEGFA released from primary tumor cells (45). From these results, it can be seen that hypoxia and acidic conditions are two key factors that lay the foundation for remodeling the matrix microenvironment, while also regulating tumor progression, recruitment, and activation of inflammatory cells, as well as facilitating the production of bioactive molecules.

Licensing

In the licensing phase, under the action of TDSFs and EVs, a continuous flow of regulatory/suppressive immune cells and bone marrow-derived cells (BMDCs) is activated and mobilized into the transfer sites, which start to re-educate the stromal environment of the distant secondary sites to form a soil environment suitable for CTC colonization. Exosomes play a profound role in this stage (46). Extracellular vesicles, messengers between primary tumor sites and metastatic sites, are indispensable in forming PMN. Studies have shown that extracellular vesicles are small membrane vesicles from cells during activation and apoptosis. They can be divided into at least three types: apoptotic bodies, microvesicles, and exosomes with a size ranging from 40 to 100 nm (47, 48).

Interestingly, the biological functions of exosomes are different according to their sources (49). Tumor-derived exosomes (TDEs) carry a variety of bioactive components (nucleic acid, protein, and lipid), which are effective tools for intercellular communication. Exosomal microRNAs are the major messengers to execute these functions among these bioactive components. For instance, microRNA can establish an immunosuppressive environment by changing the phenotype and function of various immune cells. It is reported that MDSCs mediate the immunosuppressive environment, and hypoxia promotes the secretion of TDEs. MDSCs ingest TDEs, and tumor exogenous miR-9 and miR-181a targeted SOCS3 and PIAS3 to activate the JAK/STAT signal pathway, thus affecting the differentiation and activation of MDSCs and enhancing its immunosuppressive effect (50, 51). TDEs could not only directly inhibit NK cells' toxicity and T cells' proliferation but also achieve immunosuppression by enhancing the immune tolerance mediated by regulatory T cells. In terms of matrix remodeling, TDEs trigger the differentiation of mesenchymal stem cells (MSCs) to carcinoma-associated fibroblasts (CAFs) *via* the TGF-β/Smad pathway (52, 53). CAFs can modify the surrounding ECM to generate an ecological niche supporting cancer cell invasion, as well as facilitate cancer cell migration and invasion so as to promote tumor occurrence, metastasis, and diffusion to malignancy (35).

Furthermore, hypoxia stimulates hypersecretion of TDEs, enhances the recruitment of TDE to macrophages, and promotes M2-like polarization. In gastric cancer, miR-135b accelerates angiogenesis due to the inhibition of FOXO1 expression from endothelial cells (54). Notably, the critical role of exosomal proteins in promoting the production of PMN and as markers of liquid biopsy should not be ignored. For example, exosomes containing metalloproteinases promote angiogenesis, exosomal PD-L1 enhances immunosuppression, and exosome-induced T-cell inhibition depends on ICAM-1-mediated adhesion (55–57). From the above description, it could be demonstrated that exosomes are reasonable and practical as liquid biopsy biomarkers.

During this period, lymphangiogenesis is critical in the PMN, in addition to immunosuppression, angiogenesis, and matrix

remodeling. Lymph node (LN) metastasis is a pivotal prognostic indicator of disease stage; thereby, the lymphatic system is considered to be a vital route of metastatic spread except for hematogenous metastasis (58). Partial tumors secrete lymphatic growth factors, which induce lymphangiogenesis and act on lymphatic vessels to boost metastasis. Namely, in the interior of the primary tumor or metastatic sites, such as sentinel LN (59), the original blood vessels form new lymphatic vessels and participate in regulating the immune response to the tumor under the action of TDSFs (60, 61). Clinical evidence indicates that tumor-derived VEGF-D and VEGF-A are key factors in the induction of premetastatic lymphangiogenesis in sentinel LN.

Moreover, since VEGF-D is associated with higher LN metastasis, it may be a potential predictor of positive LN metastasis in patients (62). Furthermore, when LN metastasis occurs, dendritic cells induce a PMN through COX-2/ep3-dependent SDF-1, suggesting that restraining this signaling axis may be an available measure to inhibit PMN formation and LN metastasis (63). Crucially, immunosuppression is facilitated by the presence of lymphatic vessels in the PMN, through which exosomes can reach mouse and human melanoma. In LN, exosomes preferentially bind CD169+ macrophages, destroy them to escape immune recognition, invade the LN cortex, and disrupt humoral immunity *via* interacting with B cells (64). Lymphatic endothelial cells (LECs), a composition of lymphatic vessels in the PMN, are regulated by TDSFs. Mechanistically, IL-6 induces the expression of HIF-1α, CCL5, and VEGF *via* the phosphorylation pathway to facilitate the recruitment, extravasation, and colonization of CCR5+ tumor cells in the niche, which lays the foundation for the smooth progress of the next stage.

Additionally, there is a self-reinforcing paracrine loop between cancer cells and LECs (65). Stromal lymphatic vessels are the primary route of metastasis in some cancers (66); moreover, the presence of LN metastasis worsens the prognosis (67). Consequently, an in-depth study on the molecular and cellular matrix and identifying critical factors in lymphangiogenesis may contribute to discovering new targets, which could be used in liquid biopsy to decrease tumor dissemination and improve prognosis.

Initiation

In the initiation phase, through epithelial–mesenchymal transformation (EMT) (68, 69), tumor cells become CTCs and infiltrate from the blood vessels of the primary site. Some of them arrive and survive at the fertile PMN, where sowing, colonization, and proliferation of tumor cells occur, eventually leading to micrometastases. Nevertheless, before the arrival of CTCs, BMDCs migrated to distant sites induced by factors of the primary tumor, such as TNF-α, TGF-β, and TDEs. BMDCs contribute to tumor vascularization and neoplastic cell migration, which are latent promoters of CTC extravasation with organotropism (70).

Tumor cells migrating from the primary site to the PMN need to go through several critical stages: intravasation, intravascular survival, extravasation, and colonization of secondary sites. CTCs acquire enhanced migratory and invasive abilities through EMT (71), which is a transient, reversible process of cell differentiation. TAMs usually play a protumoral role, providing conditions for PMN and promoting extravasation, survival, and the continuous growth of tumor cells (72). EMT, a vital sign of solid tumors, has recently been shown to be an essential driver of macrophage polarization (71). EMT-colorectal cancer (CRC) programmed cells not only stimulate the production of various cytokines, such as IL-4 and CCL2, but also deliver exosomes directly to macrophage activation signaling cascade targets that directly inhibit programmed cell death at the post-transcriptional level, thereby enhancing M2-like polarization (73–75).

TEPs are promoters and protectors of blood metastasis. Entanglements of platelets and fibrin surrounding tumor cells protect CTCs from NK lysis (76). This makes it possible for CTCs to survive within the vasculature (immune evasion) and spread from the bloodstream. Moreover, activated platelets may facilitate vessel growth and maintain vascular integrity during tumor development (77). In addition, TEPs enhance the adhesion between CTCs and vascular endothelial cells through a selectin-dependent pathway to prepare for CTC extravasation (78). The function of TEP, a biomarker trove for liquid biopsy, has been proved, especially RNA (79). Particle-swarm optimization (PSO)-enhanced algorithms diagnose cancer, exploiting selected gene panels from TEP, which has also been demonstrated for accuracy in early and advanced non-small cell lung cancer (NSCLC) diagnosis. Consequently, TEPs possess the potential value as a liquid biopsy for various clinical and investigational applications (22, 80).

Although the role of CTCs as tumor biomarkers of liquid biopsy for research and clinical diagnosis has been widely concerned (81–83), isolating CTCs is a technical challenge owing to the rarity and heterogeneity of CTCs. Nevertheless, microfluidic-based isolation technologies are expected to break this limitation and promote the transformation of cancer clinical diagnosis and treatment mode (84). Technological advances make it feasible to convert from CTC counting to the thorough analysis of the CTC gene panels, transcriptome, protein, epigenome, and various functional characteristics, which can be used to monitor prognosis, anticipate micrometastasis, and act as an auxiliary means of tumor staging (85).

Progression

In the progression phase, micrometastases attract more tumor cells to colonize, directly or indirectly promoting further microenvironment maturation by producing cytokines. This enables metastatic cancer cells to grow, invade, and progress at the site, creating a vicious cycle that culminates in macrometastases. For example, in bone metastases, there are two types of tumors: osteoblastic (bone-forming) and osteolytic (bone-lysing), of which prostate bone metastases are often the former and breast cancer bone metastases are the latter (86, 87). Several studies have shown that in osteolytic bone metastases, bone-derived chemokines and growth factors as chemoattractants, such as monocyte chemoattractant protein 1 and stromal cell-derived factor 1, could attract tumor cells to bone. Likewise, the interaction between bone marrow stromal cells and tumor cells could lead to increased production of growth factors and cytokines, further

promoting PMN formation and attracting tumor cell colonization. For instance, the ligand for receptor activator of nuclear factor kappaB or IL-6 could accelerate angiogenesis, bone destruction, and tumor growth (88). This vicious cycle between bone microenvironment and tumor cells leads to osteoclastic lesions evolving, which macroscopically manifests as malignant metastasis of the tumor, a fatal event with a poor prognosis. Therefore, there is a demand for detecting tumor cells or components of the PMN prior to macrometastases, which could be discovered by imaging, to block cancer metastasis before it is incurable.

CLINICAL APPLICATION OF LIQUID BIOPSY IN PMN

The heterogeneity of cancer cells within tumors is an essential obstacle to curative effect. Current cancer treatments, such as surgery, radiotherapy, and chemotherapy drugs, often kill healthy cells and poison patients, which cannot overcome tumor heterogeneity well (89). Therefore, it is essential to understand the molecular basis of tumors, such as the formation of PMN and the emergence of new diagnostic techniques. The current trend is to use liquid biopsy technology to obtain cancer cells or cancer-related molecules, which can explore epigenetic changes and oncogene expression based on the molecular level and flexibly apply the relevant results to clinical diagnosis and treatment. The table lists some critical molecular and cellular components in the process of PMN formation that can be detected by liquid biopsy, as well as their clinical applications (**Table 1**).

Diagnostic Value

Early detection by liquid biopsy for cancer is promising (109). In the early stages of the disease, CTCs are already circulating in the blood prior to clinical evidence of metastasis. 5-Hydroxymethylcytosine signatures in cfDNA are highly predictive for colorectal and gastric cancer as an ideal diagnostic biomarker for human cancers, which are superior to conventional biomarkers, and comparable to the 5-hydroxymethylcytosine biomarker in tissue biopsy (110). Additionally, as a liquid biopsy marker, the urine epigenetic biomarkers have manifested satisfactory sensitivity and specificity in detecting upper tract urinary carcinoma (111). The effect of extracellular vesicles and particles (EVPs) in tumor detection and determination of cancer type has been demonstrated. Analyzing the protein contents of EVPs distinguished tumors from nearby noncancerous tissue and profiling extracellular vesicle proteins obtained from plasma may also reveal cancer type.

Moreover, both tissue-derived and plasma-derived EVPs were detected with high specificity (112). As an emerging biomarker for early and minimal malignancy diagnosis, exosomal microRNA has captured people's attention because of its stability in multiple body fluids (113). Serum miR-378 levels were analyzed in 60 normal controls and 103 NSCLC patients. In NSCLC patients, exosomal miR-378 was significantly overexpressed, and its upregulation was associated with advanced TNM stage and positive LN metastasis. Additionally, the combination of serum exosomal miR-378 expression and carcinoembryonic antigen (CEA) had a high discriminating power to differentiate NSCLC subjects from controls (114). Similarly, the role of exosome-encapsulated microRNAs as a circulating diagnostic marker for low alpha-fetoprotein hepatocellular carcinoma has been demonstrated (115).

Prognostic Value

The prognostic role of CTC counts as a tool for liquid biopsy can be seen in a variety of cancers (116–118). Previous studies have reported a lack of identification of novel biomarkers associated with breast cancer (119). Research on estrogen receptor-positive breast cancer suggested that independent prognostic information

TABLE 1 | Clinical application of liquid biopsy.

	Clinical application	Reference
Exosomes and their contents		
MIF	Liver PMN formation and metastasis	(90)
Level of PD-L1	Patients with NSCLC are higher than normal people	(91)
miRNA-10b	Early diagnosis of PDAC	(92)
miR-200b, miR-200c, and miR-373	Poor outcomes in ovarian cancer	(93)
Circular RNAs	A novel potential diagnostic biomarker of CRC	(94)
Exosomes derived from M1-polarized macrophages	Immunopotentiators for a cancer vaccine	(95)
Circulating cells and inflammatory related markers		
The proportion of regulatory T cells	Identification of CRC patients versus healthy controls	(96)
EGF, macrophage-derived chemokine, IL-10, IL-6, and IL-8 levels	Predictive value in irinotecan/bevacizumab-based treatments	(97)
Quantification of Tregs and CD8+ T cells	Prognostic value	(98)
The number of EPCAM (+) CD44(+) CD47(+) MET (+) CTCs	Correlated with lower overall survival and increased number of metastatic sites	(99)
cfDNA TF profiling	Detection of early-stage colorectal carcinomas	(100)
Tumor microenvironment-derived markers		
TIMP-1 + metalloproteinases	Prediction of patients' survival	(101)
MSCs	Therapeutic production of exosomes	(102)
Transcriptomic analysis of CECs	Differentiation between healthy controls and CRC early stages	(103)
Identification and quantification of CECs	Monitoring clinical response and outcome	(104, 105)
Matrix metalloproteinase	With diagnostic value	(106)
VEGF-A and ICAM-1 variant	Prognosis value in bevacizumab treated patients	(107)
VEGF, HGF, EGF, and PDGF-AA levels	Predictive value in chemotherapy-based treated patients	(108)

CECs, circulating endothelial cells; EGF, epidermal growth factor; MIF, migration inhibitory factor; TF, transcription factor.

required for late clinical recurrence could be obtained from a single positive CTC assay (120). The presence of CTC is related to adverse prognosis in patients with metastatic CRC. While the presence of CTC weeks after surgery is not noticeably associated with CRC-related survival (CCRS) and recurrence-free survival (RFS) for patients with non-metastatic CRC, the association increases remarkably with time. Similarly, the presence of CTC in patients with optimistic preoperative staging was connected with a significant reduction in RFS and CCRS (121). In a prospective trial, CSF-derived cfDNA copy number variations were used as a surrogate for minimal residual disease (MRD) to detect disease progression (122). These phenomena may demonstrate that highly sensitive liquid biopsy assays can be applied to detect and characterize MRD (123). Blood tests based on CTC phenotype simulations can also assess overall survival and tumor metastasis in pancreatic ductal adenocarcinomas (PDAC) patients. CTC transcriptional profiling can be used not only as an independent prognostic marker but also to determine the emergence of multiple androgen receptor signaling inhibitors resistance mechanisms, which can guide the choice of treatment options (83). Besides the prognostic assessment, liquid biopsy technology can achieve individualized management of clinical patients. For instance, in stage II colon cancer, ctDNA-guided therapy reduces adjuvant chemotherapy use without compromising recurrence-free survival (124).

Therapeutic Application

The clinical utility of CTC as a marker of liquid biopsy for prognosis and monitoring of systemic treatment response was reported a decade ago (125). In recent years, the study of ctDNA, circulating cfRNA, EVs, and TEPs has also attracted much attention (126–128). The serum level of miR-378 in 73 patients with NSCLC decreased significantly after radiotherapy, which can be used as an indicator of the efficacy of radiotherapy for NSCLC (114). The effect of immunotherapy on cancer patients can be evaluated by liquid biopsy. In one study, patients who tested positive for ctDNA showed improvement in disease-free survival and overall survival when receiving adjuvant atezolizumab instead of observation (129).

Additionally, it was attractive that exosomal miRNAs conveyed the drug resistance message. Exosomes miR-3913-5p and miR-184, as biomarkers of osimertinib resistance, are suitable for NSCLC patients to detect their expression. This may be related to the abnormal activation of alternative pathways (PI3K pathway activation and RAS-MAPK pathway abnormality), indicating that miRNAs derived from peripheral blood exosomes are involved in the resistance mechanism of osimertinib through the pathway. In addition, miR-433 can inhibit cisplatin chemoresistance by regulating DNA damage and inactivating the WNT/β-catenin signaling pathway by targeting p24 transporter 5 in NSCLC. These studies suggest that miRNA can provide latent therapeutic targets for patients with NSCLC (130). The homing effect of exosomes on primary tumor cells is promising for targeted therapy. For example, PMN mimics, engineered biomaterials embedded with ovarian cancer exosomes into the peritoneal cavity of mouse models, can effectively recruit and capture free ovarian tumor cells in ascites, thereby arresting colonization in normal pelvic organs, reducing metastasis, and improving patient survival (131, 132). Furthermore, exosomes can also be used as a delivery system to load drugs and improve drug spillover in tumors (133). Generally, therapeutic applications, such as therapeutic response monitoring, targeted therapy, and drug resistance detection, have enriched remedies for cancer and are expected to enhance efficacy.

OPPORTUNITIES AND CHALLENGES OF LIQUID BIOPSY TECHNOLOGY IN CLINICAL PRACTICE

Compared with tissue biopsy and imaging diagnosis, liquid biopsy possesses the advantage of being non-invasive, repeatable, and economical, and having an early diagnosis, which could surmount the temporal and spatial heterogeneity of tumors (134). With the improvement of liquid biopsy technology, its sensitivity and operability have also been significantly strengthened. For example, CAPP-seq personalized cancer analysis technology is an economical and susceptible method to quantify ctDNA. In NSCLC, ctDNA levels are closely associated with tumor volume, distinguishing between treatment-related imaging transformations and residual disease, allowing for earlier response assessment and personalized cancer treatment (135). There are also many other detection techniques such as polymerase chain reaction-based, microfluidic methods, chip-based, next-generation sequencing-based, and fluorescence *in situ* hybridization-based (136). However, the specificity of liquid biopsy results poses some challenges. Firstly, gene mutations associated with cancer occur with age, even in people who have never experienced cancer. Therefore, while technological advances have made ctDNA testing more specific, false-positive results from its use in cancer screening can cause significant anxiety (137, 138). Secondly, widespread clinical application of liquid biopsy technology remains unrealistic because the standardization and replication of test results are challenged (139). However, advances in the characterization and detection of ctDNA and the application of single-gene and multi-gene detection methods have made the clinical application of targeted therapy possible. In addition, the application of liquid biopsy in the systemic treatment of sufferers with "ctDNA relapse" has also been noted. This is a new concept to detect cancer recurrence by detecting ctDNA after treatment, which is earlier than imaging examination (140). The advanced technology currently used for liquid biopsy is the detection of exosomes derived from cancer with biosensors, with highly specific target selection (125). Single-cell sequencing has increased the understanding of the molecular pathways involved in triggering cancer progression (141). Molecular imaging, especially when combined with liquid biopsy for screening, promises early disease localization because biochemical changes precede anatomical changes (142). The methylation patterns informed by cfDNA sequencing can be used for epigenetic variation assessment, with potential value for early detection of fatal malignancies (143). In conclusion, the emergence and development of these new technologies have contributed to the evolution of precision medicine.

CONCLUSION AND PERSPECTIVES

As a non-invasive, reproducible method, liquid biopsy has achieved remarkable success in the early detection and tracking of biomarkers. Furthermore, biological interactions between the tumor microenvironment and PMN are increasingly vital as potential mechanisms of tumor progression. In this process, the role of soluble factors, exosomes, and circulating cells from the tumor microenvironment has been emphasized as neoplastic markers for cancer diagnosis, prediction and prognosis, therapeutic response monitoring, and therapy guidance. However, the liquid biopsy technique demands a breakthrough in clinical practice. For example, the high heterogeneity and nanoscale size of exosomes pose great technical difficulties for the isolation and detection of their molecular information. There are various methods of detecting CTCs and ctDNA, and the diagnostic procedures are not standardized, which requires high enrichment technology of CTC in blood. These problems need to be overcome to achieve widespread clinical application. Early diagnosis and blocking of cancer progression before the formation of micrometastases or even PMN is a promising research direction, which requires liquid biopsy technology to break through the limitations and be flexible for clinical practice. In summary, as the three branches of liquid biopsy, CTC, ctDNA, and exosomes are crucial components for the preparation and biological function of PMN. Therefore, liquid biopsy diagnosis clarifies the biological characteristics of PMN, possibly changing the process at the initial stage of metastasis, and has tremendous potential in precision medicine.

AUTHOR CONTRIBUTIONS

ZL, XH, and QD provided direction and guidance throughout the preparation of this manuscript. YK, QD, and ZL wrote and edited the manuscript. QD, JL, NL, and YH reviewed and made significant revisions to the manuscript. SW, YZ, YR, and ZL collected and prepared the related papers. All authors read and approved the final manuscript.

REFERENCES

1. Lambert AW, Pattabiraman DR, Weinberg RA. Emerging Biological Principles of Metastasis. *Cell* (2017) 168:670–91. doi: 10.1016/j.cell.2016.11.037
2. Yu XQ, Dasgupta P, Baade P. Quantifying the Absolute Number of Cancer Deaths That Would be Avoided If Cancers Were Diagnosed Prior to Progressing to Distant Metastasis, New South Wales, Australia 1985-2014. *Int J Cancer* (2022) 150:1760–9. doi: 10.1002/ijc.33931
3. Cortés-Hernández LE, Eslami SZ, Alix-Panabières C. Circulating Tumor Cell as the Functional Aspect of Liquid Biopsy to Understand the Metastatic Cascade in Solid Cancer. *Mol Aspects Med* (2020) 72:100816. doi: 10.1016/j.mam.2019.07.008
4. Shin SH, Bode AM, Dong Z. Addressing the Challenges of Applying Precision Oncology. *NPJ Precis Oncol* (2017) 1:28. doi: 10.1038/s41698-017-0032-z
5. Mortezaee K. CXCL12/CXCR4 Axis in the Microenvironment of Solid Tumors: A Critical Mediator of Metastasis. *Life Sci* (2020) 249:117534. doi: 10.1016/j.lfs.2020.117534
6. Steeg PS. Tumor Metastasis: Mechanistic Insights and Clinical Challenges. *Nat Med* (2006) 12:895–904. doi: 10.1038/nm1469
7. Peinado H, Zhang H, Matei IR, Costa-Silva B, Hoshino A, Rodrigues G, et al. Pre-Metastatic Niches: Organ-Specific Homes for Metastases. *Nat Rev Cancer* (2017) 17:302–17. doi: 10.1038/nrc.2017.6
8. Psaila B, Lyden D. The Metastatic Niche: Adapting the Foreign Soil. *Nat Rev Cancer* (2009) 9:285–93. doi: 10.1038/nrc2621
9. Liu Y, Cao X. Characteristics and Significance of the Pre-Metastatic Niche. *Cancer Cell* (2016) 30:668–81. doi: 10.1016/j.ccell.2016.09.011
10. Fleming V, Hu X, Weber R, Nagibin V, Groth C, Altevogt P, et al. Targeting Myeloid-Derived Suppressor Cells to Bypass Tumor-Induced Immuno suppression. *Front Immunol* (2018) 9:398. doi: 10.3389/fimmu.2018.00398
11. Olmeda D, Cerezo-Wallis D, Riveiro-Falkenbach E, Pennacchi PC, Contreras-Alcalde M, Ibarz N, et al. Whole-Body Imaging of Lymphovascular Niches Identifies Pre-Metastatic Roles of Midkine. *Nat* (2017) 546:676–80. doi: 10.1038/nature22977
12. Zeng Y, Yao X, Liu X, He X, Li L, Liu X, et al. Anti-Angiogenesis Triggers Exosomes Release From Endothelial Cells to Promote Tumor Vasculogenesis. *J Extracell Vesicles* (2019) 8:1629865. doi: 10.1080/20013078.2019.1629865
13. Seibold T, Waldenmaier M, Seufferlein T, Eiseler T. Small Extracellular Vesicles and Metastasis-Blame the Messenger. *Cancers (Basel)* (2021) 13:4380. doi: 10.3390/cancers13174380
14. Bibby AC, Dorn P, Psallidas I, Porcel JM, Janssen J, Froudarakis M, et al. ERS/EACTS Statement on the Management of Malignant Pleural Effusions. *Eur Respir J* (2018) 52:1800349. doi: 10.1183/13993003.00349-2018
15. Ferrara F, Zoupanou S, Primiceri E, Ali Z, Chiriacò MS. Beyond Liquid Biopsy: Toward non-Invasive Assays for Distanced Cancer Diagnostics in Pandemics. *Biosens Bioelectron* (2022) 196:113698. doi: 10.1016/j.bios.2021.113698
16. Parikh AR, Leshchiner I, Elagina L, Goyal L, Levovitz C, Siravegna G, et al. Liquid Versus Tissue Biopsy for Detecting Acquired Resistance and Tumor Heterogeneity in Gastrointestinal Cancers. *Nat Med* (2019) 25:1415–21. doi: 10.1038/s41591-019-0561-9
17. Yi X, Ma J, Guan Y, Chen R, Yang L, Xia X. The Feasibility of Using Mutation Detection in ctDNA to Assess Tumor Dynamics. *Int J Cancer* (2017) 140:2642–7. doi: 10.1002/ijc.30620
18. Zhou H, Zhu L, Song J, Wang G, Li P, Li W, et al. Liquid Biopsy at the Frontier of Detection, Prognosis and Progression Monitoring in Colorectal Cancer. *Mol Cancer* (2022) 21:86. doi: 10.1186/s12943-022-01556-2
19. Siravegna G, Mussolin B, Venesio T, Marsoni S, Seoane J, Dive C, et al. How Liquid Biopsies can Change Clinical Practice in Oncology. *Ann Oncol* (2019) 30:1580–90. doi: 10.1093/annonc/mdz227
20. Das J, Kelley SO. High-Performance Nucleic Acid Sensors for Liquid Biopsy Applications. *Angew Chem Int Ed Engl* (2020) 59:2554–64. doi: 10.1002/anie.201905005
21. Pantel K, Alix-Panabières C. Circulating Tumour Cells in Cancer Patients: Challenges and Perspectives. *Trends Mol Med* (2010) 16:398–406. doi: 10.1016/j.molmed.2010.07.001
22. Best MG, Sol N, In 't Veld S, Vancura A, Muller M, Niemeijer AN, et al. Swarm Intelligence-Enhanced Detection of Non-Small-Cell Lung Cancer Using Tumor-Educated Platelets. *Cancer Cell* (2017) 32:238–52.e239. doi: 10.1016/j.ccell.2017.07.004
23. Yu W, Hurley J, Roberts D, Chakrabortty SK, Enderle D, Noerholm M, et al. Exosome-Based Liquid Biopsies in Cancer: Opportunities and Challenges. *Ann Oncol* (2021) 32:466–77. doi: 10.1016/j.annonc.2021.01.074
24. Cheng ML, Pectasides E, Hanna GJ, Parsons HA, Choudhury AD, Oxnard GR. Circulating Tumor DNA in Advanced Solid Tumors: Clinical Relevance and Future Directions. *CA Cancer J Clin* (2021) 71:176–90. doi: 10.3322/caac.21650
25. Mehran R, Nilsson M, Khajavi M, Du Z, Cascone T, Wu HK, et al. Tumor Endothelial Markers Define Novel Subsets of Cancer-Specific Circulating Endothelial Cells Associated With Antitumor Efficacy. *Cancer Res* (2014) 74:2731–41. doi: 10.1158/0008-5472.Can-13-2044

26. Siravegna G, Marsoni S, Siena S, Bardelli A. Integrating Liquid Biopsies Into the Management of Cancer. *Nat Rev Clin Oncol* (2017) 14:531–48. doi: 10.1038/nrclinonc.2017.14
27. Miller AM, Shah RH, Pentsova EI, Pourmaleki M, Briggs S, Distefano N, et al. Tracking Tumour Evolution in Glioma Through Liquid Biopsies of Cerebrospinal Fluid. *Nat* (2019) 565:654–8. doi: 10.1038/s41586-019-0882-3
28. Kipps E, Tan DS, Kaye SB. Meeting the Challenge of Ascites in Ovarian Cancer: New Avenues for Therapy and Research. *Nat Rev Cancer* (2013) 13:273–82. doi: 10.1038/nrc3432
29. Liebs S, Eder T, Klauschen F, Schütte M, Yaspo ML, Keilholz U, et al. Applicability of Liquid Biopsies to Represent the Mutational Profile of Tumor Tissue From Different Cancer Entities. *Oncogene* (2021) 40:5204–12. doi: 10.1038/s41388-021-01928-w
30. Cheng DT, Mitchell TN, Zehir A, Shah RH, Benayed R, Syed A, et al. Memorial Sloan Kettering-Integrated Mutation Profiling of Actionable Cancer Targets (MSK-IMPACT): A Hybridization Capture-Based Next-Generation Sequencing Clinical Assay for Solid Tumor Molecular Oncology. *J Mol Diagn* (2015) 17:251–64. doi: 10.1016/j.jmoldx.2014.12.006
31. Heitzer E, Haque IS, Roberts CES, Speicher MR. Current and Future Perspectives of Liquid Biopsies in Genomics-Driven Oncology. *Nat Rev Genet* (2019) 20:71–88. doi: 10.1038/s41576-018-0071-5
32. Vasconcelos MH, Caires HR, Ābols A, Xavier CPR, Linē A. Extracellular Vesicles as a Novel Source of Biomarkers in Liquid Biopsies for Monitoring Cancer Progression and Drug Resistance. *Drug Resist Updat* (2019) 47:100647. doi: 10.1016/j.drup.2019.100647
33. Liu W, Vivian CJ, Brinker AE, Hampton KR, Lianidou E, Welch DR. Microenvironmental Influences on Metastasis Suppressor Expression and Function During a Metastatic Cell's Journey. *Cancer Microenviron* (2014) 7:117–31. doi: 10.1007/s12307-014-0148-4
34. Ordóñez-Morán P, Huelsken J. Complex Metastatic Niches: Already a Target for Therapy? *Curr Opin Cell Biol* (2014) 31:29–38. doi: 10.1016/j.ceb.2014.06.012
35. Quail DF, Joyce JA. Microenvironmental Regulation of Tumor Progression and Metastasis. *Nat Med* (2013) 19:1423–37. doi: 10.1038/nm.3394
36. Semenza GL. Hypoxia-Inducible Factors in Physiology and Medicine. *Cell* (2012) 148:399–408. doi: 10.1016/j.cell.2012.01.021
37. Deep G, Jain A, Kumar A, Agarwal C, Kim S, Leevy WM, et al. Exosomes Secreted by Prostate Cancer Cells Under Hypoxia Promote Matrix Metalloproteinases Activity at Pre-Metastatic Niches. *Mol Carcinog* (2020) 59:323–32. doi: 10.1002/mc.23157
38. Gallagher FA, Kettunen MI, Day SE, Hu DE, Ardenkjaer-Larsen JH, Zandt R, et al. Magnetic Resonance Imaging of pH *In Vivo* Using Hyperpolarized 13C-Labelled Bicarbonate. *Nat* (2008) 453:940–3. doi: 10.1038/nature07017
39. Calcinotto A, Filipazzi P, Grioni M, Iero M, De Milito A, Ricupito A, et al. Modulation of Microenvironment Acidity Reverses Anergy in Human and Murine Tumor-Infiltrating T Lymphocytes. *Cancer Res* (2012) 72:2746–56. doi: 10.1158/0008-5472.Can-11-1272
40. Logozzi M, Angelini DF, Iessi E, Mizzoni D, Di Raimo R, Federici C, et al. Increased PSA Expression on Prostate Cancer Exosomes in In Vitro Condition and in Cancer Patients. *Cancer Lett* (2017) 403:318–29. doi: 10.1016/j.canlet.2017.06.036
41. Crane CA, Ahn BJ, Han SJ, Parsa AT. Soluble Factors Secreted by Glioblastoma Cell Lines Facilitate Recruitment, Survival, and Expansion of Regulatory T Cells: Implications for Immunotherapy. *Neuro Oncol* (2012) 14:584–95. doi: 10.1093/neuonc/nos014
42. Yu H, Kortylewski M, Pardoll D. Crosstalk Between Cancer and Immune Cells: Role of STAT3 in the Tumour Microenvironment. *Nat Rev Immunol* (2007) 7:41–51. doi: 10.1038/nri1995
43. Hiratsuka S, Watanabe A, Aburatani H, Maru Y. Tumour-Mediated Upregulation of Chemoattractants and Recruitment of Myeloid Cells Predetermines Lung Metastasis. *Nat Cell Biol* (2006) 8:1369–75. doi: 10.1038/ncb1507
44. Qian BZ, Li J, Zhang H, Kitamura T, Zhang J, Campion LR, et al. CCL2 Recruits Inflammatory Monocytes to Facilitate Breast-Tumour Metastasis. *Nat* (2011) 475:222–5. doi: 10.1038/nature10138
45. Wang D, Sun H, Wei J, Cen B, DuBois RN. CXCL1 Is Critical for Premetastatic Niche Formation and Metastasis in Colorectal Cancer. *Cancer Res* (2017) 77:3655–65. doi: 10.1158/0008-5472.Can-16-3199
46. Guo Y, Ji X, Liu J, Fan D, Zhou Q, Chen C, et al. Effects of Exosomes on Pre-Metastatic Niche Formation in Tumors. *Mol Cancer* (2019) 18:39. doi: 10.1186/s12943-019-0995-1
47. Willms E, Johansson HJ, Mäger I, Lee Y, Blomberg KE, Sadik M, et al. Cells Release Subpopulations of Exosomes With Distinct Molecular and Biological Properties. *Sci Rep* (2016) 6:22519. doi: 10.1038/srep22519
48. Marcoux G, Duchez AC, Cloutier N, Provost P, Nigrovic PA, Boilard E. Revealing the Diversity of Extracellular Vesicles Using High-Dimensional Flow Cytometry Analyses. *Sci Rep* (2016) 6:35928. doi: 10.1038/srep35928
49. Haraszti RA, Miller R, Stoppato M, Sere YY, Coles A, Didiot MC, et al. Exosomes Produced From 3D Cultures of MSCs by Tangential Flow Filtration Show Higher Yield and Improved Activity. *Mol Ther* (2018) 26:2838–47. doi: 10.1016/j.ymthe.2018.09.015
50. Jiang M, Zhang W, Zhang R, Liu P, Ye Y, Yu W, et al. Cancer Exosome-Derived miR-9 and miR-181a Promote the Development of Early-Stage MDSCs *via* Interfering With SOCS3 and PIAS3 Respectively in Breast Cancer. *Oncogene* (2020) 39:4681–94. doi: 10.1038/s41388-020-1322-4
51. Guo X, Qiu W, Liu Q, Qian M, Wang S, Zhang Z, et al. Immunosuppressive Effects of Hypoxia-Induced Glioma Exosomes Through Myeloid-Derived Suppressor Cells *via* the miR-10a/Rora and miR-21/Pten Pathways. *Oncogene* (2018) 37:4239–59. doi: 10.1038/s41388-018-0261-9
52. Webber JP, Spary LK, Sanders AJ, Chowdhury R, Jiang WG, Steadman R, et al. Differentiation of Tumour-Promoting Stromal Myofibroblasts by Cancer Exosomes. *Oncogene* (2015) 34:290–302. doi: 10.1038/onc.2013.560
53. Gu J, Qian H, Shen L, Zhang X, Zhu W, Huang L, et al. Gastric Cancer Exosomes Trigger Differentiation of Umbilical Cord Derived Mesenchymal Stem Cells to Carcinoma-Associated Fibroblasts Through TGF-β/Smad Pathway. *PloS One* (2012) 7:e52465. doi: 10.1371/journal.pone.0052465
54. Bai M, Li J, Yang H, Zhang H, Zhou Z, Deng T, et al. miR-135b Delivered by Gastric Tumor Exosomes Inhibits FOXO1 Expression in Endothelial Cells and Promotes Angiogenesis. *Mol Ther* (2019) 27:1772–83. doi: 10.1016/j.ymthe.2019.06.018
55. Chen G, Huang AC, Zhang W, Zhang G, Wu M, Xu W, et al. Exosomal PD-L1 Contributes to Immunosuppression and is Associated With Anti-PD-1 Response. *Nat* (2018) 560:382–6. doi: 10.1038/s41586-018-0392-8
56. Zhang W, Zhong W, Wang B, Yang J, Yang J, Yu Z, et al. ICAM-1-Mediated Adhesion is a Prerequisite for Exosome-Induced T Cell Suppression. *Dev Cell* (2022) 57:329–43.e327. doi: 10.1016/j.devcel.2022.01.002
57. You Y, Shan Y, Chen J, Yue H, You B, Shi S, et al. Matrix Metalloproteinase 13-Containing Exosomes Promote Nasopharyngeal Carcinoma Metastasis. *Cancer Sci* (2015) 106:1669–77. doi: 10.1111/cas.12818
58. Achen MG, Stacker SA. Molecular Control of Lymphatic Metastasis. *Ann N Y Acad Sci* (2008) 1131:225–34. doi: 10.1196/annals.1413.020
59. Farnsworth RH, Karnezis T, Shayan R, Matsumoto M, Nowell CJ, Achen MG, et al. A Role for Bone Morphogenetic Protein-4 in Lymph Node Vascular Remodeling and Primary Tumor Growth. *Cancer Res* (2011) 71:6547–57. doi: 10.1158/0008-5472.Can-11-0200
60. Tammela T, Alitalo K. Lymphangiogenesis: Molecular Mechanisms and Future Promise. *Cell* (2010) 140:460–76. doi: 10.1016/j.cell.2010.01.045
61. Saharinen P, Tammela T, Karkkainen MJ, Alitalo K. Lymphatic Vasculature: Development, Molecular Regulation and Role in Tumor Metastasis and Inflammation. *Trends Immunol* (2004) 25:387–95. doi: 10.1016/j.it.2004.05.003
62. Wakisaka N, Hasegawa Y, Yoshimoto S, Miura K, Shiotani A, Yokoyama J, et al. Primary Tumor-Secreted Lymphangiogenic Factors Induce Pre-Metastatic Lymphvascular Niche Formation at Sentinel Lymph Nodes in Oral Squamous Cell Carcinoma. *PloS One* (2015) 10:e0144056. doi: 10.1371/journal.pone.0144056
63. Ogawa F, Amano H, Eshima K, Ito Y, Matsui Y, Hosono K, et al. Prostanoid Induces Premetastatic Niche in Regional Lymph Nodes. *J Clin Invest* (2014) 124:4882–94. doi: 10.1172/jci73530
64. Pucci F, Garris C, Lai CP, Newton A, Pfirschke C, Engblom C, et al. SCS Macrophages Suppress Melanoma by Restricting Tumor-Derived Vesicle-B Cell Interactions. *Sci* (2016) 352:242–6. doi: 10.1126/science.aaf1328

65. Lee E, Fertig EJ, Jin K, Sukumar S, Pandey NB, Popel AS. Breast Cancer Cells Condition Lymphatic Endothelial Cells Within Pre-Metastatic Niches to Promote Metastasis. *Nat Commun* (2014) 5:4715. doi: 10.1038/ncomms5715
66. Karnezis T, Shayan R, Caesar C, Roufail S, Harris NC, Ardipradja K, et al. VEGF-D Promotes Tumor Metastasis by Regulating Prostaglandins Produced by the Collecting Lymphatic Endothelium. *Cancer Cell* (2012) 21:181–95. doi: 10.1016/j.ccr.2011.12.026
67. Nishida Y, Tsukushi S, Urakawa H, Sugiura H, Nakashima H, Yamada Y, et al. High Incidence of Regional and in-Transit Lymph Node Metastasis in Patients With Alveolar Rhabdomyosarcoma. *Int J Clin Oncol* (2014) 19:536–43. doi: 10.1007/s10147-013-0571-4
68. Francart ME, Lambert J, Vanwynsberghe AM, Thompson EW, Bourcy M, Polette M, et al. Epithelial-Mesenchymal Plasticity and Circulating Tumor Cells: Travel Companions to Metastases. *Dev Dyn* (2018) 247:432–50. doi: 10.1002/dvdy.24506
69. Kalluri R, Weinberg RA. The Basics of Epithelial-Mesenchymal Transition. *J Clin Invest* (2009) 119:1420–8. doi: 10.1172/jci39104
70. Kaplan RN, Riba RD, Zacharoulis S, Bramley AH, Vincent L, Costa C, et al. VEGFR1-Positive Haematopoietic Bone Marrow Progenitors Initiate the Pre-Metastatic Niche. *Nat* (2005) 438:820–7. doi: 10.1038/nature04186
71. Brabletz T, Kalluri R, Nieto MA, Weinberg RA. EMT in Cancer. *Nat Rev Cancer* (2018) 18:128–34. doi: 10.1038/nrc.2017.118
72. Noy R, Pollard JW. Tumor-Associated Macrophages: From Mechanisms to Therapy. *Immun* (2014) 41:49–61. doi: 10.1016/j.immuni.2014.06.010
73. Wei C, Yang C, Wang S, Shi D, Zhang C, Lin X, et al. Crosstalk Between Cancer Cells and Tumor Associated Macrophages is Required for Mesenchymal Circulating Tumor Cell-Mediated Colorectal Cancer Metastasis. *Mol Cancer* (2019) 18:64. doi: 10.1186/s12943-019-0976-4
74. Lin X, Wang S, Sun M, Zhang C, Wei C, Yang C, et al. miR-195-5p/NOTCH2-Mediated EMT Modulates IL-4 Secretion in Colorectal Cancer to Affect M2-Like TAM Polarization. *J Hematol Oncol* (2019) 12:20. doi: 10.1186/s13045-019-0708-7
75. Yang C, Dou R, Wei C, Liu K, Shi D, Zhang C, et al. Tumor-Derived Exosomal microRNA-106b-5p Activates EMT-Cancer Cell and M2-Subtype TAM Interaction to Facilitate CRC Metastasis. *Mol Ther* (2021) 29:2088–107. doi: 10.1016/j.ymthe.2021.02.006
76. Placke T, Kopp HG, and Salih HR. Modulation of Natural Killer Cell Anti-tumor Reactivity by Platelets. *J Innate Immun* (2011) 59:1295–300.
77. Gay LJ, Felding-Habermann B. Contribution of Platelets to Tumour Metastasis. *Nat Rev Cancer* (2011) 3:374–82. doi: 10.1159/000323936
78. Läubli H, Borsig L. Selectins Promote Tumor Metastasis. *Semin Cancer Biol* (2010) 20:169–77. doi: 10.1016/j.semcancer.2010.04.005
79. Best MG, Sol N, Kooi I, Tannous J, Westerman BA, Rustenburg F, et al. RNA-Seq of Tumor-Educated Platelets Enables Blood-Based Pan-Cancer, Multiclass, and Molecular Pathway Cancer Diagnostics. *Cancer Cell* (2015) 28:666–76. doi: 10.1016/j.ccell.2015.09.018
80. Liu L, Lin F, Ma X, Chen Z, Yu J. Tumor-Educated Platelet as Liquid Biopsy in Lung Cancer Patients. *Crit Rev Oncol Hematol* (2020) 146:102863. doi: 10.1016/j.critrevonc.2020.102863
81. Suvilesh KN, Nussbaum YI, Radhakrishnan V, Manjunath Y, Avella DM, Staveley-O'Carroll KF, et al. Tumorigenic Circulating Tumor Cells From Xenograft Mouse Models of non-Metastatic NSCLC Patients Reveal Distinct Single Cell Heterogeneity and Drug Responses. *Mol Cancer* (2022) 21:73. doi: 10.1186/s12943-022-01553-5
82. Strati A, Zavridou M, Kallergi G, Politaki E, Kuske A, Gorges TM, et al. A Comprehensive Molecular Analysis of in Vivo Isolated EpCAM-Positive Circulating Tumor Cells in Breast Cancer. *Clin Chem* (2021) 67:1395–405. doi: 10.1093/clinchem/hvab099
83. Sperger JM, Emamekhoo H, McKay RR, Stahlfeld CN, Singh A, Chen XE, et al. Prospective Evaluation of Clinical Outcomes Using a Multiplex Liquid Biopsy Targeting Diverse Resistance Mechanisms in Metastatic Prostate Cancer. *J Clin Oncol* (2021) 39:2926–37. doi: 10.1200/jco.21.00169
84. Descamps L, Le Roy D, Deman AL. Microfluidic-Based Technologies for CTC Isolation: A Review of 10 Years of Intense Efforts Towards Liquid Biopsy. *Int J Mol Sci* (2022) 23:1981. doi: 10.3390/ijms23041981
85. Chauhan A, Kaur R, Ghoshal S, Pal A. Exploration of Circulating Tumour Cell (CTC) Biology: A Paradigm Shift in Liquid Biopsy. *Indian J Clin Biochem* (2021) 36:131–42. doi: 10.1007/s12291-020-00923-4
86. Logothetis CJ, Lin SH. Osteoblasts in Prostate Cancer Metastasis to Bone. *Nat Rev Cancer* (2005) 5:21–8. doi: 10.1038/nrc1528
87. Kozlow W, Guise TA. Breast Cancer Metastasis to Bone: Mechanisms of Osteolysis and Implications for Therapy. *J Mammary Gland Biol Neoplasia* (2005) 10:169–80. doi: 10.1007/s10911-005-5399-8
88. David Roodman G. Role of Stromal-Derived Cytokines and Growth Factors in Bone Metastasis. *Cancer* (2003) 97:733–8. doi: 10.1002/cncr.11148
89. Zaimy MA, Saffarzadeh N, Mohammadi A, Pourghadamyari H, Izadi P, Sarli A, et al. New Methods in the Diagnosis of Cancer and Gene Therapy of Cancer Based on Nanoparticles. *Cancer Gene Ther* (2017) 24:233–43. doi: 10.1038/cgt.2017.16
90. Costa-Silva B, Aiello NM, Ocean AJ, Singh S, Zhang H, Thakur BK, et al. Pancreatic Cancer Exosomes Initiate Pre-Metastatic Niche Formation in the Liver. *Nat Cell Biol* (2015) 17:816–26. doi: 10.1038/ncb3169
91. Liu C, Zeng X, An Z, Yang Y, Eisenbaum M, Gu X, et al. Sensitive Detection of Exosomal Proteins *via* a Compact Surface Plasmon Resonance Biosensor for Cancer Diagnosis. *ACS Sens* (2018) 3:1471–9. doi: 10.1021/acssensors.8b00230
92. Preis M, Gardner TB, Gordon SR, Pipas JM, Mackenzie TA, Klein EE, et al. MicroRNA-10b Expression Correlates With Response to Neoadjuvant Therapy and Survival in Pancreatic Ductal Adenocarcinoma. *Clin Cancer Res* (2011) 17:5812–21. doi: 10.1158/1078-0432.Ccr-11-0695
93. Meng X, Müller V, Milde-Langosch K, Trillsch F, Pantel K, Schwarzenbach H. Diagnostic and Prognostic Relevance of Circulating Exosomal miR-373, miR-200a, miR-200b and miR-200c in Patients With Epithelial Ovarian Cancer. *Oncotarget* (2016) 7:16923–35. doi: 10.18632/oncotarget.7850
94. Pan B, Qin J, Liu X, He B, Wang X, Pan Y, et al. Identification of Serum Exosomal Hsa-Circ-0004771 as a Novel Diagnostic Biomarker of Colorectal Cancer. *Front Genet* (2019) 10:1096. doi: 10.3389/fgene.2019.01096
95. Cheng L, Wang Y, Huang L. Exosomes From M1-Polarized Macrophages Potentiate the Cancer Vaccine by Creating a Pro-Inflammatory Microenvironment in the Lymph Node. *Mol Ther* (2017) 25:1665–75. doi: 10.1016/j.ymthe.2017.02.007
96. Yun JW, Lee S, Kim HM, Chun S, Engleman EG, Kim HC, et al. A Novel Type of Blood Biomarker: Distinct Changes of Cytokine-Induced STAT Phosphorylation in Blood T Cells Between Colorectal Cancer Patients and Healthy Individuals. *Cancers (Basel)* (2019) 11:1157. doi: 10.3390/cancers11081157
97. Abajo A, Boni V, Lopez I, Gonzalez-Huarriz M, Bitarte N, Rodriguez J, et al. Identification of Predictive Circulating Biomarkers of Bevacizumab-Containing Regimen Efficacy in Pre-Treated Metastatic Colorectal Cancer Patients. *Br J Cancer* (2012) 107:287–90. doi: 10.1038/bjc.2012.242
98. Bencsikova B, Budinska E, Selingerova I, Pilatova K, Fedorova L, Greplova K, et al. Circulating T Cell Subsets are Associated With Clinical Outcome of Anti-VEGF-Based 1st-Line Treatment of Metastatic Colorectal Cancer Patients: A Prospective Study With Focus on Primary Tumor Sidedness. *BMC Cancer* (2019) 19:687. doi: 10.1186/s12885-019-5909-5
99. Baccelli I, Schneeweiss A, Riethdorf S, Stenzinger A, Schillert A, Vogel V, et al. Identification of a Population of Blood Circulating Tumor Cells From Breast Cancer Patients That Initiates Metastasis in a Xenograft Assay. *Nat Biotechnol* (2013) 31:539–44. doi: 10.1038/nbt.2576
100. Ulz P, Perakis S, Zhou Q, Moser T, Belic J, Lazzeri I, et al. Inference of Transcription Factor Binding From Cell-Free DNA Enables Tumor Subtype Prediction and Early Detection. *Nat Commun* (2019) 10:4666. doi: 10.1038/s41467-019-12714-4
101. Lee JH, Choi JW, Kim YS. Serum TIMP-1 Predicts Survival Outcomes of Invasive Breast Carcinoma Patients: A Meta-analysis. *Arch Med Res* (2011) 42:463–8. doi: 10.1016/j.arcmed.2011.09.006
102. Park KS, Bandeira E, Shelke GV, Lässer C, Lötvall J. Enhancement of Therapeutic Potential of Mesenchymal Stem Cell-Derived Extracellular Vesicles. *Stem Cell Res Ther* (2019) 10:288. doi: 10.1186/s13287-019-1398-3
103. Cima I, Kong SL, Sengupta D, Tan IB, Phyo WM, Lee D, et al. Tumor-Derived Circulating Endothelial Cell Clusters in Colorectal Cancer. *Sci Transl Med* (2016) 8:345ra389. doi: 10.1126/scitranslmed.aad7369
104. Manzoni M, Comolli G, Torchio M, Mazzini G, Danova M. Circulating Endothelial Cells and Their Subpopulations: Role as Predictive Biomarkers in Antiangiogenic Therapy for Colorectal Cancer. *Clin Colorectal Cancer* (2015) 14:11–7. doi: 10.1016/j.clcc.2014.12.002

105. Rahbari NN, Schölch S, Bork U, Kahlert C, Schneider M, Rahbari M, et al. Prognostic Value of Circulating Endothelial Cells in Metastatic Colorectal Cancer. *Oncotarget* (2017) 8:37491–501. doi: 10.18632/oncotarget.16397
106. Giussani M, Triulzi T, Sozzi G, Tagliabue E. Tumor Extracellular Matrix Remodeling: New Perspectives as a Circulating Tool in the Diagnosis and Prognosis of Solid Tumors. *Cells* (2019) 8:81. doi: 10.3390/cells8020081
107. Papachristos A, Kemos P, Katsila T, Panoilia E, Patrinos GP, Kalofonos H, et al. VEGF-A and ICAM-1 Gene Polymorphisms as Predictors of Clinical Outcome to First-Line Bevacizumab-Based Treatment in Metastatic Colorectal Cancer. *Int J Mol Sci* (2019) 20:5791. doi: 10.3390/ijms20225791
108. Inanç M, Er O, Karaca H, Berk V, Ozkan M, Saraymen R, et al. Prognostic Value of Tumor Growth Factor Levels During Chemotherapy in Patients With Metastatic Colorectal Cancer. *Med Oncol* (2012) 29:3119–24. doi: 10.1007/s12032-012-0250-8
109. Kaiser J. 'Liquid Biopsy' for Cancer Promises Early Detection. *Sci* (2018) 359:259. doi: 10.1126/science.359.6373.259
110. Li W, Zhang X, Lu X, You L, Song Y, Luo Z, et al. 5-Hydroxymethylcytosine Signatures in Circulating Cell-Free DNA as Diagnostic Biomarkers for Human Cancers. *Cell Res* (2017) 27:1243–57. doi: 10.1038/cr.2017.121
111. Xu Y, Ma X, Ai X, Gao J, Liang Y, Zhang Q, et al. A Urine-Based Liquid Biopsy Method for Detection of Upper Tract Urinary Carcinoma. *Front Oncol* (2020) 10:597486. doi: 10.3389/fonc.2020.597486
112. Hoshino A, Kim HS, Bojmar L, Gyan KE, Cioffi M, Hernandez J, et al. Extracellular Vesicle and Particle Biomarkers Define Multiple Human Cancers. *Cell* (2020) 182:1044–61.e1018. doi: 10.1016/j.cell.2020.07.009
113. Preethi KA, Selvakumar SC, Ross K, Jayaraman S, Tusubira D, Sekar D. Liquid Biopsy: Exosomal microRNAs as Novel Diagnostic and Prognostic Biomarkers in Cancer. *Mol Cancer* (2022) 21:54. doi: 10.1186/s12943-022-01525-9
114. Zhang Y, Xu H. Serum Exosomal miR-378 Upregulation is Associated With Poor Prognosis in non-Small-Cell Lung Cancer Patients. *J Clin Lab Anal* (2020) 34:e23237. doi: 10.1002/jcla.23237
115. Ghosh S, Bhowmik S, Majumdar S, Goswami A, Chakraborty J, Gupta S, et al. The Exosome Encapsulated microRNAs as Circulating Diagnostic Marker for Hepatocellular Carcinoma With Low Alpha-Fetoprotein. *Int J Cancer* (2020) 147:2934–47. doi: 10.1002/ijc.33111
116. Hugenschmidt H, Labori KJ, Brunborg C, Verbeke CS, Seeberg LT, Schirmer CB, et al. Circulating Tumor Cells are an Independent Predictor of Shorter Survival in Patients Undergoing Resection for Pancreatic and Periampullary Adenocarcinoma. *Ann Surg* (2020) 271:549–58. doi: 10.1097/sla.0000000000003035
117. Gazzaniga P, Gradilone A, de Berardinis E, Busetto GM, Raimondi C, Gandini O, et al. Prognostic Value of Circulating Tumor Cells in Nonmuscle Invasive Bladder Cancer: A CellSearch Analysis. *Ann Oncol* (2012) 23:2352–6. doi: 10.1093/annonc/mdr619
118. Antonarakis ES, Lu C, Luber B, Wang H, Chen Y, Zhu Y, et al. Clinical Significance of Androgen Receptor Splice Variant-7 mRNA Detection in Circulating Tumor Cells of Men With Metastatic Castration-Resistant Prostate Cancer Treated With First- and Second-Line Abiraterone and Enzalutamide. *J Clin Oncol* (2017) 35:2149–56. doi: 10.1200/jco.2016.70.1961
119. Tang Y, Tian W, Xie J, Zou Y, Wang Z, Li N, et al. Prognosis and Dissection of Immunosuppressive Microenvironment in Breast Cancer Based on Fatty Acid Metabolism-Related Signature. *Front In Immunol* (2022) 13:843515. doi: 10.3389/fimmu.2022.843515
120. Sparano J, O'Neill A, Alpaugh K, Wolff AC, Northfelt DW, Dang CT, et al. Association of Circulating Tumor Cells With Late Recurrence of Estrogen Receptor-Positive Breast Cancer: A Secondary Analysis of a Randomized Clinical Trial. *JAMA Oncol* (2018) 4:1700–6. doi: 10.1001/jamaoncol.2018.2574
121. van Dalum G, Stam GJ, Scholten LF, Mastboom WJ, Vermes I, Tibbe AG, et al. Importance of Circulating Tumor Cells in Newly Diagnosed Colorectal Cancer. *Int J Oncol* (2015) 46:1361–8. doi: 10.3892/ijo.2015.2824
122. Liu APY, Smith KS, Kumar R, Paul L, Bihannic L, Lin T, et al. Serial Assessment of Measurable Residual Disease in Medulloblastoma Liquid Biopsies. *Cancer Cell* (2021) 39:1519–30.e1514. doi: 10.1016/j.ccell.2021.09.012
123. Pantel K, Alix-Panabières C. Liquid Biopsy and Minimal Residual Disease - Latest Advances and Implications for Cure. *Nat Rev Clin Oncol* (2019) 16:409–24. doi: 10.1038/s41571-019-0187-3
124. Tie J, Cohen JD, Lahouel K, Lo SN, Wang Y, Kosmider S, et al. Circulating Tumor DNA Analysis Guiding Adjuvant Therapy in Stage II Colon Cancer. *N Engl J Med* (2022) 386:2261–72. doi: 10.1056/NEJMoa2200075
125. Cheng N, Du D, Wang X, Liu D, Xu W, Luo Y, et al. Recent Advances in Biosensors for Detecting Cancer-Derived Exosomes. *Trends Biotechnol* (2019) 37:1236–54. doi: 10.1016/j.tibtech.2019.04.008
126. Schwarzenbach H, Hoon DS, Pantel K. Cell-Free Nucleic Acids as Biomarkers in Cancer Patients. *Nat Rev Cancer* (2011) 11:426–37. doi: 10.1038/nrc3066
127. Anfossi S, Babayan A, Pantel K, Calin GA. Clinical Utility of Circulating non-Coding RNAs - an Update. *Nat Rev Clin Oncol* (2018) 15:541–63. doi: 10.1038/s41571-018-0035-x
128. Kalluri R, LeBleu VS. The Biology, Function, and Biomedical Applications of Exosomes. *Sci* (2020) 367:eaau6977. doi: 10.1126/science.aau6977
129. Vandekerkhove G, Lavoie JM, Annala M, Murtha AJ, Sundahl N, Walz S, et al. Plasma ctDNA is a Tumor Tissue Surrogate and Enables Clinical-genomic Stratification of Metastatic Bladder Cancer. *Nat Commun* (2021) 12:184. doi: 10.1038/s41467-020-20493-6
130. Li X, Chen C, Wang Z, Liu J, Sun W, Shen K, et al. Elevated Exosome-Derived miRNAs Predict Osimertinib Resistance in non-Small Cell Lung Cancer. *Cancer Cell Int* (2021) 21:428. doi: 10.1186/s12935-021-02075-8
131. Wu M, Wang G, Hu W, Yao Y, Yu XF. Emerging Roles and Therapeutic Value of Exosomes in Cancer Metastasis. *Mol Cancer* (2019) 18:53. doi: 10.1186/s12943-019-0964-8
132. de la Fuente A, Alonso-Alconada L, Costa C, Cueva J, Garcia-Caballero T, Lopez-Lopez R, et al. M-Trap: Exosome-Based Capture of Tumor Cells as a New Technology in Peritoneal Metastasis. *J Natl Cancer Inst* (2015) 107: djv184. doi: 10.1093/jnci/djv184
133. Liu C, Su C. Design Strategies and Application Progress of Therapeutic Exosomes. *Theranostics* (2019) 9:1015–28. doi: 10.7150/thno.30853
134. Tellez-Gabriel M, Heymann MF, Heymann D. Circulating Tumor Cells as a Tool for Assessing Tumor Heterogeneity. *Theranostics* (2019) 9:4580–94. doi: 10.7150/thno.34337
135. Newman AM, Bratman SV, To J, Wynne JF, Eclov NC, Modlin LA, et al. An Ultrasensitive Method for Quantitating Circulating Tumor DNA With Broad Patient Coverage. *Nat Med* (2014) 20:548–54. doi: 10.1038/nm.3519
136. Chang L, Li J, Zhang R. Liquid Biopsy for Early Diagnosis of non-Small Cell Lung Carcinoma: Recent Research and Detection Technologies. *Biochim Biophys Acta Rev Cancer* (2022) 1877:188729. doi: 10.1016/j.bbcan.2022.188729
137. Kulasingam V, Diamandis EP. Strategies for Discovering Novel Cancer Biomarkers Through Utilization of Emerging Technologies. *Nat Clin Pract Oncol* (2008) 5:588–99. doi: 10.1038/ncponc1187
138. Razavi P, Li BT, Brown DN, Jung B, Hubbell E, Shen R, et al. High-Intensity Sequencing Reveals the Sources of Plasma Circulating Cell-Free DNA Variants. *Nat Med* (2019) 25:1928–37. doi: 10.1038/s41591-019-0652-7
139. Geeurickx E, Hendrix A. Targets, Pitfalls and Reference Materials for Liquid Biopsy Tests in Cancer Diagnostics. *Mol Aspects Med* (2020) 72:100828. doi: 10.1016/j.mam.2019.10.005
140. Ignatiadis M, Sledge GW, Jeffrey SS. Liquid Biopsy Enters the Clinic - Implementation Issues and Future Challenges. *Nat Rev Clin Oncol* (2021) 18:297–312. doi: 10.1038/s41571-020-00457-x
141. González-Silva L, Quevedo L, Varela I. Tumor Functional Heterogeneity Unraveled by scRNA-Seq Technologies: (Trends in Cancer 6, 13-19, 2020). *Trends Cancer* (2021) 7:265. doi: 10.1016/j.trecan.2021.02.001
142. Roll W, Weckesser M, Seifert R, Bodei L, Rahbar K. Imaging and Liquid Biopsy in the Prediction and Evaluation of Response to PRRT in Neuroendocrine Tumors: Implications for Patient Management. *Eur J Nucl Med Mol Imaging* (2021) 48:4016–27. doi: 10.1007/s00259-021-05359-3
143. Liu MC, Oxnard GR, Klein EA, Swanton C, Seiden MV. Sensitive and Specific Multi-Cancer Detection and Localization Using Methylation Signatures in Cell-Free DNA. *Ann Oncol* (2020) 31:745–59. doi: 10.1016/j.annonc.2020.02.011

Conflict of Interest: The authors declare that the research was conducted in the absence of any commercial or financial relationships that could be construed as a potential conflict of interest.

this article, or claim that may be made by its manufacturer, is not guaranteed or endorsed by the publisher.

frontiers | Frontiers in Immunology

TYPE Review
PUBLISHED 25 July 2022
DOI 10.3389/fimmu.2022.908894

OPEN ACCESS

EDITED BY
Min Xue,
University of California, Riverside,
United States

REVIEWED BY
Shiqun Shao,
Zhejiang University, China
Zhili Guo,
Quantum-Si, Inc., United States

*CORRESPONDENCE
Jiuwei Cui
cuijw@jlu.edu.cn

SPECIALTY SECTION
This article was submitted to Cancer Immunity and Immunotherapy, a section of the journal Frontiers in Immunology

RECEIVED 31 March 2022
ACCEPTED 30 June 2022
PUBLISHED 25 July 2022

CITATION
Guo Y, Guo H, Zhang Y and Cui J (2022) Anaplastic lymphoma kinase-special immunity and immunotherapy. *Front. Immunol.* 13:908894. doi: 10.3389/fimmu.2022.908894

Anaplastic lymphoma kinase-special immunity and immunotherapy

Ye Guo, Hanfei Guo, Yongfei Zhang and Jiuwei Cui*

Cancer Center, The First Hospital of Jilin University, Changchun, China

Alterations in the anaplastic lymphoma kinase (*ALK*) gene play a key role in the development of various human tumors, and targeted therapy has transformed the treatment paradigm for these oncogene-driven tumors. However, primary or acquired resistance remains a challenge. *ALK* gene variants (such as gene rearrangements and mutations) also play a key role in the tumor immune microenvironment. Immunotherapy targeting the *ALK* gene has potential clinical applications. Here, we review the results of recent studies on the immunological relevance of ALK-altered tumors, which provides important insights into the development of tumor immunotherapies targeting this large class of tumors.

KEYWORDS

anaplastic lymphoma kinase, tumor microenvironment, immune evasion, immunotherapy, immune checkpoint inhibitors

Introduction

Over the past few decades, the anaplastic lymphoma kinase (*ALK*) gene has been widely known for its role in human tumorigenesis (1). Various rearrangements (fusions), mutations, amplification, and alternative splicing of the *ALK* gene have been found in anaplastic large cell lymphoma (ALCL), inflammatory myofibroblastoma (IMT), non-small cell lung cancer (NSCLC), and other human tumors (2–4) (Table 1). Currently, *ALK* gene variants are considered drug targets for these tumors. However, primary or acquired resistance to tyrosine kinase inhibitors is almost unavoidable (5). Although immunotherapy in recent years has provided new hope for patients with a variety of tumors with poor treatment efficacy, the response of these patients with *ALK* gene abnormalities to immunotherapy has not been clarified. A large retrospective study showed that patients with at least one oncogenic driver alteration (*RET*, *ROS1*, *EGFR*, or *ALK*) are less likely to benefit from immune checkpoint inhibitor (ICI) monotherapy (6). Until recently, several preclinical and clinical studies suggested that ALK rearrangement may be involved in innate and adaptive immunity through various pathways and is associated with T cell activation, cytokine release, and tumor

10.3389/fimmu.2022.908894

TABLE 1 Summary of ALK variants.

Variation type	Tumor (ALK positive rate)	Primary variation site (percentage of all ALK positive tumor)
Fusion	Anaplastic large cell lymphoma (ALCL) (60%)	NPM-ALK (80%), TPM3-ALK (12-18%)
	Non-small cell lung cancer (NSCLC) (3-7%)	EML4-ALK (80%)
	Inflammatory myofibroblastoma (IMT) (50%)	TPM3/4-ALK (95%)
	Diffuse large B-cell lymphoma (DLBCL) (rare)	CLTC-ALK
	Acute myelomonocytic leukemia (AML) (rare)	RANBP2-ALK
	Breast cancer (2.4%)	EML4-ALK
	Colorectal cancer (0.05-0.19%)	EML4-ALK, SPTBN1-ALK
	Renal cell carcinoma (<1%)	TPM3-ALK, VCL-ALK
	Thyroid carcinomas (1-3%)	STRN-ALK (50%), EML4-ALK (39%)
	Epithelioid fibrous histiocytoma (88%)	SQSTM1-ALK (52%), VCL-ALK (30%)
	Spitz tumors (10%)	DCTN1-ALK, TPM3-ALK (over 90%)
	Ovarian cancer (rare)	FN1-ALK, EML4-ALK
	Esophageal squamous cell carcinoma (ESCC) (rare)	TPM4-ALK
	Pancreatic cancer (rare)	EML4-ALK (over 50%)
Mutation	Neuroblastoma (15%)	F1174, F1245, R1275 (85%)
	Anaplastic thyroid cancer (ATC) (11%)	L1198F, G1201E
	ALK inhibitor-resistant NSCLC (30-50%)	L1196M
	ALK inhibitor-resistant ALCL	G1269A
	ALK inhibitor-resistant IMT	F1174L
Overexpression	Melanoma, Ovarian cancer, NSCLC, Breast cancer, Neuroblastoma, Astrocytoma, Glioblastoma, Ewing's sarcoma, Colorectal cancer, Retinoblastoma, Rhabdomyosarcoma	

So far, ALK fusions have been found in more than 10 kinds of tumors (both hematopoietic neoplasms and solid tumors), and more than 100 fusion partners have been reported. In most cases, ALK fusions arise from the fusion of 3′ half of ALK, which retains its kinase catalytic domain, and the 5′ portion of a different gene that provides its promoter; The mutations of ALK are located in the kinase domain; ALK overexpression has been reported in various cancer types and cell lines, but its mechanism and its relationship with tumor drivers are still unclear.

immune escape (7). In addition, chimeric antigen receptor (CAR-T) therapies and tumor vaccines targeting ALK rearrangements are under development.

Therefore, clarifying whether preferred targeted therapy, immunotherapy, or targeted combination immunotherapy is the optimal clinical treatment strategy for such patients is important. Hence, this topic will be the focus of future research in the field of ALK-altered tumor immunotherapy. This article reviews the progress on the knowledge of *ALK* gene variants in the field of immunotherapy to better understand the mechanism of ALK in the human immune response and may provide new treatment strategies for patients with *ALK* gene variants.

Physiologic role of the *ALK* oncogene and its genetic aberrations in cancer

ALK, consisting of 1,620 amino acids, is a member of the insulin receptor tyrosine kinase (RTK) superfamily, and its gene is located on chromosome 2p23 (8). ALK plays an important role in the growth and development of the mammalian nervous system; however, its expression decreases significantly after birth and remains at a low level in adulthood (9). The tissue expression of ALK in human adults is restricted to the brain, with minimal expression in the lung, colon, small intestine, and testis, as indicated by the expression data of the human protein atlas and several immunohistochemical studies (10). When somatic variations occur, ALK is expressed in tissues that do not originally express ALK, and as such the cells are abnormally activated, resulting in uncontrolled cell proliferation and tumor formation (2, 11). Because ALK expression is restricted to the nervous system, a highly immune-privileged organ, the ALK protein is a potential antigen for the immune system. Similarly, tumor-specific ALK fusions or mutants may also be recognized as neoantigens in the body. Thus, ALK-altered cancer cells may potentially trigger antibody responses in patients. ALK is also involved in innate immunity against microbial pathogens (12, 13). Preclinical and clinical studies have shown that upregulation of immune-related molecules, such as programmed cell death ligand-1 (PD-L1), is commonly observed in ALK-altered tumors (14, 15).

ALK variants affect the tumor microenvironment (TME)

The mechanisms by which ALK-altered tumors lead to immune resistance may include affecting T cell immune

responses, regulating cytokine secretion, activating immunosuppressive cells, and upregulating the expression of heterogeneous immune checkpoints (Figure 1).

Effects of ALK variants on T cell response

In ALK-positive ALCL patients, CD30 is continuously expressed in tumor cells. Compared with CD30- tumors, CD30+ tumors are characterized by downregulation of molecules involved in T cell differentiation/activation (including CD28, CD52, and CD69) and T cell receptor (TCR) signaling (16). CD3 and TCR are negatively expressed in more than 75% of cases, and CD8 expression is rare in T cells (17). In addition, two immunogenic ALK epitopes (P280-89 and p375-86) were identified to elicit cytotoxic T cell (CTL) responses *in vitro*, *in vivo*, and in human peripheral blood lymphocytes (PBLs) (18). The anti-ALK CTL generated from the PBL of healthy donors induces an antigen-specific HLA-A2.1 restricted response, which can effectively kill endogenous ALK-expressing

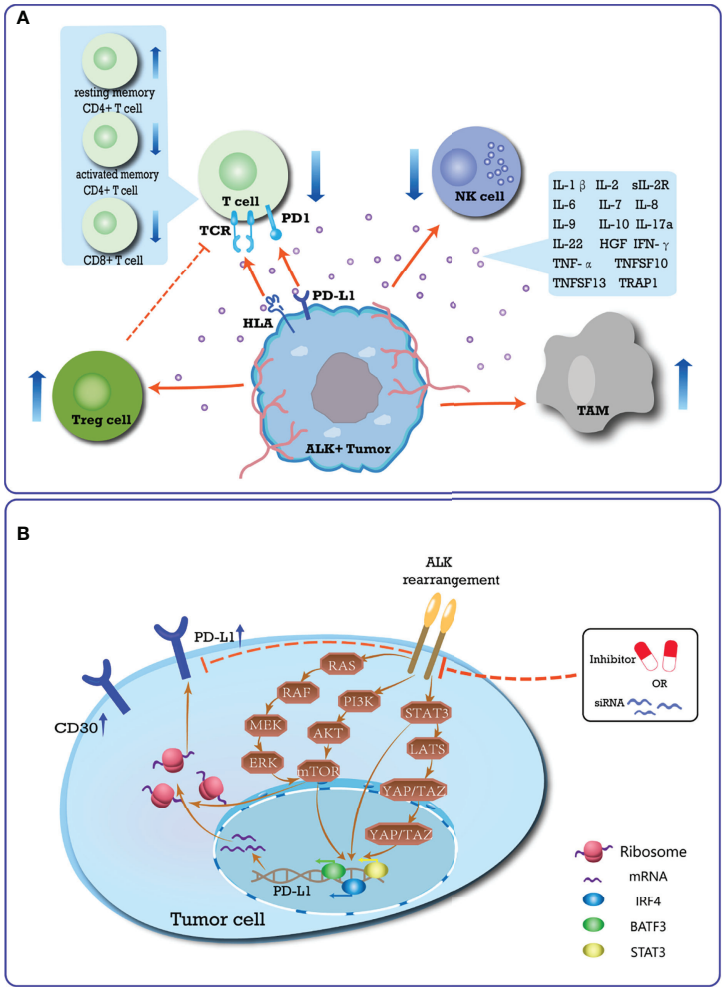

FIGURE 1
Summary of the immune-suppressive microenvironment induced by ALK-rearrangement. **(A)** Schematic diagram of the special immune TME of ALK-positive tumor. In ALK-positive tumors, CD30 is expressed continuously, and TCR signaling is inhibited. In the TME, the types of T cells changed, that is, the number of resting memory CD4+ T cells increased, while CD8+ T cells and activated memory CD4+ T cells were lacking. A variety of immunosuppressive cytokines are up-regulated, thereby inhibiting the killing ability of T cells and NK cells to tumor cells, and promoting the function of immunosuppressive cells. The special TME accumulates more Treg cells and TAM cells to promote immune evasion; **(B)** Mechanism of ALK rearrangement upregulating PD-L1 expression, which plays an essential role in mediating the process of PD-L1 expression. ALK-rearranged protein can activate STAT3, PI3K-AKT-mTOR, and MEK-ERK signaling networks, which upregulate PD-L1 expression through transcription factors acting on the promoter region of PD-L1 gene. Activated mTOR can also recruit PD-L1 transcripts to active polysomes at the post-transcriptional level. The JAK-STAT3-LATS-YAP/TAZ-PD-L1 signaling pathway has gradually been shown to play an important role in mediating ALK-induced upregulation of PD-L1 in multiple cancer cell lines. Conversely, blocking the activation of the ALK pathway inhibits the expression of PD-L1.

tumor targets. Subsequent studies using a mouse model of vaccination identified that, in healthy donors, CD8+ T cells mainly show a naive phenotype, whereas effector and memory CD8+ T cells are detected in ALK-positive ALCL patients (19). ALK-specific CD4+ T cells are detected in HLA-preselected ALCL patients using ALK-derived peptides (20). Recent studies have shown that the *in vitro* transduction of normal human CD4+ T lymphocytes by NPM-ALK leads to immortalization and malignant transformation (21). Moreover, tumor cells have the morphology and immunophenotype of primary anaplastic large cell lymphoma (21). In ALK+ NSCLC patients, Jin et al. (22) found that tumors are characterized by enriched resting memory CD4+ T cells (P<0.001), as well as a lack of CD8+ T cells (P<0.01), and activated memory CD4+ T cells (P=0.001).

Relationship between ALK variants and cytokines

Various pro-inflammatory cytokines and their receptors are significantly upregulated in ALK-positive tumors, including IL-1β, IL-2, soluble IL-2 receptor (sIL-2R), IL-6, IL-7, IL-8, IL-9, IL-10, IL-17a, IL-22, interferon (IFN)-γ, TNF-α, TNFSF10, TNFSF13, hepatocyte growth factor (HGF), CD30, and TRAP1 (23–26). IL-9 and IL-22 activate oncogenic signaling *via* the JAK3-STAT3 pathway, and neutralizing antibodies against them may inhibit the survival and clonogenicity of ALK+ ALCL cells (27, 28). Furthermore, NPM-ALK promotes the expression of other immunosuppressive signals through the activation of STAT3, including IL-10 and transforming growth factor β (TGFβ) (29). Compared with ALK- ALCL, ALK+ ALCL patients are enriched for the expression of signatures of HIF1-α target genes, IL10-induced genes, and H-ras/K-ras induced genes (30).

ALK variants activate immunosuppressive cells

Upregulation of IL6 and IL10 expression in ALK+ tumors reduce the antigen-presenting activity of dendritic cells in the TME and inhibits the function of T and NK cells (31, 32), resulting in ALK+ tumors responding to T cells and innate immunity negative effects. Upregulation of CSF1 and CCL18 expression in ALK+ tumors increase M2 tumor–associated macrophages (TAMs) in the TME that contribute to immune evasion (33–35). Previous studies have identified that ALK-mediated activation of TMEM173 (transmembrane protein 173, also known as STING) in macrophages and monocytes is related to the pathogenesis of sepsis caused by infection, and has the potential to activate macrophages and monocytes (12, 36). Recently, Jan et al. compared the immune gene expression profiles and the levels of specific immune cell populations in ALK+ and ALK- lung adenocarcinoma patients. In ALK+ tumors, the proportion of regulatory T cells was significantly increased (P < 0.0005) (35). Further analysis revealed that ALK+ tumors recruit CXCR4+ Tregs by upregulating CXCL12 and CCL22 (35, 37, 38). These studies all showed that ALK variants can activate immune suppressive cells, presenting a challenge to immune-related treatment of patients with ALK+ tumors.

ALK variants affect the expression of immunosuppressive molecules

Mutant ALK upregulates the expression of PD-L1, which may potentially confer an immunosuppressive TME, contributing to tolerance and immune evasion in cancer (39, 40). Marzec et al. (29) showed that, in an ALK+ ALCL cell model, NPM-ALK activates the transcription of STAT3 on the PD-L1 promoter. Using CRISPR/Cas9 library screening, Zhang et al. determined that PD-L1 induction is dependent on the NPM-ALK oncoprotein activation of STAT3, as well as a signalosome containing GRB2/SOS1, which activates the MEK-ERK and PI3K-AKT signaling pathways. These signaling networks ultimately induce PD-L1 expression through the action of the transcription factors IRF4 and BATF3 on the enhancer region of the *PD-L1* gene (41). A recent clinical study conducted by the MD Anderson Cancer Center of 95 patients with ALCL showed that the positive rate of PD-L1 in ALK+ ALCL patients is higher than that in ALK- cases (76% and 42%, respectively) (42). The same phenomenon was observed in patients with ALK+ NSCLC. Both *in vitro* and *in vivo* experiments have shown that the expression level of PD-L1 is positively associated with the presence of EML4-ALK in NSCLC specimens (43–46). EML4-ALK modulates PD-L1 expression *via* common downstream signaling pathways mediated by PI3K-AKT-mTOR, MEK-ERK, and STAT3 (44, 47, 48). Activated mTOR recruits PD-L1 transcripts to active polysomes at the post-transcriptional level, thereby increasing the level of PD-L1 protein without significantly increasing the mRNA levels (49, 50). STAT3 increases PD-L1 transcription by directly binding to the promoter region of the *CD274* gene (located at the 9p24.1 locus) (47). Recently, Nouri et al. (51) identified, through the kinome-wide screen of Hippo pathway regulators, that YAP/TAZ are critical in mediating ALK-induced upregulation of PD-L1 in multiple cancer cell lines. Moreover, ALK may cause enhanced immune evasion and tumorigenesis through the JAK-STAT3-LATS-YAP/TAZ-PD-L1 signaling pathway. Importantly, ALK inhibitors and ALK siRNAs effectively inhibit ALK fusion-induced PD-L1 expression in NSCLC cell models. These results confirmed the effect of ALK on PDL1 expression in NSCLC (44, 52).

Current landscape of immunotherapy of ALK-altered tumors

Various preclinical and clinical efforts are underway to identify mechanisms related to the interaction of the *ALK* gene with the tumor immune microenvironment. ICIs targeting programmed cell death ligand-1 (PD-1), PD-L1, and cytotoxic T lymphocyte-associated antigen 4 (CTLA-4) are currently the most advanced immunotherapies and have transformed the treatment paradigm for a variety of tumors, including lung cancer. However, there is no firm conclusion regarding the therapeutic effect of ICIs in patients with ALK-altered tumors. Research on tumor vaccines and chimeric antigen receptor T-Cell (CAR-T cell) therapy targeting ALK are also underway (Table 2).

Immune checkpoint inhibitors (ICIs)

In recent years, ICIs have shown remarkable therapeutic effects in various tumors. Moreover, as mentioned above, ALK variants induce the upregulation of PD-L1 expression in ALK-positive tumors. Based on these findings and *in vitro* drug trials, some scholars have speculated that anti-PD-1/PD-L1 therapy may be a promising option for NSCLC patients with upregulated PD-L1 carrying the EML4-ALK fusion gene (53). However, whether the high expression of PD-L1 affects the prognosis of

TABLE 2 Summary of ongoing trials with immunotherapy in ALK+ tumors (source: www.clinicaltrials.gov, last accessed: 30 Mar 2022).

Clinical Trial Identifier	Phase	Tumor	Study Title	Setting	N	Experimental Arm	Control Arm(s)	Primary Outcome (s)
NCT04042558	II	NSCLC	A Study Evaluating Platinum-Pemetrexed-Atezolizumab (+/-Bevacizumab) for Patients With Stage IIIB/IV Non-squamous Non-small Cell Lung Cancer With EGFR Mutations, ALK Rearrangement or ROS1 Fusion Progressing After Targeted Therapies (GFPC 06-2018)	PD-L1/anti-angiogenesis	149	Carboplatin + Pemetrexed + Atezolizumab + Bevacizumab	Carboplatin + Pemetrexed + Atezolizumab	ORR
NCT03991403	III	NSCLC	Study of Atezolizumab in Combination With Carboplatin + Paclitaxel +Bevacizumab vs With Pemetrexed + Cisplatin or Carboplatin With Stage IV NON-SQUAMOUS NON-SMALL CELL LUNG CANCER With EGFR(+) or ALK(+)	PD-L1/anti-angiogenesis	228	Atezolizumab +Carboplatin + Paclitaxel +Bevacizumab	Pemetrexed +Carboplatin/ cisplatin	PFS
NCT02393625	I	NSCLC	A Multi-center, Open-label Study to Assess the Safety and Efficacy of Combination Ceritinib (LDK378) and Nivolumab in Adult Patients With Anaplastic Lymphoma Kinase (ALK)-Positive Non-small Cell Lung Cancer (NSCLC)	PD-1	57	Ceritinib+Nivolumab		MTD and/or Recommended Dose for Expansion; ORR
NCT04425135	II	non-squamous NSCLC	Phase II Single-arm Clinical Study of Camrelizumab Combined With Apatinib Mesylate and Standard Chemotherapy (Pemetrixed +Carboplatin) in Patients With Tyrosine Kinase Inhibitor Failure in ALK-positive Advanced NSCLC	PD-1/anti-angiogenesis	59	Camrelizumab +apatinib mesylate +Pemetrixed + Carboplatin		ORR
NCT03703050	II	ALCL	Phase II Trial of Nivolumab for Pediatric and Adult Relapsing/Refractory ALK+ Anaplastic Large Cell Lymphoma, for Evaluation of Response in Patients With Progressive Disease (Cohort 1) or as Consolidative Immunotherapy in Patients in Complete Remission After Relapse (Cohort 2)	PD-1	38	Nivolumab		Best objective response rate; PFS
NCT02462538	I/II	ALCL	A "Window of Opportunity" Trial With Brentuximab Vedotin and Imatinib in Patients With Relapsed or Refractory ALK+ Anaplastic Large Cell Lymphoma or Patients Ineligible for Chemotherapy	CD30	10	Brentuximab vedotin + Imatinib		AEs
NCT02799095	I/II	Advanced Solid Tumors*	A Phase 1/2 Study of ALKS 4230 Administered Intravenously as Monotherapy and in Combination With Pembrolizumab in Subjects With Advanced Solid Tumors - ARTISTRY-1	IL-2	347	ALKS 4230 + pembrolizumab	ALKS 4230	DLT; AEs; ORR
NCT03861793	I/II	Advanced Solid Tumors*	A Phase 1/2 Study of ALKS 4230 Administered Subcutaneously as Monotherapy and in Combination With Pembrolizumab in Subjects With Advanced Solid Tumors - ARTISTRY-2 (001)	IL-2	185	ALKS 4230 +Pembrolizumab	ALKS 4230	AEs; ORR

ORR, Objective response rate; PFS, Progression-free survival; AEs, Adverse events; MTD, Maximum tolerated dose; *All eligible patients can be included in the group, no genetic requirements.

ALK+ patients remains inconclusive, and further research is needed (42, 54).

ICI monotherapy

Data from prior randomized studies indicate that immunotherapies are less effective in patients with ALK+ tumors than in those with wild-type tumors, regardless of PD-L1 expression level (55, 56). In a global "real world" study, Mazieres et al. (6) retrospectively analyzed ALK+ NSCLC patients from 10 countries and found that the objective response rate is 0% using ICI monotherapy. The proportion of ALK+ patients who experienced rapid progression within 2 months was 45.5%, which was much higher than that of patients with the wild-type gene. More recently, a multicenter retrospective study showed limited activity in patients with stage III unresectable NSCLC with driver genomic alterations treated with durvalumab (PD-L1 inhibitor) after chemoradiotherapy, especially in the ALK rearrangement subgroup. The median progression-free survival (PFS) was not reached (11.3-NR) in the KRAS-mutation vs. 8.1 month in the EGFR-mutation vs. 7.8 month in the BRAF-mutation/ALK rearrangement (P = 0.02) (57). Therefore, current research on ALK-positive patients has mainly focused on ALK inhibitor resistance (58). For patients with NSCLC, the ATLANTIC trial established an independent cohort of EGFR+/ALK+ patients to evaluate durvalumab as a third line or later treatment. The proportion of patients who achieved a response was generally lower in the cohort of patients with EGFR+/ALK+ NSCLC than in those with EGFR−/ALK− NSCLC. Nevertheless, the proportion of EGFR+/ALK+ patients with at least 25% of tumor cells expressing PD-L1 who achieved an objective response was not substantially lower than that in EGFR−/ALK− patients (12.2% vs 16.4%) (59). Recently, there was a report of a case of a 48-year-old man with ALK+ NSCLC who displayed a complete response for 16 months to nivolumab (PD-1 inhibitor) therapy in a third line setting after ceritinib (second-generation ALK inhibitor) and platin-based chemotherapy (60). Another case report showed that patients with ALK+ ALCL (PD-L1 positive) who were refractory to chemotherapy and ALK inhibitors demonstrated prolonged responses to nivolumab (61, 62). Further clinical trials are needed to verify the effectiveness of ICIs in patients with ALK + ALCL.

Some studies have analyzed the reasons for the poor effects of ICIs. A majority of ALK-positive NSCLCs lack concurrent PD-L1 expression and high levels of CD8+ tumor infiltrating lymphocytes (TILs) (63). The combined analyses of PD-L1 and CD8+ TILs show a remarkably higher proportion of PD-L1-/TIL- tumors and a lower proportion of PD-L1+/TIL+ tumors in ALK+ groups than in wild-type patients (P = 0.001), suggesting an uninflamed phenotype with immunological ignorance (22). Although a significant number of PD-1 positive CD8+ T cells were found in the ALK-positive tumor bed in early lung adenocarcinoma (64), these PD-1 expressing CD8+ T cells were functionally impaired (65) and did not express interferon-γ mRNA, which could upregulate PD-L1 expression in tumor cells (66, 67). These results indicate that the ALK-positive TME suppresses the immune function of CD8+ TILs through a PD-1/PD-L1 independent mechanism, which might lead to the inability of ALK-positive tumors to respond to PD-1/PD-L1-based immunotherapy (64). Tumor mutational burden (TMB) is an effective marker for predicting the efficacy of ICI treatment. The median TMB of ALK-positive tumor samples is only 2.29 mutations/Mb (ranging from 0.76 to 16.79 mutations/Mb) (68). The TMB (in mutations/Mb) of NSCLC patients with alteration in ALK is significantly lower than in those without (2.1 vs 7.0 mutations/Mb; P < 0.001) (69). These results suggest that the limited benefits of ICI monotherapy are attributable to the low levels of functional CD8+ TILs and TMB.

ICIs combined with ALK tyrosine kinase inhibitors (ALK-TKIs)

A preclinical study showed that *in vitro* application of ceritinib combined with a PD-L1 inhibitor in the treatment of ALK-rearranged NSCLC promotes lymphocyte proliferation and activation, inhibits PD-L1 expression, and enhances lymphocyte cytotoxicity and cell death. In the *in vivo* xenograft model, tumor volumes treated with a combination of ceritinib and a PD-L1 inhibitor (91.9%) are significantly smaller than those treated with ceritinib (84.9%) or PD-L1 (20.0%) alone (70). Some clinical trials have explored the use of ICIs in combination with ALK inhibitors (71, 72). The primary study was a phase 1/2 study (CheckMate 370) on the safety and tolerability of nivolumab plus crizotinib (first-generation ALK inhibitor) as a first-line treatment for patients with advanced ALK+ NSCLC. The high proportion (38%) of severe hepatotoxicity caused the trial to close prematurely and fail (73). Another phase Ib study evaluated the safety and preliminary antitumor activity of crizotinib plus pembrolizumab (PD-1 inhibitor) as a first-line therapy in patients with ALK+ NSCLC. Although this combination showed antitumor activity, the incidence of dose-limiting toxicities is high, especially with a higher frequency of severe transaminase level increase. Because the study was terminated early, the recommended phase II dose could not be determined (74). Therefore, for a well-designed trial, selecting a suitable combination of partner and treatment population is extremely important. Felip et al. (75) presented the results of a phase Ib trial examining ceritinib plus nivolumab in previously treated or treatment-naive ALK+ NSCLC. This combination appears to elicit activity, and high PD-L1 expression may be enriched in patients more likely to respond. Based on more toxicity findings, especially rash, a protocol amendment to switch to sequential treatment is being investigated in which ceritinib is administered as monotherapy for two cycles before combining it with

nivolumab. Two additional phase Ib studies presented at ASCO meeting show promising efficacy and acceptable safety profile of this sequential therapy. In previously treated ALK+ NSCLC, the combination of avelumab (anti-PD-L1) and lorlatinib (third-generation ALK inhibitor) showed no dose-limiting toxicity (76). In treatment-naive ALK+ NSCLC, alectinib (second-generation ALK inhibitor) should be administered 1 week prior to combination with atezolizumab (PD-L1 inhibitor). The objective response rate was 81% (95% CI 58.1–94.6), with a median PFS of 21.7 months and a median DOR of 20.3 months (77). In addition, Chalmers et al. presented a phase I trial of a combination of ipilimumab (a CTLA-4 inhibitor) and crizotinib in ALK+ NSCLC. The median PFS and overall survival (OS) were prolonged, but owing to the small number of enrolled cases (three cases), continued observation was necessary (78). Although a particularly large advantage in ORR was not observed in most combination therapies, given the long-term benefits of ICIs treatment, it remains to be seen whether PFS and OS outcomes can be prolonged in the future.

ICIs combined with anti-angiogenesis therapy

In the IMpower130 study, for ALK inhibitor-pretreated patients with ALK-sensitizing alterations, atezolizumab plus chemotherapy did not show improved overall survival versus chemotherapy alone (79). However, data from the IMpower150 study showed that the addition of atezolizumab to bevacizumab (angiogenesis inhibitor) plus chemotherapy resulted in significant improvements in PFS and OS (80). In IMpower150, the median PFS for patients with EGFR+/ALK+ status in the atezolizumab plus bevacizumab and chemotherapy (ABCP) group was 9.7 months compared with the PFS of 6.1 months in the bevacizumab plus chemotherapy (BCP) group (HR 0.59, 95% CI, 0.37–0.94). OS data were immature (not reached vs. 17.5 months; HR, 0.54; 95% 0.29–1.03). The 6- and 12-month PFS rates in the ABCP group were 65% and 37%, respectively, compared to 53% and 21% in the BCP group (80, 81). Therefore, after ALK inhibitor resistance, ABCP may be the first choice for patients with ALK+ NSCLC who are still capable of tolerating intensive therapy. The combination of ICIs and anti-vascular endothelial growth factor (VEGF) agents has significantly improved clinical outcomes in a variety of tumors compared with standard treatments (82). Multiple studies have further analyzed the synergistic mechanism between angiogenic factors such as VEGF and PD-(L)1 inhibitors, which is attributed to VEGF-mediated immunosuppression in the TME (83, 84). In addition to inducing vascular abnormalities, angiogenic factors also suppress antigen presentation and immune effector cells or augment the immunosuppressive activity of regulatory T cells, myeloid-derived suppressor cells, and tumor-associated macrophages (85–88). In the PI3K/AKT/mTOR pathway, ALK signaling promotes VEGF expression in tumors, which might enhance the sensitivity of ALK+ patients to bevacizumab (89). In ALK+ patients, CD8+ T cell tumor infiltration decreases (84) and regulatory T cells increase (90) after ALK inhibitor treatment, which induces a lower response rate to ICIs. In several clinical biomarker studies, the combination of bevacizumab and atezolizumab has been proven to overcome ICIs resistance by reversing VEGF-mediated immunosuppression and promoting CD8+ TIL in tumors (91–93). There are also reports that bevacizumab combined with targeted therapy can overcome ALK inhibitor resistance (94, 95). A recent study showed that VEGFR2 inhibition, a promising treatment strategy for oncogene-driven NSCLC, not only inhibits tumor angiogenesis but also exerts direct antiproliferative effects on cancer cells (96). In summary, it can be inferred that ICIs combined with anti-angiogenesis may be a promising treatment method.

ALK vaccine

Owing to the characteristics of ALK expression in the body, it has long been considered a potential tumor-associated antigen (TAA) (97). There are immunogenic regions located in the ALK kinase domain that can trigger specific T cell responses restricted by HLA alleles (98, 99). These findings provide a basis for peptide vaccine immunotherapy for ALK-driven tumors.

Using an ALK+ ALCL mouse model, Chiarle et al. showed that DNA vaccines with plasmids encoding a part of the ALK cytoplasmic domain elicit ALK-specific interferon-gamma responses and CD8+ T cell-mediated cytotoxicity. The combination of chemotherapy and ALK DNA vaccination significantly enhances the survival of mice challenged with ALK + lymphomas (100). In mouse models of ALK+ NSCLC, this ALK DNA vaccine induced strong systemic and intratumoral immune responses, significantly reducing tumor growth and extending the survival of treated mice. The combination of this vaccine and ALK TKI is also effective and significantly delayed tumor relapse after TKI treatment. In addition, immunotherapies, such as anti-PD-1/PD-L1 or anti-CTLA, can be used to enhance the benefits of ALK TKI and ALK vaccine combination therapy (101). Another ALK vaccine is based on ALK-overlapping peptides in splenocytes from ALK-vaccinated mice. The vaccine significantly delayed the progression of primary lung tumors in EML4-ALK transgenic mice (102). One of the technologies under study is the use of stabilized multilamellar lipid vesicles with cross-linked lipid bilayers containing an antigenic ALK variant. They can deliver antigens alone in the presence of adjuvants to form an efficient vaccine for ALK-positive glioblastomas (103). Recently, an *in vitro* test applied a novel anti-epidermal growth factor vaccine (anti-EGF VacAbs) in ALK+ NSCLC cell lines. The anti-EGF VacAbs target the B-cells to generate antibodies that neutralize circulating EGF, thus preventing its binding to EGFR. They potentiate the antitumor effects of ALK-TKIs, significantly enhancing the blockade of downstream oncogenic activation pathways, and delaying the emergence of resistance (104). These experimental results provide a powerful strategy for the treatment of ALK-

driven tumors. With the continuous progress in its research, ALK vaccines will soon enter clinical trials.

CAR-T cells & TCR-T cells

T cells engineered to express chimeric antigen receptors (CARs) have demonstrated significant activity against many tumors, and CAR-T cells have recently joined a rapidly growing repertoire of immunotherapeutics. Because ALK fusion protein is mainly expressed inside the cell, CAR-T therapy targeting ALK is currently mainly tested in neuroblastoma. It has been found that T cells expressing a CAR incorporating the single-chain variable fragment against the ALK extracellular domain lyse ALK-positive neuroblastoma cell lines. However, CAR functionality is regulated by target antigen and CAR density, and low expression of either contributes to the limited anti-tumor efficacy of ALK CAR-T (105, 106). More specific immunotherapies targeting ALCL surface markers include anti-CD30 CAR-T cells. CD30-specific CAR-T cells have been tested in mouse models and clinical trials have been initiated (107). In one case report, a patient with relapsed ALK+ ALCL achieved remission after CD30-specific CAR-T cell treatment (108). Another trial under investigation is the induction of an immunologic response in a tumor patient using mature dendritic cells transfected with a nucleic acid composition encoding NPM-ALK as a tumor antigen and loaded with a corresponding tumor antigen composition (103).

With the revolutionary breakthroughs in the field of TCR therapy in recent years, an increasing number of ALK epitopes/peptides may become suitable targets for directed immunotherapy (109, 110). An ongoing study is screening for autologous or allogeneic T cell receptor-transgenic T cells to test against ALK+/- patient-derived and cancer cell lines using *in vitro* and *in vivo* models to assess the potential utility of cytotoxic TCR-directed immunotherapies (111).

Conclusion and prospects

In summary, ALK variants play an important role in a variety of tumors, including both hematological and solid tumors. The development and application of ALK inhibitors have made outstanding contributions to the treatment of ALK + tumor patients, and it is still the main choice for first-line treatment (112). However, to date, resistance to ALK inhibitors has proven unavoidable in all cases (113). For TKIs resistant patients, the exploration of immunotherapy is currently a promising treatment direction. According to the special immunosuppressive microenvironment of ALK+ tumors, there are still huge challenges in the development and application of immunotherapeutic interventions. Based on the results of current clinical studies, ICIs monotherapy is not the preferred treatment option for TKI-resistant patients. We urgently need to explore better combined treatment options to change tumor immunosuppression to control tumors (114), such as immunotherapy combined with targeted therapy or anti-angiogenesis therapy. Nevertheless, there are still many obstacles in the process of exploration, including the understanding of the specific effects of ALK on the immune microenvironment and development of novel immunotherapy methods. Numerous studies are exploring new treatments and ways to optimize the application of immunotherapy, which may lead to greater survival benefits for the patients (Table 2).

Author contributions

YG carried out the primary literature search, drafted and revised the manuscript. HG and YZ helped modify the manuscript and participated in discussions. JC conceived and approved the final manuscript. All authors contributed to the article and approved the submitted version.

Funding

This work was supported by the National Natural Science Foundation of China (No. 81874052) and Jilin Scientific and Technological Development Program (CN) (No. 20190303146SF).

Conflict of interest

The authors declare that the research was conducted in the absence of any commercial or financial relationships that could be construed as a potential conflict of interest.

Publisher's note

References

1. Chiarle R, Voena C, Ambrogio C, Piva R, Inghirami G. The anaplastic lymphoma kinase in the pathogenesis of cancer. *Nat Rev Cancer* (2008) 8(1):11–23. doi: 10.1038/nrc2291

2. Hallberg B, Palmer RH. The role of the alk receptor in cancer biology. *Ann Oncol* (2016) 27 Suppl 3:iii4–iii15. doi: 10.1093/annonc/mdw301

3. Cao Z, Gao Q, Fu M, Ni N, Pei Y, Ou WB. Anaplastic lymphoma kinase fusions: Roles in cancer and therapeutic perspectives. *Oncol Lett* (2019) 17 (2):2020–30. doi: 10.3892/ol.2018.9856

4. Hallberg B, Palmer RH. Mechanistic insight into alk receptor tyrosine kinase in human cancer biology. *Nat Rev Cancer* (2013) 13(10):685–700. doi: 10.1038/nrc3580

5. Cameron LB, Hitchen N, Chandran E, Morris T, Manser R, Solomon BJ, et al. Targeted therapy for advanced anaplastic lymphoma kinase (Alk)-rearranged non-small cell lung cancer. *Cochrane Database Syst Rev* (2022) 1:CD013453. doi: 10.1002/14651858.CD013453.pub2

6. Mazieres J, Drilon A, Lusque A, Mhanna L, Cortot AB, Mezquita L, et al. Immune checkpoint inhibitors for patients with advanced lung cancer and oncogenic driver alterations: Results from the immunotarget registry. *Ann Oncol* (2019) 30(8):1321–8. doi: 10.1093/annonc/mdz167

7. Sankar K, Nagrath S, Ramnath N. Immunotherapy for alk-rearranged non-small cell lung cancer: Challenges inform promising approaches. *Cancers* (2021) 13 (6):1467. doi: 10.3390/cancers13061476

8. Lemmon MA, Schlessinger J. Cell signaling by receptor tyrosine kinases. *Cell* (2010) 141(7):1117–34. doi: 10.1016/j.cell.2010.06.011

9. Mao R, Zhang X, Kong Y, Wu S, Huo HQ, Kong Y, et al. Transcriptome regulation by oncogenic alk pathway in mammalian cortical development revealed by single-cell rna sequencing. *Cereb Cortex* (2021) 31(8):3911–24. doi: 10.1093/cercor/bhab058

10. Roskoski RJr. Anaplastic lymphoma kinase (Alk): Structure, oncogenic activation, and pharmacological inhibition. *Pharmacol Res* (2013) 68(1):68–94. doi: 10.1016/j.phrs.2012.11.007

11. Reshetnyak AV, Rossi P, Myasnikov AG, Sowaileh M, Mohanty J, Nourse A, et al. Mechanism for the activation of the anaplastic lymphoma kinase receptor. *Nature* (2021) 600(7887):153–7. doi: 10.1038/s41586-021-04140-8

12. Zeng L, Kang R, Zhu S, Wang X, Cao L, Wang H, et al. Alk is a therapeutic target for lethal sepsis. *Sci Transl Med* (2017) 9(412):eaan5689. doi: 10.1126/scitranslmed.aan5689

13. Damm-Welk C, Siddiqi F, Fischer M, Hero B, Narayanan V, Camidge DR, et al. Anti-alk antibodies in patients with alk-positive malignancies not expressing npm-alk. *J Cancer* (2016) 7(11):1383–7. doi: 10.7150/jca.15238

14. Glorieux C, Xia X, Huang P. The role of oncogenes and redox signaling in the regulation of pd-L1 in cancer. *Cancers* (2021) 13(17):4426. doi: 10.3390/cancers13174426

15. Wang L, Lui VWY. Emerging roles of alk in immunity and insights for immunotherapy. *Cancers* (2020) 12(2):4426. doi: 10.3390/cancers12020426

16. Bisig B, de Reynies A, Bonnet C, Sujobert P, Rickman DS, Marafioti T, et al. Cd30-positive peripheral T-cell lymphomas share molecular and phenotypic features. *Haematologica* (2013) 98(8):1250–8. doi: 10.3324/haematol.2012.081935

17. Malcolm TI, Villarese P, Fairbairn CJ, Lamant L, Trinquand A, Hook CE, et al. Anaplastic Large cell lymphoma arises in thymocytes and requires transient tcr expression for thymic egress. *Nat Commun* (2016) 7:10087. doi: 10.1038/ncomms10087

18. Passoni L, Scardino A, Bertazzoli C, Gallo B, Coluccia AM, Lemonnier FA, et al. Alk as a novel lymphoma-associated tumor antigen: Identification of 2 hla-A2.1-Restricted Cd8+ T-cell epitopes. *Blood* (2002) 99(6):2100–6. doi: 10.1182/blood.v99.6.2100

19. Passoni L, Gallo B, Biganzoli E, Stefanoni R, Massimino M, Di Nicola M, et al. *In vivo* T-cell immune response against anaplastic lymphoma kinase in patients with anaplastic Large cell lymphomas. *Haematologica* (2006) 91(1):48–55.

20. Ait-Tahar K, Barnardo MC, Pulford K. Cd4 T-helper responses to the anaplastic lymphoma kinase (Alk) protein in patients with alk-positive anaplastic Large-cell lymphoma. *Cancer Res* (2007) 67(5):1898–901. doi: 10.1158/0008-5472.CAN-06-4427

21. Congras A, Hoareau-Aveilla C, Caillet N, Tosolini M, Villarese P, Cieslak A, et al. Alk-transformed mature T lymphocytes restore early thymus progenitor features. *J Clin Invest* (2020) 130(12):6395–408. doi: 10.1172/JCI134990

22. Jin R, Liu C, Zheng S, Wang X, Feng X, Li H, et al. Molecular heterogeneity of anti-Pd-1/Pd-L1 immunotherapy efficacy is correlated with tumor immune microenvironment in East Asian patients with non-small cell lung cancer. *Cancer Biol Med* (2020) 17(3):768–81. doi: 10.20892/j.issn.2095-3941.2020.0121

23. Janik JE, Morris JC, Pittaluga S, McDonald K, Raffeld M, Jaffe ES, et al. Elevated serum-soluble interleukin-2 receptor levels in patients with anaplastic Large cell lymphoma. *Blood* (2004) 104(10):3355–7. doi: 10.1182/blood-2003-11-3922

24. Matsuyama H, Suzuki HI, Nishimori H, Noguchi M, Yao T, Komatsu N, et al. Mir-135b mediates npm-Alk-Driven oncogenicity and renders il-17-Producing immunophenotype to anaplastic Large cell lymphoma. *Blood* (2011) 118(26):6881–92. doi: 10.1182/blood-2011-05-354654

25. Yu L, Yan LL, Yang SJ. Sarcomatoid variant of alk- anaplastic Large cell lymphoma involving multiple lymph nodes and both lungs with production of proinflammatory cytokines: Report of a case and review of literature. *Int J Clin Exp Pathol* (2014) 7(8):4806–16.

26. Knorr F, Damm-Welk C, Ruf S, Singh VK, Zimmermann M, Reiter A, et al. Blood cytokine concentrations in pediatric patients with anaplastic lymphoma kinase-positive anaplastic Large cell lymphoma. *Haematologica* (2018) 103(3):477–85. doi: 10.3324/haematol.2017.177972

27. Qiu L, Lai R, Lin Q, Lau E, Thomazy DM, Calame D, et al. Autocrine release of interleukin-9 promotes Jak3-dependent survival of alk+ anaplastic Large-cell lymphoma cells. *Blood* (2006) 108(7):2407–15. doi: 10.1182/blood-2006-04-020305

28. Bard JD, Gelebart P, Anand M, Amin HM, Lai R. Aberrant expression of il-22 receptor 1 and autocrine il-22 stimulation contribute to tumorigenicity in alk+ anaplastic Large cell lymphoma. *Leukemia* (2008) 22(8):1595–603. doi: 10.1038/leu.2008.129

29. Marzec M, Zhang Q, Goradia A, Raghunath PN, Liu X, Paessler M, et al. Oncogenic kinase Npm/Alk induces through Stat3 expression of immunosuppressive protein Cd274 (Pd-L1, B7-H1). *Proc Natl Acad Sci USA* (2008) 105(52):20852–7. doi: 10.1073/pnas.0810958105

30. Iqbal J, Wright G, Wang C, Rosenwald A, Gascoyne RD, Weisenburger DD, et al. Gene expression signatures delineate biological and prognostic subgroups in peripheral T-cell lymphoma. *Blood* (2014) 123(19):2915–23. doi: 10.1182/blood-2013-11-536359

31. Liu C, Yang L, Xu H, Zheng S, Wang Z, Wang S, et al. Systematic analysis of il-6 as a predictive biomarker and desensitizer of immunotherapy responses in patients with non-small cell lung cancer. *BMC Med* (2022) 20(1):187. doi: 10.1186/s12916-022-02356-7

32. Trinchieri G. Interleukin-10 production by effector T cells: Th1 cells show self control. *J Exp Med* (2007) 204(2):239–43. doi: 10.1084/jem.20070104

33. Li Z, Wang YJ, Zhou J, Umakoshi M, Goto A. The prognostic role of M2 tumor-associated macrophages in non-Small-Cell lung cancer. *Histol Histopathol* (2022), 18474. doi: 10.14670/HH-18-474

34. Cannarile MA, Weisser M, Jacob W, Jegg AM, Ries CH, Ruttinger D. Colony-stimulating factor 1 receptor (Csf1r) inhibitors in cancer therapy. *J Immunother Cancer* (2017) 5(1):53. doi: 10.1186/s40425-017-0257-y

35. Budczies J, Kirchner M, Kluck K, Kazdal D, Glade J, Allgauer M, et al. Deciphering the immunosuppressive tumor microenvironment in alk- and egfr-positive lung adenocarcinoma. *Cancer Immunol Immunother* (2022) 71(2):251–65. doi: 10.1007/s00262-021-02981-w

36. Zhang B, Wei W, Qiu J. Alk is required for Nlrp3 inflammasome activation in macrophages. *Biochem Biophys Res Commun* (2018) 501(1):246–52. doi: 10.1016/j.bbrc.2018.04.226

37. Martinenaite E, Munir Ahmad S, Hansen M, Met O, Westergaard MW, Larsen SK, et al. Ccl22-specific T cells: Modulating the immunosuppressive tumor microenvironment. *Oncoimmunology* (2016) 5(11):e1238541. doi: 10.1080/2162402X.2016.1238541

38. Zou W. Regulatory T cells, tumour immunity and immunotherapy. *Nat Rev Immunol* (2006) 6(4):295–307. doi: 10.1038/nri1806

39. Panjwani PK, Charu V, DeLisser M, Molina-Kirsch H, Natkunam Y, Zhao S. Programmed death-1 ligands pd-L1 and pd-L2 show distinctive and restricted patterns of expression in lymphoma subtypes. *Hum Pathol* (2018) 71:91–9. doi: 10.1016/j.humpath.2017.10.029

40. Andorsky DJ, Yamada RE, Said J, Pinkus GS, Betting DJ, Timmerman JM. Programmed death ligand 1 is expressed by non-Hodgkin lymphomas and inhibits the activity of tumor-associated T cells. *Clin Cancer Res* (2011) 17(13):4232–44. doi: 10.1158/1078-0432.CCR-10-2660

41. Zhang JP, Song Z, Wang HB, Lang L, Yang YZ, Xiao W, et al. A novel model of controlling pd-L1 expression in alk(+) anaplastic Large cell lymphoma revealed by crispr screening. *Blood* (2019) 134(2):171–85. doi: 10.1182/blood.2019001043

42. Shen J, Li S, Medeiros LJ, Lin P, Wang SA, Tang G, et al. Pd-L1 expression is associated with alk positivity and Stat3 activation, but not outcome in patients with systemic anaplastic Large cell lymphoma. *Mod Pathol* (2020) 33(3):324–33. doi: 10.1038/s41379-019-0336-3

43. D'Incecco A, Andreozzi M, Ludovini V, Rossi E, Capodanno A, Landi L, et al. Pd-1 and pd-L1 expression in molecularly selected non-Small-Cell lung cancer patients. *Br J Cancer* (2015) 112(1):95–102. doi: 10.1038/bjc.2014.555

44. Ota K, Azuma K, Kawahara A, Hattori S, Iwama E, Tanizaki J, et al. Induction of pd-L1 expression by the Eml4-alk oncoprotein and downstream signaling pathways in non-small cell lung cancer. *Clin Cancer Res* (2015) 21 (17):4014–21. doi: 10.1158/1078-0432.CCR-15-0016

45. Yoneshima Y, Ijichi K, Anai S, Ota K, Otsubo K, Iwama E, et al. Pd-L1 expression in lung adenocarcinoma harboring egfr mutations or alk rearrangements. *Lung Cancer* (2018) 118:36–40. doi: 10.1016/j.lungcan.2018.01.024

46. Ma L, Lv J, Dong Y, Zhang X, Li X, Zhang H, et al. Pd-L1 expression and its regulation in lung adenocarcinoma with alk translocation. *Interdiscip Sci* (2019) 11 (2):266–72. doi: 10.1007/s12539-019-00331-0

47. Koh J, Jang JY, Keam B, Kim S, Kim MY, Go H, et al. Eml4-alk enhances programmed cell death-ligand 1 expression in pulmonary adenocarcinoma *Via* hypoxia-inducible factor (Hif)-1alpha and Stat3. *Oncoimmunology* (2016) 5(3): e1108514. doi: 10.1080/2162402X.2015.1108514

48. Hu ZY, Huang WY, Zhang L, Huang B, Chen SC, Li XL. Expression of akt and p-akt protein in lung adenocarcinoma and its correlation with pd-L1 protein and prognosis. *Ann Transl Med* (2020) 8(18):1172. doi: 10.21037/atm-20-5865

49. Sumimoto H, Takano A, Teramoto K, Daigo Y. Ras-Mitogen-Activated protein kinase signal is required for enhanced pd-L1 expression in human lung cancers. *PLoS One* (2016) 11(11):e0166626. doi: 10.1371/journal.pone.0166626

50. Lamberti G, Sisi M, Andrini E, Palladini A, Giunchi F, Lollini PL, et al. The mechanisms of pd-L1 regulation in non-Small-Cell lung cancer (Nsclc): Which are the involved players? *Cancers* (2020) 12(11):3129. doi: 10.3390/cancers12113129

51. Nouri K, Azad T, Lightbody E, Khanal P, Nicol CJ, Yang X. A kinome-wide screen using a nanoluc lats luminescent biosensor identifies alk as a novel regulator of the hippo pathway in tumorigenesis and immune evasion. *FASEB J* (2019) 33 (11):12487–99. doi: 10.1096/fj.201901343R

52. Kim SJ, Kim S, Kim DW, Kim M, Keam B, Kim TM, et al. Alterations in pd-L1 expression associated with acquisition of resistance to alk inhibitors in alk-rearranged lung cancer. *Cancer Res Treat* (2019) 51(3):1231–40. doi: 10.4143/crt.2018.486

53. Hong S, Chen N, Fang W, Zhan J, Liu Q, Kang S, et al. Upregulation of pd-L1 by Eml4-alk fusion protein mediates the immune escape in alk positive nsclc: Implication for optional anti-Pd-1/Pd-L1 immune therapy for alk-tkis sensitive and resistant nsclc patients. *Oncoimmunology* (2016) 5(3):e1094598. doi: 10.1080/2162402X.2015.1094598

54. Xie W, Medeiros LJ, Li S, Yin CC, Khoury JD, Xu J. Pd-1/Pd-L1 pathway and its blockade in patients with classic Hodgkin lymphoma and non-Hodgkin Large-cell lymphomas. *Curr Hematol Malig Rep* (2020) 15(4):372–81. doi: 10.1007/s11899-020-00589-y

55. Borghaei H, Paz-Ares L, Horn L, Spigel DR, Steins M, Ready NE, et al. Nivolumab versus docetaxel in advanced nonsquamous non-Small-Cell lung cancer. *N Engl J Med* (2015) 373(17):1627–39. doi: 10.1056/NEJMoa1507643

56. Peters S, Gettinger S, Johnson ML, Janne PA, Garassino MC, Christoph D, et al. Phase ii trial of atezolizumab as first-line or subsequent therapy for patients with programmed death-ligand 1-selected advanced non-Small-Cell lung cancer (Birch). *J Clin Oncol* (2017) 35(24):2781–9. doi: 10.1200/JCO.2016.71.9476

57. Riudavets M, Auclin E, Mosteiro M, Dempsey N, Majem M, Lobefaro R, et al. Durvalumab consolidation in patients with unresectable stage III non-small cell lung cancer with driver genomic alterations. *Eur J Cancer* (2022) 167:142–8. doi: 10.1016/j.ejca.2022.02.014

58. Xin Yu J, Hodge JP, Oliva C, Neftelinov ST, Hubbard-Lucey VM, Tang J. Trends in clinical development for pd-1/Pd-L1 inhibitors. *Nat Rev Drug Discov* (2020) 19(3):163–4. doi: 10.1038/d41573-019-00182-w

59. Garassino MC, Cho BC, Kim JH, Mazières J, Vansteenkiste J, Lena H, et al. Durvalumab as third-line or later treatment for advanced non-Small-Cell lung cancer (Atlantic): An open-label, single-arm, phase 2 study. *Lancet Oncol* (2018) 19 (4):521–36. doi: 10.1016/s1470-2045(18)30144-x

60. Baldacci S, Gregoire V, Patrucco E, Chiarle R, Jamme P, Wasielewski E, et al. Complete and prolonged response to anti-Pd1 therapy in an alk rearranged lung adenocarcinoma. *Lung Cancer* (2020) 146:366–9. doi: 10.1016/j.lungcan.2020.05.008

61. Hebart H, Lang P, Woessmann W. Nivolumab for refractory anaplastic Large cell lymphoma: A case report. *Ann Intern Med* (2016) 165(8):607–8. doi: 10.7326/L16-0037

62. Rigaud C, Abbou S, Minard-Colin V, Geoerger B, Scoazec JY, Vassal G, et al. Efficacy of nivolumab in a patient with systemic refractory alk+ anaplastic Large cell lymphoma. *Pediatr Blood Cancer* (2018) 65(4):10.1002/pbc.26902. doi: 10.1002/pbc.26902

63. Gainor JF, Shaw AT, Sequist LV, Fu X, Azzoli CG, Piotrowska Z, et al. Egfr mutations and alk rearrangements are associated with low response rates to pd-1 pathway blockade in non-small cell lung cancer: A retrospective analysis. *Clin Cancer Res* (2016) 22(18):4585–93. doi: 10.1158/1078-0432.CCR-15-3101

64. Zeng C, Gao Y, Xiong J, Lu J, Yang J, Wang X, et al. Tumor-infiltrating Cd8 (+) T cells in alk-positive lung cancer are functionally impaired despite the absence of pd-L1 on tumor cells. *Lung Cancer* (2020) 150:139–44. doi: 10.1016/j.lungcan.2020.10.009

65. Ahmadzadeh M, Johnson LA, Heemskerk B, Wunderlich JR, Dudley ME, White DE, et al. Tumor antigen-specific Cd8 T cells infiltrating the tumor express high levels of pd-1 and are functionally impaired. *Blood* (2009) 114(8):1537–44. doi: 10.1182/blood-2008-12-195792

66. Topalian SL, Taube JM, Anders RA, Pardoll DM. Mechanism-driven biomarkers to guide immune checkpoint blockade in cancer therapy. *Nat Rev Cancer* (2016) 16(5):275–87. doi: 10.1038/nrc.2016.36

67. Garcia-Diaz A, Shin DS, Moreno BH, Saco J, Escuin-Ordinas H, Rodriguez GA, et al. Interferon receptor signaling pathways regulating pd-L1 and pd-L2 expression. *Cell Rep* (2017) 19(6):1189–201. doi: 10.1016/j.celrep.2017.04.031

68. Liu S, Huang T, Liu M, He W, Zhao Y, Yang L, et al. The genomic characteristics of alk fusion positive tumors in Chinese nsclc patients. *Front Oncol* (2020) 10:726. doi: 10.3389/fonc.2020.00726

69. Singal G, Miller PG, Agarwala V, Li G, Kaushik G, Backenroth D, et al. Association of patient characteristics and tumor genomics with clinical outcomes among patients with non-small cell lung cancer using a clinicogenomic database. *JAMA* (2019) 321(14):1391–9. doi: 10.1001/jama.2019.3241

70. Du P, Hu T, An Z, Li P, Liu L. *In vitro* and in vivo synergistic efficacy of ceritinib combined with programmed cell death ligand-1 inhibitor in anaplastic lymphoma kinase-rearranged non-Small-Cell lung cancer. *Cancer Sci* (2020) 111 (6):1887–98. doi: 10.1111/cas.14397

71. Moya-Horno I, Viteri S, Karachaliou N, Rosell R. Combination of immunotherapy with targeted therapies in advanced non-small cell lung cancer (Nsclc). *Ther Adv Med Oncol* (2018) 10:1758834017745012. doi: 10.1177/1758834017745012

72. Patel M, Jabbour SK, Malhotra J. Alk inhibitors and checkpoint blockade: A cautionary tale of mixing oil with water? *J Thorac Dis* (2018) 10(Suppl 18):S2198–S201. doi: 10.21037/jtd.2018.06.118

73. Spigel DR, Reynolds C, Waterhouse D, Garon EB, Chandler J, Babu S, et al. Phase 1/2 study of the safety and tolerability of nivolumab plus crizotinib for the first-line treatment of anaplastic lymphoma kinase translocation - positive advanced non-small cell lung cancer (Checkmate 370). *J Thorac Oncol* (2018) 13 (5):682–8. doi: 10.1016/j.jtho.2018.02.022

74. Patel SP, Pakkala S, Pennell NA, Reckamp KL, Lanzalone S, Polli A, et al. Phase ib study of crizotinib plus pembrolizumab in patients with previously untreated advanced non-small cell lung cancer with alk translocation. *Oncologist* (2020) 25(7):562–e1012. doi: 10.1634/theoncologist.2020-0034

75. Felip E, de Braud FG, Maur M, Loong HH, Shaw AT, Vansteenkiste JF, et al. Ceritinib plus nivolumab in patients with advanced alk-rearranged non-small cell lung cancer: Results of an open-label, multicenter, phase 1b study. *J Thorac Oncol* (2020) 15(3):392–403. doi: 10.1016/j.jtho.2019.10.006

76. Shaw A, Lee S-H, Ramalingam S, Bauer T, Boyer M, Costa E, et al. Avelumab (Anti–Pd-L1) in combination with crizotinib or lorlatinib in patients with previously treated advanced nsclc: Phase 1b results from javelin lung 101. *J Clin Oncol* (2018) 36:9008–. doi: 10.1200/JCO.2018.36.15_suppl.9008

77. Kim D-S, Gadgeel S, Gettinger S, Riely G, Oxnard G, Mekhail T, et al. Safety and clinical activity results from a phase ib study of alectinib plus atezolizumab in alk + advanced nsclc (Ansclc). *J Clin Oncol* (2018) 36:9009–. doi: 10.1200/JCO.2018.36.15_suppl.9009

78. Chalmers AW, Patel S, Boucher K, Cannon L, Esplin M, Luckart J, et al. Phase I trial of targeted egfr or alk therapy with ipilimumab in metastatic nsclc with long-term follow-up. *Target Oncol* (2019) 14(4):417–21. doi: 10.1007/s11523-019-00658-0

79. West H, McCleod M, Hussein M, Morabito A, Rittmeyer A, Conter HJ, et al. Atezolizumab in combination with carboplatin plus nab-paclitaxel chemotherapy compared with chemotherapy alone as first-line treatment for metastatic non-squamous non-small-cell lung cancer (Impower130): A multicentre, randomised, open-label, phase 3 trial. *Lancet Oncol* (2019) 20(7):924–37. doi: 10.1016/S1470-2045(19)30167-6

80. Socinski MA, Jotte RM, Cappuzzo F, Orlandi F, Stroyakovskiy D, Nogami N, et al. Atezolizumab for first-line treatment of metastatic nonsquamous nsclc. *N Engl J Med* (2018) 378(24):2288–301. doi: 10.1056/NEJMoa1716948

81. Dhillon S, Syed YY. Atezolizumab first-line combination therapy: A review in metastatic nonsquamous nsclc. *Target Oncol* (2019) 14(6):759–68. doi: 10.1007/s11523-019-00686-w

82. Hack SP, Zhu AX, Wang Y. Augmenting anticancer immunity through combined targeting of angiogenic and pd-1/Pd-L1 pathways: Challenges and opportunities. *Front Immunol* (2020) 11:598877. doi: 10.3389/fimmu.2020.598877

83. Giannone G, Ghisoni E, Genta S, Scotto G, Tuninetti V, Turinetto M, et al. Immuno-metabolism and microenvironment in cancer: Key players for

immunotherapy. *Int J Mol Sci* (2020) 21(12):4414. doi: 10.3390/ijms21124414

84. Gaissmaier L, Christopoulos P. Immune modulation in lung cancer: Current concepts and future strategies. *Respiration* (2020), 1–27. doi: 10.1159/000510385

85. Fukumura D, Kloepper J, Amoozgar Z, Duda DG, Jain RK. Enhancing cancer immunotherapy using antiangiogenics: Opportunities and challenges. *Nat Rev Clin Oncol* (2018) 15(5):325–40. doi: 10.1038/nrclinonc.2018.29

86. Khan KA, Kerbel RS. Improving immunotherapy outcomes with anti-angiogenic treatments and vice versa. *Nat Rev Clin Oncol* (2018) 15(5):310–24. doi: 10.1038/nrclinonc.2018.9

87. Chen DS, Hurwitz H. Combinations of bevacizumab with cancer immunotherapy. *Cancer J* (2018) 24(4):193–204. doi: 10.1097/PPO.0000000000000327

88. Hegde PS, Wallin JJ, Mancao C. Predictive markers of anti-vegf and emerging role of angiogenesis inhibitors as immunotherapeutics. *Semin Cancer Biol* (2018) 52(Pt 2):117–24. doi: 10.1016/j.semcancer.2017.12.002

89. Karar J, Maity A. Pi3k/Akt/Mtor pathway in angiogenesis. *Front Mol Neurosci* (2011) 4:51. doi: 10.3389/fnmol.2011.00051

90. Pyo KH, Lim SM, Park CW, Jo HN, Kim JH, Yun MR, et al. Comprehensive analyses of immunodynamics and immunoreactivity in response to treatment in alk-positive non-Small-Cell lung cancer. *J Immunother Cancer* (2020) 8(2):e000970. doi: 10.1136/jitc-2020-000970

91. McDermott DF, Huseni MA, Atkins MB, Motzer RJ, Rini BI, Escudier B, et al. Clinical activity and molecular correlates of response to atezolizumab alone or in combination with bevacizumab versus sunitinib in renal cell carcinoma. *Nat Med* (2018) 24(6):749–57. doi: 10.1038/s41591-018-0053-3

92. Reck M, Mok TSK, Nishio M, Jotte RM, Cappuzzo F, Orlandi F, et al. Atezolizumab plus bevacizumab and chemotherapy in non-Small-Cell lung cancer (Impower150): Key subgroup analyses of patients with egfr mutations or baseline liver metastases in a randomised, open-label phase 3 trial. *Lancet Respir Med* (2019) 7(5):387–401. doi: 10.1016/S2213-2600(19)30084-0

93. Shigeta K, Datta M, Hato T, Kitahara S, Chen IX, Matsui A, et al. Dual programmed death receptor-1 and vascular endothelial growth factor receptor-2 blockade promotes vascular normalization and enhances antitumor immune responses in hepatocellular carcinoma. *Hepatology* (2020) 71(4):1247–61. doi: 10.1002/hep.30889

94. Nakasuka T, Ichihara E, Makimoto G, Maeda Y, Kiura K. Primary resistance to alectinib was lost after bevacizumab combined chemotherapy in alk-rearranged lung adenocarcinoma. *J Thorac Oncol* (2019) 14(8):e168–e9. doi: 10.1016/j.jtho.2019.03.009

95. Choudhury NJ, Young RJ, Sellitti M, Miller A, Drilon A. Lorlatinib and bevacizumab activity in alk-rearranged lung cancers after lorlatinib progression. *JCO Precis Oncol* (2020) 4:PO.20.00271. doi: 10.1200/PO.20.00271

96. Watanabe H, Ichihara E, Kayatani H, Makimoto G, Ninomiya K, Nishii K, et al. Vegfr2 blockade augments the effects of tyrosine kinase inhibitors by inhibiting angiogenesis and oncogenic signaling in oncogene-driven non-Small-Cell lung cancers. *Cancer Sci* (2021) 112(5):1853–64. doi: 10.1111/cas.14801

97. Passoni L, Gambacorti-Passerini C. Alk a novel lymphoma-associated tumor antigen for vaccination strategies. *Leuk Lymphoma* (2003) 44(10):1675–81. doi: 10.1080/1042819031000099625

98. Singh VK, Werner S, Schwalm S, Lennerz V, Ruf S, Stadler S, et al. Npm-Alk-Reactive T-cell responses in children and adolescents with npm-alk positive anaplastic Large cell lymphoma. *Oncoimmunology* (2019) 8(9):e1625688. doi: 10.1080/2162402X.2019.1625688

99. KS V, Werner S, Hackstein H, Lennerz V, Reiter A, Wolfel T, et al. Analysis of nucleophosmin-anaplastic lymphoma kinase (Npm-Alk)-Reactive Cd8(+) T cell responses in children with npm-alk(+) anaplastic Large cell lymphoma. *Clin Exp Immunol* (2016) 186(1):96–105. doi: 10.1111/cei.12842

100. Chiarle R, Martinengo C, Mastini C, Ambrogio C, D'Escamard V, Forni G, et al. The anaplastic lymphoma kinase is an effective oncoantigen for lymphoma vaccination. *Nat Med* (2008) 14(6):676–80. doi: 10.1038/nm1769

101. Voena C, Menotti M, Mastini C, Di Giacomo F, Longo DL, Castella B, et al. Efficacy of a cancer vaccine against alk-rearranged lung tumors. *Cancer Immunol Res* (2015) 3(12):1333–43. doi: 10.1158/2326-6066.CIR-15-0089

102. Blasco RBJCIR. Abstract A021: Development of an alk vaccine to treat alk-rearranged non-small cell lung cancers. *Cancer Immunology Research* (2016) 4(11 Supplement):A021–A. doi: 10.1158/2326-6066.IMM2016-A021

103. Kalamatianos T, Denekou D, Stranjalis G, Papadimitriou E. Anaplastic lymphoma kinase in glioblastoma: Detection/Diagnostic methods and therapeutic options. *Recent Pat Anticancer Drug Discov* (2018) 13(2):209–23. doi: 10.2174/1574892813666180115151554

104. Codony-Servat J, Garcia-Roman S, Molina-Vila MA, Bertran-Alamillo J, Viteri S, d'Hondt E, et al. Anti-epidermal growth factor vaccine antibodies increase the antitumor activity of kinase inhibitors in alk and ret rearranged lung cancer cells. *Transl Oncol* (2021) 14(1):100887. doi: 10.1016/j.tranon.2020.100887

105. Babar Khan M, Chakraborty S, Boockvar JA. Use of chimeric antigen receptor T cells as a potential therapeutic for glioblastoma. *Neurosurgery* (2017) 80(5):N33–N4. doi: 10.1093/neuros/nyx105

106. Walker AJ, Majzner RG, Zhang L, Wanhainen K, Long AH, Nguyen SM, et al. Tumor antigen and receptor densities regulate efficacy of a chimeric antigen receptor targeting anaplastic lymphoma kinase. *Mol Ther* (2017) 25(9):2189–201. doi: 10.1016/j.ymthe.2017.06.008

107. Hombach AA, Gorgens A, Chmielewski M, Murke F, Kimpel J, Giebel B, et al. Superior therapeutic index in lymphoma therapy: Cd30(+) Cd34(+) hematopoietic stem cells resist a chimeric antigen receptor T-cell attack. *Mol Ther* (2016) 24(8):1423–34. doi: 10.1038/mt.2016.82

108. Ramos CA, Ballard B, Zhang H, Dakhova O, Gee AP, Mei Z, et al. Clinical and immunological responses after Cd30-specific chimeric antigen receptor-redirected lymphocytes. *J Clin Invest* (2017) 127(9):3462–71. doi: 10.1172/JCI94306

109. Gaissmaier L, Elshiaty M, Christopoulos P. Breaking bottlenecks for the tcr therapy of cancer. *Cells* (2020) 9(9):2095. doi: 10.3390/cells9092095

110. Stauss HJ, Tran MGB. Tcr gene therapy: Challenges, opportunities, and future directions. *Cells* (2020) 9(12):2567. doi: 10.3390/cells9122567

111. Heather JM, Spindler MJ, Cobbold M, Gainor JF, Johnson DS, Hata AN. Anaplastic lymphoma kinase fusions as a target for tcr-directed cellular therapies. *J Immunol* (2020) 204(1 Supplement):239.10–.10.

112. Elsayed M, Christopoulos P. Therapeutic sequencing in alk(+) nsclc. *Pharm (Basel)* (2021) 14(2):80. doi: 10.3390/ph14020080

113. Smolle E, Taucher V, Lindenmann J, Jost PJ, Pichler M. Current knowledge about mechanisms of drug resistance against alk inhibitors in non-small cell lung cancer. *Cancers* (2021) 13(4):699. doi: 10.3390/cancers13040699

114. Seliger B. Combinatorial approaches with checkpoint inhibitors to enhance anti-tumor immunity. *Front Immunol* (2019) 10:999. doi: 10.3389/fimmu.2019.00999

frontiers | Frontiers in Immunology

ORIGINAL RESEARCH
published: 25 July 2022
doi: 10.3389/fimmu.2022.955390

Single-Cell Transcriptomic Analysis Reveals Macrophage–Tumor Crosstalk in Hepatocellular Carcinoma

Yunhe Liu[1†], Lin Zhang[2†], Xinyi Ju[3†], Sheng Wang[1] and Jingbo Qie[1]*

[1] Department of Clinical Laboratory Medicine, Shanghai Fifth People's Hospital, Fudan University and Institute of Biomedical Sciences, Fudan University, Shanghai, China, [2] Center of Emergency and Intensive Care Unit, Jinshan Hospital, Fudan University, Shanghai, China, [3] STEM Club, Pinetree Secondary School, British Columbia, Canada

OPEN ACCESS

Edited by:
Min Xue,
University of California, Riverside,
United States

Reviewed by:
Liu Yang,
Shanghai General Hospital, China
Yu Dong,
Shanghai Jiao Tong University, China

***Correspondence:**
Jingbo Qie
jingboqie@fudan.edu.cn

[†]These authors have contributed equally to this work

Specialty section:
This article was submitted to Cancer Immunity and Immunotherapy, a section of the journal Frontiers in Immunology

Received: 28 May 2022
Accepted: 09 June 2022
Published: 25 July 2022

Citation:
Liu Y, Zhang L, Ju X, Wang S and Qie J (2022) Single-Cell Transcriptomic Analysis Reveals Macrophage–Tumor Crosstalk in Hepatocellular Carcinoma. Front. Immunol. 13:955390. doi: 10.3389/fimmu.2022.955390

As one of the most malignant cancer, hepatocellular carcinoma (HCC) has a complex ecosystem featured by high heterogeneity. Cell crosstalk is demonstrated to be critical for HCC development. However, the cell communication orchestration in HCC remains largely unknown. Here, by analyzing the single-cell transcriptomes of the primary tumor tissues (n = 10) and tumor-adjacent tissues (n = 8) derived from 10 patients with HCC, we found that the proportions of plasmacytoid dendritic cells (pDCs) and natural killer (NK) cells were reduced and that the proportion of macrophages was increased in the immune component of the primary tumor, compared with those in the tumor-adjacent tissue. Furthermore, we found widespread communication between macrophage populations and other cell types, and this communication was remarkably strengthened in the primary tumor, especially with HCC malignant cells. In addition, the SPP1–CD44 axis was identified as a unique interaction between macrophages and HCC malignant cells. Our comprehensive portrait of cell communication patterns over the HCC ecosystem reveals further insights into immune infiltration.

Keywords: hepatocellular carcinoma, crosstalk, single-cell, CellPhoneDB, interaction

INTRODUCTION

As one of the most malignant cancer, hepatocellular carcinoma (HCC) has a complex ecosystem featured by high heterogeneity (1). A thorough exploration of hepatocarcinogenesis could contribute to the illustration of mechanisms participating in HCC development and help in the exploration of effective treatment strategies for HCC.

HCC is a complex ecosystem featured by complex cell–cell communications among different heterogeneous cell types (2). The development of tumor cells for coordinated cell crosstalk patterns in the unique ecosystem. Compared with other types of cancer, HCC is strongly dependent on the immune cells' account and activity in its ecosystem (3). Thus, comprehensively exploring the states of the immune cells in the HCC ecosystem or HCC microenvironment becomes vital for immunotherapeutic strategies as well as the identification of new biomarkers of HCC. The tumor microenvironment (TME) consists of heterogeneous immune component mixtures (4, 5). With the development of HCC, a large number of immune cells transfer to the liver, interact with stromal cells, and establish an active immune environment, which can affect the progress of HCC. Therefore, it is of great significance to illustrate the composition and state of immune cells during hepatocarcinogenesis.

Due to the high heterogeneity of HCC, it remains mostly intractable to existing treatments (6). Most of the current omics technologies take the tissue blocks as the research object, resulting in the loss of important data on cell–cell communication (3). Single-cell RNA sequencing (scRNA-seq), as an emerging omics technology, can be used to study single-cell expression patterns in bulk pathological tissue, making it possible to study the relationship between the microenvironment crosstalk and the state of the diseases. Increasing studies have reported the state of cell–cell communication in TME using scRNA-seq (7–12). However, most studies focused on tumor cells' heterogeneity in HCC (13–16). A comprehensive depiction of cell crosstalk (or cell–cell communication) in HCC remains lacking.

In our study, we explored the cell crosstalk and TME in HCC by systematically analyzing the scRNA-seq dataset, GSE149614. It was demonstrated that the proportions of plasmacytoid dendritic cells (pDCs) and natural killer (NK) cells were reduced and that the proportion of macrophages was increased in the immune component of HCC, compared with those in tumor-adjacent tissues. Furthermore, we found macrophages widely communicated with the other types of cells, and this communication was remarkably strengthened in HCC, especially with HCC malignant cells. In addition, the SPP1–CD44 axis was identified as a unique interaction between macrophages and HCC malignant cells. Our findings highlighted the dynamic immune response alteration of macrophages in HCC, suggesting novel immunotherapeutic strategies against this disease.

MATERIALS AND METHODS

Single-Cell RNA Sequencing Data Processing

The scRNA-Seq Dataset of GSE149614 was obtained from the Gene Expression Omnibus (GEO) database. Cells that have <500 or >5,000 detected genes and contain mitochondrial genome >5% of total unique molecular identifiers (UMIs) were deleted. A total of 23,225 tumor-adjacent tissue cells and 22,677 HCC tissue cells were included. Considering the processing operation differences between the adjacent-tumor tissue and the tumor tissue before sequencing, the integration function based on the mutual nearest neighbors (MNNs) (17) algorithm provided by Seurat software (version 3.1.1) was used to remove the batch effect between the two datasets. Specifically, the adjacent-tumor data were used as the reference dataset, the FindAnchors function was used to find the nearest neighbor between the two datasets, and the IntegrateData function was used to remove the batch differences between the two datasets and merge them. The use of the Seurat software was continued for clustering operations. First, the merged data were normalized, and the top 2,000 variable genes were hunted for principal component analysis (PCA) dimensionality reduction (dim = 30). After that, the FindNeighbors function (principle component dim = 30) was used to construct the cell nearest neighbor network, and finally, the FindClusters function was used to perform community-based clustering of cells (Louvain; resolution = 0.5). Cell distribution was visualized by the uniform manifold approximation and projection (UMAP) method. All clusters were manually annotated according to the previous report (18).

Deferentially Expressed Genes in Specified Cell Types

To analyze the functional alteration of specified cell types, differentially expressed genes (DEGs) were obtained by FindMarkers function in Seurat (18) with fold changes ≥1.25 and *adjusted* $p < 0.05$. The volcano plot was generated by GraphPad 8.

Cell Crosstalk Analysis

CellPhoneDB (19) is a public database of receptor–ligand interactions. Here, CellPhoneDB (version 2.1.1) was utilized to explore the crosstalk of cell subtypes in HCC. The calculation of the mean value and p-value was defined by CellPhoneDB (**Table S1**). The correlation intensions between specified cell types were shown as the total mean and the number of interactions.

Definition of Macrophage Scores

To assign M1/M2 polarization estimates to macrophage cells, Gene Set Variation Analysis (GSVA) was applied using standard settings, as implemented in the GSVA package (20). The gene sets associated with the above functions were described by Azizi et al. (10) (**Table S2**).

Gene Ontology and Kyoto Encyclopedia of Genes and Genomes Pathway Functional Enrichment Analyses

Gene Ontology (GO) annotation and Kyoto Encyclopedia of Genes and Genomes (KEGG) analyses were performed and visualized using clusterProfiler and ggplot2 R package, respectively (19).

Protein–Protein Interaction Network Construction

The DEGs were mapped to the STRING database (http://strin g-db.org) to assess protein–protein interaction (PPI) within HCC

tissue (21). The PPI network was constructed using Cytoscape software (version 3.6.0).

Validation of Differential Expression of Selected Genes

To validate the expression of selected genes between tumor-adjacent tissues and HCC tissues, HCC patient's gene expression data (fragments per kilobase of transcript per million mapped reads (FPKM) processed, n = 421, including 50 normal tissues and 371 HCC tissues) from The Cancer Genome Atlas Liver Hepatocellular Carcinoma (TCGA-LIHC) database (https://xenabrowser.net/datapages/) and the Human Protein Atlas (HPA) database (https://www.proteinatlas.org/, for protein expression) (22) were used in our study.

Survival Analysis

For survival analysis, the survival data (n = 368) were downloaded from TCGA-LIHC database (https://xenabrowser.net/datapages/). The Kaplan–Meier survival curves were visualized by GraphPad 8, and the survival difference between groups was tested by a log-rank test (23).

RESULTS

Landscape of the Cell Composition in Non-Tumor and Tumor Tissues

The scRNA-Seq dataset of GSE149614 was obtained from the GEO database. After data processing, 23,225 cells from tumor-adjacent tissues (control, n = 8) and 22,677 cells from HCC tissues (n = 10) were used for further analysis. To explore the landscape of the cell composition, the classification of cells and identification of marker genes were performed as in a previous study (18). The cells were divided into 30 clusters through UMAP dimensionality reduction (**Figures 1A**, **S1**), and the frequency of cell types is shown in **Figure 1B**.

Then, 11 cell types were identified among the 30 clusters, including 4 types of non-immune cells and 7 types of immune cells (**Figure 1C**). Non-immune cells were mainly composed of endothelial cells (Es; CDH5, SPARC, TM4SF1, and INSR), hepatic stellate cells (HSCs; RGS5, COL1A1, ACTA2, and PDGFRB), apparently normal epithelial cells (KRT18, KRT19, and EPCAM), and hepatocyte or HCC malignant cells (**Figure 1C**). Immune cells primarily consisted of macrophages

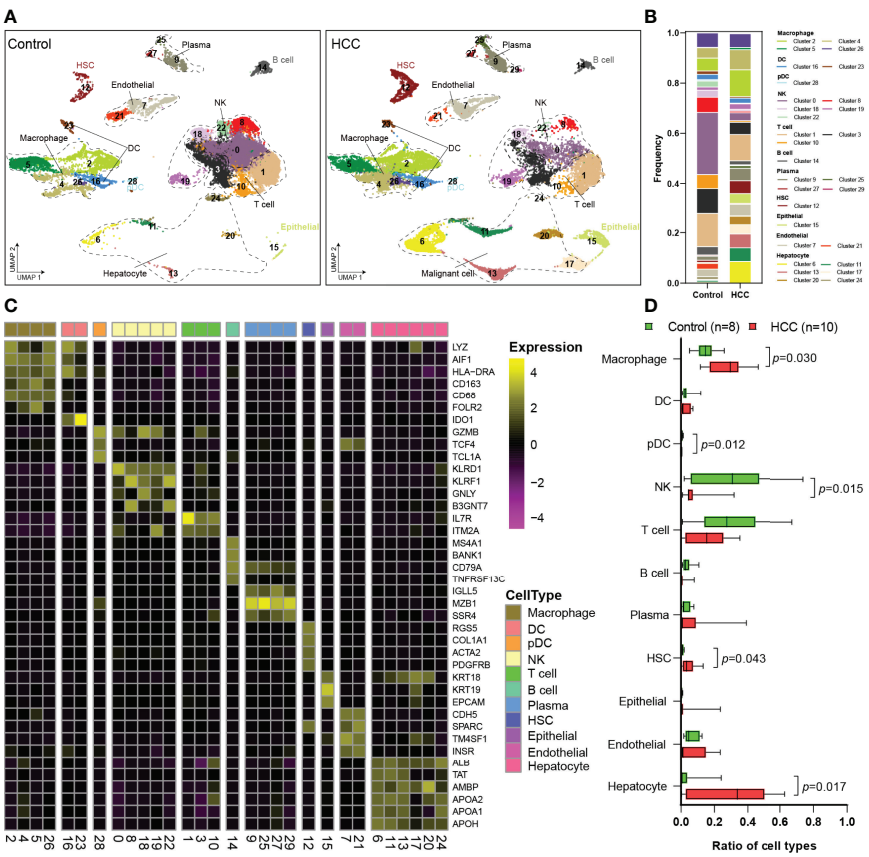

FIGURE 1 | Single-cell atlas of the HCC and tumor-adjacent tissues. **(A)** Overview of the cell clusters based on scRNA-seq data from tumor-adjacent and HCC tissues (UMAP). **(B)** The frequency of cells in each cluster. **(C)** Heatmap showing the expression of marker genes in the indicated cell types. The bottom bars label the clusters corresponding to specific cell types, and the number in brackets corresponds to the cluster number in panel **(A, D)** Histogram indicating the proportion of cells. HCC, hepatocellular carcinoma; scRNA-seq, single-cell RNA sequencing; UMAP, uniform manifold approximation and projection.

(LYZ, AIF1, HLA-DRA, CD163, CD68, and FOLR2), DCs (LYZ, AIF1, HLA-DRA, and IDO1), pDCs (GZMB, TCF4, and TCL1A), NK cells (KLRD1, KLRF1, GNLY, and B3GNT7), T cells (IL7R and ITM2A), B cells (MS4A1, BANK1, CD79A, and TNFRSF13C), and plasma cells (IGLL1, MZB1, and SSR4) (**Figure 1C**). Then, the proportions of each cell type were calculated in tumor-adjacent tissues (n = 8) and HCC (n = 10) (**Figure 1D**). We found that the proportions of pDCs and NK cells in tumor tissues were significantly decreased and the proportions of T cells and B cells were also obviously decreased (**Figure 1D**). Consistent with the previous report (2), we found that the proportion of macrophages was significantly increased in our data.

Differentially Expressed Genes in Specific Cell Types

Next, DEGs of non-immune cells (**Figure S2**) and immune cells (**Figure 2**) between tumor-adjacent tissues and HCC were identified, and the top dysregulated genes were marked. Then, we focused on the immune cells significantly changed in tumor tissues, including NK cells and macrophages.

In NK cells, 54 upregulated and 7 downregulated genes were identified in HCC, most of which had been reported to be involved in the p53 signaling pathway and cell cycles, such as CCNB1, CCNB2, CDK1, PTTG1, PLK1, MAD2L1, GTSE1, and TOP2A. These genes and related pathways were demonstrated to maintain NK cell homeostasis (24). Moreover, some other DEGs, including HSPA1A, HSPA1B, HSPA5, HSPA6, IFNG, CD8B, and KIR2DL3, were reported to participate in antigen processing and presentation. The above DEGs may affect the nature of NK cells and contribute to the immune escape of HCC.

In macrophages, 25 DEGs were screened out, consisting of 9 upregulated and 16 downregulated. Interestingly, most of the DEGs were membrane proteins or secretory proteins, contributing to immune response. For example, SPP1 (also known as OPN), a glycoprotein secreted by macrophages, was reported to mediate HCC malignant cell–macrophage communication (25). CLEC4E, which is located in the cell membrane of the macrophages, regulates macrophage polarization by enhancing endoplasmic reticulum stress response and inhibiting cholesterol efflux (26).

Cell–Cell Communication in Hepatocellular Carcinoma

To uncover the cellular crosstalk in tumor-adjacent tissues and HCC tissues, the analysis of receptor–ligand interactions was performed through CellPhoneDB (**Table S1**). The correlation intensions between cell A (x-axis) and cell B (y-axis) were shown as the total mean and the number of interactions. The results showed that myeloid-derived cells (macrophages and DCs) widely communicated with the other types of cells, and this communication was remarkably strengthened in HCC, especially with HCC malignant cells (**Figure 3A**). This finding, coupled with the result in **Figure 1D**, triggered us to study the communication between macrophages and hepatocytes or HCC malignant cells *via* receptor–ligand interactions. The results clearly showed that macrophages communicated with all the types of cells using SPP1, especially SPP1–CD44 interaction, which was not identified in tumor-adjacent tissues, suggesting the role of macrophage-derived SPP1 in the progress of HCC (**Figure 3B**). SPP1 was a well-studied oncogene in HCC, and previous studies were primarily concerned with the role of

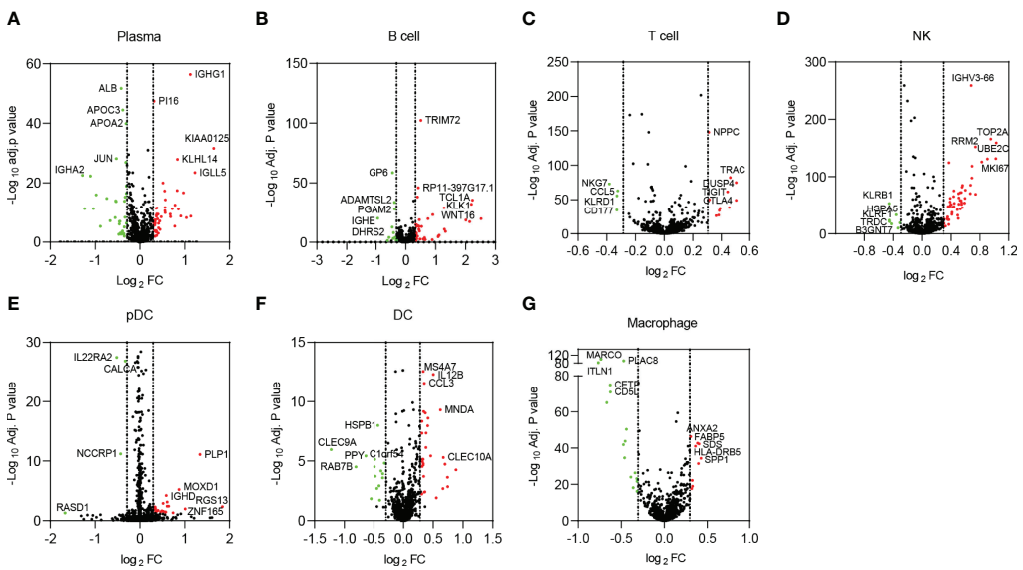

FIGURE 2 | DEGs in immune cells. **(A)** Plasma cells. **(B)** B cells. **(C)** T cells. **(D)** NK cells. **(E)** pDCs. **(F)** DCs. **(G)** Macrophages. The dots in red represent upregulated genes, and the dots in green represent downregulated genes. DEGs, differentially expressed genes; NK, natural killer; pDCs, plasmacytoid dendritic cells.

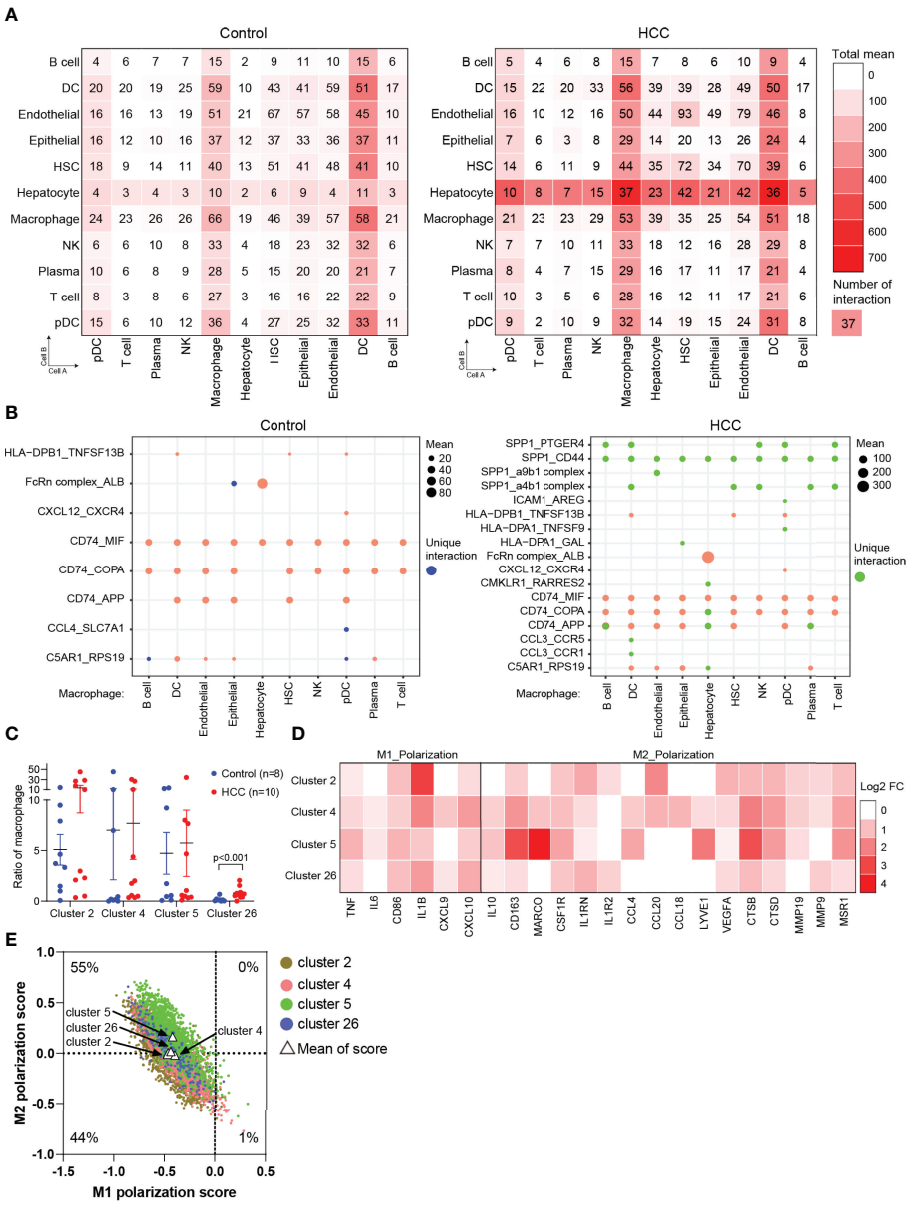

FIGURE 3 | Cell crosstalk in HCC. **(A)** The strength of cell crosstalk shown as total mean and number of interactions. **(B)** Cell crosstalk based on ligand–receptor interaction in the non-tumor and tumor tissues (significant mean >10). **(C)** Ratio of macrophages of clusters 2, 4, 5, and 26 in the individuals. **(D)** The phenotype of macrophages in HCC. **(E)** Scatterplots showing M1 and M2 scores for each color-coded cluster of macrophages. HCC, hepatocellular carcinoma.

tumor cell-intrinsic SPP1. The most recent study indicated that tumor cell-intrinsic SPP1 could promote macrophages to M2-like tumor-associated macrophages (TAMs) by mediating the crosstalk between HCC malignant cells and macrophages. Our findings further noted there may be a mutually reinforcing cycle.

To further verify the result from **Figure 1D**, we analyzed the proportion of macrophages (clusters 2, 4, 5, and 26) in tumor-adjacent and HCC groups. The results observed a significant enrichment of macrophages in tumors compared with tumor-adjacent tissues (**Figure 3C**). Then, we attempted to distinguish M1 and M2 macrophages from clusters 2, 4, 5, and 26. We found that the marker genes of M1 macrophages (FCGR3A) and M2 macrophages (CD163) were all expressed in clusters 2, 4, 5, and 26, in accordance with a previous report (18). Therefore, we analyzed and calculated M1 and M2 polarization scores of clusters 2, 4, 5, and 26 using macrophage polarization-related gene sets (**Table S2**) (18). It was demonstrated that all the clusters of macrophages have an M2-like phenotype (**Figures 3D, E**).

Gene Ontology and Kyoto Encyclopedia of Genes and Genomes Pathway Analysis and Protein–Protein Interaction Network Construction

For a deeper insight into the biological alteration of HCC malignant cells and macrophages, we performed GO and KEGG pathway enrichment analyses. KEGG analysis showed that the DEGs in HCC malignant cells were mainly enriched in metabolism-related pathways, including glutathione metabolism, tyrosine metabolism, and retinol metabolism (**Figure 4A**). GO analysis indicated that the DEGs significantly enriched in metabolic process, as well as apoptosis signaling pathways (**Figure 4A**). For macrophages, we found that the DEGs were mainly enriched in cell adhesion molecules, phagosome, and immune-related pathways by KEGG analysis, and lipid transport and growth-related process (**Figure 4B**). Furthermore, we constructed the PPI networks using the DEGs in HCC malignant cells and macrophages. Coincidentally, SPP1 and CD44 were both the top hub genes in their respective PPI network. So we merged these two PPI networks using the genes directly interacting with SPP1 or CD44 (**Figure 4C**). The new network indicated many potential signaling axes that mediate the crosstalk between HCC malignant cells and macrophages, which need further validation.

Determination of the Expression and Prognostic Role of SPP1 and CD44 in Hepatocellular Carcinoma

According to the findings above, we further analyzed the expression of SPP1 and CD44 in HCC using TCGA-LIHC database. The results suggested that SPP1 and CD44 expression was significantly upregulated in HCC tissues than in normal tissues (**Figure 5A**). Then, the expression of SPP1 and CD44 at the protein level was also analyzed using the HPA database. The immunohistochemistry (IHC) results showed that the protein expression of SPP1 and CD44 in HCC was significantly higher than that in normal tissues (**Figure 5B**). We were surprised to find a close association between the expression of SPP1 and CD44, suggesting the potential regulation relationship between SPP1 and CD44, which needs to be further verified (**Figure 5C**). Furthermore, we also downloaded the survival data from TCGA-LIHC dataset. By combining the expression data and survival data, we found that high expression of SPP1 significantly indicated poor prognosis in HCC, but high expression of CD44 was not (**Figure 5D**). Finally, we divided the patients into $SPP1^{high}/CD44^{high}$ (n = 89) and the other group (n = 275). The survival result showed the worse prognosis of patients with dual high expression of SPP1 and

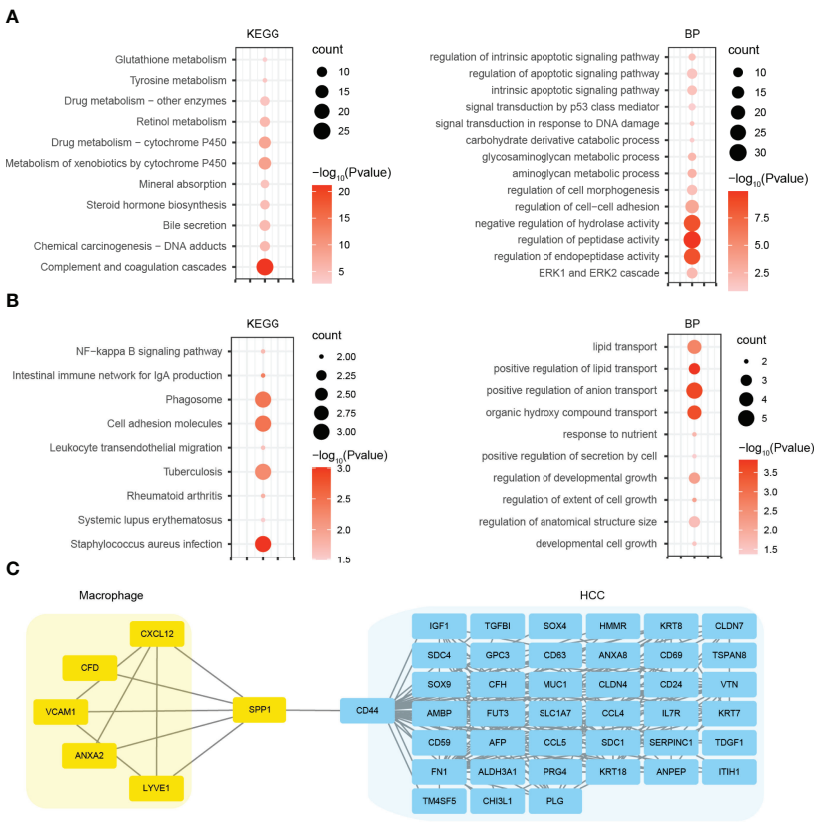

FIGURE 4 | GO and KEGG pathway analyses and PPI network construction. **(A)** KEGG and GO BP analyses using the DEGs of HCC malignant cells. **(B)** KEGG and GO BP analyses using the DEGs of macrophages. **(C)** PPI network using the genes directly interacting with SPP1 or CD44. GO, Gene Ontology; KEGG, Kyoto Encyclopedia of Genes and Genomes; PPI, protein–protein interaction; BP, biological process; DEGs, differentially expressed genes; HCC, hepatocellular carcinoma.

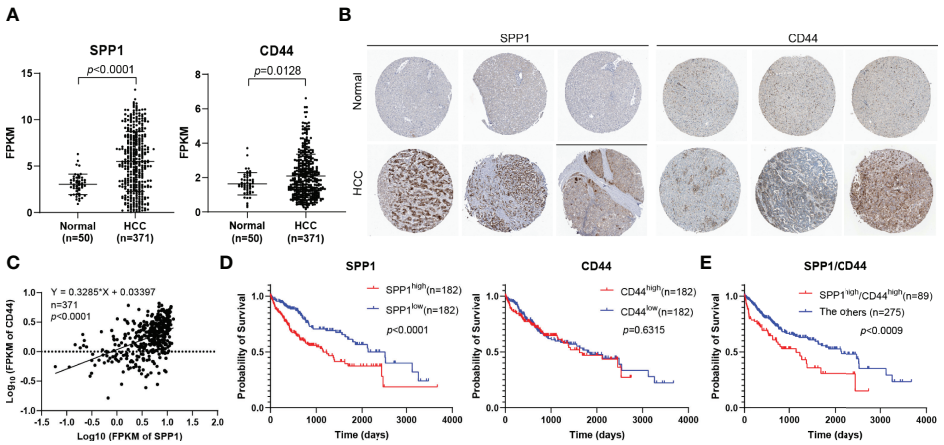

FIGURE 5 | Determination of the expression and prognostic role of SPP1 and CD44 in HCC. **(A)** The mRNA expression of SPP1 and CD44 in HCC from the TCGA-LIHC database. **(B)** IHC staining of SPP1 and CD44 in normal and HCC tissues from HPA database. **(C)** The correlation of the expression of SPP1 and CD44 in HCC (n = 424) from TCGA-LIHC database. **(D, E)** Kaplan–Meier survival curve of SPP1 and CD44 in HCC from TCGA-LIHC database. HCC, hepatocellular carcinoma; TCGA-LIHC, The Cancer Genome Atlas Liver Hepatocellular Carcinoma; IHC, immunohistochemistry; HPA, Human Protein Atlas.

CD44, indicating the pro-tumor role of the SPP1/CD44 axis in the progress of HCC (**Figure 5E**).

DISCUSSION

Despite the advances in surveillance and treatment strategies, the clinical outcomes of HCC remain unsatisfactory, mainly because of the lack of in-depth understanding of heterogeneity (27). Hence, we focused on the exploration of the intratumoral heterogeneity in HCC. Here, we characterized the ecosystems of tumor-adjacent and HCC tissues by bioinformatics analysis of single-cell transcriptomic data, revealing a distinct immune ecosystem in HCC. We found that the proportions of pDCs and NK cells were decreased and the proportion of macrophages was increased in the immune component.

Immunotherapy is a promising approach that stimulates immune cells to enhance their anticancer activity (28). Crosstalk among different cell types plays a crucial part in the efficacy of immunotherapy. Therefore, CellPhoneDB was used to explore cell–cell communications. We found that there was obviously an interaction between HCC malignant cells and macrophages, which may compromise antitumor immunity. Liver macrophages (Mϕs) mainly consist of resident Kupffer cells and MoMϕs. The TME of HCC regulates the polarization of macrophages, resulting in M2-like macrophages with immunosuppressive properties. In this study, we tried to identify the phenotype of macrophages (clusters 2, 4, 5, and 26). We found the marker genes of M1 macrophages (FCGR3A) and M2 macrophages (CD163) were all expressed in clusters 2, 4, 5, and 26, in accordance with a previous report (18). Therefore, we analyzed clusters 2, 4, 5, and 26 using macrophage polarization-related gene sets. It was demonstrated that all the clusters of macrophages have an M2-like phenotype.

Using CellPhoneDB database, we also identified multiple ligand–receptor interactions mediating cell crosstalk, including FcRn complex–albumin (ALB) and SPP1–CD44 between macrophages and HCC malignant cells. FcRn complex–ALB interaction exists in normal liver tissues. However, the strength of interaction was enhanced in HCC. It was demonstrated that hepatocytes used FcRn complex receptors to bind ALB to maintain its normal growth and metabolism. With the progress of HCC, malignant cells consumed a large amount of nutrients for proliferation or invasion, mainly by binding more ALB (29). The upregulated expression of FcRn was identified in a number of cancers, suggesting the importance of ALB recruitment driven by FcRn (30) and the recycling and transcytosis of ALB regulated by FcRn (31, 32). In addition to FcRn complex–ALB interaction, we found that macrophages communicated with all the types of cells using SPP1, especially SPP1–CD44 interaction, which was not identified in normal tissues, suggesting the role of macrophage-derived SPP1 in the progress of HCC (**Figure 3B**). SPP1 was a well-studied oncogene in HCC, and previous studies were primarily concerned with the role of tumor cell-intrinsic SPP1. The most recent study indicated that HCC cells could secrete SPP1 into TME and bind to CD44 of macrophages, resulting in M2-phenotype TAM polarization of macrophages. Our findings further noted that there may be a mutually reinforcing cycle.

In conclusion, our study characterizes the heterogeneity of the tumor ecosystem between tumor-adjacent and HCC tissues, especially the crosstalk between immune cells and HCC malignant cells. Moreover, we identify the SPP1–CD44 axis as a unique interaction between macrophages and HCC malignant

cells. Our comprehensive portrait of cell communication patterns over the HCC ecosystem reveals further insights into immune infiltration and more effective therapeutic targets for immunotherapies in patients with HCC.

DATA AVAILABILITY STATEMENT

The datasets presented in this study can be found in online repositories. The names of the repository/repositories and accession number(s) can be found in the article/ **Supplementary Material**.

AUTHOR CONTRIBUTIONS

JQ conceived and supervised the study. YL and LZ collected and analyzed the data. SW and JQ wrote the manuscript. XJ and JQ revised the manuscript. All authors read and approved the manuscript and agreed to be accountable for all aspects of the research in ensuring that the accuracy or integrity of any part of the work is appropriately investigated and resolved.

SUPPLEMENTARY MATERIAL

The Supplementary Material for this article can be found online at: https://www.frontiersin.org/articles/10.3389/fimmu.2022.955390/full#supplementary-material

Supplementary Figure 1 | Overview of the cell clusters based on scRNA-seq data using total cells 23,225 cells from tumor-adjacent tissues (control, n = 8), and 22,677 cells from HCC tissues (n = 10).

Supplementary Figure 2 | DEGs in non-immune cells. **(A)** Endothelial cells. **(B)** Epithelial cells. **(C)** HCC malignant cells. **(D)** HSC cells.

Supplementary Table 1 | The results of cell cross-talk from CellPhoneDB.

Supplementary Table 2 | Signature related gene sets used in macrophage analysis.

REFERENCES

1. Ferlay J, Colombet M, Soerjomataram I, Mathers C, Parkin DM, Piñeros M, et al. Estimating the Global Cancer Incidence and Mortality in 2018: GLOBOCAN Sources and Methods. *Int J Cancer* (2019) 144(8):1941–53. doi: 10.1002/ijc.31937
2. Zhang SW, Liu ZH, Wu D, Chen LM, Xie L. Single-Cell RNA-Seq Analysis Reveals Microenvironmental Infiltration of Plasma Cells and Hepatocytic Prognostic Markers in HCC With Cirrhosis. *Front Oncol* (2020) 10:596318. doi: 10.3389/fonc.2020.596318
3. Prieto J, Melero I, Sangro B. Immunological Landscape and Immunotherapy of Hepatocellular Carcinoma. *Nat Rev Gastroenterol Hepatol* (2015) 12 (12):681–700. doi: 10.1038/nrgastro.2015.173
4. Zhang Z, Ma L, Goswami S, Ma J, Zheng B, Duan M, et al. Landscape of Infiltrating B Cells and Their Clinical Significance in Human Hepatocellular Carcinoma. *Oncoimmunology* (2019) 8(4):e1571388. doi: 10.1080/2162402x.2019.1571388
5. Lawal G, Xiao Y, Rahnemai-Azar AA, Tsilimigras DI, Kuang M, Bakopoulos A, et al. The Immunology of Hepatocellular Carcinoma. *Vaccines (Basel)* (2021) 9(10):1184. doi: 10.3390/vaccines9101184
6. Ho DW, Tsui YM, Sze KM, Chan LK, Cheung TT, Lee E, et al. Single-Cell Transcriptomics Reveals the Landscape of Intra-Tumoral Heterogeneity and Stemness-Related Subpopulations in Liver Cancer. *Cancer Lett* (2019) 459:176–85. doi: 10.1016/j.canlet.2019.06.002
7. Tirosh I, Izar B, Prakadan SM, Wadsworth MH2nd, Treacy D, Trombetta JJ, et al. Dissecting the Multicellular Ecosystem of Metastatic Melanoma by Single-Cell RNA-Seq. *Science* (2016) 352(6282):189–96. doi: 10.1126/science.aad0501
8. Lambrechts D, Wauters E, Boeckx B, Aibar S, Nittner D, Burton O, et al. Phenotype Molding of Stromal Cells in the Lung Tumor Microenvironment. *Nat Med* (2018) 24(8):1277–89. doi: 10.1038/s41591-018-0096-5
9. Chevrier S, Levine JH, Zanotelli VRT, Silina K, Schulz D, Bacac M, et al. An Immune Atlas of Clear Cell Renal Cell Carcinoma. *Cell* (2017) 169(4):736–49.e18. doi: 10.1016/j.cell.2017.04.016
10. Azizi E, Carr AJ, Plitas G, Cornish AE, Konopacki C, Prabhakaran S, et al. Single-Cell Map of Diverse Immune Phenotypes in the Breast Tumor Microenvironment. *Cell* (2018) 174(5):1293–308.e36. doi: 10.1016/j.cell.2018.05.060
11. Savas P, Virassamy B, Ye C, Salim A, Mintoff CP, Caramia F, et al. Single-Cell Profiling of Breast Cancer T Cells Reveals a Tissue-Resident Memory Subset Associated With Improved Prognosis. *Nat Med* (2018) 24(7):986–93. doi: 10.1038/s41591-018-0078-7
12. Guo X, Zhang Y, Zheng L, Zheng C, Song J, Zhang Q, et al. Global Characterization of T Cells in Non-Small-Cell Lung Cancer by Single-Cell Sequencing. *Nat Med* (2018) 24(7):978–85. doi: 10.1038/s41591-018-0045-3
13. Zheng C, Zheng L, Yoo JK, Guo H, Zhang Y, Guo X, et al. Landscape of Infiltrating T Cells in Liver Cancer Revealed by Single-Cell Sequencing. *Cell* (2017) 169(7):1342–56.e16. doi: 10.1016/j.cell.2017.05.035
14. Zhang Q, He Y, Luo N, Patel SJ, Han Y, Gao R, et al. Landscape and Dynamics of Single Immune Cells in Hepatocellular Carcinoma. *Cell* (2019) 179(4):829–45.e20. doi: 10.1016/j.cell.2019.10.003
15. Ma L, Hernandez MO, Zhao Y, Mehta M, Tran B, Kelly M, et al. Tumor Cell Biodiversity Drives Microenvironmental Reprogramming in Liver Cancer. *Cancer Cell* (2019) 36(4):418–30.e6. doi: 10.1016/j.ccell.2019.08.007
16. Lim CJ, Lee YH, Pan L, Lai L, Chua C, Wasser M, et al. Multidimensional Analyses Reveal Distinct Immune Microenvironment in Hepatitis B Virus-Related Hepatocellular Carcinoma. *Gut* (2019) 68(5):916–27. doi: 10.1136/gutjnl-2018-316510
17. Stuart T, Butler A, Hoffman P, Hafemeister C, Papalexi E, Mauck WM, et al. Comprehensive Integration of Single-Cell Data. *Cell* (2019) 177(7):1888–902.e21. doi: 10.1016/j.cell.2019.05.031
18. Sun Y, Wu L, Zhong Y, Zhou K, Hou Y, Wang Z, et al. Single-Cell Landscape of the Ecosystem in Early-Relapse Hepatocellular Carcinoma. *Cell* (2021) 184 (2):404–21.e16. doi: 10.1016/j.cell.2020.11.041
19. Hein DM, Deng WY, Kazmi SA, Jones AL, Kainthla R, Cantarel B, et al. Racial and Ethnic Differences in Genomic Profiling of Early Onset Colorectal Cancer. *Cancer Res* (2021) 81(13):775–8. doi: 10.1093/jnci/djac014
20. Hanzelmann S, Castelo R, Guinney J. GSVA: Gene Set Variation Analysis for Microarray and RNA-Seq Data. *BMC Bioinf* (2013) 14. doi: 10.1186/1471-2105-14-7
21. Huang K, Zhang X, Duan J, Wang R, Wu Z, Yang C, et al. STAT4 and COL1A2 are Potential Diagnostic Biomarkers and Therapeutic Targets for Heart Failure Comorbided With Depression. *Brain Res Bull* (2022) 184:68–75. doi: 10.1016/j.brainresbull.2022.03.014
22. Deng J, Lin X, Li Q, Cai XY, Wu LW, Wang W, et al. Decreased INPP5B Expression Predicts Poor Prognosis in Lung Adenocarcinoma. *Cancer Cell Int* (2022) 22(1):189. doi: 10.1186/s12935-022-02609-8
23. Shen ZF, Wu HY, Chen ZS, Hu JT, Pan JX, Kong JQ, et al. The Global Research of Artificial Intelligence on Prostate Cancer: A 22-Year Bibliometric Analysis. *Front Oncol* (2022) 12:843735. doi: 10.3389/fonc.2022.843735
24. Sohlberg E, Pfefferle A, Heggernes Ask E, Tschan-Plessl A, Jacobs B, Netskar H, et al. Perturbed NK-Cell Homeostasis Associated With Disease Severity in Chronic Neutropenia. *Blood* (2022) 139(5):704–16. doi: 10.1182/blood.2021013233

25. Liu LL, Zhang RY, Deng JW, Dai XM, Zhu XD, Fu QH, et al. Construction of TME and Identification of Crosstalk Between Malignant Cells and Macrophages by SPP1 in Hepatocellular Carcinoma. *Cancer Immunol Immun* (2022) 71(1):121–36. doi: 10.1007/s00262-021-02967-8
26. Clement M, Basatemur G, Masters L, Baker L, Bruneval P, Iwawaki T, et al. Necrotic Cell Sensor Clec4e Promotes a Proatherogenic Macrophage Phenotype Through Activation of the Unfolded Protein Response. *Circulation* (2016) 134(14):1039–51. doi: 10.1161/CIRCULATIONAHA.116.022668
27. Liang J, Chen W, Ye J, Ni C, Zhai W. Single-Cell Transcriptomics Analysis Reveals Intratumoral Heterogeneity and Identifies a Gene Signature Associated With Prognosis of Hepatocellular Carcinoma. *Biosci Rep* (2022) 42(2). doi: 10.1042/bsr20212560
28. Poureau P-G, Metges J-P. Fundamentals of Digestive Cancers Immunology, Especially Gastric and Hepatocellular CarcinomasFondamentaux De L'immunologie Des Cancers Digestifs (Gastriques Et Hépatocellulaires). *Oncologie* (2021) 23(1):47–59. doi: 10.32604/Oncologie.2021.15525
29. Swiercz R, Mo M, Khare P, Schneider Z, Ober RJ, Ward ES. Loss of Expression of the Recycling Receptor, FcRn, Promotes Tumor Cell Growth by Increasing Albumin Consumption. *Oncotarget* (2017) 8(2):3528–41. doi: 10.18632/oncotarget.13869
30. Ju C, Colgan SP, Eltzschig HK. Hypoxia-Inducible Factors as Molecular Targets for Liver Diseases. *J Mol Med (Berl)* (2016) 94(6):613–27. doi: 10.1007/s00109-016-1408-1
31. Dylewski J, Dobrinskikh E, Lewis L, Tonsawan P, Miyazaki M, Jat PS, et al. Differential Trafficking of Albumin and IgG Facilitated by the Neonatal Fc Receptor in Podocytes *In Vitro* and *In Vivo*. *PLoS One* (2019) 14(2):e0209732. doi: 10.1371/journal.pone.0209732
32. Toh WH, Louber J, Mahmoud IS, Chia J, Bass GT, Dower SK, et al. FcRn Mediates Fast Recycling of Endocytosed Albumin and IgG From Early Macropinosomes in Primary Macrophages. *J Cell Sci* (2019) 133(5). doi: 10.1242/jcs.235416

Conflict of Interest: The authors declare that the research was conducted in the absence of any commercial or financial relationships that could be construed as a potential conflict of interest.

Publisher's Note: All claims expressed in this article are solely those of the authors and do not necessarily represent those of their affiliated organizations, or those of the publisher, the editors and the reviewers. Any product that may be evaluated in this article, or claim that may be made by its manufacturer, is not guaranteed or endorsed by the publisher.

frontiers | Frontiers in Oncology

TYPE Original Research
PUBLISHED 01 August 2022
DOI 10.3389/fonc.2022.926497

OPEN ACCESS

EDITED BY
Min Xue,
University of California, Riverside,
United States

REVIEWED BY
Zhonghan Li,
University of California, Riverside,
United States
Hanjun Cheng,
Institute for Systems Biology (ISB),
United States

*CORRESPONDENCE
Iram Siddiqui
iram.siddiqui@sickkids.ca

SPECIALTY SECTION
This article was submitted to
Cancer Immunity
and Immunotherapy,
a section of the journal
Frontiers in Oncology

RECEIVED 22 April 2022
ACCEPTED 30 June 2022
PUBLISHED 01 August 2022

CITATION
Siddiqui I, Bilkey J, McKee TD, Serra S, Pintilie M, Do T, Xu J, Tsao M-S, Gallinger S, Hill RP, Hedley DW and Dhani NC (2022) Digital quantitative tissue image analysis of hypoxia in resected pancreatic ductal adenocarcinomas.
Front. Oncol. 12:926497.
doi: 10.3389/fonc.2022.926497

Digital quantitative tissue image analysis of hypoxia in resected pancreatic ductal adenocarcinomas

Iram Siddiqui[1]*, Jade Bilkey[2], Trevor D. McKee[2], Stefano Serra[3], Melania Pintilie[4], Trevor Do[2], Jing Xu[5], Ming-Sound Tsao[3], Steve Gallinger[6,7], Richard P. Hill[8], David W. Hedley[5] and Neesha C. Dhani[5]

[1]Department of Pediatric Laboratory Medicine, The Hospital for Sick Children, Toronto, ON, Canada, [2]Spatio-temporal Targeting and Amplification of Radiation Response (STTARR), University Health Network, Toronto, ON, Canada, [3]Department of Pathology, Toronto General Hospital, Toronto, ON, Canada, [4]Department of Biostatistics, The Princess Margaret Cancer Centre, Toronto, ON, Canada, [5]Department of Medical Oncology, The Princess Margaret Cancer Centre, Toronto, ON, Canada, [6]PanCuRx Translational Research Initiative, Ontario Institute for Cancer Research, Toronto, ON, Canada, [7]Hepato-Pancreatico-Biliary Surgical Oncology Program, University Health Network, Toronto, ON, Canada, [8]Medicine Program, The Princess Margaret Cancer Centre/Ontario Cancer Institute, Radiation Toronto, ON, Canada

Background: Tumor hypoxia is theorized to contribute to the aggressive biology of pancreatic ductal adenocarcinoma (PDAC). We previously reported that hypoxia correlated with rapid tumor growth and metastasis in patient-derived xenografts. Anticipating a prognostic relevance of hypoxia in patient tumors, we developed protocols for automated semi-quantitative image analysis to provide an objective, observer-independent measure of hypoxia. We further validated this method which can reproducibly estimate pimonidazole-detectable hypoxia in a high-through put manner.

Methods: We studied the performance of three automated image analysis platforms in scoring pimonidazole-detectable hypoxia in resected PDAC (n = 10) in a cohort of patients enrolled in PIMO-PANC. Multiple stained tumor sections were analyzed on three independent image-analysis platforms, Aperio Genie (AG), Definiens Tissue Studio (TS), and Definiens Developer (DD), which comprised of a customized rule set.

Results: The output from Aperio Genie (AG) had good concordance with manual scoring, but the workflow was resource-intensive and not suited for high-throughput analysis. TS analysis had high levels of variability related to misclassification of cells class, while the customized rule set of DD had a high level of reliability with an intraclass coefficient of more than 85%.

Discussion: This work demonstrates the feasibility of developing a robust, high-performance pipeline for an automated, quantitative scoring of pimonidazole-detectable hypoxia in patient tumors.

KEYWORDS

hypoxia, tumor microenvironment, ductal adenocarcinoma (PDAC), tumor heterogeneity, image analysis

Background

Histopathological tumor analysis has historically been the foundation of cancer diagnosis and prognostication. In the pursuit of targeted treatment approaches, a number of molecular analyses have now become standard pathological assays, with the most extensively used being the immunohistochemical (IHC) detection of proteins. In spite of its widespread use, however, IHC can be confounded by resource-intensive analysis (1), and poor inter-laboratory, inter-observer, and intra-observer reproducibility (2, 3). Several factors contribute to the variability of the output of IHC analyses, including the selection of appropriate tumor regions, heterogeneity in marker expression, variations in antibody performance and staining techniques, and the subjectivity and qualitative nature of traditional manual scoring (4).

Several complementary strategies have been recommended to improve on the stringency of IHC tumor analysis. These include robust guidelines around optimization of IHC staining methods, including the use of automation (5) and considerations on the issue of marker heterogeneity, as has been studied by ourselves and others (6). Finally, the validation and adoption of automated digital image analysis have the potential to provide IHC tumor analysis with the objectivity, reliability, and speed required for effective biomarker research with translation to the clinic (4). Several independent groups have already demonstrated at least equal, if not superior, performance of automated digital image analysis (DIA) versus traditional manual scoring (7, 8).

In the context of tumor hypoxia, we recently completed the quantitative scoring of pimonidazole IHC in a cohort of resected pancreatic ductal adenocarcinomas (PDAC) in patients accrued to the PIMO-PANC trial, using the adaptive, pattern-recognition, image analysis platform, Aperio Genie (1). Pimonidazole (1-[(2-hydroxy-3-piperidinyl) propyl]-2-nitromidazole hydrochloride) is an exogenous hypoxia tracer with an extensive prior use in preclinical and clinical hypoxia studies and is a well-established technique for assessing tissue hypoxia (9–11). This 2-nitroimidazole undergoes bioactive reduction to form covalent adducts with thiol-containing macromolecules in hypoxic (pO_2 < 10 mmHg) but metabolically viable cells (12, 13). Adducts are then identified using different immune-detection methods including IHC. Pimonidazole studies have historically utilized a semiquantitative, ordinal scoring system (14), which remains susceptible to bias and variability, given its basis in manual visual scoring. Another relevant limitation of ordinal scoring systems is the potential for non-linear relationships across categories, to confound correlation with biological data. The work we describe here was initiated with the primary objective of developing and validating a pipeline for image analysis that was (1) reproducible, (2) relatively user-independent, and (3) could be applied in a high-throughput manner. Further, given the emerging contributions of cancer-associated stromal cells to tumor biology and clinical behavior, we wanted a method that would be able to confidently differentiate between tumor epithelial and stromal cellular compartments (15, 16).

In our initial analysis, Aperio Genie provided a quantitative, and continuous, estimate of tumor hypoxia that had good concordance with manual scoring; analysis of five full tumor sections per each patient tumor was able to appropriately account for tumoral heterogeneity (1). However, the workflow was quite resource-intensive, with each tumor requiring its own customized analysis algorithm and settings. Further, distinguishing epithelial from stromal cells was challenging on the pixel-based Genie platform. We therefore proceeded to evaluate two other image analysis platforms that were in common use at our institution, both of which better resolve distinct cell types through improved cell segmentation algorithms. Definiens Tissue Studio utilizes a prepackaged, generic cellular segmentation methodology, with limited adaptability, while Definiens Developer allows customized modifications of cellular segmentation. We describe here the results of our comparison of quantitative tumor image analysis of pimonidazole IHC on these three platforms.

Materials and methods

Study details

PIMO-PANC (NCT01248637) is a prospective, REB-approved, single-institution trial conducted at the Princess

Margaret Cancer Centre/University Health Network. Eligible patients were 18 years or older, being considered for surgery with a presumed diagnosis of localized pancreatic ductal adenocarcinoma (PDAC). The primary objective is to evaluate the effect of hypoxia on survival of early-staged (resectable) PDAC.

Registered patients received a single dose of the hypoxia marker pimonidazole, on the day prior to surgery. Resected tumors were evaluated and processed as per institutional standard practice for a clinical diagnosis. All archived hematoxylin and eosin (H&E)-stained slides were retrospectively reviewed by an expert GI pathologist, and at least five representative tumor sections were identified. Tumor tissue selection criteria included sections containing viable tumor occupying the most surface area with minimal artifacts (such as necrosis and variations in tissue processing). Sections were cut (4 μm) from the five selected tumor blocks for pimonidazole immunohistochemical (IHC) staining and analysis with Aperio Genie (Ref 1) and Tissue Studio. Subsequently, new sections were cut and stained for PIMO immunohistochemistry from the same tumor blocks for Definiens Developer analysis. Data from Aperio Genie were used from the previous study (1), for comparison.

Pimonidazole immunohistochemistry protocol

FFPE tumor sections were dried at 60°C for 1–2 h and IHC staining completed as per the manufacturer's guidelines, using an automated slide stainer (BenchMark XT, Ventana Medical Systems) with medium antigen retrieval (CC1, Tris/borate/EDTA pH 8.0, #950-124). The dilution for pimonidazole antibody (Hypoxyprobe, Inc.) was 1:400, with incubation time of 60 min. Secondary detection was completed using Ventana ultraview Universal DAB Detection Kit (#760-500) and visualization by hydrogen peroxide substrate and 3,3′-diaminobenzidine tetrahydrochloride (DAB) chromogen. Slides were counterstained with Harris hematoxylin and Bluing in PBS, dehydrated in graded alcohol, cleared in xylene, and coverslipped in Permount. Stained sections were digitized for analysis (Aperio ScanScope, Leica Biosystems Inc., Carlsbad CA).

Quantitative image analysis

Pimonidazole IHC-stained tumor slides from 10 patients were scanned and analyzed on three independent image-analysis platforms as outlined below.

Aperio genie

Analysis was completed as described previously (1). Briefly, regions of interest (ROIs) were manually annotated on scanned images of the IHC-stained tumor slides for analysis, excluding areas of necrosis and non-neoplastic normal tissue adjacent to tumor. Classes "epithelium," "stroma," and "other" were defined and used to develop unique classifiers for each patient tumor to differentiate epithelial from stromal tumor compartments. The "other" class was used to define regions to exclude from analysis (e.g., necrosis, non-pancreatic tissue). Aperio's Positive Pixel v9 algorithm was applied to quantify hypoxic percentages (HPs) in epithelial and stromal tumor compartments (with HP-whole tumor = HP-epithelial + HP-stromal) within annotated ROIs.

Definiens tissue studio

All scanned slide images of the of the IHC-stained tumor slides were loaded into Tissue Studio (TS) 4.0 (Definiens Inc., Munich, Germany). A machine learning classifier differentiating "stroma" from "epithelium" was developed by providing examples of images of both tissue classes, as well as tissue artifact to be excluded from analysis using the decision tree algorithm. This classifier was then applied to refine regions of interest, followed by a pathologist review and manual correction of any regions incorrectly labeled by the automated classifier including manual extraction of background normal tissue. It should be noted that the manual correction was performed individually on every image from each tumor.

A stain separation algorithm was used to separate hematoxylin from the DAB signal, with nuclear segmentation being performed based on the hematoxylin signal. Cell size was estimated and simulated by growing an area of cytoplasm 2 microns from every nucleus. A threshold applied to the intensity of the DAB signal was used to differentiate between pimonidazole-positive and -negative cellular regions.

Definiens developer XD

Scanned images were manually annotated by the study pathologist to select tumor regions only. At this time, any large areas of necrosis within the tumor region were also excluded. This initial step of manual annotation of the tumor region approximately took an average of 5 min per image. A custom set of algorithms for cellular segmentation and classification was developed with direct input from a platform programmer and a study pathologist as outlined in detail below.

Development of custom classification algorithms

The white balance of respective slides was computed to correct for uneven lighting in slide scanning, and the DD stain separation algorithm was used to separate DAB and hematoxylin stains into unique image channels. Information regarding white balance and stain color coefficients was used to improve stain channel accuracy. Preliminary ROIs were then re-annotated to exclude whitespace and other obvious artifacts.

Fifty ROIs (512 × 384 microns) were randomly selected across slides from 68 patient tumors and divided into two groups. One group of 25 ROIs was designated as the *training set*, with the remaining 25 assigned as the *validation set*. Two expert GI pathologists used an open-source image editing program (GIMP, The GIMP Development Team, Retrieved from https://www.gimp.org) to independently manually annotate cells within all 50 fields as "epithelial", "stromal", or "inflammatory cell/other", further differentiating pimonidazole-positive cells as "stained" and pimonidazole-negative cells as "unstained". Cells annotated as inflammatory cell/other were excluded from hypoxia analysis. A "consensus annotation" methodology was used to resolve discrepancies between pathologists' annotations. If both pathologists' annotations agreed, or if one pathologist annotated a cell which the other did not, then the agreed or positive identification was assigned. In cases of epithelial/stromal mismatch, the cell was identified as stroma to reduce misclassification of non-epithelial cells as epithelial. Likewise, for inflammatory/other cell mismatch, any cell identified as such by one of the two pathologists was classified as inflammatory, to ensure stringency of epithelial cell discrimination.

A training set of 25 grids was used to iteratively develop a custom cell classifier algorithm with joint input from a study pathologist and a platform programmer. The hematoxylin channel was used to segment ROIs into nuclear (high hematoxylin signal) or cytoplasmic (low hematoxylin signal) segments. Nuclear segments were then classified as either "epithelial," "stromal," or "other" (which included primarily inflammatory cells) using a custom-trained, pixel-wise Random Forest classifier trained on the "consensus annotation" applied to each detected cell segment within the segmented 25 field training sets. Nuclear segments were expanded into cytoplasmic tissue segments to simulate epithelial cells, fibroblasts, and inflammatory cells/other cell bodies using cell-type-specific, sizing heuristics. Cellular segments were individually assessed using the information present in the DAB stain channel. Segments were designated pimonidazole positive if more than 50% of their mean optical density (commonly: opacity/translucency) was derived from the DAB channel (and the optical density was above a minimum threshold of 0.1). This approach was selected as it agreed with pathologist assessment of stain intensity and performed well independent of cellular density and stain concentration. Simulated cellular segments were then used to designate larger regions of tumor tissue as predominantly containing epithelial, stromal, or inflammatory cells/other. Stromal tissue regions were then further classified as "cellular" or "acellular" by subtracting the stromal cell segments based on the average size of a fibroblast and classifying the remaining stromal tissue area as "acellular."

Cell classifier validation

The derived cell segmentation and classification algorithm was then applied to the 25 fields of the validation set to calculate concordance of classification between individual pathologists (IS and SS), combined-pathologist scoring ("joint"), and DD. There was greater reliability across the two pathologists' scoring of epithelial cells (>72%) than stromal cells (>66%). When pathologists' scoring was combined to define a "consensus annotation" or "joint classification," the machine-based algorithm had an 86% alignment with manual scoring of epithelial tumor cells (Figure 1).

Cross-platform comparison and statistical analysis

A cross-platform agreement of quantitative estimates of hypoxia was analyzed in a 10-patient tumor cohort. Spearman correlation coefficients were calculated to assess the concordance between the hypoxia level for the different techniques and between epithelial hypoxia and stromal hypoxia. Mixed-effect modeling was employed to obtain the variances between patients (inter-tumor heterogeneity) and within a patient (intra-tumor heterogeneity). Based on these variances, the intraclass correlation coefficients (ICC) were calculated. The ICC is a measure of reliability ranging from 0 to 1.0; values equal to or greater than 0.85 indicate a high level of reliability across measurements. These calculations were performed using all sections and all patients available (10 patient tumors for Aperio Genie and Definiens Tissue Studio analysis; 92 patient tumors for Definiens Developer). We have calculated the ICC corresponding to analysis on one section per patient tumor, as well as with two to five sections per tumor (Table 1). All analyses were performed utilizing R 3.4 software (https://cran.r-project.org/).

Results

There were visible differences in the resolution of cellular classification across the three platforms related to the pixel-based segmentation algorithms utilized by Aperio Genie compared with the cell-based segmentation of Definiens Tissue Studio and Definiens Developer (Figure 2).

Hypoxia is variable across patient tumors

Consistent with our previous reports, pimonidazole-detectable hypoxia is variable across patient tumors and appears to exist along a continuous spectrum (1). Hypoxia levels in epithelial tumor regions are concordant with levels in stroma as measured by all three image analysis platforms (Spearman's coefficient 0.69 (Genie), 0.79 (DD), 0.88 (TS)).

Variability in quantitative estimates of hypoxia in 10 patient tumors using three different platforms is summarized in Figure 3. The range of whole-tumor HP was 0% to 26% as

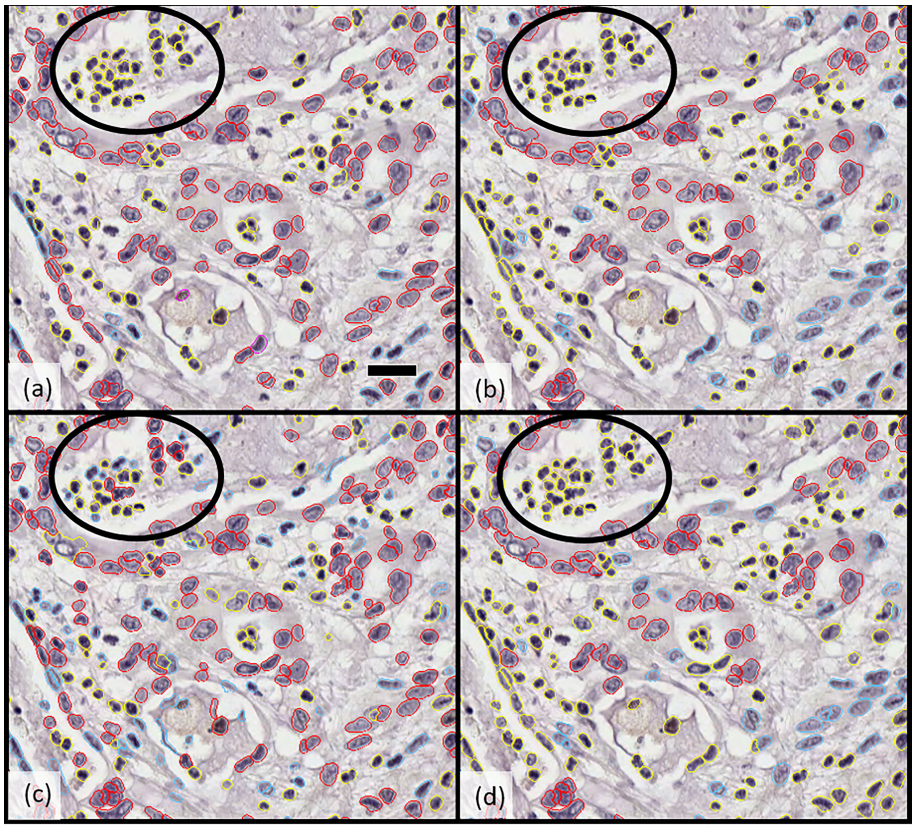

FIGURE 1
Comparison of cellular classification (epithelial vs. stromal) by **(A)** pathologist 1, **(B)** pathologist 2, **(C)** Developer algorithm v1, and **(D)** Developer algorithm v2 with epithelial cells highlighted in red and stromal cells in blue; cells excluded from analysis (including inflammatory cells, necrotic cells, and others) are indicated in yellow. Circled regions highlight the example of a region of cellular misclassification with cells identified as necrotic and coded yellow by both pathologists (to be excluded from analysis), which were classified as epithelial (red) or stromal (blue) by Developer algorithm v1. After further optimization and derivation of Developer algorithm v2, these cells were now excluded (highlight yellow). Scale bar in a) 25 microns.

measured by both (Aperio) Genie and (Definiens) Developer and 0% to 15% as measured by (Definiens) Tissue Studio. Higher levels of hypoxia were observed in the epithelial tumor compartments, with estimates of HP-epithelial ranging from 0% to 38% by Developer, 0% to 40% by Genie, and 0% to 52% by Tissue Studio. Estimates of HP-stroma were unexpectedly low using Tissue Studio (0 to 2%) in comparison with the other two platforms (0% to 14% by Genie and 0% to 19% by Developer).

TABLE 1 Reliability of estimation of hypoxia using different platforms based on number of slides evaluated.

No. of tumour sections evaluated	Intra-class co-efficient (ICC)								
	Developer			Genie			Tissue Studio		
	HPwt	HPepi	HPstr	HPwt	HPepi	HPstr	HPwt	HPepi	HPstr
1	0.728	0.736	0.713	0.678	0.702	0.567	0.325	0.308	0.059
2	0.842	0.848	0.832	0.808	0.825	0.724	0.490	0.471	0.112
3	0.889	0.893	0.882	0.863	0.876	0.797	0.591	0.572	0.159
4	0.914	0.918	0.909	0.894	0.904	0.840	0.658	0.640	0.201
5	0.930	0.933	0.925	0.913	0.922	0.868	0.706	0.690	0.240

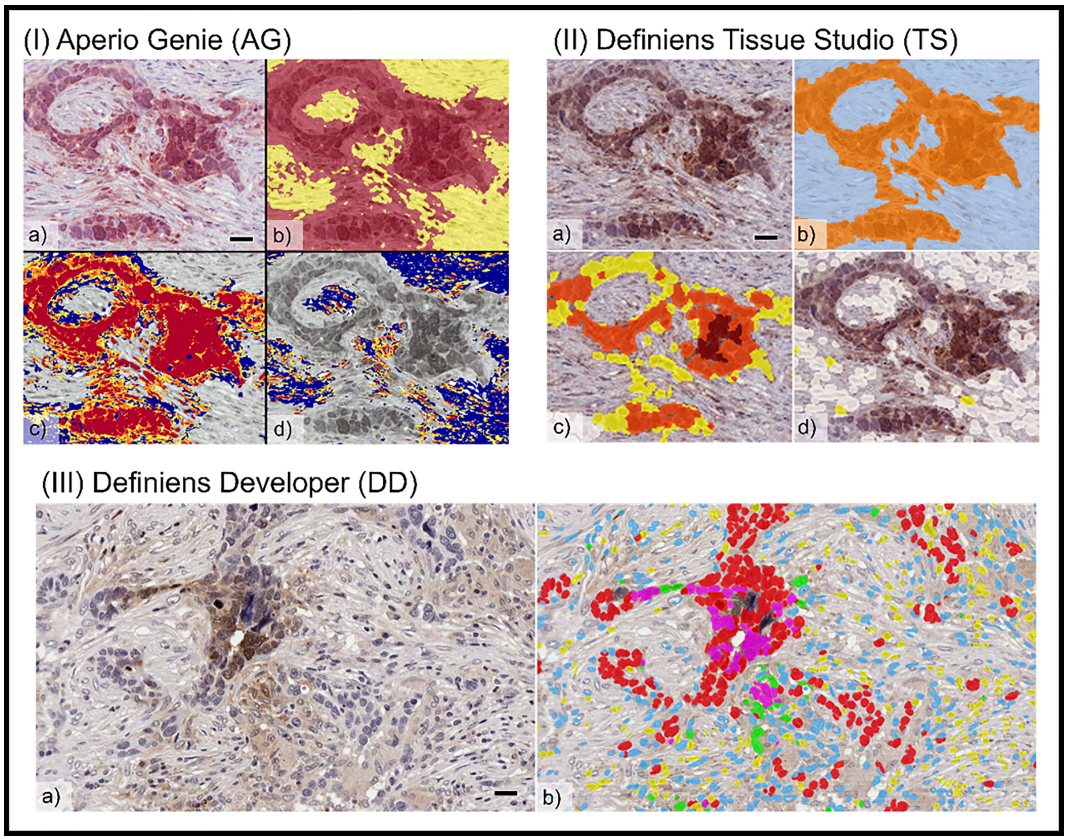

FIGURE 2
Comparison of tumor cellular classification with image overlay as processed on different image analysis platforms: (I) Aperio Genie: **(A)** pimonidazole (pimo), IHC **(B)** epithelial (red), from stroma (yellow) classification; **(C)** pimo +ve (red/orange) vs. pimo -ve (blue) in epithelial tumor; **(D)** pimo+ (red/orange) vs. pimo -ve (blue) in stromal tumor. (II) Definiens Tissue Studio: **(A)** pimonidazole IHC; **(B)** epithelial (orange) from stroma (light blue) classification; **(C)** pimo +ve (brown/orange/yellow) from pimo -ve (white) in epithelial compartment; **(D)** pimo+ (brown/orange/yellow) from pimo -ve (white) in stromal compartment; and (III) Definiens Developer: **(A)** pimonidazole IHC; **(B)** segmented cell overlay with pimo +ve epithelial cells (pink), pimo -ve epithelial cells (red), pimo +ve stromal cells (green), pimo -ve stromal cells (blue), inflammatory/other (yellow).

Factors contributing to heterogeneity of quantitative hypoxia measurements

The respective contributions of intra- and interpatient heterogeneity to the variability of the estimates of HP were evaluated by mixed-effect modeling; these results are summarized in Figure 4.

For Developer and Genie analyses, most of the variability in measurement was related to heterogeneity across different tumors, with a lower proportion of the variability being related to the heterogeneity within a particular tumor. For example, with Developer analysis, 73% of the variability inherent in measures of HP-whole tumor was interpatient variance while 27% was related to heterogeneity within a tumor; for analysis on Genie, the numbers were 68% (inter-) vs. 32% (intra), respectively. The comparatively higher inter- vs. intra-patient heterogeneity on Genie and Developer suggests that automated image analysis (AIA) estimates of tumoral hypoxia using these platforms will identify real differences in HP across patients. In contrast, most of the variability inherent in the Tissue Studio analysis was related to heterogeneity within a tumor (for HP-whole tumor, 68% intra-patient vs. 32% interpatient heterogeneity). The high level of intra-patient heterogeneity reduces the confidence with which estimates of HP by Tissue Studio approximate "true" tumoral hypoxia, and the degree to which this analysis is likely to differentiate biologically real and relevant differences in hypoxia levels across patients is low.

Hypoxia was more variable in the stromal vs. epithelial tumor compartment on all three platforms—29% vs. 26% on Developer, 43% vs. 30% on Genie, and 94% vs. 69% on Tissue Studio. This suggests that HP-epithelial, with its relatively high inter-patient and low intra-patient heterogeneity, would be the best measure to use to differentiate among tumors based on levels of pimonidazole-detectable hypoxia.

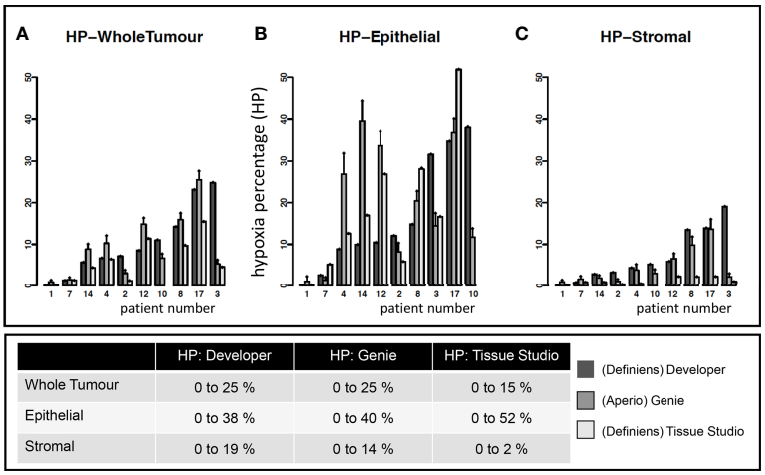

	HP: Developer	HP: Genie	HP: Tissue Studio
Whole Tumour	0 to 25 %	0 to 25 %	0 to 15 %
Epithelial	0 to 38 %	0 to 40 %	0 to 52 %
Stromal	0 to 19 %	0 to 14 %	0 to 2 %

FIGURE 3
Estimates of tumoral hypoxia by different image analysis platforms. Each point on the x-axis represents a unique study patient. Each patient (except 10) has estimates of hypoxia on Definiens Developer, Genie, and Tissue Studio as indicated by different colored bars. Y-axis shows the hypoxia percentage (HP) (i.e., pimonidazole-detected hypoxia) in specific tumor compartments: **(A)** whole tumor, **(B)** epithelial, and **(C)** stromal tumor compartments.

An additional contributor to the heterogeneity of hypoxia measurements within a given patient's tumor is the variance within and across slides. In the analysis completed on Developer, there was less variability across different sections of the same tumor compared with the variability within one section. For example, in estimating HP tumor, 25% of the variance inherent in the measure of hypoxia was related to variability across different ROIs in a given tumor section while 9% of the variance was related to variance across different sections and 66% of the variance in the measure was related to inter-patient variability (Figure 5).

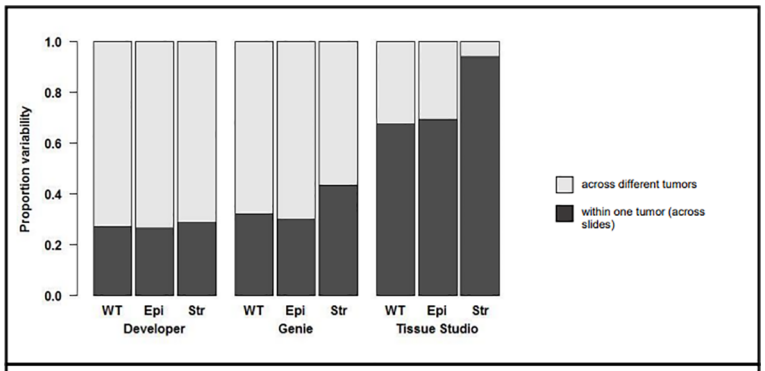

Variance	Developer (DD)			Genie (AG)			Tissue Studio(TS)		
	HP WT	HP Epi	HP Str	HP WT	HP Epi	HP Str	HP WT	HP Epi	HP Str
across tumors	73%	74%	71%	68%	70%	57%	32%	31%	6%
within a tumor	27%	26%	29%	32%	30%	43%	68%	69%	94%

Epi: epithelial
Str: stroma
WT: whole tumor

FIGURE 4
Variability in assessment of hypoxic percentage (in different tumor compartments) across platforms related to inter-patient (light gray) vs. intra-patient (dark grey) variability.

Reliability of estimates of HP based on number of sections evaluated

We calculated the intraclass correlation coefficient (ICC) using the mean of two or more values for each tumor, to understand the reliability of estimates of HP related to the number of tumor sections evaluated per patient tumor, with values equal to or greater than 0.85 indicating a high level of reliability across measurements. The results of this analysis are summarized in Table 1. As expected, ICC values increased with greater number of sections evaluated. Across the different platforms, calculated ICC was highest with Developer (0.88 for HP-stroma and 0.89 for both HP-epithelial and HP-whole tumor if three tumor sections were analyzed per patient tumor) and lowest with Tissue Studio (0.24 for HP-stroma, 0.69 for HP-epithelial, and 0.71 for HP-whole tumor if five sections were analyzed). These data suggest that analysis of three (representative) tumor sections would be sufficient to reliably estimate HP in resected pancreatic cancers using Developer but by contrast, analysis on Tissue Studio had high intra-patient variability, such that even evaluation of five tumor sections had poor reliability.

Discussion

We present here our results studying three unique image-analysis platforms with computer-based learning capabilities, for their ability to provide quantitative estimates of pimonidazole-detectable hypoxia in surgically resected pancreatic cancers. These studies add to our prior work where an extensive, iterative training process was used to develop tumor-individualized scoring algorithms for the pixel-based platform Genie. This semiquantitative strategy provided estimates of pimonidazole tumor staining that were highly concordant with manual scoring (1). Its primary limitation, however, was the need to develop a customized algorithm for each tumor analyzed, resulting in a strategy that was cumbersome and impractical for high-throughput analysis. We have now compared these results with analyses conducted on two other image analysis platforms with different cellular segmentation capabilities—Developer and Tissue Studio. Both platforms were selected for study based on their contemporary use at our institution at the time and to test the hypothesis that automated analysis platforms performing tumor/stroma differentiation at a cellular level would yield more reproducible and accurate estimates of pimonidazole staining, which could be completed in a high-throughput manner.

We observed significant variability in pimonidazole staining both within and across patient tumors, using all three platforms. Quantitation by Developer and Genie were closely aligned, but estimates of stromal hypoxia by Tissue Studio were much lower than those made on the other two platforms. Pimonidazole scoring on both Developer and Genie had greater inter-patient than intra-patient heterogeneity, suggesting that either of these techniques should be able to confidently discern differences in levels of pimonidazole-detectable hypoxia across patients. In contrast, the high intra-patient variability of Tissue Studio

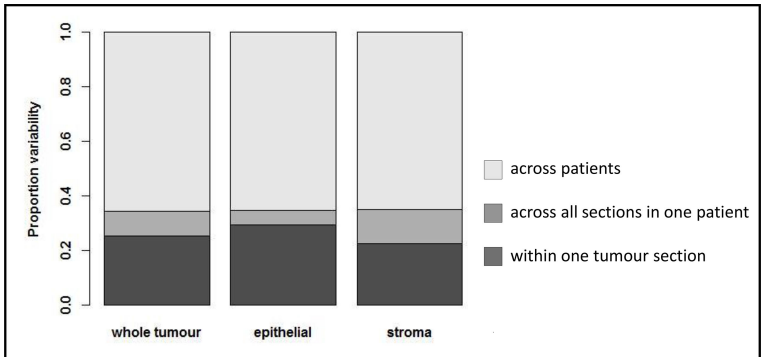

Variance	HP whole tumour	HP epithelial	HP stroma
across tumours	66%	65%	65%
across sections within same tumour	9%	5%	13%
across ROIs in one section	25%	29%	22%

FIGURE 5
Estimation of variability of hypoxia estimated by Definiens Developer analysis within given patients and across patients. HP; hypoxic percentage.

hypoxia estimates compromises the utility of this platform to discriminate biologically relevant differences in hypoxia levels across patients.

The calculated intraclass coefficients (ICCs) provided insights into the impact of increasing the number of estimates made per patient tumor on measurement reproducibility, with an ICC of 0.85 (or 85%) considered good reliability. Analysis of three sections per patient tumor on Developer was sufficient for reliable estimates of both epithelial and stromal hypoxia, in comparison with the five required for analysis on Genie. This finding likely reflects the improved accuracy of cellular classification and differentiation of epithelial from stromal cells, using Developer with its cell-based segmentation, compared with the pixel-based platform Aperio. In contrast, the low ICC estimates of the Tissue Studio analysis underscore its low reliability in architecturally complex tissue like PDAC, likely due to the inferior epithelial/stromal discrimination by tissue-level classifiers. In Developer, we were able to develop customized, pathologist-guided, and cell-based segmentation algorithms that could use random-forest-based machine learning classifiers to identify unique cell phenotypes. In contrast, Tissue Studio analyses apply a generic, tissue-level classifier to differentiate epithelial from stromal regions, and subsequently, standard, computer-vision based, nuclear segmentation algorithms are used for cellular discrimination. Although this strategy does allow for a higher degree of cellular discrimination than pixel-based platforms like Genie, the complex architecture of PDAC tumor tissue meant that several rounds of refinement and manual correction were required, limiting both the consistency and throughput of this analysis.

Although the development of the Developer rule set was time/resource intensive, once optimized, the trained classifier could be applied across hundreds of slides, with the only manual intervention being a pre-analysis annotation of tumor regions of interest, a process that took few minutes per slide. This provided an efficient and reliable workflow with significant reduction in time spent for post-segmentation ROI correction. Following annotation, whole-slide processing utilizing a tiled approach enabled the analysis of 0.5–1 slides per hour on a desktop server running two Developer CPU engines simultaneously. The time requirement for these same tasks on platforms using tissue-level classifiers with manual correction was on average 20+ hours per image, highlighting additional advantages to the cellular segmentation-based analysis methods.

We recognize that since the completion of this work, several other digital image analysis platforms have emerged with comparable capabilities and more modern interfaces than those discussed here. A similar workflow in which cellular- or tissue-level features are used to build a segmentation strategy guided by input from expert disease-site pathologists should provide similar results. In future directions from this work, the cellular segmentation map output could also be leveraged as training data for more contemporary machine learning or AI-based image analysis approaches.

Although manual scoring by expert pathologists remains the standard method of immunohistochemical analysis, its robustness and broader applicability can be deeply affected by subjectivity and interobserver variability (17). Attempts to improve on between-pathologist reproducibility and within-pathologist repeatability has led to the exploration of field-of-view analysis (18). Further semiquantitative scoring systems have been derived to convert subjective descriptions of IHC-marker expression into quantitative data. One such tiered system was historically used in prior pimonidazole-based hypoxia scoring studies and performed well in comparison with manual scoring. However, the categorization of data results in loss of information that could be inferred from continuous variables, and unless category borders are well defined *a priori*, border misclassification introduces ambiguity in analysis (4). In the specific context of hypoxia scoring, a lack of clarity with respect to biologically relevant thresholds of pimonidazole-detectable hypoxia results in the use of arbitrary cut-points to define categories. All of these issues have the potential to obscure biologically relevant differences across tumors, limiting the utility of an analysis method. It is worth mentioning that, in spite of the clearly recognized prognostic significance of tumoral hypoxia, therapeutic targeting of this microenvironmental feature has been challenging, perhaps in part due the lack of robust tools for defining patient subgroups based on tumor hypoxia levels.

Contemporary platforms of image analysis with cellular segmentation capability, and utilizing computer-based learning algorithms for rule-set development, combines the discrimination power of manual scoring by expert pathologists, with the consistency and high throughput of automated digital pathology (19). Furthermore, the whole-section analysis that is possible with automated digital pathology appears to have greater reproducibility than field-of-view, manual scoring (20). There is the further advantage that computational analyses may have greater discriminatory power than human visual perception; however, whether there is biological relevance to these differences remains to be determined.

In conclusion, we have presented in this report our workflow and preliminary results from a quantitative, automated digital image analysis that can be applied to formalin-fixed, clinical PDAC tumors in a high-throughput manner. This method has been applied to the full dataset of PIMO-PANC patient tumors to explore relationships between hypoxia and prognosis in patients with early-stage, pancreatic ductal adenocarcinoma. In future work, we will be exploring the potential to modify the current algorithms, with the input of expert pathologists, for application to other tumor types.

Data availability statement

The raw data supporting the conclusions of this article will be made available by the authors, without undue reservation.

Ethics statement

The studies involving human participants were reviewed and approved by University Health Network. The patients/participants provided their written informed consent to participate in this study.

Author contributions

IS, JB, TDM, TD carried out the research under the supervision of NCD and DWH. IS, ND and DWH planned all analysis. JB, IS, TD and TDM carried out the machine learning development and analysis. JX carried out histopathology technical support. IS, JB, TDM and NS wrote the paper with contributions from all authors. All authors approved the final manuscript.

Conflict of interest

The authors declare that the research was conducted in the absence of any commercial or financial relationships that could be construed as a potential conflict of interest.

Publisher's note

All claims expressed in this article are solely those of the authors and do not necessarily represent those of their affiliated organizations, or those of the publisher, the editors and the reviewers. Any product that may be evaluated in this article, or claim that may be made by its manufacturer, is not guaranteed or endorsed by the publisher.

Supplementary material

The Supplementary Material for this article can be found online at: https://www.frontiersin.org/articles/10.3389/fonc.2022.926497/full#supplementary-material

References

1. Dhani NC, Serra S, Pintilie M, Schwock J, Xu J, Gallinger S, et al. Analysis of the intra- and intertumoral heterogeneity of hypoxia in pancreatic cancer patients receiving the nitroimidazole tracer pimonidazole. *Br J Cancer* (2015) 113(6):864–71. doi: 10.1038/bjc.2015.284

2. Polley MY, Leung SC, McShane LM, Gao D, Hugh JC, Mastropasqua MG, et al. An international Ki67 reproducibility study. *J Natl Cancer Inst* (2013) 105 (24):1897–906. doi: 10.1093/jnci/djt306

3. Thomson TA, Hayes MM, Spinelli JJ, Hilland E, Sawrenko C, Phillips D, et al. HER-2/neu in breast cancer: interobserver variability and performance of immunohistochemistry with 4 antibodies compared with fluorescent *in situ* hybridization. *Mod Pathol* (2001) 14(11):1079–86. doi: 10.1038/modpathol.3880440

4. Meyerholz DK, Beck AP. Principles and approaches for reproducible scoring of tissue stains in research. *Lab Invest* (2018) 98(7):844–55. doi: 10.1038/s41374-018-0057-0

5. Elliott K, McQuaid S, Salto-Tellez M, Maxwell P. Immunohistochemistry should undergo robust validation equivalent to that of molecular diagnostics. *J Clin Pathol* (2015) 68(10):766–70. doi: 10.1136/jclinpath-2015-203178

6. Pintilie M, Iakovlev V, Fyles A, Hedley D, Milosevic M, Hill RP. Heterogeneity and power in clinical biomarker studies. *J Clin Oncol* (2009) 27 (9):1517–21. doi: 10.1200/JCO.2008.18.7393

7. Bankhead P, Loughrey MB, Fernandez JA, Dombrowski Y, McArt DG, Dunne PD, et al. QuPath: Open source software for digital pathology image analysis. *Sci Rep* (2017) 7(1):16878. doi: 10.1038/s41598-017-17204-5

8. Rizzardi AE, Zhang X, Vogel RI, Kolb S, Geybels MS, Leung YK, et al. Quantitative comparison and reproducibility of pathologist scoring and digital image analysis of estrogen receptor beta2 immunohistochemistry in prostate cancer. *Diagn Pathol* (2016) 11(1):63. doi: 10.1186/s13000-016-0511-5

9. Jankovic B, Aquino-Parsons C, Raleigh JA, Stanbridge EJ, Durand RE, Banath JP, et al. Comparison between pimonidazole binding, oxygen electrode measurements, and expression of endogenous hypoxia markers in cancer of the uterine cervix. *Cytom B Clin Cytom.* (2006) 70(2):45–55. doi: 10.1002/cyto.b.20086

10. Janssen HL, Haustermans KM, Sprong D, Blommestijn G, Hofland I, Hoebers FJ, et al. HIF-1A, pimonidazole, and iododeoxyuridine to estimate hypoxia and perfusion in human head-and-neck tumors. *Int J Radiat Oncol Biol Phys* (2002) 54(5):1537–49. doi: 10.1016/S0360-3016(02)03935-4

11. Ljungkvist AS, Bussink J, Kaanders JH, van der Kogel AJ. Dynamics of tumor hypoxia measured with bioreductive hypoxic cell markers. *Radiat Res* (2007) 167(2):127–45. doi: 10.1667/RR0719.1

12. Azuma C, Raleigh JA, Thrall DE. Longevity of pimonidazole adducts in spontaneous canine tumors as an estimate of hypoxic cell lifetime. *Radiat Res* (1997) 148(1):35–42. doi: 10.2307/3579536

13. Gross MW, Karbach U, Groebe K, Franko AJ, Mueller-Klieser W. Calibration of misonidazole labeling by simultaneous measurement of oxygen tension and labeling density in multicellular spheroids. *Int J Cancer* (1995) 61 (4):567–73. doi: 10.1002/ijc.2910610422

14. Raleigh JA, Chou SC, Bono EL, Thrall DE, Varia MA. Semiquantitative immunohistochemical analysis for hypoxia in human tumors. *Int J Radiat Oncol Biol Phys* (2001) 49(2):569–74. doi: 10.1016/S0360-3016(00)01505-4

15. Zhang Y, Coleman M, Brekken RA. Perspectives on hypoxia signaling in tumor stroma. *Cancers (Basel)* (2021) 13(12):3070. doi: 10.3390/cancers13123070

16. Chen Y, McAndrews KM, Kalluri R. Clinical and therapeutic relevance of cancer-associated fibroblasts. *Nat Rev Clin Oncol* (2021) 18(12):792–804. doi: 10.1038/s41571-021-00546-5

17. Aeffner F, Wilson K, Martin NT, Black JC, Hendriks CLL, Bolon B, et al. The gold standard paradox in digital image analysis: Manual versus automated scoring as ground truth. *Arch Pathol Lab Med* (2017) 141(9):1267–75. doi: 10.5858/arpa.2016-0386-RA

18. Nassar A, Cohen C, Agersborg SS, Zhou W, Lynch KA, Albitar M, et al. Trainable immunohistochemical HER2/neu image analysis: A multisite performance study using 260 breast tissue specimens. *Arch Pathol Lab Med* (2011) 135(7):896–902. doi: 10.5858/2010-0418-OAR1.1

19. Stalhammar G, Fuentes Martinez N, Lippert M, Tobin NP, Molholm I, Kis L, et al. Digital image analysis outperforms manual biomarker assessment in breast cancer. *Mod Pathol* (2016) 29(4):318–29. doi: 10.1038/modpathol.2016.34

20. Barnes M, Srinivas C, Bai I, Frederick J, Liu W, Sarkar A, et al. Whole tumor section quantitative image analysis maximizes between-pathologists' reproducibility for clinical immunohistochemistry-based biomarkers. *Lab Invest* (2017) 97(12):1508–15. doi: 10.1038/labinvest.2017.82

frontiers | Frontiers in Oncology

TYPE Review
PUBLISHED 23 August 2022
DOI 10.3389/fonc.2022.899722

OPEN ACCESS

EDITED BY
Min Xue,
University of California, Riverside,
United States

REVIEWED BY
Yajun Zhao,
Nanjing Tech University, China
Zhili Guo,
Quantum-Si, Inc., United States

*CORRESPONDENCE
Tian'an Jiang
tiananjiang@zju.edu.cn

SPECIALTY SECTION
This article was submitted to Cancer Immunity and Immunotherapy, a section of the journal Frontiers in Oncology

RECEIVED 19 March 2022
ACCEPTED 22 July 2022
PUBLISHED 23 August 2022

CITATION
Wang Y, Jiang T'a, Xie L, Wang H, Zhao J, Xu L and Fang C (2022) Effect of pulsed field ablation on solid tumor cells and microenvironment. *Front. Oncol.* 12:899722. doi: 10.3389/fonc.2022.899722

Effect of pulsed field ablation on solid tumor cells and microenvironment

Yujue Wang[1], Tian'an Jiang[1,2,3]*, Liting Xie[1,2], Huiyang Wang[1,2], Jing Zhao[1], Lei Xu[1] and Chengyu Fang[1]

[1]Department of Ultrasound Medicine, The First Affiliated Hospital, Zhejiang University School of Medicine, Hangzhou, China, [2]Key Laboratory of Pulsed Power Translational Medicine of Zhejiang Province, Hangzhou, China, [3]Zhejiang University Cancer Center, Hangzhou, China

Pulsed field ablation can increase membrane permeability and is an emerging non-thermal ablation. While ablating tumor tissues, electrical pulses not only act on the membrane structure of cells to cause irreversible electroporation, but also convert tumors into an immune active state, increase the permeability of microvessels, inhibit the proliferation of pathological blood vessels, and soften the extracellular matrix thereby inhibiting infiltrative tumor growth. Electrical pulses can alter the tumor microenvironment, making the inhibitory effect on the tumor not limited to short-term killing, but mobilizing the collective immune system to inhibit tumor growth and invasion together.

KEYWORDS

pulsed field ablation, irreversible electroporation, nanosecond pulsed electric fields, immunogenic cell death, microenvironment

Introduction

The cells demonstrate atypia as they go from normal to malignant cells, including pleomorphism, hyperchromasia, and an increase in mitotic figure. The tumor tissues also show atypia, that is, the arrangement of tumor cells becomes disordered and irregular. Changes in the tumor microenvironment have gotten a lot of attention in recent years when it comes to the occurrence and progression of cancer. The tumor microenvironment, including tumor chemical environment, immune cells, extracellular matrix (ECM), and tumor vascular system, is the tiny environment in which tumors live (1). The enhancement of tumor proliferation signal, the resistance of apoptosis, avoidance of immunity, and promotion of tumor microvascular formation are all related to the microenvironment (2).

As an emerging ablation technique, irreversible electroporation (IRE) has the advantages of good tissue selectivity, clear ablation limits, no influence of large vessel heat sink effect, short ablation time, and few postoperative complications (3). Pulsed field ablation is different from traditional thermal ablation techniques such as radiofrequency

ablation, microwave ablation, high intensity focused ultrasound therapy, etc. It is a heat-independent ablation with a delayed release of transient high-voltage electrical pulses that cause damage to the membrane structure of cells within the target ablation foci. The release of electrical pulses to tissues or cells can cause reversible or irreversible perforation of cell membranes, and apoptosis can be observed. There are several ablation techniques that perforate cells by electrical pulses to induce apoptosis, which can be classified according to the characteristics of the pulsed electric field parameters: nanosecond pulsed electric fields (nsPEF) deliver electrical pulses with very short pulse widths (in the range of 10-300 ns) and strong field strengths (20-150 kV/cm), and all pores remain small. IRE's pulse widths range from microseconds to milliseconds but its amplitudes are less than 10 kV/cm, causing a wide range of pore size variations (4, 5). High-frequency irreversible electroporation (H-FIRE) systems that split the ~100 μs monopolar pulse into a series of shorter duration ~1 μs alternating polarity pulses (6). There is also electrochemotherapy (ECT), which allows the uptake of drugs by reversible electroporation (2). Despite the different pulse parameters, IRE, nsPEF, and H-FIRE can all act through irreversible damage to the cell membrane (4–6).

Studies have shown the safety and efficacy of pulsed field ablation (7–9). Pulsed field ablation can form perforations in the membrane and induce a complex immune process that alters the local microenvironment of the tumor (10, 11). In this review, we summarize changes in tumor cells, immunogenic effects, vascularity, extracellular matrix, and chemical environment induced by electric pulses.

Changes in tumor cells

Cell signal pathway

After delivering high-voltage electric pulses to tumor cells, it kills them *via* a variety of mechanisms including cell membrane perforation, mitochondrial damage, reactive oxygen species (ROS), and DNA damage (4, 12, 13). Firstly, IRE, nsPEF, and H-FIRE all cause damage to cell membranes, resulting in osmotic imbalance and cell swelling (14, 15). And electrical pulses can also lead to DNA damage, but whether the direct effect or the indirect effect induced by apoptosis is not clear (16–18). ROS is also one of the mechanisms of damage. High levels of ROS were found after PEF treated melanoma cells (19). What needs to be emphasized is that mitochondrial damage is more studied in nsPEF, because nsPEF has shorter pulse width, increasing the possibility of causing damage to organelles, and nsPEF causes mitochondrial damage by the loss of mitochondrial membrane potential (14, 20). Thus, damage to cells through different mechanisms may lead to changes in cellular signaling pathways.

Some articles have focused on the effects of electrical pulses on cellular signaling pathways. According to one study, applying nsPEF to the human pancreatic carcinoma cell line (PANC-1) can change the protein expression of the Wnt/β-catenin signaling pathway, matrix metalloproteinases (MMP) family, and vascular endothelial growth factor (VEGF). The downstream signals of the Wnt/β-catenin signaling pathway, including hDPR1, β-catenin, and c-Myc, are dose-dependently decreased by nanosecond pulses (21). Wnt/β-Catenin has two pathways, the canonical pathway and the non-canonical, and the canonical pathway can lead to the transcription of target genes such as myc and cyclin D1, nanosecond pulses inhibit the transcription of target genes through this pathway, thereby inhibiting the proliferation of tumor cells (22). In addition to Wnt/β-catenin pathway, the expression of NF-κB pathway proteins including IKK-α, IKK-β, IκB-α, NF-κB p-65, and p-p65 is also significantly reduced (21). Not only that, the expression of proapoptotic lymphocytes/leukemia-2 (Bcl-2) family proteins (Bax, Bim, and BID) is promoted, and the expression of antiapoptotic Bcl-2 family proteins phosphorylated Bcl-2 protein (p-Bcl-2), Bcl-xL and myeloid leukemia-1 (Mcl-1) are inhibited (22, 23). The MMPs family and VEGF are also lower than those of the control group. Downgrading of MMPs and VEGF can inhibit tumor invasion and metastasis. It is explained in detail in "4. Vascularity, stroma and chemical environment ".

Sun S et al. performed IRE on human pancreatic cancer cell line AsPC-1 and BxPC-3 *in vitro* and found that IRE can trigger ROS-dependent apoptosis in pancreatic cancer through the PI3K/Akt pathway (11). Another study found that the gene expression of KRAS and EGFR pathway signaling molecules changed significantly after IRE treatment on pancreatic tumors. EGFR signaling was inhibited: (i) causing a decrease in AKT, NF-kB, and VEGF expression, which inhibited tumor growth and invasion, metastasis, etc. (ii) leading to the inhibition of JAK and STAT3, thus providing inhibition of G0 to G1 phase transformation and reducing tumor cell replication. While K-RAS was inhibited, MEK1/2, JNK, and ERK1/2 expression were down-regulated, thus inhibiting cell replication and proliferation. IRE significantly altered the cancer hallmarks and immunosuppressive biological pathways in the PDX pancreatic tumor model. And necrosis, regeneration/repair, and inflammatory signaling were significantly increased after IRE (23).

Wnt/β-Catenin, KRAS, EGFR, as well as downstream cellular pathways like MMP and VEGF were found to be downregulated after electrical pulses were applied to pancreatic cancer, and then cancer biology, including proliferation, cell death, invasion, and metastasis, all changed (Figure 1). Both IRE and nsPEF can exert anti-tumor effects by inhibiting cell replication, increasing the expression of pro-apoptotic proteins and suppressing the expression of antiapoptosis proteins, but there is not enough evidence to prove a significant difference between IRE and nsPEF in causing changes in cellular pathways.

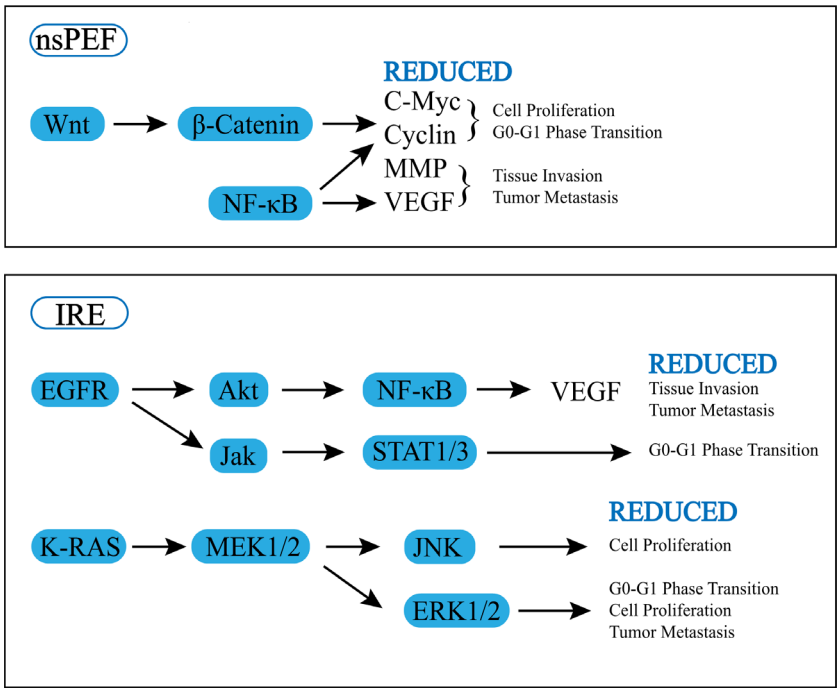

FIGURE 1
Effect of pulsed field ablation on cell signal pathway.

Cell death

Pulsed electric field ablation is known for its ability to cause apoptosis-a kind of programmed cell death. Because pro-apoptotic and anti-apoptotic factors regulate cell apoptosis, the increase in Bax, Bim, and BID and decrease in p-Bcl-2, Bcl-XL, and McL-1 after an electric pulse suggests that electroporation can promote cell apoptosis (18, 22, 24–26). Significantly increased cleavaged and active caspase 3, 7, and 9 were also detected after IRE (4, 21, 26–29), which are the markers of apoptosis. Cells exhibit the pathological characteristics of apoptosis after electrical impulses: nuclear pyknosis, nucleolysis, nuclear fragmentation, and apoptotic bodies were observed (21, 30–33).

However, during the delivery of electrical pulses, some heat will inevitably be generated. Tissues and cells exhibit distinct death features depending on their distance from the electrode needle. Generally speaking, the closer to the needle track, the easier it is to necrosis, the middle part shows irreversible electroporation, and the cells far away from the needle track are easy to form reversible perforation, which may be related to temperature, the closer the needle track is to the more heated the tissue, the more serious the thermal damage caused, which is characterized by zones of white coagulation (30, 34). The necrosis zone shows endoplasmic reticulum and nuclear membrane expansion and random DNA degradation (4, 16).

Pyroptosis and necroptosis belong to immunogenic cell death (ICD) that rely on the release of damage associated molecular patterns (DAMPs) to drive local immune responses. Pyroptosis forms intracellular inflammatory vesicles and activates caspase-1, gasdermin D (GSDMD) channels are formed on the cell surface and interleukin (IL)-1β, IL-18, and DAMP molecules are released from the cell *via* GSDMD pores, where they stimulate an immune response. Water and ion can also influx the cell from GSDMD, causing edema of the cell (4). Activation of caspase-1 and GSDMD was observed in rat liver tissue at 6 and 24 hours after electroporation, illustrating that IRE can cause pyroptosis (16). Necroptosis is initiated by the necrosome and activates the receptor interacting serine/threonine kinase 3 (RIPK3), which activates mixed lineage kinase domain-like pseudokinase (MLKL). Activated MLKL molecules aggregate and form pores in the cell membrane, allowing the release of DAMPs and the influx of water and ions, causing cellular edema and cell membrane disintegration, similar to the morphological manifestation of necrosis (4). Elevated RIP3 and MLKL were harvested after IRE, and cell morphology was observed with loss of the plasma membrane and release of organelles and chromatin, which is consistent with the morphology of necroptosis (21). Multiple modes of cell death may exist in the target area after electrical pulses, but they can change over time, and genetic analysis revealed that apoptosis was the predominant mode of cell death after H-FIRE (2000V,

100μs, bipolar pulses, a 2μs positive pulse, 5μs inter-pulse delay, 2;μs negative pulse, and a 5μs inter-pulse delay) was applied to the mouse 4T1 mammary tumor at 2 hours, while necrosis and pyroptosis were predominant by 24 hours (27). In addition, the mode of cell death can change with parameters, more energy may have greater thermal damage, more necrosis. Brock et al. conducted IRE on utilizing patient-derived xenograft (PDX) models, and found that apoptosis was evident at 500 V/cm but necrosis was more prominent at 2500 V/cm (23).

Immune response

DAMPs and immunity

Common DAMPs include the non-histone chromatin protein high mobility group box 1 (HMGB1), cell surface calcium reticulum protein (CRT), and other endoplasmic reticulum (ER) proteins, and adenosine triphosphate (ATP), which are associated with cell death. CD91, toll-like receptor 4 (TLR4), and The P2X7 receptor (P2RX7) are expressed by dendritic cells (DCs) and promote phagocytosis of dead cells, presentation of tumor antigens, and production of IL-1β, respectively (35). The release of DAMPs (ATP, calreticulin, nucleic acids and uric acid) increases with increasing pulse amplitude after IRE on cells *in vitro* (12, 29, 36–39) and causes massive immune cell aggregation in post-electroporation pancreatic cancer tissue *in vivo* (36) (Table 1). The release of DAMPs is related to the parameters of the pulses, at IRE (500-1500 V, 100 μs, 8-24 pulses) with increasing voltage, the release of DAMP increases (29), similarly, the number of DAMP releases is related to the number of pulses, after IRE (1000 V, 100 μs, 8/40/80 pulses), CRT, ATP, and HMGB1 were released most at 40 pulses and less at 8 and 80 pulses, suggesting that there may be a suitable number of pulses, neither too less nor too more, that would allow the most DAMP release, Go EJ et al. speculated that low pulses (<40) would not induce ICD and high pulses (>40) would lead to rapid cell death, thus limiting DAMP expression (38). Most of the studies about DAMP are *in vitro*, and the appropriate parameters, as well as the intensity-release dependence, may require further studies.

(i) CRT is the most abundant in the endoplasmic reticulum. After activation of ICD-related signaling pathways, it transfers from the endoplasmic reticulum to the cell membrane surface and can interact with transmembrane receptors including CD49, CD69, CD91 (also known as the low density lipoprotein (LDL) receptor-related protein-1 (LRP1)), and integrins. The most important is the CD91 molecule. CRT releases effective phagocytic signals to CD91-positive cells (mainly macrophages and DCs) and causes the production of pro-inflammatory cytokines (including IL-6 and TNF-α) (35, 40). (ii)In addition to participating in purinergic neurotransmission, ATP released from damaged cells can bind to the P2Y2 receptor of macrophages, promoting the infiltration of macrophages in tumor sites, and can also bind to the P2RX7 of DC cells, leading to DC maturation and release of IL-1β. (iii) HMGB1 can bind to protein toll-like receptor 4 (TLR-4) and receptor for advanced glycation end products (RAGE) to activate monocytes/macrophages. HMGB1 can also upregulate costimulatory molecules and major histocompatibility complex (MHC) class II to transfer immature DC to mature DC (35, 41, 42). HMGB1 stimulates neutrophils and monocytes, enabling these cells to adhere to activated vascular endothelium and migrate to inflamed tissues (43).

Electrical pulse stimulation triggers the release of DAMPs, which acts as a "find me" signal, enhances tumor immunogenicity and subsequently induces antigen-presenting cells (APC) activation. These signals enhance the ability of APC to phagocytose, process, and present tumor-derived antigens to T cells, thereby facilitating the induction of tumor-specific adaptive immunity. So, the level of these DAMPs and cells increases after pulsed electric field (29, 36–39).

Innate immune

Phagocytes

There are many phagocytic cells in the body, and the first one worth mentioning is macrophages. Macrophages have multiple functions: phagocytosis of dead cells and debris; acting as APC to process antigens and participate in adaptive immunity through MHC molecules; production and secretion of cytokines, including IL-1, IL-6, TNF-α, etc (44).

Polarized macrophages mainly exist in two distinct subsets: M1 and M2. The secreted cytokines are the key feature to distinguish the two: M1 type can secrete IL-6, IL-12 and tumor necrosis factor (TNF), M2 type can secrete IL-10, IL-1 receptor antagonist (IL-1ra), and the type II IL-1 decoy receptor. Type M1 is an effective inflammatory effector cell that can produce a large number of cytokines and kill tumor cells through the production of ROS. Type M2 is more inclined to promote angiogenesis and promote fibrosis to remodel and repair tissues (44, 45). Tumor-associated macrophages (TAM) have a phenotype and function similar to M2 macrophages, which reduce the killing of tumor cells by cytotoxic T cells and NK cells (45). Tumor cells secrete chemokine (C-C motif) ligand 2 (CCL-2) (lung tumors, breast cancer, cervical cancer, ovarian cancer, etc.) to cause the accumulation of macrophages. Low levels of CCL-2 promote tumor growth, and high levels of CCL-2 cause a large number of macrophages to accumulate and tumor destruction (45). After pancreatic ductal cell adenocarcinoma (PDAC) undergoes electroporation, the expression of CD16/32 in macrophages (a hallmark of M1 macrophages) increases and changes from a rod shape to a round shape, indicating that the formation of irreversible electroporation can induce M1 macrophages polarization of cells. In addition, positive-feedback release or expression of HMGB1 and RAGE in

TABLE 1 Effects of pulsed field ablation on tumor microenvironment.

Factors	Intervention	Parameters					Mode of action	*In vitro* or *in vivo*	Type of tumor
		V	EFS	PW	PRF	N			
DAMP									
1.CRT	IRE & RE	1000 1000 1000	– – –	100 100 100	– – –	80 40 8	24h: Increased by about 6.1 times. 24h: Increased by about 30 times. 24h: Increased by about 6.9 times	*In vitro*	The Lewis lung carcinoma (LLC, CRL-1642) (38)
2.ATP	IRE & RE	200	–	100	1	20	Within 30min: No significant difference.	*In vitro*	KRAS* (36)
		960 200 960	– – –	100 100 100	1 1 1	20 20 20	Within 30min: Increased Within 30min: Increased slightly Within 30min: Increased	*In vitro*	KRAS* (36) B16F10 (36) B16F10 (36)
		1000	–	100	–	80 40 8	24h: Increased by about 1.6 times. 24h: Increased by about 8.7 times. 24h: Increased by about 5.4 times.	*In vitro*	The Lewis lung carcinoma (LLC, CRL-1642) (38)
		500 1000	– –	100 100	1 1	20 20	Increased	*In vitro*	KPC (37)
	nsPEF	– –	7000 7000	0.2 0.2	10 10	– –	No significant difference (CT26) Increased (EL-4)	*In vitro*	EL-4 lymphoma; CT26 colon carcinoma cells (39)
3. HMGB1	IRE & RE	200 960	– –	100 100	1 1	20 20	Within 30min: No significant difference at 200V, increased at 960V.	*In vitro*	KRAS* (36)
		200 960	– –	100 100	1 1	20 20	Within 30min: No significant difference at 200V, increased at 960V.	*In vitro*	B16F10 (36)
		500–1500	–	100	–	8 16 24	24h: Increased in a strength-dependent manner.	*In vitro*	Panc-1, Bxpc-3, Pan02 (29)
		1000	–	100	–	8 40 80	24h: Increased by about 7.3 times. 24h: Increased by about 12.3 times. 24h: No increase.	*In vitro*	The Lewis lung carcinoma (38)
	nsPEF	– –	7000 7000	0.2 0.2	10 10	– –	Increased Increased	*In vitro*	EL-4 lymphoma; CT26 colon carcinoma cells (39)
4.HSP70	IRE & RE	500–1500	–	100	–	24 16 8	24h: Increased in a strength-dependent manner	*In vitro*	Panc-1, Bxpc-3, Pan02 (29)
5.Calreticulin	IRE & RE	500–1500	–	100	–	24 16 8	24h: Increased in a strength-dependent manner	*In vitro*	Panc-1, Bxpc-3, Pan02 (29)
Phagocytes									
1.Macrophages	IRE	1000	–	100	1	80	Day 7: M1 polarized and Increased in a strength-dependent manner Day 7: M2 decreased	*In vivo*	PC (29)
2.DC	IRE	1200	–	100	1	99	Day 9: No significant difference.	*In vivo*	PC (36)
3.NK	IRE	–	–	–	–	–	Day 3: decreased Day 7: increased	*In vivo*	PC (37)
	nsPEF	20000	–	0.3	4	1000	Day 8: increased	*In vivo*	HCC (56)
Cytokines and complements									
IL-1a	IRE	3000	–	70	–	90	2 h: increased	*In vivo*	HCC (51)
IL-1b	IRE	3000	–	70	–	90	2 h: increased	*In vivo*	HCC (51)
	nsPEF	30000	–	0.3	–	400	Day 7: increased	*In vivo*	PC (53)
IL-2	IRE	3000	–	70	–	90	2 h: increased	*In vivo*	HCC (51)
		–	–	–	–	–	Day 7: increased (more than Day 3 and preOP)	*In vivo*	PC (50)
	nsPEF	20000	–	0.3	4	1000	Day 8: increased	*In vivo*	HCC (56)
IL-5	nsPEF	20000	–	0.3	4	1000	Day 8: increased	*In vivo*	HCC (56)

(Continued)

TABLE 1 Continued

Factors	Intervention	Parameters					Mode of action	*In vitro* or *in vivo*	Type of tumor
		V	EFS	PW	PRF	N			
IL-6	IRE	–	–	–	–	–	Day 3: increased Day 7: decreased	*In vivo*	PC (50)
	nsPEF	20000	–	0.3	4	1000	Day 8: increased	*In vivo*	HCC (56)
		30000	–	0.3	–	400	Day 3: decreased	*In vivo*	PC (53)
IL-10	IRE	–	–	–	–	–	Day 3: increased Day 7: decreased	*In vivo*	PC (50)
		3000	–	70	–	90	2 h: increased Day 2: increased dramatically	*In vivo*	HCC (51)
	nsPEF	20000	–	0.3	4	1000	Day 8: increased	*In vivo*	HCC (56)
IL-12	IRE	3000	–	70	–	90	2 h: increased Day 2: increased dramatically	*In vivo*	HCC (51)
IL-17A	nsPEF	20000	–	0.3	4	1000	Day 8: increased	*In vivo*	HCC (56)
IL-17F	nsPEF	20000	–	0.3	4	1000	Day 8: increased	*In vivo*	HCC (56)
IL-21	nsPEF	20000	–	0.3	4	1000	Day 8: increased	*In vivo*	HCC (56)
IL-22	nsPEF	20000	–	0.3	4	1000	Day 8: increased	*In vivo*	HCC (56)
IFN-γ	IRE	–	–	–	–	–	No significant difference	*In vivo*	PC (50)
		3000	–	70	–	90	2 h: increased Day 2: increased dramatically	*In vivo*	HCC (51)
	nsPEF	20000	–	0.3	4	1000	Day 8: increased	*In vivo*	HCC (56)
TNF-α	IRE	3000	–	70	–	90	2 h: increased Day 2: increased dramatically	*In vivo*	HCC (51)
	nsPEF	30000	–	0.3	–	400	Day 7: increased	*In vivo*	PC (53)
		20000	–	0.3	4	1000	Day 8: increased	*In vivo*	HCC (56)
GM-CSF	IRE	3000	–	70	–	90	2 h: increased Day 2: increased dramatically	*In vivo*	HCC (51)
C3	IRE	–	–	–	–	–	Day 3: decreased Day 7: increased	*In vivo*	PC (50)
C4	IRE	–	–	–	–	–	Day 3: decreased Day 7: increased	*In vivo*	PC (50)
Immune-suppressive cells									
1.Treg	IRE	–	–	–	–	–	Day 3: increased Day 7: decreased	*In vivo*	PC (50)
		–	1500	90	–	–	Week 2: decreased	*In vivo*	PC (46)
		1200	–	100	1	99	Day 9: No significant difference	*In vivo*	PC (36)
	nsPEF	–	30000	0.3	–	400	Day 3: slightly increased Day 7: significantly decreased	*In vivo*	PC (53)
		–	30000	0.1	1	200	Day 4: decreased	*In vivo*	Malignant melanoma (67)
	H-FIRE	–	2500	100	–	–	Day 2: increased	*In vivo*	4T1 mammary tumor (27)
2.TAM	H-FIRE	–	2500	100	–	–	Day 2: decreased	*In vivo*	4T1 mammary tumor (27)
3.MDSC	IRE	–	1500	90	–	–	Day 14: eMDSC decreased	*In vivo*	PC (46)
	nsPEF	–	30000	0.3	–	400	Day 3&7: nMDSC & mMDSC decreased	*In vivo*	PC (53)
		–	30000	0.1	1	200	Day 4: decreased	*In vivo*	Malignant melanoma (67)
	H-FIRE	–	2500	100	–	–	Day 2: pMDSC decreased	*In vivo*	4T1 mammary tumor (27)
4.TAN	H-FIRE	–	2500	100	–	–	Day 2: decreased	*In vivo*	4T1 mammary tumor (27)
Adaptive immunity									
CD 4+ T cell	IRE	–	–	–	–	–	Week 2: increased	*In vivo*	PC (38)
		1200	–	100	1	99	Day 9: No significant difference	*In vivo*	PC (36)
		–	–	–	–	–		*In vivo*	PC (50)

(Continued)

TABLE 1 Continued

Factors	Intervention	Parameters					Mode of action	*In vitro* or *in vivo*	Type of tumor
		V	EFS	PW	PRF	N			
							Day 3: decreased Day 7: increased		
	nsPEF	–	20000	300	4	1000	Day 8: increased	*In vivo*	HCC (56)
CD 8+ T cell	IRE	1200	–	100	1	99	Day 9: increased	*In vivo*	PC (36)
		–	–	–	–	–	Day 3: decreased Day 7: increased	*In vivo*	PC (50)
		1000	–	100	–	90	increased	*In vivo*	HCC (70)
	nsPEF	–	20000	300	4	1000	Day 8: increased	*In vivo*	HCC (56)
B cell	IRE	1200	–	100	1	99	Day 9: No significant difference	*In vivo*	PC (36)
	nsPEF	–	20000	300	4	1000	Day 8: increased	*In vivo*	HCC (56)
IgA	IRE	–	–	–	–	–	Day 3&7: No significant difference	*In vivo*	PC (50)
IgG	IRE	–	–	–	–	–	Day 3: decreased Day 7: increased	*In vivo*	PC (50)
IgM	IRE	–	–	–	–	–	Day 3&7: No significant difference	*In vivo*	PC (50)
Vasculature, extracellular matrix, and chemical environment									
VEGF	nsPEF	–	20000	0.1	–	100	1h: decrease	*In vivo*	HCC (21)
CD31	IRE	1000	–	100	1	80	Day 7: increased	*In vivo*	PC (46)
		1200	–	100	1	99	Day 4: transient increase Day 6: decreased	*In vivo*	PC (36)
CD34	nsPEF	–	20000	0.1	–	100	1h: decrease	*In vivo*	Hep-3B HCC (21)
FITC-conjugated dextran	IRE	1200	–	100	1	99	Day 4: increased Day 6: decrease, but still higher than that of untreated tumors	*In vivo*	PC (36)
FAPα	IRE	1200	–	100	1	99	Day 4: decreased Day 6: rebounded back	*In vivo*	PC (36)
HABP1	IRE	1200	–	100	1	99	Day 6: decreased	*In vivo*	PC (36)
	nsPEF	1000	–	100	1	80	Day 3: decreased Day 7: decreased	*In vivo*	PC (53)
LOX	IRE	1000	–	100	1	80	Day 3: decreased Day 7: decreased	*In vivo*	PC (46)
		1200	–	100	1	99	Day 6: decreased	*In vivo*	PC (36)
α- SMA	IRE	1200	–	100	1	99	Day 6: No significant difference	*In vivo*	PC (36)
	nsPEF	1000	–	100	1	80	Day 3&7: No significant difference	*In vivo*	PC (53)
MMP	nsPEF		20000–60000	100	–	100	1 h: decrease	*In vivo*	HCC (21)
CA-IX	IRE	1200	–	100	1	99	Day 6: decreased	*In vivo*	PC (36)
HIF-1α	IRE	1200	–	100	1	99	Day 6: decreased	*In vivo*	PC (36)

V, Voltage (V); EFS, electric field intensity (V/cm); PW, Pulse width (μs); PRF, Pulse repetition frequency (Hz); N, Number of pulses; min, minutes; h, hour; HCC, hepatic cancer; PC, pancreatic cancer; RE, reversible electroporation; IRE, irreversible elecrtroporation; nsPEF, nanosecond pulsed electric fields; H-FIRE, High-frequency irreversible electroporation.

macrophages *via* the MAPK-ERK pathway promoted M1 macrophage polarization (29, 38), and M1/M2 ratio tends to increase in a strength-dependent manner (29). In addition to the MAPK - ERK pathway, a stimulator of interferon genes (STING) signaling is involved in the activation and repolarization of macrophages, one study found that this macrophage repolarization was most pronounced when tumors were treated with a combination of IRE and STING agonist (38).

After the electric pulse acts on the tissue, in addition to macrophages, the ablation zone also found the accumulation and activation of neutrophils, DC cells, and NK cells (Table 1). Like macrophages, these phagocytes can kill perforated cells (10, 36, 37, 46, 47).

Immature DC cells highly express TLRs, opsonizing receptors, etc. After receiving the DAMPs signal released by the perforated cells, the low-expressed MHC class II molecules

and costimulatory molecules are activated to become mature DC cells, which effectively present antigens in adaptive immunity (48). After electric pulse treatment of mouse KRAS* cells *in vitro*, the CD40, MHC-II, chemokine receptor (CCR) 7, and CD86 surface markers of DC cells increased relatively, which suggested the activation of DC cells (36). Combining IRE and DC vaccines for mouse pancreatic cancer, it can be found that IRE can overcome the immunosuppressive environment of pancreatic cancer, thereby enhancing the effect of DC vaccination (37).

NK cells can be defined into two subsets according to the levels of CD56 and CD 16: $CD56^{hi}$ $CD16^{\pm}$ and $CD56^{lo}$ $CD16^{hi}$, the former promoting the inflammatory response by releasing cytokines and the latter killing cells by perforin and granzyme (49). IRE can increase the concentration of mouse NK1.1 cells in the blood and tumor accumulation in animal experiments (37), and it can also cause an increase in peripheral blood NK cells in humans (50). NK cell therapy can also increase the killing effect on tumor cells. The combination of IRE ablation and NK cells can have a synergistic therapeutic effect on stage IV hepatocellular carcinoma. The combined treatment group's IL-2, tumor necrosis factor (TNF), and interferon (IFN) levels are higher in both groups than in the single treatment group. Synergistic treatment of liver cancer with IRE and NK also increases the levels of lymphocytes and Th1-type cytokine decreases the expression of alpha-fetoprotein and increases the survival time of patients (49). So, increasing NK cells will inhibit tumor growth, and electrical pulses can have a synergistic effect with NK cell therapy.

Cytokines

Chen X found IL-1a, IL-1ra, IL-1b, IL-2, IL-6, IL-8, and IL-18 levels are significantly higher 2 hours after IRE ablation. IL-4, IL-10, IL-12, TNF-a, IFN-r, granulocyte-macrophage colony-stimulating factor (GM-CSF) increased dramatically 2 days after ablation (51). Most of these cytokines can activate cytotoxic immunity, including IL-2, IL-4, IL-5, IL-6, IL-7, IL-10, IL-12, and IL-15. IL-16 and IL-17 also facilitate cellular immunity (52). And Chen X's result indicated that changes the abnormal drifted Th2 in HCC back to Th1 status (51). Zhao et al. found that after seven days the TNF-α and IL-1β levels in blood were increased, while IL-6 levels were decreased (53). IFN-γ stimulates antigen presentation and cytokine production by monocyte, and also stimulates monocyte adhesion, phagocytosis, and other effector functions. One of the most important biological activities of IL-1 is its ability to activate T lymphocytes by enhancing IL-2 production and IL-2 receptor expression. IL-6 is mainly produced by monocytes and mediates T cell activation, growth, and differentiation (52). IL-10 is a compound with both immunosuppressive and anti-angiogenic functions and is a direct inhibitor of Th1 function (54, 55). Yimingjiang et al. found significantly higher IL-10 in tumor-bearing mice after nanosecond pulses than in controls (56), while He et al. found that after IRE, IL-10 levels in pancreatic cancer increased on day 3 and decreased on day 7 (46). The immunosuppressive effect of IL-10, the function of recruitment to Treg makes IL-10 seem to promote tumor growth, while the changes in IL-10 levels after electrical pulses vary from experiment to experiment and need to be further verified (46, 51, 52, 56).

Thus, electrical pulses can activate phagocytosis, adhesion phagocytosis, activation of T lymphocytes, and induction of cytotoxic T lymphocyte (CTL) direct killer cells for immune response to post-perforation cells by triggering the secretion of pro-inflammatory cytokines *in vivo*.

Immune-suppressive cells

A large number of immunosuppressive cells are present in tumors, including T regulatory cells (Tregs), tumor-associated macrophages (TAMs), cancer-associated fibroblasts (CAFs), and myeloid-derived suppressor cells (MDSCs), and the upregulation of these cell types in tumors depends on the reciprocal signaling between these cells and tumor cells.

The production of Treg (usually $CD4+CD25^{+}Foxp3^{+}$ T cells) depends mainly on transforming growth factor-β (TGF-β) and IL-2, which negatively regulate immunity and can produce TGF-β and IL-10 to suppress immune responses (55, 57, 58). And Tregs' infiltration is negatively correlated with median survival OS in many patients with solid tumors (59). Tregs can effectively suppress effector T lymphocytes and can inhibit the function of B, NK, dendritic cells, and macrophages through different mechanisms (58, 60).

TAM has an M2 macrophage-like phenotype and promotes tumor progression through several mechanisms: secretion of VEGF, which promotes tumor angiogenesis; promotion of tumor invasion mainly through the release of metalloproteinases, matrix remodeling enzymes, and chemotactic growth factors from the environment; and suppression of innate immune responses (61).

There are mainly two types of MDSC: polymorphonuclear MDSC (P-MDSC) which resemble neutrophils morphologically and phenotypically, and monocyte MDSC (M-MDSC) which resemble monocytes. MDSC has potent immunosuppressive activity through multiple pathways: promoting Tregs' production and promoting fibroblast differentiation into cancer-associated fibroblasts (CAF) depleting L-arginine eliminates key trophic factors required for T cell proliferation, nitrates chemokines and blocks CD8+ T cells from entering the tumor, and produces immunosuppressive cytokines such as IL-10 and TGF-β (61, 62).

Unlike normal myofibroblasts, CAF does not undergo apoptosis and can release various cytokines and MMPs to hydrolyze extracellular matrix, stimulate angiogenesis and

promote tumor growth and invasion (63). (As described in 4. Vasculature, extracellular matrix, and chemical environment).

Reduction of systemic Tregs in locally advanced pancreatic cancer (LAPC) patients 2 weeks after IRE was found in clinical trials (64). However, a transient increase in Tregs on day three followed by a decrease on day seven was found in the clinical trial by He C (46). Similar results were also found in Harshul et al.'s study, where LAPC patients could have a procedure-mediated Treg attenuation between the third and fifth day after IRE (65). A reduction in Li^{-} CD^{33+} $HLA^{-}DR^{-}$ early myeloid-derived suppressor cells (eMDSC) was observed 2 weeks after IRE treatment (64). IRE combined with OX40 agonist induced a significant reduction in MDSC in primary and distant tumors (66). H-FIRE resulted in a reduction of MDSCs and TAMs in the tumor microenvironment of mammary carcinoma in mice 2 days after procedure (27). NsPEF treated with C57 malignant melanoma reduced Treg cells from 4.3% to 2.4% and MDSC by 39.0% to 19.7%, which was observed 4 days later (67). NsPEF can act on mice with pancreatic cancer after 3 days postoperative, 7 days postoperative decreased the percentage of nMDSCs and mMDSCs in the spleen, although Tregs slightly increased at 3 days postoperatively, but significantly decreased at 7 days postoperative (53), indicates that the immunosuppressed state can be reversed in this period of time, which would facilitate the combination with immunotherapy.

Therefore, electrical pulses can inhibit the proliferation of tumor-associated immune cells in the tumor microenvironment and promote anti-tumor responses to create an immune environment conducive to tumor suppression. However, the reversion of immunosuppression after IRE or nsPEF is time-dependent and this may start after day 3, but a longer and more subtle follow-up is needed to determine the time window for combination with immunotherapy.

Adaptive immunity

Adaptive immunity is achieved through regulated interactions between APC and T and B cells. Circulating antigens or APC-treated antigens are presented to T and B cells, eliciting cellular and humoral immunity, respectively. The largest T cell population in the body is the CD4+αβ T cell receptor (TCR) population. Most of these cells have a helper function and are called helper T (Th) cells, which produce many cytokines. CTL is a type of CD8+ T cells that kill target host cells through a contact-dependent mechanism: increased expression of FasL on CTL binds to Fas receptors in target tissues, participates in apoptosis, and acts on target cells by releasing substances such as perforin and granzyme. Adaptive humoral immunity is mediated by antibodies produced by plasma cells (55).

Several studies have found that electrical pulses acting on cells induce increased circulation and ablation foci of CD8+ T cells (24, 37, 46, 64, 68–70), and some experiments have found elevated CD4+ levels (38, 46, 55, 56), however, some studies has also shown no significant increase in CD4+ levels (10, 23) (Table 1). Zhao et al. found an increased CD8+ T cells and CD4+ T after nanosecond pulses acting on pancreatic cancer in mice, and a significantly higher CD8/CD3 ratio in tumors compared to controls (53). He et al. found an increase of effector CD8+ T cells, effector CD4+ T cells, and memory T cells at 7 days after IRE, despite decrease at day 3, so it can effectively induce the activation of T cells over a period of time, and the experiment also found that IRE can inhibit the growth of potential tumors through the distant effect (50). However, Dai et al. implied that IRE treatment significantly inhibited HCC growth by more CD8+ T and dendritic cells, but not CD4+ T or B cells infiltrating into the peri-ablative region. CD8+ depleted T cells induced local tumor regeneration and distant metastasis after IRE (10). Most of the IRE or nsPEF studies have activated the proliferation of CD8+T, but the proliferation of CD4+T is not obvious in some studies, revealing that CD8+ T-mediated cellular immunity plays a great role in electric pulses induced immunity. Effective T cell initiation requires several events, including: release of endogenous antigens from cancer cells, release of "danger signals" from damaged cells, processing of cancer antigens, antigens presented to naive T cells by APC, activation and proliferation of cancer-specific cytotoxic T cells (55, 69, 71). The current results suggest that pulsed electric field can promote cellular immunity through these sessions: 1) induce immunogenic death, resulting in the massive release of DAMP (29, 36, 38, 39); 2) Proliferation and activation of antigen presenting cells (29, 36, 38); 3) Activation, proliferation and function of cancer-specific cytotoxic T cells (36, 64, 66, 67, 70). In addition, Shao et al. compared IRE, thermal therapy (Heat), cryosurgery (Cryo) *in vitro*, and found that IRE can cause more protein release than other ablation. Although the released protein has 40% denatureation, T cell proliferation is still 2-3 times higher than Cryo (69). IRE induces OX40 expression in CD8+ T cells *in vivo*, and OX40 acts as a co-stimulatory molecule to increase T cell expansion and cytokine secretion (66). The combination of IRE and TLR 3/9 agonists and PD-1 blockade can effectively reverse the depletion of intratumoral CD8+T and enhance local immunity against tumors (72). Brandon et al. made a deeper exploration by combining anti-T-lymphocyte-associated protein-4 (anti-CTLA-4) therapy prior with IRE on prostate cancer to promote neoantigen-specific T-cell responses, resulting in increased numbers of splenic systemic SPAS-1+ T cells concentrated in tumors and distant sites. Circulating memory CD8+ T cells, in addition to central memory (T_{CM}) and effector memory (T_{EM}), have tissue-resident memory (T_{RM}). Endogenous SPAS-1 neoantigen-specific CD8+ T cells were increased in number and enriched in tumors following TRAMP-C2 tumor cell were attack and generated CD8+ T_{RM} cells in different tissues (68). In addition, Shi et al. treated hepatocellular carcinoma (HCC) with IRE in

combination with an anti-PD-L1 monoclonal antibody and found enhanced off-target necrosis and inflammatory infiltration, with IRE significantly increasing the inflammatory infiltration index and increasing CD8+ T infiltration not only in target tissues but also in non-target tissues (untreated tumors) (70). Immunotherapy Combined IRE induced more CD8+ T proliferation and enrichment in tumors as well as other sites than immunotherapy alone, probably because: 1) IRE increased its immunogenicity: IRE caused immunogenic death of tumor tissues, massive release of DAMPs, causing activation of APCs and presentation to T cells, leading to tumor specific T-cell population expansion and enhanced systemic antitumor effects; 2) Reversal of the immune tolerant tumor microenvironment, with M1 macrophages polarizing CD4+ Th1 cell differentiation to enhance CD8+ T cell survival and tumor infiltration; 3) IRE-induced regulation of the tumor stroma, extracellular matrix, and/or vascular system may be another reason (21, 36, 46, 53, 68, 73).

Vasculature, extracellular matrix, and chemical environment

Vasculature

Several studies have demonstrated the protective effect of ablation foci on large vessels (9, 16, 74). For example, researchers followed 158 vessels with a mean distance of 2.3 ± 2.5 mm from the treatment area and found only 7 (4.4%) with abnormal vascular changes, including stenosis and thrombosis (9). However, the effect of IRE on microvessels is uncertain, and in some studies, microvessels remain histopathologically preserved in the area after ablation and the structure is still present (75), but can show microvascular distortion, occlusion, and thrombosis when observed under electron microscopy (32), and after disruption of vascular continuity there can be hemorrhagic necrosis with infiltration of surrounding neutrophils (76), and endothelial cells are damaged significantly. Thereafter, the disrupted vessel can be recognized by new endothelial cells derived from neighboring cells and/or circulating endothelial progenitor cells (32). Non-thermal irreversible electroporation can cause a decellularizing effect of the vessel at 3 days, the vessel skeleton survives while cells are shed, however, at 7 days this skeleton has endothelial ingrowth (74).

The changes of the microvasculature after IRE are: immediate congestion (75); necrosis of endothelial cells, hemorrhage, and peripheral inflammatory response (32, 76); and there can be regeneration of new vessels (32). It is worth mentioning that in Lv et al.'s theoretical study of the effect of perforation on tumor vasculature and normal vasculature, by establishing a multilayer dielectric model, explored that rich vascular smooth muscle cells (VSMCs) might have a protective effect on normal vasculature, thus demonstrated that electroporation may have a stronger destructive effect on tumor vasculature (77).

At the level of regulation of angiogenesis, tumor growth requires nutritional support from blood vessels, and angiogenesis is influenced by the expression of pro-angiogenic factors and anti-angiogenic factors; the VEGF family, composed of six growth factors (VEGFA-F), is essential for angiogenesis (78, 79), and angiopoietin 1-2 (Ang1-2) is independent of VEGF, while Ang-2 is mainly present in vascular expressed in remodeled tissues and in the hypoxic tumor microenvironment (80). VEGF can also exert inhibitory effects on DC cells and effector T cells in driving neoangiogenesis, as well as increase TAM infiltration and the expansion of Tregs and MDSCs (78, 81–84). However, due to the overexpression of pro-angiogenic factors and less in tumors, tumor vessels exhibit functional abnormalities with abnormal leakage, rapid growth, high tortuosity, and little perivascular pericytes and smooth muscle cells coverage (78, 79). A decrease in VEGF and CD34 proteins can be detected 1 hour after nanosecond pulse treatment of pancreatic cancer (21). He et al. also found increased expression of CD31 in tumor after IRE (53). In addition, nsPEFs and everolimus (The mammalian target of rapamycin (mTOR) inhibitor) synergistically inhibited angiogenesis by decreasing the expression of vascular endothelial growth factor (VEGF), VEGF receptor (VEGFR), and CD34 (85). In addition to inhibiting the expression of pathological proangiogenic factors, a study by Zhao et al. found a transient increase in CD31 calculated tumor microvascular density microvessel density (MVD) followed by a decrease four days after IRE treatment of pancreatic cancer and an increase in microvascular permeability determined by fluorescein isothiocynate (FITC)-bound dextran (73). Therefore, pulsed electric field can inhibit the growth of tumor pathological blood vessels and blood supply around the tumor, and also preserve the permeability of functional blood vessels to a certain extent, which is conducive to the infiltration of immune cells and factors.

Extracellular matrix

In the tumor microenvironment, not only tumor cells proliferate rapidly, but also stromal deposition and remodeling as well as cancer cells and stromal cells increase, and CAFs form the main support structure of tumor tissues (1, 2). CAFs also promote cancer development by secreting growth-promoting factors such as TGF-β, stromal degrading enzymes and angiogenic factors such as MMP or VEGF, α smooth muscle actin (α-SMA) is a reliable biomarker for CAFs, and fibroblast activating protein α (FAP-α, seprase) is a surface glycoprotein that is selectively expressed on solid tumor fibroblasts. MMP hydrolyzes the extracellular matrix and its expression correlates with the aggressive phenotype of tumor cells and tumor progression (86).

Extracellular matrix and collagen structures can exist intact after IRE action because IRE acts on phospholipid bilayers (3, 74).

MMPs family proteins (MMP1, MMP2, MMP9, MMP11, MMP12, MMP14, and MMP21) are expressed at different levels of nsPEF intensity (21). In a study by Zhao et al. collagen matrix or αSMA+ CAFs were not affected by IRE, and FAP-α, hyaluronic acid (indicated by HABP1 expression levels) and lysyl oxidase (LOX, a marker of extracellular matrix stiffness) were decreased to varying degrees (36). Vasculature and collagen were still present in IRE-treated lung tissue 2 days after treatment and 28 days after a significant increase, indicating remodeling and regeneration of the mesenchyme, but decorin and heparan sulfate decreased after ablation (87).

Therefore, when electric pulses cause irreversible electroporation of cells, the presence of stromal and collagen structures can be observed histopathologically, but they can also microscopically modulate the cellular matrix and reduce the levels of CAFs and MMPs (Table 1). With the preservation of functional vessels and increased vascular permeability, softened extracellular matrix is beneficial to infiltration of inflammation and distant effects (16, 36, 53, 67).

Improving hypoxia

Tumor vessels show characteristics of tortuous, twisted, and easily occluded, and the tumor presents a relatively hypoxic state due to the rapid proliferation of tumor cells and the increase of extracellular matrix leading to the increase of tumor tissue pressure. Hypoxia leads to the accumulation of hypoxia-inducible factor 1-α (HIF-1α), which promotes further tumor angiogenesis and suppresses T-cell function (2, 88). Moreover, hypoxia increases anaerobic enzymes and lactate accumulation further reduces T and NK cell activation (89). Reversal of intratumoral hypoxia effectively increases the infiltration of immune cells. The downregulation of HIF-1α and carbonic anhydrase 9 (CA-IX) and increased vascular permeability after IRE suggest that IRE may also increase the number and action of local T cells, NK cells by alleviating tumor hypoxia (36).

Discussion

Compared with other local thermal techniques, pulsed electric field has several advantages in the regulation of the microenvironment: 1) It can protect the structure of large and medium vessels, and the elastic fibers and smooth muscle fibers in vessels can maintain the basic normal structure of vessels, with some damaged endothelial cells can be replaced (32, 74). 2) The protection of functional blood vessels makes sure the cell's "eat me" signals be found and recognized by APC (10, 29, 37, 43). 3) APC presents antigens to activate immunity, and the retained blood vessels are more conducive to the infiltration of immune cells, which may reduce the occurrence of residual cancer (10, 29, 46). 4) Triggering a shift from the innate immunosuppressive microenvironment to the immune-promoted antitumor microenvironment (27, 36, 46, 53, 64, 70). Combining pulsed electric field therapy with immunotherapy is beneficial to mobilize the body's immunity to kill tumors (37, 38, 66, 68). 5) It promotes systemic immunization and has the effect of distant effect, inhibiting tumors that may metastasize elsewhere (67, 70).

Although many studies of the effect of electric pulses on tumor microenvironment have been reported, there are still some questions that need to be addressed and more in-depth studies can be done in the future in the following areas.

1. The differences in the effects of IRE, nsPEF, and H-FIRE on cell and microenvironment need to be further studied. They have different parametric characteristics, the most prominent of which is the difference in pulse duration. They are capable of disrupting the structure of the cell membrane. However, nsPEF is characterized by high compression power, ultrashort pulse duration, fast rise time, and high electric field. When the pulse duration is shorter than the charging time of the cell membrane (mostly 100 ns), the charge cannot accumulate on the surface of the cell membrane and the applied electric field is mainly received by the membranes of intracellular organelles such as the nucleus, endoplasmic reticulum and mitochondria. When a 300 ns pulse (or longer) is applied, the pulse is long enough to allow the electric field to interact only with the plasma membrane and not the intracellular organelles (90, 91). The change of subcellular membrane potential may affect a series of signaling pathways. IRE and nsPEF are different in causing cell damage, which needs further study.
2. Even though it is the same modality, different parameters can bring about different changes. In IRE, the most studied is the voltage/field strength. Compared to a field strength of 500 V/cm, IRE using 2500 V/cm seems to be more capable of causing cellular damage, whether this is a thermal or non-thermal effect and by what exact mechanism of damage (including membrane damage, ATP depletion, mitochondrial damage, increase in ROS, DNA and protein damage) needs to be further investigated (4, 36). And changes in electric field strength bring about proportional changes in the mode of cell death, with the promotion of apoptosis evident at 500 V/cm but increased necrosis at 2500 V/cm (23), in between which there should be a suitable range of electric field strength that would keep the ablation zone within the desired range and cause more immunogenic death, but the appropriate field strength

may vary with the conductivity of the ablated tissue changes.

3. The complex cascade of responses induced by IRE, nsPEF, and H-FIRE remains to be investigated. The effect of pulsed electric fields on Wnt/β-Catenin, KRAS, EGFR, and downstream NF-κB signaling may be critical in determining therapeutic strategies, as these signals are often dysregulated in tumorigenic development (92, 93). More studies should address the complex signaling cascade response activated after pulsed electric fields.
4. The structure of antigens released by pulsed electric fields is uncertain. In experiments *in vitro*, IRE, despite releasing the highest amount of protein, which could be due to membrane rupture, was present with 40% denatured proteins, possibly related to the interactions of the high electric field, the charged amino acid residues of proteins, and solvent molecules. Alterations in the secondary structure of proteins are essential for APC processing and antigen presentation (69). Future *in vivo* experiments are still needed to evaluate the antigenic characteristics of IRE or nsPEF release, which will be important to optimize its stimulation of APC and thus the initiation and activation of T cells.
5. The effect of IRE on microvasculature remains controversial. A study found that CD31 was increased at 7 days after IRE (1000 V; 100 ms; 1 Hz; 80 pulses) in the tumor area (46), but some studies found that CD31 was increased on day 4 after IRE (200 V/960 V, 100 us, 1 Hz, 20 pulses) but fell back at day 7 (36). The difference in parameters does not seem to explain this. What is certain, however, is that IRE does preserve local vascular structures better than other thermal ablations, and in the study by Bulvik et al. there was an observed infiltration of inflammatory cells around the vessels, which was not seen with radiofrequency ablation (73). Therefore, it is important to clarify whether IRE is able to create a time window with the right number of microvessels and increased permeability, as this could provide more support for the timing of combined immunotherapy.
6. The effect of IRE on immunomodulatory activity has become an area of intensive research. However, most previous studies have provided only some descriptive data on temporal level changes in immune cells. Less has been explored regarding the precise IRE-mediated immune response.
7. Energy-based local therapies and immunotherapy can be synergistically combined is also a future direction. Pulsed electric fields can promote antigen preservation and local inflammation, and synergistic effects exist between them and immunotherapy (37, 38, 49, 66–68).

Conclusion

High voltage electrical pulses cause changes in multiple intracellular signaling pathways to inhibit replication and proliferation of tumor cells, and also kill tumor cells through multiple modes of death by necrosis, pyroptosis, and necroptosis. Pulsed electric fields can contribute to immunogenic death, increase tumor immunogenicity, reverse the immune tolerance environment, and can promote activation and proliferation of cancer-specific cytotoxic T cells acting locally and systemically.

Author contributions

Study concept and design, YW. Acquisition of data, YW, LTX, HW, JZ, LX, CF, and TJ. Writing-Original draft preparation, YW. Visualization, YW. Obtaining of funding, TJ. Technical or material support, LTX, HW, and TJ. Study supervision, TJ. All authors contributed to the article and approved the submitted version.

Funding

This study was supported by Development Project of National Major Scientific Research Instrument (82027803), National Natural Science Foundation of China (81971623), and Key Project of Natural Science Foundation of Zhejiang Province (LZ20H180001).

Conflict of interest

The authors declare that the research was conducted in the absence of any commercial or financial relationships that could be construed as a potential conflict of interest.

Publisher's note

References

1. Ivey JW, Bonakdar M, Kanitkar A, Davalos RV, Verbridge SS. Improving cancer therapies by targeting the physical and chemical hallmarks of the tumor microenvironment. *Cancer Lett* (2016) 380(1):330–9. doi: 10.1016/j.canlet

2. Donlon NE, Power R, Hayes C, Reynolds JV, Lysaght J. Radiotherapy, immunotherapy, and the tumour microenvironment: Turning an immunosuppressive milieu into a therapeutic opportunity. *Cancer Lett* (2021) 502:84–96. doi: 10.1016/j.canlet.2020.12.045

3. Chu KF, Dupuy DE. Thermal ablation of tumours: biological mechanisms and advances in therapy. *Nat Rev Cancer* (2014) 14(3):199–208. doi: 10.1038/nrc3672

4. Batista Napotnik T, Polajžer T, Miklavčič D. Cell death due to electroporation - a review. *Bioelectrochemistry* (2021) 141:107871. doi: 10.1016/j.bioelechem.2021.107871

5. Gowrishankar TR, Esser AT, Smith KC, Son RS, Weaver JC. Intracellular electroporation site distributions: modeling examples for nsPEF and IRE pulse waveforms. *Annu Int Conf IEEE Eng Med Biol Soc* (2011) 2011:732–5. doi: 10.1109/IEMBS.2011.6090166

6. Lorenzo MF, Arena CB, Davalos RV. Maximizing local access to therapeutic deliveries in glioblastoma. In: S De Vleeschouwer, editor. *Part III: Irreversible electroporation and high-frequency irreversible electroporation for the eradication of glioblastoma*. Brisbane (AU: Codon Publications (2017). Chapter 19.

7. Sutter O, Calvo J, N'Kontchou G, Nault JC, Ourabia R, Nahon P, et al. Safety and efficacy of irreversible electroporation for the treatment of hepatocellular carcinoma not amenable to thermal ablation techniques: A retrospective single-center case series. *Radiology* (2017) 284(3):877–86. doi: 10.1148/radiol.2017161413

8. Thomson KR, Cheung W, Ellis SJ, Federman D, Kavnoudias H, Loader-Oliver D, et al. Investigation of the safety of irreversible electroporation in humans. *J Vasc Interv Radiol* (2011) 22(5):611–21. doi: 10.1016/j.jvir.2010.12.014

9. Narayanan G, Bhatia S, Echenique A, Suthar R, Barbery K, Yrizarry J. Vessel patency post irreversible electroporation. *Cardiovasc Intervent Radiol* (2014) 37 (6):1523–9. doi: 10.1007/s00270-014-0988-9

10. Dai Z, Wang Z, Lei K, Liao J, Peng Z, Lin M, et al. Irreversible electroporation induces CD8+ T cell immune response against post-ablation hepatocellular carcinoma growth. *Cancer Lett* (2021) 503:1–10. doi: 10.1016/j.canlet.2021.01.001

11. Sun S, Liu Y, He C, Hu W, Liu W, Huang X, et al. Combining NanoKnife with M1 oncolytic virus enhances anticancer activity in pancreatic cancer. *Cancer Lett* (2021) 502:9–24. doi: 10.1016/j.canlet.2020.12.018

12. Polajzer T, Jarm T, Miklavcic D. Analysis of damage-associated molecular pattern molecules due to electroporation of cells *in vitro*. *Radiol Oncol* (2020) 54 (3):317–28. doi: 10.2478/raon-2020-0047

13. Hofmann F, Ohnimus H, Scheller C, Strupp W, Zimmermann U, Jassoy C. Electric field pulses can induce apoptosis. *J Membr Biol* (1999) 169(2):103–9. doi: 10.1007/s002329900522

14. Beebe SJ, Chen YJ, Sain NM, Schoenbach KH, Xiao S. Transient features in nanosecond pulsed electric fields differentially modulate mitochondria and viability. *PloS One* (2012) 7(12):e51349. doi: 10.1371/journal.pone.0051349

15. Kim HB, Sung CK, Baik KY, Moon KW, Kim HS, Yi JH, et al. Changes of apoptosis in tumor tissues with time after irreversible electroporation. *Biochem Biophys Res Commun* (2013) 435(4):651–6. doi: 10.1016/j.bbrc.2013.05.039

16. Zhang Y, Lyu C, Liu Y, Lv Y, Chang TT, Rubinsky B. Molecular and histological study on the effects of non-thermal irreversible electroporation on the liver. *Biochem Biophys Res Commun* (2018) 500(3):665–70. doi: 10.1016/j.bbrc.2018.04.132

17. Goldberg A, Rubinsky B. The effect of electroporation type pulsed electric fields on DNA in aqueous solution. *Technol Cancer Res Treat* (2010) 9(4):423–30. doi: 10.1177/153303461000900412

18. Hall EH, Schoenbach KH, Beebe SJ. Nanosecond pulsed electric fields induce apoptosis in p53-wildtype and p53-null HCT116 colon carcinoma cells. *Apoptosis* (2007) 12(9):1721–31. doi: 10.1007/s10495-007-0083-7

19. Szlasa W, Kiełbik A, Szewczyk A, Rembiałkowska N, Novickij V, Tarek M, et al. Oxidative effects during irreversible electroporation of melanoma cells-*In vitro* study. *Molecules* (2020) 26(1):154. doi: 10.3390/molecules26010154

20. Batista Napotnik T, Wu YH, Gundersen MA, Miklavčič D, Vernier PT. Nanosecond electric pulses cause mitochondrial membrane permeabilization in jurkat cells. *Bioelectromagnetics* (2012) 33(3):257–64. doi: 10.1002/bem.20707

21. Ren Z, Chen X, Cui G, Yin S, Chen L, Jiang J, et al. Nanosecond pulsed electric field inhibits cancer growth followed by alteration in expressions of NF-κB and wnt/β-catenin signaling molecules. *PloS One* (2013) 8(9):e74322. doi: 10.1371/journal.pone.0074322

22. Krishnamurthy N, Kurzrock R. Targeting the wnt/beta-catenin pathway in cancer: Update on effectors and inhibitors. *Cancer Treat Rev* (2018) 62:50–60. doi: 10.1016/j.ctrv.2017.11.002

23. Brock RM, Beitel-White N, Coutermarsh-Ott S, Grider DJ, Lorenzo MF, Ringel-Scaia VM, et al. Patient derived xenografts expand human primary pancreatic tumor tissue availability for ex vivo irreversible electroporation testing. *Front Oncol* (2020) 10:843. doi: 10.3389/fonc.2020.00843

24. Tian G, Guan J, Chu Y, Zhao Q, Jiang T. Immunomodulatory effect of irreversible electroporation alone and its cooperating with immunotherapy in pancreatic cancer. *Front Oncol* (2021) 11:712042. doi: 10.3389/fonc.2021.712042

25. Yin D, Yang WG, Weissberg J, Goff CB, Chen W, Kuwayama Y, et al. Cutaneous papilloma and squamous cell carcinoma therapy utilizing nanosecond pulsed electric fields (nsPEF). *PloS One* (2012) 7(8):e43891. doi: 10.1371/journal.pone.0043891

26. Beebe SJ, Fox PM, Rec LJ, Willis EL, Schoenbach KH. Nanosecond, high-intensity pulsed electric fields induce apoptosis in human cells. *FASEB J* (2003) 17 (11):1493–5. doi: 10.1096/fj.02-0859fje

27. Ringel-Scaia VM, Beitel-White N, Lorenzo MF, Brock RM, Huie KE, Coutermarsh-Ott S, et al. High-frequency irreversible electroporation is an effective tumor ablation strategy that induces immunologic cell death and promotes systemic anti-tumor immunity. *EBioMedicine* (2019) 44:112–25. doi: 10.1016/j.ebiom.2019.05.036

28. Zhang H, Liu K, Xue Z, Yin H, Dong H, Jin W, et al. High-voltage pulsed electric field plus photodynamic therapy kills breast cancer cells by triggering apoptosis. *Am J Transl Res* (2018) 10(2):334–51.

29. He C, Sun S, Zhang Y, Xie F, Li S. The role of irreversible electroporation in promoting M1 macrophage polarization *via* regulating the HMGB1-RAGE-MAPK axis in pancreatic cancer. *Oncoimmunology* (2021) 10(1):1897295. doi: 10.1080/2162402X.2021.1897295

30. Brock RM, Beitel-White N, Davalos RV, Allen IC. Starting a fire without flame: The induction of cell death and inflammation in electroporation-based tumor ablation strategies. *Front Oncol* (2020) 10:1235. doi: 10.3389/fonc.2020.01235

31. Zhang Z, Li W, Procissi D, Tyler P, Omary RA, Larson AC. Rapid dramatic alterations to the tumor microstructure in pancreatic cancer following irreversible electroporation ablation. *Nanomedicine (Lond)* (2014) 9(8):1181–92. doi: 10.2217/nnm.13.72

32. López-Alonso B, Hernáez A, Sarnago H, Naval A, Güemes A, Junquera C, et al. Histopathological and ultrastructural changes after electroporation in pig liver using parallel-plate electrodes and high-performance generator. *Sci Rep* (2019) 9 (1):2647. doi: 10.1038/s41598-019-39433-6

33. Zhou W, Xiong Z, Liu Y, Yao C, Li C. Low voltage irreversible electroporation induced apoptosis in HeLa cells. *J Cancer Res Ther* (2012) 8 (1):80–5. doi: 10.4103/0973-1482.95179

34. Faroja M, Ahmed M, Appelbaum L, Ben-David E, Moussa M, Sosna J, et al. Irreversible electroporation ablation: is all the damage nonthermal? *Radiology* (2013) 266(2):462–70. doi: 10.1148/radiol.12120609

35. Kroemer G, Galluzzi L, Kepp O, Zitvogel L. Immunogenic cell death in cancer therapy. *Annu Rev Immunol* (2013) 31:51–72. doi: 10.1146/annurev-immunol-032712-100008

36. Zhao J, Wen X, Tian L, Li T, Xu C, Wen X, et al. Irreversible electroporation reverses resistance to immune checkpoint blockade in pancreatic cancer. *Nat Commun* (2019) 10(1):899. doi: 10.1038/s41467-019-08782-1

37. Yang J, Eresen A, Shangguan J, Ma Q, Yaghmai V, Zhang Z. Irreversible electroporation ablation overcomes tumor-associated immunosuppression to improve the efficacy of DC vaccination in a mice model of pancreatic cancer. *Oncoimmunology* (2021) 10(1):1875638. doi: 10.1080/2162402X.2021.1875638

38. Go EJ, Yang H, Chon HJ, Yang D, Ryu W, Kim DH, et al. Combination of irreversible electroporation and STING agonist for effective cancer immunotherapy. *Cancers (Basel)* (2020) 12(11):3123. doi: 10.3390/cancers12113123

39. Rossi A, Pakhomova ON, Mollica PA, Casciola M, Mangalanathan U, Pakhomov AG, et al. Nanosecond pulsed electric fields induce endoplasmic reticulum stress accompanied by immunogenic cell death in murine models of lymphoma and colorectal cancer. *Cancers (Basel)* (2019) 11(12):2034. doi: 10.3390/cancers11122034

40. Pawaria S, Binder RJ. CD91-dependent programming of T-helper cell responses following heat shock protein immunization. *Nat Commun* (2011) 2:521. doi: 10.1038/ncomms1524

41. Messmer D, Yang H, Telusma G, Knoll F, Li J, Messmer B, et al. High mobility group box protein 1: an endogenous signal for dendritic cell maturation and Th1 polarization. *J Immunol* (2004) 173(1):307–13. doi: 10.4049/jimmunol.173.1.307

42. Dumitriu IE, Baruah P, Valentinis B, Voll RE, Herrmann M, Nawroth PP, et al. Release of high mobility group box 1 by dendritic cells controls T cell

activation *via* the receptor for advanced glycation end products. *J Immunol* (2005) 174(12):7506–15. doi: 10.4049/jimmunol.174.12.7506

43. Orlova VV, Choi EY, Xie C, Chavakis E, Bierhaus A, Ihanus E, et al. A novel pathway of HMGB1-mediated inflammatory cell recruitment that requires mac-1-integrin. *EMBO J* (2007) 26(4):1129–39. doi: 10.1038/sj.emboj.7601552

44. Shapouri-Moghaddam A, Mohammadian S, Vazini H, Taghadosi M, Esmaeili SA, Mardani F, et al. Macrophage plasticity, polarization, and function in health and disease. *J Cell Physiol* (2018) 233(9):6425–40. doi: 10.1002/jcp.26429

45. Mantovani A, Sozzani S, Locati M, Allavena P, Sica A. Macrophage polarization: tumor-associated macrophages as a paradigm for polarized M2 mononuclear phagocytes. *Trends Immunol* (2002) 23(11):549–55. doi: 10.1016/s1471-4906(02)02302-5

46. He C, Huang X, Zhang Y, Lin X, Li S. T-Cell activation and immune memory enhancement induced by irreversible electroporation in pancreatic cancer. *Clin Transl Med* (2020) 10(2):e39. doi: 10.1002/ctm2.39

47. Au JT, Mittra A, Song TJ, Cavnar M, Jun K, Carson J, et al. Irreversible electroporation facilitates gene transfer of a GM-CSF plasmid with a local and systemic response. *Surgery* (2013) 154(3):496–503. doi: 10.1016/j.surg.2013.06.005

48. Balan S, Saxena M, Bhardwaj N. Dendritic cell subsets and locations. *Int Rev Cell Mol Biol* (2019) 348:1–68. doi: 10.1016/bs.ircmb.2019.07.004

49. Alnaggar M, Lin M, Mesmar A, Liang S, Qaid A, Xu K, et al. Allogenic natural killer cell immunotherapy combined with irreversible electroporation for stage IV hepatocellular carcinoma: Survival outcome. *Cell Physiol Biochem* (2018) 48(5):1882–93. doi: 10.1159/000492509

50. He C, Wang J, Sun S, Zhang Y, Li S. Immunomodulatory effect after irreversible electroporation in patients with locally advanced pancreatic cancer. *J Oncol* (2019) 2019:9346017. doi: 10.1155/2019/9346017

51. Chen X, Ren Z, Yin S, Xu Y, Guo D, Xie H, et al. The local liver ablation with pulsed electric field stimulate systemic immune reaction against HCC with time-dependent cytokine profile. *Cytokine* (2017) 93:44–50. doi: 10.1016/j.cyto.2017.05.003

52. Borish LC, Steinke JW. 2. cytokines and chemokines. *J Allergy Clin Immunol* (2003) 111(2 Suppl):S460–75. doi: 10.1067/mai.2003.108

53. Zhao J, Chen S, Zhu L, Zhang L, Liu J, Xu D, et al. Antitumor effect and immune response of nanosecond pulsed electric fields in pancreatic cancer. *Front Oncol* (2021) 10:621092. doi: 10.3389/fonc.2020.621092

54. Li X, Xu K, Li W, Qiu X, Ma B, Fan Q, et al. Immunologic response to tumor ablation with irreversible electroporation. *PloS One* (2012) 7(11):e48749. doi: 10.1371/journal.pone.0048749

55. Bonilla FA, Oettgen HC. Adaptive immunity. *J Allergy Clin Immunol* (2010) 125(2 Suppl 2):S33–40. doi: 10.1016/j.jaci.2009.09.017

56. Yimingjiang M, Tuergan T, Chen X, Wen H, Shao Y, Zhang R, et al. Comparative analysis of immunoactivation by nanosecond pulsed electric fields and PD-1 blockade in murine hepatocellular carcinoma. *Anal Cell Pathol (Amst)* (2020) 2020:9582731. doi: 10.1155/2020/9582731

57. Teicher BA. Transforming growth factor-beta and the immune response to malignant disease. *Clin Cancer Res* (2007) 13(21):6247–51. doi: 10.1158/1078-0432.CCR-07-1654

58. Sakaguchi S, Yamaguchi T, Nomura T, Ono M. Regulatory T cells and immune tolerance. *Cell* (2008) 133(5):775–87. doi: 10.1016/j.cell.2008.05.009

59. Petersen RP, Campa MJ, Sperlazza J, Conlon D, Joshi MB, Harpole DHJr, et al. Tumor infiltrating Foxp3+ regulatory T-cells are associated with recurrence in pathologic stage I NSCLC patients. *Cancer* (2006) 107(12):2866–72. doi: 10.1002/cncr.22282

60. Whiteside TL. FOXP3+ treg as a therapeutic target for promoting anti-tumor immunity. *Expert Opin Ther Targets* (2018) 22(4):353–63. doi: 10.1080/14728222.2018.1451514

61. Cassetta L, Pollard JW. Tumor-associated macrophages. *Curr Biol* (2020) 30(6):R246–8. doi: 10.1016/j.cub.2020.01.031

62. Kumar V, Patel S, Tcyganov E, Gabrilovich DI. The nature of myeloid-derived suppressor cells in the tumor microenvironment. *Trends Immunol* (2016) 37(3):208–20. doi: 10.1016/j.it.2016.01.004

63. Belli C, Trapani D, Viale G, D'Amico P, Duso BA, Della Vigna P, et al. Targeting the microenvironment in solid tumors. *Cancer Treat Rev* (2018) 65:22–32. doi: 10.1016/j.ctrv.2018.02.004

64. Scheffer HJ, Stam AGM, Geboers B, Vroomen LGPH, Ruarus A, de Bruijn B, et al. Irreversible electroporation of locally advanced pancreatic cancer transiently alleviates immune suppression and creates a window for antitumor T cell activation. *Oncoimmunology* (2019) 8(11):1652532. doi: 10.1080/2162402X.2019.1652532

65. Pandit H, Hong YK, Li Y, Rostas J, Pulliam Z, Li SP, et al. Evaluating the regulatory immunomodulation effect of irreversible electroporation (IRE) in pancreatic adenocarcinoma. *Ann Surg Oncol* (2019) 26(3):800–6. doi: 10.1245/s10434-018-07144-3

66. Zhang QW, Guo XX, Zhou Y, Wang QB, Liu Q, Wu ZY, et al. OX40 agonist combined with irreversible electroporation synergistically eradicates established tumors and drives systemic antitumor immune response in a syngeneic pancreatic cancer model. *Am J Cancer Res* (2021) 11(6):2782–801.

67. Zhang X, Zhang Y, Chen J, Wu Y, Zhang J, Wang J. Nanosecond pulsed electric field inhibits malignant melanoma growth by inducing the change of systemic immunity. *Med Oral Patol Oral Cir Bucal* (2019) 24(4):e555–61. doi: 10.4317/medoral.22976

68. Burbach BJ, O'Flanagan SD, Shao Q, Young KM, Slaughter JR, Rollins MR, et al. Irreversible electroporation augments checkpoint immunotherapy in prostate cancer and promotes tumor antigen-specific tissue-resident memory CD8+ T cells. *Nat Commun* (2021) 12(1):3862. doi: 10.1038/s41467-021-24132-6

69. White SB, Zhang Z, Chen J, Gogineni VR, Larson AC. Early immunologic response of irreversible electroporation versus cryoablation in a rodent model of pancreatic cancer. *J Vasc Interv Radiol* (2018) 29(12):1764–9. doi: 10.1016/j.jvir.2018.07.009

70. Shi X, O'Neill C, Wang X, Chen Y, Yu Y, Tan M, et al. Irreversible electroporation enhances immunotherapeutic effect in the off-target tumor in a murine model of orthotopic HCC. *Am J Cancer Res* (2021) 11(6):3304–19.

71. Mellman I, Coukos G, Dranoff G. Cancer immunotherapy comes of age. *Nature* (2011) 480(7378):480–9. doi: 10.1038/nature10673

72. Babikr F, Wan J, Xu A, Wu Z, Ahmed S, Freywald A, et al. Distinct roles but cooperative effect of TLR3/9 agonists and PD-1 blockade in converting the immunotolerant microenvironment of irreversible electroporation-ablated tumors. *Cell Mol Immunol* (2021) 18(12):2632–47. doi: 10.1038/s41423-021-00796-4

73. Bulvik BE, Rozenblum N, Gourevich S, Ahmed M, Andriyanov AV, Galun E, et al. Irreversible electroporation versus radiofrequency ablation: A comparison of local and systemic effects in a small-animal model. *Radiology* (2016) 280(2):413–24. doi: 10.1148/radiol.2015151166

74. Phillips M, Maor E, Rubinsky B. Nonthermal irreversible electroporation for tissue decellularization. *J Biomech Eng* (2010) 132(9):091003. doi: 10.1115/1.4001882

75. Lee YJ, Lu DS, Osuagwu F, Lassman C. Irreversible electroporation in porcine liver: acute computed tomography appearance of ablation zone with histopathologic correlation. *J Comput Assist Tomogr* (2013) 37(2):154–8. doi: 10.1097/RCT.0b013e31827dbf9b

76. Long G, Bakos G, Shires PK, Gritter L, Crissman JW, Harris JL, et al. Histological and finite element analysis of cell death due to irreversible electroporation. *Technol Cancer Res Treat* (2014) 13(6):561–9. doi: 10.7785/tcrtexpress.2013.600253

77. Lv Y, Zhang Y, Rubinsky B. Molecular and histological study on the effects of electrolytic electroporation on the liver. *Bioelectrochemistry* (2019) 125:79–89. doi: 10.1016/j.bioelechem.2018.09.007

78. Tonini T, Rossi F, Claudio PP. Molecular basis of angiogenesis and cancer. *Oncogene* (2003) 22(42):6549–56. doi: 10.1038/sj.onc.1206816

79. Carmeliet P, Jain RK. Angiogenesis in cancer and other diseases. *Nature* (2000) 407(6801):249–57. doi: 10.1038/35025220

80. Nasarre P, Thomas M, Kruse K, Helfrich I, Wolter V, Deppermann C, et al. Host-derived angiopoietin-2 affects early stages of tumor development and vessel maturation but is dispensable for later stages of tumor growth. *Cancer Res* (2009) 69(4):1324–33. doi: 10.1158/0008-5472.CAN-08-3030

81. Rahma OE, Hodi FS. The intersection between tumor angiogenesis and immune suppression. *Clin Cancer Res* (2019) 25(18):5449–57. doi: 10.1158/1078-0432.CCR-18-1543

82. Oyama T, Ran S, Ishida T, Nadaf S, Kerr L, Carbone DP, et al. Vascular endothelial growth factor affects dendritic cell maturation through the inhibition of nuclear factor-kappa b activation in hemopoietic progenitor cells. *J Immunol* (1998) 160(3):1224–32.

83. Ohm JE, Gabrilovich DI, Sempowski GD, Kisseleva E, Parman KS, Nadaf S, et al. VEGF inhibits T-cell development and may contribute to tumor-induced immune suppression. *Blood* (2003) 101(12):4878–86. doi: 10.1182/blood-2002-07-1956

84. Wada J, Suzuki H, Fuchino R, Yamasaki A, Nagai S, Yanai K, et al. The contribution of vascular endothelial growth factor to the induction of regulatory T-cells in malignant effusions. *Anticancer Res* (2009) 29(3):881–8.

85. Dai J, Wu S, Kong Y, Chi Z, Si L, Sheng X, et al. Nanosecond pulsed electric fields enhance the anti-tumour effects of the mTOR inhibitor everolimus against melanoma. *Sci Rep* (2017) 7:39597. doi: 10.1038/srep39597

86. Hofmeister V, Vetter C, Schrama D, Bröcker EB, Becker JC. Tumor stroma-associated antigens for anti-cancer immunotherapy. *Cancer Immunol Immunother* (2006) 55(5):481–94. doi: 10.1089/bioe.2021.0014

87. Fujimori M, Kimura Y, Ueshima E, Dupuy DE, Adusumilli PS, Solomon SB, et al. Lung ablation with irreversible electroporation promotes immune cell

infiltration by sparing extracellular matrix proteins and vasculature: Implications for immunotherapy. *Bioelectricity* (2021) 3(3):204–14. doi: 10.1089/bioe.2021.0014

88. Doedens AL, Stockmann C, Rubinstein MP, Liao D, Zhang N, DeNardo DG, et al. Macrophage expression of hypoxia-inducible factor-1 alpha suppresses T-cell function and promotes tumor progression. *Cancer Res* (2010) 70(19):7465–75. doi: 10.1158/0008-5472.CAN-10-1439

89. Brand A, Singer K, Koehl GE, Kolitzus M, Schoenhammer G, Thiel A, et al. LDHA-associated lactic acid production blunts tumor immunosurveillance by T and NK cells. *Cell Metab* (2016) 24(5):657–71. doi: 10.1016/j.cmet.2016.08.011

90. Schoenbach KH, Joshi R, Kolb J, Buescher S, Beebe S. Subcellular effects of nanosecond electrical pulses. *Conf Proc IEEE Eng Med Biol Soc* (2004) 2004:5447–50. doi: 10.1109/IEMBS.2004.1404522

91. Breton M, Mir LM. Microsecond and nanosecond electric pulses in cancer treatments. *Bioelectromagnetics* (2012) 33(2):106–23. doi: 10.1002/bem.20692

92. Sigismund S, Avanzato D, Lanzetti L. Emerging functions of the EGFR in cancer. *Mol Oncol* (2018) 12(1):3–20. doi: 10.1002/1878-0261.12155

93. Drosten M, Barbacid M. Targeting the MAPK pathway in KRAS-driven tumors. *Cancer Cell* (2020) 37(4):543–50. doi: 10.1016/j.ccell.2020.03.013

Frontiers in Immunology

Explores novel approaches and diagnoses to treat immune disorders.

The official journal of the International Union of Immunological Societies (IUIS) and the most cited in its field, leading the way for research across basic, translational and clinical immunology.

Discover the latest Research Topics

See more →

Frontiers

Avenue du Tribunal-Fédéral 34
1005 Lausanne, Swizerland
frontiersin.org

Contact us

+41 (0)21 510 17 00
frontiersin.org/about/contact